



# Kent Academic Repository

**Brown, Oliver (2015) *Novel Dissymmetric Copper Bis(thiosemicarbazone) Complexes for Medical Diagnostic Imaging by Positron Emission Tomography.* Doctor of Philosophy (PhD) thesis, University of Kent,.**

## Downloaded from

<https://kar.kent.ac.uk/53590/> The University of Kent's Academic Repository KAR

## The version of record is available from

## This document version

UNSPECIFIED

## DOI for this version

## Licence for this version

UNSPECIFIED

## Additional information

## Versions of research works

### Versions of Record

If this version is the version of record, it is the same as the published version available on the publisher's web site. Cite as the published version.

### Author Accepted Manuscripts

If this document is identified as the Author Accepted Manuscript it is the version after peer review but before type setting, copy editing or publisher branding. Cite as Surname, Initial. (Year) 'Title of article'. To be published in *Title of Journal*, Volume and issue numbers [peer-reviewed accepted version]. Available at: DOI or URL (Accessed: date).

## Enquiries

If you have questions about this document contact [ResearchSupport@kent.ac.uk](mailto:ResearchSupport@kent.ac.uk). Please include the URL of the record in KAR. If you believe that your, or a third party's rights have been compromised through this document please see our [Take Down policy](https://www.kent.ac.uk/guides/kar-the-kent-academic-repository#policies) (available from <https://www.kent.ac.uk/guides/kar-the-kent-academic-repository#policies>).

**Novel Dissymmetric Copper  
Bis(thiosemicarbazone) Complexes for Medical  
Diagnostic Imaging by Positron Emission  
Tomography.**

A thesis is submitted to  
the University of Kent at Canterbury  
in partial fulfilment of the requirements for the degree of  
Doctor of Philosophy

By

Oliver Brown

June 2015

I dedicate this thesis to Isabella-Rose

*May this inspire you that anything is possible with a little determination and the support of such awesome family and friends.*

## **Declaration**

No part of this thesis has been submitted by me or anyone else in support of an application for any other degree or qualification at the University of Kent or at any other University.

A handwritten signature in black ink, consisting of a stylized 'O' and 'B' followed by a long, wavy horizontal line.

Oliver Brown

## Acknowledgements

I would like to express my sincere thanks to my supervisor, Prof. Mike Went for all his assistance and encouragement that enabled to pass through 3 years of blood, sweat and tears which enabled me to submit a thesis.

With a huge amount of gratitude I would like to thank Nikki for her love, support and standing beside me through the ups and downs of this PhD.

My eternal thanks go out to my family, particularly my parents (Sharon and Thomas) who without their belief, encouragement and support, this thesis would not have been possible. A particular mention should go to my Grandfather who from a very young age has always pushed me to chase success. My love and thanks go out to my siblings Sophie, Victoria and Joseph for all their support over the years.

I would like to thank Dr. Vicky Mason, for giving me the opportunity to get involved in Outreach. Without this opportunity completing a self-funded PhD would have been very tough, also I would not have grown so much as a person.....but may have had less grey hairs.

I would like to thank all my fellow outreach demonstrators for being such a joy to work with, including the frequent grillings for being a Chemist in a Physicist dominated team.

I also would like to thank all my fellow students in the lab 310 who made it a pleasure to work. A particular thanks to Trevor who rode the 3 year roller-coaster of research alongside me.

My thanks go out to everyone in 104, who made the office such a fantastic place to be particularly, Chris who was always at hand for an emergency pint or a beasting on the climbing wall.

To all the academics, technical staff and administration staff in the school of Physical Sciences, you are all awesome! I shall miss you all.

Thanks to Prof. Phil Blower and Julia Baguña Torres for their assistance with making my research applicable to such a fantastic application, of which potentially great good can be achieved. With great gratitude, I would like to extend a second thank you to Julia for collecting all the reduction potential data on my copper complexes.

Special thanks go out to Kevin Howland from Biosciences, who very kindly ran a vast number of mass spectrometry samples for me.

For running analysing a sample by X-ray diffraction I would like to thank Prof. Derek Tocher from UCL.

## Abstract

Bis(thiosemicarbazone) ligand derivatives (Figure 1) and their metal complexes (Figure 2) have long been of interest as they have applications as anticonvulsants, super-oxide dismutase-like radical scavengers, in the investigation of Alzheimer's disease and diagnostic imaging.

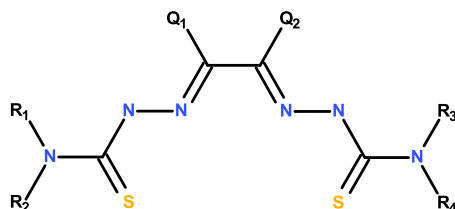


Figure 1

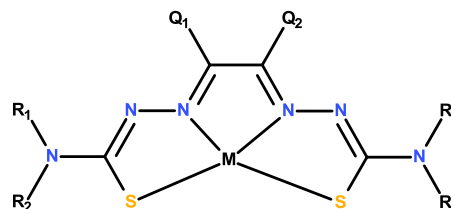


Figure 2

Copper (II) bis(thiosemicarbazone) derivatives have been used extensively in the imaging of oxygen deficient (hypoxic) cells for the detection and imaging of cancerous tissues and heart disease via Positron Emission Tomography (PET). It is possible to fine tune the bis(thiosemicarbazone) complexes redox potentials and lipophilicity by altering the substituents on the  $Q_1$  and  $Q_2$  position and the  $R_1$ ,  $R_2$ ,  $R_3$  and  $R_4$  locations respectively. To date only symmetric bis(thiosemicarbazone) ligands ( $R_1=R_3$ ,  $R_2=R_4$ ) have been evaluated for hypoxia imaging. This thesis reports the synthesis of dissymmetric ligands ( $R_1\neq R_3$ ,  $R_2\neq R_4$ ) in order to gain further control of the properties of the complexes and therefore the locations they will migrate to. A range of ligands has also been synthesised for the monitoring of copper metabolism within the brain for the investigation of Alzheimer's disease and other neurodegenerative disorders. Ligand synthesis has been achieved by controlling the condensation reactions between dicarbonyl compounds and 4-substituted-3-thiosemicarbazides. Synthesis via an alternative acetal protecting method has also been investigated.

Thirty bis(thiosemicarbazone) ligands have been successfully synthesised, of which thirteen are symmetric and seventeen dissymmetric. From this library of ligands, eighteen copper complexes have been synthesised along with twenty zinc complexes. The zinc complexes have the potential to act as convenient precursors for the rapid synthesis of radio-copper complexes via a transmetalation method.

All ligands, complexes and intermediates have been fully characterised by a range of techniques including IR spectroscopy, Raman spectroscopy, NMR spectroscopy, UV-vis spectroscopy, elemental analysis and mass spectroscopy. A new cyclic by-product from the ligand synthesis has also been isolated and fully characterised.

# Table of contents

<b>Declaration</b> .....	<b>ii</b>
<b>Acknowledgements</b> .....	<b>iii</b>
<b>Abstract</b> .....	<b>iv</b>
<b>Table of contents</b> .....	<b>v</b>
<b>Abbreviations</b> .....	<b>x</b>
<b>1. Introduction</b> .....	<b>1</b>
1.1. Nuclear medicine .....	1
1.1.1. Diagnosis .....	1
1.1.2. Therapy .....	2
1.1.3. Types of radioactive decay.....	2
1.2. Single Photon Emission Computed Tomography (SPECT) .....	5
1.3. Positron Emission Tomography (PET) .....	7
1.4. Copper radioisotopes in nuclear medicine. ....	10
1.5. Bis(thiosemicarbazone) ligands .....	15
1.6. Complexes of bis(thiosemicarbazone) pro-ligands.....	23
1.6.1. Copper bis(thiosemicarbazone) complexes.....	23
1.6.2. Applications of copper bis(thiosemicarbazone) complexes .....	24
1.6.2.1. Hypoxia imaging.....	25
1.6.2.2. Imaging copper metabolism for the investigation of neurodegenerative disorders..	38
1.6.3. Zinc bis(thiosemicarbazone) complexes .....	40
1.6.3.1. Transmetalation .....	41
1.7. Thesis hypothesis, aims and objectives .....	42
1.7.1. Hypothesis.....	45
1.7.2. Aims.....	46
1.7.3. Objectives.....	46
<b>2. Synthesis of symmetric and dissymmetric bis(thiosemicarbazone) ligands. ....</b>	<b>47</b>
2.1. Introduction .....	47
2.1.1. Abbreviations used to describe the bis(thiosemicarbazone) ligands .....	47
2.1.2 Abbreviations for the intermediates .....	50
2.2. Synthesis of dissymmetric bis(thiosemicarbazone) ligands by the protecting approach.....	51
2.2.1. Method of synthesis .....	52
2.2.2. Characterisation data for ligands synthesised by the protection method .....	54
2.2.3. Monitoring the de-protection of PADA via spectral methods.....	55

2.2.4. Attempts to synthesise dissymmetric ligands from DMB.....	59
2.2.5. Synthetic methods .....	65
2.2.6. NMR spectral data .....	66
2.2.7. Discussion.....	66
2.3. Ligands with Me/H backbones.....	69
2.3.1. Symmetric ligands with Me/H backbones .....	69
2.3.2. Methods .....	70
2.3.3. Characterisation data for symmetric ligands with Me/H backbones .....	71
2.3.4. Spectral examples of a symmetric ligand with a Me/H backbone.....	73
2.3.5. Discussion.....	75
2.3.6. Dissymmetric ligands with Me/H backbones.....	77
2.3.7. Synthesis of the PADA-mono-substituted-3-thiosemicarbazone intermediates.....	79
2.3.8. Methods .....	79
2.3.9. Characterisation data for the PADA-mono-substituted-3-thiosemicarbazone intermediates.....	80
2.3.10. Spectral examples of a PADA-mono-substituted-3-thiosemicarbazone intermediate	81
2.3.11. Discussion.....	83
2.3.12. Dissymmetric ligands from PADA-Me=O .....	87
2.3.13. Dissymmetric ligands from PADA-Et=O .....	90
2.3.14. Dissymmetric ligands from PADA-Ph=O .....	92
2.3.15 Spectral examples of a dissymmetric ligand with a Me/H backbone .....	94
2.3.16. Discussion.....	96
2.4. Ligands with Me/Me backbones.....	99
2.4.1. Symmetric ligands with Me/Me backbones .....	99
2.4.2. Methods .....	100
2.4.3. Characterisation data for symmetric ligands with Me/Me backbones .....	101
2.4.4. Spectral examples of a symmetric ligand with a Me/Me backbone.....	102
2.4.5. Discussion.....	104
2.4.6. Dissymmetric ligands with Me/Me backbones.....	107
2.4.7. Synthesis of the BDO-mono-substituted-3-thiosemicarbazone intermediates .....	108
2.4.8. Characterisation data for the BDO-mono-substituted-3-thiosemicarbazone intermediates.....	109
2.4.9. Spectral examples of a BDO-mono-substituted-3-thiosemicarbazone intermediate ..	110
2.4.10. Discussion.....	112
2.4.11. Dissymmetric ligands from the BDO-mono-substituted-3-thiosemicarbazone intermediates.....	113



2.4.12. Characterisation data for the dissymmetric ligands from the BDO-mono-substituted-3-thiosemicarbazone intermediates.....	114
2.4.13. Spectral examples of a dissymmetric ligand with a Me/Me backbone .....	115
2.4.14. Discussion.....	117
2.5. Ligands with Me/Et backbones .....	118
2.5.1. Symmetric ligands with Me/Et backbones .....	119
2.5.2. Methods.....	119
2.5.3. Characterisation data for symmetric ligands with Me/Et backbones .....	120
2.5.5. Discussion.....	124
2.5.6. Dissymmetric ligands with Me/Et backbones.....	125
2.5.7. Synthesis of the PDO-mono-substituted-3-thiosemicarbazone intermediates.....	127
2.5.8. Methods .....	127
2.5.9. Characterisation data for the PDO-mono-substituted-3-thiosemicarbazone intermediates.....	128
2.5.10. Spectral examples of a PDO-mono-substituted-3-thiosemicarbazone intermediate	129
2.5.11. Discussion.....	131
2.5.13. Dissymmetric ligands from PDO-NH <sub>2</sub> =O, PDO-Me=O and PDO-Et=O .....	135
2.5.14. Methods.....	135
2.5.15. Characterisation data for dissymmetric ligands from PDO-NH <sub>2</sub> =O, PDO-Me=O and PDO-Et=O .....	137
2.5.16. Spectral examples of a dissymmetric ligand with a Me/Et backbone .....	139
2.5.17. Discussion.....	140
2.6. Formation of a PDO-NH <sub>2</sub> =O cyclic by-product .....	144
2.6.1. Method .....	146
2.6.2. Characterisation data and tentative assignments for PDO-NH <sub>2</sub> =O cyclic.....	146
2.6.3. Proposition of the cyclic by products structure .....	146
2.6.4. Validation of the proposed structure of PDO-NH <sub>2</sub> =O cyclic .....	147
2.6.5. Summary .....	150
2.7. Ligands with H/H backbones.....	151
2.7.1. Symmetric ligands with H/H backbones .....	151
2.7.1. Methods .....	152
2.7.2. Characterisation data for symmetric ligands with H/H backbones .....	153
2.7.3. Spectral examples of a symmetric ligand with an H/H backbone .....	153
2.7.4. Discussion.....	155
2.7.5. Attempts to synthesise dissymmetric ligands with H/H backbones.....	156
2.7.6. Attempts by the exploitation of carbonyl reactivity differences.....	156
2.7.7. Attempts by the acetal protection method .....	158

2.7.8. Attempts by hydrolyse DMA-Me-(OMe) <sub>2</sub> to GLY-Me=O and attach a second arm in one step.....	162
2.7.9. Discussion.....	165
2.8. Conclusion.....	167
<b>3. Synthesis of copper and zinc bis(thiosemicarbazone) complexes. ....</b>	<b>168</b>
3.1. Introduction .....	168
3.2. Copper bis(thiosemicarbazone) complexes.....	168
3.2.1. Reaction overview.....	168
3.2.2. Synthesis of copper bis(thiosemicarbazone) complexes .....	169
3.2.3. Characterisation data for copper bis(thiosemicarbazone) complexes .....	172
3.2.4. Spectral examples of copper bis(thiosemicarbazone) complexes.....	178
3.2.5. Discussion.....	182
3.3. Zinc bis(thiosemicarbazone) complexes .....	187
3.3.1. Reaction overview.....	187
3.3.2. Synthesis of zinc bis(thiosemicarbazone) complexes .....	187
3.3.3. Characterisation data for zinc bis(thiosemicarbazone) complexes .....	191
3.3.4. Spectral examples of zinc bis(thiosemicarbazone) complexes.....	198
3.3.5. Discussion.....	204
3.4. Unexpected results .....	208
3.4.1. Acetate ligand .....	208
3.4.2. Ethanol ligand .....	213
3.5. Conclusions .....	214
<b>4. Transmetalation of bis(thiosemicarbazone) complexes. ....</b>	<b>215</b>
4.1. Introduction .....	215
4.2. Transmetalation of zinc bis(thiosemicarbazone) complexes.....	216
4.2.1. Methods.....	216
4.2.2. Characterisation data for the transmetalated copper complexes.....	218
4.2.3. Spectral comparisons.....	220
4.2.4. Discussion.....	223
4.3. Zinc complexes + pyridine.....	226
4.3.1. Methods.....	226
4.3.2. Characterisation data for zinc complexes with pyridine.....	228
4.3.3. Spectral and X-ray diffraction illustrations of Zn-BDO-Me-Me-Pyridine .....	229
4.3.4. Discussion.....	234
4.4. Zn-BDO-Me-Me on PS-DMAP and PVP .....	238
4.4.1. Methods.....	238

4.4.2. Infra-red and Raman analysis of the products.....	239
4.5. Conclusions .....	243
<b>Overall conclusions and future work .....</b>	<b>245</b>
<b>Bibliography .....</b>	<b>249</b>
<b>Appendix 1 Materials used .....</b>	<b>254</b>
<b>Appendix 2 Instrumental conditions .....</b>	<b>256</b>

## Abbreviations

Abbreviation	Meaning
AD	Alzheimer's disease
ATP	Adenosine triphosphate
BBB	Blood brain barrier
BDO	2,3-Butanedione
Cr(acac) <sub>3</sub>	Chromium (III) acetylacetonate
CT	X-ray computer tomography
PS-DMAP	Dimethyl aminopyridine on polystyrene
DMA	2,2-Dimethoxyacetaldehyde
DMB	3,3-Dimethoxy-2-butanone
DMF	N,N-Dimethyl formamide
DMSO	Dimethyl sulfoxide
DNA	Deoxyribonucleic acid
ECG	Electro-cardiogram
FDG	Fluorodeoxyglucose
FTIR	Fourier transform infrared
GLY	Glyoxal
HCl	Hydrochloric acid
HIF-1	Hypoxia inducible transcription factor
HMBC	Heteronuclear multiple bond correlation
HMQC	Heteronuclear multiple-quantum correlation
keV	Kilo-electronvolt
LiBF <sub>4</sub>	Lithium tetrafluoroborate
MeV	Mega electronvolt
mmHg	Millimetre of mercury
MRI	Magnetic resonance imaging
Na <sub>2</sub> CO <sub>3</sub>	Sodium carbonate
NADH	Nicotinamide adenine dinucleotide
NADP <sup>+</sup>	Nicotinamide adenine dinucleotide phosphate (reduced)
NADPH	Nicotinamide adenine dinucleotide phosphate (oxidised)
NaI	Sodium iodide
NaOH	Sodium hydroxide
NMR	Nuclear magnetic resonance
NOESY	Nuclear overhauser effect spectroscopy
PADA	pyruvic aldehyde dimethyl acetal
PDO	2,3-Pentandione
PET	Positron emission tomography
pO <sub>2</sub>	Tissue oxygen partial pressure
PVP	Poly (4-vinyl pyridine)
RNA	Ribonucleic acid
SOD	Superoxide dismutase
SPECT	Single photo emission computed tomography
UCL	University College London

# **1. Introduction**

## **1.1. Nuclear medicine**

Nuclear medicine can be defined as the medical use of radioactive agents to diagnose and treat patients.<sup>1</sup> The radioactive agent sometimes called a radio-tracer, a term first coined by the father of nuclear medicine, George de Hevesy, in the 1920's<sup>2</sup>, is a radioactive element which is either administered in its elemental form or attached to a bio-active molecule. This bio-active molecule can be a protein, peptide or a neurotransmitter<sup>3</sup> which possess the correct interactions within the body in order to allow the radionuclide to be transported to the desired biological target. Small radiolabelled coordination complexes may also be utilised in nuclear medicine as their use may overcome problems experienced with molecules with large molecular masses such as antibodies which may lead to slow uptake in the target cells.<sup>4</sup> Once at the target site the products of the decaying radionuclide are either detected for diagnostic imaging or used to irradiate the tissue for therapeutic applications.

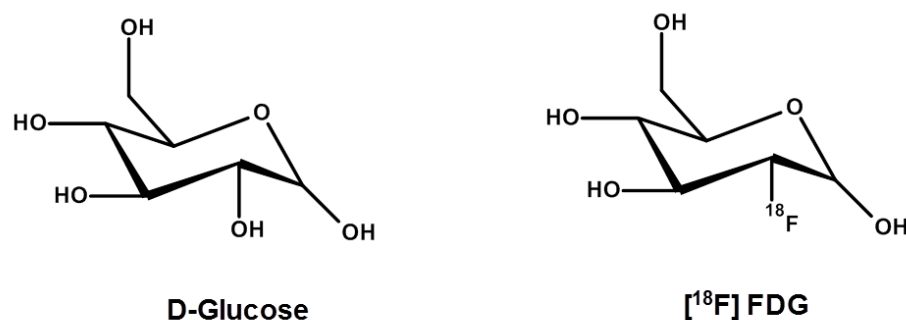
### **1.1.1. Diagnosis**

In the late 1920's Hermann Blumgart and Soma Weiss, two physicians at the Massachusetts General hospital, first pioneered diagnostic nuclear medicine by using a solution of radium-C, which is the historic name for <sup>214</sup>Bi, to study the velocity of blood. Blumgart is regarded as the father of diagnostic nuclear medicine.<sup>2</sup> Diagnostic nuclear medicine's strength lies in that it images the body's biochemistry in order to ascertain the metabolic or physiological functionality of a tissue or organ compared to other techniques commonly used in imaging procedures whose main strengths are showing anatomy.<sup>5,6</sup> The area has progressed to such an extent that almost every organ can be imaged, as there are tracers available for nearly all tissues (bone, liver, kidney, heart, lung, gastro-oesophageal tract, etc.) and fluids (blood, cerebro-spinal liquid, urinary excretion tract, etc.).<sup>7</sup> Diagnostic imaging makes up by far the majority of all nuclear medicine procedures with 85-90% of the nuclear medicine procedures being for diagnosis.<sup>1</sup> Generally, the radionuclides used in diagnostic procedures are short-lived gamma or positron emitters such as technetium-99m and fluorine-18 which aids to limit adverse effects on the patients due to the emitted radiation. Once the radiotracer has migrated to the target tissue, the products of the radioactive decay are detected by a suitable camera at many different angles around the target site and the data from the detected events is used to build up an image.

An example of a diagnostic tracer is [<sup>18</sup>F]Fluorodeoxyglucose, also known as [<sup>18</sup>F] FDG, which is a <sup>18</sup>F labelled analogue of glucose (Figure 1.1.1.1.). [<sup>18</sup>F] FDG is a substrate for the hexokinase enzyme in glucose metabolism. Hexokinase phosphorylates FDG to form two molecules (2-deoxyglucose-6-phosphate and FDG-6-phosphate) which are unable to enter the glycolysis cycle so are trapped within the cell.<sup>8</sup> This enables [<sup>18</sup>F]FDG to be used in the imaging of glucose

metabolism for the detection, staging and response monitoring of malignant and benign tumours.<sup>2, 8, 9</sup>

**Figure 1.1.1.1.** Structures of D-Glucose and [<sup>18</sup>F]Fluorodeoxyglucose based on.<sup>10, 11</sup>



### **1.1.2. Therapy**

Therapeutic nuclear medicine usually involves a single administration of a radionuclide that emits either electrons (beta minus ( $\beta^-$ ) decay) or gamma rays in order to induce the cellular destruction of any unwanted cells. The main objective of therapy is to remove the capacity of the cancer cells to multiply. High energy radiation has the ability to remove the cancer cells ability to divide and proliferate by causing damage to cells genetic material such as DNA (deoxyribonucleic acid).<sup>12</sup> This principle exploits the fact that rapidly dividing cells are particularly sensitive to radiation damage.<sup>1</sup> The first use of nuclear medicine was for therapy in 1901 where Henri Aleandre Danlos and Eugene Bloch treated a tuberculosis skin lesion by placing it in contact with radium.<sup>13</sup>

An example of a radionuclide used for therapeutic applications is <sup>131</sup>Iodine which when administered to a patient accumulates in the thyroid. This allows for the beta minus emitter to be used in thyroid cancer therapy or treatment of non-malignant thyroid disorders.<sup>1</sup> It is worth noting that radiation cannot be used in the treatment of conditions where the cells need to be stabilised or regenerated.<sup>7</sup>

### **1.1.3. Types of radioactive decay**

A radionuclide is a radioactive element that gains stability by undergoing one or more modes of radioactive decay, resulting in a loss of mass or charge.<sup>1</sup> The reasons why an element may undergo a decay process are summarised in Table 1.1.3.1.

**Table 1.1.3.1.** Nuclear transmutations based on <sup>2</sup>.

Decay Mode	Reason for instability of parent nucleus	Transformation	Example	n/p ratio change
<b>Alpha decay</b>	Too large	${}^A_Z\text{X} \rightarrow {}^{A-4}_{Z-2}\text{Y} + {}^4_2\alpha$	${}^{226}_{88}\text{Ra} \rightarrow {}^{222}_{86}\text{Rn} + {}^4_2\alpha$	Increase
<b>Beta decay</b>	Neutron rich	${}^A_Z\text{X} \rightarrow {}^A_{Z+1}\text{Y} + e^-$	${}^{14}_6\text{C} \rightarrow {}^{14}_7\text{N} + e^- + \bar{\nu}$	Decrease
<b>Positron emission</b>	Neutron deficient	${}^A_Z\text{X} \rightarrow {}^A_{Z-1}\text{Y} + e^+$	${}^{11}_6\text{C} \rightarrow {}^{11}_5\text{B} + e^+ + \nu$	Increase
<b>Electron capture</b>	Neutron deficient	${}^A_Z\text{X} + e^- \rightarrow {}^A_{Z-1}\text{Y}$	${}^{111}_{49}\text{In} + e^- \rightarrow {}^{111}_{48}\text{Cd}$	Increase
<b>Isomeric transition</b>	Excess energy	${}^A_Z\text{X}^* \rightarrow {}^A_Z\text{X} + \gamma$	${}^{99m}_{43}\text{Tc}^* \rightarrow {}^{99}_{43}\text{Tc} + \gamma$	No Change

### Alpha ( $\alpha$ ) decay

Elements with a high atomic number or with an atomic mass >210 such as <sup>238</sup>U, <sup>226</sup>Ra and <sup>230</sup>Th achieve stability by emitting alpha particles and occasionally gamma photons are emitted as well.<sup>2</sup> An alpha particle consists of two neutrons and two protons. The emission of this alpha particle results in a reduction in the nuclide's atomic and mass number which allows the nuclide to achieve a more stable state. Alpha particles have kinetic energies in the range of 4-9 MeV<sup>2</sup>. For an alpha emitting nucleus each decay will yield alpha particles with the same energy. Therefore alpha particles can be termed mono-energetic particles. Alpha particles are about 7,000 times heavier than electrons and can be stopped by organic tissue. When a collision occurs the alpha particle ionises the tissue and indirectly cuts it or allows chemical transformation which in the case of collisions with DNA or RNA can cause death to the cell.<sup>7</sup> The extremely high level of damage that alpha emitters cause coupled with their short range which limits the zone of interaction with neighbouring cells means alpha emitters have an ideal profile for use in destroying cancerous cells.<sup>7</sup> Due to the large amount of damage alpha particles can inflict, alpha emitting radiopharmaceuticals need to possess a very high level of affinity to the target site, in order to avoid undesirable damage to the rest of the body. The added down fall of alpha emitters is once they are absorbed or ingested it is impossible to detect the alpha radiation which means accidental contamination is difficult to localise which would cause problems for production,

transportation and implementation of alpha emitters for medical procedures.<sup>7</sup> The use of alpha emitters would not be first choice if another radionuclide that decays via a different route is available.

### **Beta minus ( $\beta^-$ ) decay**

Beta minus decay is when a neutron (n) in a neutron rich nucleus is converted into a proton (p), an electron ( $e^-$ ) and an anti-neutrino ( $\bar{\nu}$ ). The electron and the anti-neutrino are ejected from the nucleus. In this decay route the atomic mass of the nuclide stays constant but the atomic number increases by one. The kinetic energies of the emitted electrons can vary greatly, the range of this variation is a characteristic of the nuclide.<sup>2</sup> There is not a role in nuclear medicine for the weightless anti-neutrino, but electrons which have a continuous energy spectrum and a tendency to be absorbed by matter, are greatly useful in therapy.<sup>7</sup> When the electron is absorbed by matter X-rays are sometimes generated and the remainder of the energy is deposited as heat. This process can cause free radicals which can lead to molecular re-arrangements. This high potential for destruction coupled with their specific half-life means that beta emitters can be used for localised cell destruction.<sup>7</sup>

### **Positron ( $\beta^+$ ) decay**

Also known as beta plus decay, this type of radioactive decay is more commonly seen in elements with lower atomic numbers. Positron decay is a mechanism which allows the neutron deficient nucleus to gain increased stability by decreasing the number of positive charges (protons) it contains. In positron decay a proton in the nucleus transforms into a neutron, positron and a neutrino. The positron can be thought of as an anti-electron. The positron and the neutrino are ejected from the nucleus resulting in a daughter nuclide which comprises of a lower atomic mass number but a constant mass number. Just as with the beta decay, there is variation in the energies of the positron as their energy is dependent on how much energy is carried away by the neutrino.<sup>2</sup> Even though the neutrino is not of any use in nuclear medicine,<sup>7</sup> the gamma ray emissions which are the product of positron annihilation are of great importance for diagnostic imaging techniques such as Positron Emission Tomography (PET). After travelling a few millimetres the positron will undergo an inelastic collision with an electron which will result in both the particles undergoing annihilation.<sup>7</sup> The annihilation process causes the particles' masses to be converted into two 511 keV photons<sup>2</sup> which are emitted at  $180^\circ$  from each other.<sup>14</sup> If two detectors are placed on each side of the patient, as is done in PET, after a few disintegrations it is then possible to calculate the precise location of the source.



### **Gamma radiation**

Gamma radiation is electromagnetic radiation that is emitted from a nucleus that is in an excited state, which can be produced by the electron capture and isomeric transition mechanisms. Gamma rays are ideal for diagnosis due to their very high penetrative ability.<sup>7</sup> They can pass through large thicknesses of matter or far further in air. Gamma rays can however, be stopped or strongly attenuated with dense materials such as lead or concrete. Gamma rays can be detected by gamma cameras or used in Single Photon Emission Computed Tomography (SPECT) for diagnostic procedures.<sup>14</sup> High energy gamma radiation has also the ability to damage the DNA of cancerous cells which allows them to be routinely used in therapeutic applications for the treatment of various cancers.<sup>12</sup>

### **Electron capture**

An alternative mechanism with which a neutron deficient nucleus can become more stable is a process called electron capture. This is when an electron (usually in the K-shell) is captured by the parent nucleus resulting in a proton being converted into a neutron and a neutrino. The daughter nucleus produced has an atomic number which is one lower than the parent nucleus whilst the mass number remains unchanged. Electron capture can also produce characteristic X-rays<sup>14</sup> and/or Auger electrons, due to the vacancy in the K-shell or gamma photons produced when a daughter nucleus in an excited state falls back down to the ground state.<sup>2</sup> Auger electrons which are electrons which have been ejected from one of the atom's electronic shells have a lot less energy than  $\beta^-$  particles but show therapeutic applications due to their ability to cause destruction to only a few layers of cells.<sup>7</sup>

### **Isomeric Transition (IT)**

Isomeric transition occurs when a daughter nucleus has undergone one of the above decay routes but still remains in an excited state. This long lived metastable state, denoted by an 'm', results in the emission of gamma photons when the daughter nucleus drops to the ground state. As the ground state nuclide and the metastable nuclide only differ in energy they can be described as isomers<sup>2</sup>, hence the term isomeric transition.

## **1.2. Single Photon Emission Computed Tomography (SPECT)**

Out of approximately 40 million radiopharmaceutical based clinical scans that are made annually worldwide, 95% is comprised of SPECT scans.<sup>15</sup> The technique Single Photon Emission Tomography (SPECT) is based on using radio-nuclides that undergo decay routes resulting in the emission of gamma rays or X-rays. Technetium-99m (<sup>99m</sup>Tc), with its 140 keV gamma ray emissions, is the most commonly used radionuclide in SPECT imaging<sup>14, 15</sup> but other radio-nuclides are also used, as shown in table 1.2.1.

**Table 1.2.1.** Other commonly used radio-nuclides for SPECT Imaging, based on <sup>14</sup>.

Radionuclide	Symbol	Half-life	Emitted Photon Energies (keV)
<b>Thallium 201</b>	<sup>201</sup> Tl	73 days	≈70-80, 167
<b>Technetium 99m</b>	<sup>99m</sup> Tc	6 hours	140
<b>Iodine 123</b>	<sup>123</sup> I	13 days	159
<b>Iodine 131</b>	<sup>131</sup> I	8 days	364
<b>Indium 111</b>	<sup>111</sup> In	2.8 days	172, 245
<b>Gallium 67</b>	<sup>67</sup> Ga	78 hours	93, 184, 300, 393

When a photon is emitted by the chosen radionuclide, it radiates from the body in a random direction. The photon is then detected by a gamma camera which is fitted with a lead collimator with multiple parallel holes. The collimator only allows the photons that are emitted roughly perpendicular to the face of the gamma camera to interact with the sodium iodide (NaI) crystals and hence be detected<sup>14</sup> (Figure 1.2.2.). A projection view of the radiotracer in the body is built up by the detection of the accumulated events hence, the precision of the projection increase with longer acquisition times. In order to produce a complete image, a series of projections at successive angles need to be measured. This is achieved by the camera being mounted on a gantry that can orbit the body. Most routine clinical SPECT systems are based on dual-head variable 180 degree or variable angle cameras or triple-head variable angle cameras.<sup>2</sup> A typical angular increment is 3-6 degrees,<sup>16</sup> resulting in a total of 60 projections for a 180 degree orbit.<sup>14</sup> The total scan time of a full 360 degree is between 15-20 minutes.<sup>16</sup> Applying linear analysis to the acquired data allows a three-dimensional image of the target area to be obtained.<sup>7</sup>

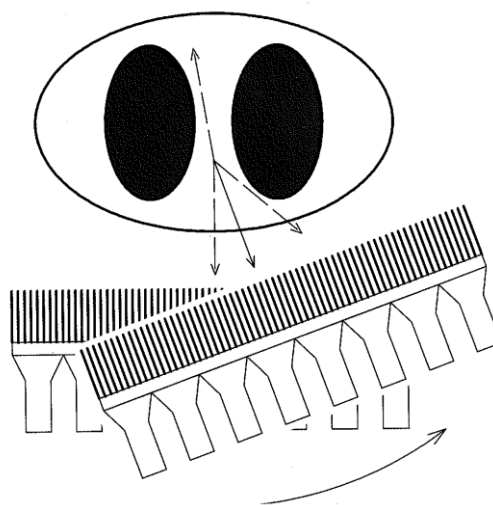


**Figure 1.2.2.** Detection of a photon by a gamma camera in SPECT, based on <sup>14</sup>. Four different emission photon trajectories are depicted. Only one (indicated by the solid line) will be detected at this camera angle because of the lead collimator.

SPECT is a less efficient method of acquiring data than methods such as Positron Emission Tomography (PET) due to only the photons that are emitted in the plane of the collimator being detected, this can be roughly 1 in 5,000, depending on the design of the collimator.<sup>2</sup> With PET, all photon pairs emitted in the same plane as the detector ring will be detected. A second disadvantage with SPECT is that each angle projection has to be measured individually while with PET all angles are acquired simultaneously.<sup>14</sup> However for preclinical small animal studies SPECT can achieve higher resolution than PET.<sup>15</sup> A number of physical effects, such as collimator blur, statistical noise, scatter and attenuation all have negative effects which ultimately limit the image quality and accuracy of a SPECT image.<sup>14</sup>

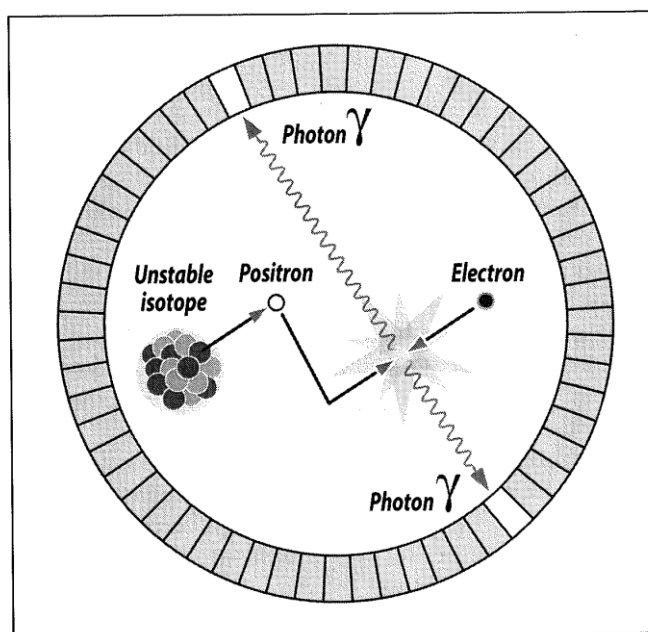
Collimator blur arises due to the collimator accepting photons with a range of incident angles instead of only the photons that are travelling exactly perpendicular to the collimator face. This causes a decrease in spatial resolution. Statistical noise arises due to the acquisition of only a limited number of photons. Photons can be scattered by tissues whilst travelling through the body, this can result in either the photon being diverted from the plane of the detector and hence not detected or the photon losing too much energy before reaching the gamma camera. If the energy loss is large enough the gamma camera will reject the event. Most photons with 140 keV of energy would be scattered rather than be absorbed.<sup>5</sup> Attenuation is when a photon that is travelling on a path that would otherwise be detected becomes either scattered or absorbed, resulting in the photon not being detected. Attenuation results in loss of quantitative accuracy and increased noise of the resulting image.<sup>14</sup> The imaging of moving organs, for example the heart, can also add difficulty in terms of image acquisition and interpretation<sup>7</sup> even though there are specific SPECT systems, such as the Cardius system (Digirad) which has been optimised for cardiac imaging.<sup>2</sup> SPECT myocardial perfusion imaging is well established as a non-invasive tool for the diagnosis of ischaemic coronary disease.<sup>16</sup> SPECT can be combined with the anatomic imaging capabilities of X-ray computed tomography (CT) to form SPECT/CT or computed tomography coronary angiography<sup>16</sup> which enables physicians to access improved diagnosis capabilities than if SPECT was used alone.<sup>1, 2, 14</sup>

### **1.3. Positron Emission Tomography (PET)**

The versatility of Positron Emission Tomography (PET) is the reason why PET is gaining popularity in functional imaging.<sup>7</sup> This is supported by the fact that between 2005 and 2011 in the UK the number of static PET scanners increased from 14 to 35.<sup>17</sup> PET relies on the detection of the decay products of, neutron-deficient, positron emitting nuclides. These nuclides can be incorporated into a pharmaceutical that is designed in order to detect a specific metabolic pathway. After emission, the particularly unstable positron, which lasts about  $10^{-10}$  seconds, interacts randomly

with the surrounding tissue. This interaction causes a loss of energy until then energy of the positron is sufficiently small, when it is able to annihilate upon collision with a free electron.<sup>2,5,7,14,18</sup> This annihilation process produces two photons of 511 KeV which corresponds to the rest mass of both the electron and positron.<sup>14</sup> The two photons are emitted at 180 degrees from each other, however the angle can be slightly more or less than 180 degrees, typically  $\pm 0.25^\circ$ , if the positron-electron system is not at rest at the moment of annihilation.<sup>2,14</sup> This process is illustrated in figure 1.3.1. The detection of a high level of coincidental events can generate an image of the distribution of the detected annihilation photons, hence the position of the positron emissions reflects the distribution of the labelled pharmaceutical. Typically, coincidental events are two photons that are detected between 6-12 nanoseconds from each other.<sup>14</sup> The distance the positron travels before annihilating is called the positron range and depends on the initial energy of the particle. A low positron energy is desirable in order to limit the positron range and optimize spatial resolution.<sup>18</sup>

**Figure 1.3.1.** A diagram of the positron emission and of the detection of both gamma photons generated by the annihilation process, based on <sup>7</sup>.



Typical to most PET scanners, the coincidental events are detected by numerous detector rings arranged in a cylindrical detector in order to make maximum use of the radiation which is emitted.<sup>14</sup> Not all emitted photons will be used in the formation of the resulting PET image. As the photons are emitted in all directions from the patient they may not be travelling in the same plane in order for them to be detected by the detector rings, even though each photon is contributing to a radiation dose to the patient. Modern PET scanners have the ability to acquire data in 2-D or 3-D modes,<sup>7</sup> in 2-D acquisitions only photon pairs detected by a single detector ring is used in the image formation whilst in the 3-D mode photons pairs detected by any combination

of detector rings are used.<sup>14</sup> The PET image is constructed by subjecting the acquisition data to algorithms, filter functions and statistical methods.<sup>14</sup> As PET does not require the use of a collimator, PET can achieve a significantly higher sensitivity than SPECT by approximately two to three orders of magnitude.<sup>19</sup> PET can also be used to quantify the absolute trace concentration in a target tissue, but before this can be achieved, the acquired data has to be subjected to corrections in order to take into account system and physical effects. The effects that need to be accounted for include, but are not limited to, detector efficiency variations, random coincidences, photon attenuation and scattered radiation.<sup>14</sup>

The PET system also suffers from a number of limitations. One limitation is that individual crystals that make up the detector may have differing light output and decay times. It is therefore necessary for each photomultiplier tube to be assessed and correction maps generated in order to ensure uniform response from the detector. Photomultiplier gain adjustments are part of the detector setup and calibration procedures.<sup>14</sup> A limitation on overall count performance is 'pulse pile up'. Pulse pile up is when two photons originating from two different annihilation events interact with the detector's crystals within a very short time frame. If this time frame is too short then the two photons cannot be distinguished as two separate photons, but only as one high energy event. If the sum of the two photons' energy is above the upper energy discrimination level then the event shall be discarded. If this is the case then both of the photons involved shall be lost. Pulse pile up can be reduced by the use of a scintillator with short decay times.<sup>14</sup> The main limitation that is faced by PET is the insurmountable resolution limit, which is due to PET detecting the products of annihilation, which occurs after the positron has travelled a few millimetres from the site of the radiotracer. The mean distance the positron can travel before annihilating can vary from a fraction of a millimetre to 4-6mm, depending on the radionuclide used.<sup>2</sup> This means that there is an unavoidable limit to the ultimate image resolution attainable by the PET technique.<sup>7</sup> Despite this resolution limit of a few millimetres, the resolution of PET images is still regarded as excellent.<sup>7,20</sup> PET is also used in animal model based research for a large number of human diseases, this is known as small-animal PET. Due to the reduction in size of the subject that is being imaged, state of the art human PET systems, with spatial resolutions of 4-6mm, are not adequate which means that there is a range of small animal PET scanner systems on the market that have spatial resolutions ranging between 1.2-2.7 mm.<sup>21</sup>

**Table 1.3.2.** Advantages and disadvantages of PET imaging based on <sup>5</sup>.

Advantages	Disadvantages
Does not require lead collimator.	Many radionuclides require to be produced on site from a cyclotron.
Uses biologically interesting radionuclides, such as <sup>11</sup> C, <sup>15</sup> O, <sup>13</sup> N.	High cost of a cyclotron, imager and radiochemistry facility.
Can accurately measure the amount of radiopharmaceutical present in a region of the body.	
Spatial resolution of about 5mm.	

For moving objects, such as the heart, gating can be used in order to improve the image quality of the objects. Gating works by synchronising the movement of the heart with a particular emission frame which can be achieved exploiting the data from an electrocardiogram (ECG).<sup>14</sup> Just like SPECT, the PET system can also be coupled with X-ray tomography to form PET-CT. PET-CT enables the functional data of PET and the anatomical data of CT to be combined together in to one image.<sup>22</sup> Another advantage that PET-CT has over PET alone is that the data acquired from the CT scanner can be used in order to correct for photon attenuation effects in PET.<sup>14</sup> PET scanners can also be combined with Magnetic Resonance Imaging (MRI) in the case of PET/MRI.<sup>17</sup> A particular benefit of this combined modality is that the high spatial and temporal resolution of MRI can compensate for the lower spatial and temporal resolution of PET. Another significant advantage of the PET/MRI systems is that they can be used to image the hallmarks of cancer by using the two complimentary techniques for validation or image one or two biological factors independently or simultaneously. One application for this powerful technique is preclinical drug development for cancers such as Glioma, the most aggressive form of brain tumour.<sup>19</sup>

#### **1.4. Copper radioisotopes in nuclear medicine.**

Copper has the versatility of a transition metal element but because its chemistry is dominated by the +1 and +2 oxidation states, copper does not suffer the complexities that a large range of oxidation states can introduce. Copper in its +1 oxidation state has a full third shell (3d<sup>10</sup>) which results in diamagnetic complexes that tend to be either colourless or yellow.<sup>23</sup> Cu(I) forms complexes without any crystal-field stabilization energy and therefore the resulting Cu(I) complexes typically lack sufficient kinetic stability for radiopharmaceutical applications<sup>24</sup> even though, there is a recent report of a stable copper (I) complex that can be used for

radiopharmaceutical applications.<sup>25</sup> Copper (II) on the other hand, has a  $3d^9$  electron configuration and forms complexes that are paramagnetic. The unsaturated d-shell gives rise to crystal field stabilisation energy that dictates preferences to coordination numbers of four, five and six. Four co-ordinate complexes typically exhibit square-planar geometries whilst five co-ordinate complexes tend to form square-pyramidal or trigonal-bipyramidal geometries, six co-ordinate complexes on the other hand exhibit octahedral configurations.<sup>23, 24, 26</sup> As copper in its 2+ oxidation state straddles the line between a hard and soft cation, most ligands that effectively chelate with  $Cu^{2+}$  tend to contain uncharged nitrogen donors and anionic sulphur or oxygen donors in order to neutralise the charge of the  $Cu^{2+}$  cation.<sup>26</sup>  $Cu(II)$  is less labile towards ligand exchange because of crystal-field stabilization energy which means that  $Cu(II)$  is the best candidate for the incorporation into radiopharmaceuticals.<sup>24</sup> *In vivo*  $Cu^{2+}$  can undergo reduction in hypoxic (oxygen deficient) tissues. This reduction is not limited to free copper ions but also can occur in a  $Cu^{2+}$  complex leading to  $Cu^+$  which is usually not as stably bound by the same ligands as  $Cu^{2+}$ . This results in a release of the copper in to the hypoxic tissue. This means that a stable  $Cu^{2+}$  complex should ideally be able to withstand reducing conditions so that no  $Cu^+$  is released from the complex and accumulating in non-target cells.<sup>27</sup> This lends  $Cu^{2+}$  complexes to the application of radio-tracer for medical imaging.

It is possible to obtain copper in the +3 oxidation state, but particularly strong  $\pi$ -donating anionic ligands are required, for example deprotonated amide nitrogen ligands.<sup>23, 24</sup> The geometry of the resulting  $3d^8$  complexes tends to be the square planar. Copper in the +3 state has not currently been observed within biology<sup>28</sup> so just copper in the +2 (cupric) and +1 (cuprous) oxidation states are applicable to biological systems,<sup>29, 30</sup> with the +2 state being the most relevant.<sup>26</sup>

Copper is a trace element, with the average adult male containing only  $\approx 100$  mg of copper<sup>30</sup> and the adult recommended daily intake being 0.9-10mg/day.<sup>31</sup> Despite the small quantity within the body copper is an essential bio-metal involved in a number of critical cell functions.<sup>32</sup> As a product of copper's ability to accept and donate electrons enzymes require copper as a cofactor for respiratory oxidation, neurotransmitter synthesis, pigment formation and iron metabolism.<sup>29, 30, 33</sup> Despite copper's importance in the cell's biology, high reactive ionic ('free') copper can exert cytotoxic effects. In order to prevent these effects cells have developed complex mechanisms in order to chaperone copper around the body to where it is required.<sup>32, 34</sup> When copper homeostasis is disrupted, the subsequent copper imbalance is a pathology that a range of diseases share, such as Wilson's disease,<sup>35</sup> neurodegenerative diseases,<sup>30, 32, 35-37</sup> cancer<sup>29</sup> and Menkes disease.<sup>23, 38</sup> Copper also has an involvement in celiac disease which is the autoimmune disease linked to an intolerance to gluten (the protein fraction of cereal grains).<sup>35, 39</sup> Wilson's disease is due to a mutation on chromosome 13 which leads to a functional deficit in the copper

transporter protein ATP7B, this results in an accumulation of copper in the liver, brain, kidneys and eyes.<sup>40</sup> The disease, which can be fatal, can be managed by the administration of penicillamine, a copper-chelating agent which controls copper levels by liberating isolated copper and facilitating its excretion.<sup>23</sup> Menkes disease is a recessive neurodegenerative disorder linked to a gene mutation on the X sex chromosome. This gene in question codes for a copper transport protein, and when the mutation is present, an inability for copper to be incorporated in to several enzymes arises which causes several biochemical pathways to malfunction.<sup>23, 38</sup>

In a nuclear medicine context copper is a highly versatile radio-nuclide due to the number of different isotopes of copper that are available, as summarised in Table 1.4.1. These different radio-isotopes of copper fortuitously have a range of different decay mechanisms which yield different decay products which can be utilised for diagnostic and therapeutic applications.<sup>41</sup> Copper isotopes could also be of interest in the new field of theranostics, where one agent can be used for both diagnostic and therapeutic applications depending on which copper isotope is incorporated in to it.<sup>18, 25</sup> Nuclear reactions can be written in a shorthand format<sup>42</sup> which is  ${}^{64}\text{Zn}(p,\alpha){}^{61}\text{Cu}$ . This format shows that the  ${}^{64}\text{Zn}$  target atom had a proton (p) collide with it. The result of this collision was the emission of an alpha particle to form an atom of  ${}^{61}\text{Cu}$ . The letters d and n represent a deuterium atom and a neutron respectively.

**Table 1.4.1.** Physical properties of copper radionuclides for imaging and therapy, based on <sup>6, 23, 24, 41, 43</sup>.

Radionuclide	T <sub>1/2</sub> (h)	Decay (%)	E <sub>p</sub> (keV)	E <sub>np</sub> (keV)	R <sub>np</sub> (mm)	Source
<sup>60</sup> Cu	0.33	β <sup>+</sup> (93) EC (7)	511 1332	873	4.4	cyclotron
<sup>61</sup> Cu	3.4	β <sup>+</sup> (62) EC (38)	511 283	527	2.6	cyclotron
<sup>62</sup> Cu	0.16	β <sup>+</sup> (98) EC (2)	511	1315	6.6	Generator/ cyclotron
<sup>64</sup> Cu	12.7	β <sup>+</sup> (18) EC (43) β <sup>-</sup> (39)	511 1346	278 190	1.4 0.95	Reactor/cyclotron
<sup>66</sup> Cu	0.09	β <sup>-</sup> (100)		1109	5.6	Reactor/cyclotron
<sup>67</sup> Cu	62	β <sup>-</sup> (100)	93	121	0.61	Reactor/cyclotron

*E<sub>p</sub>* = energy of the most abundant penetrating (γ) radiation following the corresponding decay.

*E<sub>np</sub>* = average energy of the most abundant non-penetrating (β<sup>+</sup>/β<sup>-</sup>) radiation.

*R<sub>np</sub>* = Average range of non-penetrating radiation in tissue.



## **Copper 60**

The short lived  $^{60}\text{Cu}$ , with a half-life of 20 minutes, is a radionuclide of copper that decays via  $\beta^+$  (93%) decay and electron capture (7%).  $^{60}\text{Cu}$  is not produced by a generator but via a small cyclotron by either  $^{61}\text{Ni}(p,n)^{60}\text{Cu}$  or a  $^{61}\text{Ni}(d,2n)^{60}\text{Cu}$  reaction on  $^{61}\text{Ni}$ -enriched targets.<sup>23</sup> Due to its short half live it must be synthesised on site.

## **Copper 61**

$^{61}\text{Cu}$  decays via positron emission (62%) with a mean energy range of 0.242-0.527 MeV<sup>44</sup> as well as by electron capture (38%).  $^{61}\text{Cu}$  has a half-life of 3.4 hours and large activities can be produced by using  $^{61}\text{Ni}(p,n)^{61}\text{Cu}$  using a highly enriched nickel target. The high activities of  $^{61}\text{Cu}$  produced come at a high cost due to the need for the expensive enriched  $^{61}\text{Ni}$  targets. A significantly cheaper approach is using a zinc target to utilise the  $^{64}\text{Zn}(p,\alpha)^{61}\text{Cu}$  reaction.<sup>44</sup> Due to its longer half-life, this radioisotope of copper is able to be produced off site and transported to the required location instead of having to be produced on site.

## **Copper 62**

$^{62}\text{Cu}$  undergoes  $\beta^+$  (98%) decay and owing to its short half-life (9.8 minutes)  $^{62}\text{Cu}$  can be used as a PET tracer for short timescale studies.<sup>45</sup> The half-life of  $^{62}\text{Cu}$  means that it is compatible with relatively long image acquisitions times for good counting statistics as well as being short enough in order to allow repeat scanning within an single imaging session.<sup>46</sup>  $^{62}\text{Cu}$  can be obtained by eluting it from a  $^{62}\text{Zn}/^{62}\text{Cu}$  generator or by the more expensive method of using the  $^{62}\text{Ni}(p,n)^{62}\text{Cu}$  reaction in a small cyclotron.<sup>23</sup> The  $^{62}\text{Cu}$  generator contains  $^{62}\text{Zn}$  that is produced by irradiating a copper disc in a nuclear reactor in order to perform the nuclear reaction  $^{63}\text{Cu}(p,2n)^{62}\text{Zn}$  using protons with energies between 21-26 MeV. An anion-exchange resin is used to isolate the  $^{62}\text{Zn}$  from the target copper.<sup>2, 46</sup> When dissolved in an acidic solution the  $^{62}\text{Zn}$  can be loaded on to second anion-exchange resin column and the daughter  $^{62}\text{Cu}$  can be eluted from the column when it is required. Due to the limitations of the very short half-life this radionuclide needs to be produced within a very close proximity to where it is required for use.

## **Copper 64**

The versatile  $^{64}\text{Cu}$  radionuclide undergoes a range of different decay routes which includes electron capture (43%,  $E = 1675$  and  $1346$  keV),  $\beta^-$  decay (39%,  $E = 190.2$  keV) and  $\beta^+$  decay (18%,  $E_{\text{max}} = 660$  keV,  $E_{\text{average}} = 288$  keV)<sup>43</sup> (Figure 1.4.2.).  $^{64}\text{Cu}$  yields positrons with relatively low energies that produce high-quality PET images<sup>47</sup> with spatial resolution which is equivalent to  $^{18}\text{F}$  images.<sup>25</sup> Positrons from  $^{64}\text{Cu}$  have a mean positron range of 0.7 mm and a max range of 2.2 mm

which is comparable to the mean and maximum range of positrons from  $^{18}\text{F}$  at 0.6 mm and 2.1 mm respectively.<sup>18</sup>

The electron capture decay route can yield Auger electrons which can be used for therapeutic applications,<sup>23</sup> when the copper is deposited close to the nucleus of the cell.<sup>29</sup> Its 12.7 hour half-life enables the use of more time consuming chelation methods which has allowed the development of a range of  $^{64}\text{Cu}$  containing radio-pharmaceuticals.  $^{64}\text{Cu}$  is best incorporated into a radio-pharmaceutical by the formation of a thermodynamically stable and kinetically inert coordination complex<sup>47, 48</sup> but also can be integrated in to larger bio-molecular probes based on antibodies,<sup>41, 49, 50</sup> nanoparticles or peptides.<sup>29, 41</sup> However,  $^{64}\text{CuCl}_2$  on its own has shown potential for being used as a prostate cancer tracer.<sup>51</sup>

$^{64}\text{Cu}$  has a sufficient half-life in order to allow for it to be synthesised off site and shipped to the research institution or hospital without excessive decay.<sup>26</sup>  $^{64}\text{Cu}$  can be produced by either by the  $^{64}\text{Zn}(n,p)^{64}\text{Cu}$  nuclear reaction<sup>24, 52</sup> or by using a cyclotron to exploit the  $^{64}\text{Ni}(p,n)^{64}\text{Cu}$ <sup>24, 53</sup> or the  $^{64}\text{Ni}(d, 2n)^{64}\text{Cu}$ <sup>54</sup> nuclear reactions. The  $^{64}\text{Ni}(p,n)^{64}\text{Cu}$  method in a biomedical cyclotron is by the far the most common method used to obtain  $^{64}\text{Cu}$ <sup>26</sup> and requires an expensive enriched  $^{64}\text{Ni}$  target (99.6%, natural abundance of nickel is 0.95%) which is electroplated on to a gold disk.<sup>18</sup>

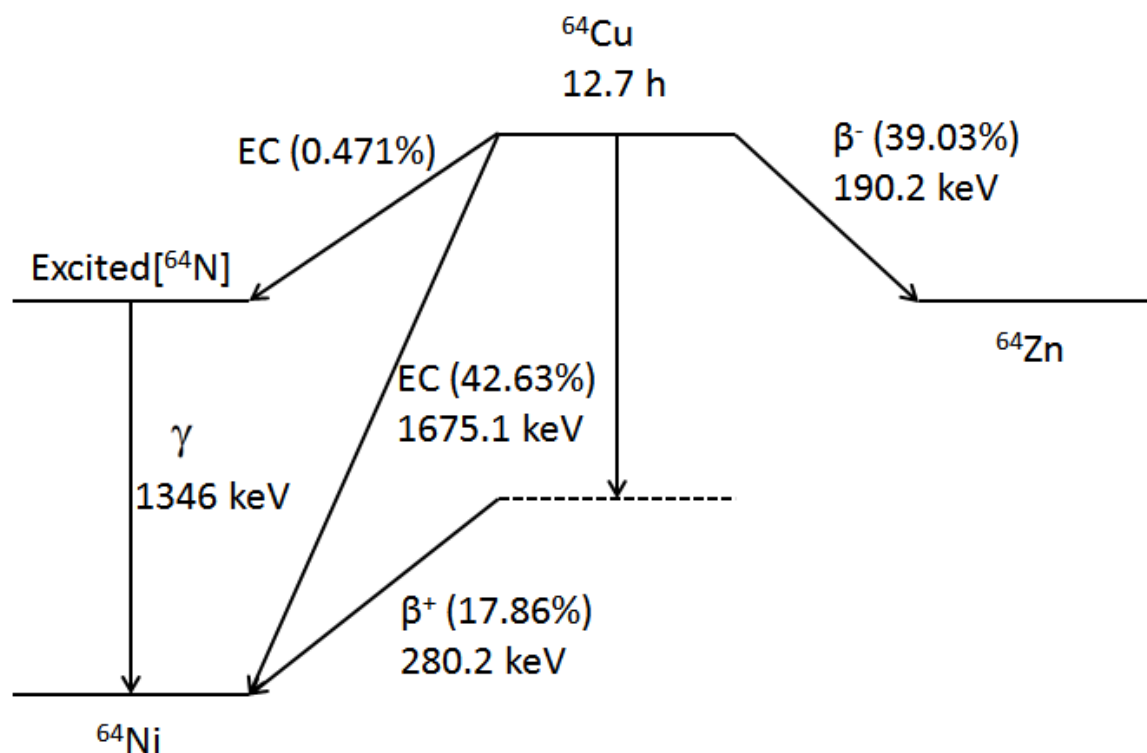


**Figure 1.4.2.** The pathways for the decays of  $^{64}\text{Cu}$  into  $^{64}\text{Ni}$  and  $^{64}\text{Zn}$  based on <sup>2, 43</sup>.

## **Copper 66**

This short lived radionuclide with a half-life of 5.1 minutes decays exclusively via  $\beta^-$  decay (100%) to produce a relatively high energy  $\beta^-$  particle (2.6 MeV) which makes  $^{66}\text{Cu}$  suitable for targeted therapy of large ( $\geq 1$  cm) tumours.<sup>23</sup>  $^{66}\text{Cu}$  can be synthesised by using a reactor with an enriched  $^{65}\text{Cu}$  target. Other systems involving nickel, copper and zinc as target materials are under investigation.

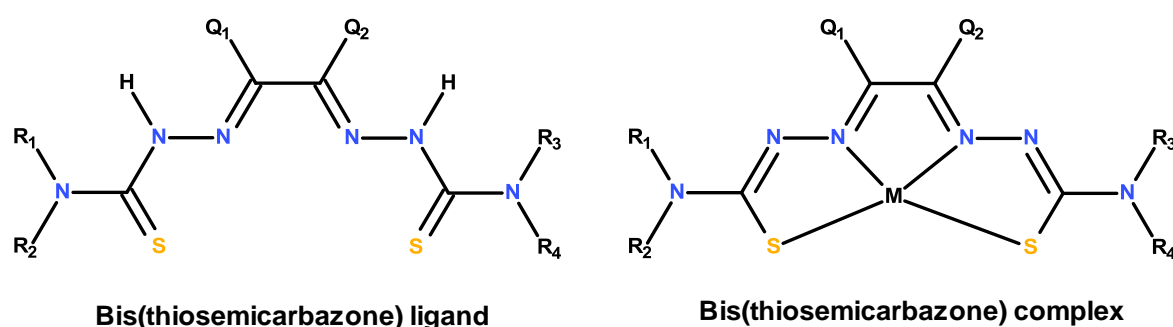
## **Copper 67**

$^{67}\text{Cu}$ , with a half-life of 62 hours, has the longest half-life of all of the radionuclides of copper. The radionuclide undergoes decay  $\beta^-$  (100%), but via four different routes which yields  $\beta^-$  emissions with energies ranging between 395 and 577 keV.<sup>55</sup> The generation of  $\beta^-$  particles makes  $^{67}\text{Cu}$  a candidate for the use in therapeutic procedures,<sup>55</sup> particularly for tumours with a diameter of 1.6 - 2.8 mm.<sup>56</sup>  $^{67}\text{Cu}$  has also been used for radio-immunotherapy using molecular antibodies and antibody fragments.<sup>29</sup> Due to the varying decay routes  $^{67}\text{Cu}$  yields gamma rays with three different energies of 91, 93 and 185 keV.<sup>23</sup> The production of these gamma rays allows the utilisation of SPECT, which permits imaging of the radioisotope destination during therapy.  $^{67}\text{Cu}$  can be produced using the  $^{67}\text{Zn}(n,p)^{67}\text{Cu}$  reaction which involves the irradiation of zinc with neutrons or by taking advantage of the  $^{64}\text{Ni}(\alpha,p)^{67}\text{Cu}$  nuclear reaction,<sup>23</sup> the latter is a less practice method.<sup>55</sup>

## **1.5. Bis(thiosemicarbazone) ligands**

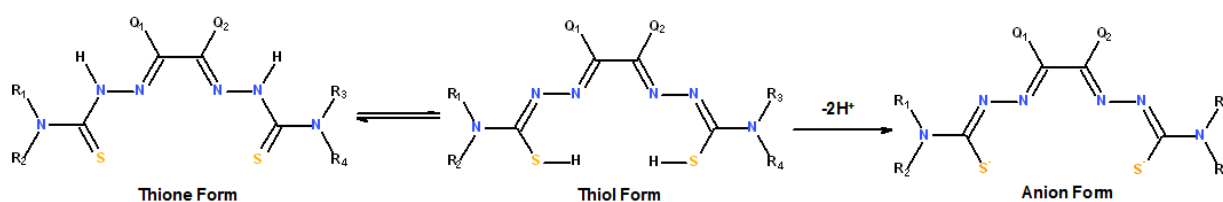
A diverse range of tetradentate bis(thiosemicarbazone) ligands and their resulting complexes have been synthesised since the 1950's,<sup>57-59</sup> however the synthesis of this class of ligands was first reported in 1902.<sup>60, 61</sup> In the 1960's they were discovered to be of use in a medicinal context due to them possessing anti-tumour properties.<sup>3, 62-64</sup> More recently bis(thiosemicarbazone) ligands that have been co-ordinated with positron-emitting isotopes, for example  $^{64}\text{Cu}$ , have been the focus of research for use as diagnostic imaging agents.<sup>65</sup> Over 60 years later, there is still considerable interest in the biological activity of both the free ligands and the related metal complexes (Figure 1.5.1.).<sup>66</sup> A summary of the history of the bis(thiosemicarbazone) ligands and their copper complexes along with their medical applications have recently been published as part of a book chapter.<sup>60</sup> Papers have also been published in the early 2000's investigating bis(selenosemicarbazone) ligands, where both the sulphur atoms are substituted for selenium atoms, for use in diagnostic imaging.<sup>67, 68</sup>

**Figure 1.5.1.** The general structures of a bis(thiosemicarbazone) pro-ligand and the resulting complex based on<sup>57, 66, 69, 70</sup>.



Bis(thiosemicarbazone) ligands should more accurately be referred to as pro-ligands due to the need to de-protonate the pro-ligand in order to expose the true ligand for chelation with a metal. The pro-ligands exist as thione-thiols tautomers which are able to bind to a metal ion either in a neutral or anionic form,<sup>71</sup> this is illustrated in (Figure 1.5.2.).

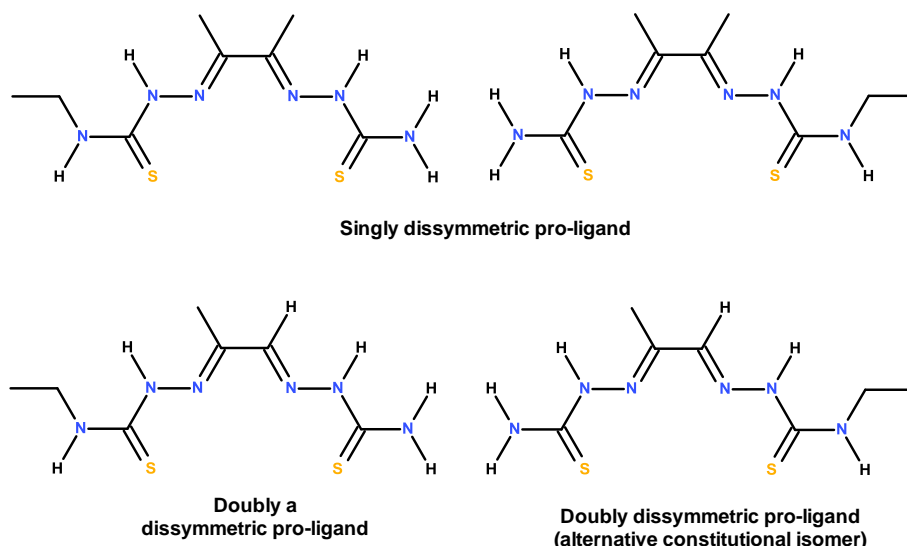
**Figure 1.5.2.** The thione, thiol and anion forms of a bis(thiosemicarbazone) pro-ligand based on<sup>71, 72</sup>.



## Synthesis

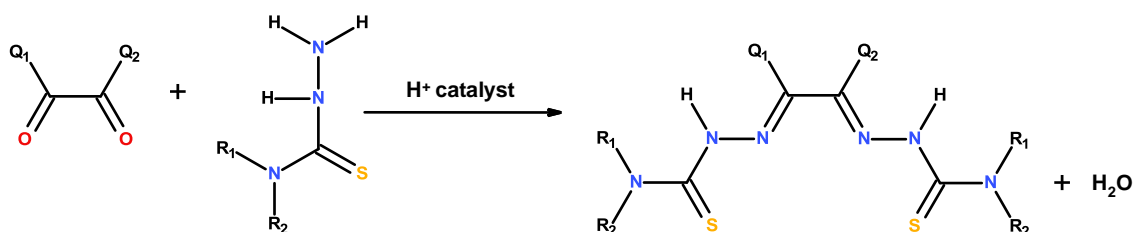
Bis(thiosemicarbazone) pro-ligands can be described as symmetric when the substituents on the terminal nitrogen atoms are the same ( $NR_1R_2 = NR_3R_4$ ). The ligand is termed as dissymmetric when the substituents on the terminal nitrogen atoms are dissimilar ( $NR_1R_2 \neq NR_3R_4$ ). Dissymmetric ligands can be further described as singly dissymmetric or doubly dissymmetric in respect to symmetry of the backbone substituents. When the substituents on the backbone are identical ( $Q_1 = Q_2$ ) they can be classed as singly dissymmetric and if they are dissimilar ( $Q_1 \neq Q_2$ ) the ligand is said to be doubly dissymmetric. Singly dissymmetric pro-ligands only have one constitutional isomer irrespective of which carbonyl group each of the two dissimilar 4-substituted-3-thiosemicarbazides react with. Doubly dissymmetric pro-ligands on the other hand, have two constitutional isomers depending on which 4-substituted-3-thiosemicarbazide reacts with which carbonyl group. Illustrations of singly and doubly dissymmetric ligands can be found below (Figure 1.5.3.).

**Figure 1.5.3.** An illustration of singly and doubly dissymmetric ligands.



Synthesis of symmetric pro-ligands is relatively simple and is widely reported.<sup>6, 59, 62, 72-78</sup> Even though a range of reaction conditions and solvents have been reported, the general principle of adding a chosen di-ketone to a warm solution (normally aqueous or ethanolic) containing at least two equivalents of a 4-substituted-thiosemicarbazide in the presence of an acid catalyst (Figure 1.5.4.) holds true. The product forms a precipitate that can be recovered via filtration and washed with a suitable solvent such as ethanol, methanol, water or diethyl ether.

**Figure 1.5.4.** The synthesis of a general symmetric bis(thiosemicarbazone) pro-ligand based on<sup>6</sup>.

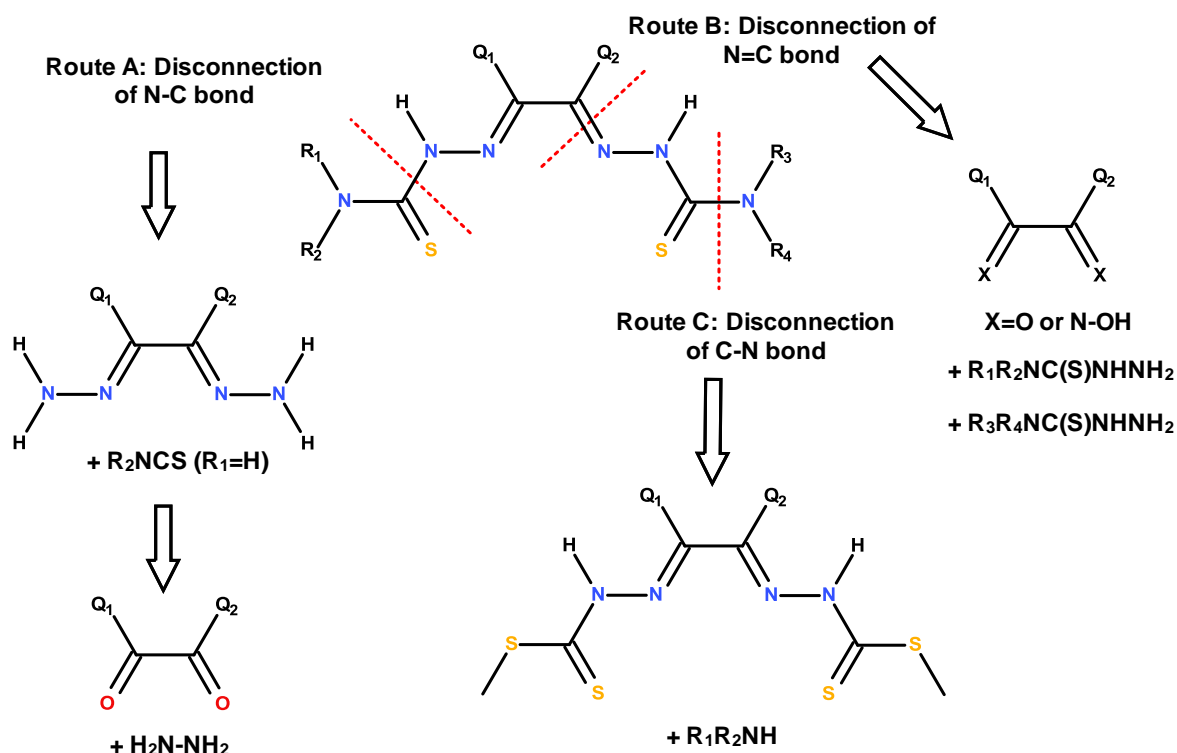


The synthesis of dissymmetric bis(thiosemicarbazone) pro-ligands however, is not as straight forward as symmetric pro-ligands. The desire to synthesize dissymmetric pro-ligands has been growing as they give the ability to gain greater control on the functionality of the pro-ligands and the resulting metal complexes. This gives the capability of making subtle adjustments to the pharmacokinetics of the complexes, which is highly advantageous when optimising any potential radio-tracer for medical applications. M. Christlieb and J. R. Dilworth published a paper<sup>66</sup> on identifying potential methods of synthesising dissymmetric bis(thiosemicarbazone) pro-ligands by retrosynthetic analysis. (Figure 1.5.5.) illustrates three potential disconnections. M. Christlieb and J. R. Dilworth illustrate the reason for making bis(thiosemicarbazone) pro-ligands by stating: ‘The

synthesis of bis(thiosemicarbazones) is challenging, but their importance in molecular imaging makes understanding their chemistry essential'.<sup>66</sup>

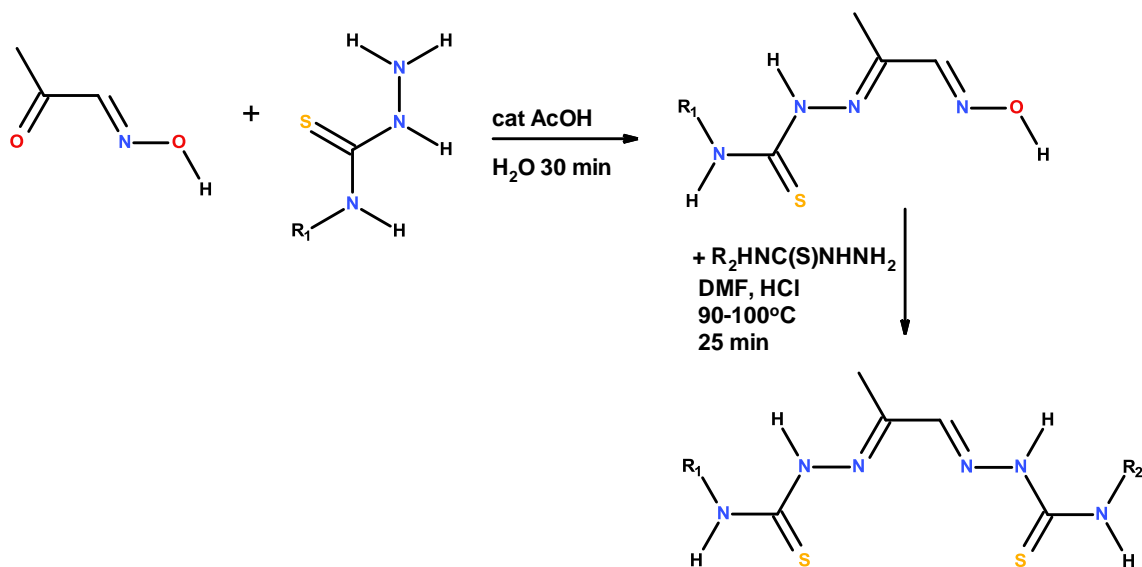
**Figure 1.5.5.** Retrosynthetic analysis of routes to dissymmetric bis(thiosemicarbazone)pro-ligands based on

66



The authors then reported their experience with each of the routes A-C. Route A was described as a potentially convenient route for dissymmetric pro-ligand synthesis and a bis(thiosemicarbazone) was successfully synthesised in a respectable yield. Reported limitations on route A includes that the strategy is restricted to 1,2-diketone-derived dihydrazones and the presence of the reactive functional groups in the isothiocyanate synthesis limits the generality of the route. A considerable problem the authors experienced was that products containing mixtures could not be separated. Route C unfortunately is limited to the synthesis of symmetric compounds as the synthesis of dissymmetric compounds is complicated by the formation of statistical mixtures. A few different methods have been reported for route B which involves the formation of a C=N. The route is the most common and is in the authors' experience is the most successful of the three routes. One method reported for route B is reacting isonitroacetone with a chosen thiosemicarbazide, exploiting that the ketone group will react first in order to give a mono-thiosemicarbazone intermediate. The intermediate is then reacted with a dissimilar thiosemicarbazide in order to yield the desired dissymmetric product. This method is illustrated in (Figure 1.5.6.).

**Figure 1.5.6.** Dissymmetric bis(thiosemicarbazone)pro-ligand synthesis, using isonitrosoacetone as a starting material, based on <sup>66</sup>.

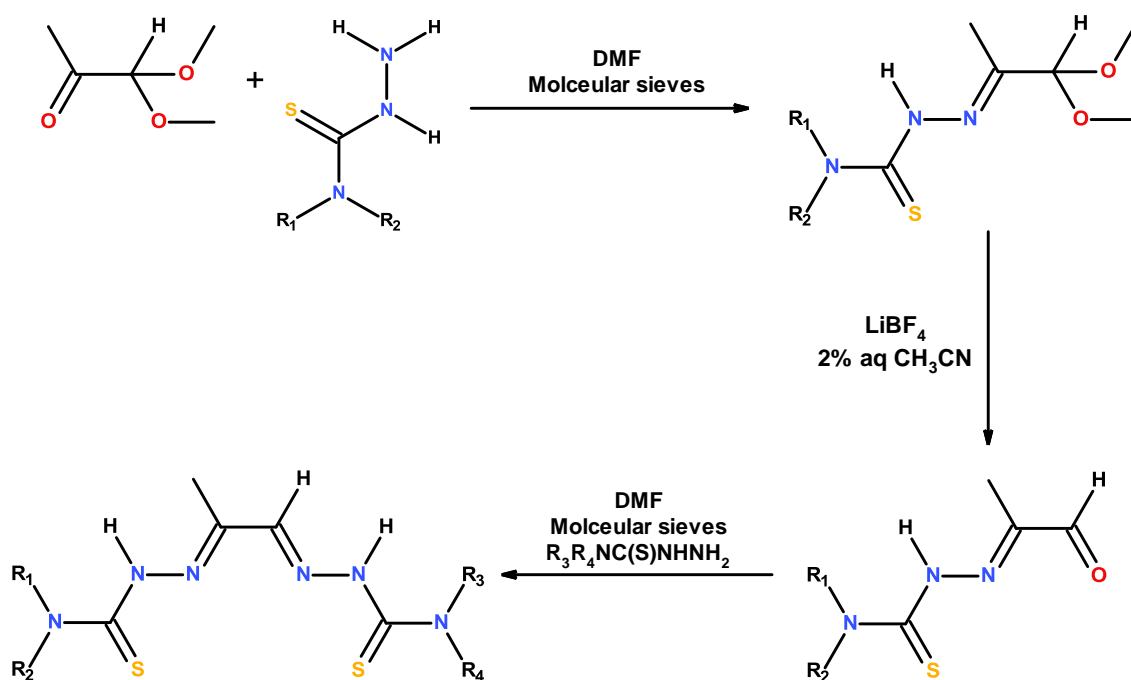


The authors successfully isolated the mono-thiosemicarbazone intermediate but then, upon reacting the intermediate with a second thiosemicarbazide, gave a product that was a mixture of symmetric and dissymmetric bis(thiosemicarbazones). An article by Green *et al.*<sup>79</sup> reported difficulty with repeating the method illustrated in (Figure 1.5.6.).

An alternative reported approach for route B is using an acetal functionality to act as protecting groups in order to ensure only one of the carbonyl groups reacts with the first thiosemicarbazide. The hydrolysis of the acetal group would then reveal the carbonyl moiety ready to be reacted with a second thiosemicarbazide. This approach is illustrated in (Figure 1.5.7.).

**Figure 1.5.7.** Dissymmetric bis(thiosemicarbazone) pro-ligand synthesis using protecting groups, based on <sup>66</sup>,

79

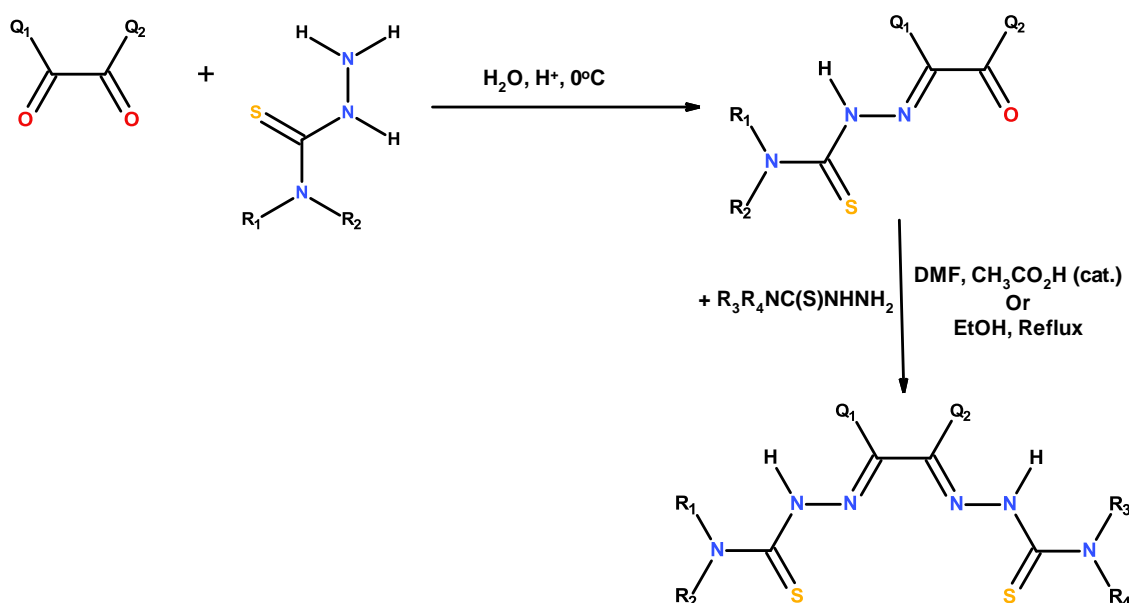


This approach has successfully been used by L. J. Ackerman *et al.*<sup>80,81</sup> and J. K. Lim *et al.*<sup>79</sup> to synthesise dissymmetric bis(thiosemicarbazones). Both authors only reported the synthesis of dissymmetric bis(thiosemicarbazones) pro-ligands that contain Q<sub>1</sub> = CH<sub>3</sub> and Q<sub>2</sub> = H substituents. J. K. Lim *et al.*<sup>79</sup> noted that their attempts to hydrolyse the acetal groups in a protic media also resulted in the hydrolysis of the imine, which lead to mixed bis(thiosemicarbazones) in the resulting product. This problem however was resolved by using the mild Lewis acid, lithium tetrafluoroborate (LiBF<sub>4</sub>), in the hydrolysis reaction that lead to a single dissymmetric bis(thiosemicarbazone) product. L. J. Ackerman *et al.*<sup>80,81</sup> also reported the successful use of LiBF<sub>4</sub>.

By far, the method that seems to be most widely adopted synthetic method for dissymmetric pro-ligands is using a di-ketone as the starting pre-cursor. In this method a cold (normally around 0°C) acidified aqueous or alcoholic solution of a chosen thiosemicarbazide is reacted with an excess of a di-ketone. This reaction exploits that, under these conditions, the thiosemicarbazide only reacts with one of the carbonyl groups on the diketone before precipitating out of solution, thus forming a mono-thiosemicarbazone intermediate. This intermediate is then reacted with a dissimilar thiosemicarbazide either in DMF at room temperature with an acetic acid catalyst<sup>82</sup> or refluxed in ethanol.<sup>57</sup> The di-ketone approach is summarised in (Figure 1.5.8.).



**Figure 1.5.8.** Dissymmetric bis(thiosemicarbazone) pro-ligand synthesis by exploiting the different reactivities of carbonyl groups on a di-ketone precursor, based on <sup>57, 65, 66, 82, 83</sup>.

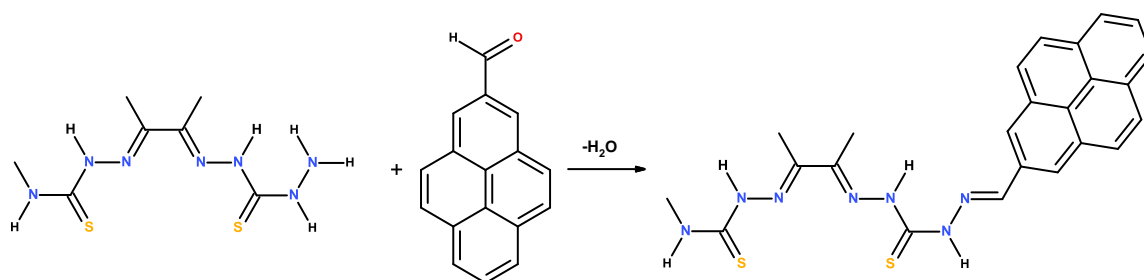


This method has been used to make dissymmetric bis(thiosemicarbazones) pro-ligands with Q<sub>1</sub> = Q<sub>2</sub> = Me,<sup>57, 65, 73, 82-85</sup> and Q<sub>1</sub> = Me, Q<sub>2</sub> = H.<sup>66, 82</sup> D. Calatayud *et al.*<sup>86</sup> attempted to synthesise ligands with Q<sub>1</sub> = Q<sub>2</sub> = Ph and R<sub>1</sub> = hydrazinequinoline, R<sub>2</sub> = H, R<sub>3</sub> = H, R<sub>4</sub> = H. Despite being able to isolate the intermediate product upon the addition of the second thiosemicarbazide, the reaction yielded a mixed product that contained the desired compound, a symmetric pro-ligand (R<sub>1</sub> = R<sub>3</sub> = H, R<sub>2</sub> = R<sub>4</sub> = hydrazinequinoline) and a cyclic by-product. Cyclic by-products have been observed by other authors such as J. Holland *et al.*<sup>57</sup> during the synthesis of a ligand from 2,3-butanedione (Q<sub>1</sub> = Q<sub>2</sub> = Me) with R<sub>1</sub> = Me, R<sub>2</sub> = Ph, R<sub>3</sub> = H, R<sub>4</sub> = H. A similar compound to Holland's where Q<sub>1</sub> = Q<sub>2</sub> = Me, R<sub>1</sub> = R<sub>3</sub> = Me and R<sub>2</sub> = R<sub>4</sub> = Ph was also observed to form a cyclic product by M. Christlieb *et al.*<sup>58</sup> However, M. Christlieb *et al.*<sup>58</sup> suggest that the bis(thiosemicarbazone) pro-ligand is able to undergo cyclisation reactions as a decomposition product instead of being formed from the intermediate. These cyclisation reactions are explained further by J. Casa *et al.*<sup>87</sup>, who attribute them to the presence of the two nucleophilic centres (R-N-H and S-H) along with a polar double bond within the two tautomeric structures of thiosemicarbazones. Mono-thiosemicarbazone intermediates where Q<sub>1</sub> = Q<sub>2</sub> = Ph seem to be particularly keen to undergo cyclization reaction as L. Alsop *et al.*<sup>59</sup> and M. Blanco *et al.*<sup>88</sup> have encountered in their work. Most of the bis(thiosemicarbazone) pro-ligands are highly hydrophobic which results in a low water solubility. There have been attempts to improve the low water solubility of these pro-ligands, for example by introducing a carbohydrate moiety<sup>89</sup> or an aromatic sulfonate<sup>82</sup> functional group into the pro-ligands' structure.

Recent publications are showing that interest is growing on attaching further larger functional groups to the R substituents of the thiosemicarbazide side arms in order to impart further desirable properties upon the pro-ligands and their resulting complexes. A hydrazonequinoline limb was introduced to a pro-ligand by D. Calatayud<sup>90</sup> in order to improve the fluorescence properties of the resulting cadmium and mercury complexes. J. Holland *et al.*<sup>91</sup> introduced a styrene moiety in order to allow the simultaneous labelling of the bis(thiosemicarbazone) with <sup>18</sup>F-fluorine and a biologically active molecule.

Attachment of these pendant functional groups is possible by synthesising a dissymmetric bis(thiosemicarbazone) that has one thiosemicarbazide arm which contains a primary amine such as thiocarbohydrazine (R=H, R'=NH<sub>2</sub>)<sup>57, 60, 65, 84, 85</sup> or 4-N-(2-<sup>t</sup>butoxycarbonylaminoethyl)-3-thiosemicarbazide.<sup>92</sup> This primary amine can then be reacted with a carbonyl functionality on the pendant group in a condensation reaction in order to produce a target functionalised bis(thiosemicarbazone) pro-ligand. This is summarised in (Figure 1.5.9.).

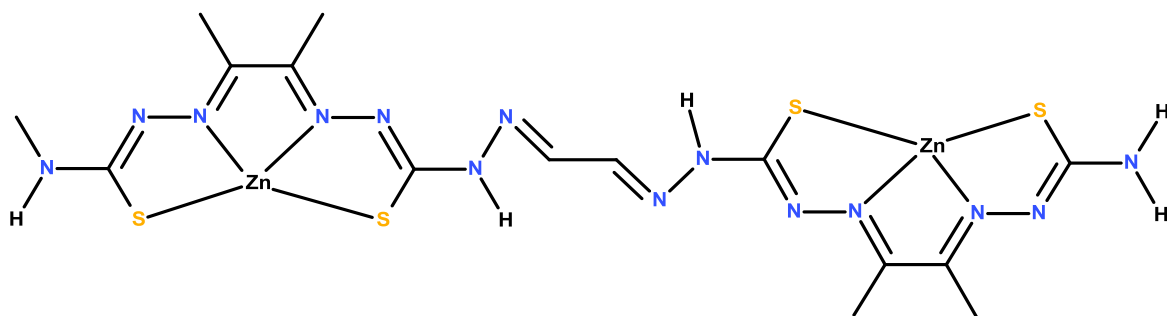
**Figure 1.5.9.** An example of a reaction between a primary amine and a carbonyl group of a pyrene fluorophore in order to yield bis(thiosemicarbazone) pro-ligand with increased functionality, based on <sup>6, 60, 84</sup>.



P. Waghorn *et al.*<sup>92</sup> added a fluorophore to bis(thiosemicarbazone) pro-ligands in order for the resulting zinc, copper and nickel complexes to be of use in fluorescence microscopy. A similar product was synthesised by S. Lim *et al.*<sup>84</sup> where the pendant functionality was the four fused aromatic ring pyrene group (Figure 1.5.9.), for the use in confocal fluorescence microscopy. R. Hueting *et al.*<sup>85</sup> used this synthesis method in order to attach a range of functional groups to the bis(thiosemicarbazone) pro-ligand, one of which was a derivative of the amino acid bombesin. A bombesin functionalised bis(thiosemicarbazone) was also synthesised by B. Paterson *et al.*<sup>73</sup> but, instead of using a primary amine, the authors used a bis(thiosemicarbazone) that contained 4,4-dimethyl-3-thiosemicarbazide (R<sub>1</sub> = Me, R<sub>2</sub> = Me). This dimethyl functional group was then reacted with a chosen carboxylic acid which contained a primary amine that acted as a linker to the bombesin molecule. A. Cowley *et al.*<sup>93</sup> used a slightly different approach by reacting the OH group of a benzoic acid functionalised thiosemicarbazide to attach the peptide lysine. There are also reports of bis(thiosemicarbazones) with a primary amine functionality being used to

synthesise bimetallic bis(thiosemicarbazone) complexes<sup>65,83</sup> (Figure 1.5.10.). Recently J. Dilworth *et al.*<sup>94</sup> have also published sulphonamide conjugates of ATSM.

**Figure 1.5.10.** A bimetallic bis(thiosemicarbazone) zinc complex, based on<sup>65</sup>.



The attachment of a radiolabelled pendant group was very recently reported by R. Hueting *et al.*<sup>95</sup> The group attached an <sup>123</sup>I labelled functionality to produce a complex (Figure 1.5.11.) that can be dual labelled for the monitoring of the fate of the ligand after the copper has dissociated it in hypoxic conditions.

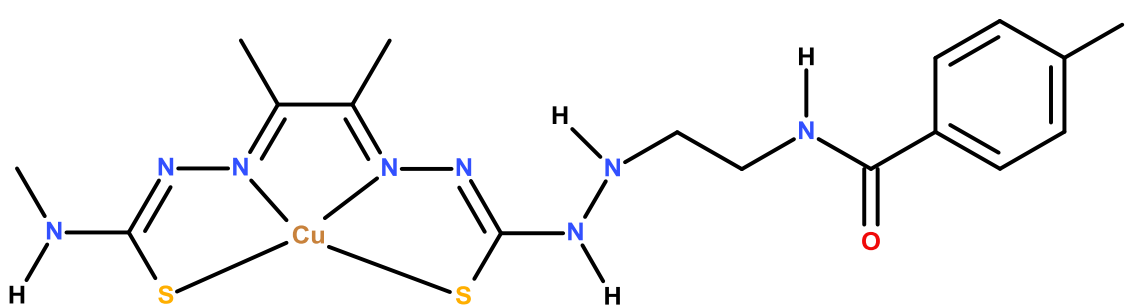


**Figure 1.5.11.** A bis(thiosemicarbazone) complex that can be labelled with <sup>64</sup>Cu either <sup>123</sup>I, based on<sup>95</sup>.

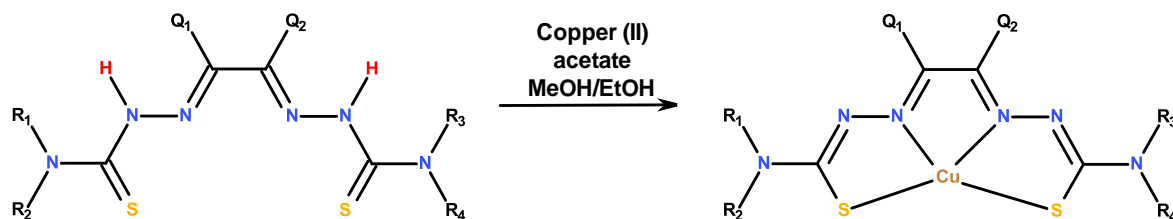
## **1.6. Complexes of bis(thiosemicarbazone) pro-ligands**

Bis(thiosemicarbazone) pro-ligands and their related compounds can be readily chelated to a range of metals in order to form complexes. Literature over the recent years reports bis(thiosemicarbazone) complexes of copper,<sup>57, 66, 69, 84, 96</sup> zinc,<sup>57, 76, 83, 84</sup> nickel,<sup>78, 80, 89</sup> platinum,<sup>97</sup> palladium,<sup>72, 98</sup> cadmium<sup>86, 90</sup> and mercury.<sup>86, 90</sup> It is also possible to make complexes of ligands that have structural similarities to bis(thiosemicarbazone) pro-ligand that chelate with gallium,<sup>99</sup> chromium<sup>100</sup> and zirconium<sup>101</sup> as well as palladium<sup>102</sup> and mercury.<sup>103</sup>

### **1.6.1. Copper bis(thiosemicarbazone) complexes**

Bis(thiosemicarbazone) pro-ligands in the presence of a copper salt such as copper acetate<sup>57, 71, 80,</sup><sup>85</sup> (when heated) or copper chloride<sup>85</sup> (at room temperature), in a methanolic or ethanolic solution, readily form the related copper complexes. This reaction is illustrated in (Figure 1.6.1.1.).

(Figure 1.6.1.1.). Formation of a bis(thiosemicarbazone) copper complex, based on<sup>57,65</sup>.



In this chelation reaction, the pro-ligand is double de-protonated by losing the two hydrogens highlighted in red (Figure 1.6.1.1.). The copper then forms two co-ordinate bonds with each of the two thione sulphur atoms and two dative bonds with the lone pairs from both the imine nitrogen atoms. The result is a neutral, lipophilic, square planar complex with the central copper ion being in the 2+ oxidation state.<sup>23, 84, 85, 104</sup> Copper (II) complexes of this class tend to yield products that are brown, reddish brown or red in appearance.<sup>57, 73, 80, 89, 91</sup>

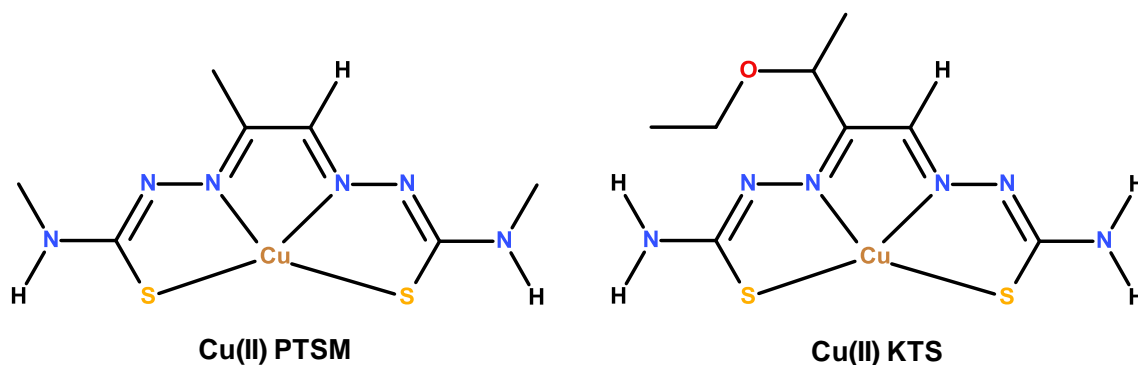
Synthesis of radio ATSM can be achieved by taking 10  $\mu\text{L}$  of an ATSM solution in dimethyl sulfoxide (1 mg/mL) and adding it to hydrochloride buffered radioactive copper chloride. The reaction takes 2 minutes. The radioactive Cu-ATSM can be eluted in ethanol using a C-18 Sep-Pak cartridge. 80% of the ethanol volume is evaporated by blowing argon gas over the solution and diluting the solution in saline prepares it for injection. HPLC and radio-TLC analysis show high radiochemical purity (>95%) and a high radio-yield (>95%) in the final product.<sup>105</sup>

### **1.6.2. Applications of copper bis(thiosemicarbazone) complexes**

When bis(thiosemicarbazone) pro-ligands are chelated with a positron emitting isotope of copper (e.g.  $^{64}\text{Cu}$  or  $^{62}\text{Cu}$ ), the resulting complex can be used as a tracer for PET. Copper bis(thiosemicarbazone) complexes have been used in the imaging of hypoxic tissues, which is the main focus of this project, but derivatives such as Cu(II)-PTSM (Figure 1.6.2.0.1.) have also been used for imaging cerebral<sup>45</sup> and myocardial perfusion (blood flow).<sup>3, 6, 23, 106</sup> The perfusion data obtained from Cu(II)-PTSM can also be coupled with the hypoxia information for Cu(II)-ATSM (Figure 1.6.2.1.2.) for evaluating lung tumours.<sup>107</sup> Cu(II)-KTS (Figure 1.6.2.0.1.) complexes have also been shown to have anti-tumour properties. When just the pro-ligand  $\text{H}_2\text{KTS}$  was administered to rats on a copper free diet the anti-tumour activity of KTS diminished, indicating that the anti-tumour activity was probably attributed to Cu(II)-KTS.<sup>60</sup> The mode of action of Cu(II)-KTS is due to that it can inhibit the incorporation of thymidine into DNA and uridine into RNA, but it is also suggested it can disrupt cellular respiration and ATP (adenosine triphosphate) production.<sup>6</sup> Superoxide ( $\text{O}_2^-$ ) is a reactive oxygen species and is a factor of many disease states. Superoxide dismutase (SOD) is an endogenous enzyme that eliminates superoxide. Certain copper bis(thiosemicarbazone) complexes have shown to be SOD mimetics, with Cu(II)-ATSM (Figure 1.6.2.1.2.) displaying the highest activity.<sup>6</sup> Copper bis(thiosemicarbazone) complexes have also

been shown to possess antimicrobial activity, which is suspected to be due to redox damage as a result of the release of the reduced Cu(I) species.<sup>70</sup> In bacterial infections, copper bis(thiosemicarbazone) complexes have been shown to inhibit bacterial respiration by inhibiting NADH dehydrogenase and complex 1 in the mitochondrial electron transport chain.<sup>108</sup> In this project the focus is in the hypoxia and copper metabolism imaging.

**Figure 1.6.2.0.1.** The structures of Cu(II) PTSM and Cu(II)KTS, based on <sup>6, 60, 69</sup>.



### **1.6.2.1. Hypoxia imaging**

Hypoxia is a term to describe when there is insufficient oxygen to meet the metabolic needs of a tissue.<sup>105, 109</sup> Hypoxia is normally defined as the oxygen tension at which the metabolic demand in stoma, endothelial cells and tumour cells exceeds the supply.<sup>110</sup> Hypoxia can be caused when the vascular supply is interrupted such as in a stroke or myocardial infraction or when a tumour outgrows its vascular supply.<sup>109</sup>

When a healthy tissue suddenly loses its oxygen supply to the point that there is insufficient oxygen for oxidative phosphorylation, the cells die either by necrosis (un-programmed cell death) or apoptosis (cell initiated death). This occurs in conditions such as strokes, myocardial infraction or when there is poor perfusion in arthritic joints.<sup>109</sup> Tissues in tumours become hypoxic gradually, however, instead of the cells dying they start to adapt to the lack of oxygen by up-regulating the production of more than 100 proteins that promote their survival and increases the aggressiveness of hypoxic cells.<sup>105, 111, 112</sup> The most important regulatory factor of the hypoxia signalling pathway activity in cells is the protein hypoxia-inducible transcription factor 1 (HIF-1) which mediates adaptive responses to reduced oxygen availability. It has been suggested that HIF-1 could be used as a reliable intrinsic marker for tumour hypoxia and prognosis.<sup>113, 114</sup> These proteins cause the slowing of the rate of cellular growth by directing the mitochondria to undergo glycolysis (the anaerobic conversion of glucose to adenosine triphosphate (ATP)), inhibit apoptosis and promote metastasis (cell spreading).<sup>109</sup> Hypoxia also may down regulate the expression of adhesion molecules which facilitates tumour cell detachments. Hypoxia in tumours was first

described by R. Thomlinson and L. Gray, who observed that heterogeneous regions of hypoxic cells formed just beyond the diffusion distance of oxygen from blood vessels (100-150  $\mu\text{m}$ ) adjacent to the necrotic core.<sup>115, 116</sup> Nearly all solid tumours consist of either hypoxic (serve or intermediate) or anoxic (no oxygen present) cells and the presence of hypoxia does not depend on tumour size, stage, pathology or nodal status.<sup>112</sup> Tumour hypoxia occurs from three distinct causes: 1) perfusion related (acute) inadequate blood flow; 2) diffusion related (chronic) hypoxia caused by increased oxygen diffusion distance ( $\approx 150\text{-}200 \mu\text{m}$ ) due to the imbalance of tumour growth and vascular neogenesis (new growth of blood vessels); 3) anemic hypoxia which may be caused by tumour-related cachexia (wasting away) or treatment.<sup>105, 117-121</sup> Tumour hypoxia is a spatial and temporal heterogeneous phenomenon, resulting from the combined effect of many factors such as tumour type, tumour volume, disease site (specific organ or tissue), regional micro-vessel density, blood flow, oxygen diffusion and consumption rates.<sup>113</sup>

The presence of hypoxia can lead to negative effects on the response of the tumour to treatment by chemotherapy, surgery or radiotherapy.<sup>122</sup> In 1955, Thomlinson and Gray suggested that human epithelial tumours may be hypoxic and therefore radio-resistant.<sup>116, 121</sup> Commonly studied cells lines were found to be roughly half-maximally resistant to ionising radiation when moderately hypoxic.<sup>121</sup> Resistance to chemotherapy is a consequence of compromised drug delivery activity in a hypoxic/acidic tumour. The acidity of the hypoxic cells comes from the accumulation of lactic acid which is a by-product of anaerobic respiration.<sup>123</sup> Surgery resistance occurs because hypoxia promotes the mobility and invasion of the tumour cells meaning the tumour is likely to have spread (metastasis) by the time of treatment.<sup>122</sup> Hypoxia induced resistance to radiotherapy was first shown in 1909 by G. Schwarz when he demonstrated that the skin's response to radiation was markedly decreased if applied to an area with reduced blood flow which was caused by compression.<sup>124, 125</sup> In radio therapy ionising radiation damages the DNA of the tumours cells. The damage occurs in several ways, the most common is that the double strand is broken by radical products that are in the vicinity of the DNA. The radical needs to then react with oxygen in order to make the damage permanent. If there is insufficient oxygen to achieve this, small thiols can repair radical damage.<sup>109, 114, 118, 126</sup> It has been determined that the radiation dose has to be 2.8-3 times higher in the absence of oxygen compared with the presence of oxygen in order to achieve the same biological effect.<sup>110</sup> It has been shown that modifying tumour hypoxia by breathing hyperbaric oxygen or carbogen (95% oxygen and 5% carbon dioxide) can be beneficial during treatment, however it was noted that benefits differ between and within tumour sites.<sup>117</sup> This has led to the suggestion that hypoxia imaging could potentially be used in selecting which cancer patients would benefit from treatments that overcome, circumvent or take advantage of the presence of hypoxia. Imaging could also be used to document whether or not and to what extent re-oxygenation occurs in tumours during radiotherapy.<sup>105</sup> There is an idea that

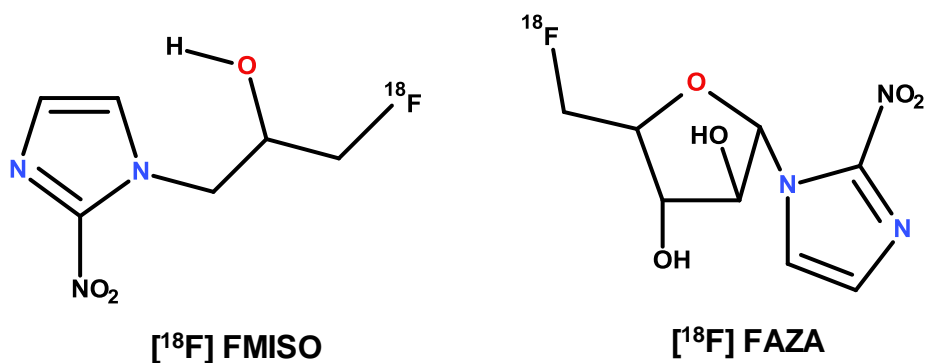
potentially could overcome the problems with hypoxia induced radio-resistance in order to improve the effectiveness of radio therapy. The idea of dose painting correlates the dose of radio therapy that a particular region of the tumour receives against the level of the hypoxia that each tumour region experiences i.e. increasing the dose to areas with increased hypoxia. This concept is still in its infancy and success will depend on the solving of challenges such as accurate conversion of hypoxia measurements into effective doses and accounting for the variations of PET hypoxia tracers in accurately reporting hypoxic information.<sup>120, 127-129</sup> Dose painting could also prevent some patients from receiving unnecessary treatments and their consequential side effects as well as supporting the use of hypoxia selective drugs like tirapazamine or nimorazole which are hypoxic radio-sensitizers.<sup>112</sup>

There is no specific value for oxyhaemoglobin ( $O_2Hb$ ) concentration, haemoglobin saturation percentage or tissue oxygen partial pressure ( $pO_2$ ) that defines the transition from normoxia to hypoxia. Arterial  $pO_2$  is typically stated at 75 mm Hg while venous blood normally averages 40 mm Hg.<sup>121</sup> The biological consequences of hypoxia depend on duration and the needs of the individual cell,<sup>109, 130</sup> which means that physoxia (the normal oxygen level in a specific tissue/organ) varies widely between different organs. For example, physoxia in the brain has a  $pO_2$  of 35 mmHg whilst physoxia in the kidneys is around 72 mmHg.<sup>122</sup> The median  $pO_2$  for lung tissues has been found to be 43 mm Hg, however the critical  $pO_2$  level where there is a negative impact upon the cellular function of the tissue is proposed to range between 8 and 10 mm Hg in most non-small-cell lung cancers.<sup>130</sup> The gold standard of measuring  $pO_2$  is the direct measurement by using a  $pO_2$  probe. These polarographic/needle electrodes can provide direct measurements of  $pO_2$  at each location point and when controlled by a computer driven stepper motor, can typically achieve one reading every 10 seconds. A distinct disadvantage of a  $pO_2$  probe is that it is an invasive technique and therefore can only be used in readily accessible tumours such as head and neck, uterine, cervix, prostate and breast tumours. The technique also only provides one dimensional information on hypoxia compared to the 3 dimensional information obtained from PET.<sup>113, 118, 127, 128, 131, 132</sup> The  $pO_2$  values obtained by these probes are also restricted by sampling error as it is not possible to extract measurements from the entire tumour in order to overcome the heterogeneous nature of tumour hypoxia. Probes cannot differentiate between necrotic (dead) and living anoxic tissue regions within the tumour.<sup>112</sup>

It is also possible to quantify hypoxia by immunohistochemical staining with hypoxic markers such as pimonidazole, which is an exogenous bio-reductive nitroimidazole compound.<sup>117, 133</sup> Immunohistochemical staining is an invasive technique and repetitive measurements of changes of hypoxic fractions after cancer treatment is not realistic in a clinical setting.<sup>112</sup> Hypoxic fraction is the fraction of the tumour that is hypoxic.<sup>122</sup> [ $^{18}F$ ] FMISO (Figure 1.6.2.1.1.) is currently the most

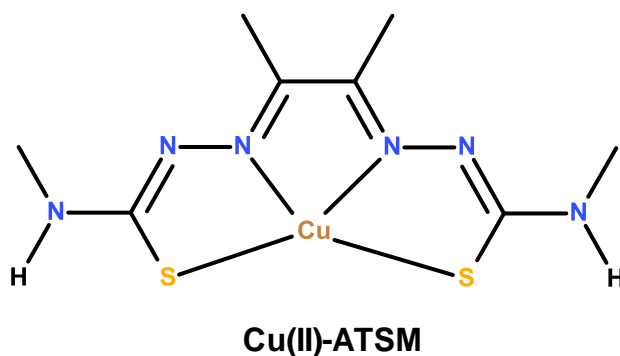
used hypoxia PET tracer in the clinic<sup>127, 128, 134</sup> and generally considered to be the gold standard for PET hypoxia imaging.<sup>110</sup> However, [<sup>18</sup>F] FAZA (Figure 1.6.2.1.1.) is becoming a more popular PET hypoxia tracer as it is more hydrophilic than [<sup>18</sup>F] FMISO, which allows faster clearance and a higher tumour-to-background ratio.<sup>112, 135</sup> The ideal PET hypoxia tracer should be able to target just cellular  $pO_2$  and not vascular  $PO_2$ , at clinically relevant oxygen concentrations only in viable cells. The tracer should be lipophilic enough to have uniform and rapid cell entry, but hydrophilic enough for rapid cell clearance from normoxic cells as well as yielding a high target-to-background ratio independent of perfusion whilst being resistant to non-hypoxia dependent metabolism.<sup>122</sup> 2-nitroimidazole derived tracers have the similar initial trapping mechanism as Cu(II)-ATSM (Figure 1.6.2.3.), in a normoxic cell the agent enters the cell and is reduced and then re-oxidised in a catalytic cycle. However in hypoxic cells the reduced nitroimidazole is not re-oxidised but instead reacts with intracellular proteins rendering it permanently trapped.<sup>136</sup>

**Figure 1.6.2.1.1.** The structure of [<sup>18</sup>F] FMISO and [<sup>18</sup>F] FAZA, based on<sup>110, 135</sup>.



The radio-copper bis(thiosemicarbazone) complex Cu(II)-ATSM (Figure 1.6.2.1.2.) can be used as a hypoxia imaging agent.

**Figure 1.6.2.1.2.** The structure of copper (II) ATSM, based on<sup>77, 126, 137</sup>.





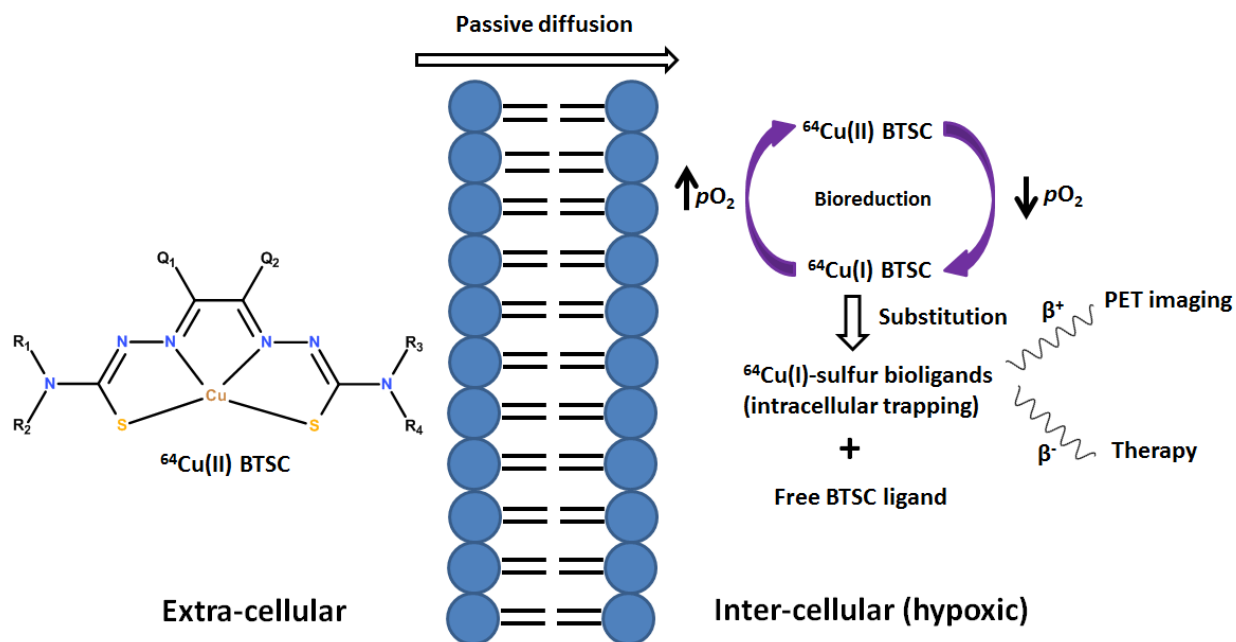
Cu(II)-ATSM has several advantages over other hypoxia PET tracers including a simpler method of synthesis, faster clearance from normoxic tissues, which allows for a reduced time between injection and imaging, as well as simpler method for quantification.<sup>138</sup> It is possible to select the copper isotope which best suits the application in terms of half-life and decay products.<sup>136</sup>

As Cu(II)-ATSM is neutral and lipophilic it is highly membrane permeable and can freely diffuse in and out of cells. When in the cell the Cu(II)-ATSM gets reduced by intracellular agents (such as NADH and NADPH) to form Cu(I)-ATSM. In normoxic cells the Cu(I)-ATSM is substantially stable and capable of resisting Cu(I) dissociation and therefore can be re-oxidised to Cu(II)-ATSM which is free to diffuse back out of the cell, however in hypoxic cell the Cu(I)-ATSM cannot be re-oxidised causing the negatively charged complex to be trapped within the cell.<sup>6, 105, 109, 130, 138-140</sup>

Related copper complexes that dissociate rapidly when reduced to Cu(I), such as Cu-PSTM, show no selectivity for hypoxia but deposits copper into cells and tissues in proportion to their delivery, making Cu(II)-PTSM an effective blood flow tracer.<sup>41</sup> K.Price *et al.*<sup>141</sup> expanded this theory by adding that for the two complexes Cu(II)-ATSM and Cu(II)-GTSM the data strongly suggested that two complexes may be taken into cells by both passive and facilitated (protein carrier mediated) mechanisms. Also the authors observed that both the complexes rapidly effluxed from cells through active mechanisms, even though it was not known if it was the ionic copper or the intact complexes that was being observed.

Cu(II) and Cu(I) show different co-ordination geometries and therefore different affinities for different donor atoms. As Cu(I) is only weakly chelated to ATSM it can become substituted by macromolecular bio-ligands present inside the cell, causing the copper to be trapped within hypoxic cells.<sup>126</sup> However cellular metabolism can wash Cu(I) that has become dissociated from ATSM out of the cells, preventing copper retention (Figure 1.6.2.1.3.), despite the presence of hypoxia.<sup>122</sup>

**Figure 1.6.2.1.3.** The suspected mechanism of hypoxia selectivity of copper bis(thiosemicarbazone) complexes, based on<sup>43, 126, 130, 142</sup>.

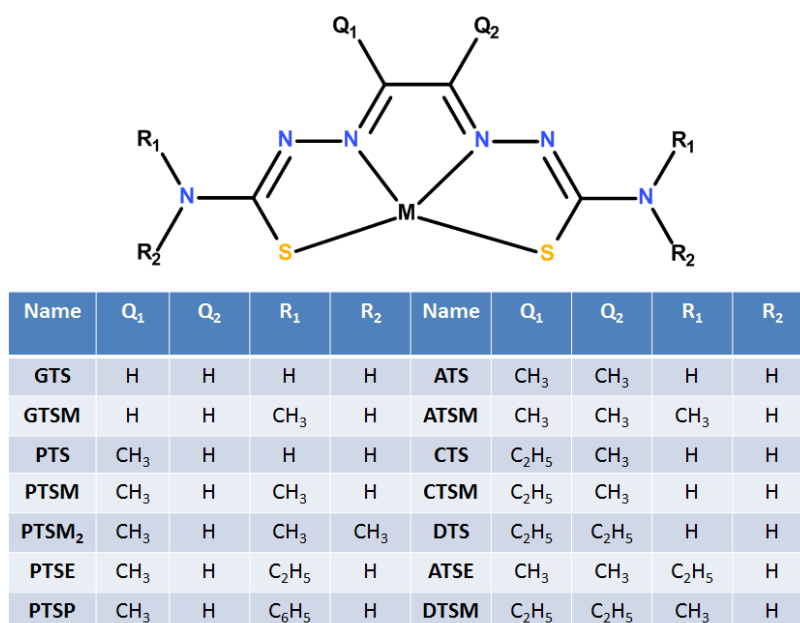


J. Dearling and A. Packard published a paper in 2010 with some thoughts on the mechanism of cellular trapping of Cu(II)-ATSM.<sup>136</sup> The authors explain that there is a range of factors contributing to the trapping of Cu(II)-ATSM in hypoxic cells. They then go on to state that the complex is transiently trapped through reduction of the Cu(II) by cellular thiols to form [Cu(I)-ATSM], which decreases the complexes lipophilicity and increases its residence time within the cell. This results in an increased likelihood that the reduced [Cu(I)-ATSM] complex will dissociate or interact with the mitochondria causing the copper to become trapped within the cell. The cellular trapping mechanism is described as biphasic, with the first phase being the reduction/oxidation cycle involving cellular thiols and molecular oxygen and the second phase being the interactions with proteins within the mitochondria leading to more permanent retention of the tracer. This biphasic mechanism may explain some of the early data that showed that 1-2 hours post injection Cu(II)-ATSM accumulation does not represent hypoxia within the tumour but 16-20 hours post injection the location of Cu(II)-ATSM correlates well with alternative methods of hypoxia detection e.g. [<sup>18</sup>F]FMISO tracers and Eppendorf oxygen electrodes. The authors suggest that this biphasic mechanism may also be responsible for the differences seen in tissue uptake and site of reduction for different cells lines because of the variation in their metabolism. The investigators concluded that experimental data on the trapping mechanism is still not complete and a number of questions about the trapping mechanism still remain unanswered which need to be answered in order to fully understand and exploit this potentially very useful tracer. A very recent investigation by R. Hueting<sup>95</sup> and co-workers attempted to shed light on the fate of the dissociated ligands. A complex was synthesised that had very similar physicochemical characteristics to Cu-ATSM which could be labelled with <sup>64</sup>Cu or <sup>123</sup>I (Figure

1.5.11.). The team showed unequivocal evidence that *in vitro* the complexes undergo rapid dissociation but unfortunately the complex was not retained effectively in the hypoxic areas of the tumour. A study by F. Shaughnessy *et al.*<sup>143</sup> investigated if changes in the antioxidant glutathione, which is the most abundant intercellular thiol, whose redox status changes in cancer cells and ischaemic myocardium, changed the hypoxia selectivity of [<sup>64</sup>Cu] Cu-ATSM. It was found that modification of glutathione levels did not impact on the pharmacokinetics or hypoxia selectivity of [<sup>64</sup>Cu] Cu-ATSM. A slightly earlier investigation by P. Bernard *et al.*<sup>144</sup> used UV/visible spectroscopy to establish if Cu(II)-ATSM is stable in the presence of glutathione. The results showed that the Cu(II)-ATSM is stable in the presence of glutathione, indicating that glutathione is not a strong enough reducing agent in order to reduce Cu(II)-ATSM.

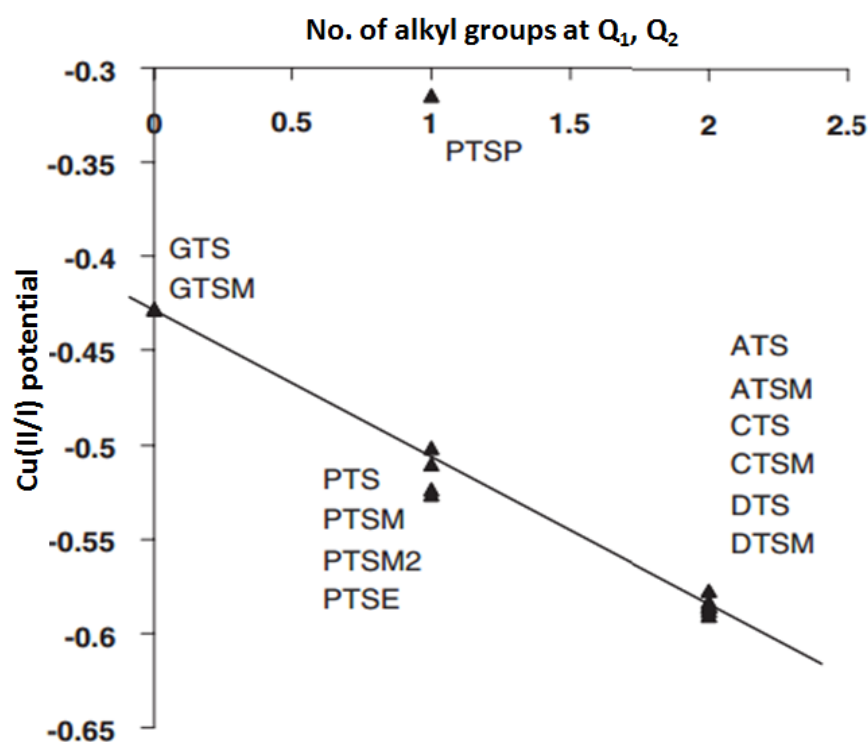
The mechanism and selectivity of copper bis(thiosemicarbazone) is a complex one, which is believed to be dependent on many factors such as lipophilicity, planarity, molecular weight, pK<sub>a</sub> and redox potential.<sup>123</sup> As copper bis(thiosemicarbazone) complexes have very low water solubility, the determination of reliable pK<sub>a</sub> values experimentally has not been possible.<sup>123</sup> Investigations into the structure activity relationships of copper bis(thiosemicarbazone) complex was initially carried out by J. Dearling *et al.*<sup>77, 145</sup> and then later P. Blower *et al.*<sup>69</sup>, R. Maurer *et al.*<sup>146</sup> and J. Holland *et al.*<sup>123</sup> used density functional theory (DFT) in order to further understand the hypoxia selectivity of the copper bis(thiosemicarbazone) complexes. The studies were undertaken in order to investigate if the lowering of the redox potential of a copper bis(thiosemicarbazone) complex would result in the complex only being trapped in a more reducing environment than normal, like hypoxic cells. The complexes that were tested along with their name designations are illustrated in (Figure 1.6.2.1.4.).

**Figure 1.6.2.1.4.** Structures and name designations of bis(thiosemicarbazone) complexes, based on<sup>69, 77, 145</sup>.



The investigations showed that altering the substituents at the diimine backbone ( $Q_1$  and  $Q_2$  positions) primarily controlled the redox potential of the complex, i.e. the potential that the copper (II) in the complex would be reduced resulting in the release of copper (I) in to the hypoxic cell. If an electron donating group is at one or both Q positions the complex will have an intermediate or low reduction potential respectively. However, if a substituent with poor electron donating ability (i.e. hydrogens) were at the Q positions then the reduction potential would be high, this is illustrated in (Figure 1.6.2.1.5.). Alkyl substitutions on the terminal amino groups ( $R_1$  and  $R_2$  positions) do not significantly affect the redox potential or the hypoxia selectivity.<sup>6</sup>

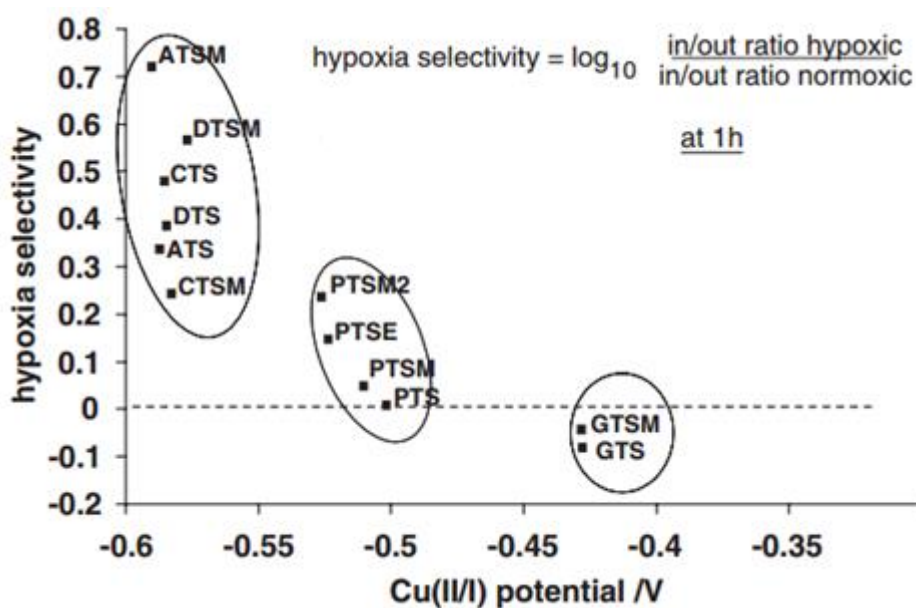
**Figure 1.6.2.1.5.** Effect of backbone alkylation on Cu(II/I) redox potential, based on<sup>69,77</sup>.



The lipophilicity of the copper can be controlled by adding more lipophilic/ less lipophilic substituents on the terminal amino positions ( $R_1$  and  $R_2$ ) which will influence where in the body the complex will migrate to. Lipophilicity was shown not to correlate with cellular uptake either under hypoxic or normoxic conditions or with hypoxia selectivity.<sup>77</sup>

It was shown that complexes with lower redox potentials are more hypoxic selective e.g. Cu-ATSM, while complexes with higher redox potentials such as Cu-GTS have little or no hypoxia selectivity (Figure 1.6.2.1.6.).

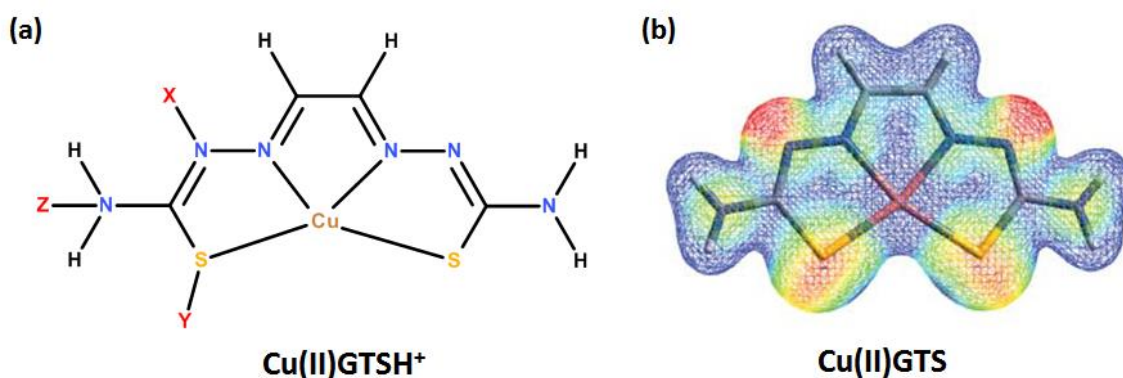
**Figure 1.6.2.1.6.** The relationship of the redox potential of the copper bis(thiosemicarbazone) and hypoxic selectivity in cultured cells, based on <sup>69,77</sup>.



There is a very strong grouping based on number of carbons on the backbone, the group far left with the lowest redox potential and highest hypoxia selectivity all have 2-4 carbons on the backbone substituents (Me/Me, Me/Et and Et/Et). The middle group all have one carbon on the backbone (Me/H) and the group to the far right, which has little or no hypoxia selectivity, only have two hydrogens (H/H) on the backbone.

Through using DFT calculations it was found that the most stable conjugate acid results from protonation at the X position. Protonation at the Y and Z position leads to a decrease in the conjugate acid stability by 58.0 and 73.3 kJ mol<sup>-1</sup> respectively when compared to X (Figure 1.6.2.1.7(a)). Figure 1.6.2.1.7. image (b) shows the electrostatic potentials of Cu(II)GTS. The red indicates regions of net negative charge. All the Cu(II) complexes were found to be highly acidic and consequently will only be protonated in strongly acidic conditions.<sup>123</sup>

**Figure 1.6.2.1.7.** (a) Illustration of the potential protonation sites for Cu(II)GTSH<sup>+</sup>. (b) Illustration of electrostatic potential of Cu(II) GTS, based on.<sup>123</sup>



The work by P. Blower *et al.*<sup>69</sup> suggested a path forward by analysing dissymmetric ligands which should give greater control on hypoxia selectivity. Quasi-combinatorial synthesis was investigated which resulted in a product containing a number of symmetric and dissymmetric pro-ligands.

A study by R. Hueting *et al.*<sup>147</sup> yielded evidence to question the common thoughts on the hypoxia selectivity mechanism of [<sup>64</sup>Cu] Cu-ATSM. Radio-copper retention in cancer cells *in vivo* and *in vitro* after administration of [<sup>64</sup>Cu] Cu-ATSM and [<sup>64</sup>Cu] Cu-acetate was measured. The results showed that the distribution of <sup>64</sup>Cu from [<sup>64</sup>Cu] Cu-ATSM and [<sup>64</sup>Cu] Cu-acetate was very similar which suggests that retention of radio-copper could be effected by copper metabolism rather than being solely a direct indicator of hypoxia.

Early work by Y. Fujibayashi<sup>148</sup> and co-workers compared [<sup>64</sup>Cu] Cu-ATSM with [<sup>11</sup>C] acetate, a regional perfusion tracer, to visualise hypoxic rat heart tissue. It was discovered that in ischemic regions (areas of reduced blood supply to tissues), where there was low uptake of [<sup>11</sup>C] acetate, there was a high accumulation of [<sup>64</sup>Cu] Cu-ATSM compared to normal regions. Furthermore areas of low blood flow, low uptake of [<sup>11</sup>C] acetate, are surrounded by regions that have a high uptake of [<sup>64</sup>Cu] Cu-ATSM indicated that these hypoxic regions contain viable myocardial tissue. J. Lewis and co-workers undertook studies to further illustrate that the uptake of [<sup>60</sup>Cu] Cu-ATSM significantly increases in hypoxic tissue.<sup>149, 150</sup>

The first report of Cu-ATSM being used in a human study was in 2000 where [<sup>62</sup>Cu] Cu-ATSM was used in subjects who had lung cancer. Intense uptake was observed in all lung cancer patients reaching a plateau within a few minutes after injection. However, the distribution of [<sup>62</sup>Cu] Cu-ATSM was different from that of FDG or blood flow.<sup>151</sup> The hypoxic selectivity of a large number of Cu(II)-bis(thiosemicarbazone) complexes was correlated with their reduction potential, stability of the Cu(I) species and the pKa values. The data gathered supports that intercellular reduction of Cu(II) to a Cu(I) species can lead to two distinct patterns of behaviour. Non-hypoxia selective complexes undergo rapid acid catalysed dissociation but for hypoxia selective complexes they are resistant to dissociation allowing for back-oxidation by molecular oxygen in normal tissues.<sup>126</sup> Lewis *et al.*<sup>150</sup> used a canine ischaemic myocardial model to show that [<sup>64</sup>Cu] Cu-ATSM has a half-life of 7-8 minutes. The hypoxia selectivity of the copper bis(thiosemicarbazone) complexes arises from a delicate balance between enzyme-mediated one-electron reduction and subsequent back-oxidation by di-oxygen in normal tissue against protonation and ligand dissociation in hypoxic tissues.<sup>126</sup> The first clinical study undertaken compared the quality of images obtained when using [<sup>60</sup>Cu] Cu-ATSM and [<sup>64</sup>Cu] Cu-ATSM for imaging a cohort of ten women with cervical carcinoma on separate days. Image quality was assessed qualitatively and the tumour-to-muscle activity ratio was measured for each tracer. The study found that a 925MBq dose of [<sup>64</sup>Cu] Cu-ATSM produced images with less noise and therefore a higher quality than the images obtained by a 740MBq dose

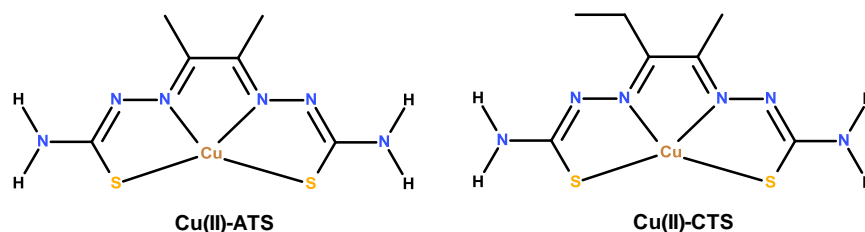
of [<sup>60</sup>Cu] Cu-ATSM.<sup>132, 138, 140, 152</sup> The authors selected the respective doses in order to achieve the same number of decays in the 30- to 60-min-postinjection scan.<sup>152</sup> Results from toxicology studies in animals and patient monitoring indicated that the doses used for both isotopes in the study were safe to be clinically employed.<sup>60</sup> One of the biggest drawbacks of [<sup>64</sup>Cu] Cu-ATSM is that it has a perceived high log*P* (around 1.5-1.6) and a high liver uptake. The most successful modification in order to overcome the high lipophilicity was the introduction of a glucose molecule as a pendant arm to ATSM to yield a water soluble complex with a log*P* of 0.5 without affecting its hypoxia selectivity.<sup>20, 153, 154</sup> Bio-distribution in preclinical mice models show that early uptake occurs in the heart (8.75%) and brain (10.46%) which then diminished to 3.81% and 3.34% respectively after 40 minutes post injection. A similar uptake pattern was observed in the kidneys but with a far greater initial uptake (23.45%). Liver uptake gradually increased from 7.75% (1 minute post injection) to 29.83% (40 minutes post injection). From this it was suspected that the metabolism of ATSM occurs in the liver and the kidneys. In human studies activity was seen in the liver, kidneys and spleen, however very little trace was detected in the bladder and bowel despite the proposed site of metabolism being the liver and kidneys. Human data showed that the kidneys received a much lower dose, which was just above background. It is recommended that the liver should be the human dose limiting organ for dose calculations.<sup>139, 155</sup>

In the application of Cu-ATSM acting as an imaging agent for myocardial infarctions, it has been shown that Cu-ATSM is not retained in necrotic tissue, thus Cu-ATSM can be used to differentiate between hypoxic, viable tissue and non-functional, dead, myocardial tissue.<sup>110</sup> [<sup>61</sup>Cu] Cu-ATSM was used by T. Bradshaw *et al.*<sup>156</sup> along with two other tracers in order to measure and compare the spatial distributions of three biological properties, glucose metabolism ([<sup>18</sup>F] FDG), cellular proliferation ([<sup>18</sup>F] FLT) and hypoxia ([<sup>61</sup>Cu] Cu-ATSM), in canine tumours. It was concluded that the relationship of glucose metabolism, proliferation and hypoxia was heterogeneous across the two tumour types tested. The uptake of [<sup>64</sup>Cu] Cu-ATSM is highest in anoxic cell but is also significant in normoxic cells, but after this initial period the uptake of [<sup>64</sup>Cu] Cu-ATSM is dependent on cell line and the oxygenation conditions which can lead retention to decrease in some circumstances.<sup>157</sup> Yuan and colleagues evaluated [<sup>64</sup>Cu] Cu-ATSM as a hypoxia imaging agent and concluded that Cu-ATSM may be a valid hypoxia imaging agent for some tumour types, but cannot be extrapolated to all tumour types therefore it cannot be used as a universal hypoxia marker which prevented widespread acceptance of Cu-ATSM as a hypoxia PET tracer.<sup>122</sup> Cu-ATSM has also been evaluated in patients with rectal and cervical cancer.<sup>158</sup> K. Chao *et al.*<sup>159</sup> demonstrated the feasibility of using Cu-ATSM PET coupled with CT images for the determining hypoxia of a tumour. The information gathered can then be used for intensity-modulated radiation therapy (IMRT) or dose painting which would allow the escalation of radiation dose to the tumour whilst maintaining low doses to the surrounding normal tissue.

K. Matsumoto *et al.*<sup>160</sup> showed that when directly compared [<sup>64</sup>Cu] Cu-ATSM and [<sup>18</sup>F] FMISO under different levels of hypoxia only resulted in a positive correlation with [<sup>18</sup>F] FMISO uptake while [<sup>64</sup>Cu] Cu-ATSM was found to not be able to detect the varying changes in hypoxia. So despite some clinical uses for [<sup>64</sup>Cu] Cu-ATSM, more studies are required in order to confirm that [<sup>64</sup>Cu] Cu-ATSM is truly a hypoxia specific tracer.<sup>112</sup> A more recent investigation by S. Carlin *et al.*<sup>161</sup> compared the hypoxia selectivity of [<sup>64</sup>Cu] Cu-ATSM with three other hypoxia tracers ([<sup>18</sup>F] FMISO, [<sup>18</sup>F] FAZA and [<sup>18</sup>F]-HX4). The highest tumour uptake was observed with [<sup>64</sup>Cu] Cu-ATSM with little renal clearance. However, the distribution of [<sup>64</sup>Cu] Cu-ATSM did not correlate with the immunohistochemistry hypoxia markers which cast further doubt on the hypoxia selectivity of [<sup>64</sup>Cu] Cu-ATSM. A selected review by M. Bourgeois<sup>162</sup> and co-workers also compared [<sup>64</sup>Cu] Cu-ATSM and [<sup>18</sup>F] FMISO. The conclusion of the authors was despite [<sup>64</sup>Cu] Cu-ATSM having less favourable dosimetry than [<sup>18</sup>F] FMISO because of the associated β<sup>-</sup> emission from <sup>64</sup>Cu, [<sup>64</sup>Cu] Cu-ATSM was found to be superior in terms of imaging performance. [<sup>18</sup>F] FMISO has a slow *in vivo* accumulation and a weak image contrast of the hypoxic area.

An investigation carried out by V. Keremans *et al.*<sup>163</sup> showed that the use of anaesthetic and carrier gas can influence the tumour uptake of hypoxia imaging agents, [<sup>64</sup>Cu] Cu-ATSM, [<sup>99m</sup>Tc] HL91 and [<sup>18</sup>F]-FMISO.<sup>20</sup> Handley *et al.*<sup>164</sup> used the rat isolated heart model<sup>165, 166</sup>, the same model that was used by Y. Fujubayashi<sup>74</sup> and co-workers to show that the retention of [<sup>62</sup>Cu] Cu-ATSM was inversely correlated with the accumulation of a myocardial blood flow tracer, in order to screen structural variants of [<sup>62</sup>Cu] Cu-ATSM for the application of cardiac hypoxia. Handley made the structural variants at the Q<sub>1</sub>, Q<sub>2</sub>, R<sub>1</sub> and R<sub>2</sub> positions (Figure 1.6.2.5.). Out of the nine Cu-ATSM analogues [<sup>64</sup>Cu] Cu-ATS and [<sup>64</sup>Cu] Cu-CTS (Figure 1.6.2.1.8.) demonstrated better cardiac hypoxia selectivity and imaging characteristics than the current lead hypoxia tracers, [<sup>64</sup>Cu] Cu-ATSM and [<sup>18</sup>F]-FMISO. Their improvement in imaging performance is due to their reduced lipophilicity which improves their rate of washout from normoxic tissues and increases hypoxic-to-normoxic tissue contrast. The redox potentials of the both copper complexes remained similar to [<sup>64</sup>Cu] Cu-ATSM.

**Figure 1.6.2.1.8.** The structure of copper (II) ATS and copper (II) CTS, based on<sup>145, 164</sup>.





M. Handley<sup>167</sup> and co-workers have also used a novel, low cost, reusable incubation system in order to quantify the accumulation of [<sup>64</sup>Cu] Cu-ATSM in rat heart muscle cells under oxic (95 or 21% O<sub>2</sub>/5% CO<sub>2</sub>) or hypoxic gas (95% N<sub>2</sub>/5% CO<sub>2</sub>). It was found that total cellular retention increased during hypoxia, but this was not localised in any particular compartment of the cell. At the time of publication M. Handley<sup>168</sup> reported that Cu-ATSM is the only copper bis(thiosemicarbazone) complex that has been tested for cardiac imaging. Hendley then goes on to state that development and screening of more members of the bis(thiosemicarbazone) family is essential.

[<sup>64</sup>Cu] Cu-ATSM has also been studied for targeted therapy by utilising the Auger electrons in order to deliver a cytotoxic dose to a target tissue. As the Auger electrons have a short range (≈5 μm) the radiotoxic effects are limited to the target cells.<sup>6</sup> In a preclinical trial [<sup>64</sup>Cu] Cu-ATSM was shown to increase the survival time of 50% of hamsters bearing colon cancer tumours from 20 days to 135 days with no acute toxicity side effects.<sup>6, 43, 169</sup> [<sup>61</sup>Cu] Cu-ATSM was demonstrated to have a very stable spatial distribution during radiation therapy.<sup>170</sup> M. Carter<sup>171</sup> and co-workers showed that [<sup>64</sup>Cu] Cu-ATSM and [<sup>64</sup>Cu] Cu-GTSM can be used in therapeutic applications for treating cancerous prostate cell lines. It was noted that increasing the extra-cellular copper concentration enhances the effectivity of both [<sup>64</sup>Cu] Cu-ATSM and [<sup>64</sup>Cu] Cu-GTSM and that the pro-ligands ATSM and GTSM were not toxic to cancerous prostate cells. D. Palanimuthu<sup>172</sup> also reported that certain copper bis(thiosemicarbazone) complexes, particularly complexes with only hydrogens as the backbone substituents, showed to have anti-tumour activity in mice models. The activity was similar to the anticancer drug Adriamycin. The compounds mode of action was to inhibit DNA synthesis and to induce apoptosis. A very recent article by C. Yip *et al.*<sup>130</sup> nicely summarises studies that have compared Cu-ATSM uptake against invasive measurements of tumour hypoxia as well as the results of clinical studies using Cu-ATSM as a imaging agent for non-small-cell lung cancer. One such study concluded by stating that [<sup>62</sup>Cu] Cu-ATSM is useful for predicting prognosis of patients with non-small-cell lung cancer.<sup>173</sup> A general overview of Cu-ATSM in the evaluation of hypoxia in clinical oncology is presented by.<sup>132</sup>

An interesting study by D. Williamson and co-workers.<sup>132, 174</sup> tested [<sup>64</sup>Cu] Cu-ATSM and [<sup>64</sup>Cu] Cu-ATSE (Figure 1.6.2.1.4.) as imaging agents for brain hypoxia, however despite the ability of the tracers to rapidly enter and efflux from the brain there was no significant accumulation of either tracer in the hypoxic lesions.

### **1.6.2.2. Imaging copper metabolism for the investigation of neurodegenerative disorders**

Imbalances in copper homeostasis can be identified in a range of inherited and acquired pathological conditions such as Wilson's disease, Alzheimer's disease (AD) and cancer.<sup>29</sup> Over 95% of AD cases are sporadic and only 2-7% of cases are genetically determined.<sup>36</sup> Alzheimer's disease is a fatal progressive neurodegenerative disease and is the most common form of dementia. Dementia is defined as the loss of ordered neural function leading ultimately to synaptic failure and neuronal death. The loss of neural function can manifest in loss of abilities like storing new memory, impairment of judgement or reasoning abilities and language, to name but a few.<sup>175-178</sup> Alzheimer's disease is characterised by the presence of extracellular amyloid plaques which are composed of insoluble amyloid  $\beta$  peptides, which consists of 39-43 amino acid residues.<sup>6, 29, 31, 76, 179</sup> It is believed that reactive oxygen species from copper metabolism can promote cross linking and aggregation of amyloid  $\beta$  peptides.<sup>180</sup>

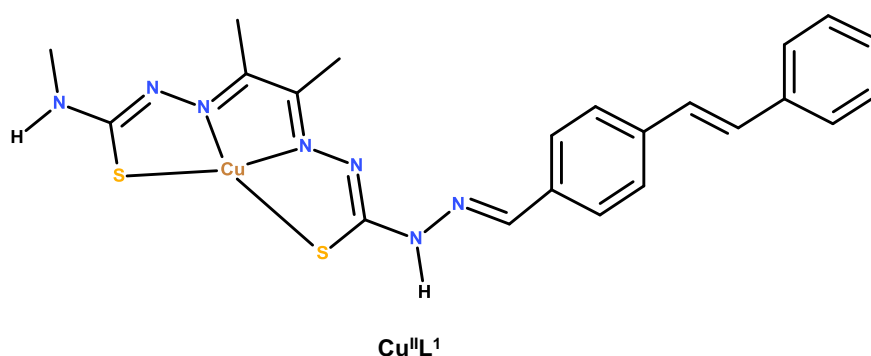
The amyloid  $\beta$  peptide is generated from the breakdown of a large transmembrane protein called the amyloid precursor protein.<sup>31</sup> However, the presence of amyloid  $\beta$  plaques do not consistently correlate with cognitive impairment leading some to argue that the smaller soluble oligomeric species are the toxic species that are responsible for neuronal death.<sup>176</sup> Currently AD is diagnosed by tests that establish progressive impairment of memory and at least one other area of cognition and definite diagnosis is only obtained by post mortem investigations of the presence of plaques and neurofibrillary tangles.<sup>179</sup> The highly insoluble neurofibrillary tangles contain hyper-phosphorylated forms of the normally soluble tau protein.<sup>181</sup>

Both the peptides and proteins can isolate and reduce copper, and the elevated copper deposition has been observed in these plaques.<sup>29</sup> Along with copper, metals such zinc and iron have significantly elevated concentration in the brain of sufferers of AD and other neurodegenerative diseases when compared to brains of the same age without a neurodegenerative condition.<sup>182</sup> In fact aggregated amyloid  $\beta$  peptides have been described as metal sinks due to their abnormally high content of Cu, Zn and Fe.<sup>6, 31</sup> It is thought that copper binding is involved in the aggregation of the A $\beta$  peptide which has developed interest in high affinity copper chelators for therapeutic applications. Other potential pharmacotherapeutic targets for AD are nicely reported by Y. Biran and co-authors.<sup>182</sup> Copper bis(thiosemicarbazone) complexes, such as Cu-GTSM due to its ability to cross the blood brain barrier (BBB) and release copper in to cells, are of interest as potential diagnostic PET tracers.<sup>29</sup> These complexes can be used to image changes in copper homeostasis and transport in diseases such as Alzheimer's disease, other dementias, Menkes' disease and Wilson's disease.<sup>41</sup>

Copper bis(thiosemicarbazone) complexes have been of interest on both the diagnostic and therapeutic front for AD and other neurodegenerative diseases. In terms of therapy, P. Donnelly, K. Price and co-workers<sup>76, 180</sup> tested a number of copper and zinc bis(thiosemicarbazone) complexes derivatives in order to ascertain which complexes could transport the metal across the blood brain barrier and release the metal in to the brain resulting in an increase of metal bioavailability. This modulation of bioavailability then could lead to potential therapeutic effects by the reduction of secreted amyloid  $\beta$  peptide. The results showed a 100-200 fold increase in copper levels<sup>178</sup> and a 10 fold increase in zinc levels. The administration of the copper complexes resulted in the decrease of extracellular amyloid  $\beta$  peptides. The authors concluded by stating that both copper and zinc bis(thiosemicarbazone) derivatives have potential as therapeutic agents for AD. Cu-GTSM has shown to have potential use as a clinical treatment as it has the ability to increase intracellular copper concentrations by several hundred fold which leads to signalling pathways which inhibits the glycogen synthase kinase enzyme which regulates the accumulation of amyloid  $\beta$  aggregates.<sup>181, 183</sup> Increasing the intercellular copper concentrations also allows Cu-GTSM to decrease the level of tau phosphorylation.<sup>181</sup>

Cu-GTSM is easier to reduce than Cu-ATSM because of the hydrogen substituents on the imine carbons, whilst still processing membrane permeability, it can be reduced in most cells thus allowing transportation of Cu species to the brain. A significant uptake (40%) of [<sup>64</sup>Cu] Cu-GTSM was shown in transgenic mice compared to [<sup>64</sup>Cu] Cu-ATSM.<sup>184</sup> This approach does not directly measure AD pathologies (A $\beta$  plaques or neuronal dysfunction) however, it does have the potential to offer complementary information to other diagnostic procedures.<sup>176</sup> A slightly different approach was to develop a copper bis(thiosemicarbazone) complex Cu<sup>II</sup>L<sup>1</sup> (Figure 1.6.2.2.1.) which is functionalised with an A $\beta$  plaque targeting stilbene group.

**Figure 1.6.2.2.1.** The structure of copper complex Cu<sup>II</sup>L<sup>1</sup>, based on <sup>176, 185</sup>.



The copper complex was added to human AD brain tissue and examined by fluorescent microscopy. The results were compared to immune A $\beta$  staining methods that showed strong co-localisation.<sup>176, 185</sup> This approach was further explored by J. Hickey *et al.*<sup>179</sup> who synthesised three

copper complexes with similar structures to  $\text{Cu}^{\text{II}}\text{L}^1$  of which two of them successfully bound to amyloid  $\beta$  plaques.

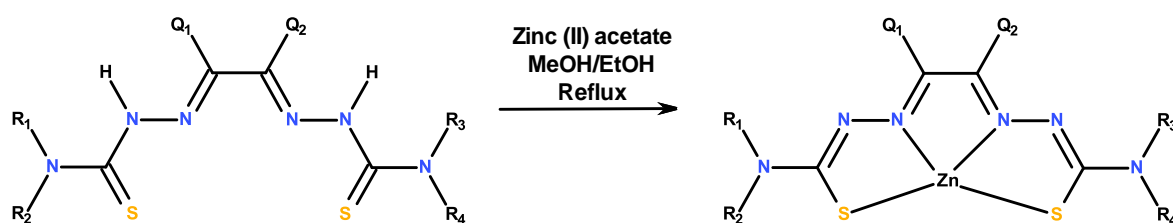
Another functionalised copper bis(thiosemicarbazone) complex was also synthesised by J. Holland and co-workers<sup>186</sup> for the diagnosing Parkinson's disease. The complex contained dopamine and tropinone like groups, as these groups are present in most Parkinson's disease imaging agents. Cu-ATSM has also got potential therapeutic applications in the treatment of Amyotrophic Lateral Sclerosis.<sup>187</sup> Cu-ATSM has also been used to assess oxidative stress in a variety of neurodegenerative disorders such as Parkinson's disease.<sup>132</sup> Oxidative stress is the imbalance in redox couples such as  $\text{NADPH}/\text{NADP}^+$ , causing a disparity between the productions of oxygen reactive species and protecting antioxidant species.<sup>188</sup>

### **1.6.3. Zinc bis(thiosemicarbazone) complexes**

Generally zinc bis(thiosemicarbazone) complexes can be readily made by refluxing a chosen bis(thiosemicarbazone) pro-ligand in ethanol or methanol whilst in the presence of Zinc (II) acetate as shown in (Figure 1.6.3.1.) The product can be recovered by filtration and washed with a solvent such as diethyl ether or methanol. Although the resulting product is commonly a yellow/orange colour, some red products have also been reported.<sup>57, 83, 91, 185, 189</sup> According to the literature, this reflux method seems to be the most popular method however there are two different methods that are worth mentioning. Firstly, Donnelly *et al.*<sup>76</sup> reported an alternative method where the pro-ligand was dissolved in a small quantity of DMF along with zinc (II) acetate and stirred at room temperature for 1 hour. The product precipitated out of solution upon the addition of water and was washed with ethanol and diethyl ether. Secondly, V. Bocokic *et al.*<sup>190</sup> combined the construction of the ligand and the chelation of the zinc all in one reaction. This was done by reacted a mono-thiosemicarbazone intermediate with a dissimilar thiosemicarbazide and zinc (II) acetate at once.

Studies on Zn-ATSM ( $\text{Q}_1=\text{Q}_2=\text{Me}$ ,  $\text{R}_1=\text{R}_3=\text{Me}$ ,  $\text{R}_2=\text{R}_4=\text{H}$ ) by Cowley *et al.*<sup>189</sup> shows that zinc can form a 5<sup>th</sup> coordination bond with an oxygen atom in a solvent molecule of DMSO. This 5<sup>th</sup> bond is axial and produces a complex that has a square pyramidal geometry.

**Figure 1.6.3.1.** Formation of a zinc bis(thiosemicarbazone) complex, based on<sup>57, 83</sup>.



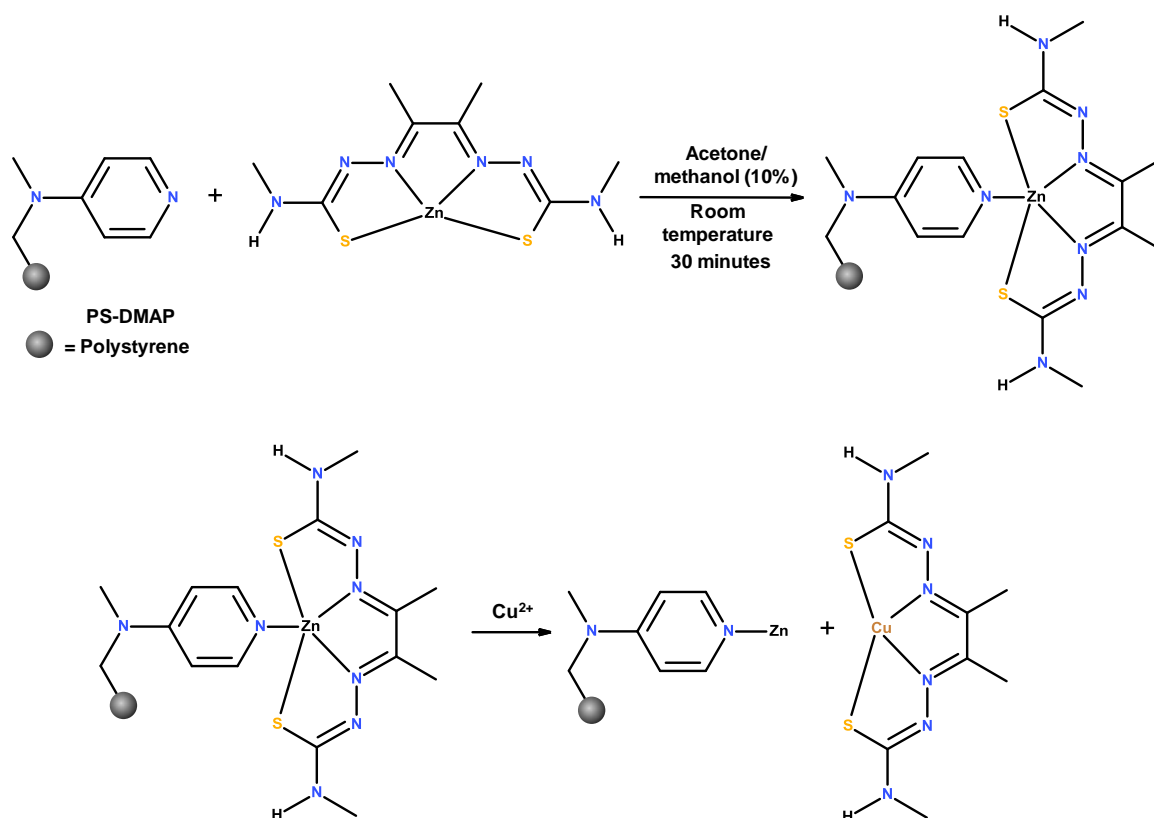
Zinc bis(thiosemicarbazone) complexes are of interest for a number of reasons, firstly they are weakly fluorescent which allows their uptake and intracellular distribution within cells to be tracked by fluorescence microscopy.<sup>76, 83, 84, 91, 189, 191</sup> Secondly due to zinc bis(thiosemicarbazone) complexes being diamagnetic they can be characterised by NMR something which is not possible with the related paramagnetic copper complexes.<sup>57</sup> Finally the zinc complexes can be convenient precursors in the production of the related radio-copper bis(thiosemicarbazone) complexes by transmetalation. S. Kadwoaki<sup>75</sup> and co-workers have recently showed that a zinc bis(thiosemicarbazone) complex shows promise for acting as an oral antidiabetic agent.

### **1.6.3.1. Transmetalation**

In 1992, K. Matsumoto *et al.*<sup>192</sup> and in 1993, H. Saji *et al.*<sup>193</sup> published the first reports on the use of the transmetalation approach.<sup>57</sup> M. Chrislieb *et al.*<sup>83</sup> reported that when a chosen zinc bis(thiosemicarbazone) complex is added to one equivalent of copper(II) in aqueous methanol the transmetalated copper bis(thiosemicarbazone) complex is rapidly formed. This principle lends itself to be translated in to the rapid synthesis of copper bis(thiosemicarbazone) complexes by using polymer bound zinc bis(thiosemicarbazone) complexes as the precursor. The transmetalation process relies on the fact that the zinc complexes are constrained in a pseudo-square-planar conformation which allows the zinc to form an axial fifth coordination bond with another donor atom, just like in A. Cowley *et al.*<sup>189</sup> Instead of a solvent molecule of DMSO, a fifth bond can be formed between the zinc atom and the nitrogen lone pair of a pyridine functionality which is attached to a solid polystyrene polymer support. Upon addition of a Cu<sup>2+</sup> solution the copper undergoes transmetalation with the zinc in the complex in order to form a copper bis(thiosemicarbazone). As the Jahn-Teller distortion disfavors the coordination of the axial fifth bond in the resulting copper complex, the copper-pyridine bond does not form leading to only the transmetalated square planar copper bis(thiosemicarbazone) complex to be released from the resin.<sup>137, 183</sup> This process is illustrated in (Figure 1.6.3.1.1.).

Betts *et al.*<sup>137</sup> used a 4-(dimethylamino)pyridine (DAMP)- functionalised polystyrene resin that was cross-linked with 2% divinylbenzene. Loading of the chosen zinc bis(thiosemicarbazone) on to the resin was achieved by stirring the resin in an acetone/methanol (10%) solution of zinc complex at room temperature for 30 minutes. The resin was then recovered via filtration, washed in order to remove any unbound zinc complex and dried.

**Figure 1.6.3.1.1.** Formation of a zinc bis(thiosemicarbazone) complex, based on<sup>137</sup>.



J. Holland *et al.*<sup>57</sup> studied the kinetics of the copper transmetalation with a glucose functionalised zinc bis(thiosemicarbazone) complex and found that the second-order reaction was very rapid and upon efficient mixing can be completed within 1 second at room temperature. A study by A. Aphaiwong *et al.*<sup>194</sup> involved testing a number of different polymers for application in zinc-copper transmetalation reactions. The authors concluded that out of the polymers that they tested a pyridine functionality was found to be optimal and that further work to improve loading and release of metal ligands from their polymeric supports is warranted. A slightly older report of solid phase synthesis has been found for the production of [<sup>18</sup>F]FDG by using a solid bound FDG substrate which is selectively cleaved upon reaction with [<sup>18</sup>F] fluoride ions.<sup>10</sup>

## **1.7. Thesis hypothesis, aims and objectives**

Reports of the evaluation of copper bis(thiosemicarbazone) complexes for the diagnosis of hypoxia via positron emission tomography have been dominated by the symmetric complexes. Even though the majority of reports are in respect to Cu-ATSM other symmetric complexes have been investigated<sup>69, 77, 123, 164, 168</sup>. These other symmetric complexes are structurally similar to Cu-ATSM except having different substituents at the Q<sub>1</sub>, Q<sub>2</sub>, R<sub>1</sub> and R<sub>2</sub> positions. These substituents are typically H, CH<sub>3</sub>, CH<sub>2</sub>CH<sub>3</sub> and C<sub>6</sub>H<sub>5</sub> (Figure 1.6.2.1.4.). As mentioned earlier in this chapter the

Q<sub>1</sub> and Q<sub>2</sub> positions influence the reduction potential of the copper complexes which dictates in which environments the copper complexes release their radio copper ion. Independently the R<sub>1</sub> and R<sub>2</sub> positions control the lipophilicity of the complexes which prescribes where in the body the copper complexes will migrate to. The ideal copper complex will be lipophilic enough in order to passively diffuse through the cell membrane but hydrophilic enough to allow faster clearance from non-target cells resulting in a higher target to background ratio. By synthesising dissymmetric copper bis(thiosemicarbazone) complexes with different substituents on the two terminal amines, the greater the range of complexes with slightly different lipophilicity values that can be evaluated for hypoxia selectively. If a range of copper complexes can be screened the more likely it is to find a complex which is superior to the symmetric complexes, or at the very least will suggest further complex designs for the next generation of bis(thiosemicarbazone) copper complexes. Additionally, if a copper complex is synthesised that has the correct reduction potential and is lipophilic enough to cross the blood brain barrier then that complex could be utilised for the application of brain imaging for investigating neurodegenerative disorders.

With this in mind, the main focus of this thesis is investigating the synthesising of dissymmetric copper complexes to fill this gap. From previous work by P.J. Blower *et al.*<sup>69</sup> and J. Dearling *et al.*<sup>77</sup> it is known that complexes with two alkyl groups on the Q<sub>1</sub> and Q<sub>2</sub> positions have a lower reduction potential and a higher hypoxia selectivity. Therefore, it is desirable to synthesise copper complexes with Me/Me and Me/Et on the backbone with R<sub>1</sub> and R<sub>2</sub> substituents with varying lipophilicity for the evaluation of hypoxia imaging. A secondary aim is to synthesise copper complexes with Me/H and H/H on the Q<sub>1</sub> and Q<sub>2</sub> positions and more lipophilic R<sub>1</sub> and R<sub>2</sub> substituents, as these are expected to have less negative reduction potentials which could allow the complexes to deposit their radio copper ion in to the brain irrespective of hypoxia.

The initial aim of this project is to establish a suitable method for the synthesis of the dissymmetric bis(thiosemicarbazone) ligands. There are a handful of methods reported in the literature.<sup>66</sup> Out of these, the method of using acetal protecting groups and the method of exploiting the reactivity of carbonyl groups are going to be investigated in order to determine which method is most suitable for this project. Throughout the synthesis of each class of dissymmetric ligands the related symmetric complexes are also going to be synthesised to act as both a comparison of pharmacokinetic properties, but also to establish knowledge about the synthesis and characterisation of that class of ligands which can be applied to the case of the dissymmetric ligands. Once a ligand is reacted with radio-copper to form a radio complex there is very little time for lengthy purification procedures as the copper complex is constantly decaying. So in order to cut down the need for purification procedures post radio labelling the target purity for each ligand is  $\geq 95\%$ .

From the literature, the method that seems to be most used for synthesising copper bis(thiosemicarbazone) complexes, in the milligram to gram scale, is refluxing the chosen bis(thiosemicarbazone) ligand in a solvent such as ethanol<sup>80</sup> and methanol<sup>57</sup> with a copper (II) salt such as copper acetate. Of course for these methods to work the ligands must at least be moderately soluble in methanol or ethanol. As the aim of this project is to synthesise ligands with a range of lipophilicity values an objective is to devise a method that can be applied to the entire ligand library which produces complexes with high purity and reasonable yield. Due to NMR spectroscopy not being available for the analysis of the copper complexes, high purity will be regarded as CHN analysis within +/- 0.3 of the theoretical percentage. These objectives will also be set for the synthesis of zinc (II) bis(thiosemicarbazone) complexes. It is desirable to synthesise zinc complexes from the library of ligands because, besides most of them being expected to be novel, they can act as potential precursors for the rapid synthesis of their related copper complexes via the transmetalation reaction.<sup>57, 137</sup> A further objective is to determine if the transmetalation synthetic approach can be applied to the range of ligands that are to be synthesised in this project.

Due to restrictions in the facilities that are available, it will not be possible to routinely synthesise radio copper complexes. The complexes will be synthesised using stable copper and zinc isotopes for the purposes of synthesis optimisation and comprehensive characterisation of each complex. Characterisation data shall be collected on all intermediates, ligands and complexes. There is not currently a source of comprehensive unified characterisation data for the bis(thiosemicarbazone) ligands and their related complexes. The techniques that shall be utilised shall be NMR spectroscopy (except for paramagnetic copper complexes). Vibrational spectroscopy in the form of infrared and Raman spectroscopy which can be used as a very quick verification of the identity of a product, but also for establishing if zinc complexes have been successfully loaded upon polymers for the transmetalation investigation. Mass spectrometry will give compelling evidence that the desired copper or zinc complex have been successfully produced. Uv-vis lambda max and extinction coefficients shall also be collected. In order to establish the purity of the ligands and the complexes produced, CHN analysis shall be employed.

Once fully characterised by the techniques listed above, the next objective is to collect logP and reduction potentials for each of the copper complexes. This work shall be carried out by collaborating with the Division of Imaging Sciences and Biomedical Engineering at King's College London. The data will give an indication of the lipophilicity of the complexes and at what level of hypoxia the copper (II) complexes will be reduced so that the radio copper ion can be deposited within the hypoxic environment. The logP value for each copper complex will be determined by synthesising the related <sup>64</sup>Cu complex and partitioning it between water and octanol phases. The



partition coefficient shall be established by using a gamma counter to count the proportion of the complex in each the water and octanol phase. It is expected that the redox potential shall be obtained using cyclic voltammetry.

From the logP data and reduction potential of each copper complex, a list of copper complexes candidates can be compiled for screening in the isolated heart model<sup>164-166</sup> in order to establish the hypoxia selectivity of the candidate complexes. J. Dearling *et al.*<sup>77</sup> reports that Cu-ATSM, with a Cu(II/I) reduction potential of -0.59V and a logP of 1.48, had the greatest hypoxia selectivity at 60 minutes post injection out of the range of symmetric copper complexes tested. The experiment set up used a glassy carbon electrode, a Pt gauze auxiliary electrode and an Ag/AgCl reference electrode. It is also suggested that for a copper bis(thiosemicarbazone) complex to be hypoxia selective it has to have a reduction potential below -0.5V. Copper complexes synthesised in this project with a reduction potential of below -0.5V would be candidates for screening in the isolated heart model. The priority complexes would be any which have a lower reduction potential than Cu-ATSM (-0.59V). For the copper complexes that J. Dearling *et al.*<sup>77</sup> screened which showed hypoxia selectivity, the Log P range of these complexes was 0.65-2.69. The non-hypoxic selective complexes had a Log P of 0.45-0.84. With this in mind it is suggested that the copper complexes that are synthesised in this project with a Log P in the range of 0.65-2.69 are of interest for screening. The ones with Log P values at the top end of this range or higher than 2.69 should be regarded as priority complexes. An interesting result with PTSP was obtained; PTSP has Me/H on the backbone and H/Ph substituents on the terminal amine. Despite having a relatively high reduction potential of -0.3, PTSP showed a small level of hypoxia selectivity. Synthesis of dissymmetric complexes with Me/H on the backbone containing phenyl substituents on the terminal amine will be worth evaluating for hypoxia selectivity.

Copper complexes which would be candidates for the application of brain imaging for the investigation of neurodegenerative disorders would be any complexes whose lipophilicity values are at the higher end of the range for the all synthesised complexes and who possess reduction values of above -0.5V. A potential way of screening these candidate complexes would be *in vivo* rat testing in order to determine, via PET, the proportion of the radio copper complex that is able to migrate to and remain within the brain. Using what has been discussed above the hypothesis, aim and objectives for this thesis are set out as:

### **1.7.1. Hypothesis**

The use of radio labelled dissymmetric copper bis(thiosemicarbazone) complexes offers the opportunity to achieve superior imaging capabilities in diagnostic imaging of hypoxia by positron emission tomography, than currently used symmetric copper bis(thiosemicarbazone) complexes.

### **1.7.2. Aims**

The aims derived from the hypothesis of this thesis are:

1. Synthesise a range of dissymmetric bis(thiosemicarbazone) ligands.
2. Create a library of symmetric bis(thiosemicarbazone) ligands related to the planned dissymmetric ligands.
3. Explore the coordination of copper (II) ions with the library of bis(thiosemicarbazone) ligands.
4. Collect characterisation data on all ligands, complexes and intermediates that were created.
5. Evaluate the copper complexes pharmacokinetics in order to establish candidates for biological screening.

### **1.7.3. Objectives**

From the aims the following objectives have been set out:

1. Compare the acetal protection method and the exploitation of carbonyl reactivity method for synthesis of dissymmetric bis(thiosemicarbazone) ligands with a target purity of  $\geq 95\%$ .
2. Produce a library of symmetric ligands using previously reported methods.
3. Where possible, optimise the synthetic methods for both the synthesis of dissymmetric and symmetric ligands.
4. Improve the synthesis of copper complexes so that it is suitable for the entire library of bis(thiosemicarbazone) ligands.
5. Synthesise a range of zinc (II) bis(thiosemicarbazone) complexes for the evaluation of an alternative copper complex synthetic approach via transmetalation.
6. Characterise all ligands, intermediates and complexes by NMR (except copper complexes), IR and Raman spectroscopy. Obtain CHN analysis on all ligands and complexes which are believed to be novel. Utilise mass spectrometry for the analysis of novel zinc and copper complexes.
7. Collaborate with the Division of Imaging Sciences and Biomedical Engineering at King's College London to obtain lipophilicity and redox potentials for the library of copper complexes produced.
8. Based on lipophilicity and redox data send King's College candidates for biological screening using the isolated heart model<sup>164-166</sup> in order to determine hypoxia selectivity.
9. Based on lipophilicity and redox data send King's College candidates for the evaluation of brain up take and retention.

## **2. Synthesis of symmetric and dissymmetric bis(thiosemicarbazone) ligands.**

### **2.1. Introduction**

This chapter reports the synthesis and characterisation of a range of symmetric and dissymmetric bis(thiosemicarbazones). The primary consideration was to synthesise the ligands with a high level of purity irrespective of yield in order for the ligands to be of use in a radio-pharmaceutical application. The ligands are split in to four broad groups depending what substituents are present at the Q<sub>1</sub> and Q<sub>2</sub> positions of the backbone precursor. 30 ligands have been synthesised with 13 being symmetric and 17 being dissymmetric ligands. Out of the 17 dissymmetric ligands 2 are singly dissymmetric and 15 are doubly dissymmetric. Alongside these a new cyclic by product was observed and is reported in this chapter.

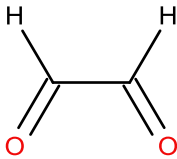
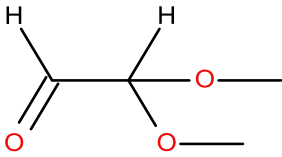
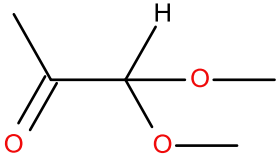
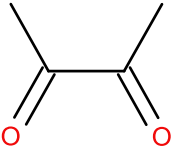
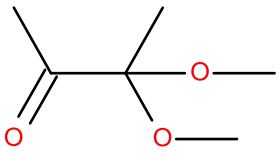
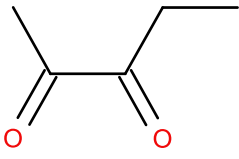
#### **2.1.1. Abbreviations used to describe the bis(thiosemicarbazone) ligands**

A new abbreviation system has been devised in order to clearly show the subtle variation between the ligands.

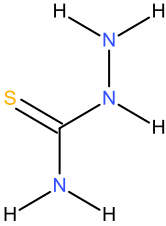
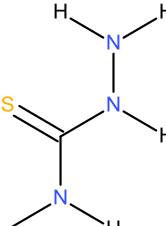
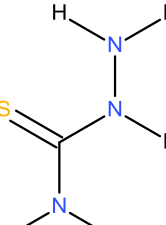
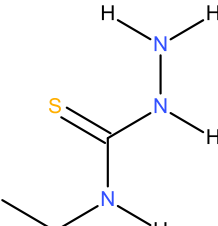
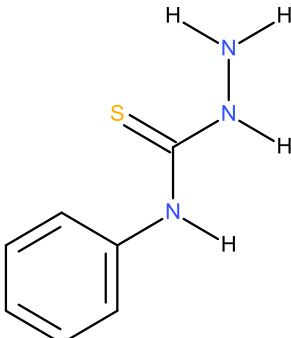
The abbreviation contains three components in a specific order all with a hyphen between them:

1. An abbreviation to represent the backbone used to form the imine substituents (Q<sub>1</sub>-Q<sub>2</sub>).
2. Substituents on the terminal amine of the 4-substituted-3-thiosemicarbazide that was reacted with the carbonyl group on the methyl ketone.
3. Substituents on the terminal amine of the 4-substituted-3-thiosemicarbazide that was reacted with the remaining ketone/ aldehyde.

The abbreviations used to represent the backbones are:

Abbreviation	Chemical Name	Chemical Structure
GLY	Glyoxal	
DMA	2,2-dimethoxyacetaldehyde	
PADA	Methylglyoxal-1,1-dimethyl acetal Or pyruvic aldehyde dimethyl acetal	
BDO	2,3-butanedione	
DMB	3,3-dimethoxy-2-butanone	
PDO	2,3-pentandione	

The abbreviations used to describe substituents on the terminal nitrogen of the 4-substituted-3-thiosemicarbazide are:

Abbreviation	Chemical Name	Chemical Structure
NH <sub>2</sub>	Thiosemicarbazide	
Me	4-methyl-3-thiosemicarbazide	
(Me) <sub>2</sub>	4,4-dimethyl-3-thiosemicarbazide	
Et	4-ethyl-3-thiosemicarbazide	
Ph	4-phenyl-3-thiosemicarbazide	

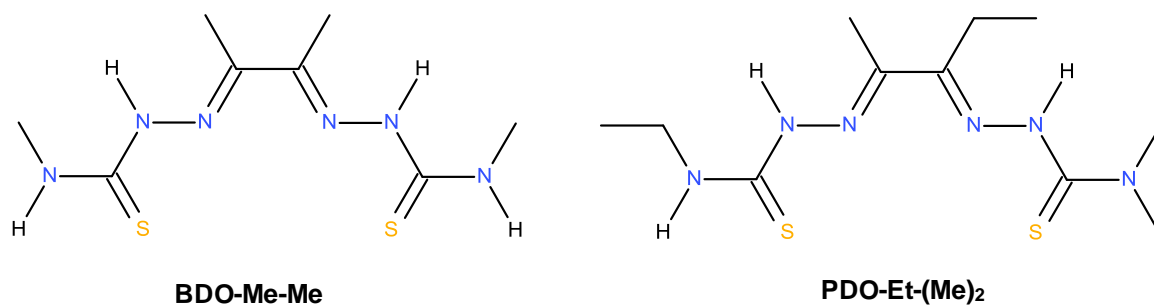


**Figure 2.1.1.1.** Examples of the abbreviations used for the bis(thiosemicarbazone) ligands.

### **2.1.2 Abbreviations for the intermediates**

In the case of the synthesis of the dissymmetric bis(thiosemicarbazone) ligands an intermediate mono-substituted thiosemicarbazone was prepared first. An abbreviation is constructed by using:

1. The abbreviation to represent the backbone used to form the imine substituents
2. Substituents on the terminal nitrogen of the 4-substituted-3-thiosemicarbazide that was reacted with the carbonyl group on the methyl ketone.
3. The symbol '=O' is attached to show the presence of an unreacted ketone/ aldehyde.

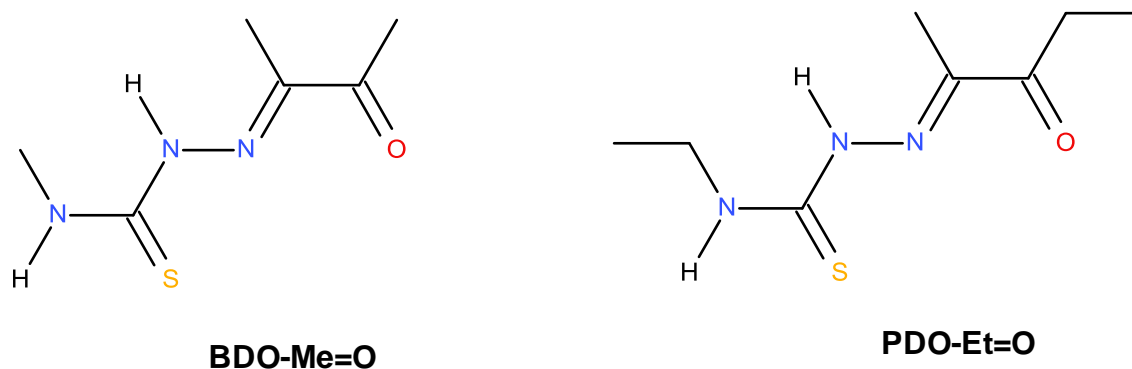
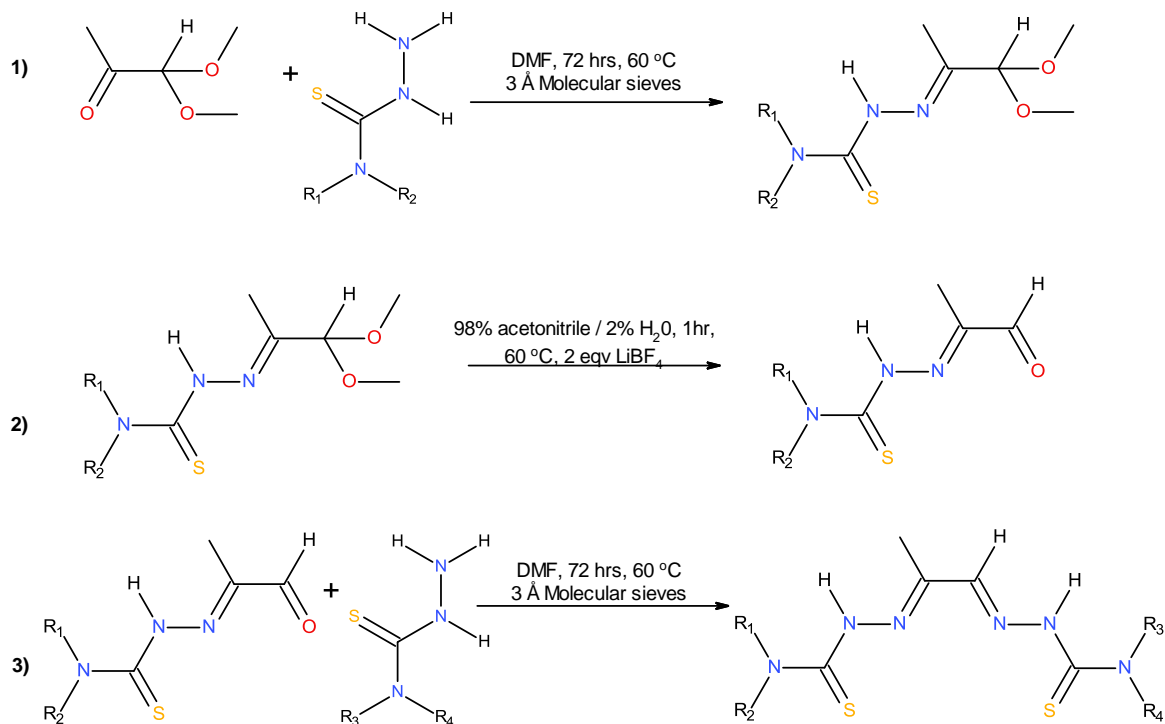


**Figure 2.1.2.1.** Examples of the abbreviations used for the of mono-substituted thiosemicarbazone intermediates.

## **2.2. Synthesis of dissymmetric bis(thiosemicarbazone) ligands by the protecting approach.**

The synthesis of some dissymmetric ligands with Me/H on the backbone was initially attempted by using the acetal protecting approach as described in the literature.<sup>66, 79-81, 195</sup> The approach first attempted is summarised in the figure 2.2.0.1.



	R <sub>1</sub>	R <sub>2</sub>	R <sub>3</sub>	R <sub>4</sub>
PADA-Me-NH <sub>2</sub>	CH <sub>3</sub>	H	H	H
PADA-NH <sub>2</sub> -Me	H	H	CH <sub>3</sub>	H

**Figure 2.2.0.1.** The reaction conditions first used in the acetal protection approach.

For the purposes of this section the resulting product, when a 4-substituted-3-thiosemicarbazide is reacted with PADA shall be given the abbreviation PADA-R<sub>1,2</sub>-(OMe)<sub>2</sub> in order to distinguish between when the acetal protecting groups are present and when they are absent (PADA-R<sub>1,2</sub>=O). This is illustrated below (Figure 2.1.0.2.).

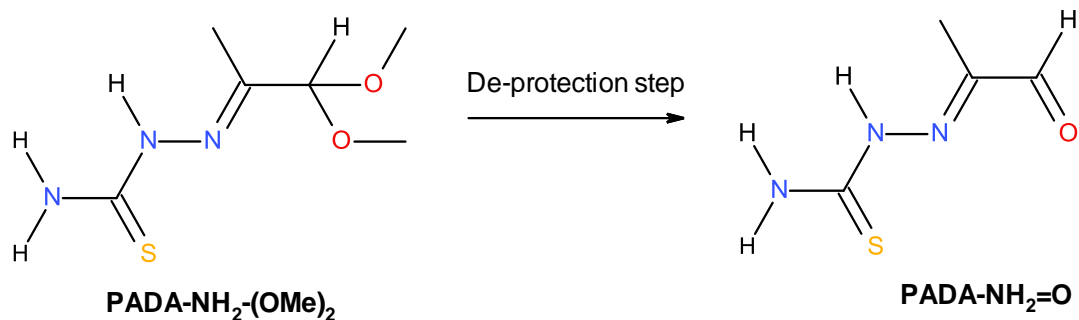


**Figure 2.1.0.2.** Example of the abbreviations used for the mono-substituted thiosemicarbazone intermediates with Me/H on the backbone.

All protected intermediates derived from DMB shall also be giving abbreviation DMB- $R_{1,2}$ -(OMe)<sub>2</sub> but once the protected intermediate undergoes a de-protecting step the abbreviation shall revert back to BDO-  $R_{1,2}$ =O, to keep in line with abbreviations that are used throughout.

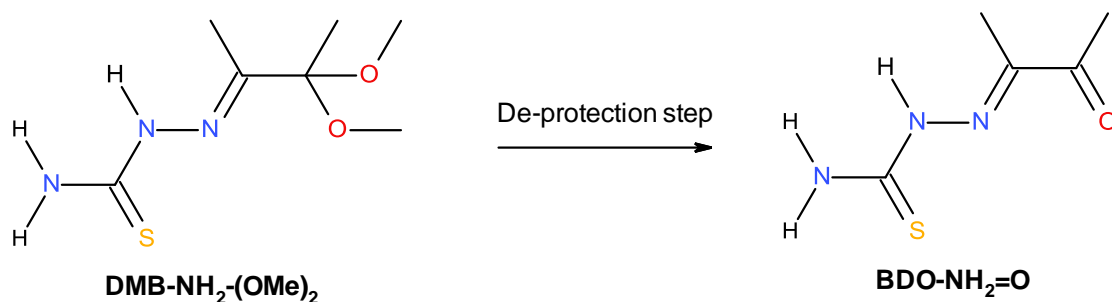


**Figure 2.1.0.3.** Example of the abbreviations used for the mono-substituted thiosemicarbazone intermediates with Me/Me on the backbone.

## **2.2.1. Method of synthesis**

### **Synthesis of PADA-Me-NH<sub>2</sub>:**

#### **PADA-Me-(OMe)<sub>2</sub>:**

4-methyl-3-thiosemicarbazide (1.315 g, 0.013 mol) was dissolved in DMF (40 mL), followed by the addition of methylglyoxal-1,1-dimethylacetal (1.5 mL, 0.012 mol, 1.5 g). The resulting solution was left to stir (3 days). The volume of DMF was reduced under vacuum until a viscous solution was formed. A small amount of diethyl ether was added to the solution and then cooled on ice overnight. The precipitate was isolated, washed with diethyl ether (4 x 1 mL) and dried. A clear crystalline solid (0.585 g) was recovered (24% yield).

#### **PADA-Me=O:**

PADA-Me-(OMe)<sub>2</sub> (0.146 g, 0.0007 mol) was dissolved in an acetonitrile solution (15 mL, 98% acetonitrile, 2% de-ionised water). LiBF<sub>4</sub> (0.139 g, 0.0015 mol) was added and the resulting solution was left to stir (60 °C, 1 hour). To the solution a saturated solution of Na<sub>2</sub>CO<sub>3</sub> (30 mL) was



added rapidly resulting in the formation of a bright yellow solution. The product was extracted with diethyl ether (3 x 50 mL) and the organic solution was dried over magnesium sulfate. The magnesium sulfate was filtered off and the solvent was removed. A brown solid (0.084 g) was recovered (75% yield).

#### **PADA-Me-NH<sub>2</sub>:**

Freshly activated molecular sieves (3 Å, 0.051 g) was added to DMF (10 mL, 60 °C), followed by the addition of PADA-Me=O (0.083 g, 0.0005 mol) and thiosemicarbazide (0.049 g, 0.0005 mol). The solution was left to stir (60 °C, 6 hours) then allowed to continue stirring overnight (room temperature). Removed the DMF under vacuum and the crude product was washed with ethyl acetate (1 x 14 mL, 1 x 7 mL, 1 x 3.5 mL) and a little acetone. The solid was then dried. A white solid (0.042 g) was recovered (36 % yield).

#### **Synthesis of PADA-NH<sub>2</sub>-Me**

##### **PADA-NH<sub>2</sub>-(OMe)<sub>2</sub>:**

Freshly activated molecular sieves (3 Å, 0.801 g) was added to DMF (15 mL, 60 °C), followed by the addition of thiosemicarbazide (0.770 g, 0.0084 mol). This was followed by the addition of methylglyoxal-1,1-dimethylacetal (1 mL, 0.0083 mol, 1 g). The resulting solution was left to stir (room temperature, 3 days). The molecular sieves were filtered off and the DMF was removed under vacuum. The crude product was washed with a little diethyl ether and dried. An off white solid (0.769 g) was recovered (48% yield).

##### **PADA-NH<sub>2</sub>=O:**

PADA-NH<sub>2</sub>-(OMe)<sub>2</sub> (0.754 g, 0.004 mol) was dissolved in an acetonitrile solution (15 mL, 98% acetonitrile, 2% de-ionised water, 60 °C). LiBF<sub>4</sub> (0.720 g, 0.008 mol) was added and the resulting solution was left to stir (60 °C, 1 hour). A saturated solution of Na<sub>2</sub>CO<sub>3</sub> (30 mL) was added rapidly resulting in the formation of a brown/orange solution. The product was extracted with diethyl ether (1 x 50 mL, 2 x 25 mL) and the organic solution was dried over magnesium sulfate. The magnesium sulfate was filtered off and the solvent was removed. A brown solid (0.137 g) was recovered (24% yield).

##### **PADA-NH<sub>2</sub>-Me:**

Freshly activated molecular sieves (3 Å, 0.075 g) was added to DMF (17 mL, 60 °C), followed by the addition of PADA-NH<sub>2</sub>=O (0.131 g, 0.0009 mol) and 4-methyl-3-thiosemicarbazide (0.101 g, 0.0010 mol). The heat was turned off and the solution was left to stir (3 days, cooling down to room temperature). The molecular sieves were filtered off and the DMF was removed under

vacuum. The crude product was washed with a little ethyl acetate and diethyl ether (1 x 25 mL) and dried. A sawdust coloured solid (0.130 g) was recovered (62% yield).

### **2.2.2. Characterisation data for ligands synthesised by the protection method**

As this method of synthesis was superseded by a different method most the characterisation data collected was just enough to ascertain the likely structure of the product.

#### **PADA-Me-(OMe)<sub>2</sub>:**

**<sup>1</sup>H NMR** (DMSO-*d*<sub>6</sub>, 400 MHz): δ= 10.19 (s, 1 H, N-NH), 8.94 (q, 1 H, H<sub>3</sub>C-NH, J= 4.4 Hz), 4.49 (s, 1 H, O-CH), 3.25 (s, 6 H, O-CH<sub>3</sub>), 2.93 (d, 3 H, HN-CH<sub>3</sub>, J= 4.4 Hz), 1.78 (s, 3 H, N=C-CH<sub>3</sub>). **<sup>13</sup>C {<sup>1</sup>H} NMR** (DMSO-*d*<sub>6</sub>, 100 MHz): δ= 179.57 (C=S), 148.60 (C=N), 106.87 (HC-O), 55.16 (O-CH<sub>3</sub>), 31.39 (HN-CH<sub>3</sub>), 11.17 (N=C-CH<sub>3</sub>). **IR (neat):** cm<sup>-1</sup>= 3279 (m), 3227 (w), 2936 (w), 1537 (m), 1504 (m), 1435 (m), 1410 (m), 1366 (m), 1325 (m), 1271 (m), 1213 (m), 1192 (m), 1115 (m), 1072 (s), 1057 (s), 986 (s), 949 (s), 860 (m), 660 (m), 559 (s), 494 (m). **Raman (neat), laser = 784.15 nm:** cm<sup>-1</sup>= 1642 (s), 1539 (w), 1499 (w), 1450 (w), 1437 (w), 1324 (w), 1277 (w), 1224 (w), 1156 (w), 1062 (w), 1044 (w), 1022 (w), 985 (m), 963 (w), 860 (s), 799 (s), 660 (w), 632 (w), 582 (m), 573 (s), 495 (w), 435 (w), 354 (w), 308 (m), 272 (m). **Melting point:** >84-88 °C.

#### **PADA-Me=O:**

**<sup>1</sup>H NMR** (DMSO-*d*<sub>6</sub>, 400 MHz): δ= 11.18 (s, 1 H, N-NH), 9.32 (s, 1 H, O=CH), 9.01 (m, 1 H, H<sub>3</sub>C-NH), 2.99 (d, 3 H, HN-CH<sub>3</sub>, J= 4.8 Hz), 1.90 (s, 3 H, N=C-CH<sub>3</sub>). **<sup>13</sup>C {<sup>1</sup>H} NMR** (DMSO-*d*<sub>6</sub>, 100 MHz): δ= 192.16 (C=O), 179.46 (C=S), 145.93 (C=N), 31.69 (HN-CH<sub>3</sub>), 9.68 (N=C-CH<sub>3</sub>). **IR (neat):** cm<sup>-1</sup>= 3352 (w), 3173 (m), 2963 (w), 2843 (w), 1694 (m), 1593 (m), 1537 (m), 1504 (m), 1410 (m), 1369 (m), 1200 (s), 1146 (m), 1111 (m), 1047 (s), 1001 (s), 856 (m), 789 (m), 665 (s), 594 (s), 569 (s), 534 (s), 503 (m).

#### **PADA-Me-NH<sub>2</sub>:**

**<sup>1</sup>H NMR** (DMSO-*d*<sub>6</sub>, 400 MHz): δ= 11.67 (s, 1 H, N-NH), 10.36 (s, 1 H, N-NH), 8.50 (q, 1 H, H<sub>3</sub>C-NH, J= 4.4 Hz), 8.29 (s, 1 H C-NH), 7.88 (s, 1 H C-NH), 7.62 (s, 1 H, N=CH), 2.95 (d, 3 H, HN-CH<sub>3</sub>, J= 4.4 Hz), 2.10 (s, 3 H, N=C-CH<sub>3</sub>). **<sup>13</sup>C {<sup>1</sup>H} NMR** (DMSO-*d*<sub>6</sub>, 100 MHz): δ= 178.79 (C=S), 178.63 (C=S), 147.54 (C=N), 142.97 (C=N), 31.58 (HN-CH<sub>3</sub>), 11.52 (N=C-CH<sub>3</sub>). **IR (neat):** cm<sup>-1</sup>= 3414 (w), 3138 (w), 2984 (w), 1605 (w), 1533 (m), 1501 (m), 1464 (w), 1337 (w), 1267 (w), 1213 (m), 1069 (s), 924 (m), 833 (m), 799 (m), 658 (w), 623 (m), 565 (m).

### **PADA-NH<sub>2</sub>-(OMe)<sub>2</sub>:**

<sup>1</sup>H NMR (DMSO-*d*<sub>6</sub>, 400 MHz): δ= 10.21 (s, 1 H, N-NH), 8.23 (s, 1 H, C-NH), 7.72 (s, 1 H, C-NH), 4.48 (s, 1 H, O-CH), 3.24 (s, 6 H, O-CH<sub>3</sub>), 1.78 (s, 3 H, N=C-CH<sub>3</sub>). <sup>13</sup>C {<sup>1</sup>H} NMR (DMSO-*d*<sub>6</sub>, 100 MHz): δ= 179.90 (C=S), 149.02 (C=N), 106.78 (HC-O), 55.16 (O-CH<sub>3</sub>), 11.21 (N=C-CH<sub>3</sub>).

### **PADA-NH<sub>2</sub>=O:**

<sup>1</sup>H NMR (DMSO-*d*<sub>6</sub>, 400 MHz): δ= 11.12 (s, 1 H, N-NH), 9.31 (s, 1 H, O=CH), 8.78 (s, 1 H, C-NH), 8.38 (s, 1 H, C-NH), 1.90 (s, 3 H, N=C-CH<sub>3</sub>). <sup>13</sup>C {<sup>1</sup>H} NMR (d<sub>6</sub>-DMSO, 100 MHz): δ= 192.46 (C=O), 180.52 (C=S), 146.30 (C=N), 9.70 (N=C-CH<sub>3</sub>).

### **PADA-NH<sub>2</sub>-Me:**

<sup>1</sup>H NMR (DMSO-*d*<sub>6</sub>, 400 MHz): δ= 11.69 (s, 1 H, N-NH), 10.33 (s, 1 H, N-NH), 8.38 (quartet overlapping a singlet, 1 H, H<sub>3</sub>C-NH, J= 4.4 Hz), 8.35 (singlet overlapping a quartet, 1 H C-NH), 7.60 (s, 1 H C-NH), 7.61 (s, 1 H, N=CH), 2.95 (d, 3 H, HN-CH<sub>3</sub>, J= 4.4 Hz), 2.04 (s, 3 H, N=C-CH<sub>3</sub>). <sup>13</sup>C {<sup>1</sup>H} NMR (DMSO-*d*<sub>6</sub>, 100 MHz): δ= 179.27 (C=S), 178.24 (C=S), 148.02 (C=N), 142.55 (C=N), 31.47 (HN-CH<sub>3</sub>), 11.62 (N=C-CH<sub>3</sub>).

### **2.2.3. Monitoring the de-protection of PADA via spectral methods**

Figure 2.2.3.1. shows a <sup>1</sup>H spectrum of PADA-Me-(OMe)<sub>2</sub> shows the presence of the protecting acetal groups, as seen by the singlet at 3.25 ppm with an integral of six protons corresponding to the six hydrogen atoms on both the acetal groups. An indirect indicator of the presence of the protecting groups is the singlet at 4.49 ppm which is due to the hydrogen labelled 'E', if the product was PADA-Me=O or PADA-Me with a second 4-substituted-3-thiosemicarbazide bound, 'E' would be expected to shift to roughly 9.3 ppm or 7.6 ppm respectively.

**Figure 2.2.3.1.** A  $^1\text{H}$  spectrum of  $\text{PADA-Me-(OMe)}_2$ , with assigned peaks.  $\text{PADA-Me-(OMe)}_2$  was obtained by the reacting methylglyoxal-1,1-dimethyl acetal with 4-methyl-3-thiosemicarbazide.

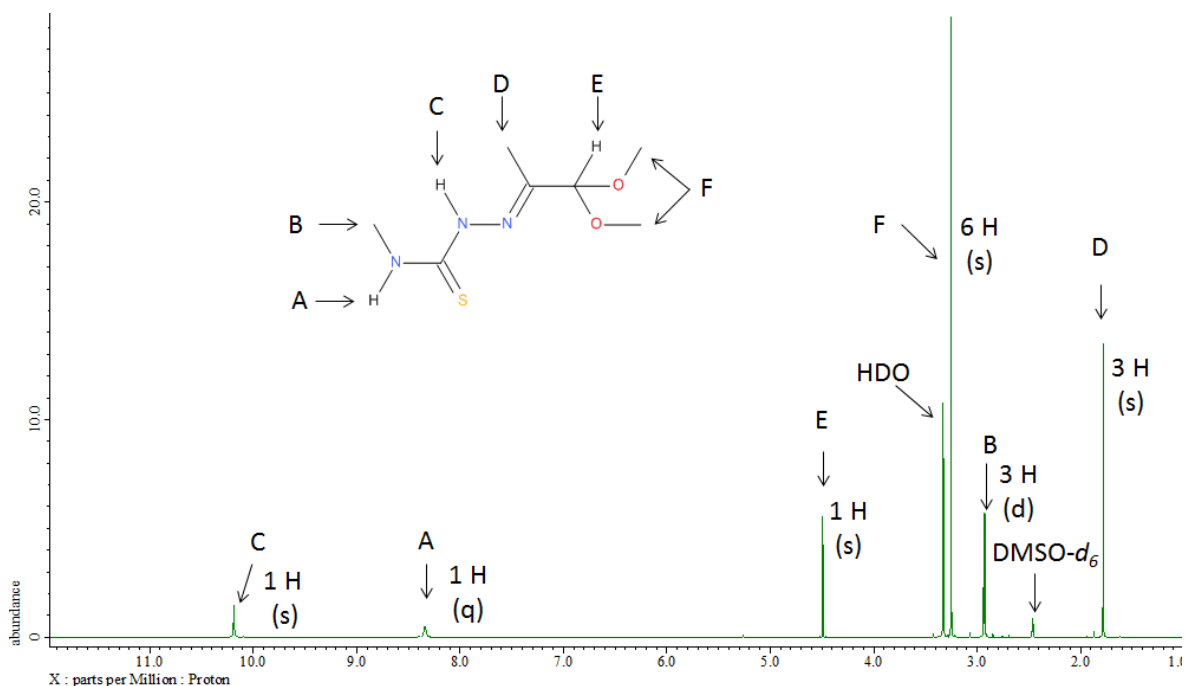
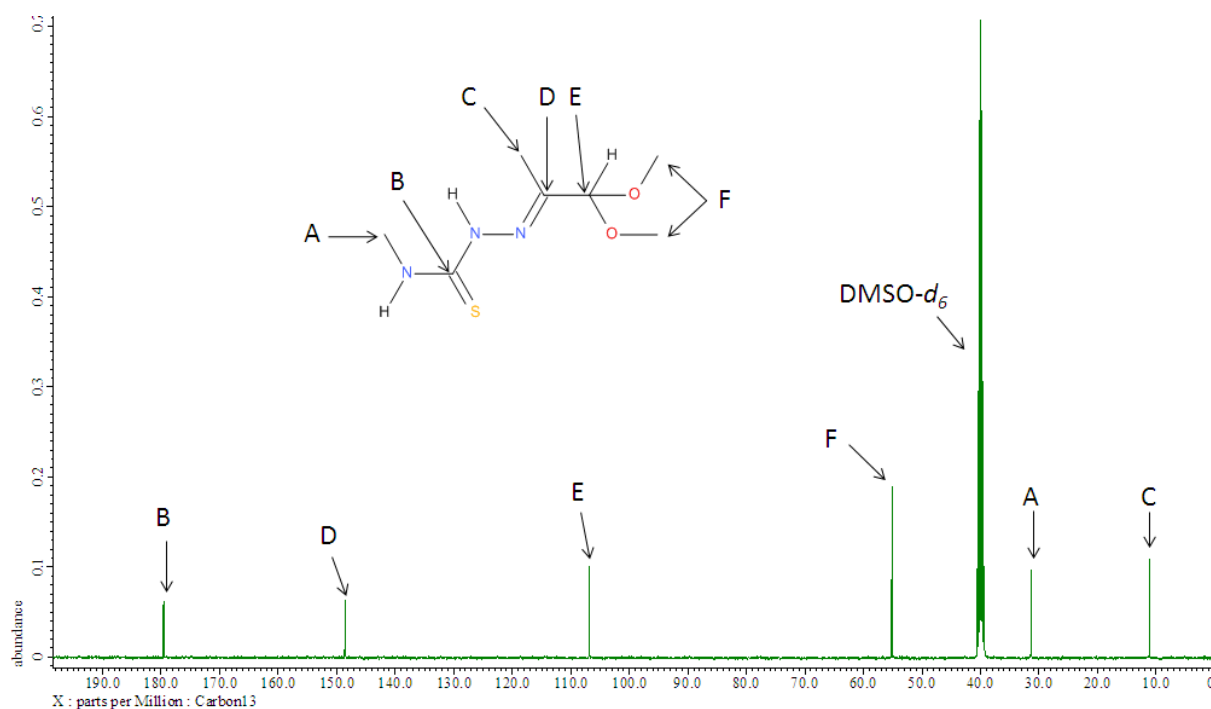


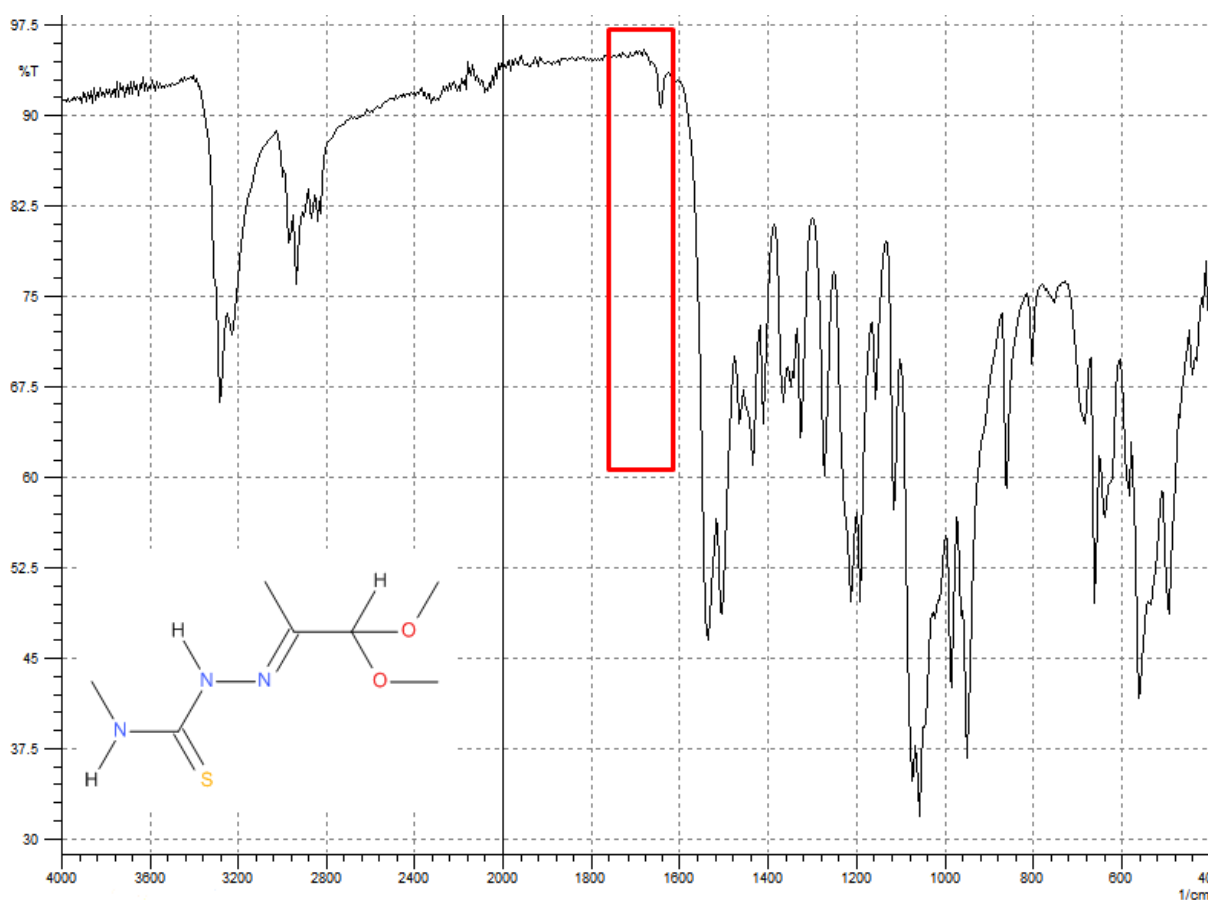
Figure 2.2.3.2. is a  $^{13}\text{C}$  spectrum of  $\text{PADA-Me-(OMe)}_2$  which further supports the presence of the acetal protecting groups. The main peak of interest is the peak at 55.16 ppm which is due to the carbons in position 'F'. Similar to what was seen in the  $^1\text{H}$  spectrum above, if the product was  $\text{PADA-Me=O}$  or  $\text{PADA-Me}$  with a second 4-substituted-3-thiosemicarbazide attached environment 'E' would shift to circa 192 ppm or 142-148 ppm respectively.

**Figure 2.2.3.2.** A  $^{13}\text{C}$  spectrum of  $\text{PADA-Me-(OMe)}_2$ , with assigned peaks.



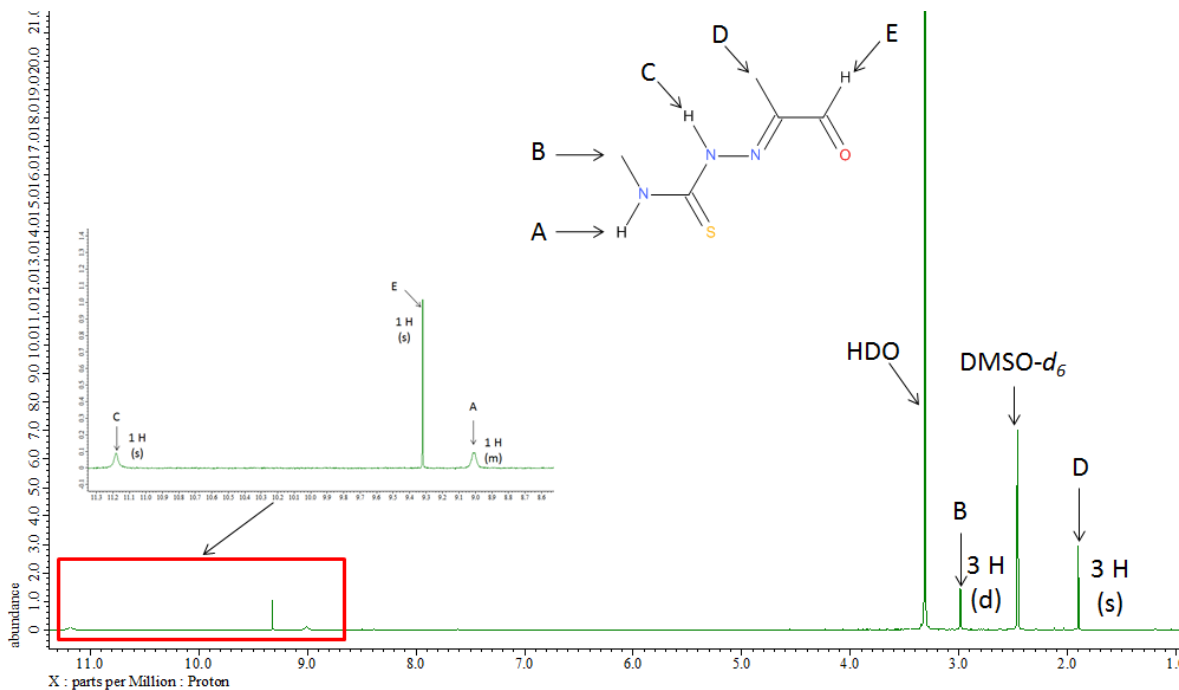
IR spectroscopy (Figure 2.2.3.3.) was used to further corroborate the presence of PADA-Me-(OMe)<sub>2</sub>, but due to the limitation of the technique the only thing that can be ascertained with any level of confidence is that there is no strong absorption between 1800-1600 cm<sup>-1</sup>, which would be the expected position of a peak due to the C=O bond of the aldehyde group of PADA-Me=O (indicated by the red box). Unlike the NMR spectra above FTIR cannot easily be used to confirm the presence of PADA-Me-(OMe)<sub>2</sub> nor the absence of a symmetric or dissymmetric complete ligand, but it can be used relatively easily to show the presence of the carbonyl group as a result of a successful de-protection step.

**Figure 2.2.3.3.** A FTIR spectrum of PADA-Me-(OMe)<sub>2</sub>. The red box highlights the absence of a C=O bond indicating that the two acetal functionalities are present.



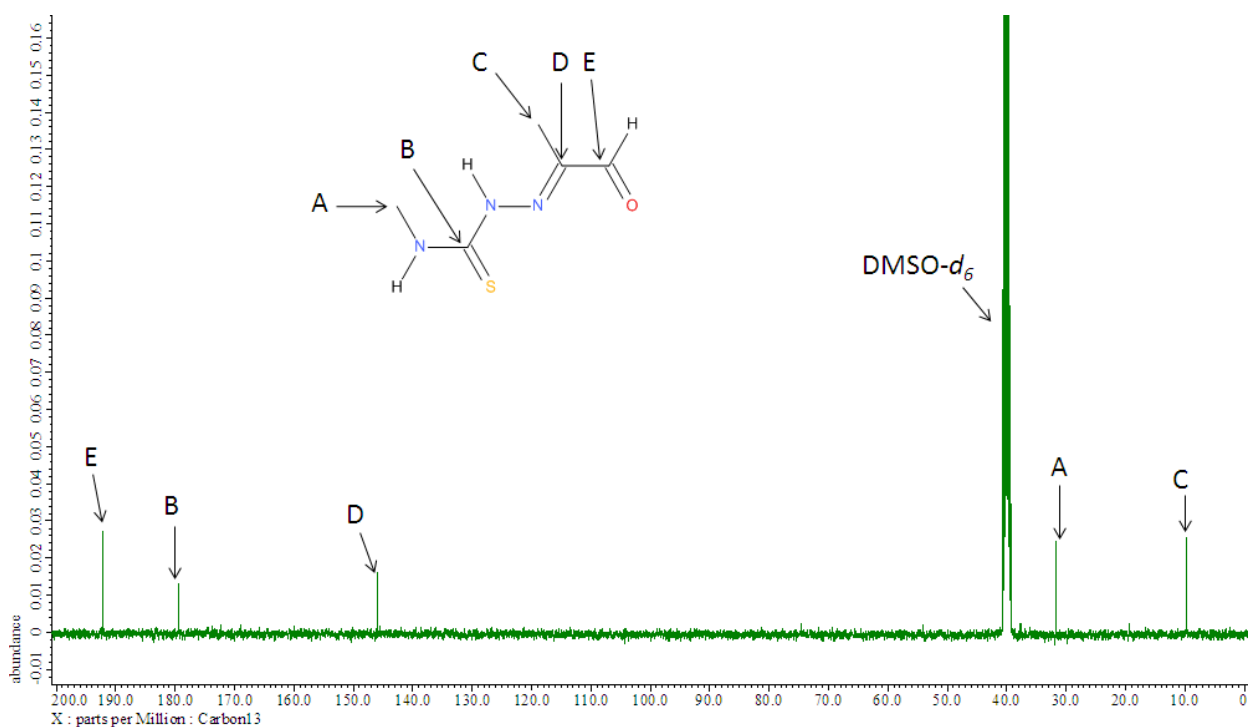
The <sup>1</sup>H spectrum of PADA-Me=O (figure 2.2.3.4.) clearly shows the complete absence of the acetal hydrogen environment previously seen at 3.25 ppm, as well as the singlet labelled 'E' which was situated at 4.49 ppm and has now shifted downfield to 9.32 ppm. All these changes in the spectra are expected and are consistent for PADA-Me=O<sup>79</sup>.

**Figure 2.2.3.4.** A  $^1\text{H}$  spectrum of PADA-Me=O, with assigned peaks. PADA-Me=O was obtained by using  $\text{LiBF}_4$  to cleave the acetal functionalities of PADA-Me-(OMe) $_2$ .



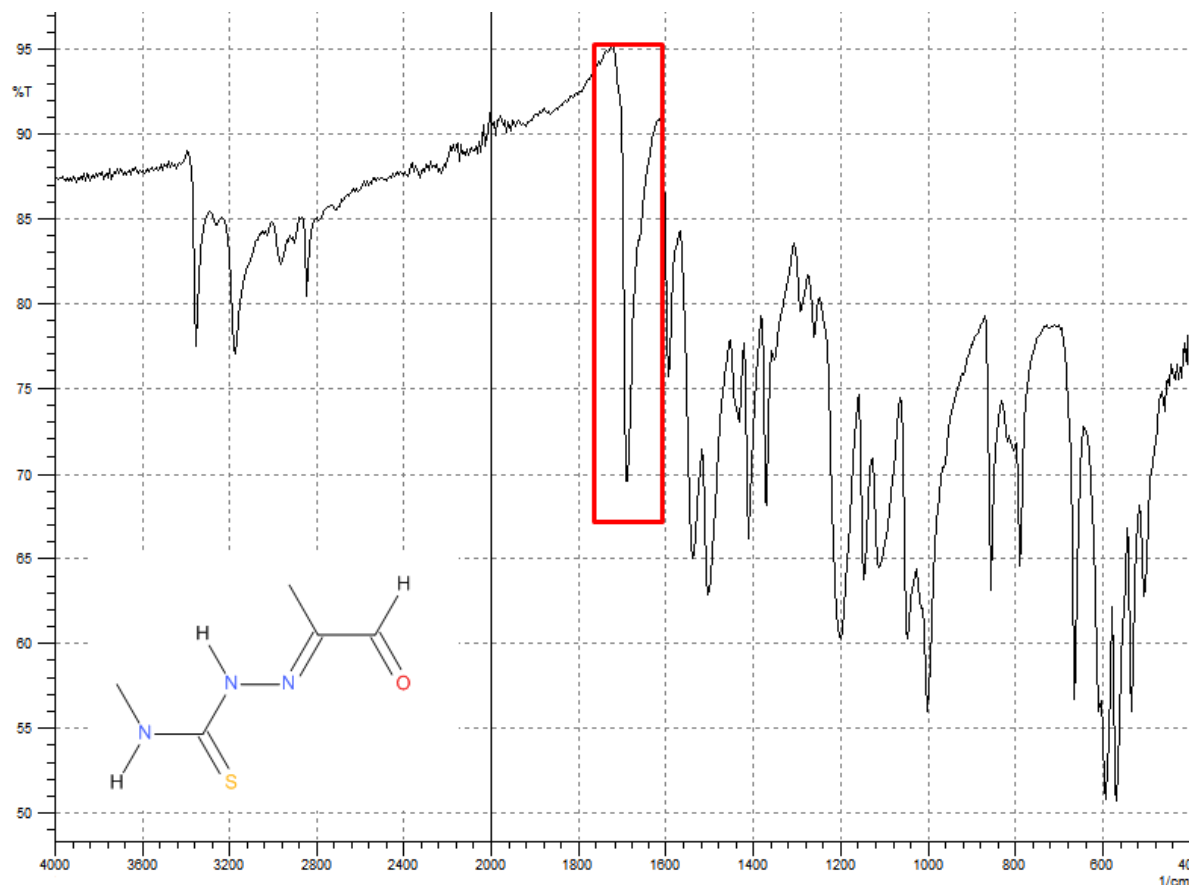
The  $^{13}\text{C}$  spectrum of PADA-Me=O (figure 2.2.3.5.) shows the peak locations related to PADA-Me=O. Firstly the carbon peak for the acetal carbons at 55.16 ppm has vanished, also environment 'E' has shifted downfield to 192.16 ppm indicating the presence of a C=O group.

**Figure 2.2.3.5.** A  $^{13}\text{C}$  spectrum of PADA-Me=O, with assigned peaks. Carbon environment E illustrates that the acetal protecting groups have been successfully removed.



Finally the FTIR spectrum of PADA-Me=O (Figure 2.2.3.6.) clearly shows the presence of a strong absorption at  $1694\text{ cm}^{-1}$  (indicated by the red box), this further indicates the presence of the C=O bond of the carbonyl group on the aldehyde.

**Figure 2.2.3.6.** A FTIR spectrum of PADA-Me=O. The red box highlights the presence of a C=O bond indicating that the two acetal functionalities have been successfully removed.

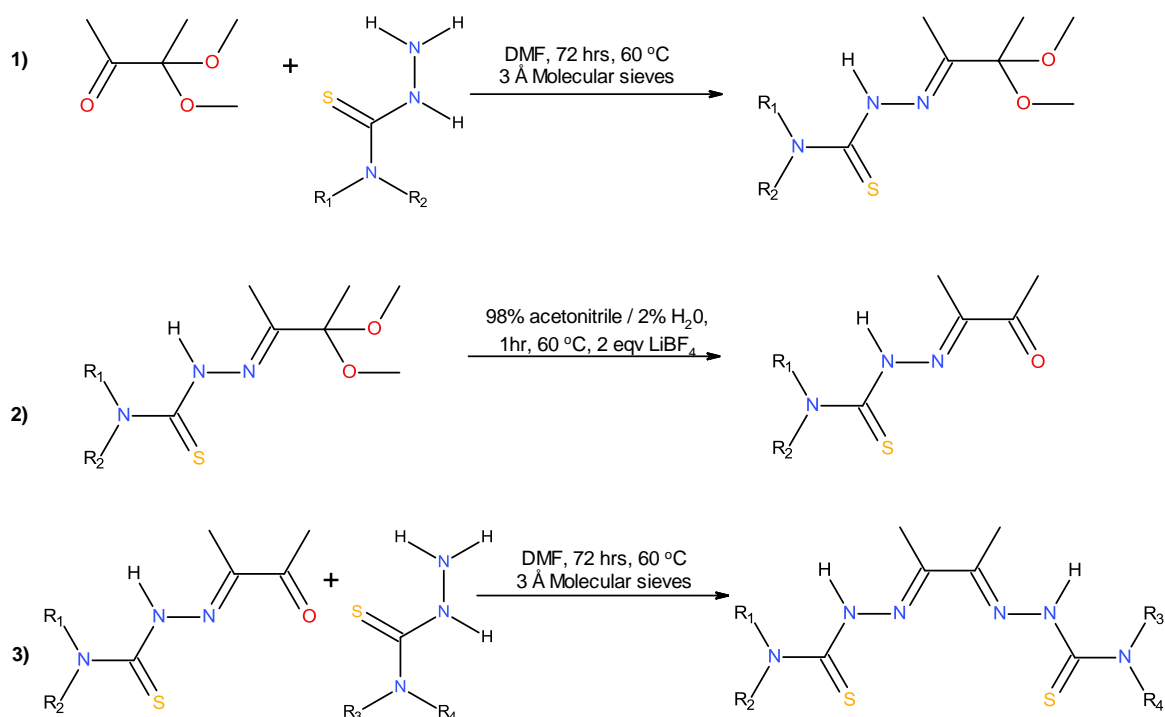


Proton NMR data has been reported for compounds PADA-Me-(OMe)<sub>2</sub>, PADA-Me=O, PADA-Me-NH<sub>2</sub>, PADA-NH<sub>2</sub>-(OMe)<sub>2</sub>, PADA-NH<sub>2</sub>=O, PADA-NH<sub>2</sub>-Me by J. Lim *et al.*,<sup>79</sup> of which the data collected show strong agreement to the figures published. The literature value for the melting point for PADA-Me-(OMe)<sub>2</sub> is reported as  $87\text{--}88^\circ\text{C}$ <sup>79</sup> which is in accord with the value of  $84\text{--}88^\circ\text{C}$  observed. This corroboration by the literature increases confidence in that the molecules are correctly identified and that the synthesis of dissymmetric bis(thiosemicarbazone) ligands via the deprotection approach is achievable.

#### **2.2.4. Attempts to synthesise dissymmetric ligands from DMB**

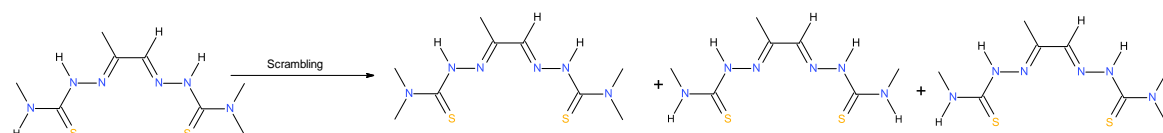
Using the same protecting method that was used to synthesise dissymmetric ligands from PADA, attempts were undertaken to synthesis dissymmetric ligands from DMB in order to obtain ligands with two methyl groups on the backbone.

Figure 2.2.4.1. Illustrates the planned synthetic route first attempted for the synthesis of dissymmetric ligands from DMB.



**Figure 2.2.4.1.** Summary of the reaction conditions first used.

The first intermediate that was attempted was BDO-NH<sub>2</sub>-(OMe)<sub>2</sub>. The reaction conditions in figure 2.2.4.1. was used, but the product turned out not to be the one that was expected. The identity of this unknown product was not able to be solved. Subsequent reactions were run with similar reaction conditions as figure 2.2.4.1. but with different temperature and stir time parameters. Throughout the method development process, heating above 60 °C was avoided and where possible, this exposure was limited to the shortest length of time. The reason for this was that the literature<sup>57, 66, 79, 81</sup> reported that dissymmetric bis(thiosemicarbazone) ligands under certain conditions were prone to scrambling resulting in a product that contained a mixture of the target dissymmetric bis(thiosemicarbazone) and related symmetric bis(thiosemicarbazones). This idea is illustrated in figure 2.2.4.2.



**Figure 2.2.4.2.** Illustration of the products of scrambling.

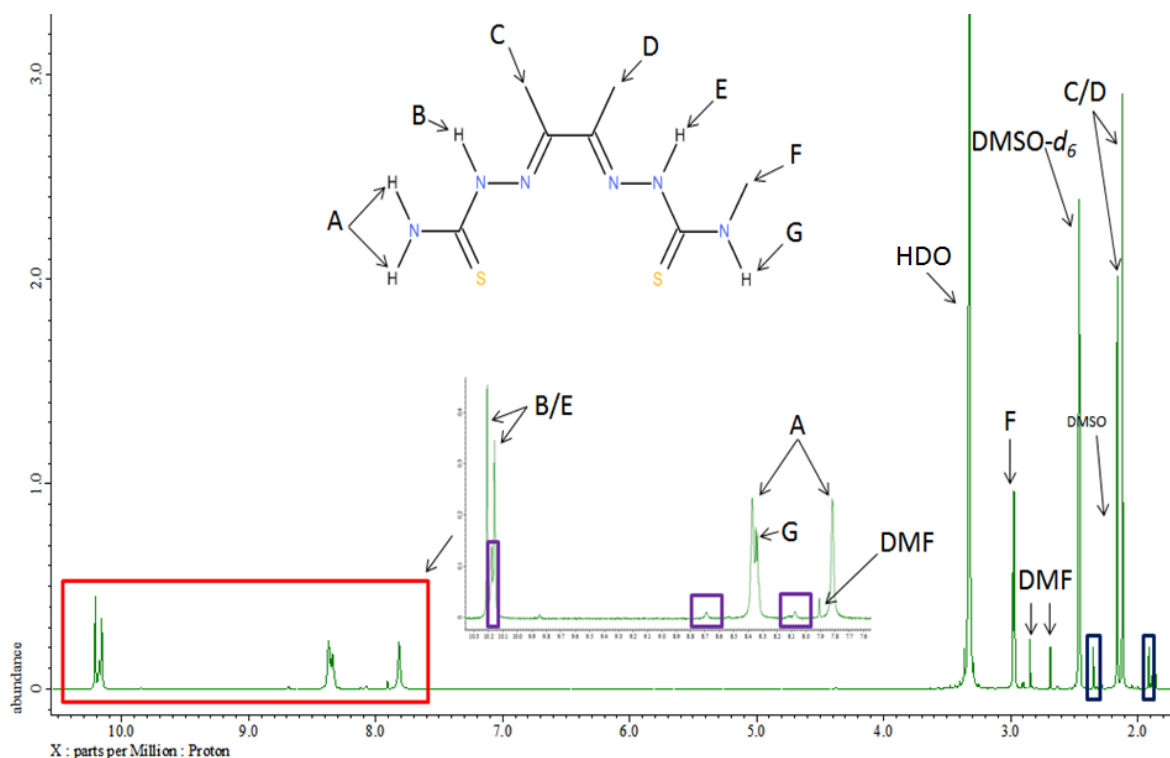
A range of temperature and stir profiles was used. Some conditions that were tried was stirring at room temperature for 72 hours and stirring at 60 °C for 6 hours. All these attempts failed to yield the desired product and only produced either unreacted reagents or a more complex mixture of unreacted reagents with small proportions of what was thought to be BDO-NH<sub>2</sub>=O and BDO-NH<sub>2</sub>-NH<sub>2</sub>. One attempt that was partially successful yielded a product that turned out to be a mixture



of BDO-NH<sub>2</sub>=O and BDO-NH<sub>2</sub>-NH<sub>2</sub> with estimated proportions of 85% and 15% respectively. This partially successful attempt was not run with any significant alteration in conditions except a slightly larger excess of DMB.

The crude BDO-NH<sub>2</sub>=O was then reacted with 4-methyl-3-thiosemicarbazide in a 1:1 stoichiometric ratio (see reaction 3 Figure.2.2.4.1.). The reaction duration was altered from 72 hours to 6 hours as PADA-Me-NH<sub>2</sub> was successfully synthesised when stirred at 60 °C for only 6 hours followed by stirring overnight at room temperature. The resulting product contained predominantly BDO-NH<sub>2</sub>-Me with signs of BDO-NH<sub>2</sub>=O and BDO-NH<sub>2</sub>-NH<sub>2</sub> impurities. The proportions of the impurities were not able to be estimated due the BDO-NH<sub>2</sub>-NH<sub>2</sub> peaks lying beneath the BDO-NH<sub>2</sub>-Me peaks. This is illustrated in the <sup>1</sup>H NMR spectrum below (Figure 2.2.4.3.). The blue boxes show the peaks that are due to the presence of BDO-NH<sub>2</sub>=O and the purple boxes show the peaks that are due to the presence of BDO-NH<sub>2</sub>-NH<sub>2</sub>. The singlet at 2.12 ppm has a larger integral than is expected due to the two methyl groups on the backbone of the BDO-NH<sub>2</sub>-NH<sub>2</sub> impurity, owing to each environment having very similar chemical shifts.

**Figure 2.2.4.3.** An assigned <sup>1</sup>H NMR spectrum of BDO-NH<sub>2</sub>-Me synthesised by the acetal protecting approach. The spectrum suggests the presence of BDO-NH<sub>2</sub>=O (blue boxes) and BDO-NH<sub>2</sub>-NH<sub>2</sub> (purple boxes).



In order to achieve a greater purity of either BDO-NH<sub>2</sub>-(OMe)<sub>2</sub> or BDO-NH<sub>2</sub>=O the reaction solvent was changed to ethanol with the hope that one of the desired intermediates would precipitate out of solution upon its formation resulting in a purer intermediate. Due to the low solubility of

thiosemicarbazide in ethanol, the 4-substituted-thiosemicarbazide was changed to 4-methyl-thiosemicarbazide due to its higher solubility in ethanol (Figure 2.2.4.4.).

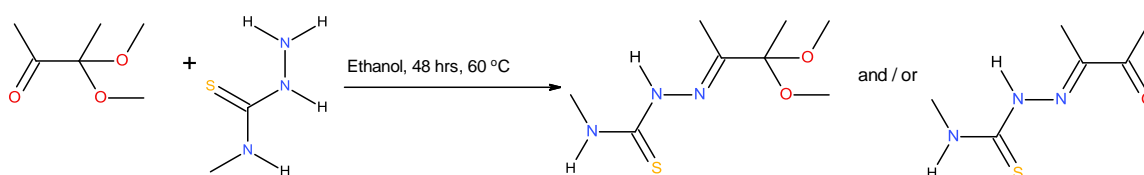


**Figure 2.2.4.4.** Figure showing the changes made to the reaction conditions.

When treating the reaction solution three products were recovered. Each time a precipitate was observed it was filtered off and bottled, the reaction mixture was put back on the heat and stirred. The first precipitate was formed in the reaction mixture while it was at 60 °C, which was identified as the symmetric ligands BDO-Me-Me. After the filtrate was kept in the freezer for 36 hours the second precipitate formed which was unreacted 4-methyl-3-thiosemicarbazide. The solvent in the resulting filtrate was allowed to evaporate to yield the third product, which was a mixture of BDO-Me-(OMe)<sub>2</sub> and unreacted 4-methyl-3-thiosemicarbazide. This third product was then washed with diethyl ether in an attempt to remove the 4-methyl-3-thiosemicarbazide, but when the washed product was analysed again it was found that it was the ratio of BDO-Me-(OMe)<sub>2</sub> that had reduced.

With all the previous observations taken in to account the following reaction methods (Figure 2.2.4.5) were devised for the synthesis of BDO-Me-(OMe)<sub>2</sub> and BDO-Me=O.

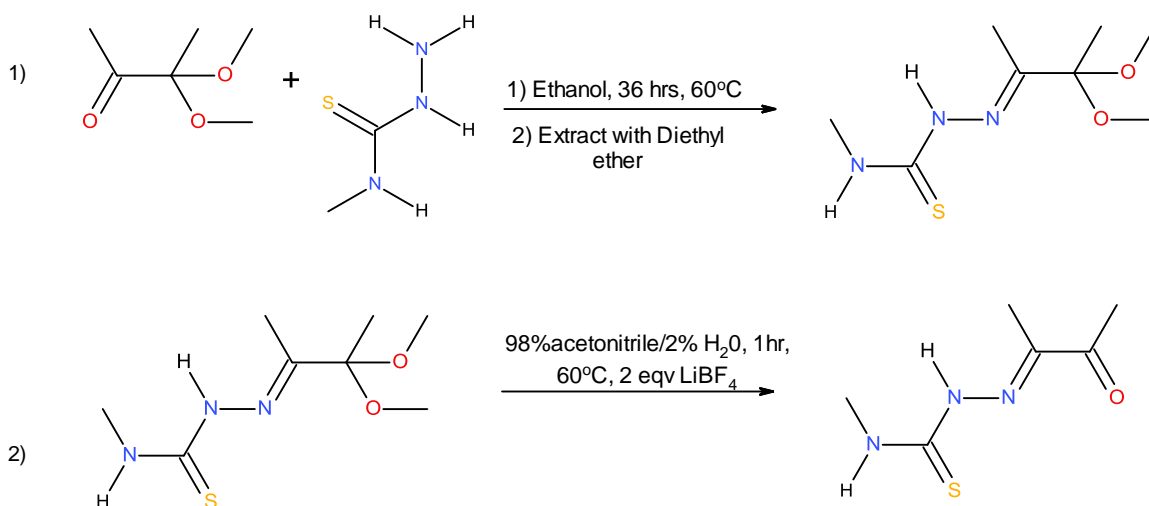


**Figure 2.2.4.5.** The reactions conditions used for the synthesis of BDO-Me-(OMe)<sub>2</sub> (1) and BDO-Me=O (2).

The <sup>1</sup>H spectrum (Figure 2.2.4.6.) of the product from reaction 1 shows the peaks that would be expected given the target molecules structure. From the spectrum it is possible to see that there are a few impurity peaks. The product contains some unreacted 4-methyl-3-thiosemicarbazide

despite using a slight excess of 3,3-dimethoxy-2-butanone, these peaks are highlighted with purple boxes.

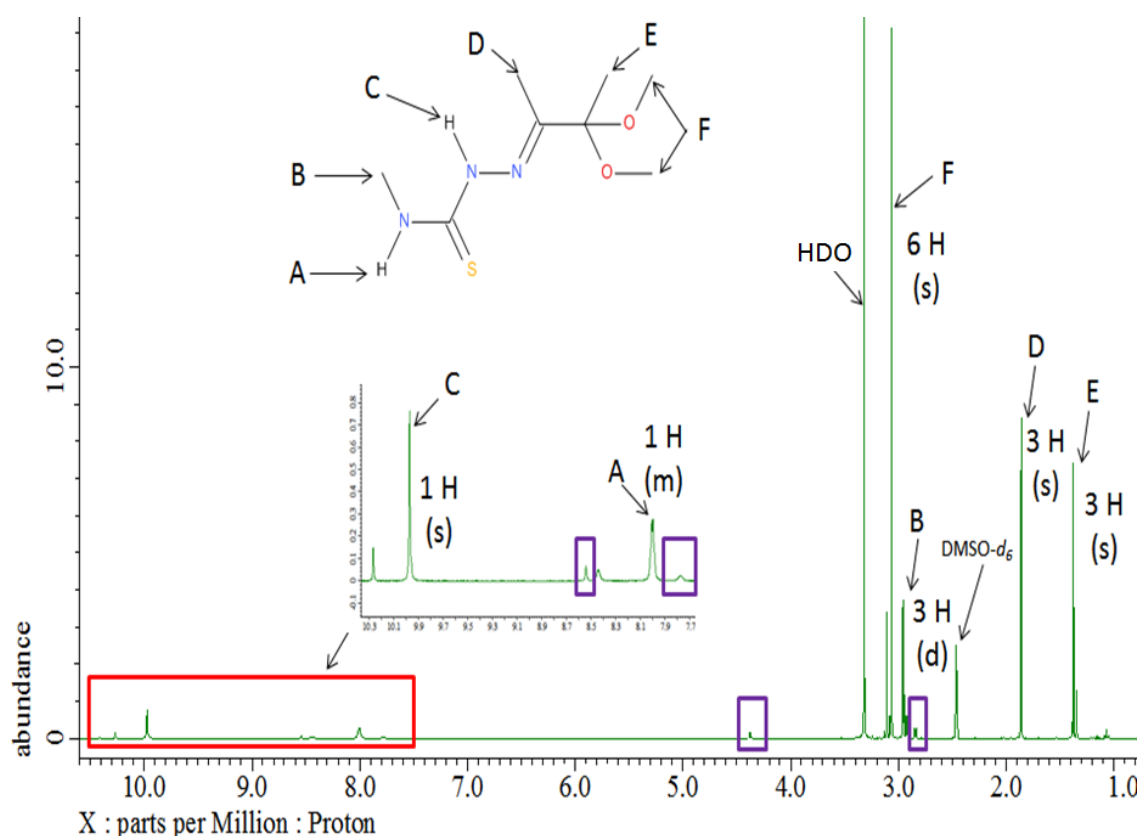


**Figure 2.2.4.6.** An assigned  $^1\text{H}$  NMR spectrum of the novel compound  $\text{DMB-Me-(OMe)}_2$ .  $\text{DMB-Me-(OMe)}_2$  was obtained by the reacting 3,3-dimethoxy-2-butanone with 4-methyl-3-thiosemicarbazide. The purple boxes suggest a small presence of unreacted 4-methyl-3-thiosemicarbazide.

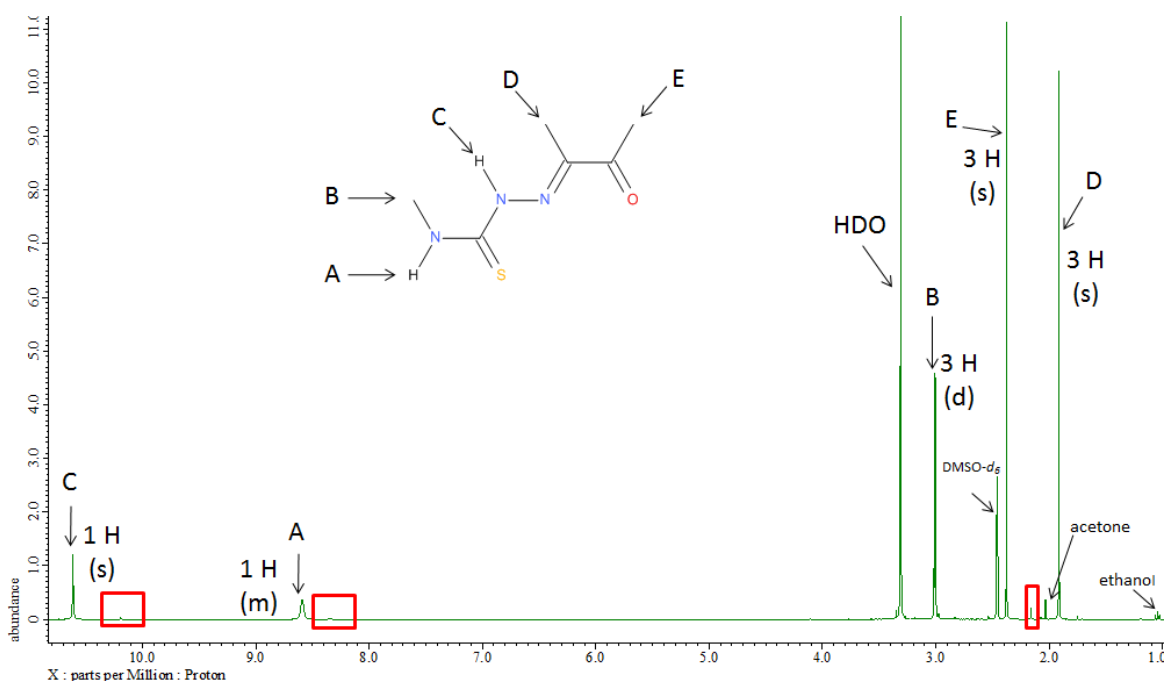


**Figure 2.2.4.7.** An assigned  $^1\text{H}$  NMR spectrum of  $\text{BDO-Me=O}$ .  $\text{BDO-Me=O}$  was obtained by using  $\text{LiBF}_4$  to cleave the acetal functionalities of  $\text{DMB-Me-(OMe)}_2$ .

The  $^1\text{H}$  spectrum of BDO-Me=O (Figure 2.2.4.7.) shows that the target intermediate for reaction 2 was successfully synthesised with a good level of purity. The only significant impurity that is present is BDO-Me-Me (highlighted by red boxes) in a quantity of around 1%, this value was estimated by using the NMR integrals. There is a trace of ethanol present which was carried over from the reaction solvent. It is suspected that the water peak comes from the slightly wet DMSO- $d_6$  which was used as the NMR solvent. A slight trace of acetone can be seen which is carryover from the cleaning of the NMR tubes.

The FTIR spectrum of BDO-Me=O (Figure 2.2.4.8.), helps support that the product is in its de-protected form and not in its protected form as DMB-Me-(OMe) $_2$ . The spectrum shows a strong absorbance at  $1670\text{ cm}^{-1}$  which corresponds to the C=O bond of the ketone carbonyl group.

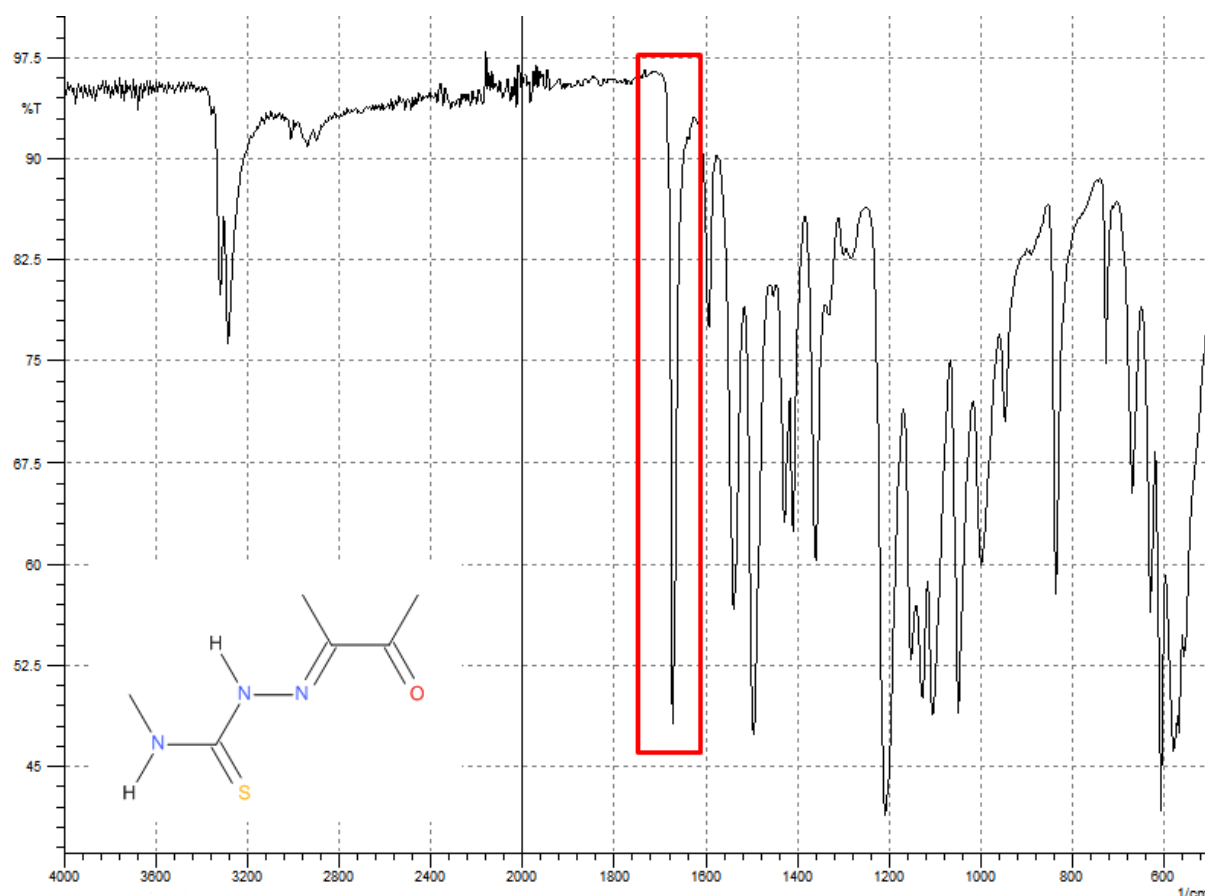


**Figure 2.2.4.8.** A FTIR spectrum of BDO-Me=O, synthesised by successfully deprotecting DMB-Me-(OMe) $_2$ . The red box illustrates the presence of the deprotected carbonyl functionality.

The synthesis was not taken any further due to an alternative method of synthesis was discovered<sup>57</sup>. This method managed to synthesise intermediates (e.g. BDO-Me=O) without the need of a protecting group by exploiting the reactivity differences of a selected di-ketone (e.g.

2,3-butandione). A dissimilar 4-substituted-3-thiosemicarbazide was then reacted to produce the desired dissymmetric ligand. Following this method it was possible to produce dissymmetric ligands with greater yields and purity whilst removing the requirement for a de-protection step and in doing so reducing the overall synthesis time from start to finish. It was decided to abandon using the protection method and to pursue this new method.

### **2.2.5. Synthetic methods**

#### **DMB-Me-(OMe)<sub>2</sub>**

4-methyl-3-thiosemicarbazide (0.890 g, 0.0085 mol) was dissolved in ethanol (30 mL, 60 °C), followed by the addition of 3,3-dimethoxy-2-butanone (1.25 mL, 0.0093 mol, 1.23 g). The resulting solution was left to stir (60 °C, 36 hours). The precipitate was filtered off and discarded. The solvent was removed and the resulting solid was extracted with diethyl ether (1 x 50 mL, 2 x 25 mL). The diethyl ether was removed and the remaining solid was dried. A white solid (0.308 g) was recovered (17% yield).

#### **BDO-NH<sub>2</sub>=O**

Freshly activated molecular sieves (3 Å, 0.808 g) were added to DMF (15 mL, 60 °C), followed by the addition of thiosemicarbazide (0.773 g, 0.0085 mol) and 3,3-dimethoxy-2-butanone (1.5 mL, 0.011 mol, 1.48 g). The resulting solution was left to stir (60 °C, 3 days). The molecular sieves plus any solid by-products were filtered off, the DMF under was removed under vacuum and the sample was dried. A brown solid (0.342 g) was recovered (20% yield).

#### **BDO-Me=O**

DMB-Me-(OMe)<sub>2</sub> (2.357 g, 0.011 mol) were dissolved in an acetonitrile solution (30 mL, 98% acetonitrile / 2% de-ionised water, 60 °C). LiBF<sub>4</sub> (1.969 g, 0.021 mol) was added and the resulting solution was left to stir (60 °C, 1 hour). A saturated solution of Na<sub>2</sub>CO<sub>3</sub> (40 mL) was added rapidly resulting in the formation of a bright yellow solution. The solution was left to stir (10 minutes). The product was extracted with diethyl ether (4 x 50 mL) and the organic solution was dried over magnesium sulfate (4 large spatulas). The magnesium sulfate was filtered off and the solvent was removed. The pale yellow solid was extracted with hot diethyl ether (1 x 25 mL, 1 x 50 mL). The mixture was cooled in the freezer and the precipitate was removed by filtration. The solid was left to dry. A light yellow solid (0.212 g) was recovered (11% yield).

#### **BDO-NH<sub>2</sub>-Me**

Freshly activated molecular sieves (3 Å, 0.060 g) was added to DMF (18 mL, 60 °C), followed by the addition of BDO-NH<sub>2</sub>=O (0.170 g, 0.0008 mol) and 4-methyl-3-thiosemicarbazide (0.088 g, 0.0008 mol). The heat was turned off and the solution was left to stir (cooling down to room temperature, 6 hours). The molecular sieves were filtered off and the DMF was removed under

vacuum. The crude product was washed with a little acetone and dried. A brown solid (0.158 g) was recovered (80% yield).

### **2.2.6. NMR spectral data**

#### **DMB-Me-(OMe)<sub>2</sub>**

<sup>1</sup>H NMR (DMSO-*d*<sub>6</sub>, 400 MHz): δ= 9.98 (s, 1 H, N-NH), 8.01 (m, 1 H, H<sub>3</sub>C-NH), 3.06 (s, 6 H, O-CH<sub>3</sub>), 2.96 (d, 3 H, HN-CH<sub>3</sub>, J= 4.8 Hz), 1.86 (s, 3 H, N=C-CH<sub>3</sub>), 1.37 (s, 3 H, O-C-CH<sub>3</sub>).

#### **BDO-NH<sub>2</sub>=O**

<sup>1</sup>H NMR (DMSO-*d*<sub>6</sub>, 400 MHz): δ= 10.56 (s, 1 H, N-NH), 8.69 (s, 1 H, C-NH), 8.07 (s, 1 H, C-NH), 2.35 (s, 3 H, O=C-CH<sub>3</sub>), 1.91 (s, 3 H, N=C-CH<sub>3</sub>). <sup>13</sup>C {<sup>1</sup>H} NMR (DMSO-*d*<sub>6</sub>, 100 MHz): δ= 198.20 (C=O), 180.30 (C=S), 146.40 (C=N), 25.31 (O=C-CH<sub>3</sub>), 10.59 (N=C-CH<sub>3</sub>).

#### **BDO-Me=O**

<sup>1</sup>H NMR (DMSO-*d*<sub>6</sub>, 400 MHz): δ= 10.61 (s, 1 H, N-NH), 8.59 (m, 1 H, H<sub>3</sub>C-NH), 3.01 (d, 3 H, HN-CH<sub>3</sub>, J= 4.8 Hz), 2.38 (s, 3 H, O=C-CH<sub>3</sub>), 1.92 (s, 3 H, N=C-CH<sub>3</sub>).

#### **BDO-NH<sub>2</sub>-Me**

<sup>1</sup>H NMR (DMSO-*d*<sub>6</sub>, 400 MHz): δ= 10.21 (s, 1 H, N-NH), 10.16 (s, 1 H, N-NH), 8.37 (singlet overlapping a quartet, 1 H C-NH), 8.34 (quartet overlapping a singlet, 1 H, H<sub>3</sub>C-NH, J= 4.4 Hz), 7.82 (s, 1 H C-NH), 2.97 (d, 3 H, HN-CH<sub>3</sub>, J= 4.4 Hz), 2.16 (s, 3 H, N=C-CH<sub>3</sub>), 2.12 (s, 3 H, N=C-CH<sub>3</sub>). <sup>13</sup>C {<sup>1</sup>H} NMR (DMSO-*d*<sub>6</sub>, 100 MHz): δ= 179.33 (C=S), 178.97 (C=S), 148.92 (C=N), 148.43 (C=N), 31.74 (HN-CH<sub>3</sub>), 12.26 (N=C-CH<sub>3</sub>), 12.07 (N=C-CH<sub>3</sub>).

The above results are in accord to literature reports of BDO-Me=O,<sup>57, 190</sup> which was synthesised by an alternative synthetic route. Characterisation data for compounds BDO-NH<sub>2</sub>=O, BDO-Me=O and BDO-NH<sub>2</sub>-Me shows strong agreement to the same compounds that are reported later in this chapter which were synthesised by the synthetic route reported by J. Holland *et al.*<sup>57</sup> It is believed that this is the first reports of the compound DMB-Me-(OMe)<sub>2</sub>.

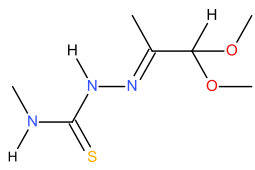
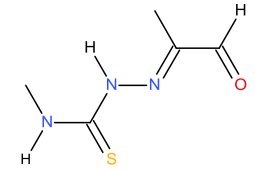
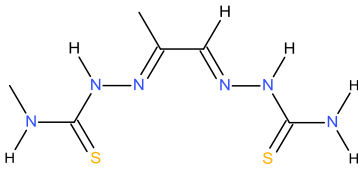
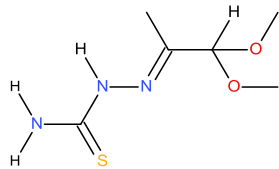
### **2.2.7. Discussion**

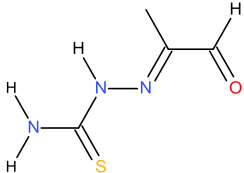
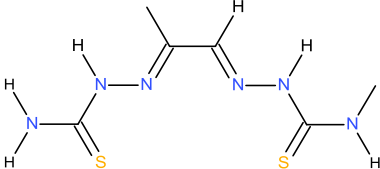
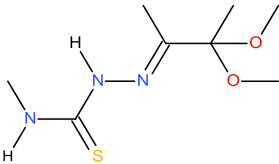
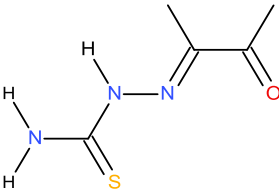
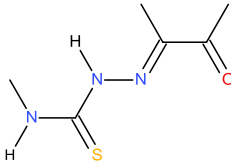
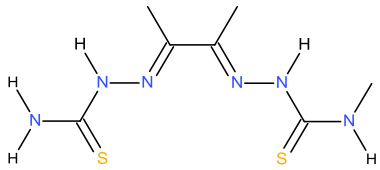
Using acetal groups for a protection based approach for the synthesis of dissymmetric bis(thiosemicarbazones) is possible, table 2.2.7.1. summarises the compounds synthesised during in this section. However, numerous problems were encountered such as the clean cleavage of the acetal functionalities with LiBF<sub>4</sub> was often found to be labour intensive and temperamental. The presence of the acetal protection prevented the use of acid catalysts resulting in long reaction times, often up to three days. If the reaction conditions resulted in the successful cleavage of the acetal groups the resulting sample often contained a mixture of dissymmetric, symmetric and intermediate products. The multiple poor yielding steps (sometimes as low as 11%) meant that

the resulting ligands were often recovered in unworkably small quantities. Limits in the equipment that was available made running the samples in DMF undesirable as the removal of DMF could only be achieved on a vacuum line for long periods, using temperatures above 60°C. This raised concerns about increase the risk of potential scrambling of the ligands. Once the DMF was fully removed a very crude, often a sludge like product was obtained. The absence of a suitable purification method made the ligands unsuitable for the use in a medical context.

Based on these issues it was decided to back away from this approach and focus on the development of the exploitation of the di-carbonyl method.<sup>57</sup> If the above issues could be rectified in order to give a method that gives a pure compound with a higher yield and preferably in a reduced time span, the protection based method may be of greater use. However, it is unlikely to outperform the exploitation of the di-carbonyl method in terms of producing a clean ligand in a relatively short time period without the need for labour intensive methods.

**Table 2.2.7.1.** A summary of the compounds synthesised during the investigation of the acetal protecting approach.

Ligand	Novel	Yield
<p><b>PADA-Me-(OMe)<sub>2</sub></b></p> 	No <sup>79, 80</sup>	24%
<p><b>PADA-Me=O</b></p> 	No <sup>79, 80</sup>	75%
<p><b>PADA-Me-NH<sub>2</sub></b></p> 	No <sup>79</sup>	36%
<p><b>PADA-NH<sub>2</sub>-(OMe)<sub>2</sub></b></p> 	No <sup>79</sup>	48%

<p style="text-align: center;"><b>PADA-NH<sub>2</sub>=O</b></p> 	No <sup>79</sup>	24%
<p style="text-align: center;"><b>PADA-NH<sub>2</sub>-Me</b></p> 	No <sup>79</sup>	62%
<p style="text-align: center;"><b>DMB-Me-(OMe)<sub>2</sub></b></p> 	Yes	73%
<p style="text-align: center;"><b>BDO-NH<sub>2</sub>=O</b></p> 	No <sup>196, 197</sup>	22%
<p style="text-align: center;"><b>BDO-Me=O</b></p> 	No <sup>57, 73, 83</sup>	66%
<p style="text-align: center;"><b>BDO-NH<sub>2</sub>-Me</b></p> 	No <sup>196, 198, 199</sup>	55%



## **2.3. Ligands with Me/H backbones**

### **Application**

This class of ligands is of interest for the application of monitoring the copper trafficking within the brain in order to study neurodegenerative diseases such as Alzheimer's disease, as described in the introduction. In order to achieve this, the ligand once chelated with copper must be lipophilic enough to cross the blood–brain barrier (BBB). The complex must also have a redox potential that allows the copper to be deposited in the brain, irrespective of hypoxic or normoxic conditions. Once the radio-copper has been deposited the copper's migration can be monitored via PET.

To keep the redox potential within an appropriate range, it is desirable to make ligands with hydrogen and a methyl group on the backbone. In order to achieve the lipophilicity required to cross the blood-brain barrier, a range of ligands was made with varying combinations of 4-substituted-3-thiosemicarbazides that have relatively lipophilic substituents such as methyl, ethyl, dimethyl and phenyl.

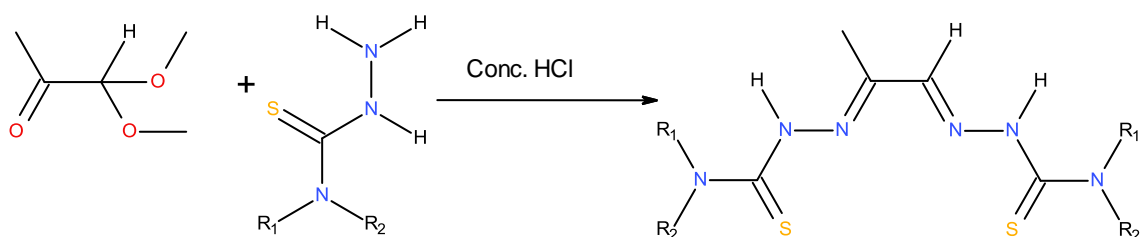
The main aim was to make a number of different ligands that fulfilled the above criteria for screening in order to establish the optimal ligand configuration or to suggest further refinement of the ligands' substituents.

### **2.3.1. Symmetric ligands with Me/H backbones**

#### **Overview of reaction**

The synthesis of this subgroup of ligands requires one equivalent of methylglyoxal-1,1-dimethyl acetal (PADA) to be reacted with two equivalents (in excess) of a chosen 4-substituted-3-thiosemicarbazide, under acidic conditions, in water at 50 °C to give the desired symmetric ligand (Figure 2.3.1.1). Using this method four ligands were synthesised (Figure 2.3.1.2).

**Figure 2.3.1.1.** The general reaction for the synthesis of symmetric ligands with Me/H backbones.



	R <sub>1</sub>	R <sub>2</sub>
PADA-Me-Me	CH <sub>3</sub>	H
PADA-(Me) <sub>2</sub> -(Me) <sub>2</sub>	CH <sub>3</sub>	CH <sub>3</sub>
PADA-Et-Et	CH <sub>2</sub> CH <sub>3</sub>	H
PADA-Ph-Ph	C <sub>6</sub> H <sub>5</sub>	H

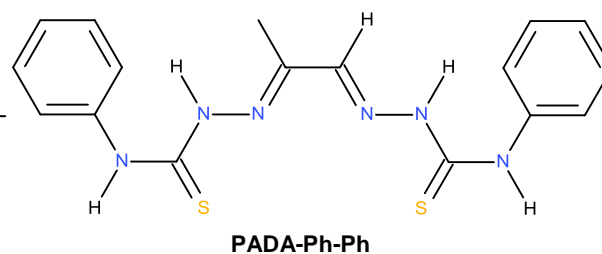
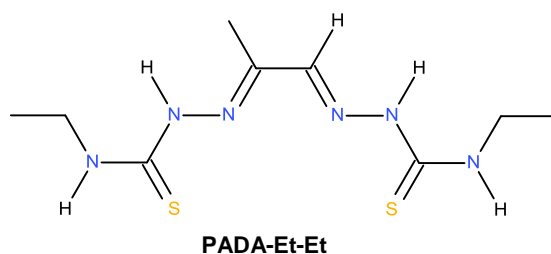
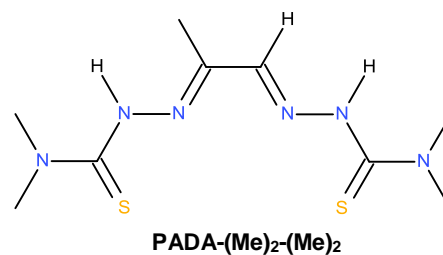
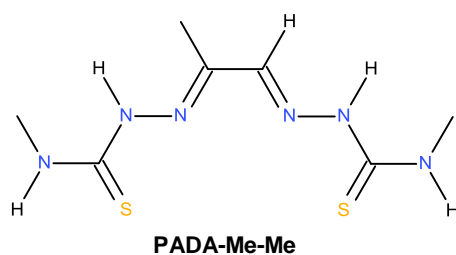


**Figure 2.3.1.2.** Structures of the symmetric ligands with Me/H backbones that were synthesised.

## 2.3.2. Methods

### PADA-Me-Me

4-methyl-3-thiosemicarbazide (1.100 g, 0.0105 mol) was dissolved in de-ionised water (40 mL, 50 °C) and HCl (32%, 2 drops) was added. Methylglyoxal-1,1-dimethylacetal (0.58 mL, 0.0048 mol, 0.566 g) was added rapidly and left to stir (50 °C, 5 minutes). The precipitate was removed by filtration and washed with de-ionised water (50 mL, room temperature and 50 mL, 80 °C). The crude product was dissolved in DMSO (17 mL). The solution was filtered, recrystallised with de-ionised water (34 mL). The precipitate was removed via filtration, washed with water (50 mL) and left to dry. A cream solid (0.858 g) was recovered (73% yield).

### **PADA-(Me)<sub>2</sub>-(Me)<sub>2</sub>**

4,4-dimethyl-3-thiosemicarbazide (0.321 g, 0.0027 mol) was dissolved in de-ionised water (50 mL, 50 °C) and HCl (32%, 2 drops) was added. Methylglyoxal-1,1-dimethylacetal (0.15 mL, 0.0012 mol, 0.15 g) was added rapidly and left to stir (50 °C, 1 hour). The precipitate was removed by filtration and washed with de-ionised water (50 mL, room temperature and 50 mL, 80 °C). The crude product was dissolved in DMSO (3 mL). The solution was filtered, and the product was recrystallised with de-ionised water (6 mL). The precipitate was recovered by filtration, washed with water (50 mL) and dried. A yellow solid (0.065 g) was recovered (20% yield).

### **PADA-Et-Et**

4-ethyl-3-thiosemicarbazide (1.251 g, 0.0105 mol) was dissolved in de-ionised water (50 mL, 50 °C). The insoluble particulates were filtered and HCl was added (32%, 2 drops). Methylglyoxal-1,1-dimethylacetal (0.58 mL, 0.0048 mol, 0.57 g) was added rapidly and left to stir (50 °C, 5 minutes). The precipitate was removed by filtration and washed with de-ionised water (50 mL). The crude product was dissolved in DMSO (35 mL). The solution was filtered and the product was recrystallised with de-ionised water (70 mL). The precipitate was isolated via filtration, washed with water (50 mL) and dried. A yellowish white solid (0.870 g) was recovered (66% yield).

### **PADA-Ph-Ph**

4-phenyl-3-thiosemicarbazide (0.439 g, 0.00263 mol) was dissolved in de-ionised water/ethanol solution (25 mL water, 13 mL ethanol, 50 °C). The insoluble particulates were filtered and HCl (32%, 2 drops) was added. Methylglyoxal-1,1-dimethylacetal (0.15 mL, 0.0012 mol, 0.146 g) was added rapidly and left to stir (50 °C, 5 minutes). The precipitate was removed by filtration and washed with de-ionised water (50 mL, room temperature and 50 mL, 80 °C). The crude product was dissolved in DMSO (15 mL). The solution was filtered, the product was recrystallised with de-ionised water (30 mL). Precipitate filtered and washed with water (50 mL) and dried. The sample was further washed with ethanol (2 x 25 mL), de-ionised water (50 mL, 80 °C) and dried. A mustard coloured solid (0.244 g) was recovered (55% yield).

## **2.3.3. Characterisation data for symmetric ligands with Me/H backbones**

### **PADA-Me-Me**

<sup>1</sup>H NMR (DMSO-*d*<sub>6</sub>, 400 MHz): δ= 11.73 (s, 1 H, N-NH), 10.33 (s, 1 H, N-NH), 8.49 (m, 1 H, H<sub>3</sub>C-NH, J= 4.4 Hz), 8.38 (m, 1 H H<sub>3</sub>C-NH, J= 4.8 Hz), 7.62 (s, 1 H, N=CH), 2.94 (two overlapping doublets, 6 H, HN-CH<sub>3</sub>, J= 4.4 Hz), 2.12 (s, 3 H, N=C-CH<sub>3</sub>). <sup>13</sup>C {<sup>1</sup>H} NMR (DMSO-*d*<sub>6</sub>, 100 MHz): δ= 178.76 (C=S), 178.22 (C=S), 147.63 (C=N), 142.40 (C=N), 31.58 (HN-CH<sub>3</sub>), 31.47 (HN-CH<sub>3</sub>), 11.62 (N=C-CH<sub>3</sub>). IR (neat): cm<sup>-1</sup>= 3302 (w), 3142 (w), 1531 (s), 1489 (s), 1431 (m), 1408 (m), 1354 (w), 1213 (s), 1152

(m), 1088 (s), 1024 (s), 914 (m), 820 (m), 548 (s), 517 (m). **Raman (neat):**  $\text{cm}^{-1}$  = 2909 (w), 1785 (w), 1657 (w), 1577 (s), 1442 (w), 1364 (w), 1279 (w), 1226 (w), 1124 (w), 1017 (w), 879 (w), 775 (w), 560 (w), 405 (w), 115 (w). **Melting point:** >214 °C (decomposed).

#### PADA-(Me)<sub>2</sub>-(Me)<sub>2</sub>

**<sup>1</sup>H NMR** (DMSO-*d*<sub>6</sub>, 400 MHz):  $\delta$  = 11.07 (s, 1 H, N-NH), 9.59 (s, 1 H, N-NH), 7.78 (s, 1 H, N=CH), 3.23 (s, 6 H, N-(CH<sub>3</sub>)<sub>2</sub>), 2.05 (s, 3 H, N=C-CH<sub>3</sub>). **<sup>13</sup>C {<sup>1</sup>H} NMR** (DMSO-*d*<sub>6</sub>, 100 MHz):  $\delta$  = 181.79 (C=S), 180.89 (C=S), 150.11 (C=N), 144.54 (C=N), 42.80 (N-(CH<sub>3</sub>)<sub>2</sub>), 42.47 (N-(CH<sub>3</sub>)<sub>2</sub>), 11.37 (N=C-CH<sub>3</sub>). **IR (neat):**  $\text{cm}^{-1}$  = 3404 (w), 2922 (w), 1533 (s), 1490 (m), 1362 (m), 1328 (s), 1281 (m), 1229 (s), 1150 (s), 1113 (m), 1057 (m), 1022 (m), 905 (s), 785 (m), 542 (m). **Raman (neat):**  $\text{cm}^{-1}$  = 2917 (w), 1581 (s), 1436 (w), 1381 (w), 1281 (w), 1237 (m), 1132 (w), 1027 (w), 864 (w), 718 (w), 546 (w), 438 (w), 394 (w), 171 (w), 107 (w). **Melting point:** >106 °C (decomposed).

#### PADA-Et-Et

**<sup>1</sup>H NMR** (DMSO-*d*<sub>6</sub>, 400 MHz):  $\delta$  = 11.65 (s, 1 H, N-NH), 10.24 (s, 1 H, N-NH), 8.52 (t, 1 H, H<sub>2</sub>C-NH, J = 6.0 Hz), 8.41 (t, 1 H H<sub>2</sub>C-NH, J = 6.0 Hz), 7.62 (s, 1 H, N=CH), 3.52 (m, 4 H, H<sub>2</sub>C-NH), 2.13 (s, 3 H, N=C-CH<sub>3</sub>), 1.07 (two overlapping triplets, 6 H, H<sub>2</sub>C-CH<sub>3</sub>, J = 7.2 Hz). **<sup>13</sup>C {<sup>1</sup>H} NMR** (DMSO-*d*<sub>6</sub>, 100 MHz):  $\delta$  = 177.65 (C=S), 177.15 (C=S), 147.66 (C=N), 142.41 (C=N), 39.01 (N-CH<sub>2</sub>), 38.87 (N-CH<sub>2</sub>), 15.01 (H<sub>2</sub>C-CH<sub>3</sub>), 14.87 (H<sub>2</sub>C-CH<sub>3</sub>), 11.38 (N=C-CH<sub>3</sub>). **IR (neat):**  $\text{cm}^{-1}$  = 3289 (m), 3161 (w), 2967 (m), 1526 (s), 1476 (s), 1427 (s), 1315 (m), 1229 (s), 1198 (s), 1096 (s), 1043 (s), 934 (s), 808 (s), 664 (m), 579 (s), 550 (s). **Raman (neat):**  $\text{cm}^{-1}$  = 3375 (w), 2936 (w), 1578 (s), 1516 (w), 1436 (w), 1365 (m), 1284 (w), 1236 (w), 1202 (w), 1132 (w), 1020 (w), 874 (w), 757 (w), 541 (w), 457 (w). **Melting point:** >220 °C (decomposed).

#### PADA-Ph-Ph

**<sup>1</sup>H NMR** (DMSO-*d*<sub>6</sub>, 400 MHz):  $\delta$  = 12.10 (s, 1 H, N-NH), 10.75 (s, 1 H, N-NH), 10.19 (s, 1 H, Ph-NH), 10.01 (s, 1 H, Ph-NH), 7.82 (s, 1 H, N=CH), 7.50 (m, 4 H, H<sub>(2,6)</sub> aryl), 7.32 (m, 4 H, H<sub>(3,5)</sub> aryl), 7.17 (m, 2 H, H<sub>(4)</sub> aryl), 2.25 (s, 3 H, N=C-CH<sub>3</sub>). **<sup>13</sup>C {<sup>1</sup>H} NMR** (DMSO-*d*<sub>6</sub>, 100 MHz):  $\delta$  = 177.30 (C=S), 176.76 (C=S), 148.49 (C=N), 143.48 (C=N), 139.48 (C<sub>(1)</sub> aryl), 139.45 (C<sub>(1)</sub> aryl), 128.66 (C<sub>(3,5)</sub> aryl), 126.55 (C<sub>(4)</sub> aryl), 126.09 (C<sub>(2,6)</sub> aryl), 11.97 (N=C-CH<sub>3</sub>). **IR (neat):**  $\text{cm}^{-1}$  = 3292 (w), 3136 (w), 2980 (w), 1595 (m), 1518 (s), 1491 (s), 1445 (m), 1350 (m), 1256 (m), 1173 (s), 1070 (m), 1026 (m), 934 (m), 750 (m), 689 (s), 640 (m), 559 (m). **Raman (neat):**  $\text{cm}^{-1}$  = 3061 (w), 1579 (s), 1433 (w), 1370 (w), 1285 (w), 1254 (m), 1178 (w), 1122 (w), 1023 (w), 942 (w), 1864 (w), 744 (w), 614 (w), 257 (w), 195 (w). **Melting point:** >177 °C (decomposed).

### 2.3.4. Spectral examples of a symmetric ligand with a Me/H backbone

Figures 2.3.4.1-4. Spectral examples of ligand PADA-(Me)<sub>2</sub>-(Me)<sub>2</sub>.

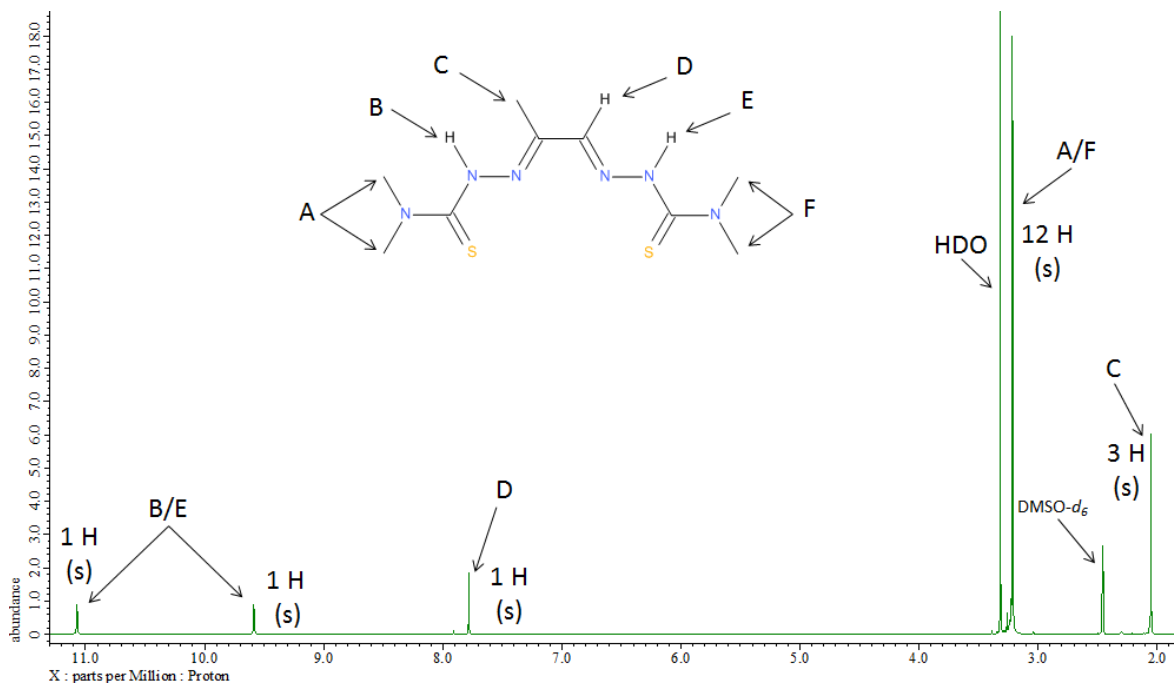


**Figure 2.3.4.1.** An assigned <sup>1</sup>H NMR spectrum of PADA-(Me)<sub>2</sub>-(Me)<sub>2</sub>. PADA-(Me)<sub>2</sub>-(Me)<sub>2</sub> was synthesised by reacting methylglyoxal-1,1-dimethylacetal with two equivalents of 4,4-dimethyl-3-thiosemicarbazide.

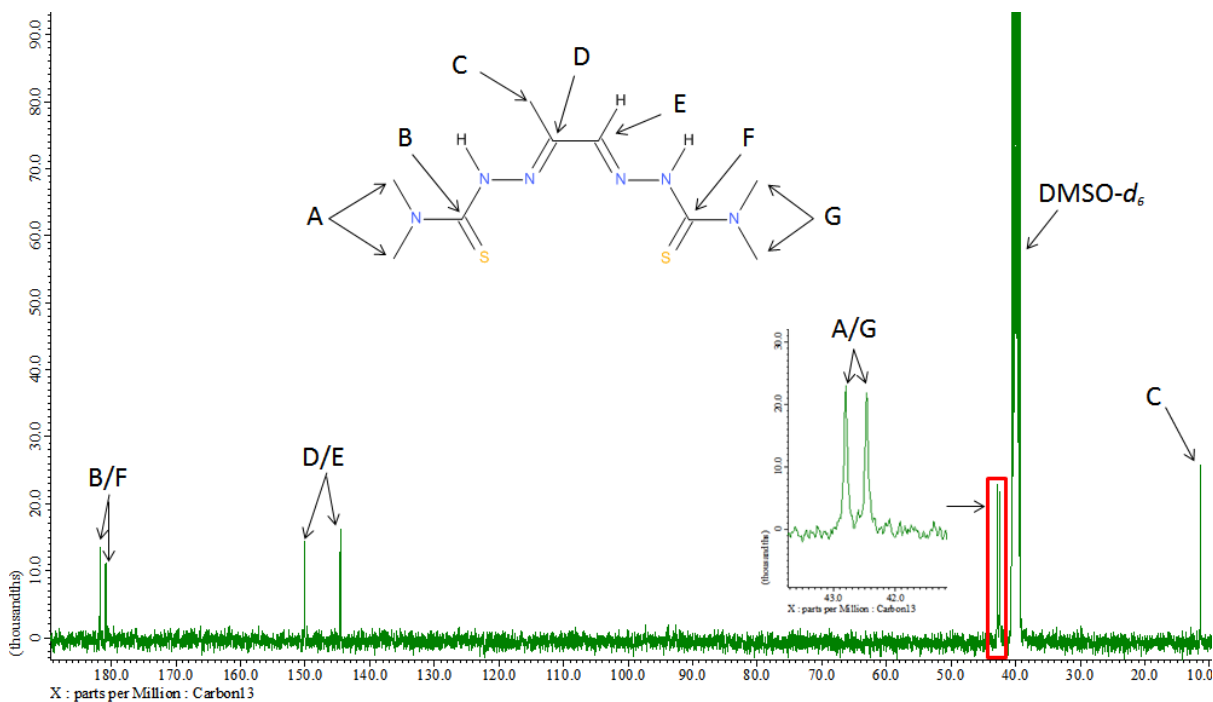


**Figure 2.3.4.2.** An assigned <sup>13</sup>C NMR spectrum of PADA-(Me)<sub>2</sub>-(Me)<sub>2</sub>.

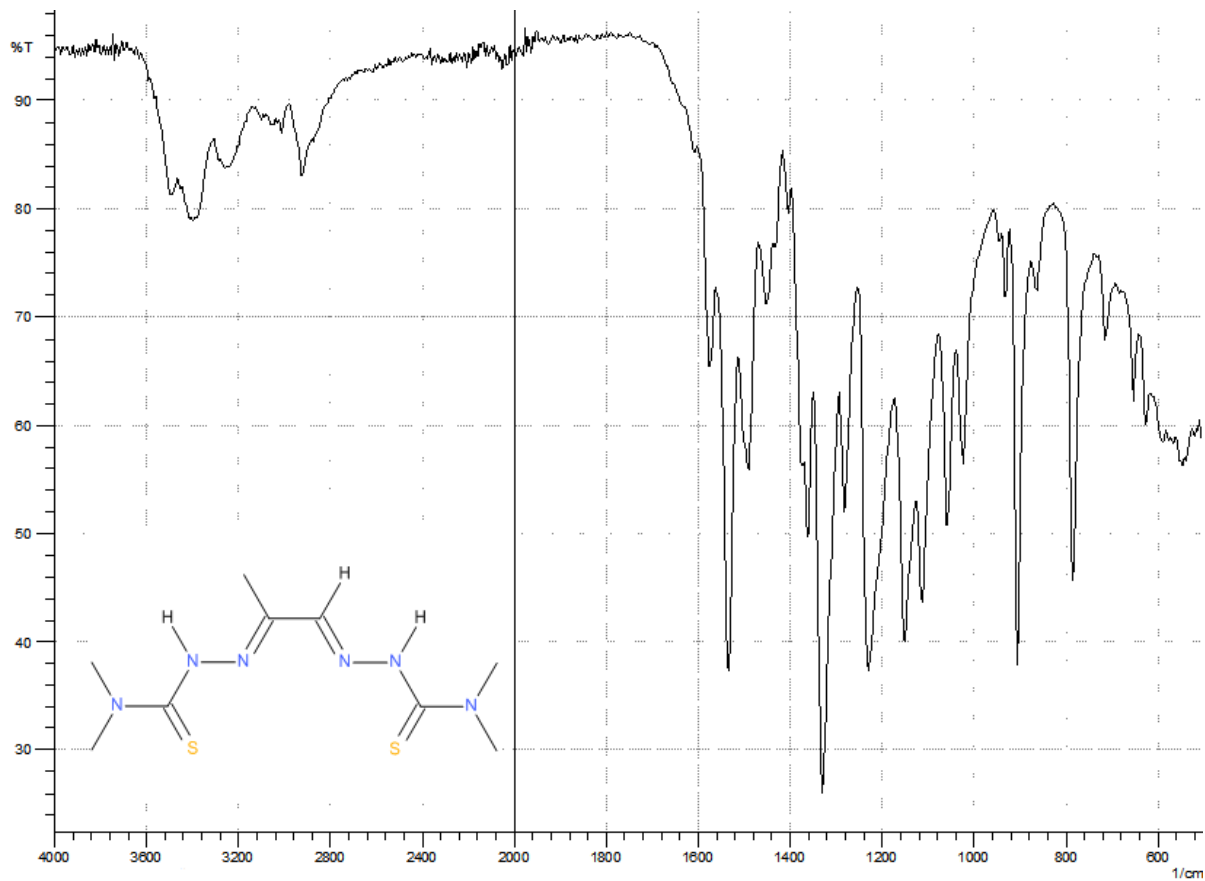


**Figure 2.3.4.3.** A FTIR spectrum of PADA-(Me)<sub>2</sub>-(Me)<sub>2</sub>.

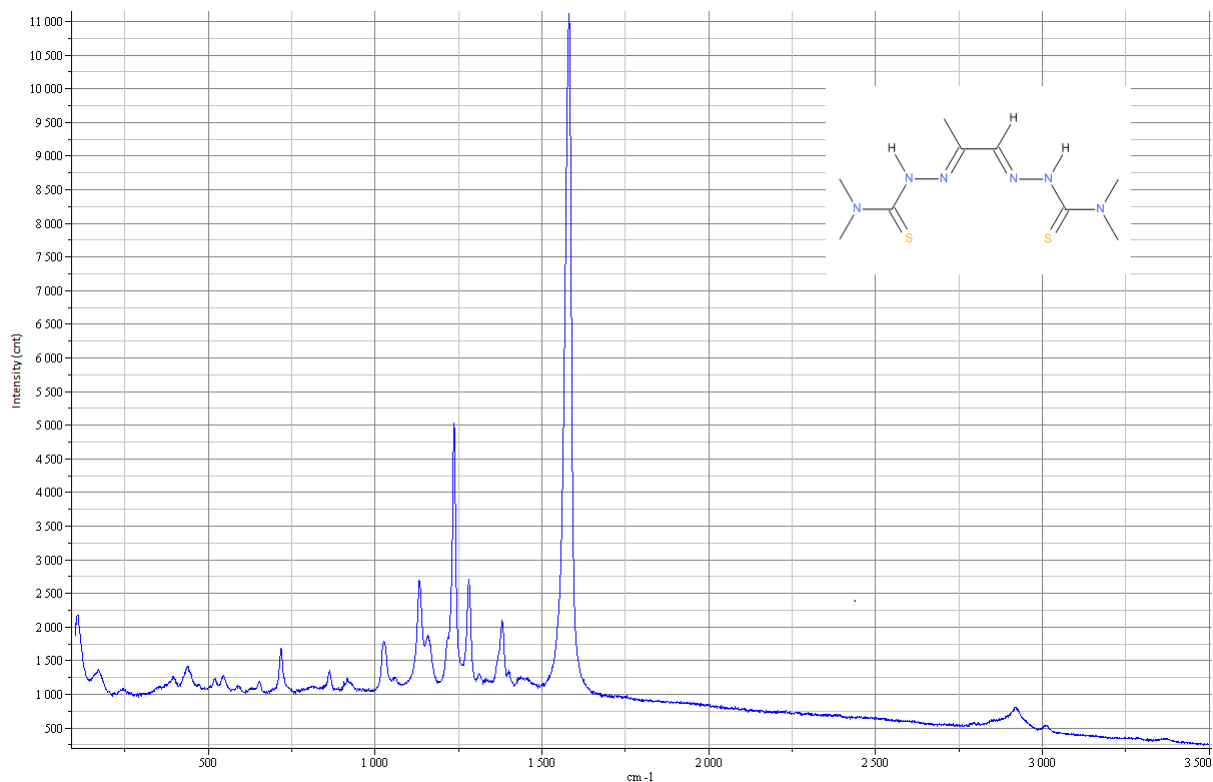


**Figure 2.3.4.4.** A Raman spectrum of PADA-(Me)<sub>2</sub>-(Me)<sub>2</sub>.

### **2.3.5. Discussion**

All four ligands were synthesised successfully and in a high purity. It is believed that the synthesis of symmetric ligands of this class by using methylglyoxal-1,1-dimethyl acetal as a precursor has not been attempted previously and as a pre-cursor it is cheaper than the methylglyoxal (Sigma-Aldrich<sup>200, 201</sup>). It was also more convenient to handle methylglyoxal-1,1-dimethyl for reactions as it comes as a neat liquid whilst methylglyoxal is only available as a 40% solution in H<sub>2</sub>O.

The only noticeable impurity is the respective mono-substituted thiosemicarbazone which is present despite the addition of a slight excess (typically 10%) of 4-substituted-3-thiosemicarbazide. By comparing the integrals of the respective ligands <sup>1</sup>H NMR spectra it is estimated that the mono-substituted thiosemicarbazone is only present in the quantity of less than 1% with the exception of PADA-Me-Me where the impurity content raises to around 2%.

No significant problems were encountered with the synthesis of these ligands, the only slight issue was adapting the amount of water used to dissolve the 4-substituted-3-thiosemicarbazides which became more challenging as the substituents on the terminal nitrogen got more lipophilic. With the 4-phenyl-3-thiosemicarbazide it was necessary to add a quantity of ethanol to the water in order to achieve full dissolution. It was important to maintain a reaction mixture that is free of insoluble particulates so when the product precipitates out of solution the insoluble impurities would not mix with the product. It is possible to run the reaction in alternate solvents, such as dimethylformamide, in which the precursors dissolve easily. The setback with this method is that the product does not precipitate out of the reaction mixture, requiring the solvent to be evaporated off, leaving behind a crude product that contains a mixture of the desired product, and undesired components such as intermediates and unreacted reagents. Later on in the project it was discovered that H<sub>2</sub>O could be added to the DMF reaction mixture to cause the product to crystallise out of solution so that it could be recovered by filtration.

It is not known if PADA's acetal groups are hydrolysed under the acidic conditions of the reaction mixture initially to form the ketone/aldehyde precursor, methylglyoxal, followed by the addition of the two 4-substituted-3-thiosemicarbazides or if the PADA-mono-substituted-3-thiosemicarbazone is formed, followed by the hydrolysis of the acetal groups to a aldehyde which is then able to react with the second 4-substituted-3-thiosemicarbazide.

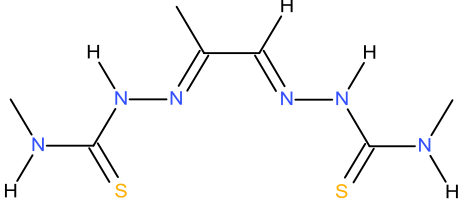
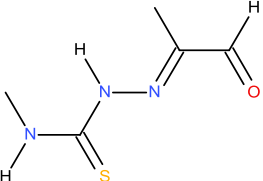
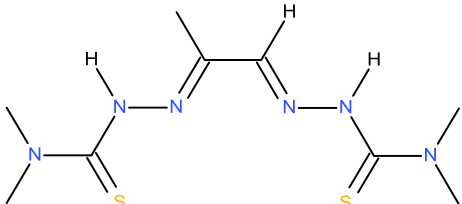
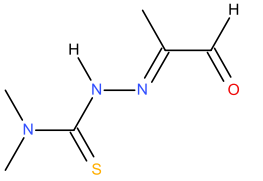
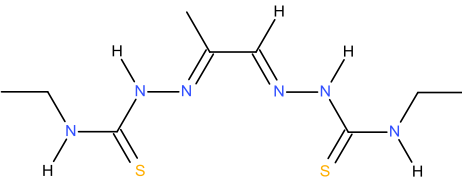
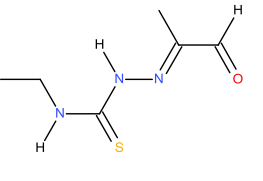
There has been a report of PADA's acetal groups being used as protecting groups<sup>79</sup> in the synthesis of dissymmetric ligands, but in protic media the acetal groups were easily hydrolysed resulting in a mixture of bis(thiosemicarbazones). This observation, coupled with all the NMR spectra of the successfully synthesised ligands shown no trace of the mono-substituted-3-

thiosemicarbazone of PADA where the protecting groups are intact may indicate that the hydrolysis of PADA's acetal groups occurs first.

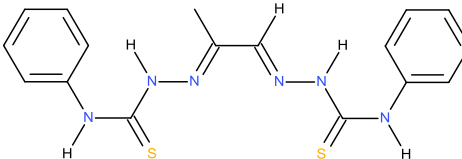
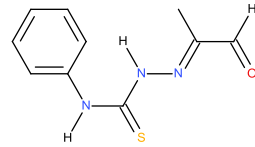
There are a large number of reports of symmetric ligands with Me/H on the backbone.<sup>6, 45, 63, 69, 77, 82, 106, 123, 145, 146, 164, 202</sup> However, the scope of these reports is aimed towards biological screening for the use as imaging agents or other pharmaceutical applications. Due to this characterisation data such as NMR, IR or Raman data have not been identified in these articles. However, data obtained from ligands with different substituents on the imine backbone and/or terminal amine that can be linked to the literature can be used to corroborate peak positions and assignments are feasible. For ligands of this class, on comparison to data from related ligands, there is confidence in the data obtained and assignments of that data.

The table (Table 2.3.5.1.) below illustrates all four ligands, what the main impurity is and an estimate of the percentage.

**Table 2.3.5.1.** Summary of purity for the symmetric ligands with Me/H backbones.

Ligand	Novel	Yield	Main impurity	Estimated impurity *
<p><b>PADA-Me-Me</b></p> 	<p>No<sup>6, 45, 63, 66, 69, 77, 80, 106, 123, 145, 146, 164, 203, 204</sup></p>	73%		2%
<p><b>PADA-(Me)<sub>2</sub>-(Me)<sub>2</sub></b></p> 	<p>No<sup>6, 69, 77, 145, 146</sup></p>	22%		Less than 1%
<p><b>PADA-Et-Et</b></p> 	<p>No<sup>63, 69, 77, 145, 146, 164</sup></p>	66%		Less than 1%



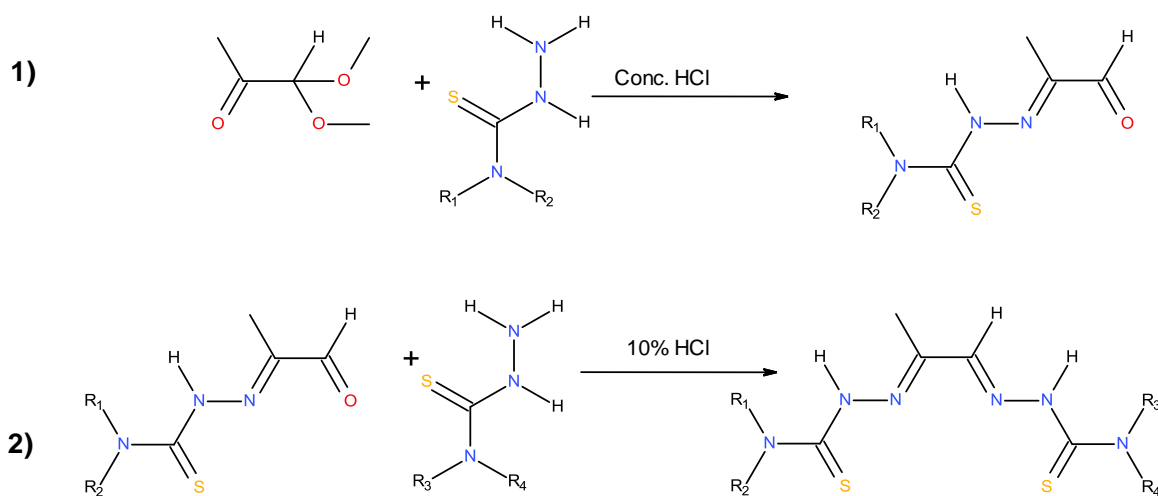
<b>PADA-Ph-Ph</b> 	No <sup>69,77,</sup> 145, 146	55%		Less than 1%
--	----------------------------------	-----	---	-----------------

\*Estimated by <sup>1</sup>H NMR spectra on an average of three integrals where possible. Typically the integrals were taken from the peaks due to the N=CH, N=C-CH<sub>3</sub> and N-NH environments.

### 2.3.6. Dissymmetric ligands with Me/H backbones

#### Overview of reaction

The synthesis of the dissymmetric ligands firstly requires the synthesis of a PADA-mono-substituted-3-thiosemicarbazone intermediate. This intermediate is synthesised by reacting PADA and a 4-substituted-3-thiosemicarbazone in the stoichiometric ratio of 1:1 under acidic conditions. Once isolated the intermediate is then reacted with 1 equivalent of a dissimilar 4-substituted-3-thiosemicarbazone catalysed under slightly acidic conditions to produce the desired dissymmetric ligand (Figure 2.3.6.1.).



	R <sub>1</sub>	R <sub>2</sub>	R <sub>3</sub>	R <sub>4</sub>
PADA-Me-NH <sub>2</sub>	CH <sub>3</sub>	H	H	H
PADA-Me-(Me) <sub>2</sub>	CH <sub>3</sub>	H	CH <sub>3</sub>	CH <sub>3</sub>
PADA-Me-Et	CH <sub>3</sub>	H	CH <sub>2</sub> CH <sub>3</sub>	H
PADA-Me-Ph	CH <sub>3</sub>	H	C <sub>6</sub> H <sub>5</sub>	H
PADA-Et-NH <sub>2</sub>	CH <sub>2</sub> CH <sub>3</sub>	H	H	H
PADA-Et-Me	CH <sub>2</sub> CH <sub>3</sub>	H	CH <sub>3</sub>	H
PADA-Et-(Me) <sub>2</sub>	CH <sub>2</sub> CH <sub>3</sub>	H	CH <sub>3</sub>	CH <sub>3</sub>

PADA-Et-Ph	CH <sub>2</sub> CH <sub>3</sub>	H	C <sub>6</sub> H <sub>5</sub>	H
PADA-Ph-NH <sub>2</sub>	C <sub>6</sub> H <sub>5</sub>	H	H	H
PADA-Ph-Me	C <sub>6</sub> H <sub>5</sub>	H	CH <sub>3</sub>	H
PADA-Ph-(Me) <sub>2</sub>	C <sub>6</sub> H <sub>5</sub>	H	CH <sub>3</sub>	CH <sub>3</sub>
PADA-Ph-Et	C <sub>6</sub> H <sub>5</sub>	H	CH <sub>2</sub> CH <sub>3</sub>	H

**Figure 2.3.6.1.** The general reaction for the synthesis of dissymmetric ligands with Me/H backbones.

**Figure 2.3.6.2-4.** Illustration of the dissymmetric ligands with Me/H backbones that have been synthesised.

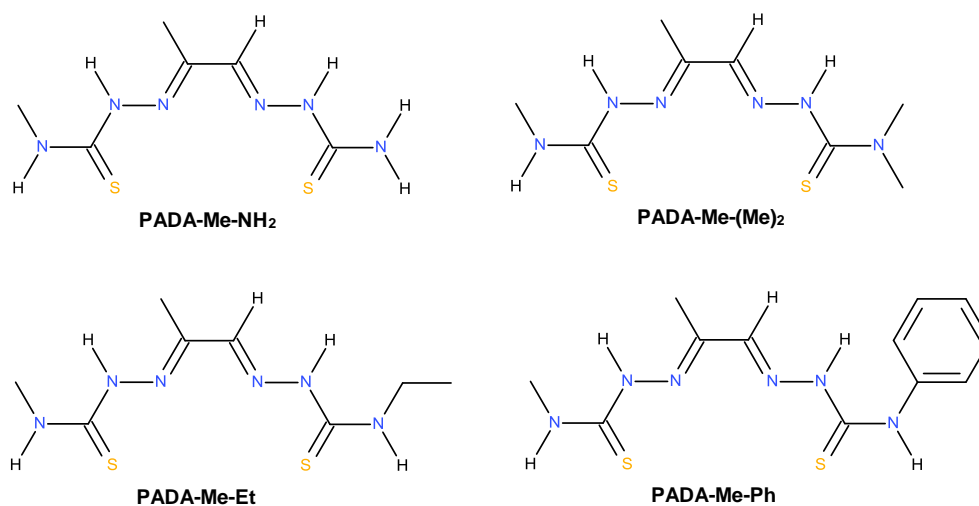


**Figure 2.3.6.2.** Dissymmetric ligands from PADA-Me=O.

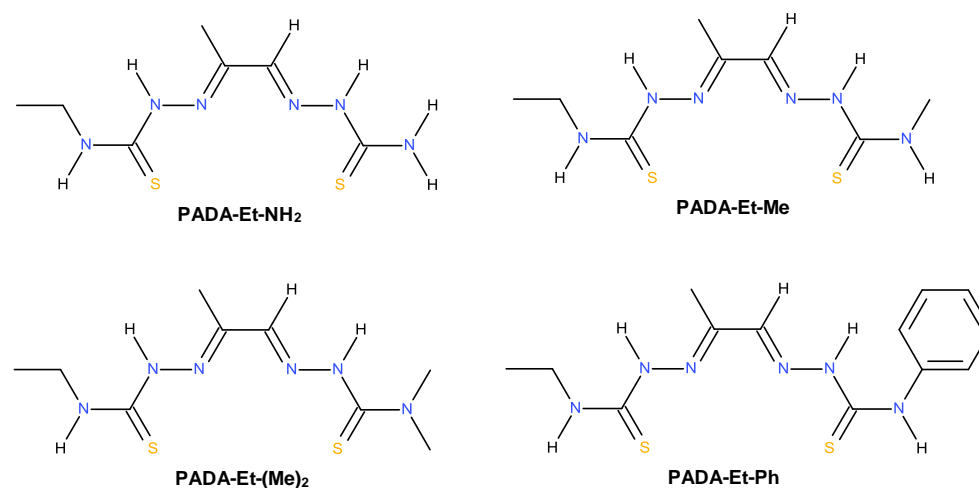


**Figure 2.3.6.3.** Dissymmetric ligands from PADA-Et=O.

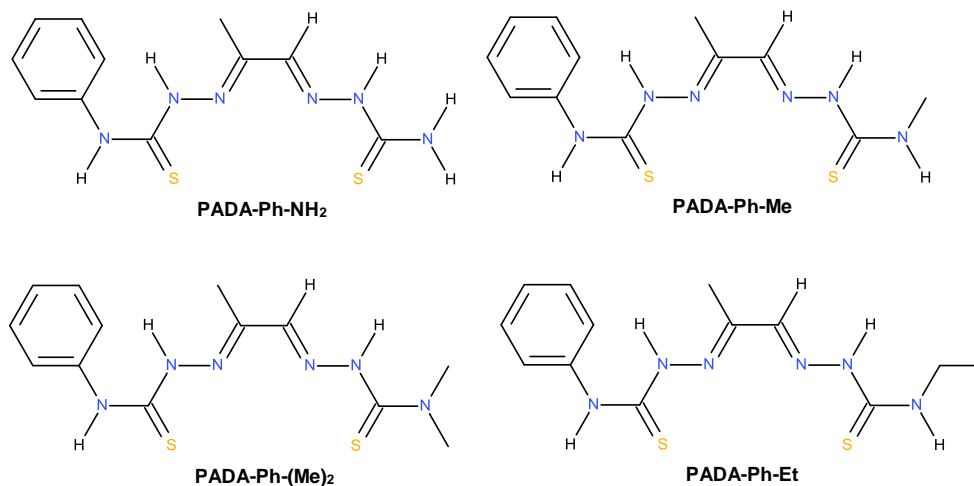


**Figure 2.3.6.4.** Dissymmetric ligands from PADA-Ph=O.

### **2.3.7. Synthesis of the PADA-mono-substituted-3-thiosemicarbazone intermediates**

In order to make the twelve dissymmetric ligands, these three intermediates had to be successfully synthesised (Figure 2.3.7.1.).

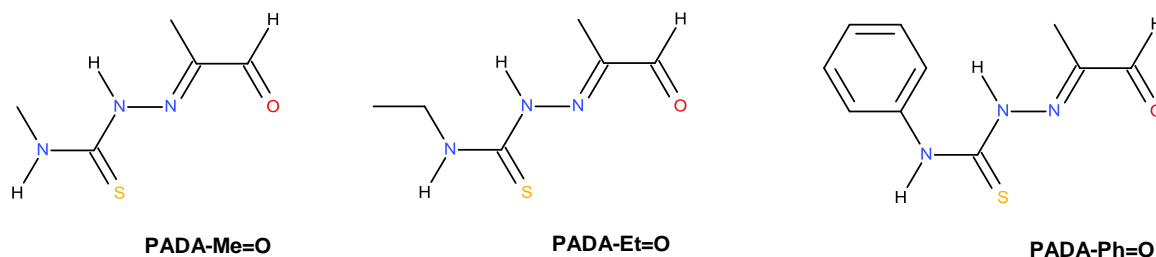


**Figure 2.3.7.1.** Structures of the three PADA-mono-substituted-3-thiosemicarbazone intermediates.

### **2.3.8. Methods**

#### **PADA-Me=O**

4-methyl-3-thiosemicarbazide (2.500 g, 0.024 mol) was dissolved in de-ionised water (100 mL, 50 °C) and HCl (32%, 5 drops) was added. Methylglyoxal-1,1-dimethylacetal (8.70 mL, 0.072 mol, 8.49 g) was added rapidly and vigorously stirred (50 °C, 5 minutes). The precipitate was recovered via filtration, washed with de-ionised water (10 x 50 mL) and dried. A yellow solid (2.473 g) was recovered (65% yield).

#### **PADA-Et=O**

4-ethyl-3-thiosemicarbazide (2.288 g, 0.0192 mol) was dissolved in de-ionised water (200 mL, warm), the insoluble particulates was filtered off and then the solution was cooled to room temperature. HCl was added (32%, 8 drops) followed by the rapid addition of methylglyoxal-1,1-dimethylacetal (6.96 mL, 0.058 mol, 6.79 g). The solution was vigorously stirred (50 °C, 1 hour).

The precipitate was recovered via filtration, washed with de-ionised water (8 x 50 mL) and dried. A pale yellow solid (2.047 g) was recovered (62% yield).

#### PADA-Ph=O

4-phenyl-3-thiosemicarbazide (0.803 g, 0.0048 mol) was dissolved in de-ionised water/ethanol solution (50 mL water, 25 mL ethanol, 50 °C). The insoluble particulates were filtered off and HCl (32%, 3 drops) was added. Methylglyoxal-1,1-dimethylacetal (1.74 mL, 0.0144 mol, 1.698 g) was added rapidly and the solution was vigorously stirred (50 °C, 5 minutes). The precipitate was recovered via filtration, washed with de-ionised water (2 x 50 mL) and dried. A yellow solid (0.821 g) was recovered (77% yield).

### 2.3.9. Characterisation data for the PADA-mono-substituted-3-thiosemicarbazone intermediates

#### PADA-Me=O

$^1\text{H NMR}$  (DMSO- $d_6$ , 400 MHz):  $\delta$ = 11.16 (s, 1 H, N-NH), 9.32 (s, 1 H, O=CH), 8.98 (m, 1 H, H<sub>3</sub>C-NH, J= 4.4 Hz), 2.98 (d, 3 H, HN-CH<sub>3</sub>, J= 4.4 Hz), 1.90 (s, 3 H, N=C-CH<sub>3</sub>).  $^{13}\text{C } \{^1\text{H}\}$  NMR (DMSO- $d_6$ , 100 MHz):  $\delta$ = 192.10 (C=O), 179.45 (C=S), 145.94 (C=N), 31.67 (HN-CH<sub>3</sub>), 9.66 (N=C-CH<sub>3</sub>). **IR (neat):**  $\text{cm}^{-1}$ = 3350 (m), 3171 (m), 2845 (w), 1692 (m), 1593 (m), 1537 (m), 1504 (s), 1410 (m), 1369 (m), 1200 (s), 1146 (m), 1113 (m), 1047 (s), 1001 (s), 856 (s), 789 (m), 665 (s), 592 (s), 569 (s), 534 (s). **Raman (neat):**  $\text{cm}^{-1}$ = 3354 (w), 3179 (w), 2921 (w), 2848 (w), 1696 (m), 1577 (s), 1433 (w), 1278 (w), 1227 (w), 1192 (w), 1116 (w), 1045 (w), 856 (w), 783 (w), 567 (w), 357 (w), 296 (w), 237 (w). **Melting point:** >156 °C (decomposed).

#### PADA-Et=O

$^1\text{H NMR}$  (DMSO- $d_6$ , 400 MHz):  $\delta$ = 11.08 (s, 1 H, N-NH), 9.34 (s, 1 H, O=CH), 9.01 (t, 1 H, H<sub>2</sub>C-NH, J= 5.6 Hz), 3.56 (dq, 2 H, H<sub>2</sub>C-NH, J= 7.2, 5.6 Hz), 1.90 (s, 3 H, N=C-CH<sub>3</sub>), 1.03 (t, 6 H, H<sub>2</sub>C-CH<sub>3</sub>, J= 7.2 Hz).  $^{13}\text{C } \{^1\text{H}\}$  NMR (DMSO- $d_6$ , 100 MHz):  $\delta$ = 191.18 (C=O), 178.41 (C=S), 146.00 (C=N), 39.19 (N-CH<sub>2</sub>), 14.54 (H<sub>2</sub>C-CH<sub>3</sub>), 9.68 (N=C-CH<sub>3</sub>). **IR (neat):**  $\text{cm}^{-1}$ = 3319 (w), 3142 (m), 2976 (w), 2835 (w), 1688 (s), 1587 (m), 1541 (s), 1489 (m), 1422 (m), 1368 (m), 1279 (m), 1188 (s), 1126 (s), 1086 (m), 1059 (m), 1007 (m), 939 (m), 849 (m), 710 (m), 660 (s), 538 (w). **Raman (neat):**  $\text{cm}^{-1}$ = 3325 (w), 3146 (w), 2910 (w), 2835 (w), 1686 (m), 1586 (s), 1437 (w), 1367 (w), 1331 (w), 1272 (w), 1183 (w), 1145 (w), 1121 (w), 1060 (w), 1008 (w), 938 (w), 811 (w), 776 (w), 668 (w), 626 (w), 578 (w), 540 (w), 374 (w). **Melting point:** >132-134°C.

#### PADA-Ph=O

$^1\text{H NMR}$  (d<sub>6</sub>-DMSO, 400 MHz):  $\delta$ = 11.49 (s, 1 H, N-NH), 10.57 (s, 1 H, Ph-NH), 9.45 (s, 1 H, O=CH), 7.53 (m, 2 H, H<sub>(2,6)</sub> aryl), 7.36 (m, 2 H, H<sub>(3,5)</sub> aryl), 7.20 (m, 1 H, H<sub>(4)</sub> aryl), 1.97 (s, 3 H, N=C-CH<sub>3</sub>).  $^{13}\text{C}$

**$\{^1\text{H}\}$  NMR** (DMSO- $d_6$ , 100 MHz):  $\delta$ = 192.57 (C=O), 178.24 (C=S), 146.53 (C=N), 139.48 (C<sub>(1)</sub> aryl), 139.11 (C<sub>(1)</sub> aryl), 128.33 (C<sub>(3,5)</sub> aryl), 126.40 (C<sub>(4)</sub> aryl), 126.24 (C<sub>(2,6)</sub> aryl), 9.88 (N=C-CH<sub>3</sub>). **IR (neat)**:  $\text{cm}^{-1}$ = 3277 (w), 3150 (m), 2968 (w), 2851 (w), 1697 (m), 1593 (m), 1520 (s), 1495 (s), 1447 (m), 1425 (m), 1366 (m), 1229 (m), 1167 (s), 1157 (s), 1119 (m), 1016 (m), 935 (m), 831 (m), 748 (m), 698 (s), 615 (s), 590 (s). **Raman (neat)**:  $\text{cm}^{-1}$ = 3283 (w), 3068 (w), 2918 (w), 2860 (w), 1695 (s), 1590 (s), 1518 (m), 1448 (w), 1346 (w), 1292 (m), 1227 (m), 1146 (m), 1117 (m), 1030 (w), 1005 (s), 933 (w), 834 (w), 770 (w), 752 (m), 680 (w), 617 (m), 607 (m), 448 (w), 411 (w), 269 (w).  
**Melting point**: >151 °C (decomposed).

### **2.3.10. Spectral examples of a PADA-mono-substituted-3-thiosemicarbazone intermediate**

**Figures 2.3.10.1-4.** Spectral examples of the PADA-mono-substituted-3-thiosemicarbazone intermediate PADA-Et=O.

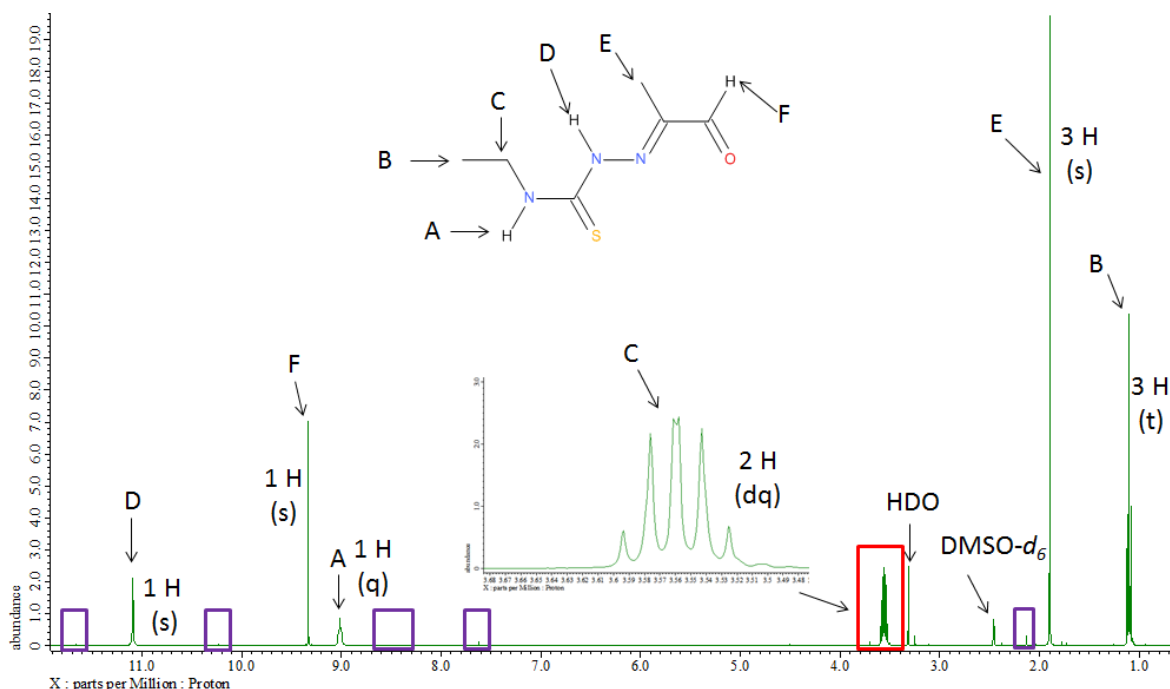


**Figure 2.3.10.1.** An assigned  $^1\text{H}$  NMR spectrum of PADA-Et=O, synthesised by the exploitation of carbonyl reactivity approach by reacting excess methylglyoxal-1,1-dimethylacetal with one equivalent of 4-ethyl-3-thiosemicarbazide. The purple boxes suggest a small impurity of PADA-Et-Et.

The purple boxes indicate a small presence of the related symmetric bis(thiosemicarbazone), in this example it is PADA-Et-Et. This is commonly seen in the other intermediate forming reactions of this class.

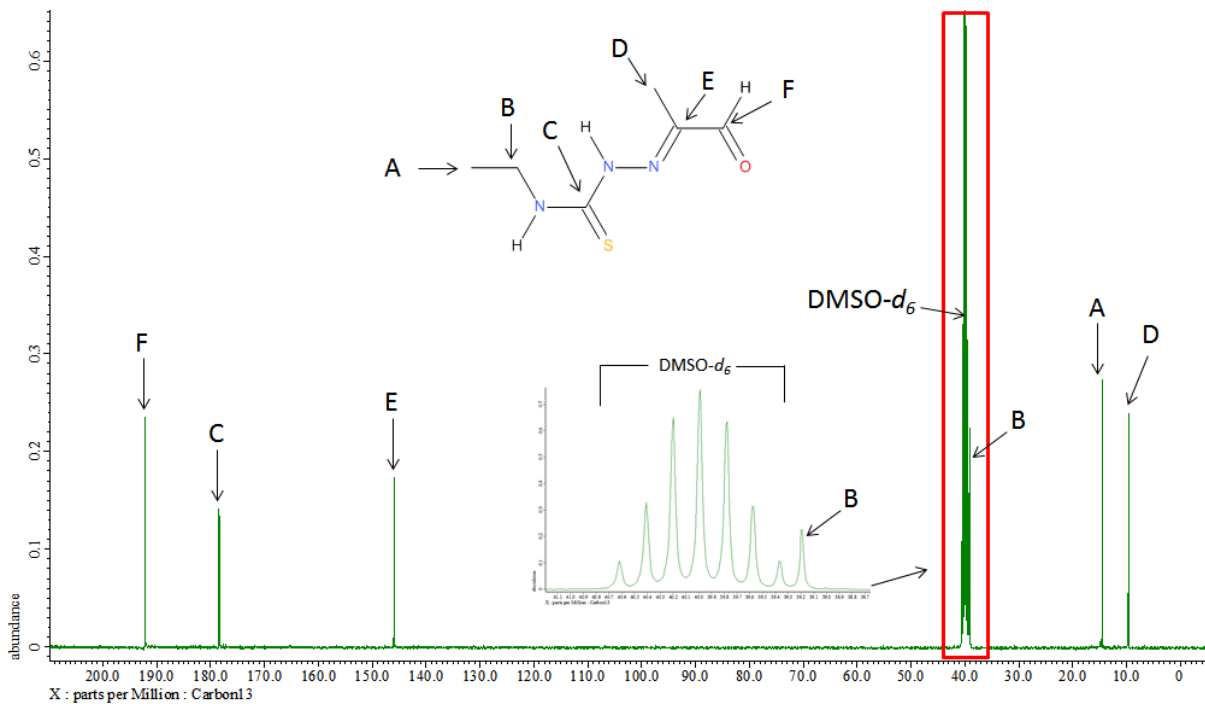


Figure 2.3.10.2. An assigned  $^{13}\text{C}$  NMR spectrum of PADA-Et=O.

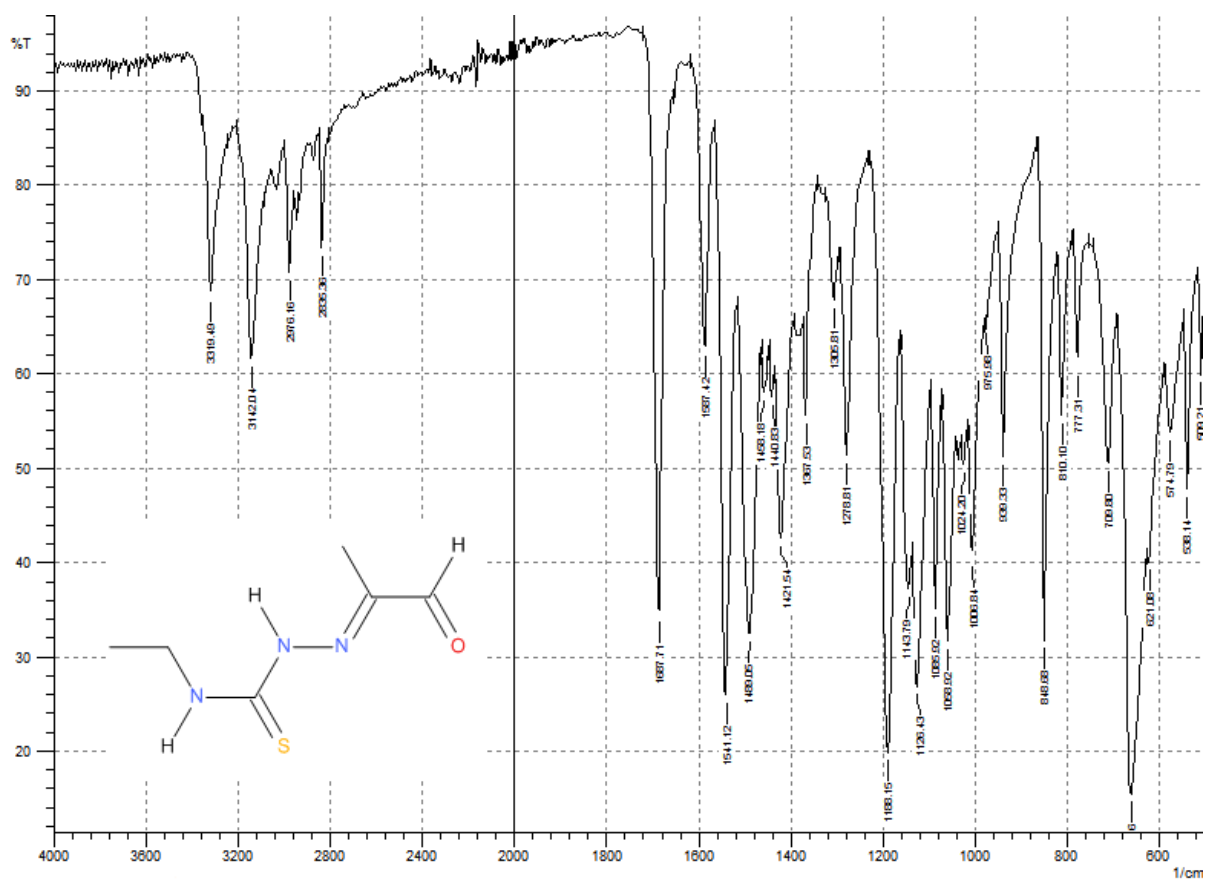
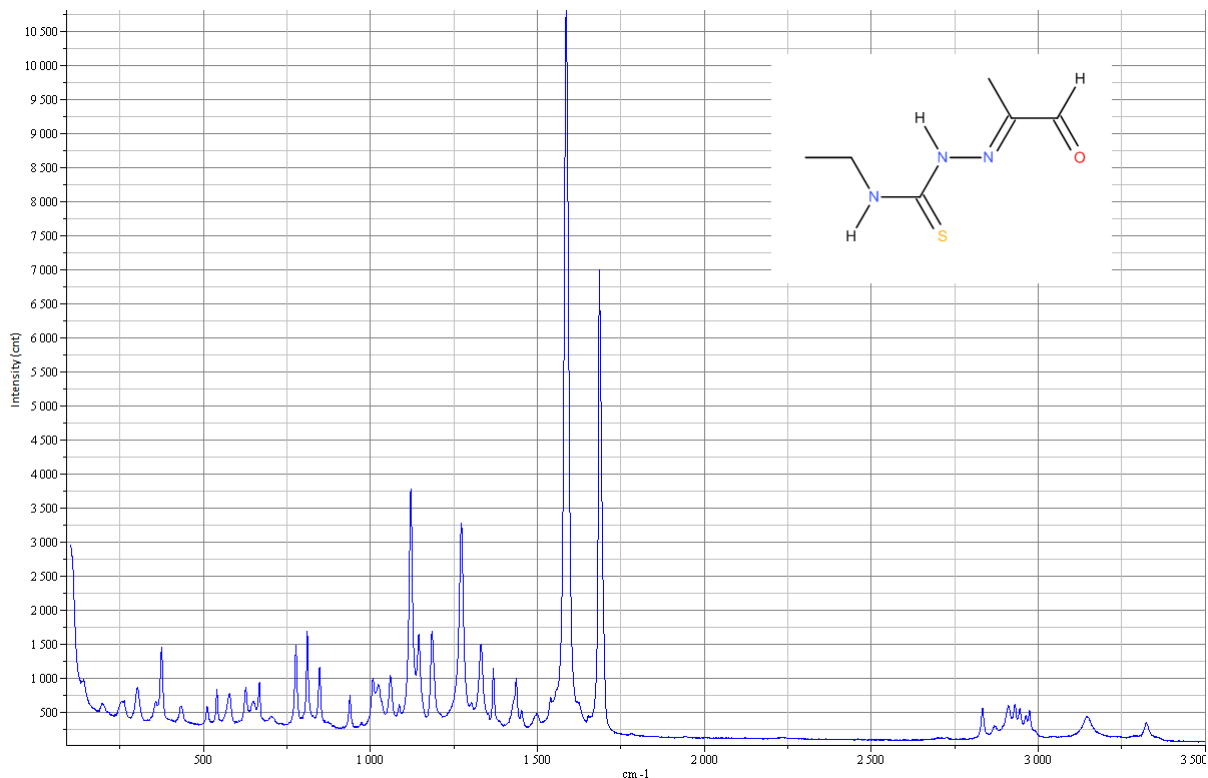


Figure 2.3.10.3. A FTIR spectrum of PADA-Et=O.



**Figure 2.3.10.4.** A Raman spectrum of PADA-Et=O.

### **2.3.11. Discussion**

All three intermediates were successfully made with a good level of purity. Obtaining the intermediates of this class by this method (Figure 2.3.6.1.) is believed to be novel. The only reports of methods found in the literature were either using methyl glyoxal as a precursor<sup>82</sup> or PADA followed by hydrolysis of the protecting acetal groups in a separate reaction by using  $\text{LiBF}_4$ .<sup>79-81</sup> For the same reasons for the symmetric ligands of this class, PADA was used because it was readily available from investigating the synthesis of dissymmetric ligands via the protection approach and also that PADA is cheaper than methyl glyoxal.

Using the method illustrated in (Figure 2.3.6.1.) it is theoretically possible that the formation of the mono-substituted-3-thiosemicarbazone could take two isomeric forms depending on which carbonyl group the chosen 4-substitued-3-thiosemicarbazide reacts with. The diagram below illustrates these forms (Figure 2.3.11.1.):

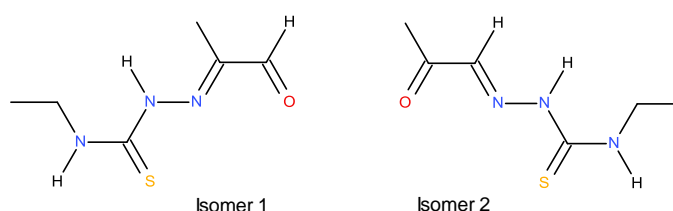


**Figure 2.3.11.1.** An Illustration of the isomeric forms of the mono-substituted-3-thiosemicarbazone intermediates.

By consulting the respective NMR spectra of the successfully synthesised intermediates it is possible to conclude that the intermediates are in the form of isomer 1. There are two peaks that relate to the environments that allows this to be claimed, the first is the singlets found between 9.32-9.45 ppm which relates to the O=C-H environments. The second is the singlets found between 1.90-1.97 ppm which relates to the N=C-CH<sub>3</sub> environments. If the intermediates were present in the same arrangement as isomer 2 then we would observe two different sets of peaks, the first owing to the N=C-H environment which would be expected between 7.61-7.84 ppm. The second set of peaks due to the O=C-CH<sub>3</sub> environment which would be predicted between 2.28-2.38 ppm. All of the NMR spectra contain a small presence of these peaks but it is thought that these are due to the formation of the related symmetric ligands as there are extra peaks that relate just to the symmetric ligands extra environments (Figure 2.3.10.1.). If this was not the case then a second peak would be present in the carbon spectra owing to the presence of a second carbonyl group, which is absent. Even though it must be highlighted that it is possible that isomer 2 is present, but in very small proportions that are not detectable in the carbon spectra. If this was the situation then it is still reasonable to claim that the vast majority of the intermediate is still present in the form of isomer 1.

The NMR spectra of the respective ligands suggest that the main impurity tends to be the symmetric ligand of the respective mono-substituted-3-thiosemicarbazone despite the addition of excess PADA (typically 3 equivalents). By comparing the <sup>1</sup>H NMR integrals of the intermediate and the symmetric by-product it is estimated that the symmetric by-product does not occur in the three intermediate samples in quantities larger than 5%. In the case of the synthesis of PADA-Ph=O there is sign of one or more impurities in low proportions which are absent in the NMR spectra of PADA-Me=O and PADA-Et=O. No investigation was taken to identify these other impurities, these impurities may be cyclisation products PADA-Ph=O of which similar structures have been observed in the literature.<sup>57-59, 87, 88, 205</sup>

Attempts were made to synthesise the intermediate PADA-NH<sub>2</sub>=O by using a similar method to the other three, but it was found that the formation of PADA-NH<sub>2</sub>-NH<sub>2</sub> as a by-product is a little more favourable giving rise to an elevated level of contamination of the desirable intermediate by the PADA-NH<sub>2</sub>-NH<sub>2</sub> product. When the reaction was run at 50 °C it was found that PADA-NH<sub>2</sub>-NH<sub>2</sub> became the major product (circa 90 %) and the desired PADA-NH<sub>2</sub>=O intermediate only present in about 10 % despite the presence of the large excess of PADA. The same reaction was run at room temperature instead of 50 °C and it was found that the resulting product contained only about 13 % of the symmetric by-product and the PADA-NH<sub>2</sub>=O intermediate became the major product at 87 %. One explanation for this is that the evaluated temperature coupled with the effects of the NH<sub>2</sub> substituent increases the reactivity of the aldehyde group so that it has a



similar reactivity to the methyl ketone making the formation of the PADA-NH<sub>2</sub>-NH<sub>2</sub> by product more favourable than the formation of the PADA-NH<sub>2</sub>=O intermediate. This was not seen with the other 4-substituted-3-thiosemicarbazides so it is reasonable to suggest that this is due to a property unique to thiosemicarbazide. As the brief was to make lipophilic ligands the decision was made to not pursue the clean synthesis of the PADA-NH<sub>2</sub>=O intermediate as the NH<sub>2</sub> substituent is likely to make the resulting ligand more hydrophilic instead of lipophilic. It was however, possible to make isomers with NH<sub>2</sub> substituents from the intermediates already synthesised, without the need for the PADA-NH<sub>2</sub>=O intermediate. For example, PADA-Me-NH<sub>2</sub> can be synthesised from the intermediate PADA-Me=O which is the isomer of PADA-NH<sub>2</sub>-Me. If it was found that the presence of the NH<sub>2</sub> substituent is favourable then the clean synthesis of the PADA-NH<sub>2</sub>=O intermediate can be revisited.

It was decided not to attempt the synthesis of the intermediate PADA-(Me)<sub>2</sub>=O due to the high cost of 4,4-dimethyl-3-thiosemicarbazide, coupled with the expected low yields which would give un-workable quantities of intermediate. However, if ligands from the PADA-(Me)<sub>2</sub>=O intermediate was desirable then this synthesis can be pursued.

Despite two of out of the three intermediates being previously reported in the literature<sup>79-81</sup> there is scarce information in terms of characterisation data for the intermediates as the authors seem to only report data for the final ligand/complex. There is a report of NMR (<sup>1</sup>H + <sup>13</sup>C) data for the intermediate PADA-Me=O.<sup>206</sup> The NMR data reported was all in accord with the data obtained except for two proton peak assignments. The literature assignments for the proton environments at 11.18 and 9.36 were N-NH and O=CH respectively. This thesis reports the proton environments at 11.16 and 9.32 were O=CH and N-NH respectively. HMQC NMR spectrum shows a coupling between the O=CH proton at 9.32 ppm and O=CH at 192.10 ppm. Also the HMBC NMR spectrum shows that the peak 9.32 has a coupling to the backbone environments C-CH<sub>3</sub> and C-CH<sub>3</sub> but no coupling between these carbon environments and the proton peak at 11.16. This supports the assignments for the proton environments at 11.18 and 9.36 being N-NH and O=CH respectively. Despite no literature NMR data for the other two intermediates, their proton and carbon peak positions show strong similarity for the positions reported for PADA-Me=O, discounting any expected shift in the peaks and extra peaks due to varying substituents on the terminal amine. There are reports of NMR data for the intermediate BDO-Ph=O<sup>57, 83, 190</sup> and BDO-Et=O<sup>57</sup> which can be used for a partial comparison to the intermediates PADA-Ph=O and PADA-Et=O respectively. Excluding the peaks attributing to the structural variations of the two intermediates BDO-Ph=O and PADA-Ph=O, the NMR data is in accord to the peak locations and assignments for the novel PADA-Ph=O intermediate. This is also the case for BDO-Et=O and PADA-Et=O.

J. Holland *et al.*<sup>57</sup> has attempted to assign the carbon environments in the NMR spectra of BDO-Ph=O of which the meta and ortho assignments agree with the above assignments. However there is a discrepancy between the assignments for the peaks at 139.48 and 126.40ppm. J. Holland *et al.*<sup>57</sup> assigned the two peaks as C<sub>4</sub> aryl and C<sub>1</sub> aryl respectively while this thesis assigns the peaks at 139.48 and 126.40 ppm as C<sub>1</sub> aryl and C<sub>4</sub> aryl respectively. The reason the latter assignments are believed to be true is that HMQC NMR data on 4-Phenylthiosemicarbazide shows couplings to support these assignments.

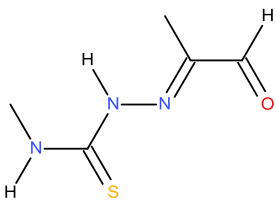
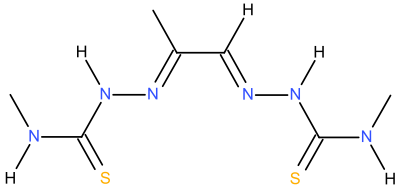
It was not possible to find any reports of IR data for the intermediates of this class, this was even the case for the well reported intermediates with Me/Me on the backbone where only NMR data or mass spectrometry data is reported. The IR spectra of all three samples show peaks in the regions expected for the characteristic functional groups (Table 2.3.11.2.). These assignments were made based on reported IR data of bis(thiosemicarbazone) ligands<sup>78,80</sup> and IR spectroscopy text books.<sup>207, 208</sup>

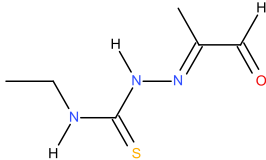
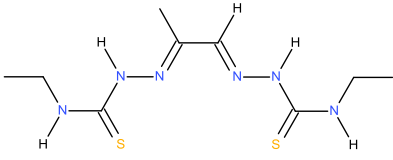
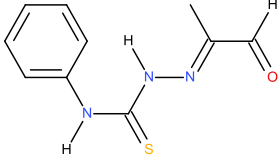
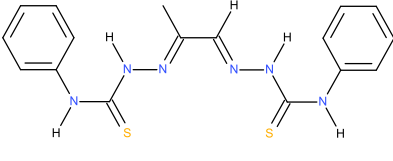
Intermediate	N-H	C=O	C=N	C=S
PADA-Me=O	3352	1697	1537	831
PADA-Et=O	3319	1687	1541	848
PADA-Ph=O	3277	1692	1519	856

**Table 2.3.11.2.** Tentative assignment of IR peaks of key functional groups in PADA-mono-substituted-3-thiosemicarbazone intermediates.

The table below (Table 2.3.11.3.) illustrates all three intermediates, what the main impurity is and an estimate of percentage impurity.

**Table 2.3.11.3.** Summary of purity for the PADA-mono-substituted-3-thiosemicarbazone intermediates, synthesised by the exploitation of carbonyl reactivity approach.

Intermediate	Novel	Yield	Main impurity	Estimated impurity *
PADA-Me=O 	No <sup>79-</sup> 82	65%		1%

<p>PADA-Et=O</p> 	No <sup>80</sup>	62%		2%
<p>PADA-Ph=O</p> 	Yes	77%		5%

\*Estimated by <sup>1</sup>H NMR spectra on an average of three integrals where possible. Typically the integrals were taken from the peaks due to the N=CH, N=C-CH<sub>3</sub> and N-NH environments.

### **2.3.12. Dissymmetric ligands from PADA-Me=O**

#### **Methods**

##### **PADA-Me-NH<sub>2</sub>**

PADA-Me=O (0.510 g, 0.0032 mol) was dissolved in DMF (3 mL) and filtered. Thiosemicarbazide (0.292 g, 0.0032 mol) was dissolved in DMF (10 mL), HCl (10%, 2 drops) was added and filtered. The two solutions were combined and left to stir (room temperature, 5 hours). De-ionised water (26 mL) was added, the precipitate was filtered off and washed with de-ionised water (50 mL, room temperature and 50 mL, 80 °C). The crude product was dissolved in DMSO (10 mL) the resulting solution was filtered and recrystallised with de-ionised water (20 mL). The precipitate was recovered via filtration, washed with de-ionised water (50 mL, room temperature and 50 mL, 80 °C) and dried. A white solid (0.456 g) was recovered (61% yield).

##### **PADA-Me-(Me)<sub>2</sub>**

PADA-Me=O (0.255 g, 0.0016 mol) was dissolved in DMF (1.5 mL) and filtered. 4,4-dimethyl-3-thiosemicarbazide (0.191 g, 0.0016 mol) was dissolved in DMF (3 mL), HCl (10%, 1 drop) was added and filtered. The two solutions were combined and left to stir (room temperature, 5 hours). De-ionised water (9 mL) was added, the precipitate was filtered off and washed with de-ionised water (50 mL, room temperature and 50 mL, 80°C). The crude product was dissolved in DMSO (9 mL), filtered and recrystallised with de-ionised water (18 mL). The precipitate was recovered by filtration, washed with de-ionised water (50 mL) and dried. A yellow solid (0.158 g) was recovered (38% yield).

### PADA-Me-Et

PADA-Me=O (0.255 g, 0.0016 mol) was dissolved in DMF (1 mL) and filtered. 4-ethyl-3-thiosemicarbazide (0.191 g, 0.0016 mol) was dissolved in DMF (5 mL), HCl (10%, 1 drop) was added and filtered. The two solutions were combined and left to stir (room temperature, 5 hours). De-ionised water (12 mL) was added, the precipitate was filtered and washed with de-ionised water (50 mL, room temperature and 50 mL, 80 °C). The crude product was dissolved in DMSO (6 mL), filtered and recrystallised with de-ionised water (12 mL). The precipitate was recovered by filtration, washed with de-ionised water (50 mL) and dried. A cream solid (0.191 g) was recovered (46% yield).

### PADA-Me-Ph

PADA-Me=O (0.255 g, 0.0016 mol) was dissolved in DMF (2 mL) and filtered. 4-phenyl-3-thiosemicarbazide (0.268 g, 0.0016 mol) was dissolved in DMF (2.5 mL), HCl (10%, 1 drop) was added and filtered. The two solutions were combined and left to stir (room temperature, 5 hours). De-ionised water (9 mL) was added, the precipitate was filtered and washed with de-ionised water (50 mL, room temperature and 50 mL, 80 °C). The crude product was dissolved in DMSO (12 mL), filtered and recrystallised with de-ionised water (24 mL). The precipitate was recovered by filtration, washed with ethanol (2 x 25mL), de-ionised water (50 mL, 80 °C) and dried. An off white solid (0.313 g) was recovered (63% yield).

### Characterisation data for dissymmetric ligands from PADA-Me=O

#### PADA-Me-NH<sub>2</sub>

<sup>1</sup>H NMR (DMSO-*d*<sub>6</sub>, 400 MHz): δ= 11.66 (s, 1 H, N-NH), 10.35 (s, 1 H, N-NH), 8.50 (q, 1 H, H<sub>3</sub>C-NH, J= 4.8 Hz), 8.28 (s, 1 H C-NH), 7.87 (s, 1 H C-NH), 7.61 (s, 1 H, N=CH), 2.94 (d, 3 H, HN-CH<sub>3</sub>, J= 4.8 Hz), 2.09 (s, 3 H, N=C-CH<sub>3</sub>). <sup>13</sup>C {<sup>1</sup>H} NMR (DMSO-*d*<sub>6</sub>, 100 MHz): δ= 178.76 (C=S), 178.59 (C=S), 147.54 (C=N), 142.95 (C=N), 31.58 (HN-CH<sub>3</sub>), 11.52 (N=C-CH<sub>3</sub>). IR (neat): cm<sup>-1</sup>= 3414 (w), 3148 (m), 1988 (w), 1607 (m), 1531 (s), 1497 (s), 1458 (m), 1364 (m), 1335 (m), 1269 (m), 1217 (s), 1155 (m), 1070 (s), 924 (m), 833 (s), 656 (m), 565 (s). Raman (neat): cm<sup>-1</sup>= 2915 (w), 1672 (w), 1600 (m), 1585 (s), 1374 (w), 1336 (w), 1268 (w), 1223 (w), 1126 (w), 1013 (w), 878 (w), 792 (w), 481 (w), 307 (w), 219 (w). Elemental analysis: Found: C, 31.1; H, 5.1; N, 36.1. Calc. for C<sub>6</sub>H<sub>12</sub>N<sub>6</sub>S<sub>2</sub>: C, 31.0; H, 5.1; N, 36.2%. Melting point: >217 °C (decomposed).

#### PADA-Me-(Me)<sub>2</sub>

<sup>1</sup>H NMR (DMSO-*d*<sub>6</sub>, 400 MHz): δ= 11.19 (s, 1 H, N-NH), 10.41 (s, 1 H, N-NH), 8.45 (q, 1 H, H<sub>3</sub>C-NH, J= 4.4 Hz), 7.72 (s, 1 H, N=CH), 3.21 (s, 6 H, HN-(CH<sub>3</sub>)<sub>2</sub>), 2.95 (d, 3 H, HN-CH<sub>3</sub>, J= 4.4 Hz), 2.05 (s, 3

H, N=C-CH<sub>3</sub>). <sup>13</sup>C {<sup>1</sup>H} NMR (DMSO-*d*<sub>6</sub>, 100 MHz): δ= 181.06 (C=S), 178.82 (C=S), 147.56 (C=N), 143.95 (C=N), 42.96 (N-(CH<sub>3</sub>)<sub>2</sub>), 31.56 (HN-CH<sub>3</sub>), 11.65 (N=C-CH<sub>3</sub>). IR (neat): cm<sup>-1</sup>= 3306 (m), 3200 (m), 2999 (w), 1589 (w), 1526 (s), 1495 (s), 1406 (m), 1354 (m), 1273 (s), 1225 (s), 1142 (m), 1107 (s), 1045 (s), 966 (m), 935 (s), 878 (m), 812 (m), 658 (m), 623 (s), 584 (s), 565 (s). Raman (neat): cm<sup>-1</sup>= 1589 (m), 1570 (s), 1417 (m), 1363 (m), 1295 (m), 1275 (m), 1225 (m), 1143 (m), 1064 (m), 1016 (m), 876 (m), 744 (m), 583 (w), 314 (w), 131 (w). Elemental analysis: Found: C, 37.0; H, 6.2; N, 32.2. Calc. for C<sub>8</sub>H<sub>16</sub>N<sub>6</sub>S<sub>2</sub>: C, 36.9; H, 6.2; N, 32.3%. Melting point: >205 °C (decomposed).

#### PADA-Me-Et

<sup>1</sup>H NMR (DMSO-*d*<sub>6</sub>, 400 MHz): δ= 11.68 (s, 1 H, N-NH), 10.33 (s, 1 H, N-NH), 8.50 (q, 1 H, H<sub>3</sub>C-NH, J= 4.4 Hz), 8.42 (t, 1 H H<sub>2</sub>C-NH, J= 6.0 Hz), 7.62 (s, 1 H, N=CH), 3.52 (dq, 2 H, H<sub>2</sub>C-NH, J=7.2, 6.0 Hz), 2.94 (d, 3 H, N-CH<sub>3</sub>, J= 4.4 Hz), 2.13 (s, 3 H, N=C-CH<sub>3</sub>), 1.08 (t, 3 H, H<sub>2</sub>C-CH<sub>3</sub>, J= 7.2 Hz). <sup>13</sup>C {<sup>1</sup>H} NMR (DMSO-*d*<sub>6</sub>, 100 MHz): δ= 178.75 (C=S), 177.17 (C=S), 147.64 (C=N), 142.44 (C=N), 38.86 (N-CH<sub>2</sub>), 31.58 (N-CH<sub>3</sub>), 15.01 (H<sub>2</sub>C-CH<sub>3</sub>), 11.68 (N=C-CH<sub>3</sub>). IR (neat): cm<sup>-1</sup>= 3374 (w), 3316 (w), 3165 (w), 2988 (w), 1537 (s), 1497 (s), 1435 (m), 1412 (m), 1327 (m), 1219 (s), 1159 (m), 1084 (s), 1042 (m), 935 (m), 814 (m), 664 (m), 619 (m), 546 (s). Raman (neat): cm<sup>-1</sup>= 2902 (w), 1580 (s), 1518 (w), 1364 (w), 1284 (w), 1220 (w), 1130 (w), 1016 (w), 879 (w), 773 (w), 572 (w), 461 (w), 307 (w), 236 (w), 180 (w). Elemental analysis: Found: C, 37.0; H, 6.25; N, 32.2. Calc. for C<sub>8</sub>H<sub>16</sub>N<sub>6</sub>S<sub>2</sub>: C, 36.9; H, 6.2; N, 32.3%. Melting point: >220 °C (decomposed).

#### PADA-Me-Ph

<sup>1</sup>H NMR (DMSO-*d*<sub>6</sub>, 400 MHz): δ= 12.06 (s, 1 H, N-NH), 10.40 (s, 1 H, N-NH), 9.97 (s, 1 H, Ph-NH), 8.55 (q, 1 H, CH<sub>3</sub>-NH, J=4.4 Hz), 7.73 (s, 1 H, N=CH), 7.48 (d, 2 H, H<sub>(2,6)</sub> aryl, J=8.0 Hz), 7.33 (dd, 2 H, H<sub>(3,5)</sub> aryl, J=8.0 Hz), 7.17 (dd, 1 H, H<sub>(4)</sub> aryl, J=8.0 Hz), 2.96 (d, 3 H, N-CH<sub>3</sub>, J= 4.4 Hz), 2.18 (s, 3 H, N=C-CH<sub>3</sub>). <sup>13</sup>C {<sup>1</sup>H} NMR (DMSO-*d*<sub>6</sub>, 100 MHz): δ= 178.79 (C=S), 176.68 (C=S), 147.50 (C=N), 143.50 (C=N), 139.44 (C<sub>(1)</sub> aryl), 128.63 (C<sub>(3,5)</sub> aryl), 126.53 (C<sub>(4)</sub> aryl), 126.06 (C<sub>(2,6)</sub> aryl), 31.61 (N-CH<sub>3</sub>), 11.71 (N=C-CH<sub>3</sub>). IR (neat): cm<sup>-1</sup>= 3331 (w) cm<sup>-1</sup>, 3285 (w) cm<sup>-1</sup>, 3136 (w) cm<sup>-1</sup>, 2988 (w) cm<sup>-1</sup>, 1589 (w) cm<sup>-1</sup>, 1541 (s) cm<sup>-1</sup>, 1499 (s) cm<sup>-1</sup>, 1449 (m) cm<sup>-1</sup>, 1400 (m) cm<sup>-1</sup>, 1356 (m) cm<sup>-1</sup>, 1315 (m) cm<sup>-1</sup>, 1263 (m) cm<sup>-1</sup>, 1200 (s) cm<sup>-1</sup>, 1072 (s) cm<sup>-1</sup>, 934 (m) cm<sup>-1</sup>, 745 (m) cm<sup>-1</sup>, 691 (m) cm<sup>-1</sup>, 665 (m) cm<sup>-1</sup>, 635 (m) cm<sup>-1</sup>, 569 (s) cm<sup>-1</sup>. Raman (neat): cm<sup>-1</sup>= 3044 (w) cm<sup>-1</sup>, 1585 (s) cm<sup>-1</sup>, 1513 (w) cm<sup>-1</sup>, 1367 (w) cm<sup>-1</sup>, 1278 (w) cm<sup>-1</sup>, 1236 (w) cm<sup>-1</sup>, 1118 (w) cm<sup>-1</sup>, 1016 (w) cm<sup>-1</sup>, 934 (w) cm<sup>-1</sup>, 873 (w) cm<sup>-1</sup>, 745 (w) cm<sup>-1</sup>, 638 (w) cm<sup>-1</sup>, 410 (w) cm<sup>-1</sup>, 290 (w) cm<sup>-1</sup>, 224 (w) cm<sup>-1</sup>. Elemental analysis: Found: C, 46.7; H, 5.1; N, 27.2. Calc. for C<sub>12</sub>H<sub>16</sub>N<sub>6</sub>S<sub>2</sub>: C, 46.7; H, 5.2; N, 27.25%. Melting point: >205 °C (decomposed).

### **2.3.13. Dissymmetric ligands from PADA-Et=O**

#### **Methods**

##### **PADA-Et-NH<sub>2</sub>**

PADA-Et=O (0.554 g, 0.0032 mol) was dissolved in DMF (2 mL) and filtered. Thiosemicarbazide (0.292 g, 0.0032 mol) was dissolved in DMF (10 mL), HCl (10%, 2 drops) was added and filtered. The two solutions were combined and left to stir (room temperature, 5 hours). De-ionised water (24 mL) was added, the precipitate was filtered off and washed with de-ionised water (50 mL, room temperature and 50 mL, 80 °C). The crude product was dissolved in DMSO (25 mL), filtered and recrystallised with de-ionised water (50 mL). The precipitate was recovered by filtration, washed with de-ionised water (50 mL, room temperature and 50 mL, 80 °C), and dried. An off white solid (0.386 g) was recovered (49% yield).

##### **PADA-Et-Me**

PADA-Et=O (0.554 g, 0.0032 mol) was dissolved in DMF (2 mL) and filtered. 4-methyl-3-thiosemicarbazide (0.337 g, 0.0032 mol) was dissolved in DMF (6 mL), HCl (10%, 2 drops) was added and filtered. The two solutions were combined and left to stir (room temperature, 5 hours). De-ionised water (50 mL) was added, a gelatinous precipitate was recovered by filtration and washed with de-ionised water (50 mL, room temperature and 50 mL, 80 °C). The crude product was left on the water pump until its volume decreased then dissolved in DMSO (6 mL), filtered and recrystallised with de-ionised water (60 mL). The waxy gelatinous precipitate was recovered by filtration, washed with de-ionised water (50 mL, room temperature and 50 mL, 80 °C), and dried. The product was further washed with de-ionised water (50 mL, room temperature and 50 mL, 80 °C), and dried. A yellowish white solid (0.118 g) was recovered (14% yield).

##### **PADA-Et-(Me)<sub>2</sub>**

PADA-Et=O (0.277 g, 0.0016 mol) was dissolved in DMF (1.5 mL) and filtered. 4,4-dimethyl-3-thiosemicarbazide (0.191 g, 0.0016 mol) was dissolved in DMF (3 mL), HCl (10%, 1 drop) was added and filtered. The two solutions were combined and left to stir (room temperature, 5 hours). De-ionised water (24 mL) was added, the precipitate was filtered and washed with de-ionised water (2 x 50 mL). The crude product was dissolved in DMSO (7 mL), filtered and recrystallised with de-ionised water (14 mL). The precipitate was recovered by filtration, washed with de-ionised water (50 mL, 80 °C) and dried. A yellow solid (0.117 g) was recovered (27% yield).

## Characterisation data for dissymmetric ligands from PADA-Et=O

### PADA-Et-NH<sub>2</sub>

**<sup>1</sup>H NMR** (DMSO-*d*<sub>6</sub>, 400 MHz): δ = 11.65 (s, 1 H, N-NH), 10.26 (s, 1 H, N-NH), 8.53 (t, 1 H H<sub>2</sub>C-NH, J = 6.0 Hz), 8.28 (s, 1 H, C-NH), 7.88 (s, 1 H, C-NH), 7.62 (s, 1 H, N=CH), 3.52 (dq, 2 H, H<sub>2</sub>C-NH, J = 7.2, 6.0 Hz), 2.09 (s, 3 H, N=C-CH<sub>3</sub>), 1.07 (t, 3 H, H<sub>2</sub>C-CH<sub>3</sub>, J = 7.2 Hz). **<sup>13</sup>C {<sup>1</sup>H} NMR** (DMSO-*d*<sub>6</sub>, 100 MHz): δ = 178.57 (C=S), 177.67 (C=S), 147.62 (C=N), 142.93 (C=N), 38.99 (N-CH<sub>2</sub>), 14.87 (H<sub>2</sub>C-CH<sub>3</sub>), 11.53 (N=C-CH<sub>3</sub>). **IR (neat)**: cm<sup>-1</sup> = 3292 (w), 3148 (m), 2982 (m), 1593 (m), 1530 (s), 1493 (s), 1456 (m), 1352 (m), 1310 (m), 1269 (m), 1202 (s), 1090 (s), 926 (m), 829 (s), 662 (m), 548 (s). **Raman (neat)**: cm<sup>-1</sup> = 2978 (w), 2908 (w), 1583 (s), 1425 (w), 1350 (w), 1270 (w), 1209 (w), 1128 (w), 1014 (w), 936 (w), 874 (w), 800 (w), 483 (w), 307 (w), 209 (w). **Elemental analysis**: Found: C, 34.0; H, 5.8; N, 34.0. Calc. for C<sub>7</sub>H<sub>14</sub>N<sub>6</sub>S<sub>2</sub>: C, 34.1; H, 5.7; N, 34.1%. **Melting point**: >207 °C (decomposed).

### PADA-Et-Me

**<sup>1</sup>H NMR** (DMSO-*d*<sub>6</sub>, 400 MHz): δ = 11.71 (s, 1 H, N-NH), 10.24 (s, 1 H, N-NH), 8.53 (t, 1 H H<sub>2</sub>C-NH, J = 6.0 Hz), 8.39 (q, 1 H, H<sub>3</sub>C-NH, J = 4.4 Hz), 7.62 (s, 1 H, N=CH), 3.52 (dq, 2 H, H<sub>2</sub>C-NH, J = 7.2, 6.0 Hz), 2.95 (d, 3 H, N-CH<sub>3</sub>, J = 4.4 Hz), 2.12 (s, 3 H, N=C-CH<sub>3</sub>), 1.07 (t, 3 H, H<sub>2</sub>C-CH<sub>3</sub>, J = 7.2 Hz). **<sup>13</sup>C {<sup>1</sup>H} NMR** (DMSO-*d*<sub>6</sub>, 100 MHz): δ = 178.23 (C=S), 177.69 (C=S), 147.70 (C=N), 142.37 (C=N), 39.00 (N-CH<sub>2</sub>), 31.47 (N-CH<sub>3</sub>), 14.87 (H<sub>2</sub>C-CH<sub>3</sub>), 11.62 (N=C-CH<sub>3</sub>). **IR (neat)**: cm<sup>-1</sup> = 3366 (w), 3129 (w), 2982 (w), 1518 (s), 1491 (s), 1425 (m), 1364 (m), 1242 (m), 1204 (s), 1076 (s), 1040 (m), 914 (m), 812 (m), 631 (m), 600 (m), 540 (s). **Raman (neat)**: cm<sup>-1</sup> = 1581 (s), 1434 (w), 1362 (w), 1328 (w), 1275 (w), 1204 (w), 1125 (w), 1023 (w), 917 (w), 873 (w), 774 (w), 598 (w), 420 (w), 298 (w), 211 (w). **Elemental analysis**: Found: C, 37.0; H, 6.3; N, 32.2. Calc. for C<sub>8</sub>H<sub>16</sub>N<sub>6</sub>S<sub>2</sub>: C, 36.9; H, 6.2; N, 32.3%. **Melting point**: >220 °C (decomposed).

### PADA-Et-(Me)<sub>2</sub>

**<sup>1</sup>H NMR** (DMSO-*d*<sub>6</sub>, 400 MHz): δ = 11.18 (s, 1 H, N-NH), 10.36 (s, 1 H, N-NH), 8.46 (t, 1 H H<sub>2</sub>C-NH, J = 6.0 Hz), 7.75 (s, 1 H, N=CH), 3.52 (dq, 2 H, H<sub>2</sub>C-NH, J = 7.2, 6.0 Hz), 3.21 (s, 6 H, HN-(CH<sub>3</sub>)<sub>2</sub>), 2.05 (s, 3 H, N=C-CH<sub>3</sub>), 1.08 (t, 3 H, H<sub>2</sub>C-CH<sub>3</sub>, J = 7.2 Hz). **<sup>13</sup>C {<sup>1</sup>H} NMR** (DMSO-*d*<sub>6</sub>, 100 MHz): δ = 181.00 (C=S), 177.76 (C=S), 147.57 (C=N), 144.09 (C=N), 42.90 (HN-(CH<sub>3</sub>)<sub>2</sub>), 39.00 (N-CH<sub>2</sub>), 14.87 (H<sub>2</sub>C-CH<sub>3</sub>), 11.67 (N=C-CH<sub>3</sub>). **IR (neat)**: cm<sup>-1</sup> = 3341 (w), 3134 (m), 2988 (m), 1589 (w), 1526 (s), 1489 (s), 1410 (m), 1348 (m), 1269 (s), 1206 (s), 1140 (m), 1049 (s), 920 (s), 868 (m), 806 (m), 783 (m), 660 (m), 625 (m), 581 (m) cm<sup>-1</sup>. **Raman (neat)**: cm<sup>-1</sup> = 2936 (w), 1575 (s), 1361 (w), 1284 (w), 1274 (w), 1206 (w), 1143 (w), 1102 (w), 1016 (w), 964 (w), 934 (w), 870 (w), 742 (w), 626 (w), 308 (w). **Elemental analysis**: Found: C, 39.4; H, 6.7; N, 30.6. Calc. for C<sub>9</sub>H<sub>18</sub>N<sub>6</sub>S<sub>2</sub>: C, 39.4; H, 6.6; N, 30.6%. **Melting point**: >180 °C (decomposed).

### **2.3.14. Dissymmetric ligands from PADA-Ph=O**

#### **Methods**

##### **PADA-Ph-NH<sub>2</sub>**

PADA-Ph=O (0.354 g, 0.0016 mol) was dissolved in DMF (2.5 mL) and filtered. Thiosemicarbazide (0.146 g, 0.0016 mol) was dissolved in DMF (5 mL), HCl (10%, 1 drop) was added and filtered. The two solutions were combined and left to stir (room temperature, 5 hours). De-ionised water (15 mL) was added, the precipitate was filtered and washed with de-ionised water (50 mL, room temperature and 50 mL, 80 °C). The crude product was dissolved in DMSO (7 mL), filtered and recrystallised with de-ionised water (14 mL). The precipitate was recovered by filtration, washed with de-ionised water (50 mL, room temperature and 50 mL, 80 °C), and dried. An off yellowish white solid (0.273 g) was recovered (58% yield).

##### **PADA-Ph-Me**

PADA-Ph=O (0.354 g, 0.0016 mol) was dissolved in DMF (2.5 mL) and filtered. 4-methyl-3-thiosemicarbazide (0.168 g, 0.0016 mol) was dissolved in DMF (4 mL), HCl (10%, 1 drop) was added and filtered. The two solutions were combined and left to stir (room temperature, 5 hours). De-ionised water (13 mL) was added, the precipitate was filtered and washed with de-ionised water (50 mL, room temperature and 50 mL, 80 °C). The crude product was dissolved in DMSO (10 mL), filtered and recrystallised with de-ionised water (20 mL). The precipitate was recovered by filtration, washed with de-ionised water (50 mL, room temperature and 50 mL, 80 °C), and dried. An off cream solid (0.319 g) was recovered (65% yield).

##### **PADA-Ph-Et**

PADA-Ph=O (0.354 g, 0.0016 mol) was dissolved in DMF (2.5 mL) and filtered. 4-ethyl-3-thiosemicarbazide (0.191 g, 0.0016 mol) was dissolved in DMF (5 mL), HCl (10%, 1 drop) was added and filtered. The two solutions were combined and left to stir (room temperature, 5 hours). De-ionised water (15 mL) was added, the precipitate was filtered and washed with de-ionised water (50 mL, room temperature and 50 mL, 80 °C). The crude product was dissolved in DMSO (11 mL), filtered and recrystallised with de-ionised water (22 mL). The precipitate was recovered by filtration, washed with de-ionised water (50 mL, room temperature and 50 mL, 80 °C), and dried. A yellowish cream solid (0.309 g) was recovered (60% yield).



## Characterisation data for dissymmetric ligands from PADA-Ph=O

### PADA-Ph-NH<sub>2</sub>

<sup>1</sup>H NMR (DMSO-*d*<sub>6</sub>, 400 MHz): δ= 11.70 (s, 1 H, N-NH), 10.71 (s, 1 H, N-NH), 10.15 (s, 1 H, Ph-NH), 8.32 (s, 1 H, C-NH), 7.92 (s, 1 H, C-NH), 7.71 (s, 1 H, N=CH), 7.50 (d, 2 H, *H*<sub>(2,6)</sub> aryl, J=8.0 Hz), 7.31 (dd, 2 H, *H*<sub>(3,5)</sub> aryl, J=8.0 Hz), 7.15 (dd, 1 H, *H*<sub>(4)</sub> aryl, J=8.0 Hz), 2.16 (s, 3 H, N=C-CH<sub>3</sub>). <sup>13</sup>C {<sup>1</sup>H} NMR (DMSO-*d*<sub>6</sub>, 100 MHz): δ= 178.71 (C=S), 177.27 (C=S), 148.54 (C=N), 142.93 (C=N), 139.48 (C<sub>(1)</sub> aryl), 128.64 (C<sub>(3,5)</sub> aryl), 126.09 (C<sub>(4)</sub> aryl), 125.91 (C<sub>(2,6)</sub> aryl), 11.77 (N=C-CH<sub>3</sub>). IR (neat): cm<sup>-1</sup>= 3449 (w), 3296 (w), 3157 (m), 2974 (w), 1595 (m), 1516 (s), 1493 (s), 1447 (m), 1366 (m), 1335 (m), 1267 (m), 1250 (m), 1179 (s), 1090 (s), 1069 (m), 1024 (m), 935 (m), 824 (m), 756 (m), 694 (s), 588 (s). Raman (neat): cm<sup>-1</sup>= 3054 (w), 1580 (w), 1373 (w), 1277 (w), 1253 (w), 1172 (w), 1124 (w), 1017 (w), 937 (w), 870 (w), 781 (w), 758 (w), 608 (w), 423 (w), 259 (w), 206 (w). Elemental analysis: Found: C, 44.7; H, 4.8; N, 28.5. Calc. for C<sub>11</sub>H<sub>14</sub>N<sub>6</sub>S<sub>2</sub>: C, 44.9; H, 4.8; N, 28.55%. Melting point: >215 °C (decomposed).

### PADA-Ph-Me

<sup>1</sup>H NMR (DMSO-*d*<sub>6</sub>, 400 MHz): δ= 11.77 (s, 1 H, N-NH), 10.70 (s, 1 H, N-NH), 10.14 (s, 1 H, Ph-NH), 8.43 (q, 1 H, H<sub>3</sub>C-NH, J= 4.4 Hz), 7.71 (s, 1 H, N=CH), 7.50 (d, 2 H, *H*<sub>(2,6)</sub> aryl, J=8.0 Hz), 7.31 (dd, 2 H, *H*<sub>(3,5)</sub> aryl, J=8.0 Hz), 7.15 (dd, 1 H, *H*<sub>(4)</sub> aryl, J=8.0 Hz), 2.96 (d, 3 H, N-CH<sub>3</sub>, J= 4.4 Hz), 2.20 (s, 3 H, N=C-CH<sub>3</sub>). <sup>13</sup>C {<sup>1</sup>H} NMR (DMSO-*d*<sub>6</sub>, 100 MHz): δ= 178.29 (C=S), 177.23 (C=S), 148.63 (C=N), 142.39 (C=N), 139.48 (C<sub>(1)</sub> aryl), 128.64 (C<sub>(3,5)</sub> aryl), 126.06 (C<sub>(4)</sub> aryl), 125.89 (C<sub>(2,6)</sub> aryl), 31.49 (N-CH<sub>3</sub>), 11.87 (N=C-CH<sub>3</sub>). IR (neat): cm<sup>-1</sup>= 3291 (w), 3157 (w), 2999 (w), 1595 (w), 1518 (s), 1495 (s), 1477 (s), 1447 (m), 1352 (m), 1250 (m), 1173 (s), 1090 (m), 1038 (m), 932 (m), 797 (m), 748 (m), 687 (m), 559 (s). Raman (neat): cm<sup>-1</sup>= 1577 (s), 1514 (w), 1367 (w), 1286 (w), 1247 (w), 1174 (w), 1128 (w), 1020 (w), 934 (w), 874 (w), 773 (w), 602 (w), 541 (w), 435 (w), 194 (w). Elemental analysis: Found: C, 46.6; H, 5.2; N, 27.6. Calc. for C<sub>12</sub>H<sub>16</sub>N<sub>6</sub>S<sub>2</sub>: C, 46.7; H, 5.2; N, 27.25%. Melting point: >210 °C (decomposed).

### PADA-Ph-Et

<sup>1</sup>H NMR (DMSO-*d*<sub>6</sub>, 400 MHz): δ= 11.71 (s, 1 H, N-NH), 10.69 (s, 1 H, N-NH), 10.15 (s, 1 H, Ph-NH), 8.47 (t, 1 H H<sub>2</sub>C-NH, J= 6.0 Hz), 7.71 (s, 1 H, N=CH), 7.50 (d, 2 H, *H*<sub>(2,6)</sub> aryl, J=8.0 Hz), 7.32 (dd, 2 H, *H*<sub>(3,5)</sub> aryl, J=8.0 Hz), 7.15 (dd, 1 H, *H*<sub>(4)</sub> aryl, J=8.0 Hz), 3.54 (dq, 2 H, H<sub>2</sub>C-NH, J=7.2, 6.0 Hz), 2.21 (s, 3 H, N=C-CH<sub>3</sub>), 1.09 (t, 3 H, H<sub>2</sub>C-CH<sub>3</sub>, J= 7.2 Hz). <sup>13</sup>C {<sup>1</sup>H} NMR (DMSO-*d*<sub>6</sub>, 100 MHz): δ= 177.24 (C=S), 148.63 (C=N), 142.42 (C=N), 139.48 (C<sub>(1)</sub> aryl), 128.64 (C<sub>(3,5)</sub> aryl), 126.06 (C<sub>(4)</sub> aryl), 125.90 (C<sub>(2,6)</sub> aryl), 38.90 (N-CH<sub>2</sub>), 15.00 (H<sub>2</sub>C-CH<sub>3</sub>), 11.93 (N=C-CH<sub>3</sub>). IR (neat): cm<sup>-1</sup>= 3294 (w), 3132 (m), 2970 (w), 1591 (w), 1518 (s), 1491 (s), 1447 (m), 1335 (m), 1277 (m), 1227 (s), 1182 (s), 1123 (m),

1072 (m), 937 (m), 787 (m), 748 (m), 696 (s), 635 (m), 577 (s). **Raman (neat):**  $\text{cm}^{-1}$  = 2966 (w), 1582 (s), 1445 (w), 1372 (w), 1253 (w), 1177 (m), 1125 (w), 1019 (w), 924 (w), 865 (w), 751 (w), 527 (w), 419 (w), 293 (w), 206 (w). **Elemental analysis:** Found: **C**, 48.3; **H**, 5.6; **N**, 26.0. Calc. for  $\text{C}_{13}\text{H}_{18}\text{N}_6\text{S}_2$ : **C**, 48.4; **H**, 5.6; **N**, 26.0%. **Melting point:**  $>207^\circ\text{C}$  (decomposed).

### 2.3.15 Spectral examples of a dissymmetric ligand with a Me/H backbone

**Figures 2.3.15.1-4.** Spectral examples of the dissymmetric ligand PADA-Me-Ph.

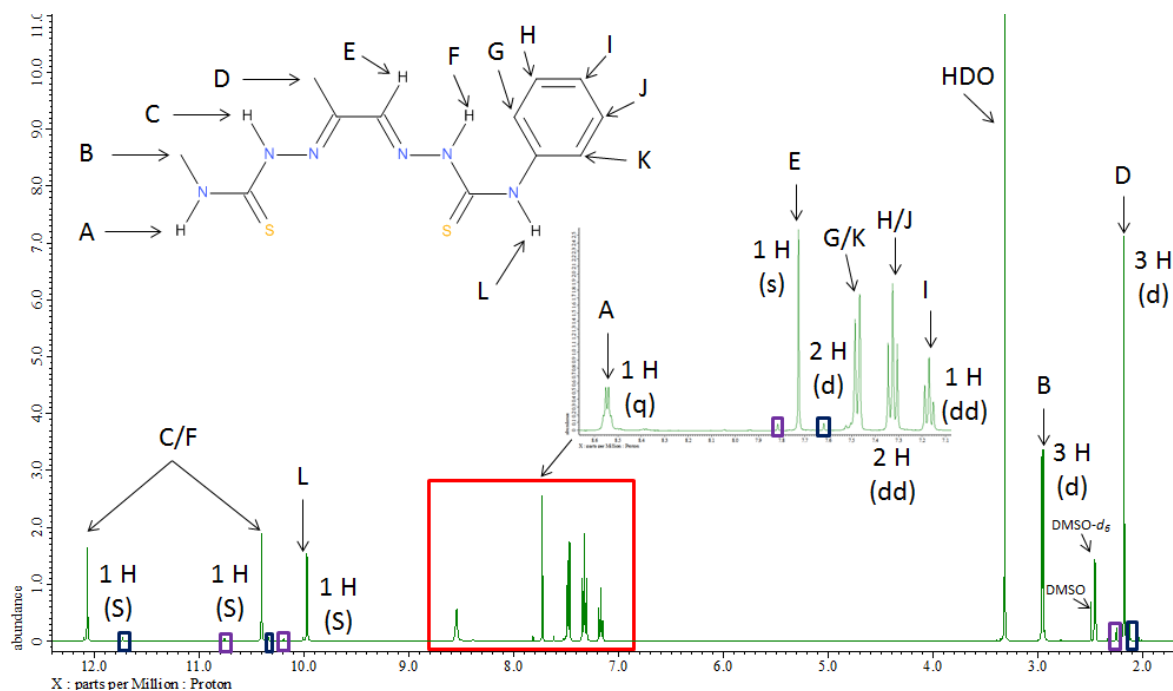


**Figure 2.3.15.1.** An assigned  $^1\text{H}$  NMR spectrum of PADA-Me-Ph, successfully synthesised by reacting PADA-Me-O with 4-phenyl-3-thiosemicarabzide. The spectrum suggests a small presence of PADA-Ph-Ph (purple box) and PADA-Me-Me (Blue box). This is commonly seen in other dissymmetric ligand reactions of this class.

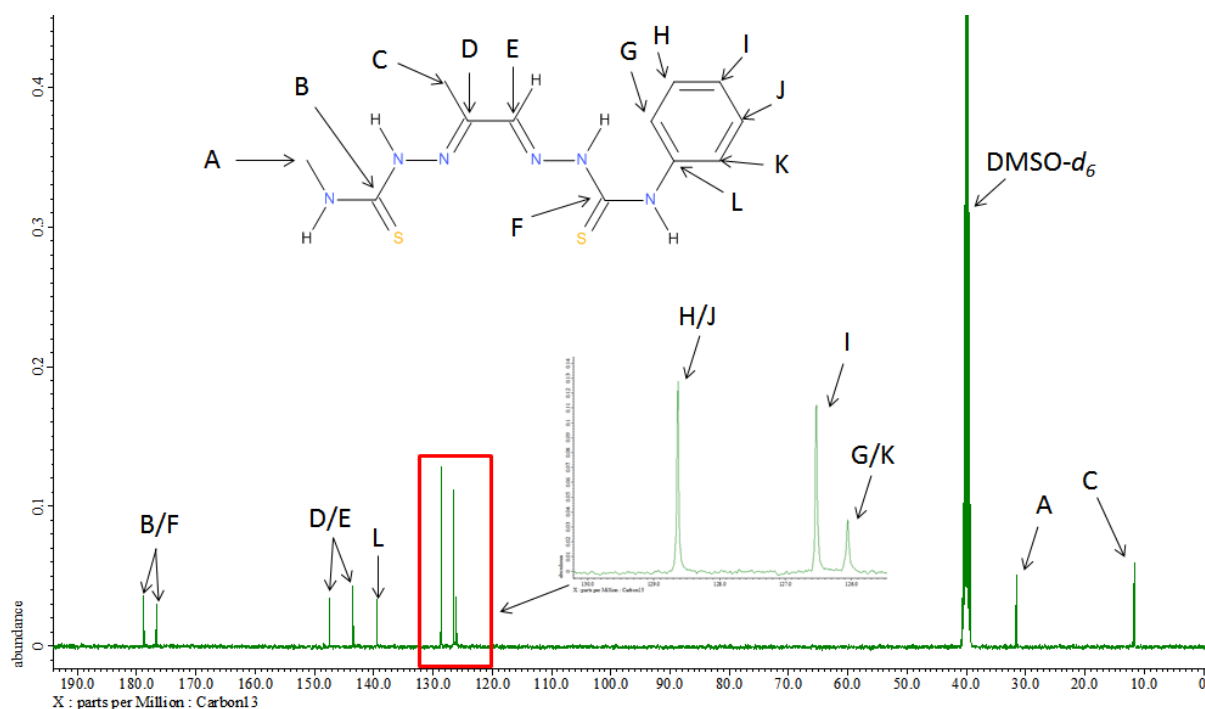


**Figure 2.3.15.2.** An assigned  $^{13}\text{C}$  NMR spectrum of PADA-Me-Ph.

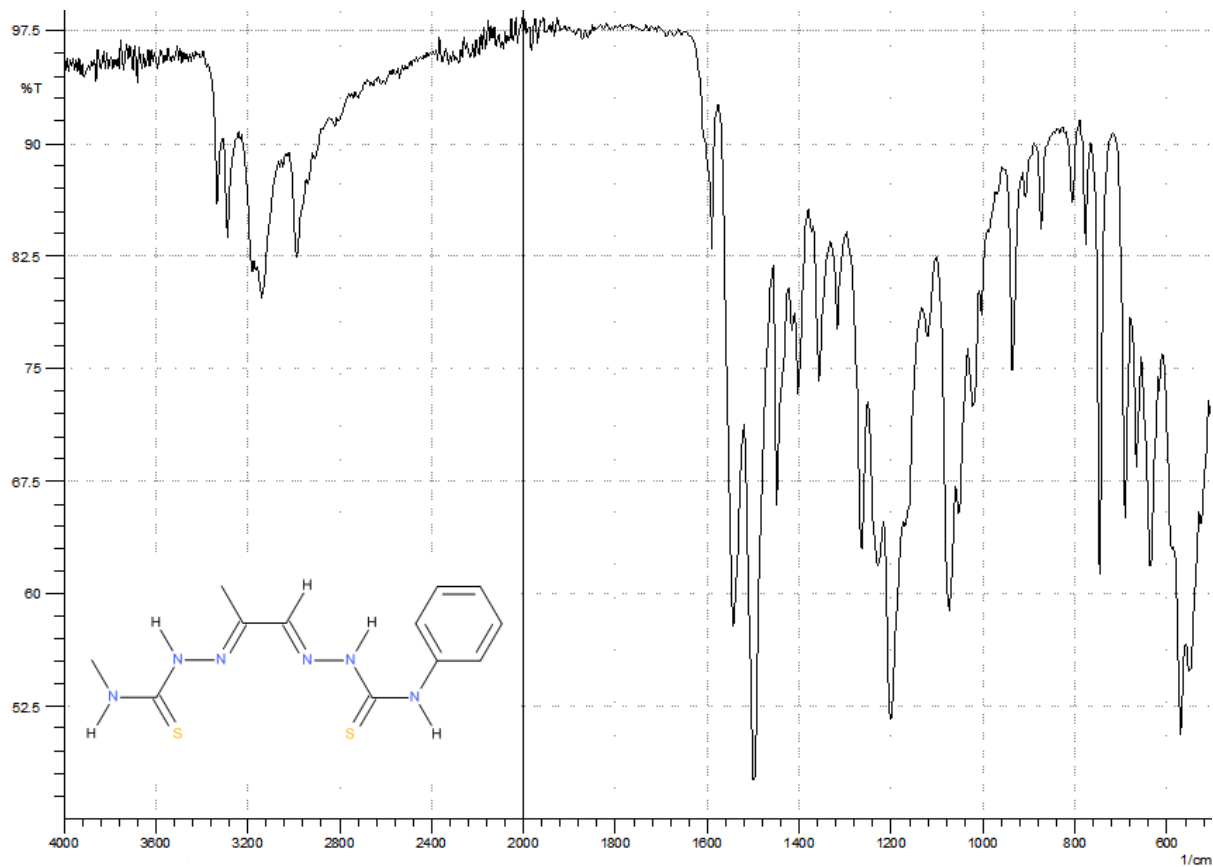


Figure 2.3.15.3. A FTIR spectrum of PADA-Me-Ph.

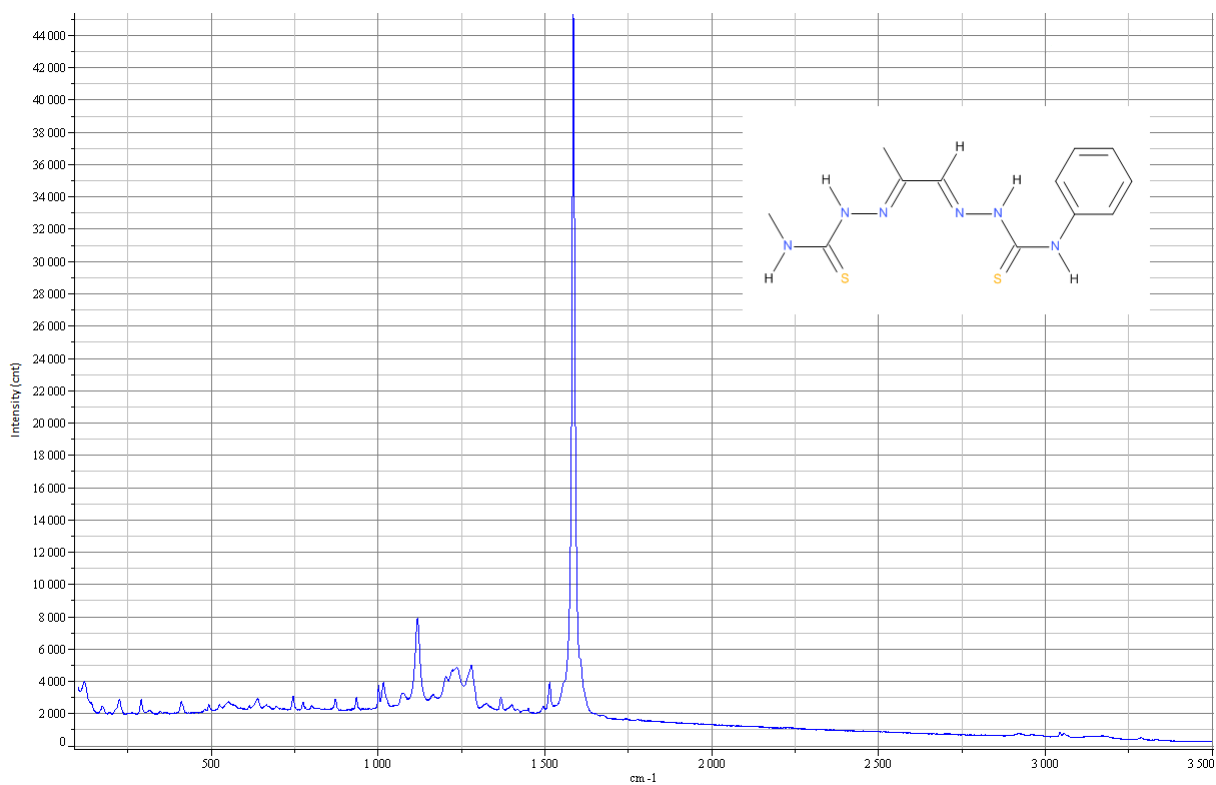


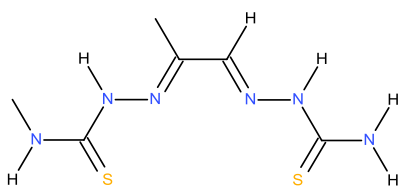
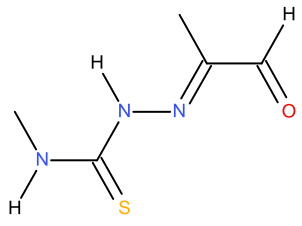
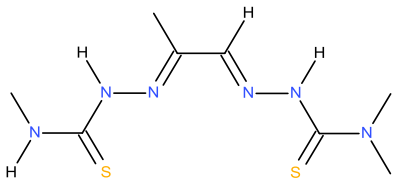
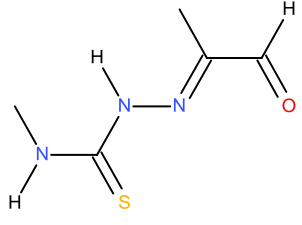
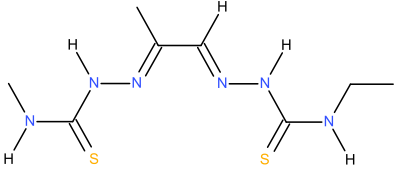
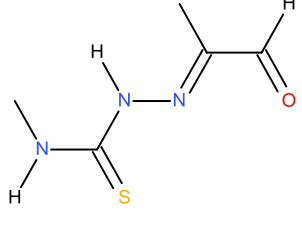
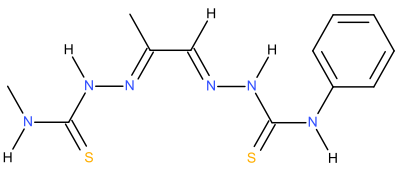
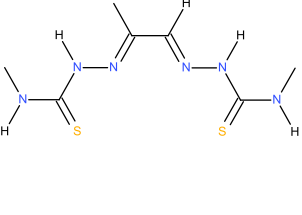
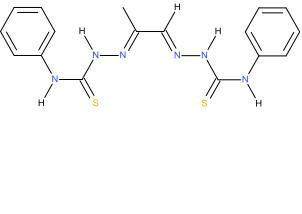
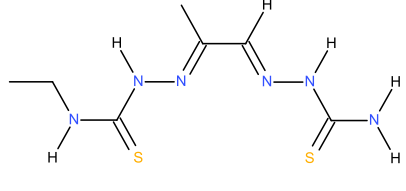
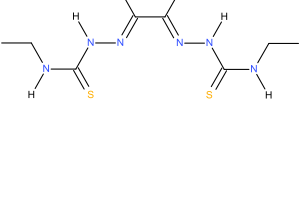
Figure 2.3.15.4. A Raman spectrum of PADA-Me-Ph.

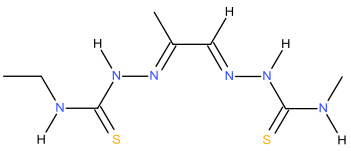
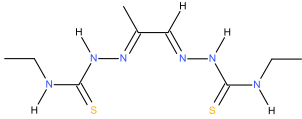
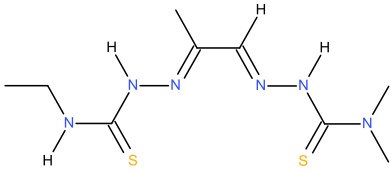
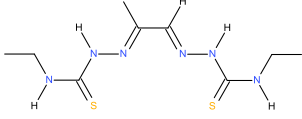
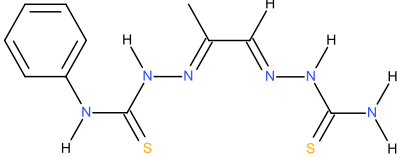
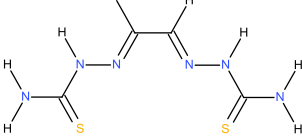
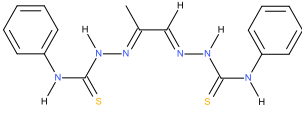
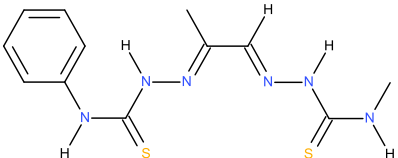
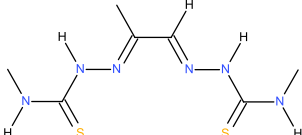
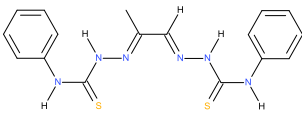
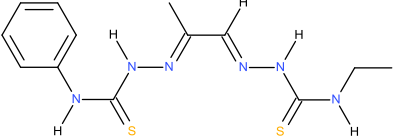
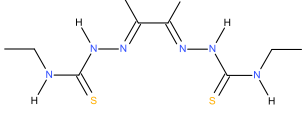
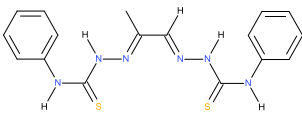
### **2.3.16. Discussion**

All ten ligands were synthesised with varying levels of purity by following a slightly altered version of a previously reported method.<sup>82</sup> Most of the ligands are expected to present in purity of in an excess of 90% except for the ligands synthesised from PADA-Ph=O where the purity percentage falls mostly to the high 80% mark. Despite almost identical reaction conditions attempts to synthesise ligands PADA-Ph-(Me)<sub>2</sub> and PADA-Et-Ph resulted in large impurity (10-25%) of the symmetric ligand PADA-Ph-Ph. One explanation for this is could be that 4-phenyl-3-thiosemicarbazide has the ability to displace the thiosemicarbazone from the intermediate hence promoting the 'scrambling' of the dissimilar arms. It was decided to not pursue the synthesis of the PADA-Ph-(Me)<sub>2</sub> and PADA-Et-Ph ligands. The table below (Table 2.3.16.1.) illustrates all twelve dissymmetric ligands, what the main impurity is and an estimate of percentage impurity.

There is a little more published characterisation data for the dissymmetric ligands of this class. The proton and carbon NMR data of PADA-Me-(Me)<sub>2</sub> has been reported before.<sup>206</sup> The data that was collected in this project closely agrees with the reported literature. This was also the case for PADA-Et-Me which also matched the reported literature<sup>81</sup> in terms of peak positions. One discrepancy was the assignment of the peaks at 8.53 ppm and 8.39 ppm. The literature reported the 8.53 ppm peak as a doublet and the 8.39 ppm position as a triplet and assigning them as the *NHCH*<sub>3</sub> and *NHC*<sub>2</sub>H<sub>5</sub> environments respectively. In this project the 8.53 ppm peak resembled a triplet and the one at 8.39 ppm as a quartet. Based on these splitting patterns the 8.53 peak was assigned as the *NHC*<sub>2</sub>H<sub>5</sub> proton and the peak at 8.39 as the *NHCH*<sub>3</sub> environment. These assignments are backed up in other ligands synthesised with methyl and/or ethyl groups on the terminal amine. In the same article<sup>81</sup> a melting point for PADA-Et-Me was given as 228-230°C which is similar to the melting point of 220°C observed however it was suspected that instead of melting the ligand decomposed as the sample started to turn brown. Infrared data was reported by L. Ackerman *et al.*<sup>80</sup> for ligands PADA-Me-Et and PADA-Et-Me. The recorded IR positions show close agreement the C=S bond however there was discrepancies of a few tens of wavenumbers for the C=N, R-N-H and N-N-H bonds.

**Table 2.3.16.1.** Summary of purity for the dissymmetric Ligands with CH<sub>3</sub>/H backbones, synthesised by the exploitation of carbonyl reactivity approach.

Ligand	Novel	Yield	Main impurity	Estimated impurity *
<b>PADA-Me-NH<sub>2</sub></b> 	No <sup>79</sup>	61%		Less than 1%
<b>PADA-Me-(Me)<sub>2</sub></b> 	No <sup>82</sup>	38%		Less than 1%
<b>PADA-Me-Et</b> 	No <sup>66, 80</sup>	46%		Less than 1%
<b>PADA-Me-Ph</b> 	Yes	63%	 	3%  3%
<b>PADA-Et-NH<sub>2</sub></b> 	Yes	49%		3%

<p><b>PADA-Et-Me</b></p> 	No <sup>80</sup> , 81	14%		Not possible to obtain an integral due to overlapping peaks.
<p><b>PADA-Et-(Me)<sub>2</sub></b></p> 	Yes	27%		7%
<p><b>PADA-Ph-NH<sub>2</sub></b></p> 	Yes	58%	 	2% 4%
<p><b>PADA-Ph-Me</b></p> 	Yes	65%	 	7% 5%
<p><b>PADA-Ph-Et</b></p> 	Yes	60%	 	5% 5%

\*Estimated by <sup>1</sup>H NMR spectra on an average of three integrals where possible. Typically the integrals were taken from the peaks due to the N=CH, N=C-CH<sub>3</sub> and N-NH environments.

## 2.4. Ligands with Me/Me backbones

### Application

This class of ligands along with ligands with Me/Me backbones are of interest for the imaging of hypoxia tissues which can be pathologies in a range of diseases including heart disease and cancer.<sup>105, 109, 111</sup> In order to do this, the complex must be able to migrate to the tissue and be reduced in hypoxic conditions, but not in normoxic conditions. The reduction of the ligand will allow the release and trapping of the copper radioisotope which can then be detected via PET.

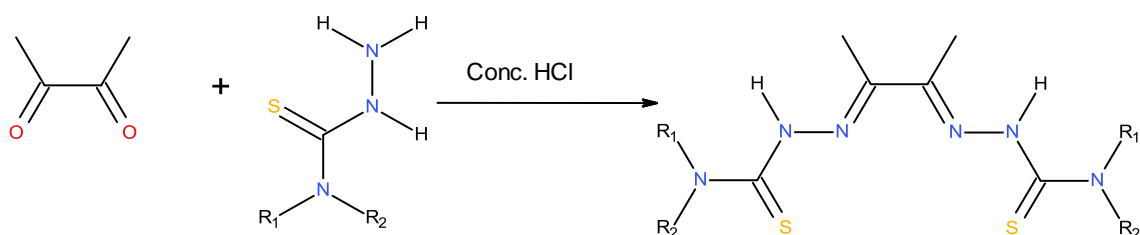
It has been found that ligands made from di-ketones with Me/Me or Me/Et on the backbone have redox potential in the appropriate range. The more lipophilic the substituents on the 4-substituted-3-thiosemicarbazide arm; the slower the clearance from normoxic cells and thus the longer it takes to achieve a suitable hypoxic: normoxic ratio in order to give informative images.

The aim was to synthesise a range of ligands with Me/Me or Me/Et on the backbone and with 4-substituted-3-thiosemicarbazide arms with a restricted number of methyl/ethyl substituents in order to control lipophilicity.

### 2.4.1. Symmetric ligands with Me/Me backbones

#### Overview of reaction

The synthesis of this subgroup of ligands requires one equivalent of 2,3-butanedione (BDO) to be reacted with two equivalent of a chosen 4-substituted-3-thiosemicarbazide under acidic conditions in water, at circa 60°C, to give the desired symmetric ligand (Figure 2.4.1.1.). A total of four ligands were synthesised (Figure 2.4.1.2.).



	R <sub>1</sub>	R <sub>2</sub>
BDO-NH <sub>2</sub> -NH <sub>2</sub>	H	H
BDO-Me-Me	CH <sub>3</sub>	H
BDO-(Me) <sub>2</sub> -(Me) <sub>2</sub>	CH <sub>3</sub>	CH <sub>3</sub>
BDO-Et-Et	CH <sub>2</sub> CH <sub>3</sub>	H

Figure 2.4.1.1. The general reaction for the synthesis of symmetric ligands with Me/Me backbones.

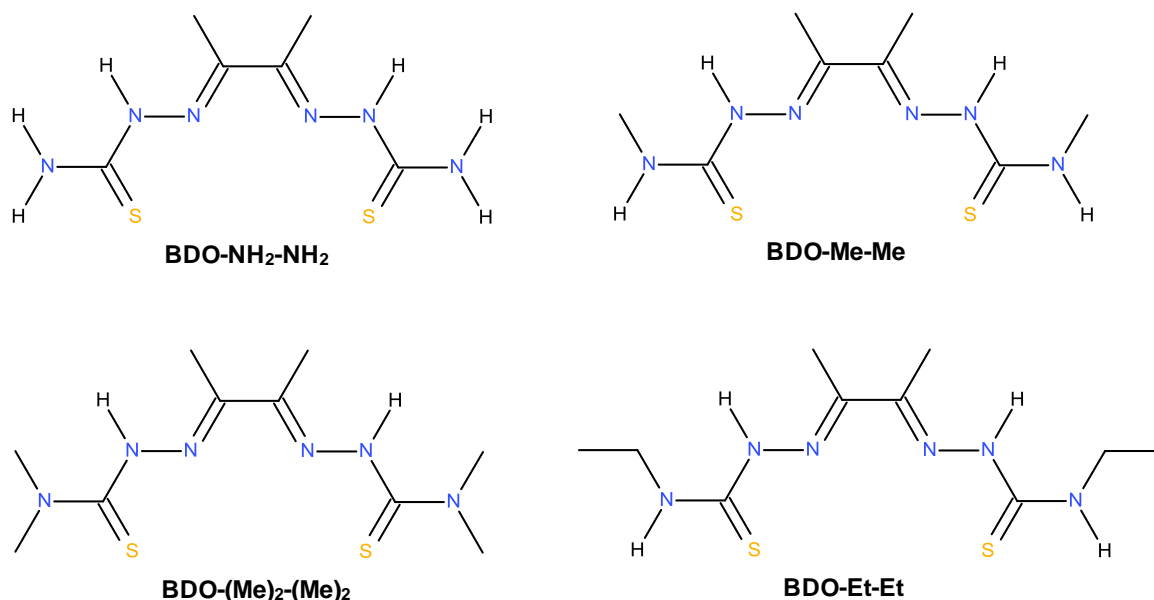


**Figure 2.4.1.2.** Structures of the symmetric ligands with Me/Me backbones that were synthesised.

## **2.4.2. Methods**

### **BDO-NH<sub>2</sub>-NH<sub>2</sub>**

Thiosemicarbazide (0.388 g, 0.004 mol) was dissolved in de-ionised water (10 mL, 60 °C). HCl (32%, 1 drop) was added, followed by the rapid addition of 2,3-butanedione (0.17 mL, 0.002 mol, 0.17 g) and the solution was left to stir (60 °C, 1 hour). The precipitate was recovered by filtration and washed with de-ionised water (50 mL, room temperature and 50 mL, 80 °C). The solid was dried. An off white solid (0.448 g) was recovered (96% yield).

### **BDO-Me-Me**

4-methyl-3-thiosemicarbazide (1.789 g, 0.017 mol) was dissolved in ethanol (50 mL, 72 °C). HCl (32%, 5 drops) was added followed by the rapid addition of 2,3-butanedione (0.7 mL, 0.0080 mol, 0.687 g). The solution was left to stir (72 °C, 1 hour). The precipitate was filtered off and washed with ethanol (3 x 30 mL) and diethyl ether (3 x 30 mL). The solid was dried. The crude product was dissolved in DMSO (55 mL), filtered and recrystallised with de-ionised water (30 mL). The precipitated was recovered by filtration, washed with acetone (25 mL), and dried. An off white solid (1.618 g) was recovered (78% yield).

### **BDO-(Me)<sub>2</sub>-(Me)<sub>2</sub>**

4,4-dimethyl-3-thiosemicarbazide (0.262 g, 0.0022 mol) was dissolved in de-ionised water (15 mL, 60 °C). HCl (32%, 1 drop) was added followed by the rapid addition of 2,3-butanedione (0.09 mL, 0.0010 mol, 0.088 g). The solution was left to stir (60 °C, 5 minutes). The precipitate was filtered off and washed with de-ionised water (50 mL, room temperature and 50 mL, 80 °C). The solid was dried. A yellow/orange solid (0.147 g) was recovered (51% yield).



### **BDO-Et-Et**

4-ethyl-3-thiosemicarbazide (0.316 g, 0.0027 mol) was dissolved in de-ionised water (13 mL, 60 °C) and filtered off the insoluble particulates. HCl (32%, 1 drop) was added followed by the rapid addition of 2,3-butanedione (0.10 mL, 0.0011 mol, 0.098 g). The solution was left to stir (60 °C, 1 hour). The precipitate was filtered off and washed with de-ionised water (50 mL, room temperature and 50 mL, 80 °C). The solid was dried. An off white solid (0.189 g) was recovered (60% yield).

### **2.4.3. Characterisation data for symmetric ligands with Me/Me backbones**

#### **BDO-NH<sub>2</sub>-NH<sub>2</sub>**

**<sup>1</sup>H NMR** (DMSO-*d*<sub>6</sub>, 400 MHz): δ= 10.17 (s, 1 H, N-NH), 8.35 (s, 1 H, C-NH), 8.37 (s, 2 H, C-NH), 7.81 (s, 2 H, C-NH), 2.04 (s, 6 H, N=C-CH<sub>3</sub>). **<sup>13</sup>C {<sup>1</sup>H} NMR** (DMSO-*d*<sub>6</sub>, 100 MHz): δ= 179.36 (C=S), 148.84 (C=N), 12.12 (N=C-CH<sub>3</sub>). **IR (neat)**: cm<sup>-1</sup>= 3404 (s), 3246 (m), 3184 (s), 3146 (s), 1587 (s), 1489 (s), 1454 (s), 1369 (s), 1290 (s), 1248 (m), 1153 (m), 1082 (m), 1013 (s), 947 (m), 831 (s), 716 (m), 650 (m), 598 (s). **Raman (neat)**: cm<sup>-1</sup>= 2916 (w), 1608 (s), 1590 (m), 1377 (w), 1335 (m), 1126 (m), 1004 (w), 856 (w), 758 (w), 467 (w), (Fluorescence present). **Melting point**: >215 °C (decomposed).

#### **BDO-Me-Me**

**<sup>1</sup>H NMR** (DMSO-*d*<sub>6</sub>, 400 MHz): δ= 10.20 (s, 2 H, N-NH), 8.34 (m, 2 H, H<sub>3</sub>C-NH, J= 4.4 Hz), 2.97 (d, 6 H, HN-CH<sub>3</sub>, J= 4.4 Hz), 2.16 (s, 6 H, N=C-CH<sub>3</sub>). **<sup>13</sup>C {<sup>1</sup>H} NMR** (DMSO-*d*<sub>6</sub>, 100 MHz): δ= 178.95 (C=S), 148.51 (C=N), 31.74 (HN-CH<sub>3</sub>), 12.21 (N=C-CH<sub>3</sub>). **IR (neat)**: cm<sup>-1</sup>= 3356 (m), 3233 (m), 2936 (w), 1688 (w), 1612 (w), 1543 (s), 1485 (s), 1350 (m), 1215 (m), 1169 (m), 1128 (m), 1070 (m), 955 (m), 816 (s), 640 (m), 540 (s). **Raman (neat)**: cm<sup>-1</sup>= 1605 (s), 1548 (w), 1383 (w), 1325 (w), 1239 (w), 1130 (w), 1003 (w), 846 (w), 736 (w), 583 (w), 458 (w), 398 (w), 320 (w), 271 (w), 209 (w). **Melting point**: >219 °C (decomposed).

#### **BDO-(Me)<sub>2</sub>-(Me)<sub>2</sub>**

**<sup>1</sup>H NMR** (DMSO-*d*<sub>6</sub>, 400 MHz): δ= 9.48 (s, 2 H, N-NH), 3.23 (s, 12 H, N-(CH<sub>3</sub>)<sub>2</sub>), 2.09 (s, 6 H, N=C-CH<sub>3</sub>). **<sup>13</sup>C {<sup>1</sup>H} NMR** (DMSO-*d*<sub>6</sub>, 100 MHz): δ= 182.25 (C=S), 150.29 (C=N), 42.75 (N-(CH<sub>3</sub>)<sub>2</sub>), 11.60 (N=C-CH<sub>3</sub>). **IR (neat)**: cm<sup>-1</sup>= 3323 (w), 2926 (w), 1526 (s), 1452 (m), 1423 (m), 1366 (m), 1312 (s), 1200 (s), 1161 (s), 1125 (s), 1099 (s), 1055 (m), 893 (m), 773 (s), 633 (m), 509 (m). **Raman (neat)**: cm<sup>-1</sup>= 3327 (w), 2927 (w), 1578 (s), 1545 (w), 1378 (w), 1364 (w), 1295 (w), 1206 (w), 1133 (w), 1011 (w), 909 (w), 816 (w), 703 (w), 581 (w), 514 (w), 424 (w), 117 (w). **Melting point**: >170 °C (decomposed).

## BDO-Et-Et

$^1\text{H}$  NMR (DMSO- $d_6$ , 400 MHz):  $\delta$ = 10.11 (s, 2 H, N-NH), 8.39 (t, 2 H, H<sub>2</sub>C-NH, J= 6.0 Hz), 3.55 (dq, 4 H, H<sub>2</sub>C-NH, J=7.2, 6.0 Hz), 2.16 (s, 6 H, N=C-CH<sub>3</sub>), 1.07 (t, 6 H, H<sub>2</sub>C-CH<sub>3</sub>, J= 7.2 Hz).  $^{13}\text{C}$  { $^1\text{H}$ } NMR (DMSO- $d_6$ , 100 MHz):  $\delta$ = 177.88 (C=S), 148.48 (C=N), 39.08 (N-CH<sub>2</sub>), 14.91 (H<sub>2</sub>C-CH<sub>3</sub>), 12.22 (N=C-CH<sub>3</sub>). IR (neat):  $\text{cm}^{-1}$ = 3347 (m), 3211 (w), 2967 (w), 2884 (w), 1686 (w), 1614 (w), 1522 (s), 1485 (s), 1385 (m), 1362 (m), 1308 (m), 1258 (m), 1213 (m), 1167 (m), 1130 (s), 1065 (m), 970 (m), 943 (m), 812 (m), 665 (m), 544 (s). Raman (neat):  $\text{cm}^{-1}$ = 3214 (w), 2984 (w), 1606 (s), 1533 (w), 1395 (w), 1342 (w), 1256 (w), 1208 (w), 1127 (w), 1005 (w), 840 (w), 746 (w), 462 (w), 398 (w), 299 (w), 198 (w). Melting point: >223 °C (decomposed).

### 2.4.4. Spectral examples of a symmetric ligand with a Me/Me backbone

Figures 2.4.4.1-4 Spectral examples of ligands BDO-Me-Me.

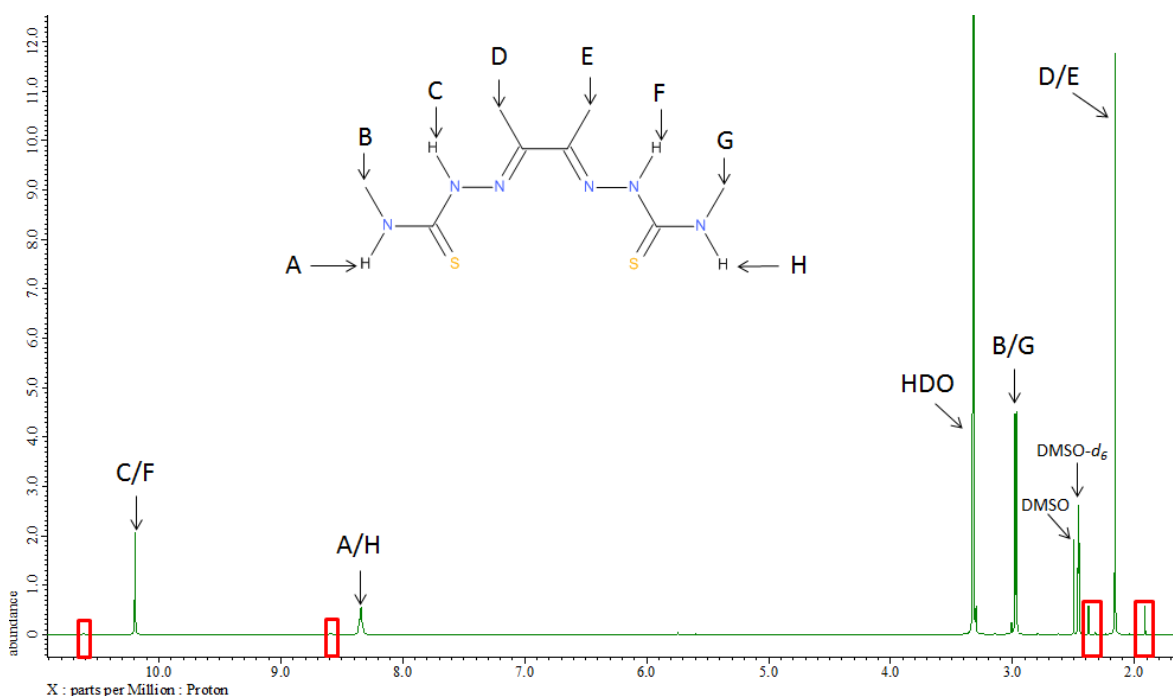


**Figure 2.4.4.1.** An assigned  $^1\text{H}$  NMR spectrum of BDO-Me-Me. BDO-Me-Me was synthesised by reacting 2,3-butanedione with 4-methyl-3-thiosemicarbazide. The red boxes highlight a small presence of BDO-Me=O.

The presence of the corresponding mono-substituted-3-thiosemicarbazone is very typical in the synthesis of this class of ligand.

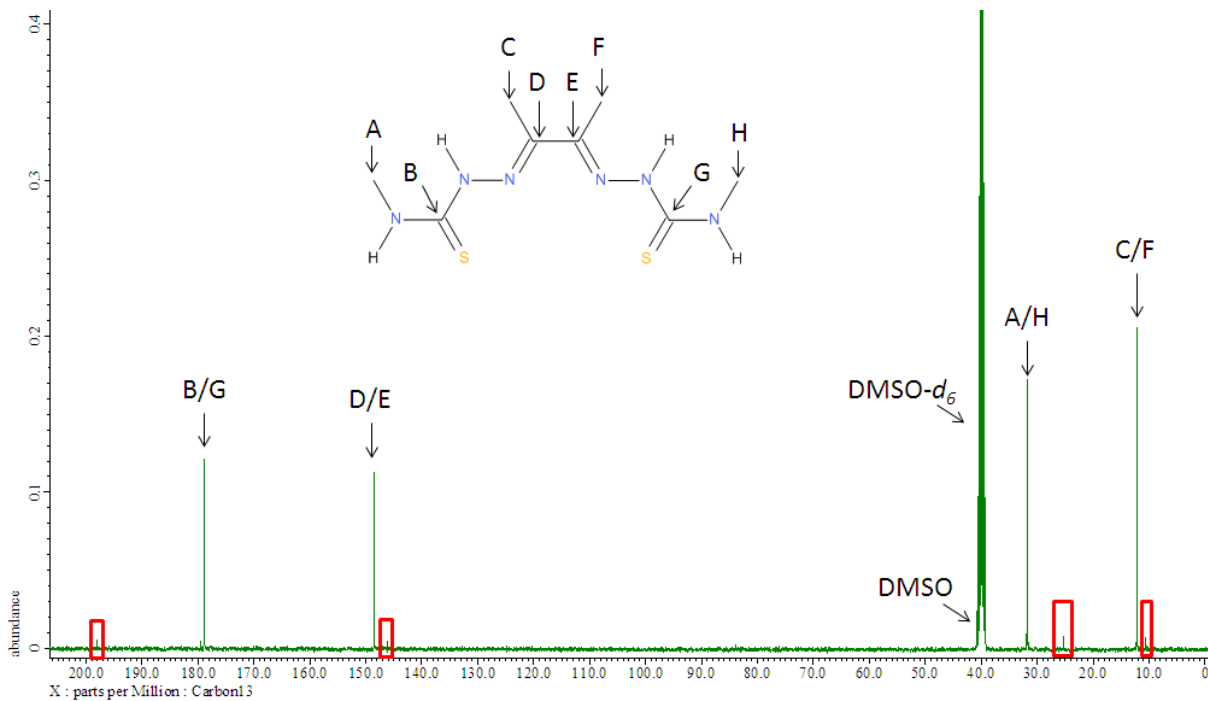


**Figure 2.4.4.2.** An assigned  $^{13}\text{C}$  NMR spectrum of BDO-Me-Me. The red boxes highlight a small presence of BDO-Me=O.

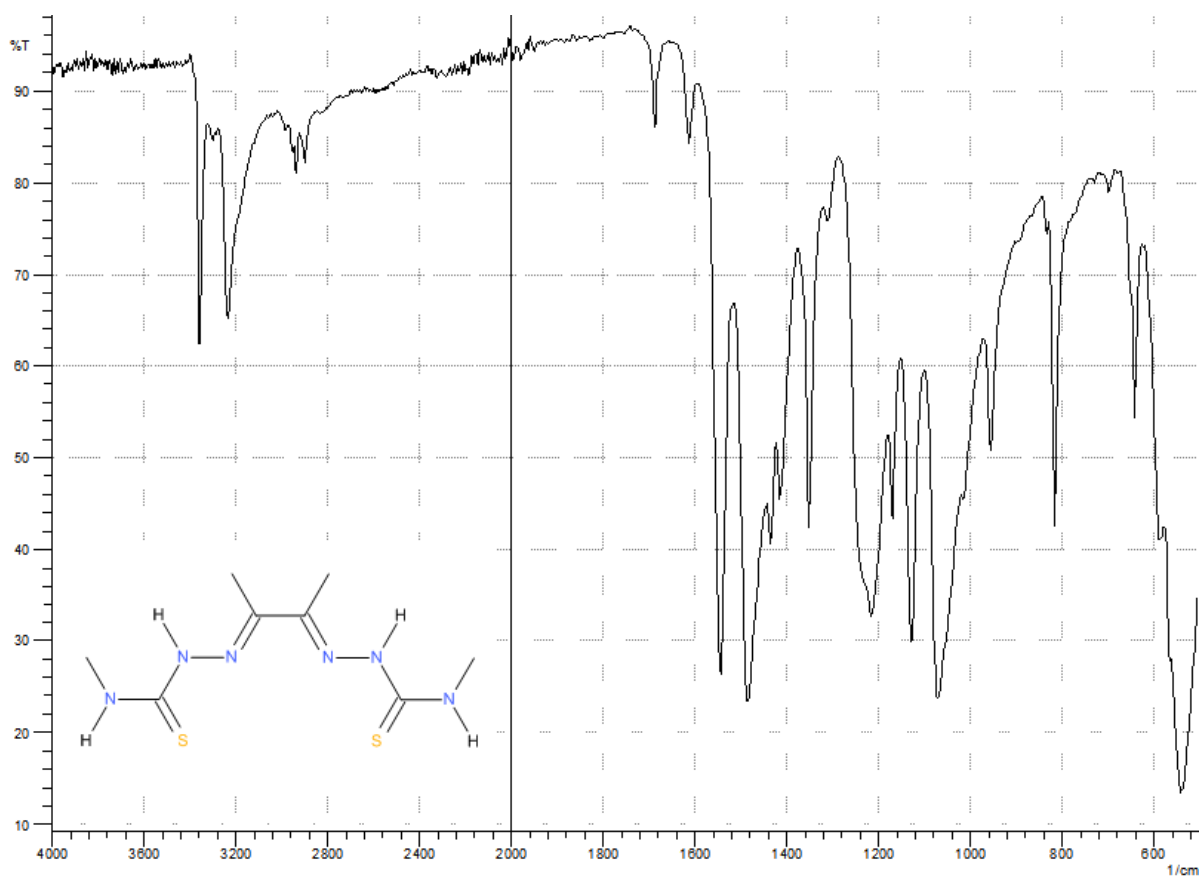


**Figure 2.4.4.3.** A FTIR spectrum of BDO-Me-Me.

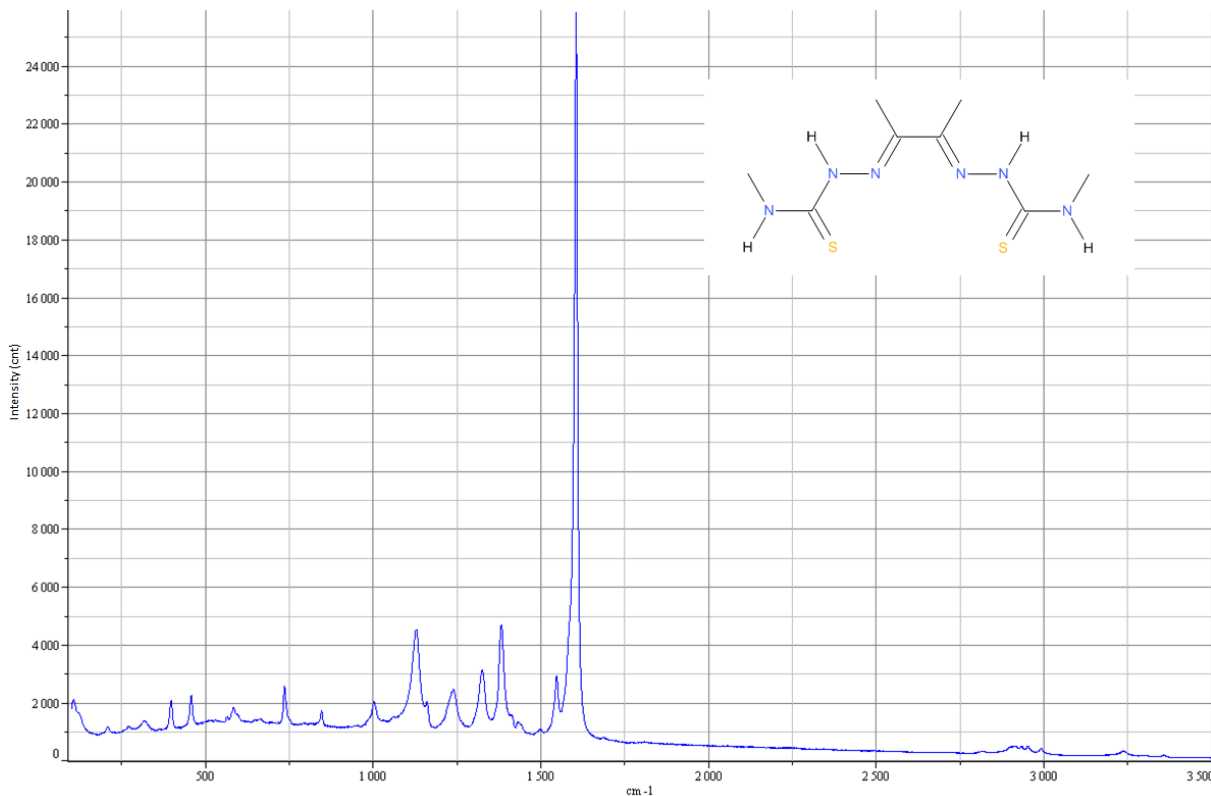
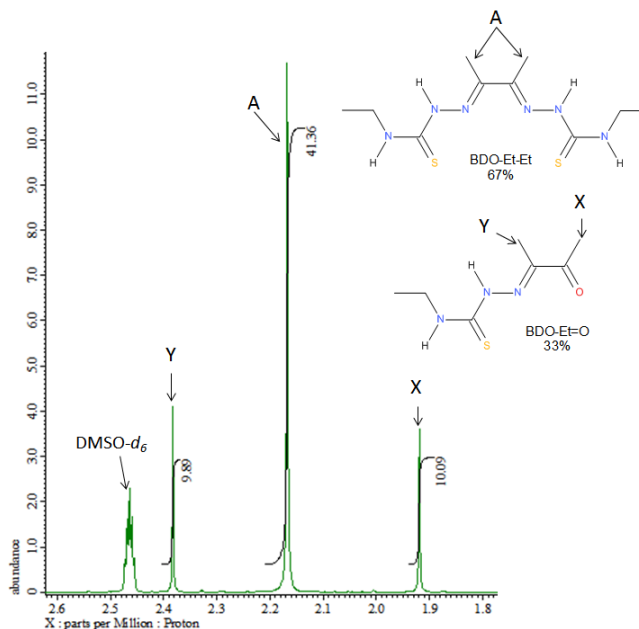


**Figure 2.4.4.4.** A Raman spectrum of BDO-Me-Me.

### **2.4.5. Discussion**

The target ligands have been made with a respectable yield by following the well reported methods in the literature.<sup>6, 57, 75, 77, 96</sup> The synthesis of this class of ligand was the first to be attempted as symmetric ligands with Me/Me on the backbone are one of the most reported bis(thiosemicarbazones) ligands in the literature. This gave a convenient starting point for the synthesis of dissymmetric ligands with a variety of backbone substituents.

The synthesis of this type of class of ligands seems to be particularly plagued with the presence of the mono-substituted-3-thiosemicarbazone as an impurity in far higher proportions that has been observed with either the corresponding symmetric ligands with Me/H or Me/Et groups on the backbone. This is particularly observed in the synthesis of BDO-Et-Et where the impurity content was a disappointing 33% (Figure 2.4.5.1.); even when a 20% excess of 4-ethyl-3-thiosemicarbazide was used coupled with a reaction run time of one hour. It should be noted that the DMSO/H<sub>2</sub>O recrystallisation step was removed for this synthesis because the re-crystallised product produced very small particulates which the majority of the sample was unable to be isolated through filtration. The DMSO/H<sub>2</sub>O recrystallisation step was also removed from the synthesis method for BDO-NH<sub>2</sub>-NH<sub>2</sub>, because BDO-NH<sub>2</sub>-NH<sub>2</sub> has a very low solubility in DMSO.

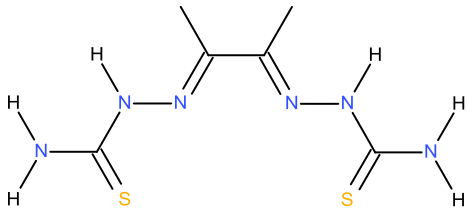
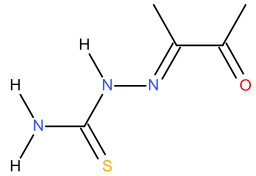
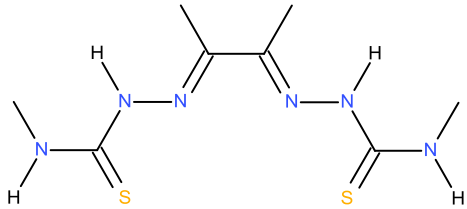
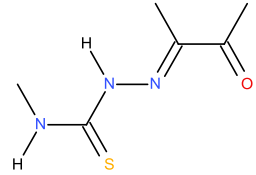
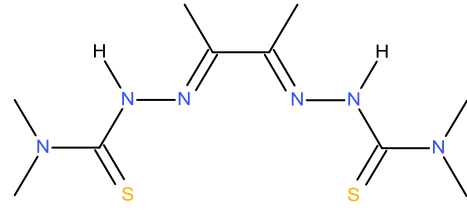
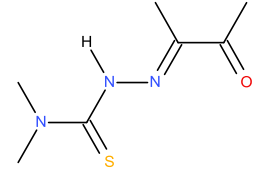


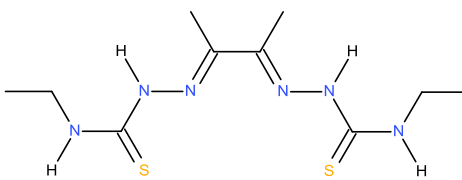
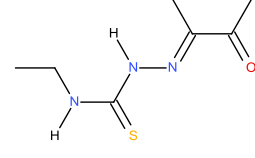
**Figure 2.4.5.1.** A section of a  $^1\text{H}$  NMR of BDO-Et-Et showing the significant impurity content of BDO-Et=O.

The addition of an excess of 4-substituted-3-thiosemicarbazide seems to be of limited use when attempting to reduce the mono-substituted-3-thiosemicarbazone impurity. A reaction was run in order to synthesize BDO-Me-Me in the presence of a 50% excess of 4-methyl-3-thiosemicarbazide with a reaction time of five hours. The resulting product still had roughly a 14% impurity of BDO-Me=O. Various solvents have been used in washing steps ranging from water, ethanol, water and hot water, none of which resulting in the complete removal of the impurity. A DMSO/H<sub>2</sub>O recrystallisation step is thought to improve the purity, but a toll is paid in regards to yield, the magnitude of the toll is dependent on the ligand's structure. It has been observed that ligands containing 4,4-dimethyl-3-thiosemicarbazide seem to be partially prone to significant loss with the DMSO/H<sub>2</sub>O recrystallisation step. No meaningful relationship has been detected between reactions conditions (excess of arm, run time, temperature) and impurity content of product. It may be possible to use preparatory HPLC in order to further purify the ligands, but due to restraints on equipment this avenue was not explored.

Despite the numerous reports of the symmetric ligands of this class in the literature (Table 2.4.5.2.) there seems to be only a small amount of characterisation data for just the ligand instead of the resulting copper complex. The Infra-red data reported for BDO-NH<sub>2</sub>-NH<sub>2</sub><sup>96</sup>, BDO-Me-Me<sup>75, 78, 146</sup> and BDO-(Me)<sub>2</sub>-(Me)<sub>2</sub><sup>78</sup> all agree with the data obtained from the synthesised ligands in this project. Proton NMR data for BDO-Me-Me published by S. Kadowaki *et al.*<sup>75</sup> shows very strong agreement to NMR data reported above. Unfortunately, no characterisation data was identified from the literature in regards to BDO-Et-Et.

As the symmetric ligands have been reported in a number of publications (Table 2.4.5.2.) and as the dissymmetric ligands are the main focus in respect of the proposed application/screening it was decided to avoid spending long periods of time improving the yield and purity of the synthesis and concentrate on the clean synthesis of the dissymmetric ligands. Also, it is expected that if it is not possible to completely remove the mono-substituted-3-thiosemicarbazone impurities, the complex formation step should remove the impurity. This is expected because when sample is mixed with the chosen copper salt then symmetric/dissymmetric ligand will form a complex with the copper and will precipitate out of solution, leaving the un-complexed mono-substituted-3-thiosemicarbazone impurity in solution. It is worth noting that there are reports in the literature<sup>209</sup> of some mono-substituted-3-thiosemicarbazones forming complexes, which also have some biological activity. The table below (Table 2.4.5.2.) illustrates all four ligands, what the main impurities are and an estimate of the percentage.

Ligand	Novel	Yield	Main impurity	Estimated impurity *
<p>BDO-NH<sub>2</sub>-NH<sub>2</sub></p> 	<p>No<sup>69, 77,</sup> 123, 145, 146, 164</p>	63%		6%
<p>BDO-Me-Me</p> 	<p>No<sup>6, 57, 69,</sup> 70, 75-78, 123, 145, 146, 164, 172, 189, 203, 204</p>	78%		6%
<p>BDO-(Me)<sub>2</sub>-(Me)<sub>2</sub></p> 	<p>No<sup>78, 203</sup></p>	51%		9%

<b>BDO-Et-Et</b> 	No <sup>69, 76,</sup> 164, 203	<b>67%</b>		<b>7%</b>
---	-----------------------------------	------------	---	-----------

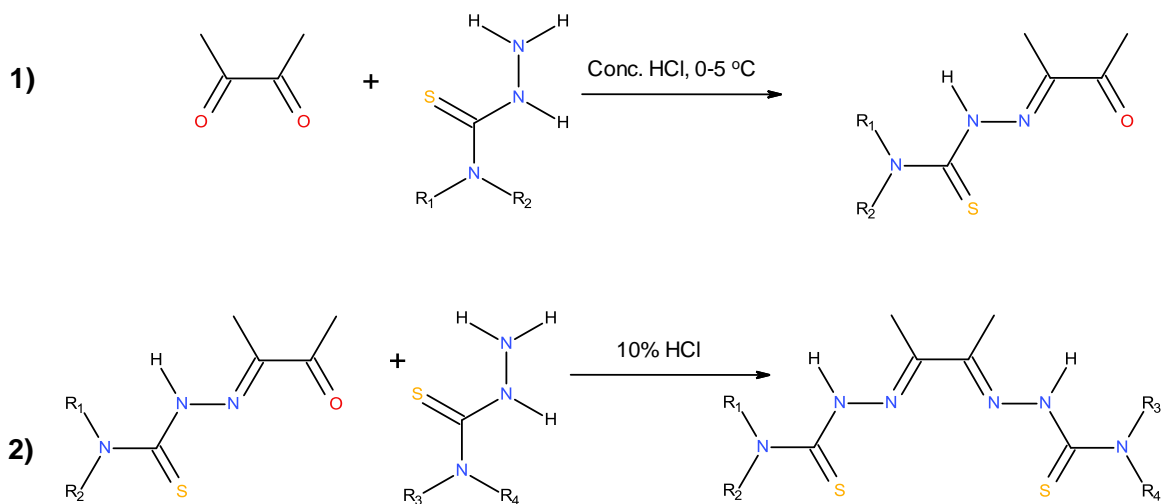
\*Estimated by <sup>1</sup>H NMR spectra on an average of three integrals where possible. Typically this was to include the integrals from the peaks due to the N=C-CH<sub>3</sub> and N-NH environments.

**Table 2.4.5.2.** Summary of purity for the symmetric Ligands with Me/Me backbones.

## 2.4.6. Dissymmetric ligands with Me/Me backbones

### Overview of reaction

The synthesis of the dissymmetric ligands requires the synthesis of three mono-substituted-3-thiosemicarbazone intermediates. These intermediates are synthesised by reacting BDO and a 4-substituted-3-thiosemicarbazone in the stoichiometric ratio of 1:1 at reduced temperatures and under acidic conditions. Once isolated the intermediate is then reacted with 1 equivalent of a dissimilar 4-substituted-3-thiosemicarbazone catalysed under slightly acidic conditions to produce the desired dissymmetric ligand (Figure 2.4.6.1.). The two ligands that were synthesised are shown in the figure below (Figure 2.4.6.2.).



	R <sub>1</sub>	R <sub>2</sub>	R <sub>3</sub>	R <sub>4</sub>
BDO-Me-NH <sub>2</sub>	CH <sub>3</sub>	H	H	H
BDO-NH <sub>2</sub> -(Me) <sub>2</sub>	H	H	CH <sub>3</sub>	CH <sub>3</sub>

**Figure 2.4.6.1.** The general reaction for the synthesis of dissymmetric ligands with Me/Me backbones.





### BDO-(Me)<sub>2</sub>=O

4,4-dimethyl-3-thiosemicarbazide (0.500 g, 0.0042 mol) was dissolved in de-ionised water (60 mL). Solution cooled (4 °C) over ice, followed by the addition of HCl (32%, 2 drops). 2,3-butanedione (0.36 mL, 0.041 mol, 0.35 g) was added rapidly and vigorously stirred (5 °C, 1 hour). The precipitate was recovered via filtration, washed with de-ionised water (2 x 30 mL). The crude product was dissolved in ethanol (15 mL, hot). The resulting solution was filtered and left to recrystallise in a freezer. The crystalline solid was filtered off, washed with petroleum ether (bp range: 40 – 60 °C, 2 x 10 mL) and left to dry. A bright yellow crystalline solid (0.191 g) was recovered (25% yield).

### 2.4.8. Characterisation data for the BDO-mono-substituted-3-thiosemicarbazone intermediates

#### BDO-NH<sub>2</sub>=O

<sup>1</sup>H NMR (DMSO-*d*<sub>6</sub>, 400 MHz): δ= 10.54 (s, 1 H, N-NH), 8.67 (s, 1 H, C-NH), 8.05 (s, 1 H, C-NH), 2.33 (s, 3 H, O=C-CH<sub>3</sub>), 1.90 (s, 3 H, N=C-CH<sub>3</sub>). <sup>13</sup>C {<sup>1</sup>H} NMR (DMSO-*d*<sub>6</sub>, 100 MHz): δ= 198.15 (C=O), 180.27 (C=S), 146.39 (C=N), 25.28 (O=C-CH<sub>3</sub>), 10.59 (N=C-CH<sub>3</sub>). IR (neat): cm<sup>-1</sup>= 3443 (m), 3323 (m), 3165 (m), 1682 (s), 1587 (s), 1504 (s), 1452 (m), 1418 (m), 1364 (m), 1290 (m), 1107 (s), 1045 (m), 993 (m), 949 (m), 853 (s), 712 (m), 621 (s), 608 (s), 556 (s). Raman (neat): cm<sup>-1</sup>= 3445 (w), 3323 (w), 3175 (w), 3000 (w), 2956 (w), 2905 (w), 1675 (s), 1605 (s), 1462 (w), 1426 (w), 1371 (w), 1307 (w), 1284 (w), 1107 (s), 1045 (w), 1008 (w), 946 (w), 846 (w), 741 (w), 608 (w), 464 (w), 315 (w), 143 (w). Melting point: >173 °C (decomposed).

#### BDO-Me=O

<sup>1</sup>H NMR (DMSO-*d*<sub>6</sub>, 400 MHz): δ= 10.61 (s, 1 H, N-NH), 8.59 (m, 1 H, H<sub>3</sub>C-NH, J= 4.4 Hz), 3.01 (d, 3 H, HN-CH<sub>3</sub>, J= 4.4 Hz), 2.38 (s, 3 H, O=C-CH<sub>3</sub>), 1.91 (s, 3 H, N=C-CH<sub>3</sub>). <sup>13</sup>C {<sup>1</sup>H} NMR (DMSO-*d*<sub>6</sub>, 100 MHz): δ= 198.04 (C=O), 179.49 (C=S), 146.49 (C=N), 31.94 (HN-CH<sub>3</sub>), 25.31 (O=C-CH<sub>3</sub>), 10.57 (N=C-CH<sub>3</sub>). IR (neat): cm<sup>-1</sup>= 3285 (m), 1670 (s), 1593 (w), 1537 (m), 1495 (s), 1427 (m), 1410 (s), 1360 (m), 1207 (s), 1152 (s), 1126 (s), 1105 (s), 1047 (s), 999 (m), 835 (m), 725 (w), 667 (m), 629 (m), 606 (s), 577 (s). Raman (neat): cm<sup>-1</sup>= 3289 (w), 2919 (w), 1671 (m), 1591 (s), 1409 (w), 1367 (w), 1304 (w), 1213 (w), 1128 (w), 1106 (w), 1000 (w), 947 (w), 836 (w), 725 (w), 609 (w), 578 (w), 318 (w). Melting point: >149 °C (decomposed).

#### BDO-(Me)<sub>2</sub>=O

<sup>1</sup>H NMR (DMSO-*d*<sub>6</sub>, 400 MHz): δ= 9.85 (s, 1 H, N-NH), 3.27 (s, 6 H, N-(CH<sub>3</sub>)<sub>2</sub>), 2.28 (s, 3 H, O=C-CH<sub>3</sub>), 1.91 (s, 3 H, N=C-CH<sub>3</sub>). <sup>13</sup>C {<sup>1</sup>H} NMR (DMSO-*d*<sub>6</sub>, 100 MHz): δ= 197.81 (C=O), 182.39 (C=S), 147.05 (C=N), 43.16 (N-(CH<sub>3</sub>)<sub>2</sub>), 24.83 (O=C-CH<sub>3</sub>), 10.07 (N=C-CH<sub>3</sub>). IR (neat): cm<sup>-1</sup>= 3362 (w), 2920

(w), 1670 (s), 1578 (m), 1537 (m), 1429 (m), 1354 (s), 1290 (s), 1198 (s), 1150 (s), 1107 (s), 1063 (s), 1005 (m), 901 (m), 804 (s), 702 (m), 611 (m), 602 (m), 527 (s). **Raman (neat):**  $\text{cm}^{-1}$  = 3364 (w), 2923 (w), 1669 (s), 1580 (s), 1364 (m), 1342 (m), 1289 (w), 1194 (m), 1150 (w), 1009 (m), 946 (w), 903 (w), 805 (w), 701 (w), 633 (w), 603 (w), 525 (w), 457 (w), 370 (w), 217 (w). **Melting point:**  $>129^\circ\text{C}$  (decomposed).

#### **2.4.9. Spectral examples of a BDO-mono-substituted-3-thiosemicarbazone intermediate**

**Figures 2.4.9.1-4.** Spectral examples of the BDO-mono-substituted-3-thiosemicarbazone intermediate BDO-NH<sub>2</sub>=O.

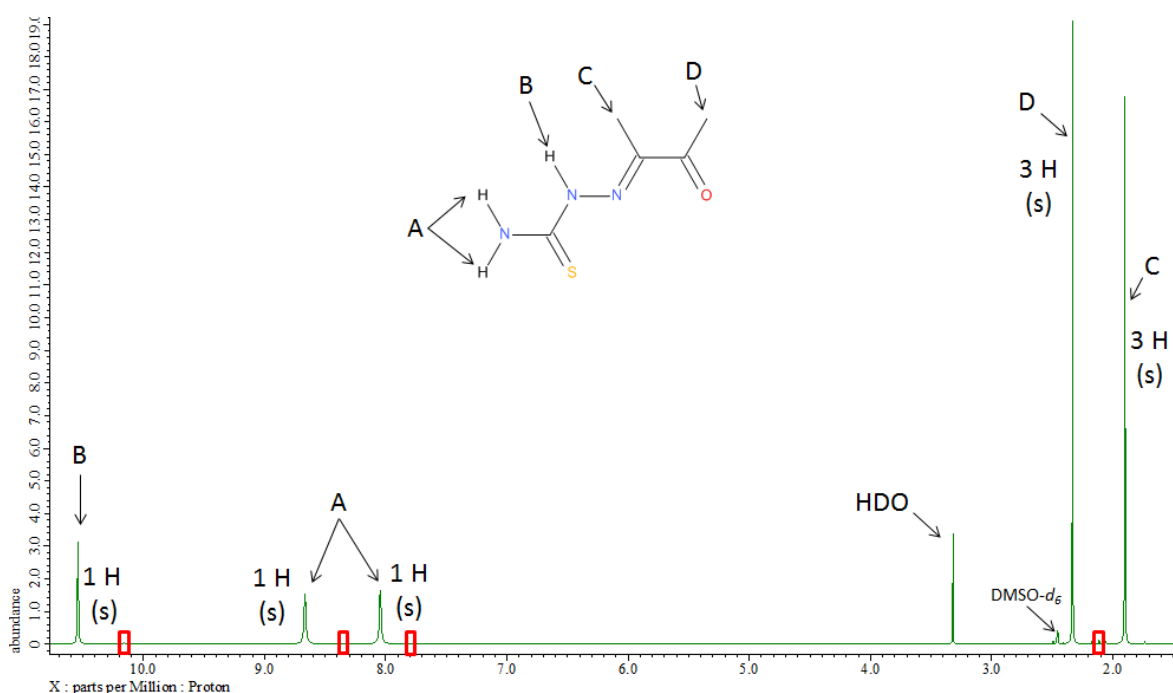


**Figure 2.4.9.1.** An assigned <sup>1</sup>H NMR spectrum of BDO-NH<sub>2</sub>=O. BDO-NH<sub>2</sub>=O was synthesised by reacting 2,3-butanedione with thiosemicarbazide at 5<sup>o</sup>C. The red boxes indicate a very small presence of BDO-NH<sub>2</sub>-NH<sub>2</sub>. This is consistent with the rest of the reactions synthesising BDO based intermediates.

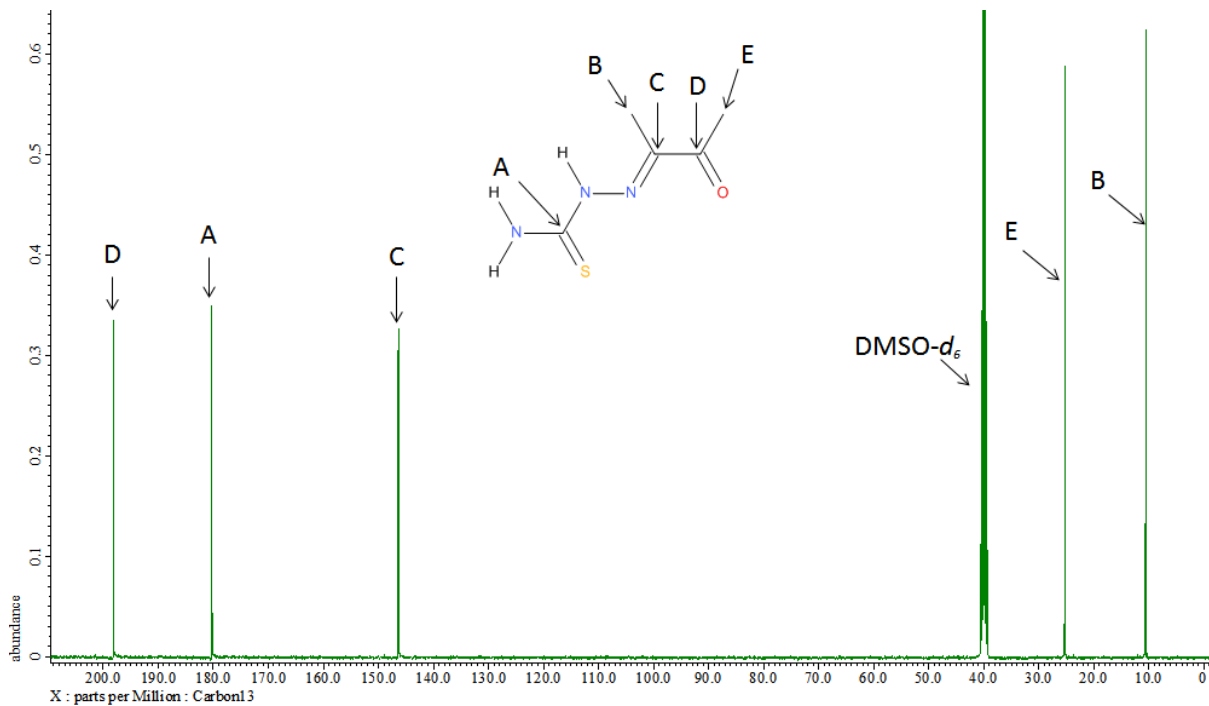


Figure 2.4.9.2. An assigned  $^{13}\text{C}$  NMR spectrum of BDO-NH<sub>2</sub>=O.

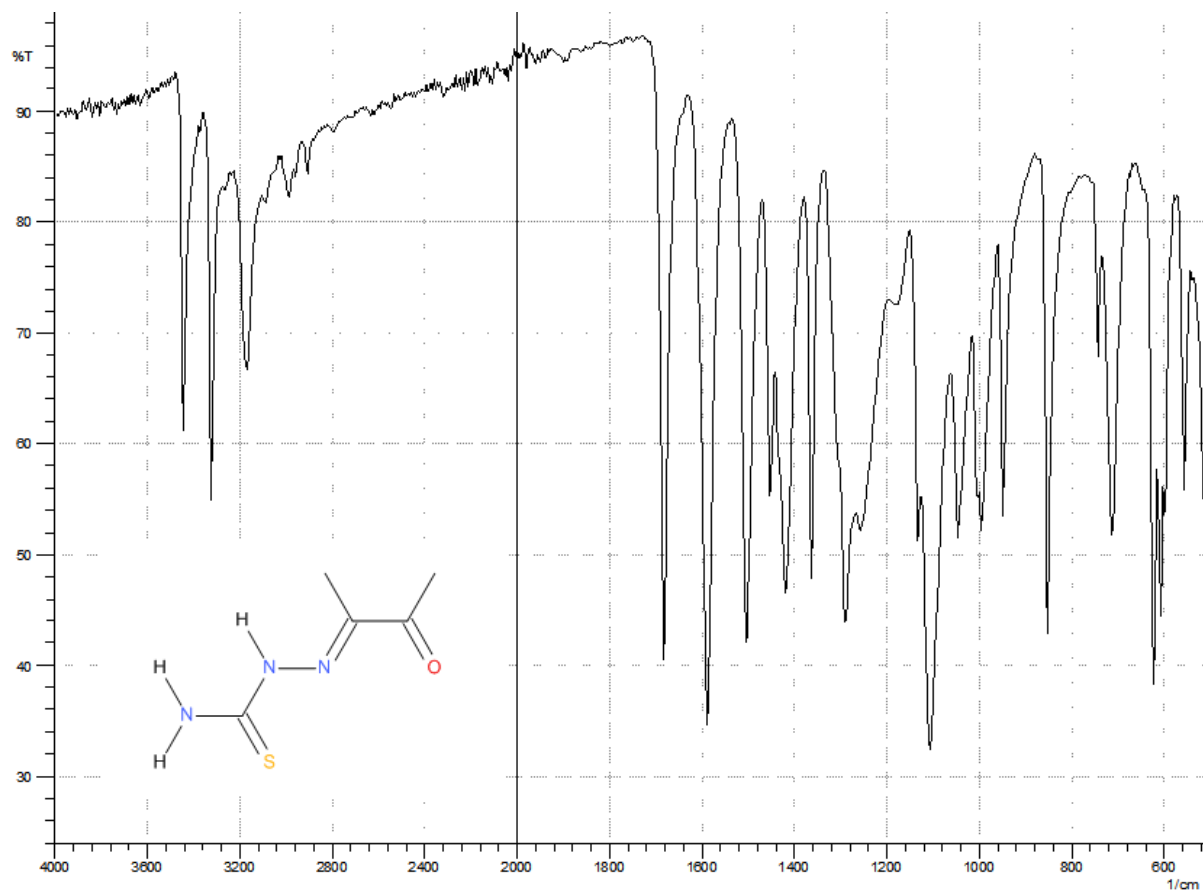
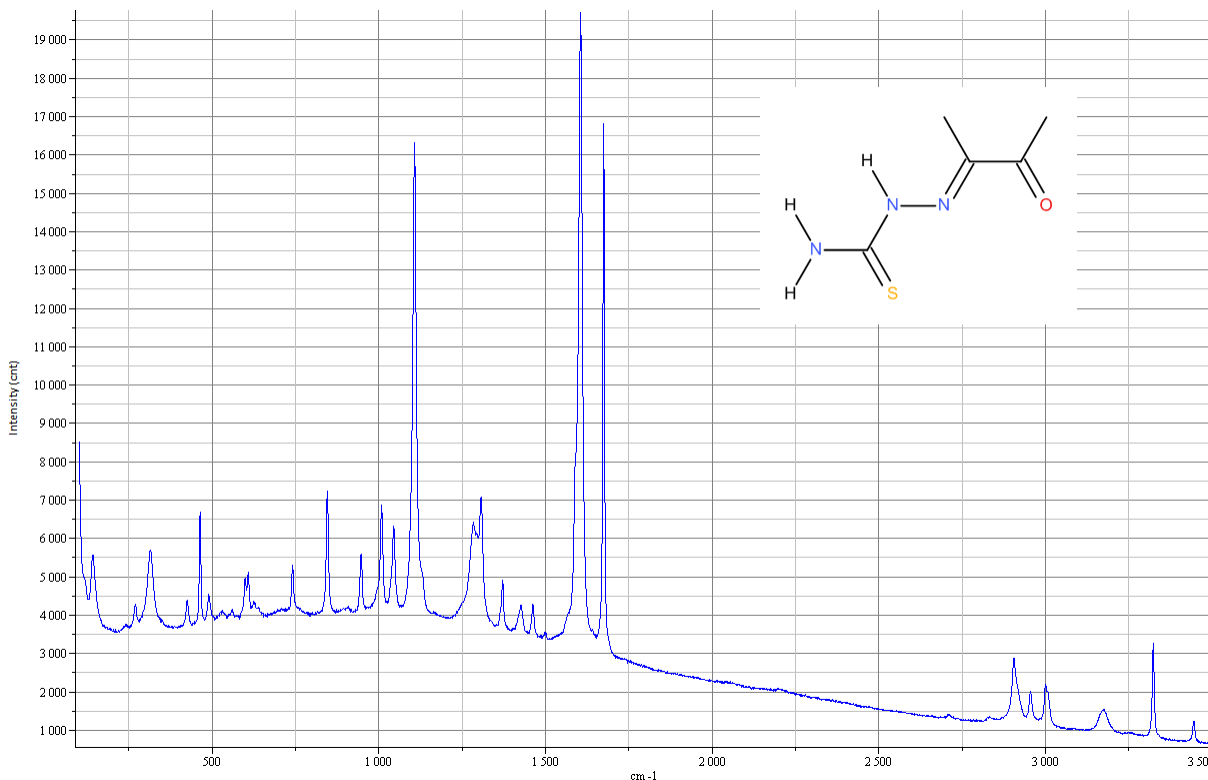


Figure 2.4.9.3. A FTIR spectrum of BDO-NH<sub>2</sub>=O.

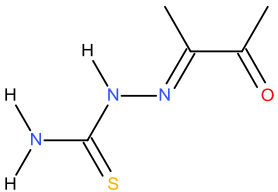
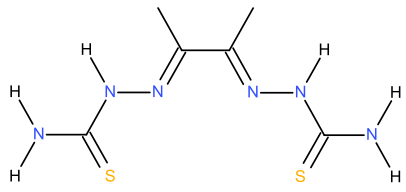
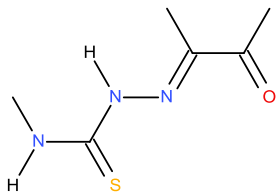
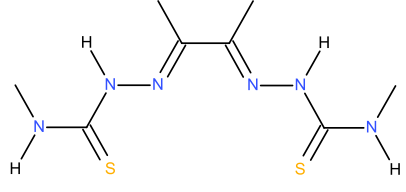
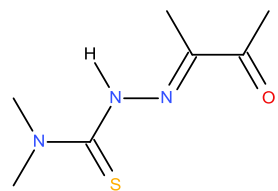
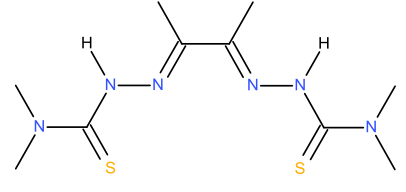


**Figure 2.4.9.4.** A Raman spectrum of BDO-NH<sub>2</sub>=O.

### **2.4.10. Discussion**

All three intermediates were successfully made in high purity by using methods as per the published literature.<sup>57, 66, 73</sup> No significant problems had to be overcome during the synthesis. As observed in the PADA-mono-substituted-3-thiosemicarbazones synthesis, the main impurity tends to be the respective symmetric ligand. The only thing to note is the low yield for the synthesis of BDO-(Me)<sub>2</sub>=O. A depressed yield is consistently observed in reactions involving 4,4-dimethyl-3-thiosemicarbazide. Fortunately in the case of the BDO backbone it is inconsequential which order the 4-substituted-3-thiosemicarbazide arms are attached. This coupled with 4,4-dimethyl-3-thiosemicarbazide being relatively precious and low yielding, it is preferable to choose to synthesise a higher yielding intermediate first then attach the 4,4-dimethyl-3-thiosemicarbazide arm. There are numerous reports of proton and carbon NMR data in the literature<sup>57, 73, 83, 190</sup> of which the data obtained in this project close agreement with. Unfortunately no infrared data was reported in these articles. J. Holland *et al.*<sup>57</sup> reported the melting point of BDO-Me=O as 157-159°C which is close to the melting point obtained of 149°C. At 149°C signs of decomposition were observed, browning of the solid/liquid. The report does not state if the sample melted properly or showed signs of decomposition. As BDO-(Me)<sub>2</sub>=O is believed to be novel no characterisation is available, it was also not possible to locate data for BDO-NH<sub>2</sub>=O. However, the data obtained from these intermediates is in accord with BDO-Me=O when the structural alterations are ignored.

Table 2.4.10.1. Reports the intermediates that have been successfully made along with the main impurity present and at what proportion this impurity is estimated at.

Intermediate	Novel	Yield	Main impurity	Estimated impurity *
<p>BDO-NH<sub>2</sub>=O</p> 	No <sup>196, 197</sup>	43%		1%
<p>BDO-Me=O</p> 	No <sup>57, 73, 83</sup>	42%		1%
<p>BDO-(Me)<sub>2</sub>=O</p> 	Yes	18%		1%

\*Estimated by <sup>1</sup>H NMR spectra on an average of three integrals where possible. Typically this was to include the integrals from the peaks due to the N=C-CH<sub>3</sub> and N-NH environments.

**Table 2.4.10.1.** Summary of purity for the PDO-mono-substituted-3-thiosemicarbazone intermediates, synthesised by the exploitation of carbonyl reactivity approach.

### **2.4.11. Dissymmetric ligands from the BDO-mono-substituted-3-thiosemicarbazone intermediates**

#### **Methods**

##### **BDO-Me-NH<sub>2</sub>**

Thiosemicarbazide (0.158 g, 0.0017 mol) was dissolved in ethanol (50 mL, 50 °C) and added HCl (10%, 1 drop). BDO-Me=O (0.300 g, 0.0017 mol) added to the solution and left to stir (50 °C, 5 hours). The precipitate was recovered by filtration, dissolved in DMSO (5 mL) and recrystallised

with de-ionised water (5 mL). The precipitate was filtered off, washed with a little amount of acetone and dried. A white solid (0.145 g) was recovered (35% yield).

#### **BDO-NH<sub>2</sub>-(Me)<sub>2</sub>**

BDO-NH<sub>2</sub>=O (0.255 g, 0.0016 mol) was dissolved in DMF (1.5 mL) and filtered. 4,4-dimethyl-3-thiosemicarbazide (0.191 g, 0.0016 mol) dissolved in DMF (2.5 mL), HCl (10%, 2 drops) was added and filtered. The two solutions were combined and left to stir (room temperature, 5 hours). De-ionised water (33 mL) was added, the precipitate was recovered by filtration and washed with de-ionised water (50 mL, room temperature and 50 mL, 80 °C). The crude product was dissolved in DMSO (3 mL), filtered and recrystallised with de-ionised water (6 mL). The precipitate was filtered off, washed with de-ionised water (50 mL, room temperature and 50 mL, 80 °C) and dried. A yellow solid (0.170 g) was recovered (41% yield).

#### **2.4.12. Characterisation data for the dissymmetric ligands from the BDO-mono-substituted-3-thiosemicarbazone intermediates**

##### **BDO-Me-NH<sub>2</sub>**

<sup>1</sup>H NMR (DMSO-*d*<sub>6</sub>, 400 MHz): δ= 10.19 (s, 2 H, N-NH), 8.37 (singlet overlapped with a quartet, 1 H, C-NH), 8.34 (quartet overlapped with a singlet, 1 H, H<sub>3</sub>C-NH, J= 4.4 Hz), 7.82 (s, 1 H, C-NH), 2.97 (d, 3 H, HN-CH<sub>3</sub>, J= 4.4 Hz), 2.16 (s, 3 H, N=C-CH<sub>3</sub>), 2.12 (s, 3 H, N=C-CH<sub>3</sub>). <sup>13</sup>C {<sup>1</sup>H} NMR (DMSO-*d*<sub>6</sub>, 100 MHz): δ= 179.32 (C=S), 178.97 (C=S), 148.92 (C=N), 148.43 (C=N), 31.74 (HN-CH<sub>3</sub>), 12.26 (N=C-CH<sub>3</sub>), 12.07 (N=C-CH<sub>3</sub>). IR (neat): cm<sup>-1</sup>= 3414 (m), 3352 (w), 3215 (m), 3150 (m), 1605 (m), 1553 (m), 1489 (s), 1362 (m), 1288 (m), 1231 (m), 1169 (m), 1142 (m), 1080 (s), 953 (m), 854 (m), 826 (m), 716 (m), 644 (m), 565 (s), 544 (s). Raman (neat): cm<sup>-1</sup>= 3212 (w), 2913 (w), 1604 (s), 1589 (m), 1461 (w), 1374 (m), 1329 (w), 1237 (w), 1123 (w), 1005 (w), 854 (w), 747 (w), 461 (w), 398 (w), 216 (w). Elemental analysis: Found: C, 34.2; H, 5.8; N, 34.0. Calc. for C<sub>7</sub>H<sub>14</sub>N<sub>6</sub>S<sub>2</sub>: C, 34.1; H, 5.7; N, 34.1%. Melting point: >215 °C (decomposed).

##### **BDO-NH<sub>2</sub>-(Me)<sub>2</sub>**

<sup>1</sup>H NMR (DMSO-*d*<sub>6</sub>, 400 MHz): δ= 10.18 (s, 1 H, N-NH), 9.49 (s, 1 H, N-NH), 8.38 (s, 1 H, C-NH), 7.83 (s, 1 H, C-NH), 3.22 (s, 6 H, N-(CH<sub>3</sub>)<sub>2</sub>), 2.11 (s, 3 H, N=C-CH<sub>3</sub>), 2.10 (s, 3 H, N=C-CH<sub>3</sub>). <sup>13</sup>C {<sup>1</sup>H} NMR (DMSO-*d*<sub>6</sub>, 100 MHz): δ= 182.16 (C=S), 179.35 (C=S), 150.00 (C=N), 148.96 (C=N), 42.80 (N-(CH<sub>3</sub>)<sub>2</sub>), 11.96 (N=C-CH<sub>3</sub>), 11.70 (N=C-CH<sub>3</sub>). IR (neat): cm<sup>-1</sup>= 3395 (w), 3221 (m), 3148 (m), 1591 (m), 1545 (m), 1460 (m), 1412 (m), 1396 (m), 1368 (m), 1261 (m), 1221 (m), 1134 (m), 1103 (m), 1055 (m), 968 (m), 847 (m), 708 (m), 606 (m), 515 (s). Raman (neat): cm<sup>-1</sup>= 2913 (w), 1603 (m), 1586 (s), 1498 (w), 1463 (w), 1397 (w), 1371 (w), 1338 (m), 1263 (w), 1229 (w), 1128 (m), 1110 (w), 1006 (w), 850 (w), 736 (w), 612 (w), 461 (w). Elemental analysis: Found: C, 36.9; H, 6.2; N, 32.3. Calc. for C<sub>8</sub>H<sub>16</sub>N<sub>6</sub>S<sub>2</sub>: C, 36.9; H, 6.2; N, 32.2%. Melting point: >192 °C (decomposed).

### 2.4.13. Spectral examples of a dissymmetric ligand with a Me/Me backbone

Figures 2.4.13.1-4. Spectral examples of the dissymmetric ligand BDO-NH<sub>2</sub>-(Me)<sub>2</sub>.

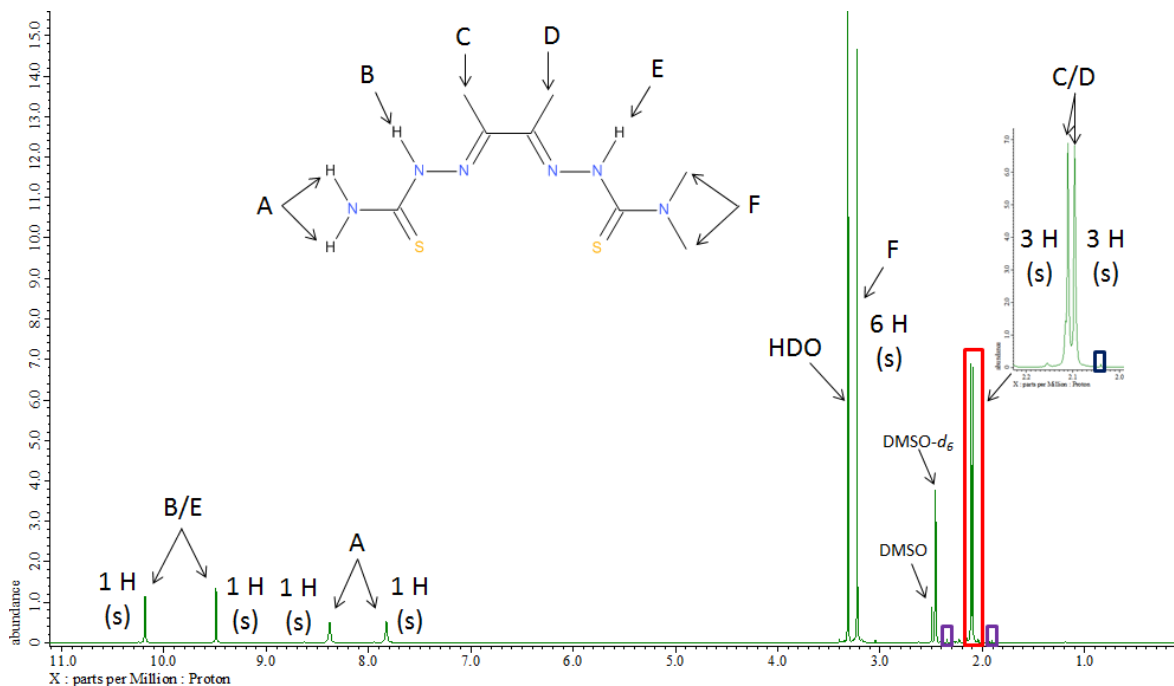


**Figure 2.4.13.1.** An assigned <sup>1</sup>H NMR spectrum of BDO-NH<sub>2</sub>-(Me)<sub>2</sub>. This ligand was successfully synthesised by the exploitation of carbonyl reactivity approach by reacting BDO-NH<sub>2</sub>=O with 4,4-dimethyl-3-thiosemicarbazide. The purple and blue boxes indicate a very small presence of BDO-NH<sub>2</sub>=O and BDO-NH<sub>2</sub>-NH<sub>2</sub> respectively.

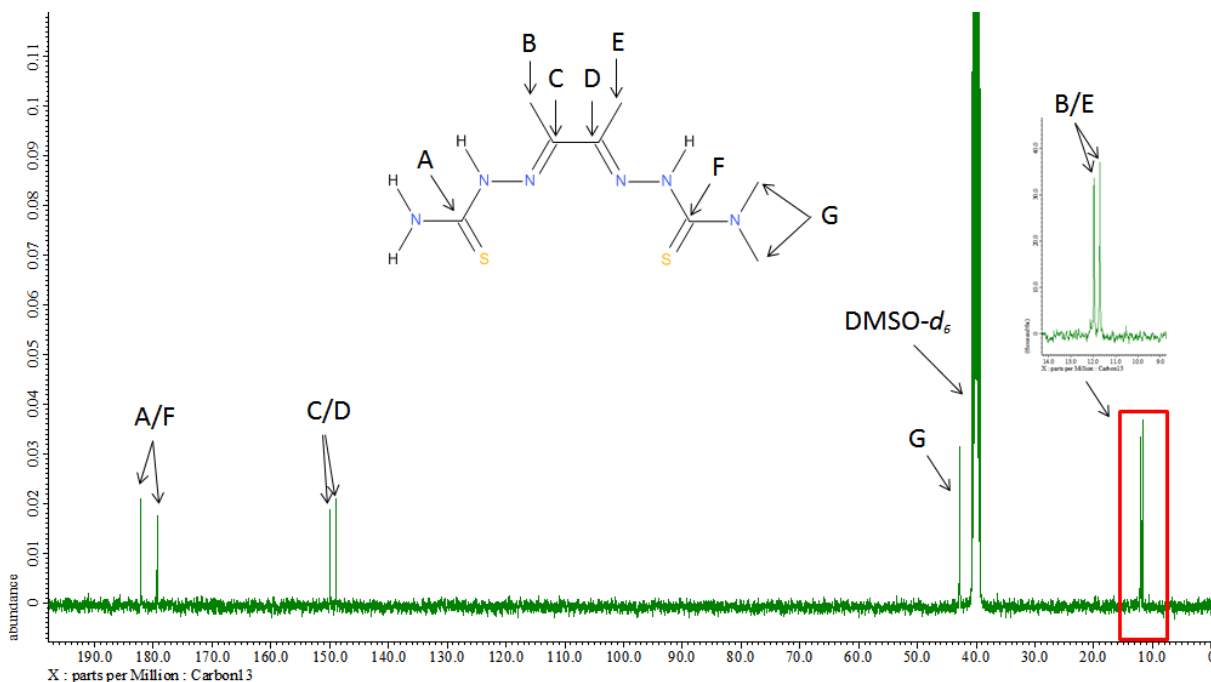


**Figure 2.4.13.2.** An assigned <sup>13</sup>C NMR spectrum of BDO-NH<sub>2</sub>-(Me)<sub>2</sub>.

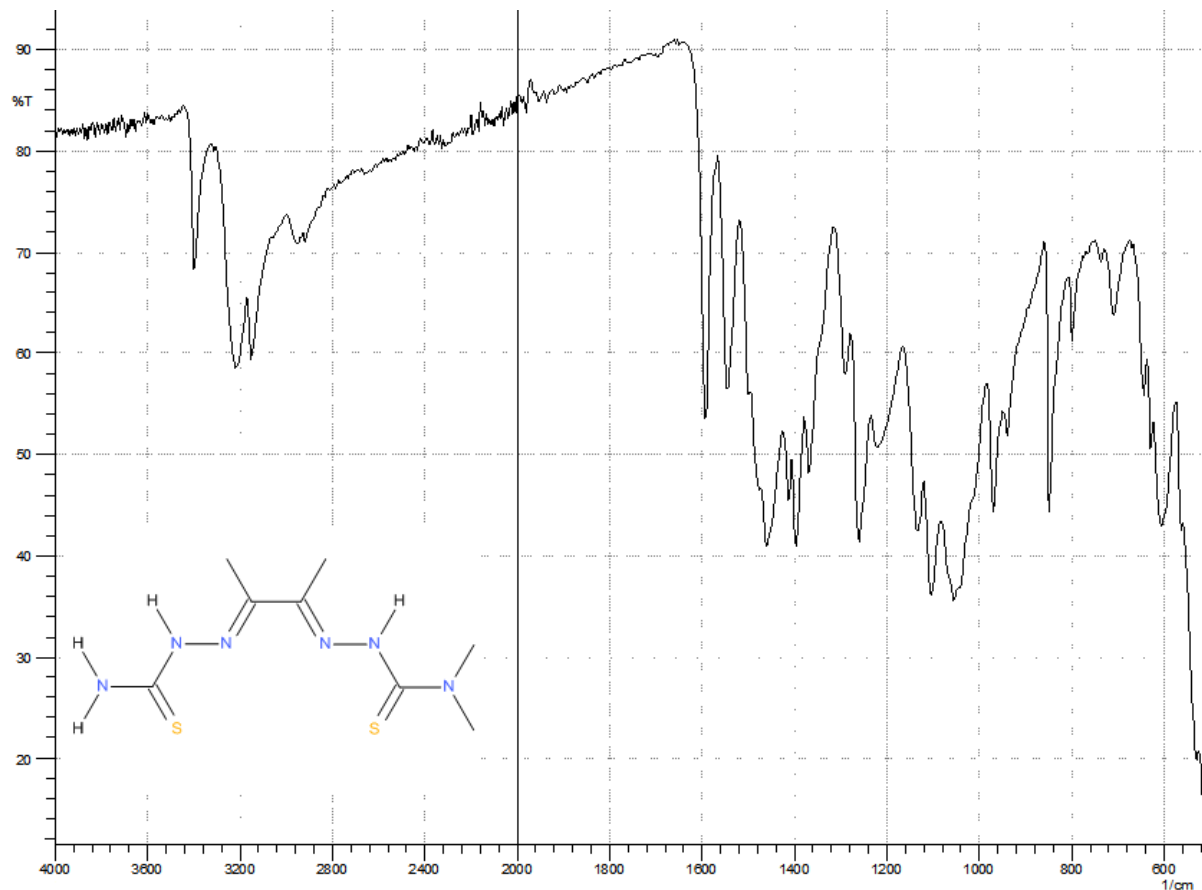


Figure 2.4.13.3. A FTIR spectrum of  $BDO-NH_2-(Me)_2$ .

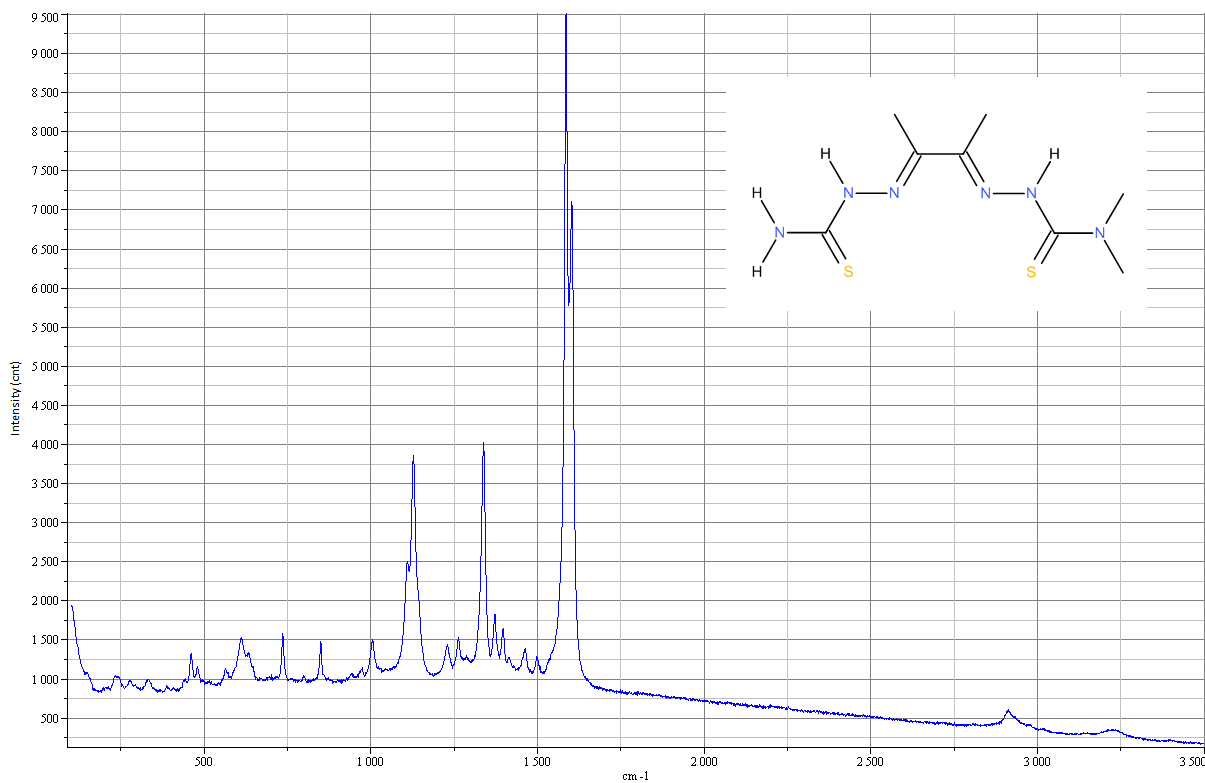


Figure 2.4.13.4. A Raman spectrum of  $BDO-NH_2-(Me)_2$ .

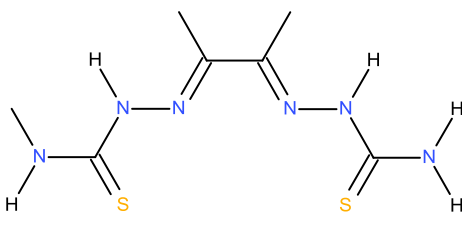
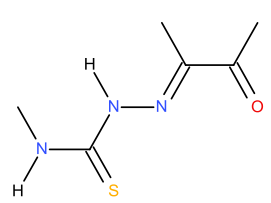
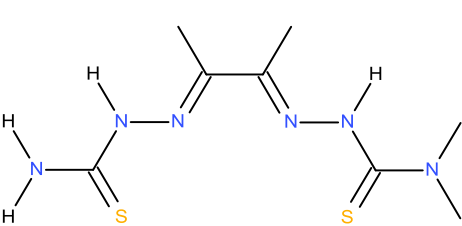
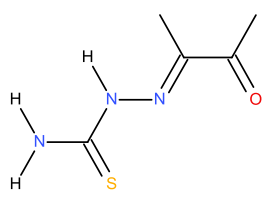


#### **2.4.14. Discussion**

Both the dissymmetric ligands were made successfully and in high purity by following the method reported by G. Buncic *et al.*<sup>82</sup> which was also the method used when synthesising dissymmetric ligands with H/Me on the backbone. Once the BDO-mono-substituted-3-thiosemicarbazone intermediate was isolated in a relatively high purity, the attachment of a second dissimilar 4-substituted-3-thiosemicarbazone was relatively straight forward. The attempt to synthesise BDO-(Me)<sub>2</sub>-Me was an exception. Both intermediates that could be used to make this ligand, BDO-(Me)<sub>2</sub>=O and BDO-Me=O were obtained with a high level of purity. It is worth re-emphasising that as all ligands with BDO backbones, it does not matter which order the two dissimilar 4-substituted-3-thiosemicarbazones are attached. It was found that the constructing a dissymmetric ligand from BDO-(Me)<sub>2</sub>=O was not feasible. The two main reasons were that 4,4-dimethyl-3-thiosemicarbazide is significantly more expensive than any of the other 4-substituted-3-thiosemicarbazones and secondly that the reaction to create the BDO-(Me)<sub>2</sub>=O intermediate had a considerably low yield. Both attempts to synthesise BDO-(Me)<sub>2</sub>-Me/ BDO-Me-(Me)<sub>2</sub> using either BDO-(Me)<sub>2</sub>=O and BDO-Me=O respectively failed to produce the desired product. On closer inspection of the <sup>1</sup>H NMR spectra of both products all the expected peaks were present (plus some impurity peaks), but the integrals of the peaks did not add up to what was expected. After a significant amount of time on this problem, a suitable explanation for this observation still has not been reached. This reaction requires further investigation, but due to the heavy cost of the synthesis, the decision was made to concentrate on the synthesis of dissymmetric ligands with different back bones.

Despite BDO-Me-NH<sub>2</sub> being cited in the literature,<sup>198, 199</sup> it was not possible to find any characterisation data for the ligand. It is believed that BDO-NH<sub>2</sub>-(Me)<sub>2</sub> has not been reported before. However, the ligands BDO-Me-(Me)<sub>2</sub> has been reported before<sup>73, 82, 190</sup> and despite the ligand not being one of those that have been synthesised in this project, the NMR characterisation data can be used as a partial comparison. The NMR data reported<sup>73, 190</sup> show an acceptable level of similarity to the NMR data for BDO-Me-NH<sub>2</sub> and BDO-NH<sub>2</sub>-(Me)<sub>2</sub> when the structural variations are discounted.

Table 2.4.14.1. reports the two dissymmetric ligands that have been successfully made along with the main impurity present and at what proportion this impurity is estimated at.

Ligand	Novel	Yield	Main impurity	Estimated impurity *
<p>BDO-Me-NH<sub>2</sub></p> 	No <sup>196, 198, 199</sup>	35%		2%
<p>BDO-NH<sub>2</sub>-(Me)<sub>2</sub></p> 	Yes	41%		Less than 1%

\*Estimated by <sup>1</sup>H NMR spectra on an average of three integrals where possible. Typically this was to include the integrals taken from the peaks due to the N=C-CH<sub>3</sub> and N-NH environments.

**Table 2.4.14.1.** Summary of purity for the dissymmetric Ligands with Me/Me backbones, synthesised by the exploitation of carbonyl reactivity approach.

## 2.5. Ligands with Me/Et backbones

### Application

This class of ligands along with ligands with Me/Me backbones are of interest for the imaging of hypoxic tissues which can be a common pathology in a range of diseases including heart disease and cancer.<sup>109, 113, 115</sup> In order to achieve this, the complex must be able to migrate to the tissue and be reduced only in hypoxic conditions but not in normoxic conditions. The reduction of the ligand will allow the release and trapping of the copper radioisotope ion which can then be detected via PET.

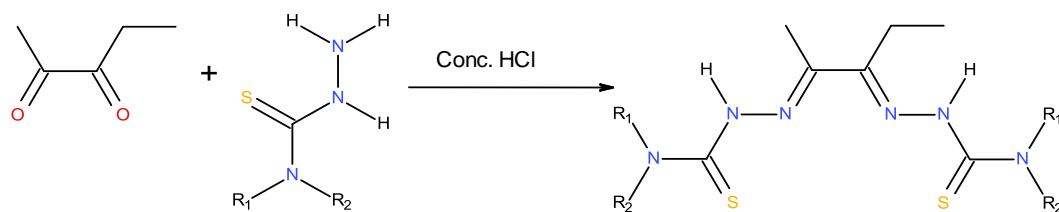
It is expected that ligands made from di-ketones with Me/Me or Me/Et on the backbone have redox potential in the appropriate range. The more lipophilic the substituents on the 4-substituted-3-thiosemicarbazide arm; the slower the clearance from normoxic and thus the longer it takes to achieve a suitable hypoxic: normoxic ratio in order to give informative images.

The aim is to synthesise a range of ligands with Me/Me or Me/Et on the backbone and with 4-substituted -3-thiosemicarbazide arms with a limited number of methyl/ethyl substituents.

## 2.5.1. Symmetric ligands with Me/Et backbones

### Overview of reaction

The synthesis of this subgroup of ligands requires one equivalent of 2,3-pentanedione (PDO) to be reacted with two equivalents of a chosen 4-substituted-3-thiosemicarbazide, under acidic conditions, in water at 60°C to give the desired symmetric ligand (Figure 2.5.1.1.). Three symmetric ligands have been synthesised (Figure 2.5.1.2.).



	R <sub>1</sub>	R <sub>2</sub>
PDO-NH <sub>2</sub> -NH <sub>2</sub>	H	H
PDO-Me-Me	CH <sub>3</sub>	H
PDO-Et-Et	CH <sub>2</sub> CH <sub>3</sub>	H

Figure 2.5.1.1. The general reaction for the synthesis of symmetric ligands with Me/Et backbones.

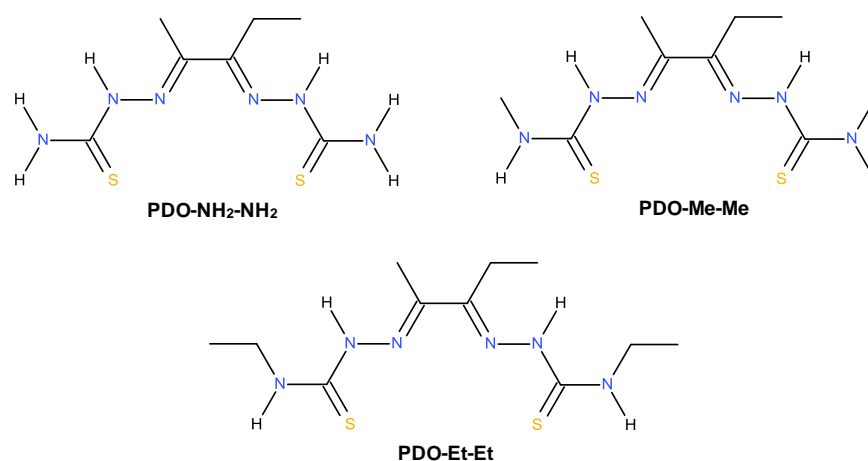


Figure 2.5.1.2. Structures of the symmetric ligands with Me/Et backbones that were synthesised.

## 2.5.2. Methods

### PDO-NH<sub>2</sub>-NH<sub>2</sub>

Thiosemicarbazide (0.775 g, 0.0085 mol) was dissolved in de-ionised water (50 mL, 60 °C). HCl (32%, 5 drops) was added, then 2,3-pentanedione (0.44 mL, 0.0042 mol, 0.42 g) was added rapidly and left to stir (60 °C, 1 hour). The precipitate was filtered and washed with diethyl ether (2 x 25 mL). The crude product was dissolved in DMSO (12 mL), filtered and recrystallised with de-ionised water (24 mL). The precipitate was recovered by filtration, washed with a small quantity of water and dried. A white solid (0.652 g) was recovered (63% yield).

### PDO-Me-Me

4-methyl-3-thiosemicarbazide (0.894 g, 0.0085 mol) was dissolved in de-ionised water (50 mL, 60 °C). HCl (32%, 5 drops) was added, then 2,3-pentanedione (0.44 mL, 0.0042 mol, 0.42 g) was added rapidly and left to stir (60 °C, 1 hour). The precipitate was filtered and washed with diethyl ether (2 x 25 mL). The crude product was dissolved in DMSO (15 mL), filtered and recrystallised with de-ionised water (30 mL). The precipitate was recovered by filtration, washed with a small quantity of water, diethyl ether (2 x 25 mL) and dried. A white solid (0.474 g) was recovered (78% yield).

### PDO-Et-Et

4-ethyl-3-thiosemicarbazide (1.013 g, 0.0085 mol) was dissolved in ethanol (50 mL, 60 °C). HCl (32%, 5 drops) was added, then 2,3-pentanedione (0.44 mL, 0.0042 mol, 0.42 g) was added rapidly and left to stir (60 °C, 1 hour). The precipitate was filtered and washed with diethyl ether (2 x 25 mL). The crude product was dissolved in DMSO (12 mL), filtered and recrystallised with de-ionised water (24 mL). The precipitate was recovered by filtration, washed with a quantity of water and dried. A creamy white solid (0.729 g) was recovered (57% yield).

## 2.5.3. Characterisation data for symmetric ligands with Me/Et backbones

### PDO-NH<sub>2</sub>-NH<sub>2</sub>

<sup>1</sup>H NMR (DMSO-*d*<sub>6</sub>, 400 MHz): δ= 10.32 (s, 1 H, N-NH), 10.19 (s, 1 H, N-NH), 8.38 (s, 2 H, C-NH<sub>2</sub>), 7.79 (s, 1 H, C-NH), 7.79 (s, 1 H, C-NH), 2.81 (q, 2H, C-CH<sub>2</sub>, J= 7.6 Hz), 2.10 (s, 3 H, N=C-CH<sub>3</sub>), 0.84 (t, 3 H, C-CH<sub>2</sub>-CH<sub>3</sub>, J=7.2 Hz). <sup>13</sup>C {<sup>1</sup>H} NMR (DMSO-*d*<sub>6</sub>, 100 MHz): δ= 179.40 (C=S), 179.36 (C=S), 152.68 (C=N), 147.81 (C=N), 17.46 (C-CH<sub>2</sub>), 12.23 (N=C-CH<sub>3</sub>), 11.56 (C-CH<sub>2</sub>-CH<sub>3</sub>). IR (neat): cm<sup>-1</sup>= 3418 (w), 3202 (m), 3152 (m), 2986 (m), 1599 (s), 1493 (s), 1447 (s), 1366 (w), 1290 (m), 1244 (m), 1155 (m), 1086 (s), 1059 (m), 988 (m), 924 (w), 841 (m), 793 (w), 642 (m), 590 (m). Raman (neat): cm<sup>-1</sup>= 2908 (w), 1604 (s), 1589 (s), 1473 (w), 1366 (w), 1345 (m), 1308 (w), 1246 (w), 1125 (s), 1054 (w), 989 (w), 923 (w), 865 (w), 744 (w), 467 (w). Melting point: >202 °C (decomposed).

### PDO-Me-Me

<sup>1</sup>H NMR (DMSO-*d*<sub>6</sub>, 400 MHz): δ= 10.32 (s, 1 H, N-NH), 10.18 (s, 1 H, N-NH), 8.31 (quartet overlapping a quartet, 1 H, H<sub>3</sub>C-NH, J= 4.8 Hz), 8.30 (quartet overlapping a quartet, 1 H, H<sub>3</sub>C-NH, J= 4.4 Hz), 2.98 (m, 6 H, HN-CH<sub>3</sub>), 2.87 (q, 2H, C-CH<sub>2</sub>, J= 7.2 Hz), 2.14 (s, 3 H, N=C-CH<sub>3</sub>), 0.90 (t, 3 H, C-CH<sub>2</sub>-CH<sub>3</sub>, J=7.2 Hz). <sup>13</sup>C {<sup>1</sup>H} NMR (DMSO-*d*<sub>6</sub>, 100 MHz): δ= 178.89 (C=S), 152.36 (C=N), 147.53 (C=N), 31.74 (HN-CH<sub>3</sub>), 31.70 (HN-CH<sub>3</sub>), 17.25 (C-CH<sub>2</sub>), 12.29 (N=C-CH<sub>3</sub>), 11.35 (C-CH<sub>2</sub>-CH<sub>3</sub>). IR (neat): cm<sup>-1</sup>= 3308 (w), 2938 (w), 1539 (s), 1477 (s), 1460 (s), 1433 (s), 1410 (m), 1354 (m), 1219 (s), 1169 (m), 1128 (s), 1086 (s), 1065 (s), 1042 (s), 991 (m), 826 (m), 781 (m), 660 (m), 608 (m),

565 (s). **Raman (neat):**  $\text{cm}^{-1}$  = 3379 (w), 2936 (w), 1598 (m), 1573 (s), 1390 (m), 1336 (w), 1296 (w), 1235 (w), 1160 (w), 1134 (w), 1026 (w), 992 (w), 734 (w), 673 (w), 577 (w), 453 (w), 324 (w).

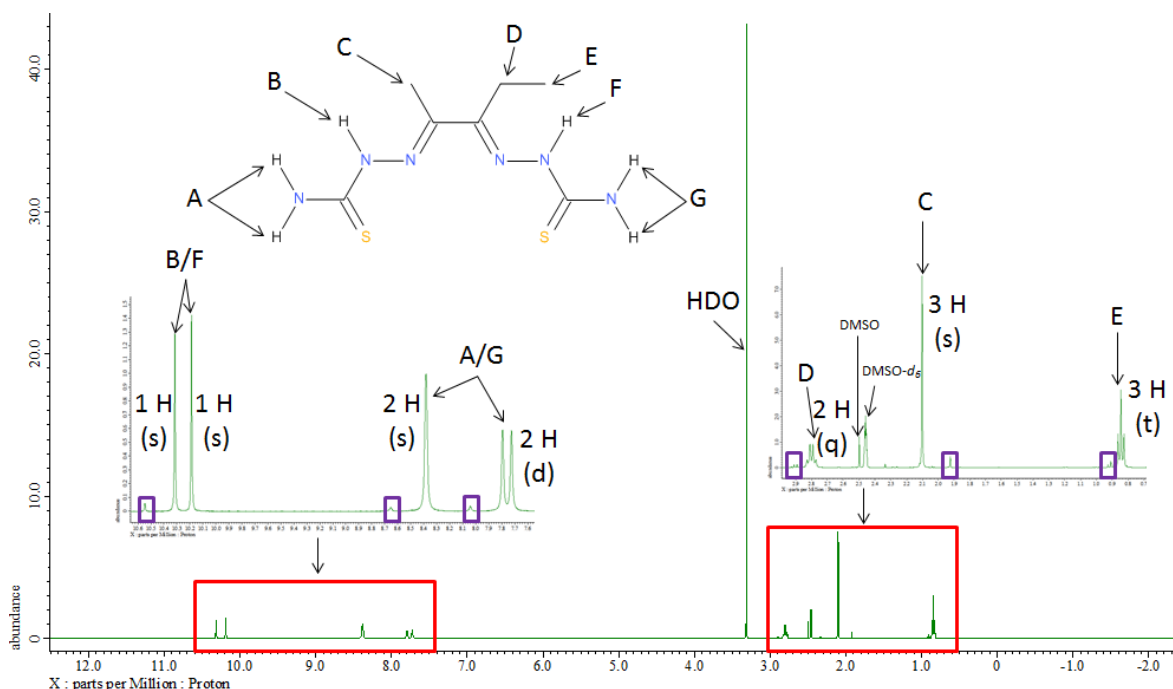
**Melting point:** >217 °C (decomposed).

### PDO-Et-Et

**$^1\text{H}$  NMR** (DMSO- $d_6$ , 400 MHz):  $\delta$  = 10.26 (s, 1 H, N-NH), 10.13 (s, 1 H, N-NH), 8.35 (t, 1 H,  $\text{H}_2\text{C-NH}$ ,  $J$  = 6.0 Hz), 8.29 (t, 1 H,  $\text{H}_2\text{C-NH}$ ,  $J$  = 6.0 Hz), 3.55 (dq, 4 H,  $\text{HN-CH}_2$ ,  $J$  = 7.2, 6.0 Hz), 2.86 (q, 2H, C- $\text{CH}_2$ ,  $J$  = 7.2 Hz), 2.15 (s, 3 H, N=C- $\text{CH}_3$ ), 1.09 (two overlapping triplets, 6 H, N- $\text{CH}_2\text{-CH}_3$ ,  $J$  = 7.2), 0.86 (t, 3 H, C- $\text{CH}_2\text{-CH}_3$ ,  $J$  = 7.2 Hz).  **$^{13}\text{C}$  { $^1\text{H}$ } NMR** (DMSO- $d_6$ , 100 MHz):  $\delta$  = 177.92 (C=S), 152.28 (C=N), 147.51 (C=N), 39.10 (HN- $\text{CH}_2$ ), 39.08 (HN- $\text{CH}_2$ ), 17.41 (C- $\text{CH}_2$ ), 14.89 (N- $\text{CH}_2\text{-CH}_3$ ), 12.35 (N=C- $\text{CH}_3$ ), 11.38 (C- $\text{CH}_2\text{-CH}_3$ ). **IR (neat):**  $\text{cm}^{-1}$  = 3345 (w), 3211 (w), 2967 (w), 2880 (w), 1522 (s), 1491 (s), 1437 (s), 1385 (m), 1306 (m), 1261 (m), 1209 (s), 1167 (m), 1136 (s), 1078 (m), 1061 (s), 959 (m), 924 (m), 818 (m), 783 (m), 658 (m), 530 (s). **Raman (neat):**  $\text{cm}^{-1}$  = 2876 (w), 1600 (s), 1531 (w), 1400 (w), 1346 (w), 1247 (w), 1208 (w), 1128 (w), 1048 (w), 992 (w), 738 (w), 675 (w), 458 (w), 306 (w), 200 (w). **Elemental analysis:** Found: C, 43.7; H, 7.3; N, 27.8. Calc. for  $\text{C}_{11}\text{H}_{22}\text{N}_6\text{S}_2$ : C, 43.6; H, 7.3; N, 27.7%. **Melting point:** >215 °C (decomposed).

### 2.5.4. Spectral examples of a symmetric Ligand with a Me/Et backbone

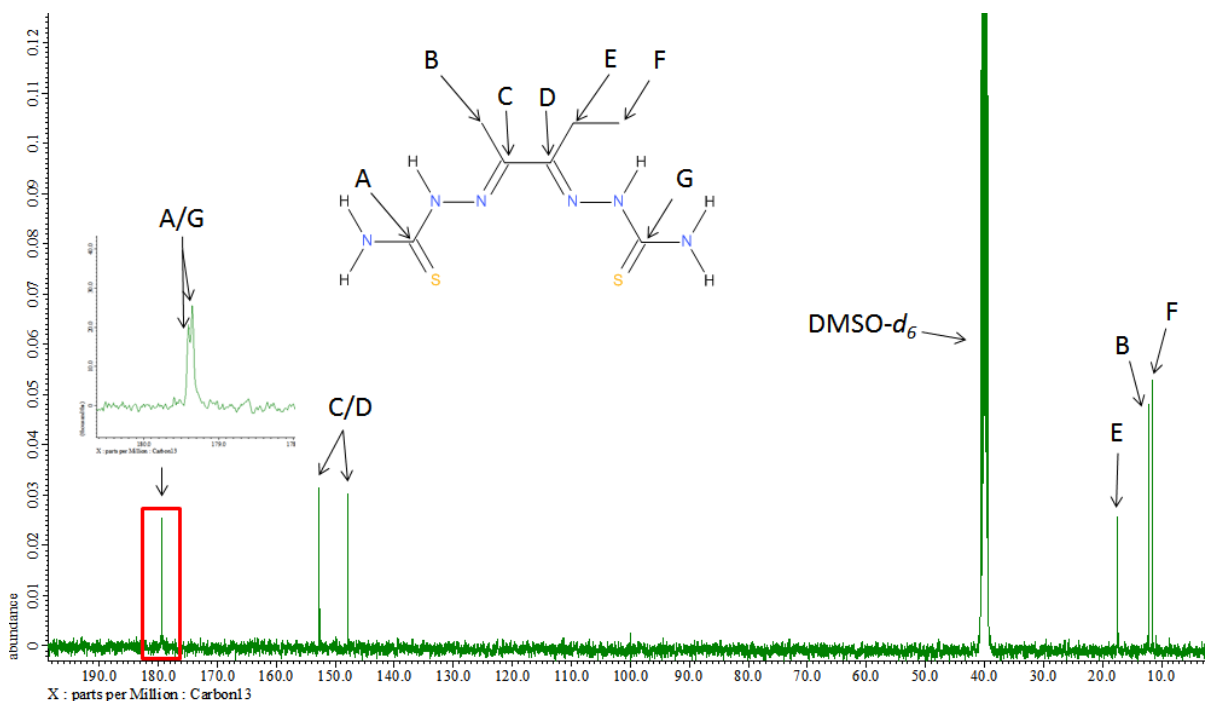
Figures 2.5.4.1-4. Spectral examples of ligand PADA-NH<sub>2</sub>-NH<sub>2</sub>.



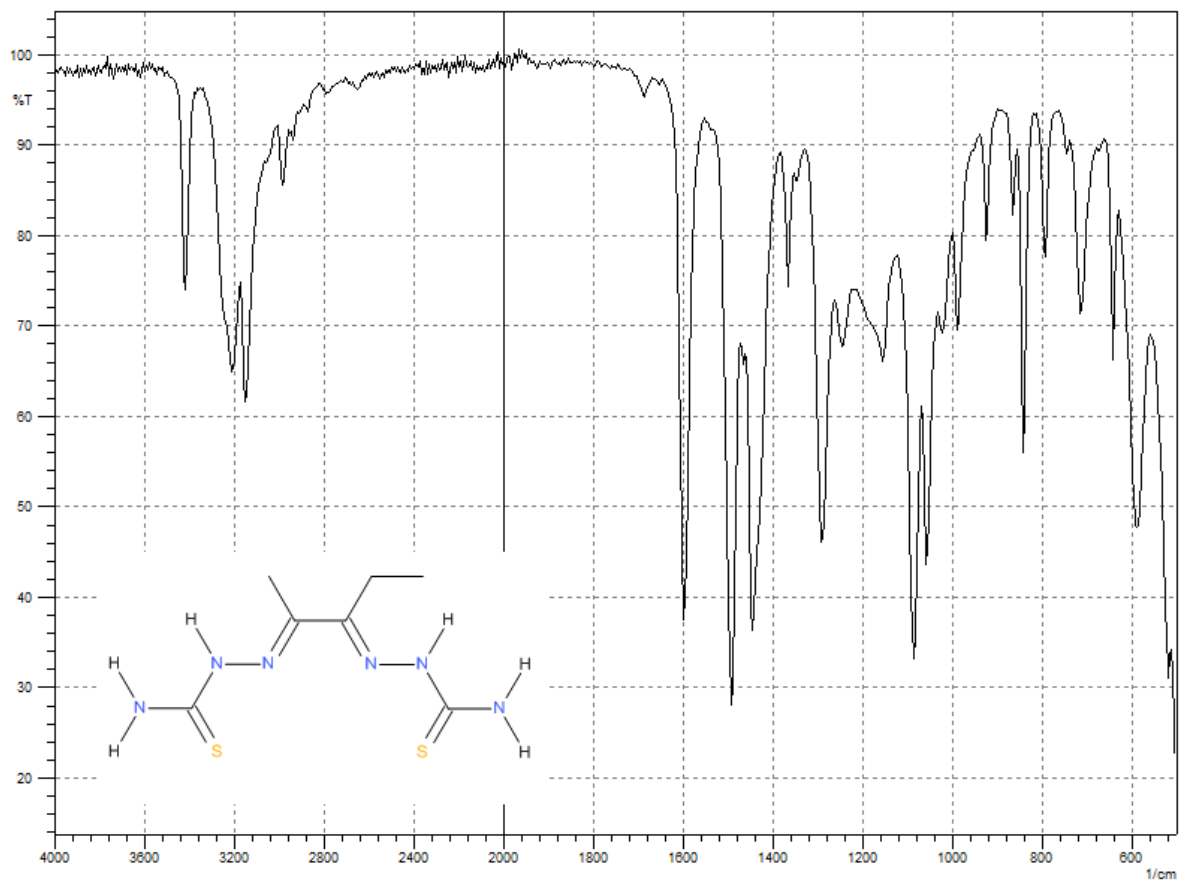
**Figures 2.5.4.1.** An assigned  $^1\text{H}$  NMR spectrum of  $\text{PDO-NH}_2\text{-NH}_2$ . The  $\text{PDO-NH}_2\text{-NH}_2$  ligand was produced by reacting 2,3-pentanedione with thiosemicarbazide. The purple boxes indicate a small presence of  $\text{PDO-NH}_2\text{-O}$ . This is typical throughout the synthesis of this class of ligands.

An interesting observation worth noting is that when the thiosemicarbazide is bound to the PDO backbone the terminal  $\text{NH}_2$  groups are seen as a singlet and a doublet of equal integrals. This is

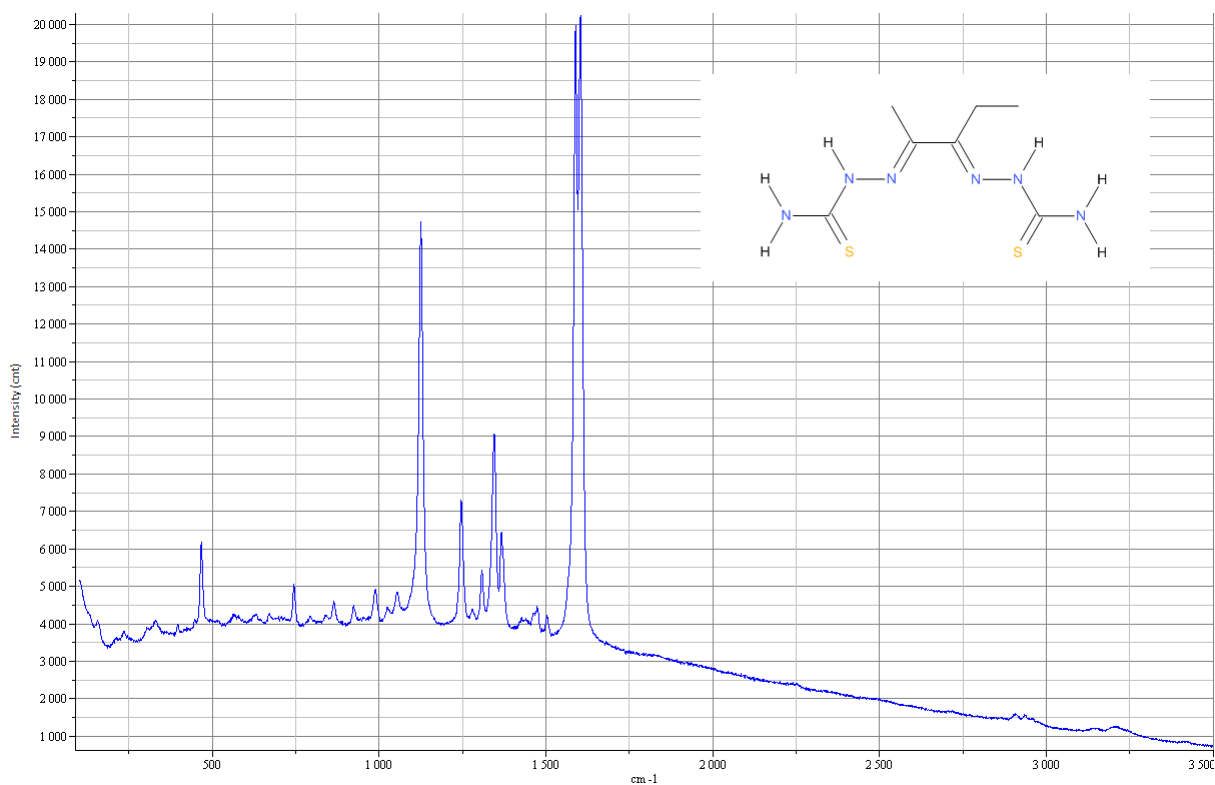
not observed with the other backbones when the  $\text{NH}_2$  group is seen as two singlets with equal integrals. As this phenomenon is only observed with the PDO backbone it is reasonable to predict that the doublet is due to the  $\text{NH}_2$  group of the 4-ethyl-3-thiosemicarbazide that has reacted with the carbonyl group of the ethyl ketone. It is thought that the ethyl group induces some level of hindered rotation of the  $\text{NH}_2$  group and in doing so allows the NMR spectrometer to resolve two slightly different proton environments. No further investigation was undertaken, but a possible investigation that could be undertaken is reacting 2 equivalents of thiosemicarbazide with 3,4-hexane-dione to see if the singlet is replaced by a second doublet. Some variable temperature NMR studies could also be undertaken in order to establish if heating up the sample would result in the doublet being observed as a singlet.



**Figure 2.5.4.2.** An assigned  $^{13}\text{C}$  NMR spectrum of PDO- $\text{NH}_2$ - $\text{NH}_2$ .



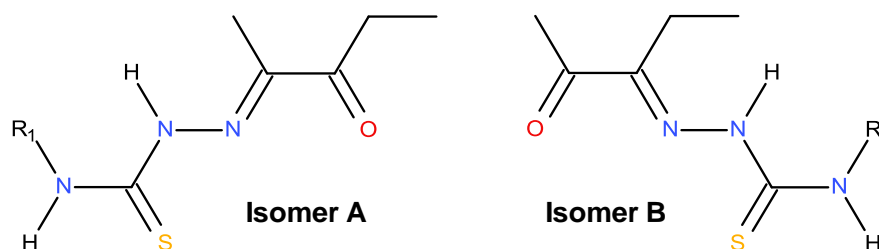
**Figure 2.5.4.3.** A FTIR spectrum of PDO-NH<sub>2</sub>-NH<sub>2</sub>.



**Figure 2.5.4.4.** A Raman spectrum of PDO-NH<sub>2</sub>-NH<sub>2</sub>.

### 2.5.5. Discussion

All three ligands were successfully synthesised in high purity. It is estimated that none of the three ligands have a purity, in respect to impurities related to the bis-(thiosemicarbazones), of less than 95%. Symmetric ligands of this class have been reported before therefore methods are well described.<sup>23, 77, 164</sup> It seems that alongside the normal expected intermediate a different isomeric form of the mono-substituted-3-thiosemicarbazone intermediate is being formed as a minor product. The general structures of the two expected impurities are shown below (Figure 2.5.5.1.).

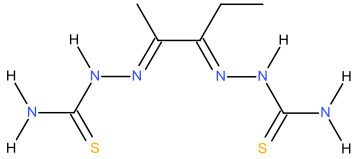
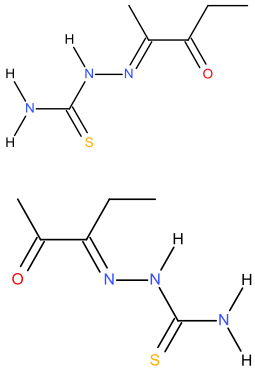
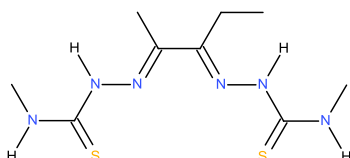
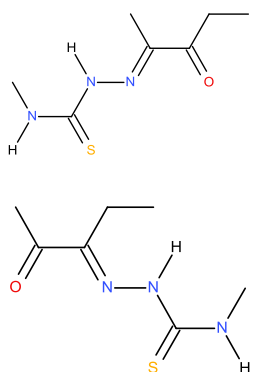
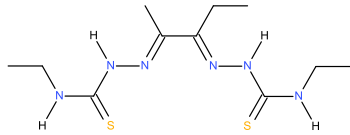
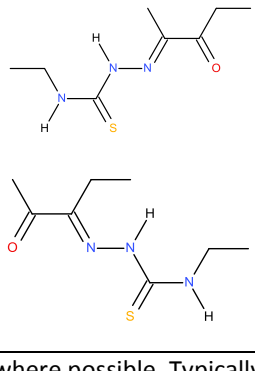


**Figure 2.5.5.1.** The two expected impurities in the synthesis of the symmetric ligands with Me/Et backbones.

It is hypothesized that the ethyl substituent on the di-ketone reduces the reactivity difference between the two ketones causing the formation of the new intermediate to become favourable. Discussion of this new intermediate will be addressed in the intermediate section below (section 2.5.11.).

Despite symmetric ligands with Me/Et on the backbone have been reported by numerous articles<sup>69, 77, 145, 146, 164</sup> for biological screening studies for the use of these ligands for hypoxia imaging, there is no NMR or IR/Raman characterisation data reported alongside the biological results. Structural based searching of databases, such as SciFinder, did not locate any characterisation data on these compounds. By comparing the data from this class of ligands with data of ligands with different backbones/amine substituents it is believed that data has been assigned accurately. Table 2.5.5.2. below illustrates all three ligands, what the main impurities are and an estimate of the percentage.



Ligand	Novel	Yield	Main impurity	Estimated impurity*
<p><b>PDO-NH<sub>2</sub>-NH<sub>2</sub></b></p> 	No <sup>69, 77,</sup> 145, 146, 164	63%		4%  1%
<p><b>PDO-Me-Me</b></p> 	No <sup>69, 77,</sup> 145, 146, 164	78%		2%  Less than 1%
<p><b>PDO-Et-Et</b></p> 	Yes	18%		3%  1%

\*Estimated by <sup>1</sup>H NMR spectra on an average of three integrals where possible. Typically this was to include the integrals from the peaks due to the N=C-CH<sub>3</sub> and N-NH environments.

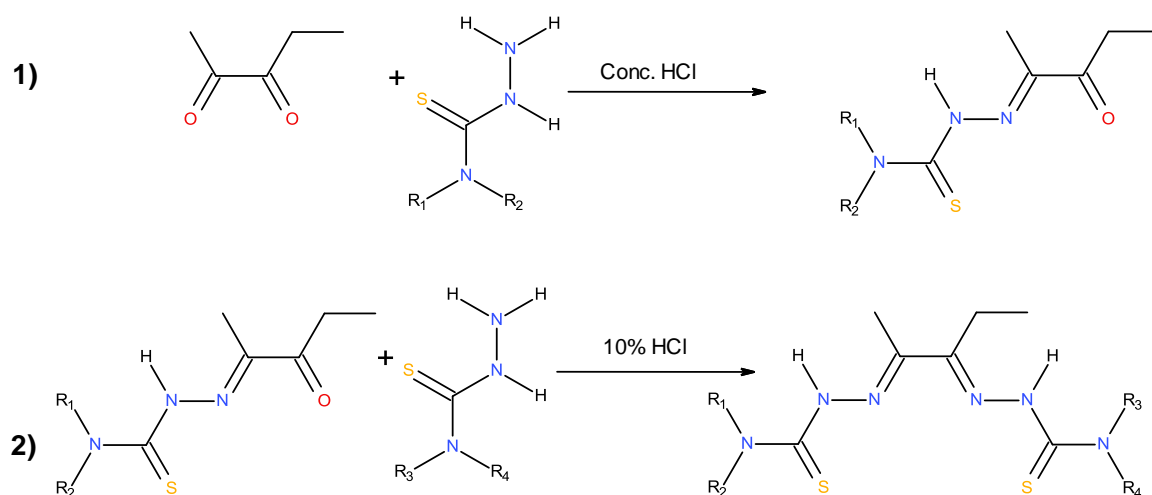
**Table 2.5.5.2.** Summary of purity for the symmetric Ligands with Me/Et backbones, synthesised by the exploitation of carbonyl reactivity approach.

## **2.5.6. Dissymmetric ligands with Me/Et backbones**

### **Overview of reaction**

The synthesis of the dissymmetric ligands firstly requires the synthesis of PDO based mono-substituted-3-thiosemicarbazone intermediates. These intermediates are synthesised by reacting PDO and a 4-substituted-3-thiosemicarbazone in the stoichiometric ratio of 1:1 at reduced temperatures and under acidic conditions. Once isolated the intermediate is then reacted with 1

equivalent of a dissimilar 4-substituted-3-thiosemicarbazone catalysed under slightly acidic conditions to produce the desired dissymmetric ligand (Figure 2.5.6.1.).



	R <sub>1</sub>	R <sub>2</sub>	R <sub>3</sub>	R <sub>4</sub>
PDO-NH <sub>2</sub> -Me	H	H	CH <sub>3</sub>	H
PDO-NH <sub>2</sub> -(Me) <sub>2</sub>	H	H	CH <sub>3</sub>	CH <sub>3</sub>
PDO-NH <sub>2</sub> -Et	H	H	CH <sub>2</sub> CH <sub>3</sub>	H
PDO-Me-NH <sub>2</sub>	CH <sub>3</sub>	H	H	H
PDO-Et-NH <sub>2</sub>	CH <sub>2</sub> CH <sub>3</sub>	H	H	H

**Figure 2.5.6.1.** The general reaction for the synthesis of dissymmetric ligands with Me/Et backbones.

Figures 2.5.6.2-3. Structures of the dissymmetric ligands with Me/Et backbones that have been synthesised.

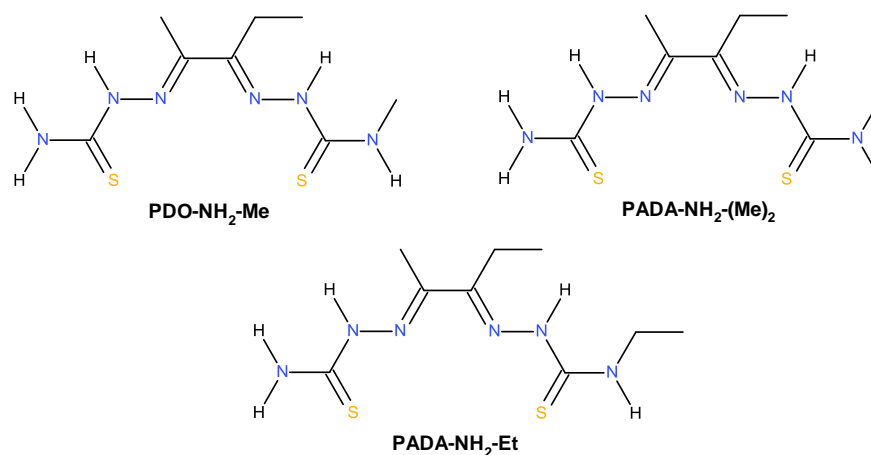


**Figure 2.5.6.2.** Dissymmetric ligands from PDO-NH<sub>2</sub>=O.

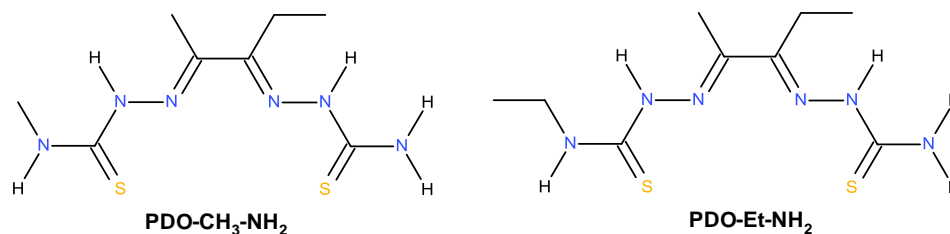


**Figure 2.5.6.2.** Dissymmetric ligands from PDO-Me=O and PDO-Et=O.

### **2.5.7. Synthesis of the PDO-mono-substituted-3-thiosemicarbazone intermediates**

In order to make the five dissymmetric ligands, these three intermediates had to be successfully synthesised (Figure 2.5.7.1.).

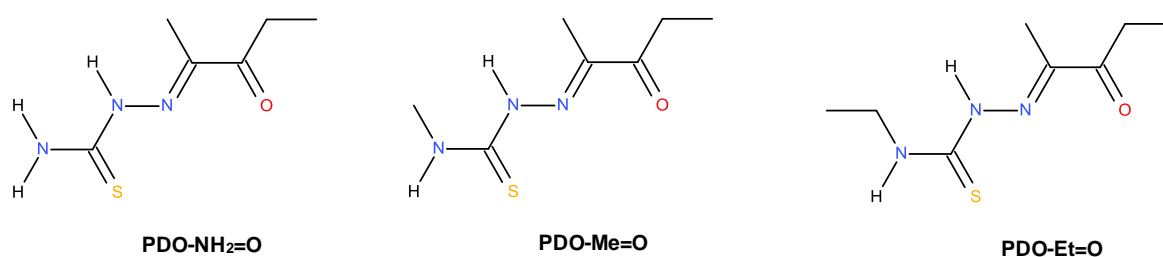


**Figure 2.5.7.1.** Structures of the three PDO-mono-substituted-3-thiosemicarbazone intermediates that have been synthesised by the exploitation of carbonyl reactivity approach.

### **2.5.8. Methods**

#### **PDO-NH<sub>2</sub>=O**

Thiosemicarbazide (1.55 g, 0.017 mol) was dissolved in de-ionised water (200 mL, warm). Solution cooled (10°C) over ice, followed by the addition of HCl (32%, 20 drops). 2,3-pentanedione (7.12 mL, 0.068 mol, 6.81 g) was added rapidly and vigorously stirred (10°C, 10 minutes). The precipitate was recovered via filtration, washed with de-ionised water (2 x 50 mL) and dried. An off white solid (1.957g) was recovered (66% yield).

#### **PDO-Me=O**

4-methyl-3-thiosemicarbazide (1.788 g, 0.017 mol) was dissolved in a solution of de-ionised water (200 mL) and ethanol (80 mL). The solution was cooled (-10°C) in a salt/ice bath (300g ice, 100g table salt), followed by the addition of HCl (32%, 6 drops). 2,3-pentanedione (3.56 mL, 0.034 mol, 3.41 g) was added rapidly and vigorously stirred (circa -10°C, 5 minutes). The precipitate was recovered via filtration, washed with de-ionised water (4 x 50 mL) and dried. An off white solid (1.572g) was recovered (49% yield).

### PDO-Et=O

4-ethyl-3-thiosemicarbazide (1.013 g, 0.085 mol) dissolved in a solution of de-ionised water (100 mL) and ethanol (60 mL). The solution was cooled (-12°C) in a salt/ice bath (300g ice, 100g table salt), followed by the addition of HCl (32%, 3 drops). 2,3-pentanedione (1.78 mL, 0.017 mol, 1.70 g) was added rapidly and vigorously stirred (circa -11°C, 4 minutes). The precipitate was recovered via filtration, washed with de-ionised water (3 x 50 mL) and dried. An off white solid (0.862g) was recovered (50% yield).

### 2.5.9. Characterisation data for the PDO-mono-substituted-3-thiosemicarbazone intermediates

#### PDO-NH<sub>2</sub>=O

<sup>1</sup>H NMR (DMSO-*d*<sub>6</sub>, 400 MHz): δ= 10.55 (s, 1 H, N-NH), 8.66 (s, 1 H, C-NH), 8.04 (s, 1 H, C-NH), 2.90 (q, 2H, C-CH<sub>2</sub>, J= 7.2 Hz), 1.92 (s, 3 H, N=C-CH<sub>3</sub>), 0.90 (t, 3 H, C-CH<sub>2</sub>-CH<sub>3</sub>, J=7.2 Hz). <sup>13</sup>C {<sup>1</sup>H} NMR (DMSO-*d*<sub>6</sub>, 100 MHz): δ= 200.71 (C=O), 180.25 (C=S), 145.90 (C=N), 29.64 (C-CH<sub>2</sub>), 10.88 (N=C-CH<sub>3</sub>), 8.68 (C-CH<sub>2</sub>-CH<sub>3</sub>). IR (neat): cm<sup>-1</sup>= 3412 (w), 3302 (m), 3177 (m), 2984 (w), 1688 (s), 1593 (s), 1491 (m), 1422 (m), 1362 (m), 1233 (s), 1090 (s), 1043 (s), 932 (m), 843 (m), 797 (m), 700 (m), 590 (s), 552 (s). Raman (neat): cm<sup>-1</sup>= 3302 (w), 3192 (w), 2986 (w), 2945 (w), 2919 (w), 2898 (w), 1683 (m), 1614 (s), 1464 (w), 1364 (w), 1258 (w), 1103 (m), 1091 (m), 1045 (m), 930 (w), 838 (w), 602 (w), 487 (w), 461 (w), 410 (w), 313 (w). Melting point: >165 °C (decomposed).

#### PDO-Me=O

<sup>1</sup>H NMR (DMSO-*d*<sub>6</sub>, 400 MHz): δ= 10.58 (s, 1 H, N-NH), 8.55 (q, 1 H, H<sub>3</sub>C-NH, J= 4.8 Hz), 3.00 (d, 3 H, HN-CH<sub>3</sub>, J= 4.8 Hz), 2.93 (q, 2H, C-CH<sub>2</sub>, J= 7.2 Hz), 1.93 (s, 3 H, N=C-CH<sub>3</sub>), 0.93 (t, 3 H, C-CH<sub>2</sub>-CH<sub>3</sub>, J=7.2 Hz). <sup>13</sup>C {<sup>1</sup>H} NMR (DMSO-*d*<sub>6</sub>, 100 MHz): δ= 200.54 (C=O), 179.48 (C=S), 145.60 (C=N), 31.91 (HN-CH<sub>3</sub>), 29.59 (C-CH<sub>2</sub>), 10.84 (N=C-CH<sub>3</sub>), 8.62 (C-CH<sub>2</sub>-CH<sub>3</sub>). IR (neat): cm<sup>-1</sup>= 3379 (w), 3210 (w), 2982 (w), 1682 (s), 1541 (s), 1499 (s), 1429 (m), 1406 (m), 1375 (m), 1360 (m), 1207 (s), 1146 (s), 1107 (s), 1088 (s), 1055 (m), 1034 (s), 932 (m), 835 (m), 797 (m), 652 (m), 559 (s). Raman (neat): cm<sup>-1</sup>= 3322 (w), 2940 (w), 1684 (m), 1677 (m), 1600 (s), 1367 (w), 1203 (m), 1143 (w), 1115 (w), 1090 (w), 1047 (m), 831 (m), 649 (w), 561 (w), 415 (w), 315 (w). Melting point: >136-141 °C.

#### PDO-Et=O

<sup>1</sup>H NMR (DMSO-*d*<sub>6</sub>, 400 MHz): δ= 10.51 (s, 1 H, N-NH), 8.60 (t, 1 H, H<sub>2</sub>C-NH, J= 6.0 Hz), 3.58 (dq, 2 H, HN-CH<sub>2</sub>, J=7.6, 6.0 Hz), 2.93 (q, 2H, C-CH<sub>2</sub>, J= 7.2 Hz), 1.93 (s, 3 H, N=C-CH<sub>3</sub>), 1.11 (t, 3 H, N-CH<sub>2</sub>-CH<sub>3</sub>, J=7.6), 0.93 (t, 3 H, C-CH<sub>2</sub>-CH<sub>3</sub>, J=7.2 Hz). <sup>13</sup>C {<sup>1</sup>H} NMR (DMSO-*d*<sub>6</sub>, 100 MHz): δ= 200.53 (C=O), 178.47 (C=S), 145.65 (C=N), 39.27 (HN-CH<sub>2</sub>), 29.59 (C-CH<sub>2</sub>), 14.66 (N-CH<sub>2</sub>-CH<sub>3</sub>), 10.86 (N=C-CH<sub>3</sub>), 8.60 (C-CH<sub>2</sub>-CH<sub>3</sub>). IR (neat): cm<sup>-1</sup>= 3345 (w), 3188 (w), 2974 (w), 1686 (s), 1612 (w), 1537 (s), 1499

(s), 1427 (m), 1364 (m), 1190 (s), 1155 (m), 1117 (m), 1092 (m), 1038 (s), 949 (m), 824 (m), 800 (m), 600 (s), 563 (s). **Raman (neat):**  $\text{cm}^{-1}$  = 3346 (w), 2913 (w), 1683 (w), 1611 (w), 1448 (w), 1366 (w), 1265 (w), 1189 (w), 1153 (w), 1115 (w), 1039 (w), 819 (w), 654 (w), 560 (w), 304 (w). **Melting point:** >103-104 °C.

### 2.5.10. Spectral examples of a PDO-mono-substituted-3-thiosemicarbazone intermediate

**Figures 2.5.10.1-4.** Spectral examples of the PADA-mono-substituted-3-thiosemicarbazone intermediate PDO-Me=O.

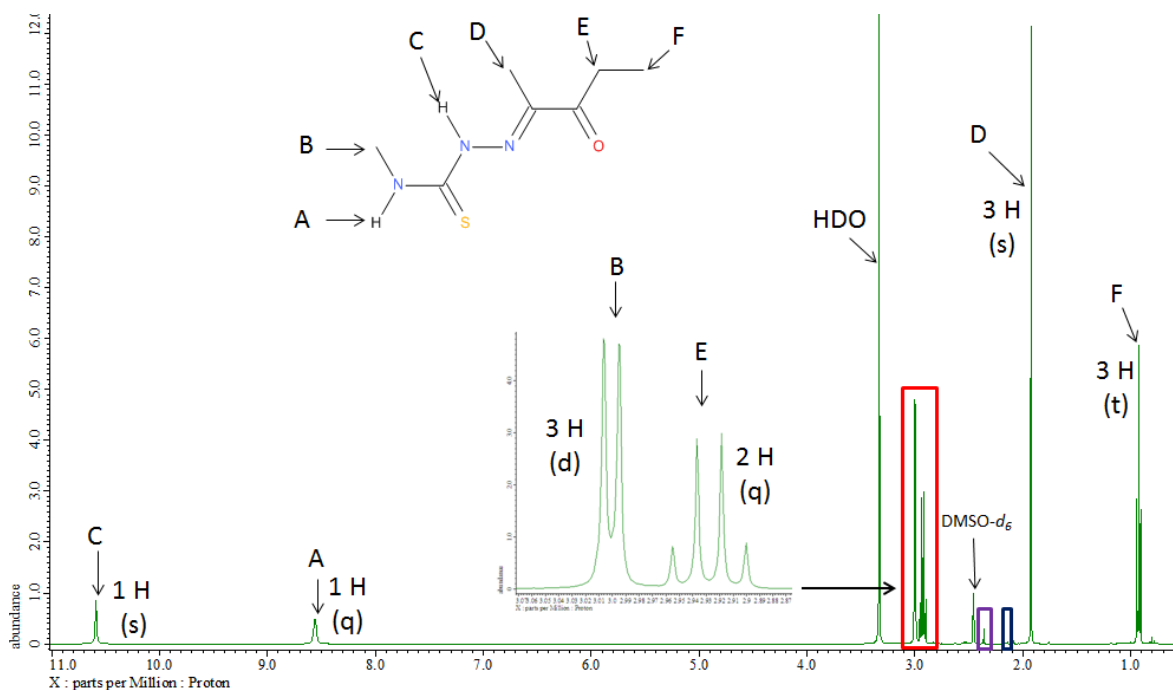


**Figure 2.5.10.1.** An assigned  $^1\text{H}$  NMR spectrum of the novel compound PDO-Me=O, which was successfully synthesised by the exploitation of carbonyl reactivity approach. This involved reacting 2,3-pentanedione with 4-methyl-3-thiosemicarbazide at  $-10^\circ\text{C}$ .

The purple box illustrates the presence of a second isomeric form of the target intermediate. This intermediate forms when the chosen 4-substituted-3-thiosemicarbazide reacts with the carbonyl group of the ethyl ketone instead of the methyl ketone. Due to the similarity of both of these isomeric forms most the related NMR peaks either overlap or cannot be fully resolved. The  $^1\text{H}$  environment 'D' is the most effective environment to use in order to distinguish between the two isomeric forms of the PDO-mono-substituted-3-thiosemicarbazone intermediates. The presence of this second intermediate is common in the synthesis of the PDO-mono-substituted-3-thiosemicarbazone intermediates. The blue box indicates a very small presence of the related symmetric bis(thiosemicarbazone), in this example it is PDO-Me-Me.

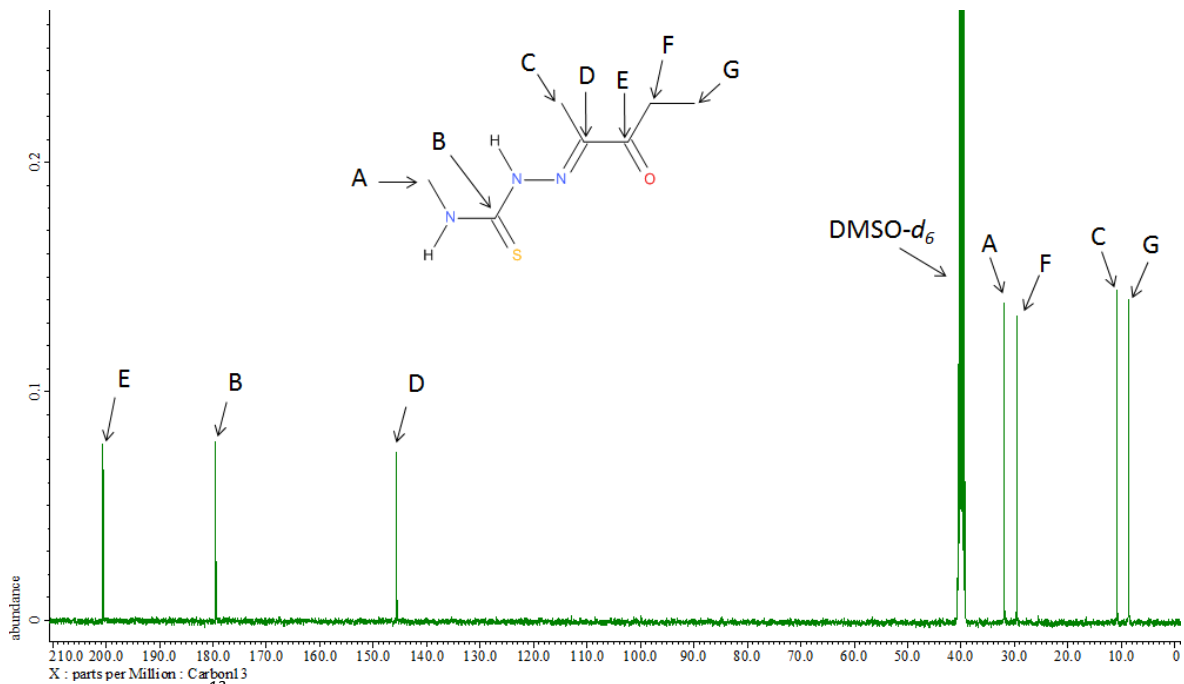


Figure 2.5.10.2. A  $^{13}\text{C}$  NMR spectrum of PDO-Me=O.

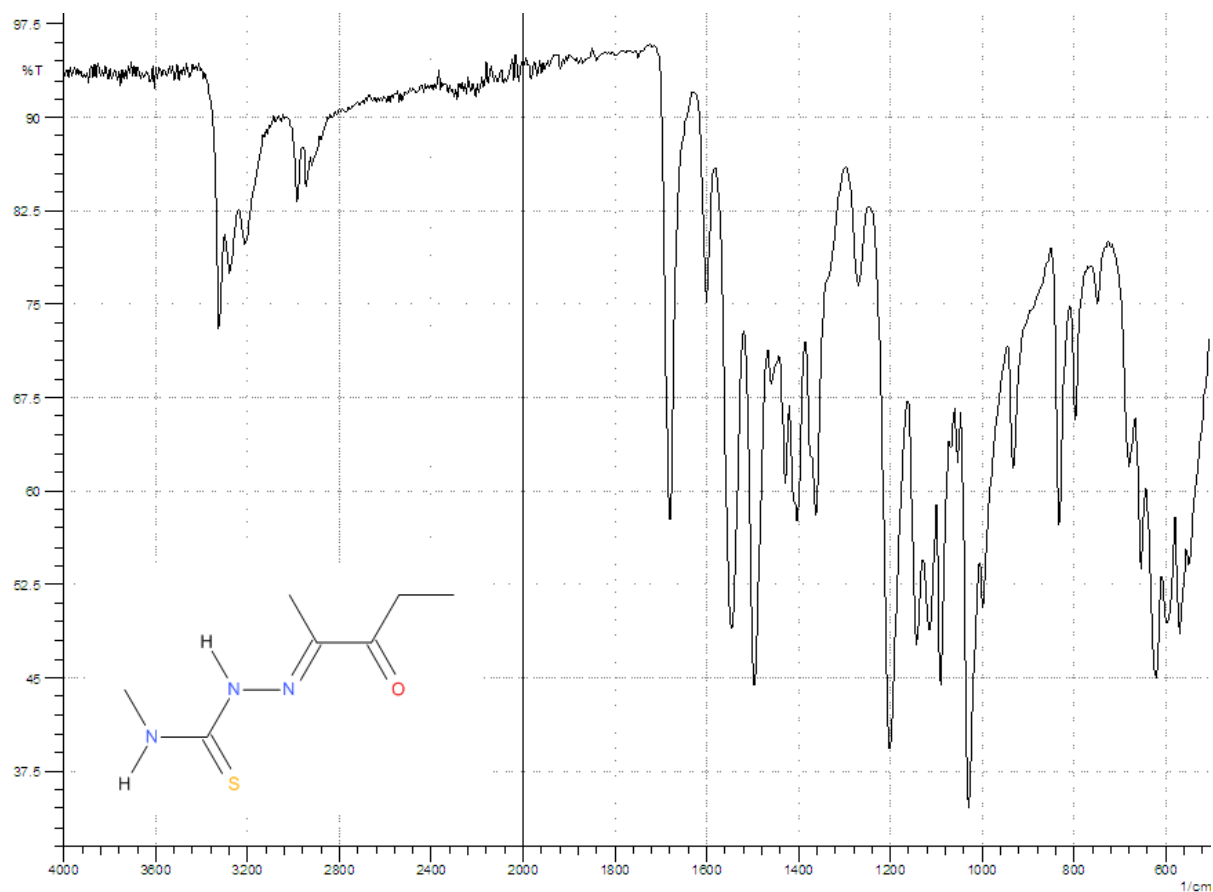
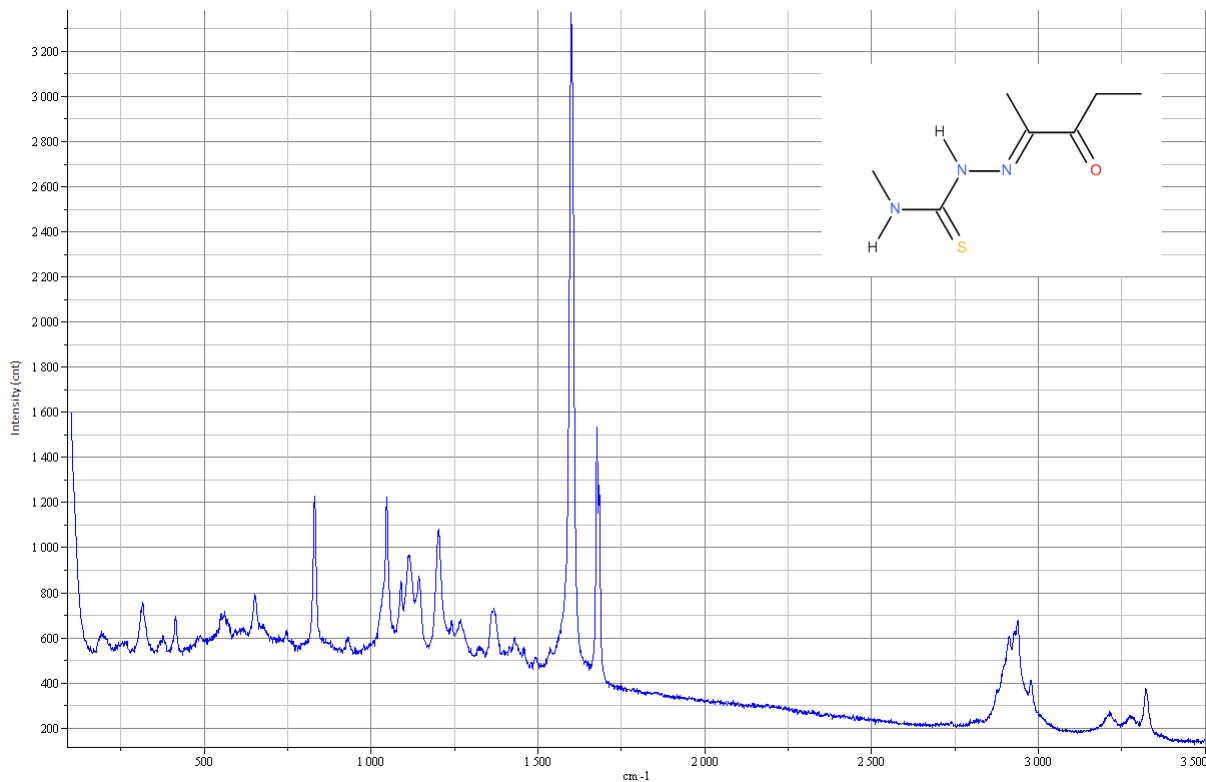


Figure 2.5.10.3. A FTIR spectrum of PDO-Me=O.



**Figure 2.5.10.4.** A Raman spectrum of PDO-Me=O.

### **2.5.11. Discussion**

All three intermediates were successfully synthesised with an acceptable level of purity. It is believed that no one has reported intermediates of this class before. The method of synthesis was adapted from procedures that have been reported for the synthesis of intermediates with Me/Me on the backbone.<sup>57, 66, 73</sup> The NMR data is very close in agreement to the NMR data reported by J. Holland *et al.*<sup>57</sup> for the intermediates with Me/Me on the backbone, when structural variations have been discounted. The Infrared and Raman spectra of each of the intermediates of this class also contain common peaks in the regions that N-H, C=O, C=N and C=S peaks have been identified for other intermediates (Table 2.3.11.2.).

Evidence of a second isomeric form of the intermediate was present in all NMR spectra, this second intermediate arises when the amine of the chosen 4-substituted-3-thiosemicarbazide reacts with the ethyl carbonyl group of the 2,3-pentandione instead of the methyl carbonyl group. It was initially expected that the amine would preferentially attack the ethyl ketone of 2,3-pentandione as the ethyl group would be more effective at stabilising the partial positive charge on the carbonyl carbon than the corresponding methyl carbonyl group. If this was the case then the intermediate containing an unreacted methyl carbonyl group instead of an unreacted ethyl group would be observed. It is expected that steric effects may cause the formation of the intermediate bound through the methyl ketone to be more favourable.

It was found that if the reaction mixture was cooled to below 0°C (typically -10/-12°C) the formation of the second isomeric intermediate was reduced. There seems to be a limit of how

much you can cool the solution as just after  $-12^{\circ}\text{C}$  the 4-substituted-3-thiosemicarbazide either precipitates out of solution or the solution mixture freezes. In the case of thiosemicarbazide it was noted that the solution cannot be cooled much below  $10^{\circ}\text{C}$  before the arm starts to precipitate out of solution. The formation of this intermediate impurity will undoubtedly lead to the formation of an isomeric mixture of dissymmetric ligands when a dissimilar 4-substituted-3-thiosemicarbazide is attached. If tests show that there is a significant difference in the pharmacokinetics or bio-distribution between the two isomeric forms of the dissymmetric ligands then it will be necessary to revise the method in order to further reduce or stop the formation of the intermediate impurity.

It is clear that one of the two isomeric forms of the intermediate was formed in a significantly larger proportion than the other but in order to ascertain what the structure of the final ligand was at the end of the synthesis, it was important to identify which ligand intermediate was formed as the major product. This is illustrated in the reaction figure below (Figure 2.5.11.1.).

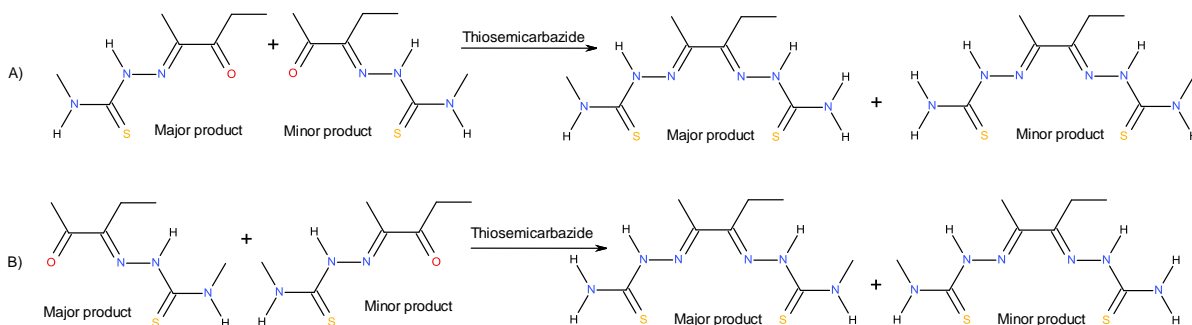


**Figure 2.5.11.1.** Illustrates what the major products will be depending on what the major isomer is.

Figure 2.5.11.2. shows a HMBC NMR spectra of PDO-Me=O which it was hoped, would help prove which isomeric form of the intermediate was the major product. It is predicted that the intermediate that is marked as the major product in reaction 'A' above (Figure 2.5.11.1.) is correct.



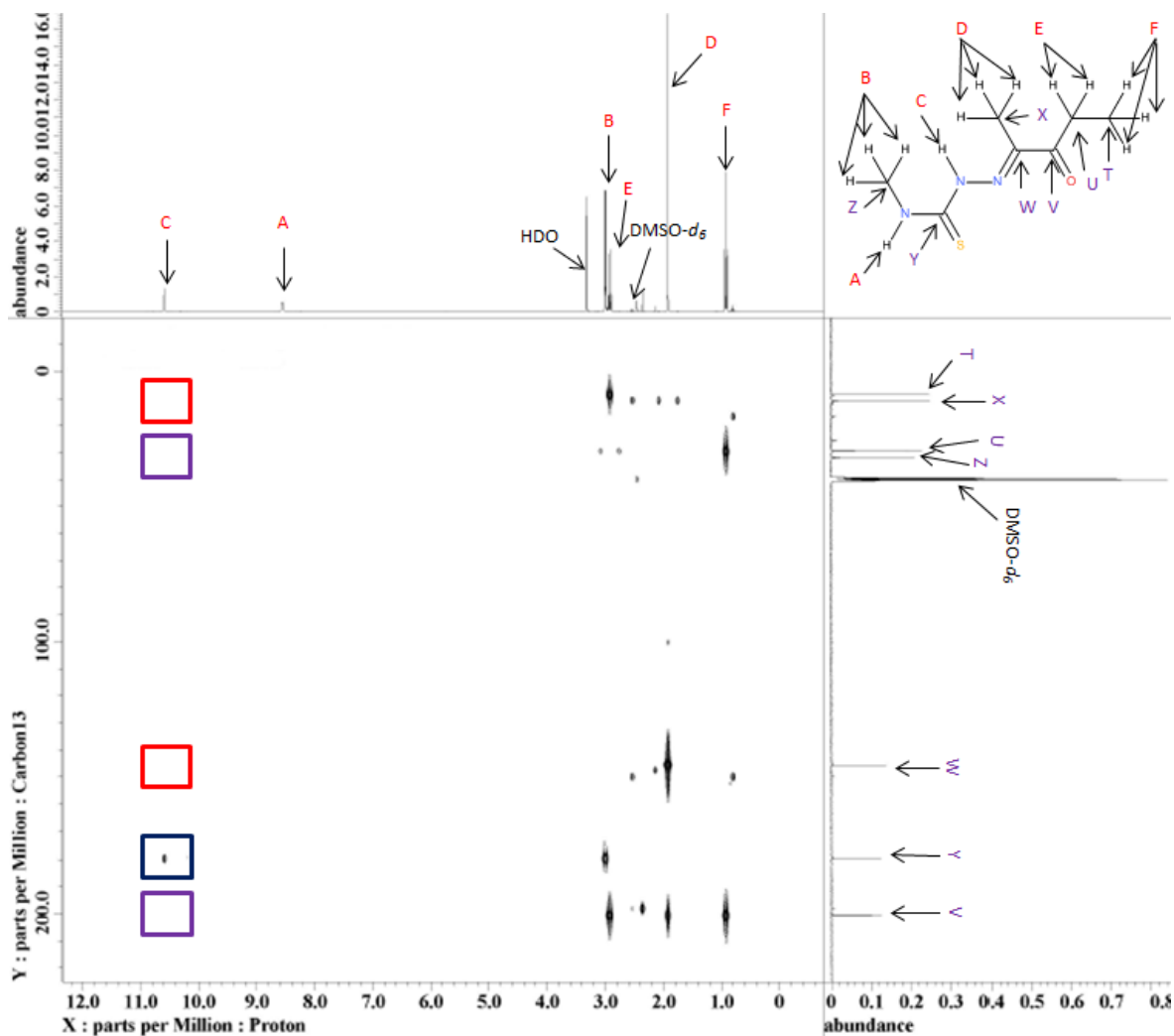


**Figure 2.5.11.2.** A HMBC spectrum of PDO-Me=O. HMBC was not able to help elucidate the identity of the major isomer of PDO-Me=O.

Unfortunately the expected long range carbon/hydrogen couplings between proton 'C' with carbon 'W' and 'X' were not present. These absent coupling locations that would support that reaction A (Figure 2.5.11.1.) is correct are marked by the red boxes. If reaction B (Figure 2.5.11.1.) was correct then it would be expected that long range carbon/hydrogen couplings between proton 'C' with carbon 'V' and 'U' would be observed, these are indicated by the purple boxes. These couplings are also absent. One explanation for this could be that because proton 'C' is directly bonded to a nitrogen atom that this is weakening the long range carbon/hydrogen couplings to such an extent that they are no longer detectable. This theory is backed up by the coupling marked with the blue box which shows a weak coupling between proton 'C' and carbon 'Y'. This coupling is a lot weaker than other strong coupling that are observed over a similar number of bond lengths, for example the coupling between proton 'D' and carbon 'W' is significantly stronger even though the coupling being observed over one bond length (H-C-C) which has the same number of bond lengths as between proton 'C' and carbon 'W' (H-N-C). The only difference is the atoms which the bond is between.

However, it is possible to indirectly support that the reaction A (Figure 2.5.11.1.) is correct by looking at the  $^1\text{H}$  and  $^{13}\text{C}$  NMR peaks and comparing the major NMR peaks of the intermediate sample against the expected peaks for each isomeric form. The table below (Table 2.5.11.3.) illustrates this, the example intermediate used for comparison is PDO-Me=O. Both PDO-NH<sub>2</sub>=O and PDO=Et=O both show major NMR peaks in very similar positions to PDO-Me=O showing that all intermediates follow reaction A (Figure 2.5.11.1).

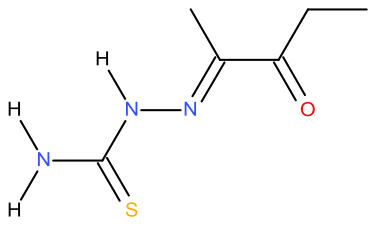
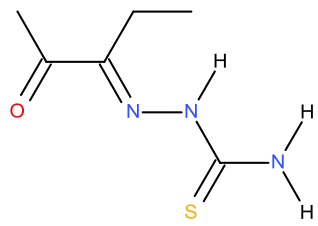
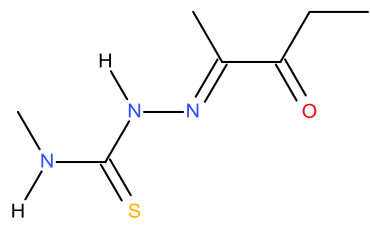
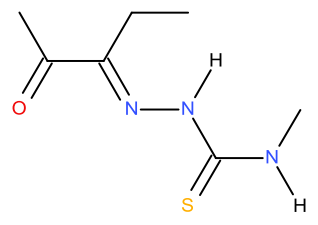
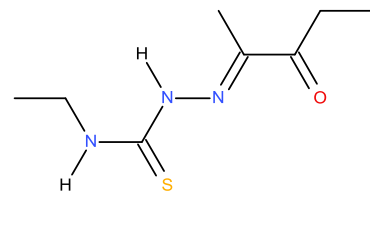
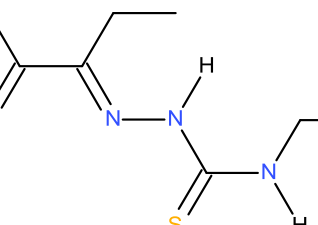
Environment	Observed peaks In PDO-Me=O	Expected peak if reaction A is correct	Expected peak if reaction B is correct
	<b>Major peaks</b>		
$\text{CH}_2\text{-C=O}$	2.93 ppm	≈2.6-7 ppm	Minor peak
$\text{CH}_2\text{-C=O}$	29.59 ppm	≈28.7-9	Minor peak
$\text{CH}_3\text{-C=N}$	1.93 ppm	≈1.9 ppm	Minor peak
$\text{CH}_3\text{-C=N}$	10.85 ppm	≈9.9-10.6 ppm	Minor peak
	<b>Minor peaks</b>		
$\text{CH}_3\text{-C=O}$	2.36 ppm	Minor peak	≈2.3-4 ppm
$\text{CH}_3\text{-C=O}$	25.59 ppm	Minor peak	24.8-25.3≈ ppm
$\text{CH}_2\text{-C=N}$	2.54 ppm	Minor peak	2.0-9 ppm
$\text{CH}_2\text{-C=N}$	16.67 ppm	Minor peak	17.0-5 ppm

**Table 2.5.11.3.** Summarises the expected major NMR peaks that would be present depending on which intermediate is the major product.

Previous data in the literature relating to PDO based intermediates was not able to found, as it is believed that no PDO-mono-substituted-3-thiosemicarbazone intermediate has been isolated to date. This means that the only data available that can be used to help determine which isomeric form is correct is data corresponding to BDO-mono-substituted-3-thiosemicarbazone intermediates. By looking at the  $\text{CH}_3\text{-C=O}$ ,  $\text{CH}_3\text{-C=N}$ ,  $\text{CH}_2\text{-C=O}$  and  $\text{CH}_2\text{-C=N}$  environments, the position of the spectral peaks can be predicted, which can be used to propose the major configuration of the PDO based intermediates. The observed peaks agree with the peaks expected for reaction A (Figure 2.5.11.1) and disagrees with the peaks expected for reaction B (Figure 2.5.11.1). Table 2.5.11.3. supports the theory that the substituted-3-thiosemicarbazide forms an imine bond with the methyl carbon preferentially over the ethyl carbon. However, this conclusion must be treated with caution as only NMR spectroscopy has been used. Unfortunately all three intermediate products formed powders which were not suitable for analysis by X-ray diffraction.

If it is accepted that the conclusion is correct then this may advocate that the methyl ketone is still slightly more reactive than the ethyl ketone. This may be an important consideration in the respect of the clean synthesis of Me/Et dissymmetric ligands.

**Table 2.5.11.4.** Reports the intermediates that have been successfully made along with the main impurity present and at what proportion this impurity is estimated at.

Intermediate	Novel	Yield	Main impurity	Estimated impurity *
<p><b>PDO-NH<sub>2</sub>=O</b></p> 	Yes	66%		9%
<p><b>PDO-Me=O</b></p> 	Yes	49%		4%
<p><b>PADA-Et=O</b></p> 	Yes	50%		10%

\*Estimated by <sup>1</sup>H NMR spectra on an average of three integrals where possible. Typically this was to include the integrals from the peaks due to the N=C-CH<sub>3</sub> and N-NH environments.

**Table 2.5.11.4.** Summary of purity for the PDO-mono-substituted-3-thiosemicarbazone intermediates.

### **2.5.13. Dissymmetric ligands from PDO-NH<sub>2</sub>=O, PDO-Me=O and PDO-Et=O**

#### **2.5.14. Methods**

##### **PDO-NH<sub>2</sub>-Me**

PDO-NH<sub>2</sub>=O (0.277 g, 0.0016 mol) was dissolved in DMF (3 mL). 4-methyl-3-thiosemicarbazide (0.168 g, 0.0016 mol) was dissolved in DMF (4 mL) and HCl (10%, 1 drop) was added. The two

solutions were combined and left to stir (room temperature, 5 hours). De-ionised water (14 mL) was added, the precipitate was filtered and washed with de-ionised water (50 mL). The crude product was dissolved in DMSO (8 mL) and recrystallised with de-ionised water (16 mL). The precipitate was filtered off, washed with de-ionised water (50 mL), ethanol (5 x 10 mL) and dried. A yellow/white solid (0.275 g) was recovered (66% yield).

#### **PDO-NH<sub>2</sub>-(Me)<sub>2</sub>**

PDO-NH<sub>2</sub>=O (0.452 g, 0.0026 mol) was dissolved in DMF (2 mL) and filtered. 4,4-dimethyl-3-thiosemicarbazide (0.310 g, 0.0026 mol) was dissolved in DMF (4 mL), HCl (10%, 2 drops) was added and filtered. The two solutions were combined and left to stir (room temperature, 5 hours). De-ionised water (37 mL) was added and solution was put in the freezer (10 minutes). The precipitate was filtered off and washed with de-ionised water (50 mL, room temperature and 50 mL, 80 °C). The crude product was dissolved in DMSO (3.5 mL), filtered and recrystallised with de-ionised water (60 mL). The precipitate was recovered by filtration, washed with de-ionised water (2 x 50 mL) and dried. A yellow solid (0.171 g) was recovered (24% yield).

#### **PDO-NH<sub>2</sub>-Et**

PDO-NH<sub>2</sub>=O (0.277 g, 0.0016 mol) was dissolved in DMF (3 mL). 4-ethyl-3-thiosemicarbazide (0.191 g, 0.0016 mol) was dissolved in DMF (5 mL) and added HCl (10%, 1 drop) was added. The two solutions were combined and left to stir (room temperature, 5 hours). De-ionised water (14 mL) was added, the precipitate was filtered off and washed with de-ionised water (50 mL). The crude product was dissolved in DMSO (8 mL), filtered and recrystallised with de-ionised water (16 mL). The precipitate was recovered by filtration, washed with de-ionised water (50 mL), ethanol (5 x 10 mL) and dried. A yellowish-white solid (0.168 g) was recovered (38% yield).

#### **PDO-Me-NH<sub>2</sub>**

PDO-Me=O (0.599 g, 0.0032 mol) was dissolved in DMF (2 mL) and filtered. Thiosemicarbazide (0.292 g, 0.0032 mol) was dissolved in DMF (10 mL), HCl (10%, 2 drops) was added and filtered. The two solutions were combined and left to stir (room temperature, 5 hours). De-ionised water (24 mL) was added, the precipitate was filtered off and washed with de-ionised water (50 mL, room temperature and 50 mL, 80 °C). The crude product was dissolved in DMSO (31 mL), filtered and recrystallised with de-ionised water (62 mL). The precipitate was recovered by filtration, washed with de-ionised water (50 mL, room temperature and 50 mL, 80 °C) and dried. An off white solid (0.597 g) was recovered (72% yield).

## PDO-Et-NH<sub>2</sub>

PDO-Et=O (0.322 g, 0.0016 mol) dissolved in DMF (2.5 mL) and filtered. Thiosemicarbazide (0.146 g, 0.0016 mol) dissolved in DMF (5.5 mL), added HCl (10%, 1 drop) and filtered. The two solutions were combined and left to stir (room temperature, 5 hours). De-ionised water (16 mL) was added, filtered off precipitate and washed with de-ionised water (50 mL, room temperature and 50 mL, 70°C). The crude product was dissolved in DMSO (14 mL), filtered and recrystallised with de-ionised water (28 mL). Filtered off precipitate, washed de-ionised water (50 mL) and dried. A white solid (0.237 g) was recovered (54% yield).

## 2.5.15. Characterisation data for dissymmetric ligands from PDO-NH<sub>2</sub>=O, PDO-Me=O and PDO-Et=O

### PDO-NH<sub>2</sub>-Me

**<sup>1</sup>H NMR** (DMSO-*d*<sub>6</sub>, 400 MHz): δ= 10.37 (s, 1 H, N-NH), 10.19 (s, 1 H, N-NH), 8.40 (s, 1 H, C-NH), 8.32 (q, 1 H, H<sub>3</sub>C-NH, J= 4.8 Hz), 7.74 (s, 1 H, C-NH), 2.97 (d, 3 H, HN-CH<sub>3</sub>, J= 4.8 Hz), 2.80 (q, 2H, C-CH<sub>2</sub>, J= 7.6 Hz), 2.10 (s, 3 H, N=C-CH<sub>3</sub>), 0.84 (t, 3 H, C-CH<sub>2</sub>-CH<sub>3</sub>, J=7.2 Hz). **<sup>13</sup>C {<sup>1</sup>H} NMR** (DMSO-*d*<sub>6</sub>, 100 MHz): δ= 179.28 (C=S), 178.93 (C=S), 152.24 (C=N), 147.92 (C=N), 31.76 (HN-CH<sub>3</sub>), 17.38 (C-CH<sub>2</sub>), 12.38 (N=C-CH<sub>3</sub>), 11.45 (C-CH<sub>2</sub>-CH<sub>3</sub>). **IR (neat)**: cm<sup>-1</sup>= 3424 (w), 3223 (w), 2982 (w), 1603 (m), 1551 (m), 1491 (s), 1437 (m), 1366 (w), 1290 (m), 1231 (m), 1144 (m), 1082 (s), 1063 (s), 989 (w), 926 (w), 841 (m), 775 (w), 563 (m). **Raman (neat)**: cm<sup>-1</sup>= 2935 (w), 1603 (s), 1457 (w), 1378 (w), 1336 (w), 1247 (w), 1145 (w), 1124 (w), 1048 (w), 992 (w), 925 (w), 741 (w), 484 (w), 456 (w), 327 (w), 226 (w). **Elemental analysis**: Found: C, 36.9; H, 6.2; N, 32.3. Calc. for C<sub>8</sub>H<sub>16</sub>N<sub>6</sub>S<sub>2</sub>: C, 36.8; H, 6.1; N, 32.2%. **Melting point**: >198 °C (decomposed).

### PDO-NH<sub>2</sub>-(Me)<sub>2</sub>

**<sup>1</sup>H NMR** (DMSO-*d*<sub>6</sub>, 400 MHz): δ= 10.18 (s, 1 H, N-NH), 10.53 (s, 1 H, N-NH), 8.38 (s, 1 H, C-NH), 7.74 (s, 1 H, C-NH), 3.22 (s, 6 H, N-(CH<sub>3</sub>)<sub>2</sub>), 2.77 (q, 2H, C-CH<sub>2</sub>, J= 7.6 Hz), 2.08 (s, 3 H, N=C-CH<sub>3</sub>), 0.88 (t, 3 H, C-CH<sub>2</sub>-CH<sub>3</sub>, J=7.6 Hz). **<sup>13</sup>C {<sup>1</sup>H} NMR** (DMSO-*d*<sub>6</sub>, 100 MHz): δ= 182.39 (C=S), 179.32 (C=S), 153.32 (C=N), 147.88 (C=N), 42.95 (N-(CH<sub>3</sub>)<sub>2</sub>), 17.04 (C-CH<sub>2</sub>), 12.01 (N=C-CH<sub>3</sub>), 10.92 (C-CH<sub>2</sub>-CH<sub>3</sub>). **IR (neat)**: cm<sup>-1</sup>= 3410 (w), 3229 (m), 3148 (w), 2974 (w), 2932 (w), 1593 (m), 1541 (m), 1483 (s), 1433 (s), 1260 (m), 1105 (s), 1076 (m), 1055 (s), 1020 (m), 989 (m), 926 (m), 843 (m), 511 (s). **Raman (neat)**: cm<sup>-1</sup>= 2934 (w), 1600 (s), 1583 (s), 1495 (w), 1458 (w), 1396 (w), 1367 (w), 1345 (w), 1246 (w), 1126 (m), 1111 (w), 991 (w), 732 (w), 633 (w), 603 (w), 461 (w), 386 (w), 332 (w). **Elemental analysis**: Found: C, 39.3; H, 6.2; N, 30.6. Calc. for C<sub>9</sub>H<sub>18</sub>N<sub>6</sub>S<sub>2</sub>: C, 39.4; H, 6.2; N, 30.6%. **Melting point**: >180 °C (decomposed).

### PDO-NH<sub>2</sub>-Et

**<sup>1</sup>H NMR** (DMSO-*d*<sub>6</sub>, 400 MHz): δ= 10.29 (s, 1 H, N-NH), 10.19 (s, 1 H, N-NH), 8.40 (singlet overlapping a triplet, 1 H, C-NH), 8.60 (triplet overlapping a singlet, 1 H, H<sub>2</sub>C-NH, J= 6.0 Hz), 7.74 (s, 1 H, C-NH), 3.54 (dq, 2 H, HN-CH<sub>2</sub>, J=7.2, 6.0 Hz), 2.80 (q, 2H, C-CH<sub>2</sub>, J= 7.2 Hz), 2.14 (s, 3 H, N=C-CH<sub>3</sub>), 1.09 (t, 3 H, N-CH<sub>2</sub>-CH<sub>3</sub>, J=7.2), 0.84 (t, 3 H, C-CH<sub>2</sub>-CH<sub>3</sub>, J=7.2 Hz). **<sup>13</sup>C {<sup>1</sup>H} NMR** (DMSO-*d*<sub>6</sub>, 100 MHz): δ= 179.28 (C=S), 177.90 (C=S), 152.19 (C=N), 147.86 (C=N), 39.35 (HN-CH<sub>2</sub>), 17.04 (C-CH<sub>2</sub>), 14.89 (N-CH<sub>2</sub>-CH<sub>3</sub>), 12.39 (N=C-CH<sub>3</sub>), 11.44 (C-CH<sub>2</sub>-CH<sub>3</sub>). **IR (neat)**: cm<sup>-1</sup>= 3428 (w), 3210 (w), 2982 (w), 1601 (m), 1537 (m), 1493 (s), 1435 (m), 1290 (m), 1213 (m), 1146 (m), 1080 (s), 1059 (m), 926 (w), 837 (m), 777 (w), 716 (w), 652 (w), 565 (m), 517 (m). **Raman (neat)**: cm<sup>-1</sup>= 2934 (w), 1599 (s), 1589 (m), 1532 (w), 1457 (w), 1395 (w), 1368 (w), 1345 (w), 1247 (w), 1215 (w), 1120 (m), 1049 (w), 991 (w), 741 (w), 463 (w), 318 (w). **Elemental analysis**: Found: C, 39.5; H, 6.5; N, 30.55. Calc. for C<sub>9</sub>H<sub>18</sub>N<sub>6</sub>S<sub>2</sub>: C, 39.4; H, 6.6; N, 30.6%. **Melting point**: >218 °C (decomposed).

### PDO-Me-NH<sub>2</sub>

**<sup>1</sup>H NMR** (DMSO-*d*<sub>6</sub>, 400 MHz): δ= 10.29 (s, 1 H, N-NH), 10.21 (s, 1 H, N-NH), 8.39 (s, 1 H, C-NH), 8.27 (q, 1 H, H<sub>3</sub>C-NH, J= 4.8 Hz), 7.80 (s, 1 H, C-NH), 2.98 (d, 3 H, HN-CH<sub>3</sub>, J= 4.8 Hz), 2.87 (q, 2H, C-CH<sub>2</sub>, J= 7.2 Hz), 2.10 (s, 3 H, N=C-CH<sub>3</sub>), 0.85 (t, 3 H, C-CH<sub>2</sub>-CH<sub>3</sub>, J=7.2 Hz). **<sup>13</sup>C {<sup>1</sup>H} NMR** (DMSO-*d*<sub>6</sub>, 100 MHz): δ= 179.35 (C=S), 178.96 (C=S), 152.89 (C=N), 147.48 (C=N), 31.80 (HN-CH<sub>3</sub>), 17.36 (C-CH<sub>2</sub>), 12.21 (N=C-CH<sub>3</sub>), 11.53 (C-CH<sub>2</sub>-CH<sub>3</sub>). **IR (neat)**: cm<sup>-1</sup>= 3408 (m), 3337 (w), 3229 (m), 3150 (m), 2978 (w), 2938 (w), 1603 (m), 1541 (m), 1491 (s), 1464 (s), 1439 (s), 1364 (m), 1227 (m), 1144 (m), 1082 (s), 1059 (s), 860 (m), 826 (m), 797 (m), 640 (m), 509 (s). **Raman (neat)**: cm<sup>-1</sup>= 2937 (w), 1604 (s), 1591 (m), 1591 (w), 1380 (w), 1341 (w), 1232 (w), 1144 (w), 1123 (m), 1024 (w), 985 (w), 737 (w), 675 (w), 481 (w), 460 (w). **Elemental analysis**: Found: C, 36.8; H, 6.2; N, 32.2. Calc. for C<sub>8</sub>H<sub>16</sub>N<sub>6</sub>S<sub>2</sub>: C, 36.9; H, 6.2; N, 32.3%. **Melting point**: >202 °C (decomposed).

### PDO-Et-NH<sub>2</sub>

**<sup>1</sup>H NMR** (DMSO-*d*<sub>6</sub>, 400 MHz): δ= 10.30 (s, 1 H, N-NH), 10.15 (s, 1 H, N-NH), 8.38 (s, 1 H, C-NH), 8.28 (t, 1 H, H<sub>2</sub>C-NH, J= 6.0 Hz), 7.80 (s, 1 H, C-NH), 3.55 (dq, 2 H, HN-CH<sub>2</sub>, J=7.2, 6.0 Hz), 2.86 (q, 2H, C-CH<sub>2</sub>, J= 7.2 Hz), 2.10 (s, 3 H, N=C-CH<sub>3</sub>), 1.09 (t, 3 H, N-CH<sub>2</sub>-CH<sub>3</sub>, J=7.2), 0.86 (t, 3 H, C-CH<sub>2</sub>-CH<sub>3</sub>, J=7.2 Hz). **<sup>13</sup>C {<sup>1</sup>H} NMR** (DMSO-*d*<sub>6</sub>, 100 MHz): δ= 179.37 (C=S), 177.94 (C=S), 152.77 (C=N), 147.47 (C=N), 39.07 (HN-CH<sub>2</sub>), 17.48 (C-CH<sub>2</sub>), 14.89 (N-CH<sub>2</sub>-CH<sub>3</sub>), 12.20 (N=C-CH<sub>3</sub>), 11.50 (C-CH<sub>2</sub>-CH<sub>3</sub>). **IR (neat)**: cm<sup>-1</sup>= 3410 (w), 3333 (w), 3219 (m), 3152 (m), 2978 (w), 1601 (m), 1531 (m), 1493 (s), 1466 (s), 1439 (s), 1385 (m), 1292 (m), 1250 (m), 1207 (s), 1167 (m), 1146 (m), 1080 (s), 1059 (s), 860 (m), 818 (m), 797 (m), 652 (m), 501 (s). **Raman (neat)**: cm<sup>-1</sup>= 2953 (w), 1602 (s), 1589 (m), 1533 (w), 1456 (w), 1393 (w), 1373 (w), 1347 (w), 1248 (w), 1214 (w), 1146 (w), 1122 (w), 1027 (w), 990

(w), 741 (w), 464 (w), 306 (w). **Elemental analysis:** Found: C, 39.3; H, 6.5; N, 30.55. Calc. for  $C_9H_{18}N_6S_2$ : C, 39.4; H, 6.6; N, 30.6%. **Melting point:** >200 °C (decomposed).

### 2.5.16. Spectral examples of a dissymmetric ligand with a Me/Et backbone

**Figures 2.5.16.1-4.** Spectral examples of the dissymmetric ligand PDO-Me-NH<sub>2</sub>.

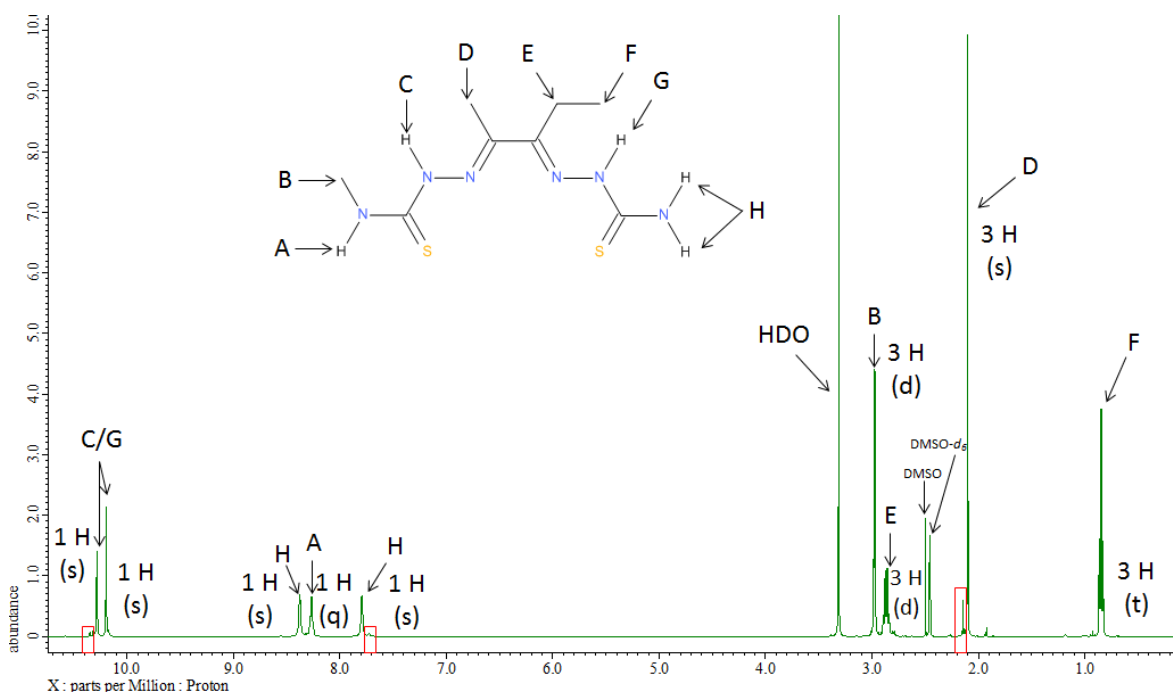


**Figure 2.5.16.1.** An assigned  $^1H$  NMR spectrum of PDO-Me-NH<sub>2</sub>, which was successfully synthesised by reacting PDO-Me=O with thiosemicarbazide. The red boxes show a small presence of the ligand PDO-NH<sub>2</sub>-Me, which is due to the 4-methyl-3-thiosemicarbazide reacting with the second isomeric form of PDO-Me=O (Isomer B, Figure 2.5.5.1.).

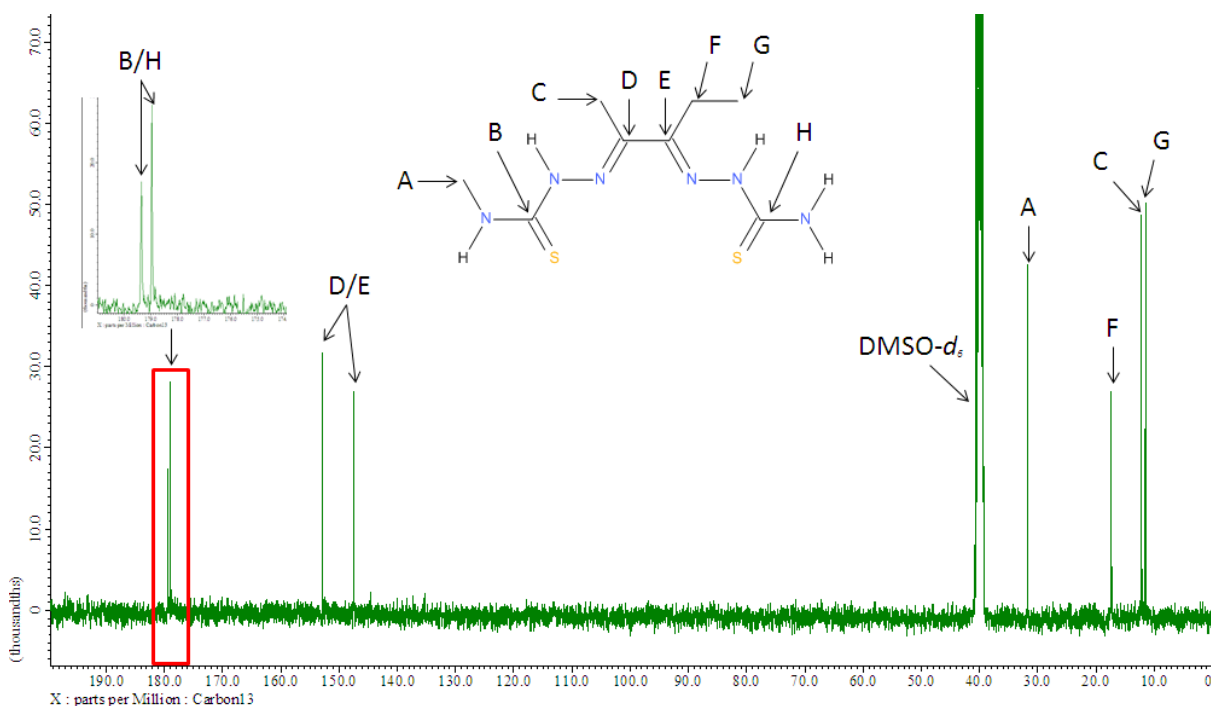


**Figure 2.5.16.2.** An assigned  $^{13}C$  NMR spectrum of PDO-Me-NH<sub>2</sub>.

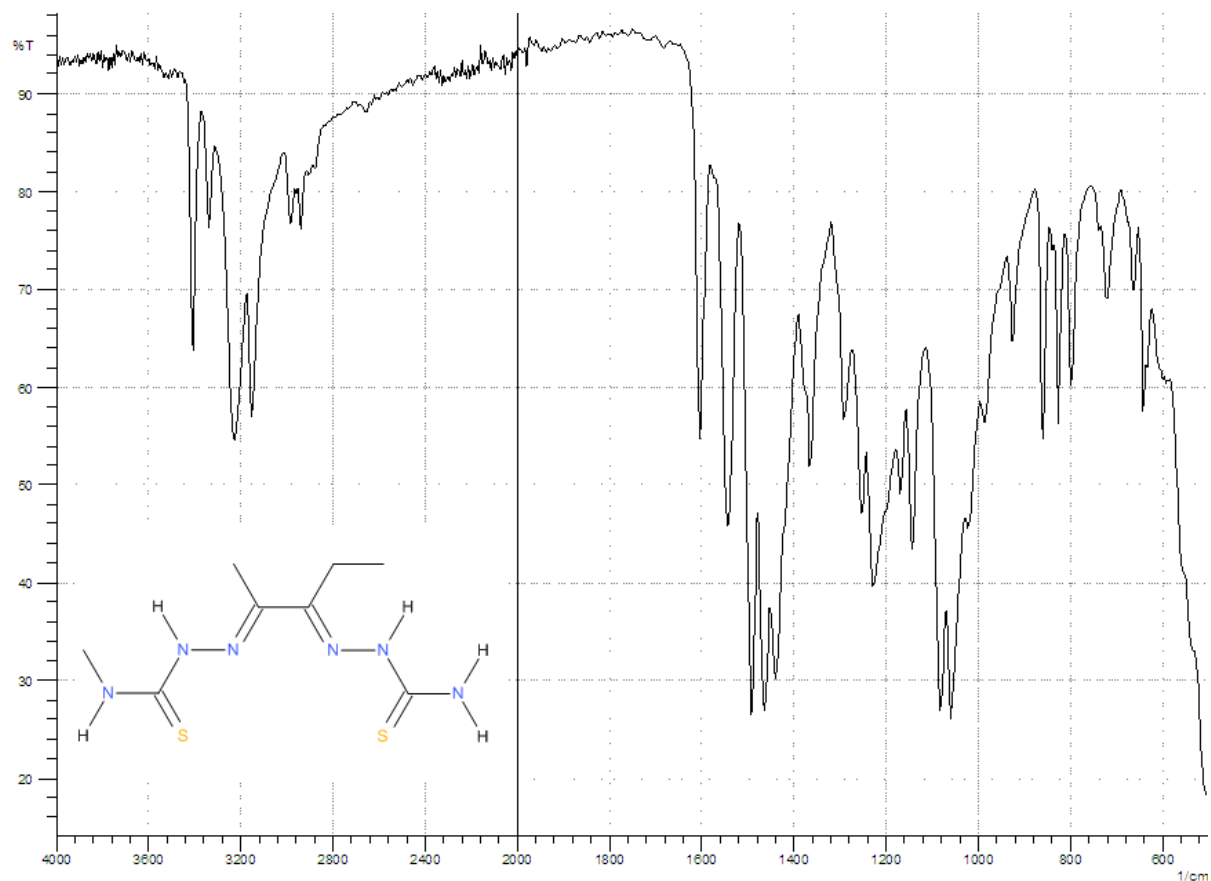


Figure 2.5.16.3. A FTIR spectrum of PDO-Me-NH<sub>2</sub>.

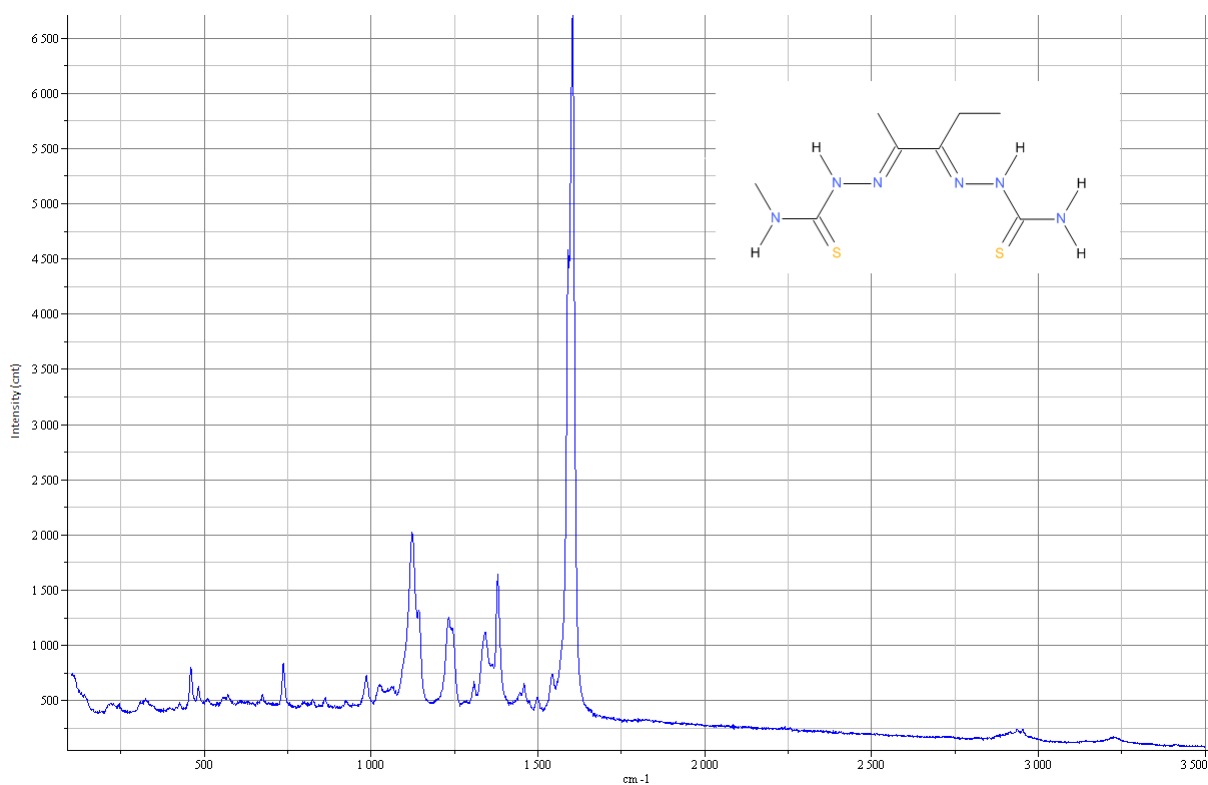


Figure 2.5.16.4. A Raman spectrum of PDO-Me-NH<sub>2</sub>.

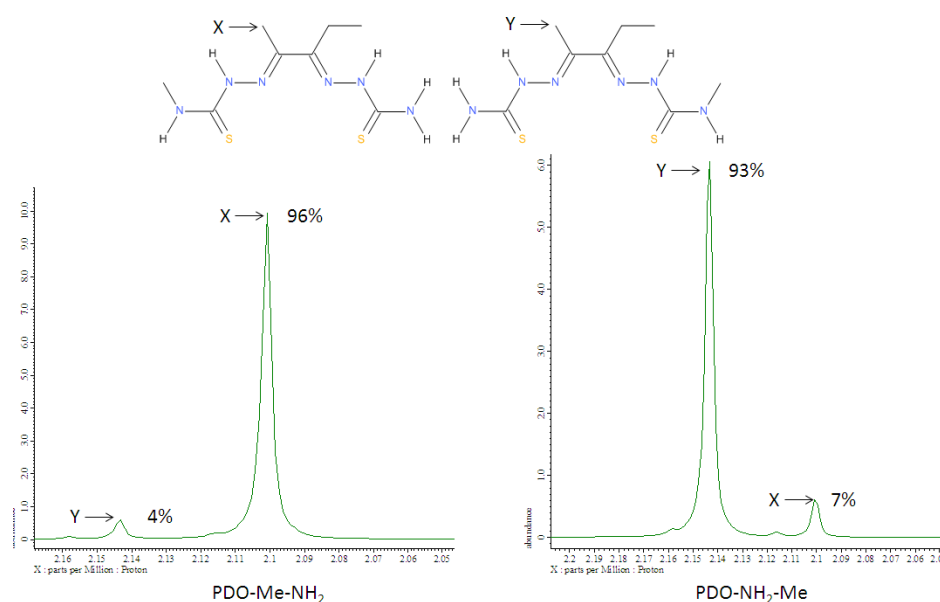
### 2.5.17. Discussion

All five ligands were made with an acceptable level of purity. No reports have been found of any attempts to synthesise dissymmetric ligands with Me/Et on the imine backbone so it is believed



that all five ligands are novel. The same method was successfully used for reacting the PDO intermediate with a dissimilar 4-substituted-3-thiosemicarbazide as was used for the ligands with Me/Me and Me/H on the backbone. Due to lack of published data on these ligands, the only possible comparison that could be made is with other ligands made in this project. Assignments made for NMR, IR and Raman for other ligands with different backbones/ amine substituents seem to hold roughly true with this class of ligands as well.

As predicted the main impurity peaks suggests the presence of the isomeric form of the target ligand. Just by using NMR spectroscopy, it is possible to confirm the presence of these impurities and determine their relative proportions by using the N=C-CH<sub>3</sub> environment. Other peaks in the spectra tend to partially or fully overlap owing to very similar chemical environments. When overlapping of peaks occurred it was not possible to determine reliable integrals. Some of the isomeric forms of the ligands have already been synthesised as they are also target ligands, where this is the case it is possible to directly compare the positions of their NMR peaks. This is illustrated by the by the <sup>1</sup>H NMR peaks of the N=C-CH<sub>3</sub> environments of PDO-Me-NH<sub>2</sub> and PDO-NH<sub>2</sub>-Me showing the presence of the second isomeric form of the target ligand (Figure 2.5.17.1).

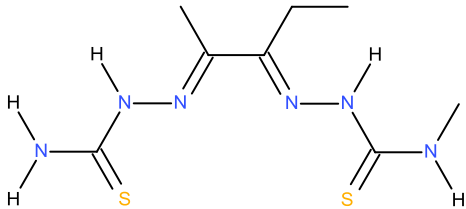
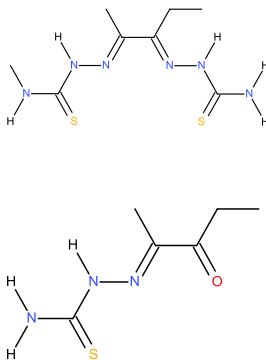
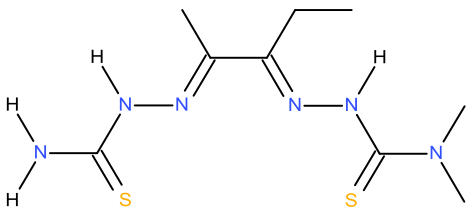
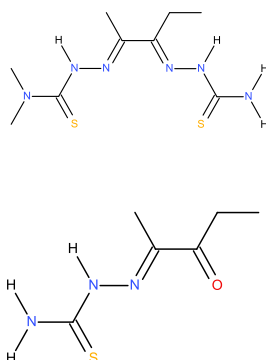


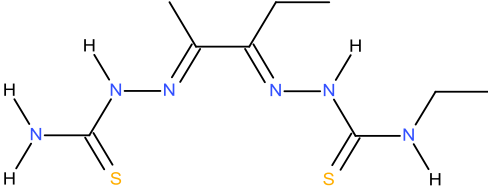
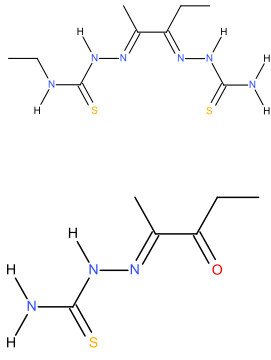
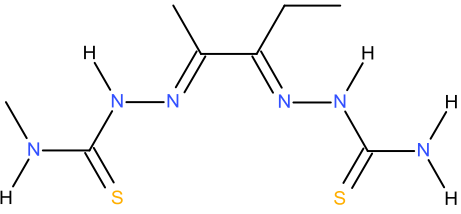
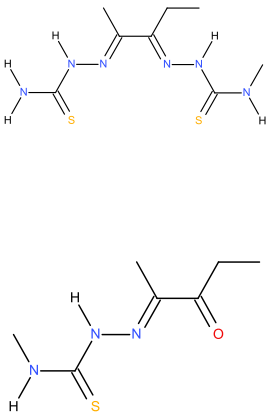
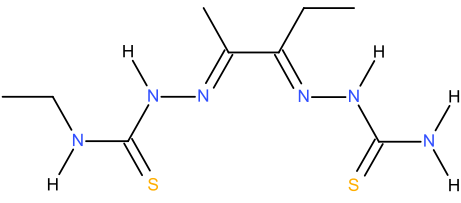
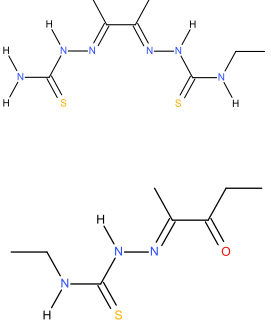
**Figure 2.5.17.1. Left:** <sup>1</sup>H NMR peaks of the N=C-CH<sub>3</sub> environment of PDO-Me-NH<sub>2</sub> showing a small presence of PDO-NH<sub>2</sub>-Me. **Right:** <sup>1</sup>H NMR peaks of the N=C-CH<sub>3</sub> environment of PDO-NH<sub>2</sub>-Me showing the presence of PDO-Me-NH<sub>2</sub>.

There was also evidence of a small proportion of unreacted intermediates which have been seen throughout. To echo what was said earlier, as these ligands are to be initially screened for their appropriateness as hypoxia imaging agents, a small presence of an isomeric impurity should not be detrimental to the screening process. If it was found that each isomeric form had significantly

different pharmacokinetics or bio-distribution, it would then be necessary to revisit the method of synthesis in order to synthesize ligands with greater purity.

Melting point data was collected on all the bis(thiosemicarbazone) ligands and their respective intermediates. It was found that all that all the ligands and most of the intermediates showed signs of decomposition before they melted. The exceptions to this was the intermediates PDO-Me=O, PDO-Et=O, DMA-Me-(OMe)<sub>2</sub> and PADA-Me-(OMe)<sub>2</sub> which melted to form a transparent liquid. When the ligands and intermediates decomposed they started to turn from a white/off white or light yellow colour to a brown solid. The decomposition temperature was taken at the point when the sample first started to turn brown or discolour. For a couple of ligands, the sample was continued to be heated past the temperature where signs of decomposition was shown, it was witnessed that the solid would continue to turn browner and then will eventually melt and form a brownish black liquid. The range of decomposition temperatures that was collected for all the intermediates and ligands was 138-192°C and 180-250°C respectively. Table 2.5.17.2. reports the five dissymmetric ligands that have been successfully made along with the main impurity present and at what proportion this impurity is estimated at.

Ligand	Novel	Yield	Main impurity	Estimated impurity *
<p style="text-align: center;"><b>PDO-NH<sub>2</sub>-Me</b></p> 	Yes	66%		<p style="text-align: center;">7%</p> <p style="text-align: center;">Less than 1%</p>
<p style="text-align: center;"><b>PDO-NH<sub>2</sub>-(Me)<sub>2</sub></b></p> 	Yes	24%		<p style="text-align: center;">5-13%</p> <p style="text-align: center;">Less than 1%</p>

<p style="text-align: center;"><b>PDO-NH<sub>2</sub>-Et</b></p>  <p>The structure shows a central 1,2-dimethyl-3-ethyl-1,3-butadiene backbone. Each terminal carbon of the diene is coordinated to a nitrogen atom, which is double-bonded to a sulfur atom. Each nitrogen atom also has two hydrogen atoms attached, forming a secondary amine group.</p>	Yes	38%	 <p>Two chemical structures are shown. The top one is the same as the main structure. The bottom one is a similar structure but with a carbonyl group (=O) instead of an ethyl group on the right-hand carbon of the diene backbone.</p>	<p style="text-align: right;">6%</p> <p style="text-align: right;">Less than 1%</p>
<p style="text-align: center;"><b>PDO-Me-NH<sub>2</sub></b></p>  <p>The structure shows a central 1,2-dimethyl-3-ethyl-1,3-butadiene backbone. Each terminal carbon of the diene is coordinated to a nitrogen atom, which is double-bonded to a sulfur atom. Each nitrogen atom also has one hydrogen atom and one methyl group attached.</p>	Yes	72%	 <p>Two chemical structures are shown. The top one is the same as the main structure. The bottom one is a similar structure but with a carbonyl group (=O) instead of an ethyl group on the right-hand carbon of the diene backbone.</p>	<p style="text-align: right;">3%</p> <p style="text-align: right;">2%</p>
<p style="text-align: center;"><b>PDO-Et-NH<sub>2</sub></b></p>  <p>The structure shows a central 1,2-dimethyl-3-ethyl-1,3-butadiene backbone. Each terminal carbon of the diene is coordinated to a nitrogen atom, which is double-bonded to a sulfur atom. Each nitrogen atom also has one hydrogen atom and one ethyl group attached.</p>	Yes	54%	 <p>Two chemical structures are shown. The top one is the same as the main structure. The bottom one is a similar structure but with a carbonyl group (=O) instead of an ethyl group on the right-hand carbon of the diene backbone.</p>	<p style="text-align: right;">9%</p> <p style="text-align: right;">3%</p>

\*Estimated by <sup>1</sup>H NMR spectra on an average of the integral from the peaks due to the N=C-CH<sub>3</sub> environment. No other peaks yielded usable integrals.

**Table 2.5.17.2.** Summary of purity for the dissymmetric Ligands with Me/Et backbones, synthesised by the exploitation of carbonyl reactivity approach.

## 2.6. Formation of a PDO-NH<sub>2</sub>=O cyclic by-product

The first reaction conditions used to attach 4-methyl-3-thiosemicarbazide to PDO-NH<sub>2</sub>=O was to dissolve the reagents in water and run the reaction at 60 °C with a drop of 10% HCl (Figure 2.6.0.1.). The <sup>1</sup>H NMR spectrum of the first attempt to synthesise PDO-NH<sub>2</sub>-Me (Figure 2.6.0.2.) showed a relatively high presence of a previously un-encountered by-product.

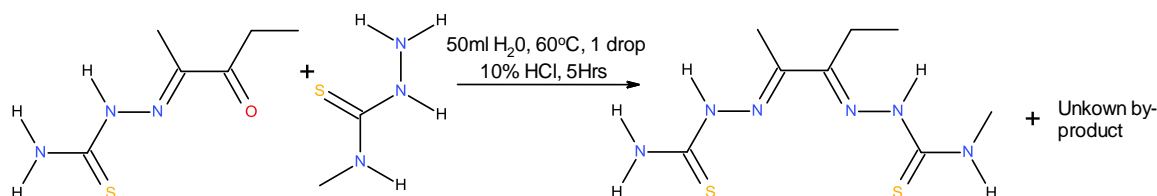


**Figure 2.6.0.1.** A reaction scheme showing the conditions used when the unknown by-product was first observed.

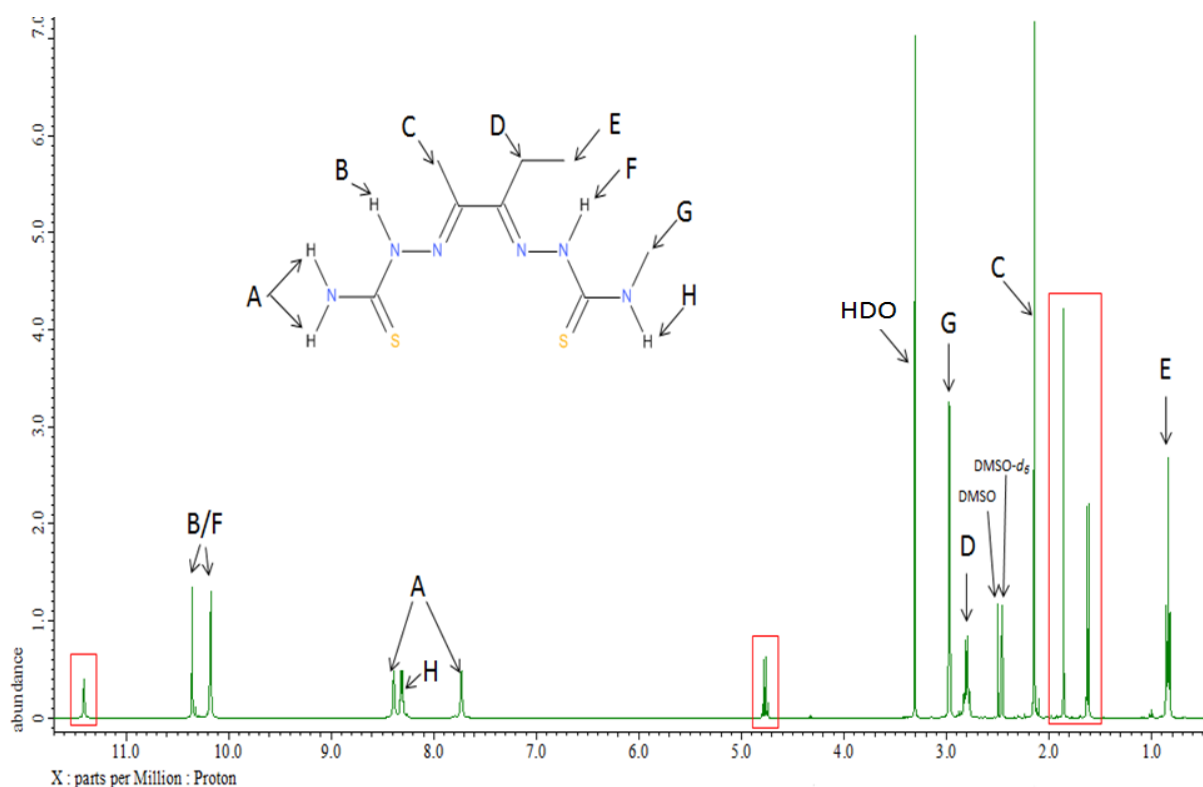


**Figure 2.6.0.2.** A <sup>1</sup>H NMR spectrum of PDO-NH<sub>2</sub>-Me attempt 1, showing the presence an unfamiliar by-product (red boxes).

It is possible to see that PDO-NH<sub>2</sub>-Me was successfully synthesised. The red boxes highlight the presence of an unfamiliar by-product in relatively high proportions. A similar reaction using PDO-Me=O and thiosemicarbazide did not show signs of a new by-product. On consultation of the literature, there were reports of bis(thiosemicarbazone) ligands forming cyclic by-products and that some of these cyclic by-products are produced from mono-substituted-3-thiosemicarbazone intermediates.<sup>57-59, 87, 88</sup>

In an attempt to avoid the formation of this by-product the reaction was ran without acid and at room temperature. As the PDO-NH<sub>2</sub>=O intermediate does not fully dissolve in water at room temperature the reagents has to be dissolved in the minimum volume of DMF. The resulting product was a mixture of roughly 50% of the target molecule with the rest of the sample comprising up of the unreacted intermediate and 4-methyl-3-thiosemicarbazide however, the suspected cyclic by-product was absent. This is illustrated in Figure 2.6.0.3.

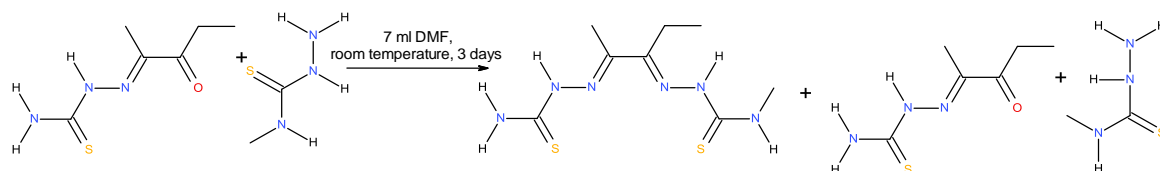


**Figure 2.6.0.3.** Reaction conditions that yielded no by-product.

As this new by-product was not observed in the synthesis of the intermediate PDO-NH<sub>2</sub>=O, which involves the presence of much higher concentrations of HCl, a hypothesis was formed that the acid was not responsible for the formation of this new by-product. The previous reaction was repeated with the presence of HCl and was only stirred for 5 hours at room temperature (Figure 2.6.0.4.). The resulting product contained roughly 92% of the target ligand and the impurities where the common ones observed throughout the synthesis of this class of ligand. The new by-product was completely absent from the resulting solid.

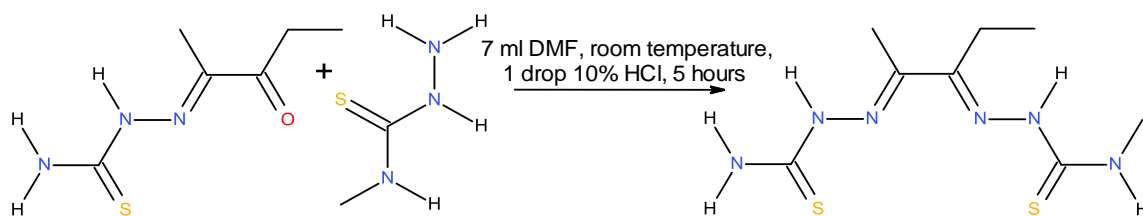


**Figure 2.6.0.4.** Successful synthesis of the dissymmetric ligand PDO-NH<sub>2</sub>-CH<sub>2</sub> without the presence of the unknown by-product.

In order characterise the new by-product, and to discover if it is indeed cyclic, the by-product was purposely synthesised (Figure 2.6.0.5.).

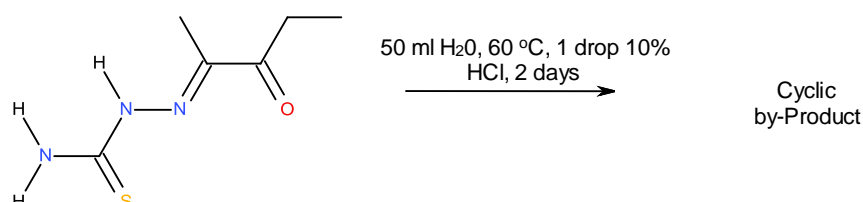


**Figure 2.6.0.5.** Conditions used to cleanly synthesise the unknown by-product.

A yellow solid, with a high purity was produced and the solid was subjected to a range of NMR experiments in order to elucidate the structure.

### 2.6.1. Method

#### PDO-NH<sub>2</sub>=O cyclic

PDO-NH<sub>2</sub>=O (0.277 g, 0.0016 mol) was dissolved in de-ionised water (50 mL, 60 °C) and any insoluble particulates was removed by filtration. HCl (10%, 1 drop) was then added and the solution was left to stir (60 °C, 2 days). The precipitate was filtered off and washed with de-ionised water (100 mL) and dried. A yellow solid (0.135 g) was recovered (35% yield).

#### 2.6.2. Characterisation data and tentative assignments for PDO-NH<sub>2</sub>=O cyclic

<sup>1</sup>H NMR (DMSO-*d*<sub>6</sub>, 400 MHz): δ= 11.41 (s, 1 H, C-NH), 10.18 (s, 1 H, N-NH), 4.77 (q, 1 H, C=CH, J=

7.6 Hz), 1.86 (s, 3 H, N=C-CH<sub>3</sub>), 1.62 (d, 3 H, C=CH-CH<sub>3</sub>, J=7.6 Hz). <sup>13</sup>C {<sup>1</sup>H} NMR (DMSO-*d*<sub>6</sub>, 100 MHz): δ= 179.10 (C=S), 147.76 (C=N), 127.27 (N-C=CH), 101.44 (C=CH), 18.52 (N=C-CH<sub>3</sub>), 11.22 (C=CH-CH<sub>3</sub>). IR (neat): cm<sup>-1</sup>= 3244 (m), 1713 (m), 3129 (m), 2945 (m), 1653 (m), 1607 (m), 1545 (s), 1470 (m), 1445 (m), 1423 (m), 1398 (m), 1354 (m), 1296 (m), 1219 (s), 1140 (m), 1094 (m), 1061 (s), 1034 (m), 735 (s), 671 (s), 617 (s), 546 (s). Raman (neat): cm<sup>-1</sup>= 2910 (w), 1653 (m), 1605 (m), 1595 (w), 1536 (w), 1432 (w), 1370 (w), 1347 (w), 1298 (w), 1244 (w), 1212 (m), 1127 (w), 1059 (w), 932 (w), 673 (w), 623 (w), 544 (w), 502 (m), 416 (w), 364 (w), 196.3 (w), 109 (w).

(Fluorescence was present). Elemental analysis: Found: C, 46.3; H, 5.9; N, 26.95. Calc. for C<sub>6</sub>H<sub>9</sub>N<sub>3</sub>S<sub>1</sub>: C, 46.4; H, 5.8; N, 27.1%. Melting point: >196 °C (decomposed).

#### 2.6.3. Proposition of the cyclic by products structure

Using the above techniques the structure of the cyclic by-product (Figure 2.6.3.1.) is proposed.

The cyclic by-product shall be referred to from now on as PDO-NH<sub>2</sub> cyclic.

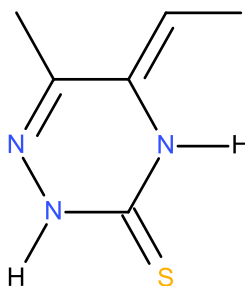


**Figure 2.6.3.1.** The proposed structure of PDO-NH<sub>2</sub> cyclic.

Therefore the proposed reaction scheme (Figure 2.6.3.2.) is:

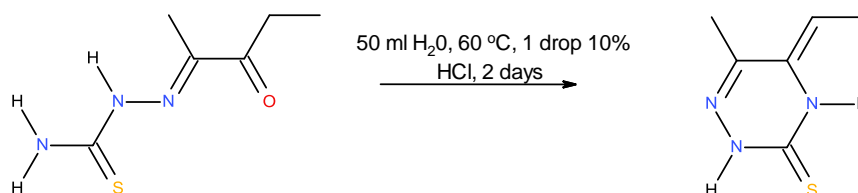


**Figure 2.6.3.2.** The reaction scheme of PDO-NH<sub>2</sub> cyclic.

#### 2.6.4. Validation of the proposed structure of PDO-NH<sub>2</sub>=O cyclic

The proton NMR spectrum (Figure 2.6.4.1), below supports the proposed structure of PDO-NH<sub>2</sub> cyclic as all the integrals and splitting patterns one would expect corresponding to the proposed structure are present. The key difference in this spectrum that is not seen in spectra of ligands or intermediates with a Me/Et backbone is the quartet environment marked 'B' which is centered at 4.77 ppm. This peak suggests the presence of a double bond as the chemical shift is within the range of a typical alkene. The existence of a carbon-carbon double bond would only allow a single hydrogen at the 'B' location, the integral of 1H agrees with the suggestion that the carbon double bond is between carbon position 'C' and 'D' (Figure 2.6.4.2.). The doublet marked 'C' (Figure 2.6.4.1.) is consistent with the splitting pattern you would expect when a methyl substituent is coupled with a C=CH group, according to the 2In+1 rule, where I is the spin quantum number and n is the number of adjacent hydrogen atoms. This coupled with the absence of the quartet centred at 2.90 ppm relating to the CH<sub>2</sub>-CH<sub>3</sub> environment, further supports a single hydrogen at the 'B' location. The absence of a hydrogen from the C-NH<sub>2</sub> environment, which is normally expected between 8 and 9 ppm, coupled with the single N-H location shifting from 8-9 ppm to 10.2 ppm supports that one of the terminal hydrogen atoms of the C-NH<sub>2</sub> group of PDO-NH<sub>2</sub>=O has been removed. This backs-up that the nitrogen of the remaining C-NH group is likely to be singly bound to another atom, most likely the carbon of the ketone carbonyl group.

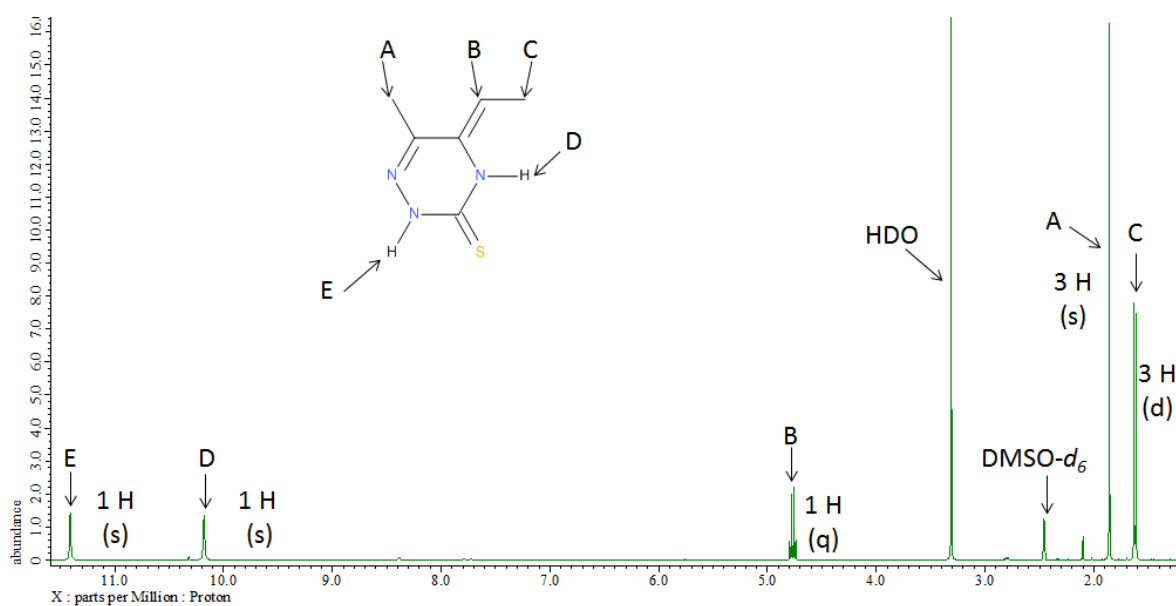


**Figure 2.6.4.1.** An assigned <sup>1</sup>H NMR spectrum of PDO-NH<sub>2</sub>=O cyclic.

The first supporting aspect of the carbon spectrum below (Figure 2.6.4.2.) is that the peak normally located at 200 ppm has shifted down to 130 ppm, this indicates that the ketone carbonyl group is no longer present. As the C=N group is typically found at chemical shifts of around 145 ppm, it reasonable to suggest that carbon 'C' is in a similar environment which is slightly less electron withdrawing e.g. C-N. The presence of the double bond between carbons 'C' and 'D' is also bound to have an effect of the position of peak 'C'. The most notable environment due to this

double bond is position 'D' which is in the region which suggests carbon 'D' is in a similar site to  $R_2C=CH_2$ .

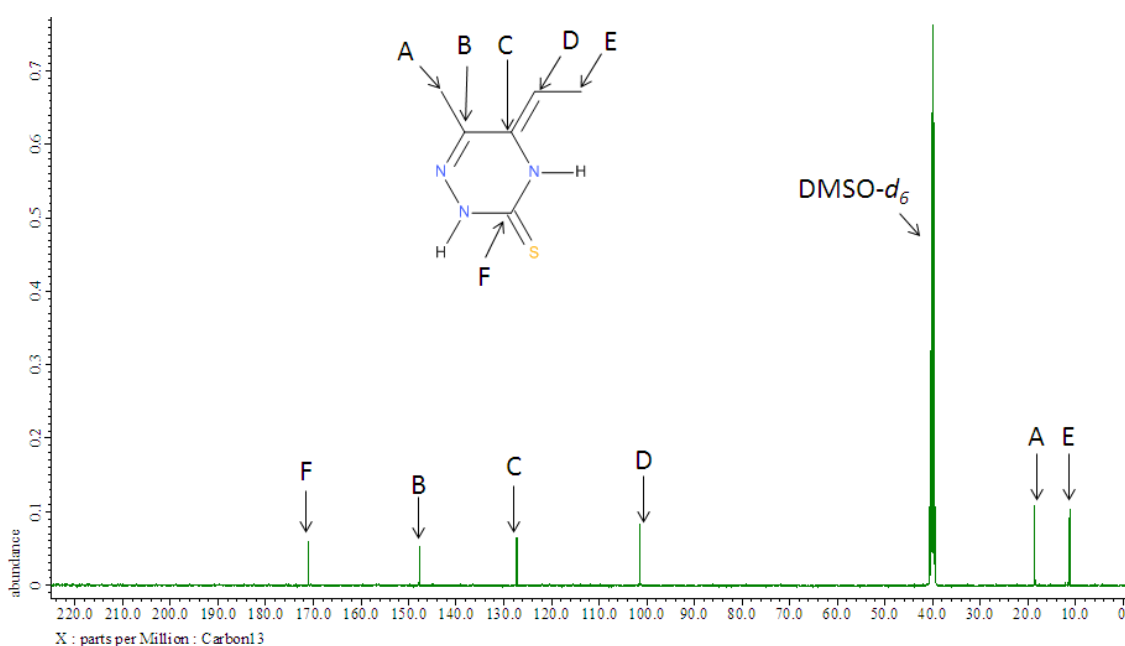


**Figure 2.6.4.2.** An assigned  $^{13}C$  NMR of spectrum of PDO-NH<sub>2</sub>=O cyclic.

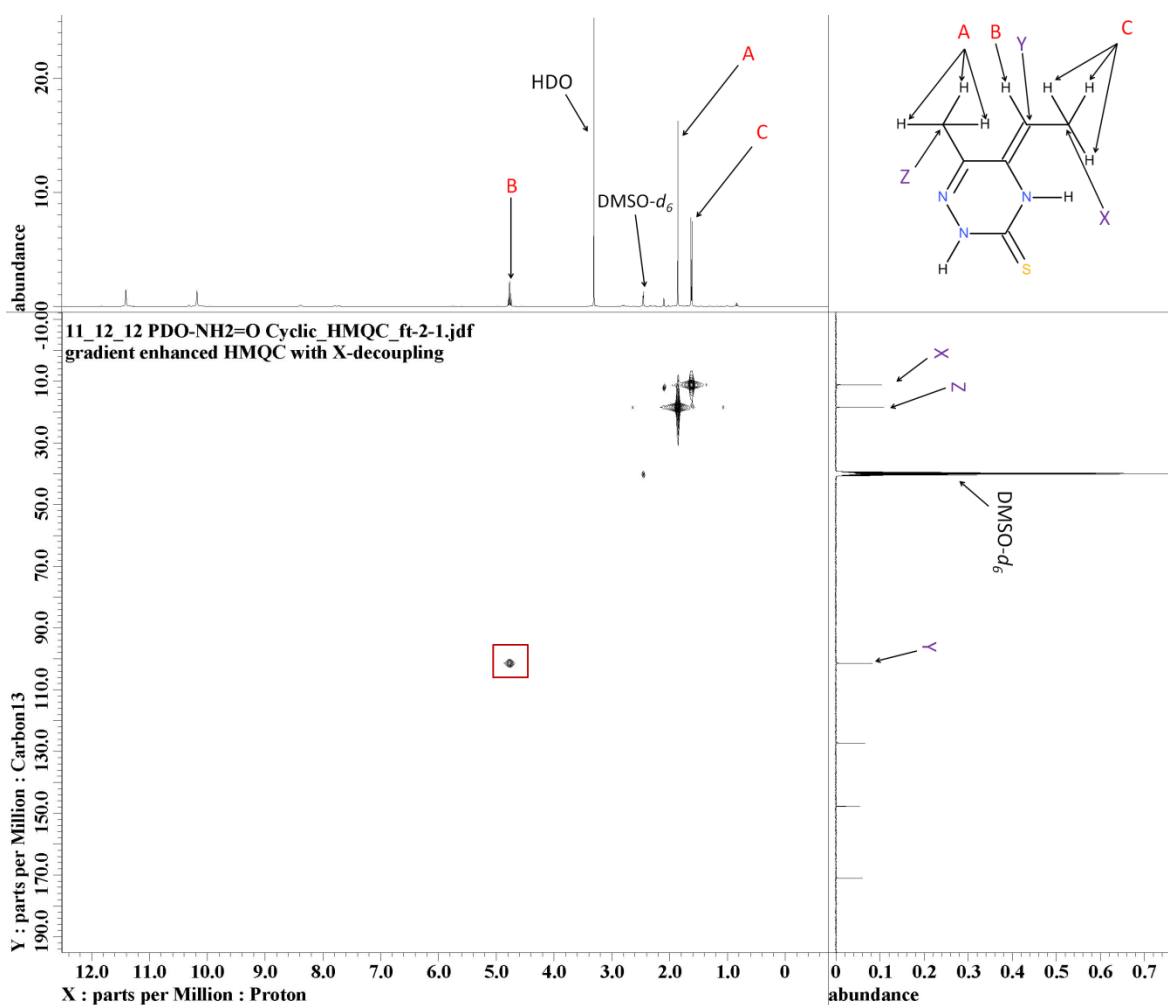


**Figure 2.6.4.3.** A HMQC NMR spectrum of PDO-NH<sub>2</sub>=O cyclic, supporting the presence the double bond within the enamine functionality of PDO-NH<sub>2</sub>=O cyclic.



The above HMQC NMR spectrum (Figure 2.6.4.3.) makes it possible to determine which of the hydrogen environments (labelled by the letters A-C) are directly bound to which carbon locations (labelled by the letters Y-Z). Firstly the spectra confirms that both the hydrogen locations 'A' and 'C' are bound to carbon 'Z' and carbon 'X' respectively in order to form two CH<sub>3</sub> groups on the backbone of the molecule. A strong piece of evidence to the structure of this by product is that the HMQC spectra shows that the single proton 'B' is directly bound to carbon 'Y', illustrated by the red box, which supports the presence of a double carbon bond. There is no coupling data present that advocates a different structure.

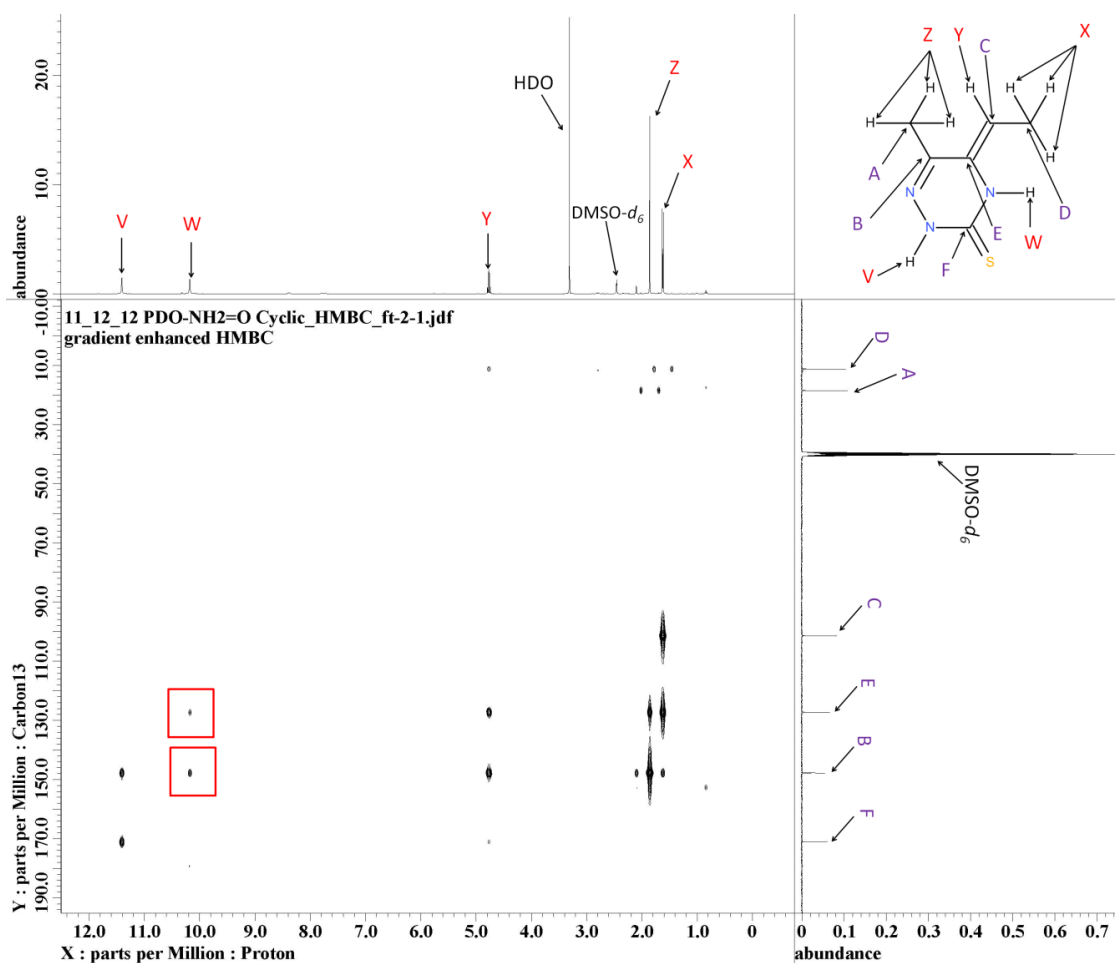


**Figure 2.6.4.4.** A HMBC NMR spectrum of PDO-NH<sub>2</sub>=O cyclic, supporting the cyclic confirmation of PDO-NH<sub>2</sub>=O cyclic.

This HMBC spectrum (Figure 2.6.4.4.) makes it possible to look at the couplings between hydrogen atoms (labelled by the letters V-Z) and carbons (labelled by the letters A-F) which are not directly attached to each other. By looking at the spectra, the couplings are consistent with those which are expected for the proposed structure and there are no extra couplings which suggest a different structure. The two most informative couplings are indicated by the red boxes. These coupling show that the hydrogen 'W' is bound in a location that allows it to have a detectable coupling with carbons 'B' and 'E'. This is very strong evidence that the nitrogen which the hydrogen is bound is linked to carbon 'E'. The only discrepancy present is that a coupling is

expected between hydrogen 'W' and carbon 'F', this may just be due to this particular coupling being particularly weak, which results in the interaction not being detected. The interaction must be unique to the C(=S)-N(-H)-C environment as a coupling is observed between carbon 'F' and hydrogen 'V'. An article by J. Adams *et al.*<sup>205</sup> reports the same cyclic by-product. There is very little information about the synthesis of this compound, but the proton NMR data matches.

### **Proposed mechanism for the formation of PDO-NH<sub>2</sub> cyclic:**

The following scheme (Figure 2.6.4.5.) sets out the suggested mechanism of the formation of the PDO-NH<sub>2</sub> cyclic by-product, which is formed when the amine nitrogen attacks the carbonyl carbon. This is followed by a series of proton transfer steps in order to form the cyclic by-product. It is expected that the cyclic by-product should be in some level of equilibrium with the other mechanistic products, but as the NMR shows no significant extra peaks then it can be assumed that the equilibrium is in favour of the final cyclic by product.

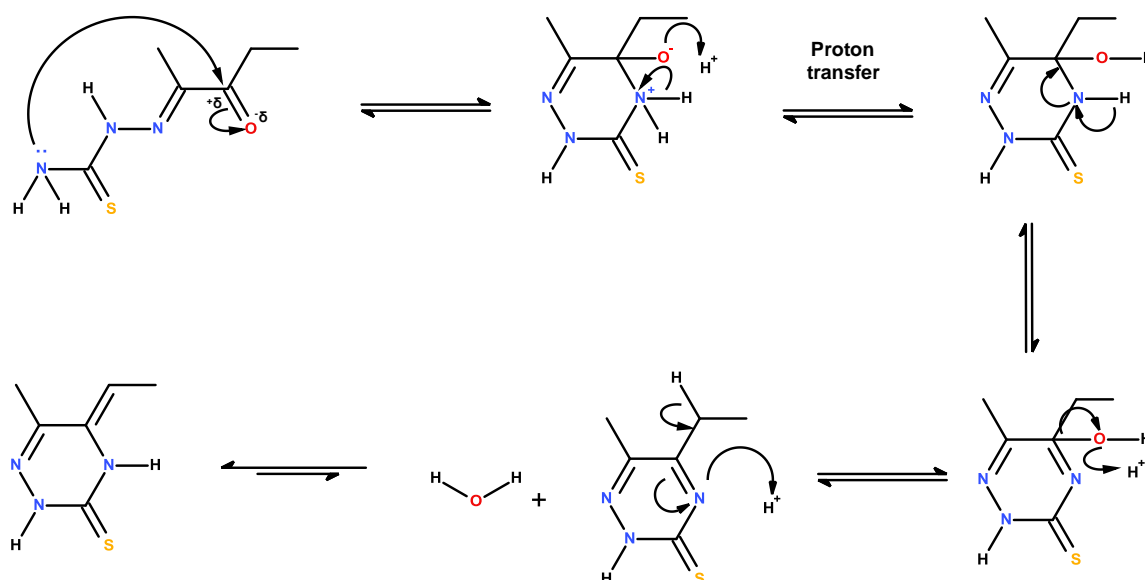


**Figure 2.6.4.5.** The proposed mechanism for the formation of PDO-NH<sub>2</sub>=O cyclic.

### **2.6.5. Summary**

All the spectra strongly support the proposed structure of PDO-NH<sub>2</sub> cyclic (Figure 2.6.5.1.). This is validated by NMR data that has previously been reported.<sup>205</sup> There are no other feasible alternative structures that also satisfy the experimental data.

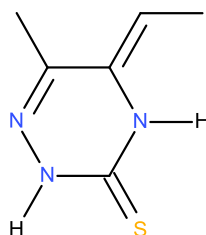


**Figure 2.6.5.1.** The proposed structure of PDO-NH<sub>2</sub> cyclic.

## **2.7. Ligands with H/H backbones**

### **Application**

It was hoped that the synthetic methods applied for the synthesis of dissymmetric ligands covered in the previous sections could be easily transferred to the synthesis of dissymmetric ligands with H/H on the backbone. This class of ligand may have the desired properties in be of interest in the study of copper trafficking within the brain, similar to the hopes for the ligands with Me/H on the backbone.

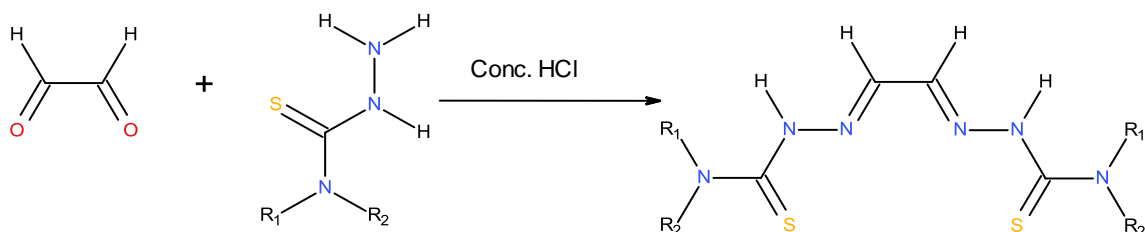
The literature has reported that the symmetric copper complex of Gly-Me-Me is able to cross the blood brain barrier. After being reduced by intracellular processes the copper becomes available to the cell<sup>182</sup>. With this in mind it hoped that synthesising a range of dissymmetric ligands with H/H on the backbone for biological screening would identify the most effective ligand to use for the above application. Donnelly *et al.*<sup>76</sup> has previously investigated a range of symmetric bis(thiosemicarbazone) complexes, including the three ligands with H/H on the backbone, but for a therapeutic application instead of investigation of neurodegenerative diseases, such as Alzheimer's disease. With these two pieces of research in mind it was decided to try to attempt the synthesis of dissymmetric ligands with H/H on the backbone and, if successful, make a range of ligands with relatively lipophilic substituents on the side arms so that the resulting complexes can cross the blood brain barrier and deposit radio-copper in the brain. The radio-copper can then be monitored via PET in order to investigate the migration of the copper in neurodegenerative disorders in order to elucidate the cellular mechanisms which could present a potential target for therapy. The chemistry reported by B. Paterson *et al.*<sup>73</sup> gives rise to an interest in dissymmetric ligands that contain a dimethyl side arm, as these could be potentially useful for the synthesis of dual labelled complexes. GLY-Me-(Me)<sub>2</sub> is a ligand that is of interest for this application and therefore GLY-Me-(Me)<sub>2</sub> is the initial target dissymmetric ligand to synthesise.

### **2.7.1. Symmetric ligands with H/H backbones**

Even though the main focus is the synthesis of dissymmetric ligands, two symmetric ligands were synthesised in order to establish the precursors' chemistry and their NMR spectroscopy and vibrational spectra.

#### **Overview of reaction**

The synthesis of this subgroup of ligands requires glyoxal (GLY) to be combined with a chosen 4-substituted-3-thiosemicarbazide under acidic conditions in water or a water/ethanol solution at circa 60°C to give the desired symmetric ligand (Figure 2.7.1.1.). Two ligands were synthesised (Figure 2.7.1.2.).



	R <sub>1</sub>	R <sub>2</sub>
GLY-Et-Et	CH <sub>2</sub> CH <sub>3</sub>	H
GLY-Ph-Ph	C <sub>6</sub> H <sub>5</sub>	H

**Figure 2.7.1.1.** The general reaction for the synthesis of symmetric ligands with H/H backbones.

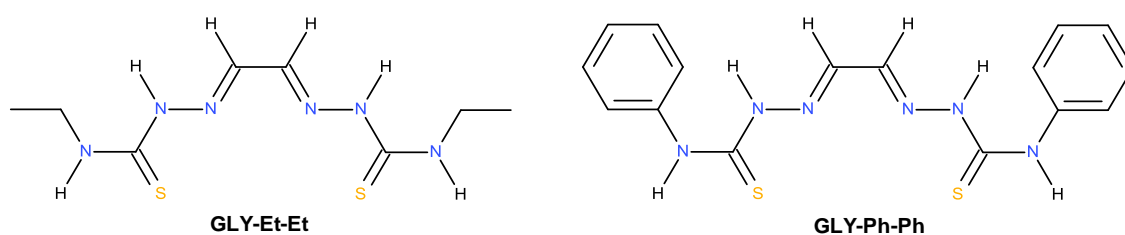


**Figure 2.7.1.2.** Structures of the symmetric ligands with H/H backbones that were synthesised.

## 2.7.1. Methods

### GLY-Et-Et

4-Ethyl-3-thiosemicarbazide (1.311 g, 0.011 mol) was dissolved in de-ionised water (75 mL, 50 °C). HCl (32%, 3 drops) was added, followed by the rapid addition of glyoxal (40 wt. % solution, 0.58 mL, 0.005 mol) and the solution was left to stir (50 °C, 10 minutes). The precipitate was recovered by filtration and washed with de-ionised water (4 x 50 mL). The solid was dried. A cream solid (1.286 g) was recovered (99% yield).

### GLY-Ph-Ph

4-phenyl-3-thiosemicarbazide (1.840 g, 0.011 mol) was dissolved in an ethanol solution (de-ionised water 100 mL, ethanol 52 mL, 50 °C). HCl (32%, 8 drops) was added followed by the rapid addition of glyoxal (40 wt. % solution, 0.58 mL, 0.005 mol). The solution was left to stir (50 °C, 10 minutes). The precipitate was filtered off and washed with de-ionised water (4 x 50 mL). The solid was dried. A creamy brown solid (1.762 g) was recovered (99% yield).

## 2.7.2. Characterisation data for symmetric ligands with H/H backbones

### GLY-Et-Et

$^1\text{H NMR}$  (DMSO- $d_6$ , 400 MHz):  $\delta$ = 11.67 (s, 2 H, N-NH), 8.50 (t, 1 H, C-NH,  $J$ = 6.0 Hz), 7.68 (s, 2 H, N=C-H), 3.49 (dq, 4 H,  $\text{H}_2\text{C-NH}$ ,  $J$ =7.2, 6.0 Hz), 1.06 (t, 6 H,  $\text{H}_2\text{C-CH}_3$ ,  $J$ = 7.2 Hz).  $^{13}\text{C}\{^1\text{H}\}$  NMR (DMSO- $d_6$ , 100 MHz):  $\delta$ = 176.96 (C=S), 140.60 (C=N), 38.92 (N- $\text{CH}_2$ ), 14.89 ( $\text{H}_2\text{C-CH}_3$ ). IR (neat):  $\text{cm}^{-1}$ = 3370 (m), 3130 (m), 2982 (m), 1570 (w), 1514 (s), 1470 (m), 1373 (w), 1323 (m), 1281 (m), 1207 (s), 1070 (s), 1040 (m), 961 (w), 908 (m), 806 (m), 692 (w), 642 (m), 623 (s), 538 (s), 426 (m). Raman (neat):  $\text{cm}^{-1}$ = 3370 (w), 3128 (w), 1589 (s), 1526 (m), 1413 (w), 1301 (w), 1166 (m), 1148 (w), 1119 (w), 1046 (w), 924 (w), 791 (w), 420 (w), 207 (w), 142 (w). Melting point: >210 °C (decomposed).

### GLY-Ph-Ph

$^1\text{H NMR}$  (DMSO- $d_6$ , 400 MHz):  $\delta$ = 12.12 (s, 2 H, N-NH), 10.17 (s, 2 H, Ph-NH), 7.86 (s, 2 H, N=C-H), 7.51 (d, 4 H,  $\text{H}_{(2,6)}$  aryl), 7.32 (dd, 4 H,  $\text{H}_{(3,5)}$  aryl), 7.16 (t, 2 H,  $\text{H}_{(4)}$  aryl).  $^{13}\text{C}\{^1\text{H}\}$  NMR (DMSO- $d_6$ , 100 MHz):  $\delta$ = 176.55 (C=S), 141.24 (C=N), 139.40 ( $\text{C}_{(1)}$  aryl), 128.61 ( $\text{C}_{(3,5)}$  aryl), 126.08 ( $\text{C}_{(2,6)}$  aryl), 125.89 ( $\text{C}_{(4)}$  aryl). IR (neat):  $\text{cm}^{-1}$ = 3296 (m), 3154 (w), 2988 (w), 1595 (m), 1537 (s), 1504 (s), 1443 (m), 1383 (m), 1308 (w), 1252 (s), 1184 (s), 1082 (m), 1026 (m), 937 (m), 924 (m), 899 (w), 770 (m), 748 (s), 689 (s), 658 (m), 613 (m), 581 (s), 494 (s), 469 (s). Raman (neat):  $\text{cm}^{-1}$ = 1588 (s), 1546 (w), 1512 (w), 1301 (w), 1212 (w), 1169 (s), 1121 (w), 1002 (w), 930 (w), 768 (w), 745 (w), 652 (w), 349 (w), 335 (w), 261 (w), 224 (w), 197 (w). Melting point: >250 °C (decomposed).

## 2.7.3. Spectral examples of a symmetric ligand with an H/H backbone

Figures 2.7.3.1-4. Spectral examples of ligand GLY-Ph-Ph.

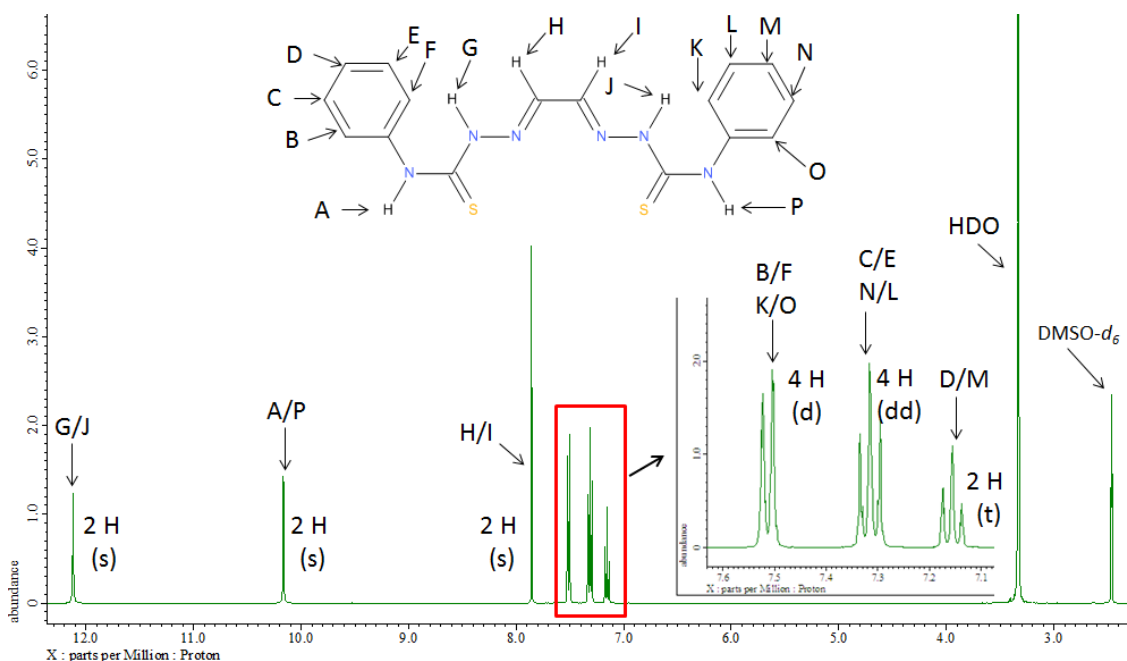


**Figure 2.7.3.1.** An assigned  $^1\text{H NMR}$  spectrum of GLY-Ph-Ph. This ligand was synthesised by reacting glyoxal with 4-phenyl-3-thiosemicarbazide.

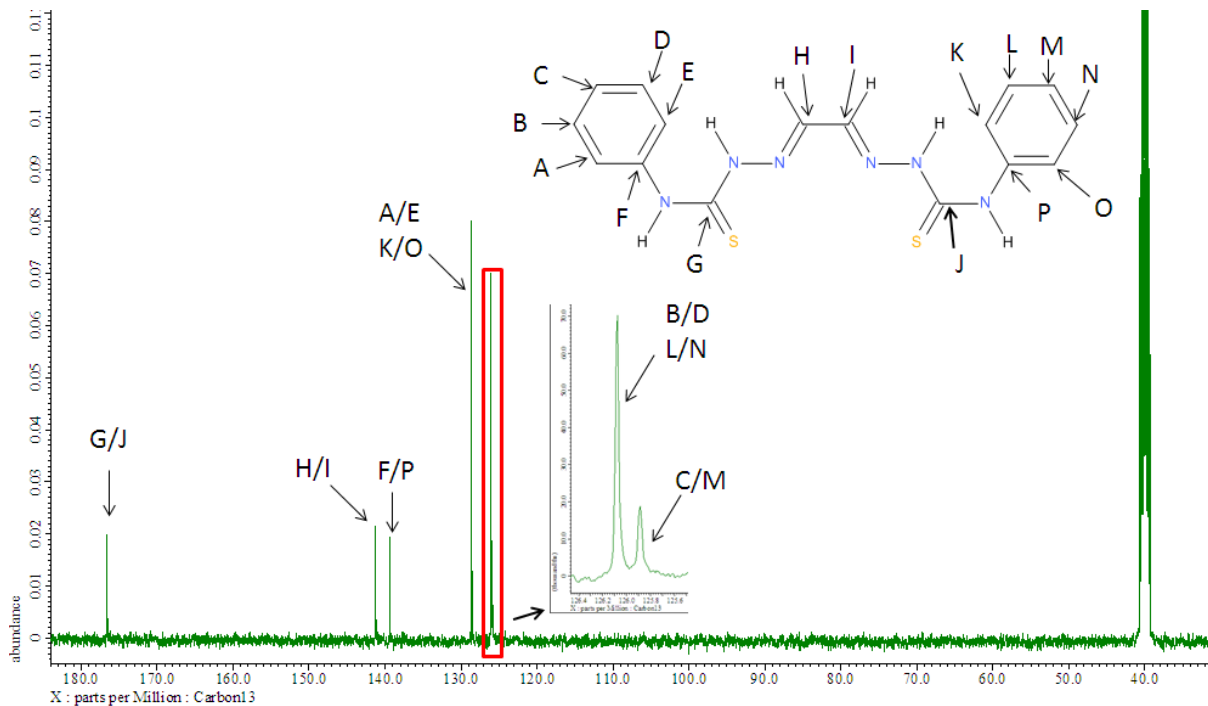


**Figure 2.7.3.2.** A assigned  $^{13}\text{C}$  NMR spectrum of GLY-Ph-Ph.

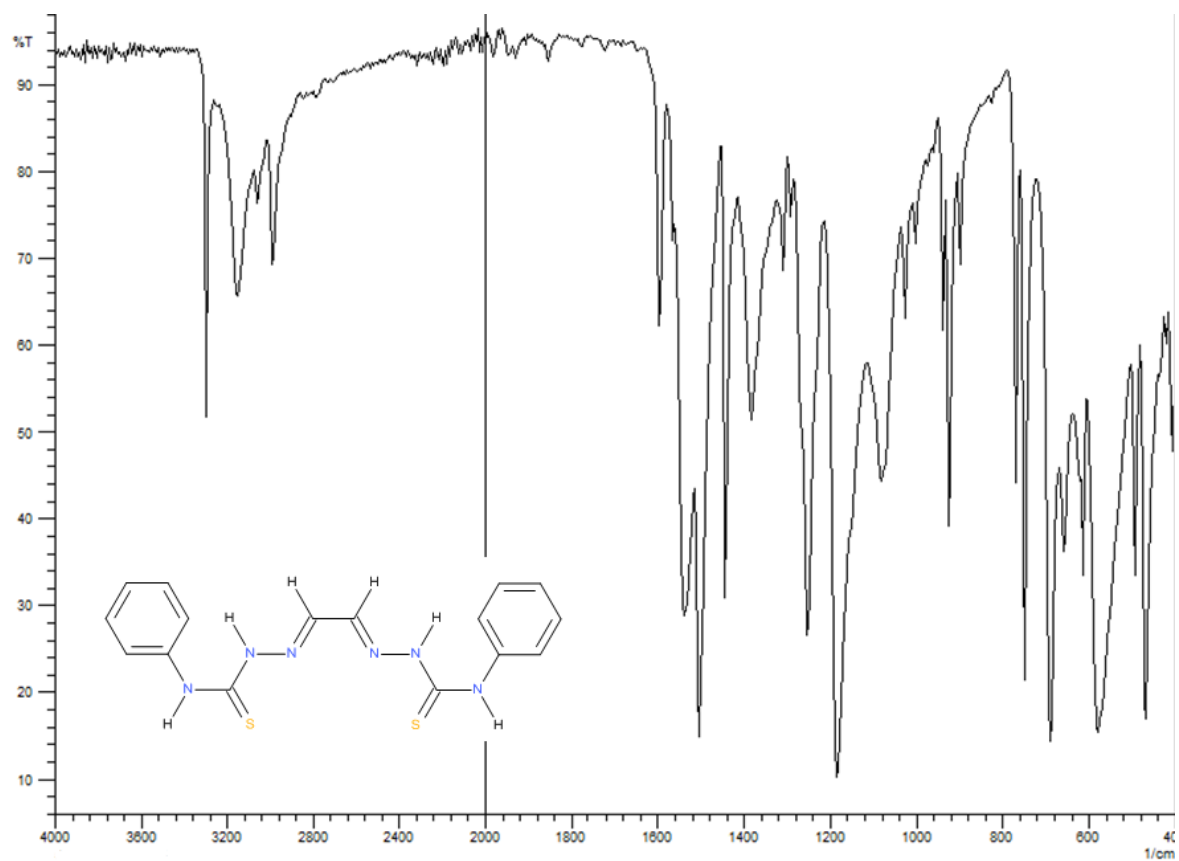


**Figure 2.7.3.3.** A FTIR spectrum of GLY-Ph-Ph.

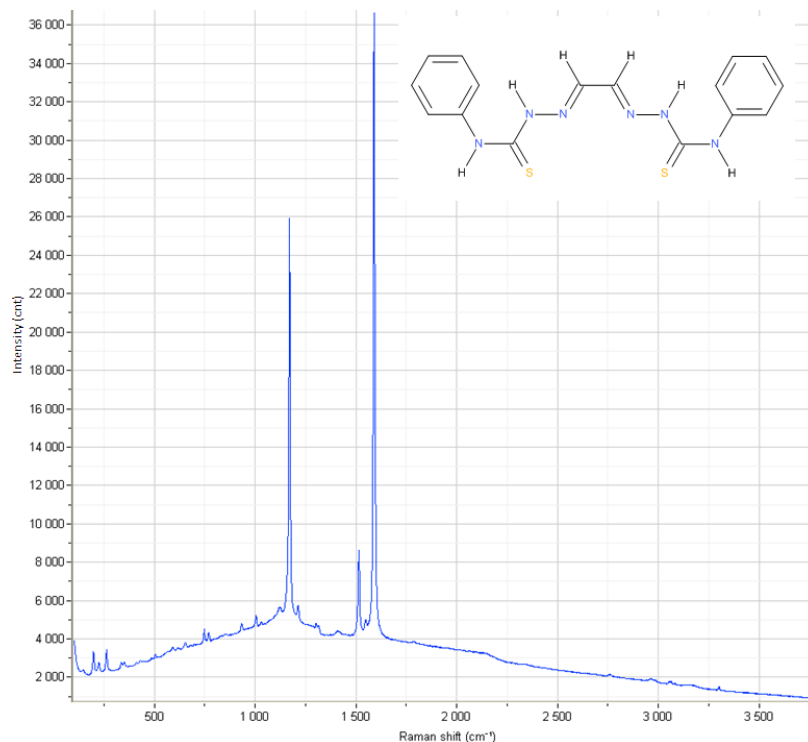


**Figure 2.7.3.4.** A Raman spectrum of GLY-Ph-Ph.

### 2.7.4. Discussion

The synthetic method of both GLY-Et-Et and GLY-Ph-Ph was similar to the synthesis of previous symmetric ligands that have been reported in this chapter. Both products were recovered with excellent yields and with no signs of significant impurities in their NMR spectra (Table 2.7.4.1.). The NMR data recorded for GLY-Ph-Ph is in close agreement with the literature<sup>76</sup> and the NMR and IR data for GLY-Et-Et is also a good fit to the literature values.<sup>210</sup> No further reports on any characterisation data could be found for GLY-Et-Et or GLY-Ph-Ph.

**Table 2.7.4.1.** A summary of purity for the symmetric ligands with H/H backbones.

Ligand	Novel	Yield	Main impurity	Estimated impurity*
<p style="text-align: center;"><b>GLY-Et-Et</b></p>	No <sup>76</sup> , 180, 210	99%		1%
<p style="text-align: center;"><b>GLY-Ph-Ph</b></p>	No <sup>76</sup> , 180	99%		Not possible to determine due to overlapping peaks

\*Estimated by <sup>1</sup>H NMR spectra using the integrals of the N=CH environments.

### 2.7.5. Attempts to synthesise dissymmetric ligands with H/H backbones

Two synthetic approaches were attempted in the pursuit of the synthesis of dissymmetric ligands with H/H on the backbone. The first was using the exploitation of carbonyl reactivity which has been successfully used to synthesise the dissymmetric ligands in sections 2.3.-2.5. The second method used was using acetal protecting approach, a method which was explored in section 2.2.

### 2.7.6. Attempts by the exploitation of carbonyl reactivity differences

#### Overview of reaction

The first attempts used the same principal as all the previous mono-substituted-3-thiosemicarbazone intermediates were synthesised by, which involved reacting a 4-substituted-3-thiosemicarbazide with one of the carbonyl groups of the backbone precursor (glyoxal). The second unreacted carbonyl group's reactivity should reduce enough so that the formation of the symmetric bis(thiosemicarbazones) would not be favourable, thus resulting in the creation of a pure mono-substituted-3-thiosemicarbazone. Once this mono-substituted-3-thiosemicarbazone intermediate was isolated then it could be reacted with a dissimilar 4-substituted-3-thiosemicarbazide to yield the desired dissymmetric ligand (Figure 2.7.6.1.). This rationale was backed up by a paper written by P. Waghorn *et al.*<sup>92</sup> which claimed that the mono-methyl-3-thiosemicarbazone of glyoxal had been achieved by using a method that was briefly reported, which seems to be almost identical method which had been implemented in the formation of previous intermediate mono-substituted-3-thiosemicarbazones reported in this chapter.

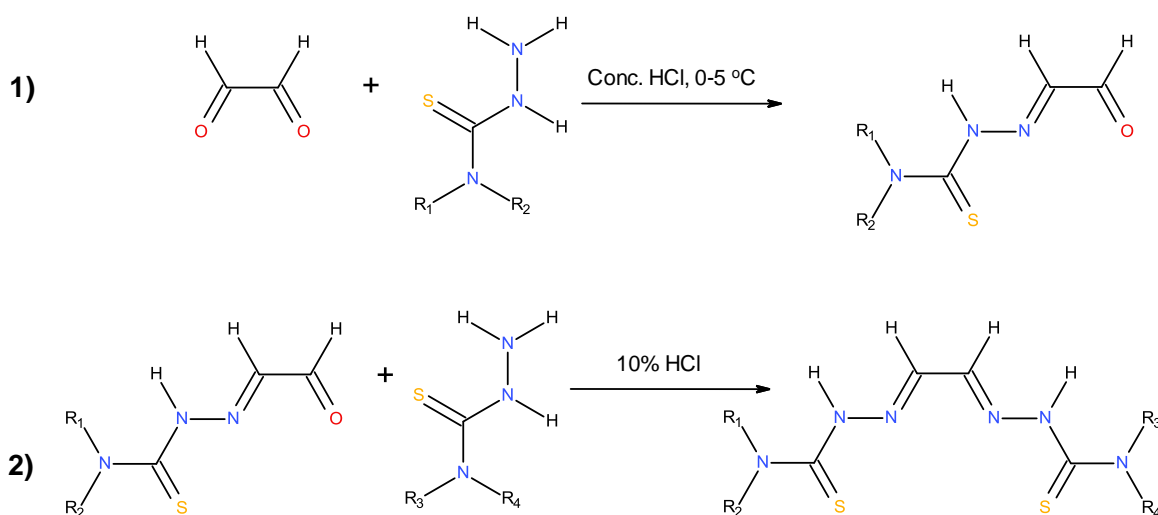


**Figure 2.7.6.1.** The proposed method for the synthesis of dissymmetric ligands with H/H backbones.



**Method of the first attempt to synthesise GYL-Me=O:**

4-methyl-3-thiosemicarbazide (1.157 g, 0.011 mol) was dissolved in de-ionised water (100 mL). The solution was cooled (2.6 °C) over ice, followed by the addition of HCl (32%, 5 drops). The solution was cooled further (0.7 °C). Glyoxal (40 wt. % solution, 5.05 mL, 0.044 mol) was added rapidly and vigorously stirred (5 °C, 10 minutes). The precipitate was recovered via filtration, washed with de-ionised water (4 x 50 mL) and dried. A yellow solid (0.485 g) was recovered.

**Result:**

Disappointingly, despite excess of backbone, the product recovered was by the vast majority the symmetric ligand GLY-Me-Me with only a very small proportion being the desired intermediate GLY-Me=O. The estimated proportions of both these products were 94-93% and 6-7% respectively.

**Alteration 1:**

The above method was repeated but instead of cooling the reaction between 5.0-0.7 °C the reaction would be cooled to below 0 °C using a salt/ice bath because of this, the reaction solvent had to be changed to an ethanol/water mixture in order to stop the reaction mixture freezing. The excess of glyoxal backbone was increased and the overall reactions proportions were scaled up but the volume of HCl was kept the same. The justification for this was hopefully to make the formation of GLY-Me=O more favourable than GLY-Me-Me and even if this was not successful there should be enough GLY-Me=O in the resulting product in order to attempt an extraction method.

**Method of the first alteration for the synthesis GYL-Me=O:**

4-methyl-3-thiosemicarbazide (2.314 g, 0.022 mol) was dissolved in water/ethanol solution (200 mL de-ionised water, 120mL ethanol). The solution was cooled (-10 °C) in a salt/ice bath (100 g table salt, 300 g ice), followed by the addition of HCl (32%, 5 drops). The solution was cooled further (-11.6 °C). Glyoxal (40 wt. % solution, 12.62 mL, 0.110 mol) was added rapidly and vigorously stirred (≈-11.5 °C, 15 minutes). The precipitate was recovered via filtration, washed with de-ionised water (4 x 50 mL) and dried. A yellow solid (0.430 g) was recovered.

A second precipitate formed in the filtrate which was filtered off, washed with a little water and dried. A yellowish/orange solid (0.461g) was recovered.

**Result:**

It was initially found that no precipitate had formed after 10 minutes so the reaction length was extended by a further 5 minutes. An estimate of the first product purity by NMR integrals was 90-89% GLY-Me-Me and 11-9% GLY-Me=O. Analysis of the second precipitate gave a purity estimated of 81-84% GLY-Me-Me and 16-19% GLY-Me=O.

The expectations from the alterations were supported by the results but disappointingly the difference in GLY-Me=O proportion was only small. The method was repeated with the reaction solution being cooled down to low as possible using the salt/ice bath. The minimum temperature achieved was about -17 °C but this did not improve the proportion of GLY-Me=O.

**Extraction attempts:**

Attempts to extract the GLY-Me=O from the samples was undertaken using hot water and then hot diethyl ether. Water was chosen because it has been observed that hot water could remove mono-substituted-3-thiosemicarbazones when purifying bis(thiosemicarbazone) ligands and indeed had been used for the purpose within the synthetic methods of bis(thiosemicarbazone) ligands reported earlier in this chapter. Diethyl ether was chosen because in the exploration of synthesising dissymmetric ligands with Me/Me and Me/H on the backbone by the protection approach, diethyl ether had been used to extract the desired intermediate from a mixed product. Unfortunately when extractions were attempted with either water or diethyl ether they both yielded a product that on analysis via NMR produced messy, unsolvable NMR spectra.

Based on the lack of success from the exploitation of the carbonyl groups method and without any other feasible avenue to pursue within this method, it was decided to re-visit the acetal protection approach in order to see if this approach could be successful.

**2.7.7. Attempts by the acetal protection method****Overview of plan**

The plan devised was to take 2,2-dimethoxyacetaldehyde (DMA) and react a 4-substituted-3-thiosemicarbazide to the only carbonyl group in order to produce a protected-mono-substituted-3-thiosemicarbazone with H/H on the backbone. The next step would entail finding a method to hydrolyse the acetal groups to an aldehyde functionality and attach a different 4-substituted-3-thiosemicarbazide to give a dissymmetric ligand (Figure 2.7.7.1.).

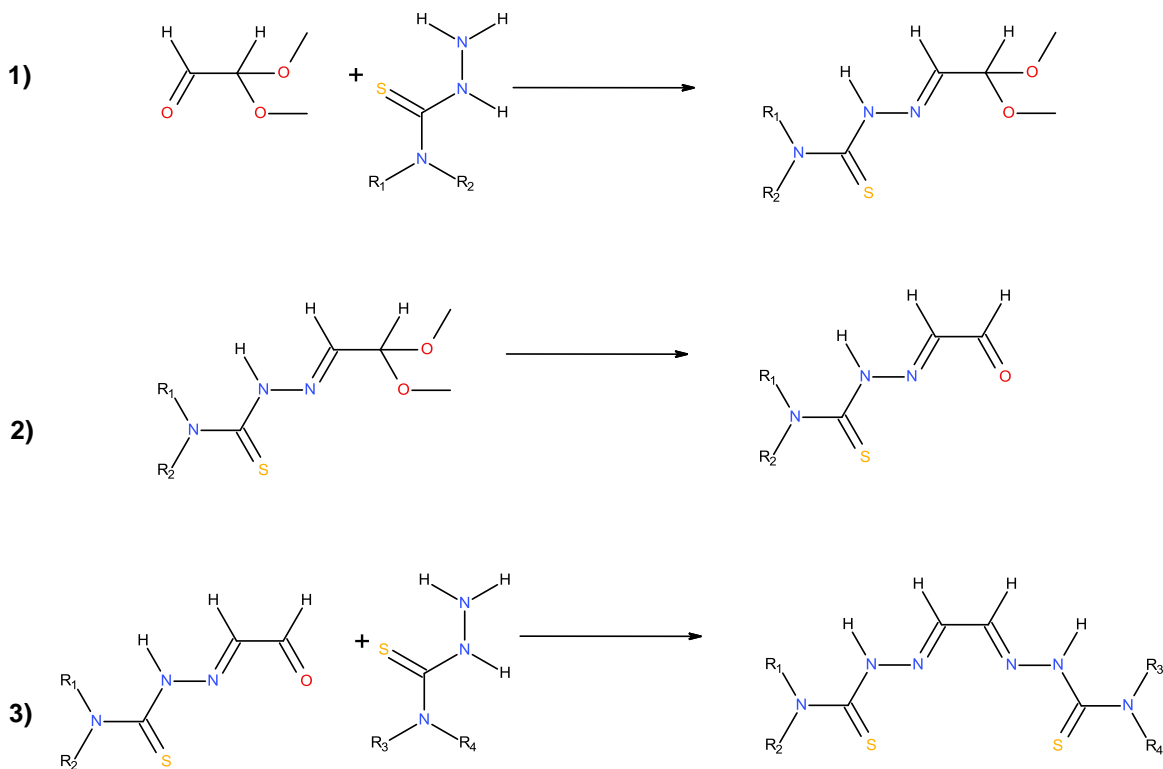


**Figure 2.7.7.1.** The proposed schematic for the synthesis of dissymmetric ligands with H/H backbones via the acetal protection method.

In order to achieve the protected-mono-substituted-3-thiosemicarbazone from reaction 1, it was decided to use water as the reaction solvent with an acid catalysis but at reduced temperature and 10 times excess of backbone in order to prevent formation of the symmetric bis(thiosemicarbazide).

#### Method of the first attempt to synthesise DMA-Me-(OMe)<sub>2</sub>:

4-methyl-3-thiosemicarbazide (0.500 g, 0.0048 mol) was dissolved in de-ionised water (30 mL). Solution cooled (7 °C) over ice, followed by the addition of HCl (32%, 1 drop). The solution was cooled further (4 °C). 2,2-dimethoxyacetaldehyde (60 wt. % solution, 8.02 mL, 0.053 mol) was added rapidly and vigorously stirred (≈2.5 °C, 1 hour). The precipitate was recovered via filtration and dried. An off white solid (0.018 g) was recovered yield (7%).

#### Result:

Overall the reaction was a success, the NMR spectra identified that DMA-Me-(OMe)<sub>2</sub> was successfully synthesised even though the yield was very low. It is believed that DMA-Me-(OMe)<sub>2</sub> is a novel compound. Via NMR it was estimated that there was a 1% impurity of GLY-Me-Me.

The reaction was scaled up by a factor of 10 in order to yield suitable quantities of intermediate in order to work with. The excess of backbone was reduced in order to prevent unnecessary wastage.

### **Method of the scaled up synthesis of DMA-Me-(OMe)<sub>2</sub>:**

4-methyl-3-thiosemicarbazide (5.000 g, 0.0475 mol) was dissolved in de-ionised water (220 mL). Solution cooled (7 °C) over ice, followed by the addition of HCl (32%, 7 drops). The solution was cooled further (3 °C). 2,2-dimethoxyacetaldehyde (60 wt. % solution, 8.02 mL, 0.053 mol) was added rapidly and vigorously stirred ( $\approx 1$  °C, 1 hour). The precipitate was recovered via filtration and dried in air. A yellow solid (3.610 g) was recovered (40% yield).

### **Result:**

The yield of the reaction increased to a more workable quantity. On analysis of the NMR spectra the product contained DMA-Me-(OMe)<sub>2</sub> and GLY-Me-Me in the quantities 98% and 2% respectively. These estimates were calculated from the integrals from the proton NMR spectra. As there was a presence of GLY-Me-Me, this suggests that a little of either the backbone or the protected intermediate can be hydrolysed to yield the undesired symmetric ligand. This should be kept in mind as a change in reaction conditions could increase the hydrolysis of the acetal protecting groups in the reaction mixture giving an increased level of undesired impurity.

The scaled up method above was tried again with all the reaction conditions being kept identical besides the drying method, which involved using an oven at 25-30 °C. The yellow product changed to a brown/yellow colour which suggests that the product is heat sensitive. The product produced turned out to contain the expected DMA-Me-(OMe)<sub>2</sub> and GLY-Me-Me, but in the proportions of 11% and 89% respectively. This heat sensitivity needs to be taken into account when drying the sample and in the design of the de-protection method.

### **Characterisation data for DMA-Me-(OMe)<sub>2</sub>**

<sup>1</sup>H NMR (DMSO-*d*<sub>6</sub>, 400 MHz):  $\delta$ = 11.30 (s, 1 H, N-NH), 8.25 (q, 1 H, C-NH, J= 4.8 Hz), 7.23 (d, 1 H, N=C-H, J= 5.6 Hz), 4.67 (d, 1 H, O-C-H, J= 5.6 Hz), 3.26 (s, 6 H, O-CH<sub>3</sub>), 2.91 (d, 3 H, N-CH<sub>3</sub>, J= 4.8 Hz). <sup>13</sup>C {<sup>1</sup>H} NMR (DMSO-*d*<sub>6</sub>, 100 MHz):  $\delta$ = 178.73 (C=S), 141.25 (C=N), 102.53 (HC-O), 53.91 (O-CH<sub>3</sub>), 31.35 (N-CH<sub>3</sub>). IR (neat): cm<sup>-1</sup>= 3256 (w), 3154 (w), 3003 (w), 2832 (w), 1553 (m), 1531 (m), 1443 (w), 1383 (w), 1337 (w), 1285 (m), 1254 (m), 1211 (w), 1188 (w), 1130 (m), 1063 (s), 1028 (m), 959 (s), 806 (w), 660 (m), 608 (m), 550 (w), 501 (w). Raman (neat): cm<sup>-1</sup>= 1633 (w), 1591 (s), 1529 (w), 1179 (m), 1143 (w), 1121 (w), 966 (w), 795 (w), 608 (w), 285 (w). Fluoresce present.

**Melting point:** 106-107 °C.

### **Spectral examples of DMA-Me-(OMe)<sub>2</sub>**

Figures 2.7.7.2-5. Spectral examples of DMA-Me-(OMe)<sub>2</sub>.

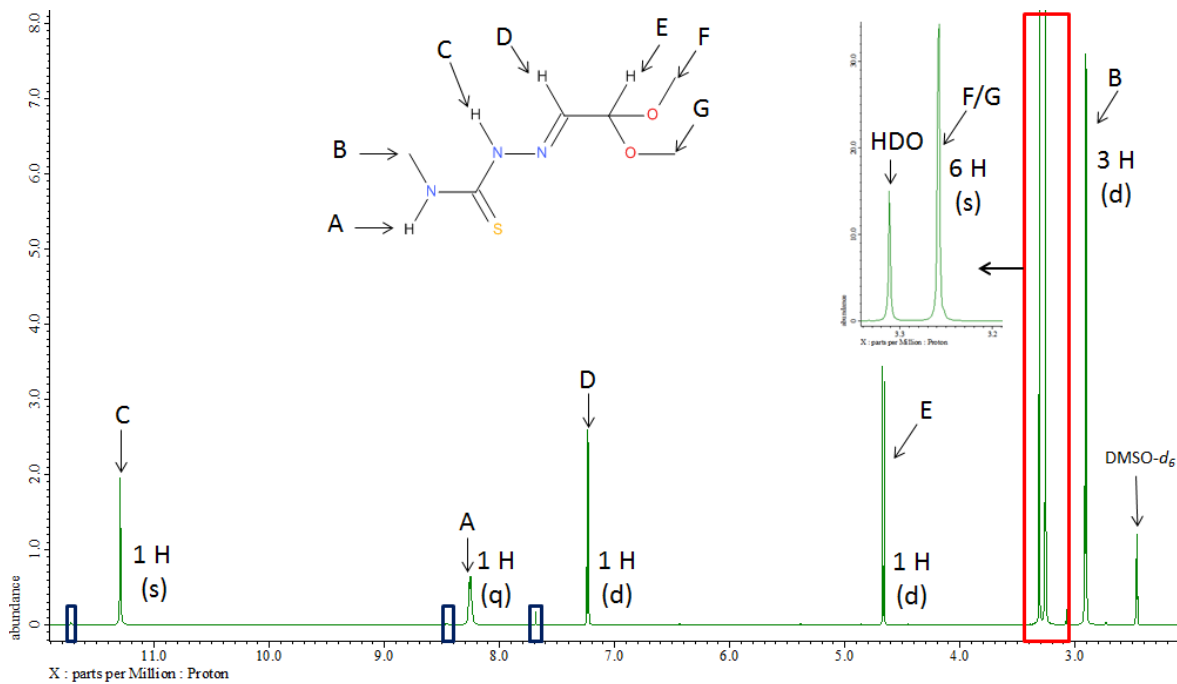


**Figure 2.7.7.2.** An assigned  $^1\text{H}$  NMR spectrum of DMA-Me-(OMe)<sub>2</sub>. This intermediate was produced by reacting 2,2-dimethoxyacetaldehyde with 4-methyl-3-thiosemicarbazide. The blue boxes suggest small presence of an impurity that is expected to be GLY-Me-Me.

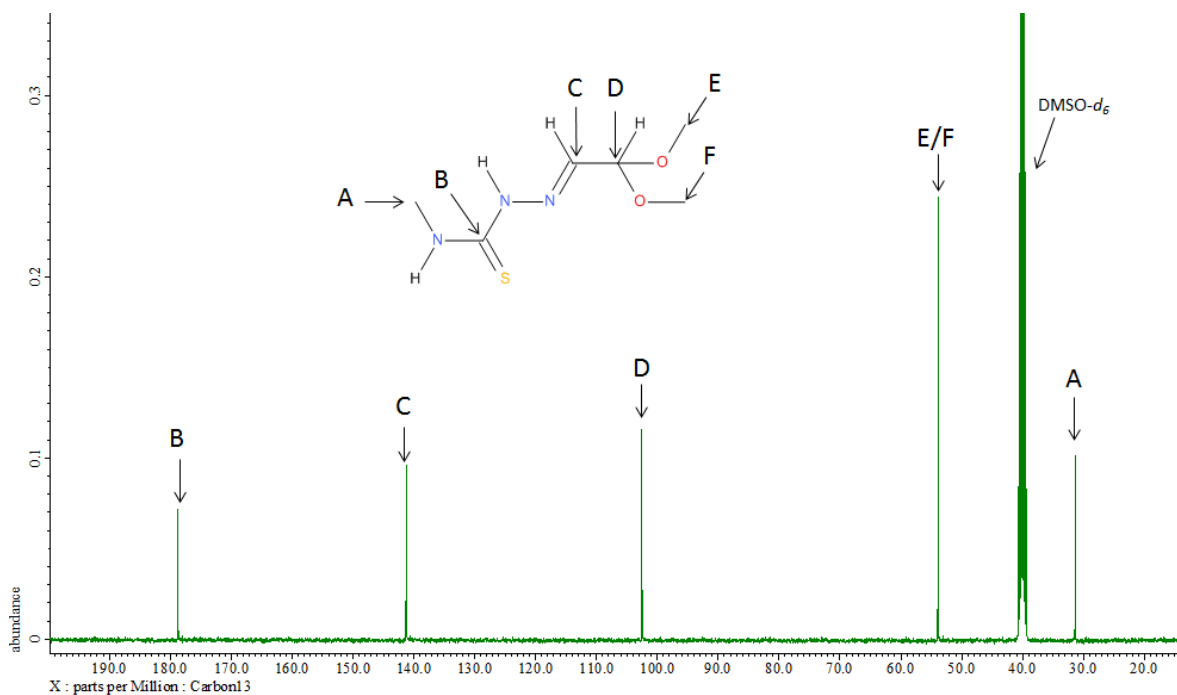


**Figure 2.7.7.3.** An assigned  $^{13}\text{C}$  NMR spectrum of DMA-Me-(OMe)<sub>2</sub>.

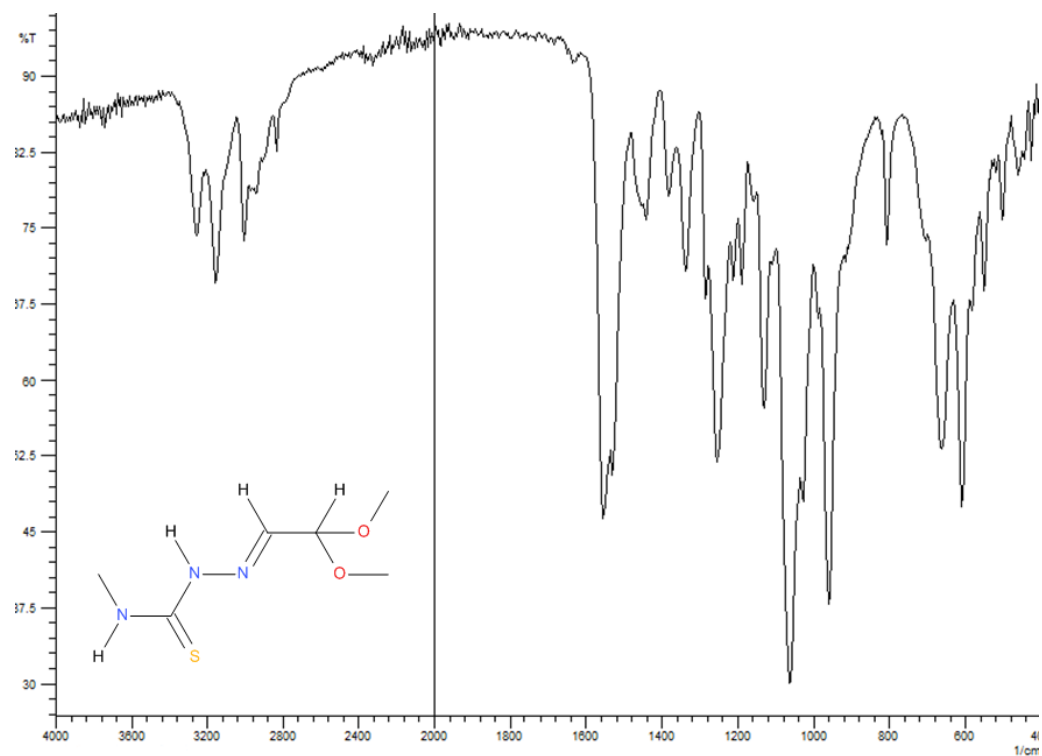


Figure 2.7.7.4. A FTIR spectrum of DMA-Me-(OMe)<sub>2</sub>.

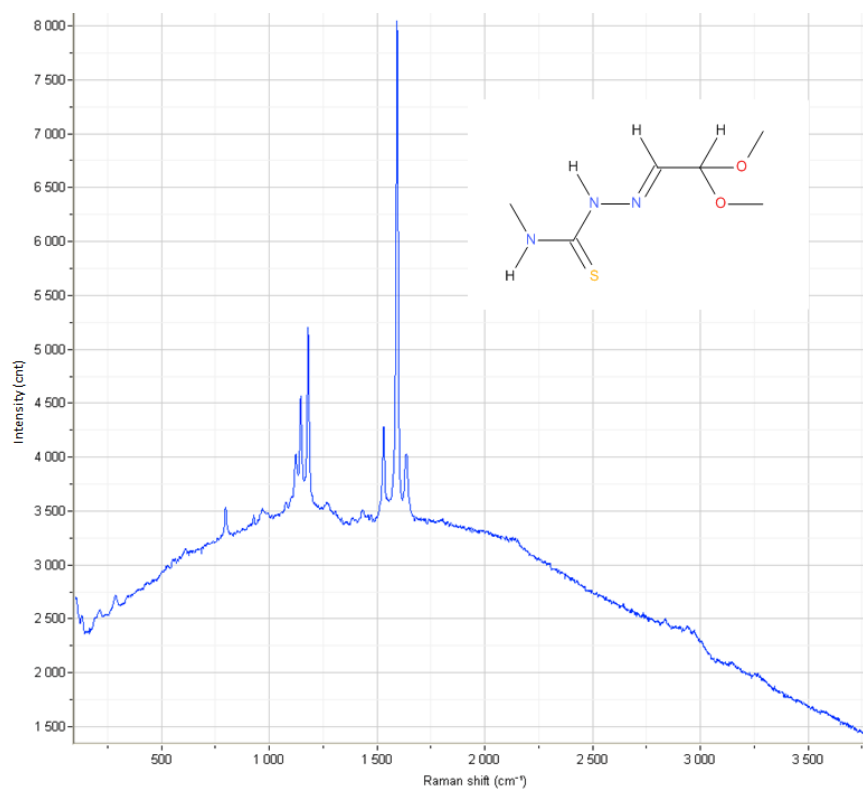


Figure 2.7.7.5. A Raman spectrum of DMA-Me-(OMe)<sub>2</sub>. Fluorescence is present.

### **2.7.8. Attempts by hydrolyse DMA-Me-(OMe)<sub>2</sub> to GLY-Me=O and attach a second arm in one step**

Taking what was learnt from hydrolysing the acetal group of PADA in the section about ligands with Me/H on the backbone, it was decided to try combining the de-protection step and attachment of the dissimilar 4-substituted-3-thiosemicarbazide together in one reaction.

**Method for the attempt of the synthesis of GLY-Me-(Me)<sub>2</sub>:**

4,4-dimethyl-3-thiosemicarbazide (0.215 g, 0.0018 mol) was dissolved in de-ionised water (25 mL). HCl (32%, 5 drops) was added followed by DMA-Me-(OMe)<sub>2</sub> (0.300g, 0.0016 mol). The stirring solution was gradually heated to 40 °C where the temperature was held with the mixture continuously stirring (40 °C, 10 minutes). The precipitate was recovered via filtration, washed with de-ionised water (50 mL) and dried in air. A pale yellow solid (0.240 g) was recovered.

**Result:**

A NMR spectrum of the product showed that the product contained roughly 7% DMA-Me-(OMe)<sub>2</sub>, 51% of GLY-Me-(Me)<sub>2</sub> and 44% of GLY-Me-Me. As it would be hard to isolate the GLY-Me-(Me)<sub>2</sub> from the mixture due to GLY-Me-Me being present, it was decided to try and alter the reaction conditions in order to encourage the purer synthesis of GLY-Me-(Me)<sub>2</sub>.

Instead of using HCl to hydrolyse the acetal groups it was decided to try using LiBF<sub>4</sub> which was used in the synthesis of dissymmetric ligands with Me/H on the back bone by J. Lim *et al.*<sup>79</sup> and L. Ackerman<sup>80, 81</sup> and co-workers.

**Method for the attempt of the synthesis of GLY-Me-(Me)<sub>2</sub> using LiBF<sub>4</sub>:**

4,4-dimethyl-3-thiosemicarbazide (0.215 g, 0.0018 mol) was dissolved in an acetonitrile solution (98% acetonitrile : 2% water, 15mL). DMA-Me-(OMe)<sub>2</sub> (0.300g, 0.0016 mol) was dissolved in an acetonitrile solution (98% acetonitrile : 2% water, 100mL, 60 °C) and a small amount of insoluble particulates were removed by filtration. The two solutions were combined, followed by the addition of LiBF<sub>4</sub> (0.337g, 0.0036 mol). The solution was left to stir (50 °C, 4 hours 50 minutes). The precipitate was recovered via filtration, washed with de-ionised water (50 mL) and dried in air. A pale yellow solid (0.126 g) was recovered.

**Result:**

A NMR spectrum of the product showed that the product contained almost 100% of GLY-Me-Me with little sign of DMA-Me-(OMe)<sub>2</sub> or GLY-Me-(Me)<sub>2</sub>.

The next attempt was to use the method which had already been used extensively to attach a dissimilar 4-substituted-3-thiosemicarbazide to a mono-substituted-3-thiosemicarbazone for the synthesis of all of the dissimilar ligands already reported in this chapter. It was hoped that the weaker acid used in this method would hydrolyse the acetal groups GLY-Me-(Me)<sub>2</sub> before catalysing the attachment of the second arm.

**Method for the attempt of the synthesis of GLY-Me-(Me)<sub>2</sub> using 10% HCl:**

DMA-Me-(OMe)<sub>2</sub> (0.300g, 0.0016 mol) was dissolved in DMF ( 1 mL) and filtered. 4,4-dimethyl-3-thiosemicarbazide (0.215 g, 0.0018 mol) was dissolved in DMF ( 2 mL, room temperature), HCl

(10%, 1 drop) was added and then the solution was filtered. The solutions were combined and left to stir (5 hours, room temperature). De-ionised water (6 mL) was added but only a tiny amount of precipitate formed (0.002 g). The filtrate was allowed to evaporate to dryness in air. An off white solid (0.282 g) was yielded.

**Result:**

When the precipitate was analysed by NMR spectroscopy the majority (77-78%) of the product was GLY-Me-Me with only 22-23% being DMA-Me-(OMe)<sub>2</sub>. There was no significant sign of the desired ligand, GLY-Me-(Me)<sub>2</sub>. The solid recovered from the filtrate gave very messy proton and carbon spectra, but evidence of GLY-Me-(Me)<sub>2</sub>, GLY-Me-Me and DMA-Me-(OMe)<sub>2</sub> could be distinguished within the spectra.

Due to the resulting failure of the combinational approach of the reactions 2 and 3 (Figure 2.7.7.1.), it was decided to attempt only hydrolysis of the acetal groups a single reaction, then attach the second arm in a separate reaction.

**Attempts by hydrolyse DMA-Me-(OMe)<sub>2</sub> to GLY-Me=O**

The first method was derived from the synthesis of symmetric ligands with Me/H on the backbone from PADA where a few drops of acid were used to hydrolyse the acetal groups.

**Method for the attempt of hydrolyse DMA-Me-(OMe)<sub>2</sub> to GLY-Me=O using 32% HCl:**

DMA-Me-(OMe)<sub>2</sub> (0.300g, 0.0016 mol) was dissolved in water (50 mL, 60 °C) and filtered. HCl (32%, 5 drops) was then added and then the solution was immediately cooled (0.3 °C). The precipitate that formed was recovered via filtration and left to dry in air. A brownish/yellow solid (0.016 g) was recovered.

**Result:**

NMR spectra of the solid showed roughly 78% of the solid was GLY-Me-Me with 17% being DMA-Me-(OMe)<sub>2</sub> and 4% being the desired ligand GLY-Me-(Me)<sub>2</sub>. The next step was to try exchanging the HCl for LiBF<sub>4</sub>.

**Method for the attempt of hydrolyse DMA-Me-(OMe)<sub>2</sub> to GLY-Me=O using LiBF<sub>4</sub>:**

DMA-Me-(OMe)<sub>2</sub> (0.300g, 0.0016 mol) was dissolved in an acetonitrile solution (98% acetonitrile : 2% water, 100 mL, 60 °C) and filtered. LiBF<sub>4</sub> (0.300 g, 0.0032 mol) was added and then the solution was immediately cooled in an ice bath (0.0 °C). When no precipitate was formed the solution was cooled further (-13.8 °C) with a salt ice bath (100 g table salt, 300 g ice). When still no precipitate formed, the solution was allowed to dry in air overnight followed by the further drying in an oven. A dark sludge like solid (0.330g) was recovered.



**Result:**

NMR of the solid showed roughly 83% of the solid was GLY-Me-Me with 6% being DMA-Me-(OMe)<sub>2</sub> and 11% being GLY-Me=O. There was no noticeable sign of GLY-Me-(Me)<sub>2</sub>. It seems that the intermediate is undergoing some sort of scrambling reaction, even in mild conditions. The decision was taken to non-longer pursue the synthesis of dissymmetric ligands with H/H on the backbone.

**2.7.9. Discussion**

A couple of different approaches have been tried in order to obtain a dissymmetric ligand with H/H on the backbone. The main problem encountered was the clean synthesis of a GLY-mono-substituted-thiosemicarbazone intermediate, which is an important pre-cursor for the formation of a pure dissymmetric ligand.

The first method that was explored, was the synthesis of the intermediate GLY-Me=O. This approach was investigated first due to first-hand success with making intermediates similar to this with different substituents on the backbone and reports in the literature<sup>92</sup> claiming that GLY-Me=O was successfully synthesised whilst using a very similar method. It seems that the unreacted aldehyde carbonyl group of the GLY-Me=O intermediate is too reactive and readily reacts with unreacted side arm, forming the undesired symmetric ligand GLY-Me-Me. As this occurs even in a huge excess of backbone it is reasonable to suggest that the unreacted aldehyde is significantly more reactive than either of the carbonyl groups of the glyoxal backbone. It was hoped that upon the cooling of the reaction mixture, a method that was used in the clean formation of other intermediates with different backbone, the reactivity of the carbonyl group on GLY-Me=O would be reduced enough so that the clean formation of GLY-Me=O would become more favourable. This method was met with only slight success, it was found that cooling the mixture did yield a product that contained a slightly elevated proportion of GLY-Me=O but the rest of the product was GLY-Me-Me by a vast majority. As the limit was met of how far the solution could be cooled by a salt/ice bath due to fears of the reaction mixture freezing, it was decided that further exploration of this method would unlikely enable the production of a clean GLY-Me=O product. It would be interesting to try the reaction in a solvent with a lower melting point in a dry ice/acetone ice bath, even though the suspicion would be that the GLY-Me=O content of the resulting product would be higher but, GLY-Me-Me would still make up the majority of the product. Disappointingly attempts to extract the GLY-Me=O from the GLY-Me=O/GLY-Me-Me product was not successful as it seems that even with the slight introduction of heat causes a product that gives unreadable NMR spectra.

The second approach investigated was the use of acetal groups to act as protecting groups in order to form a clean intermediate. To date the only reports that have been identified that have

used this approach was the in the papers by J. Lim *et al.*<sup>79</sup> and L. Ackerman *et al.*<sup>80, 81</sup> who used this approach for the synthesis of dissymmetric ligands with Me/H on the backbone. However no other evidence has been found to suggest that this method has been used in synthesis attempts of dissymmetric ligands with different substituents on the backbone. This coupled with personal experience with applying this method to the synthesis of Me/Me dissymmetric ligands (see section 2.2), did not give much hope for success at the onset. Surprisingly, the synthesis of the acetal protected intermediate was relatively straight forward, of which DMA-Me-(OMe)<sub>2</sub> was cleanly synthesised. It is believed that this is the first reports of this intermediate. The main problems arose during the attempts to de-protect and attach a second arm. It was found that it was hard to selectively de-protect the acetal-protected-intermediate without producing the undesired symmetric ligand. This result occurred even when LiBF<sub>4</sub> was used to give milder hydrolysis conditions. The successful use of the Lewis acid, LiBF<sub>4</sub>, was reported by both J. Lim *et al.*<sup>79</sup> and L. Ackerman *et al.*<sup>80, 81</sup> in the late 1990's. The reasoning behind this was that the use of a Lewis acid, instead of a harsher Brønsted acid, may help avoid scrambling reactions.

Unfortunately the use of LiBF<sub>4</sub> in the de-protection of the H/H intermediate did not help prevent the formation of GLY-Me-Me as the major product. The use of HCl and LiBF<sub>4</sub> was tried but in both cases yield mixtures that contained the acetal-protected-intermediate, the symmetric ligand GLY-Me-Me and a small proportion of the desired de-protected intermediate. As the only source of the methyl-substituted arm is in the intermediates DMA-Me-(OMe)<sub>2</sub> and GLY-Me=O, in order for GLY-Me-Me to be formed there must be some hydrolytic cleavage of the imine carbon-nitrogen double bond (C=N) within the intermediate. This allows the theory to be postulated, that the de-protected intermediate is unstable and that it is likely that very shortly after the de-protection of the acetal protected intermediate occurs, the hydrolysis of the C=N bond ensues, which gives rise to free methyl substituted side arm, yielding the undesired symmetric ligand.

Due to these failed attempts and lack of any feasible avenues to explore it was decided that the pursuit of dissymmetric H/H ligands should be abandoned for the time being. As always, if results from the biological screening identify dissymmetric H/H ligands as being ligands of significant interest, it may be necessary to re-visit the synthesis of this class of dissymmetric ligands. If it is found obligatory to revisit this synthesis, the main area that need to be address is finding a way to stabilise the de-protected intermediate or devising another synthesis approach by using an alternate disconnection.

## **2.8. Conclusion**

In this chapter 30 bis(thiosemicarbazone) ligands have been successfully synthesised of which 13 are believed to be novel. 13 of the ligands made are symmetric and 17 dissymmetric. Out of the dissymmetric ligands 2 are singly dissymmetric and 15 were doubly dissymmetric. It is believed that 5 of the intermediates used in the synthesis of the dissymmetric ligands have not been reported before. In the investigation of protection synthetic approach, 2 new protected intermediates are believed to be made.

Generally the synthesis of symmetric bis(thiosemicarbazone) ligands are reasonably straight forward and ligands of high purity with good yields can be obtained. Dissymmetric bis(thiosemicarbazone) ligands can be synthesised by using different synthetic approaches, either by exploitation of the carbonyl reactivity<sup>57, 73</sup> or by using acetal protection.<sup>79-81</sup> The method that was found to be the most successful was the method that exploited the reactivity of two the carbonyl groups. Despite the use of the exploitation of carbonyl reactivity method being prosperous, the synthesis of the dissymmetric ligands with different imine backbones and/or 4-substituted-thiosemicarbazides still hold uniquely different synthetic challenges. These challenges can involve the presence of isomeric impurities, formation of cyclic by-products as well as propensity for the thiosemicarbazide side arms to undergo scrambling. These challenges coupled with inherent difficulties common to bis(thiosemicarbazone) ligands such as poor solubility in a range of common solvents still make synthesis of any dissymmetric bis(thiosemicarbazone) ligands a major undertaking.

### 3. Synthesis of copper and zinc bis(thiosemicarbazone) complexes.

#### 3.1. Introduction

Once the bis(thiosemicarbazone) ligands had been successfully synthesised the next step was to chelate copper to the ligand in order to form a complex. As shown in Chapter 1, there is a rich source of methods describing how to make these complexes in the literature for medical imaging, the purpose of this chapter is not to investigate improving the synthesis of complexes. The primary focus of this chapter was synthesising new complexes from the ligands which are believed to be novel, in a high purity, in order to report the characterisation data for these complexes. As a practical method for gathering characterisation data, the complexes will be made with a stable metal and not a radio-isotope. An initial investigation in improving the radio complex synthesis methods has also been under taken and this is reported in Chapter 4 of this thesis.

Alongside the synthesis of copper bis(thiosemicarbazone) complexes it was decided to also synthesise zinc bis(thiosemicarbazone) complexes. The reason for this is that zinc complexes have been of interest in an alternative method for synthesising copper bis(thiosemicarbazone) complexes, where the zinc bis(thiosemicarbazone) complexes acts as the precursors. This shall be discussed in more detail in Chapter 4. Zinc bis(thiosemicarbazone) complexes have received far less attention than copper bis(thiosemicarbazone) complexes so it is believed that the vast majority of the zinc bis(thiosemicarbazone) complexes synthesised will be novel and thus their characterisation data has not yet been reported.

#### 3.2. Copper bis(thiosemicarbazone) complexes

##### 3.2.1. Reaction overview

As the bis(thiosemicarbazone) ligand becomes de-protonated upon complexation the starting bis(thiosemicarbazone) can be regarded as a pro-ligand. The de-protonation un-covers the true ligand which upon encountering a suitable metal, in this case a copper (II) salt, can chelate with the two sulphur atoms and the lone pairs from both the imine nitrogen atoms to yield a square planar, tetra dentate complex (Figure 3.2.1.1.)

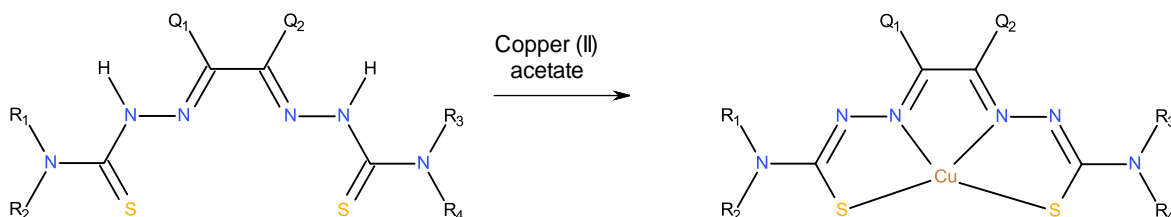


**Figure 3.2.1.1.** The general reaction for the synthesis of copper bis(thiosemicarbazone) complexes.

### **3.2.2. Synthesis of copper bis(thiosemicarbazone) complexes**

#### **Method selection:**

Most of the literature that has been used in the synthesis of dissymmetric ligands only seems to report methods for preparing very small quantities of radio-complexes in solution for biological screening. As the intention was to collect comprehensive characterisation data a method had to be used that could give a workable amount of solid product. Some methods have been published that gave workable amounts of product, however most of these required refluxing in methanol<sup>57</sup>/ethanol<sup>80</sup> or stirring in methanol at room temperature.<sup>85</sup> As this project produced a varied range of compounds it was desirable to use a method that used DMF or DMSO as the reaction solvent as these solvents were the only two solvents used in this project that can achieve full dissolution of all the ligands that have been synthesised. To this end, a method was tried from a dissertation report written by Katherine Martin<sup>211</sup> who was a third year BSc student alongside a further refined method. A method used by Samuel Stringer<sup>212</sup> in another third year BSc dissertation was also tested.

#### **K. Martin's method:**

BDO-Me-Me (0.312 g, 0.0012 mol) was added to a NaOH solution (1M, 25 mL, 50 °C), the minimum amount of DMF was added in order to achieve full dissolution. Copper (II) acetate monohydrate (0.280 g, 0.0014 mol) was dissolved in de-ionised water (10 mL). The solutions were combined and left to stir over night (whilst cooling down to room temperature). The precipitate was recovered via filtration, washed with methanol (3 x 25 mL) and de-ionised water (1 x 20 mL). The solid was dried in air. A brown solid (0.278 g) was recovered (72% yield).

#### **S. Stringer's method:**

BDO-Me-Me (0.312 g, 0.0012 mol) was added to a NaOH solution (1M, 25 mL). Copper (II) acetate monohydrate (0.280 g, 0.0014 mol) was dissolved in de-ionised water (15 mL). The copper solution was added to the suspension and left to stir over night. The solid was recovered via filtration, washed with de-ionised water (2 x 50 mL) and ethanol (1 x 50 mL). The solid was dried in air. A brown solid (0.357 g) was recovered (92% yield).

#### **Refined method:**

BDO-Me-Me (0.312 g, 0.0012 mol) was dissolved in DMF (14 mL). Copper (II) acetate monohydrate (0.280 g, 0.0014 mol) was dissolved in de-ionised water (15 mL). The two solutions were combined and further DMF (25 mL) was added to achieve full dissolution. The solution was left to stir over night. The precipitate was recovered via filtration, washed with de-ionised water

(2 x 50 mL) and ethanol (1 x 50 mL). The solid was dried in air. A brown solid (0.101 g) was recovered (26% yield).

### **Discussion**

All three methods gave a brown solid, unfortunately due to the paramagnetic properties of copper the solid could not be analysed by NMR spectroscopy in order to give an indication of purity. The S. Stringer method was discounted as being a suitable general method that could be applied to the synthesis of the remaining copper complexes because as the BDO-Me-Me did not fully dissolve in the NaOH yielding a suspension. As there was a chance that all the BDO-Me-Me ligand may not dissolved whilst being stirred overnight and therefore the ligand may not had a chance to react with the copper to form the desired complex, the product may not be as pure as it could be. The CHN data reported was significantly lower than the theoretical percentages (- 2.6%, 2.6%, 0.4% for the percentage of carbon, nitrogen and hydrogen respectively) which suggest that the product was not cleanly synthesised. The refined method was also discarded because the yield was significantly lower than the K. Martin method. The K. Martin method was selected to be used as the general method for the remaining of the copper complexes because the starting reaction mixture was a solution and not a suspension so that it can be assumed that if a precipitate forms then it should be the desired copper complex whilst any unreacted ligand should stay in solution. The amount of DMF can be changed in order to account for any differences in the remaining ligands solubility in NaOH. K. Martin's dissertation reports that her CHN analysis results agreed very closely with her theoretical percentages (within +/- 0.3%, 0.3%, 0.1% for the percentage of carbon, nitrogen and hydrogen respectively), this gives some assurance that K. Martin's method has the ability to produce pure copper complexes.

### **General methods:**

Depending on the amount of the ligand that was available the general methods used was:

#### **General method A:**

The chosen bis(thiosemicarbazone) ligand ( X g, 0.0006 mol) was added to a NaOH solution (1M, 13 mL, 50 °C), the minimum amount of DMF was added in order to achieve full dissolution. Copper (II) acetate monohydrate (0.140 g, 0.0007 mol) was dissolved in de-ionised water (5 mL). The solutions were combined and left to stir over night (whilst cooling down to room temperature). The precipitate was recovered via filtration, washed with methanol (3 x 10 mL) and de-ionised water (1 x 10 mL) .The product was dried in air.

**General method B:**

The chosen bis(thiosemicarbazone) ligand ( X g, 0.0004 mol) was added to a NaOH solution (1M, 9 mL, 50 °C), the minimum amount of DMF was added in order to achieve full dissolution. Copper (II) acetate monohydrate (0.100 g, 0.0005 mol) was dissolved in de-ionised water (3.5 mL). The solutions were combined and left to stir over night (whilst cooling down to room temperature). The precipitate was recovered via filtration, washed with methanol (3 x 7 mL) and de-ionised water (1 x 7 mL) .The product was dried in air.

The method used for each complex is summarised in table 3.2.2.1., along with the reaction yield and appearance of the product.

Complex	General method used	Yield	Appearance of product	Believed to be novel	Comments
Cu-GLY-Et-Et	A	74 %	Brown solid	No <sup>76, 141, 177, 180</sup>	
Cu-GLY-Ph-Ph	A	69%	Brown solid	No <sup>76, 141, 177, 180</sup>	
Cu-PADA-Me-Me	A	65%	Brown solid	No <sup>6, 45, 69, 77, 106, 123, 145, 146, 164</sup>	
Cu-PADA-Me-Ph	B	61%	Brown solid	Yes	
Cu-PADA-Et-Et	A	10%	Black solid	No <sup>69, 77, 145, 164</sup>	Unsure if desired complex was obtained
Cu-PADA-Et-(Me) <sub>2</sub>	B	63%	Brown solid	Yes	DMSO/H <sub>2</sub> O Recrystallisation
Cu-PADA-Ph-NH <sub>2</sub>	B	69%	Brown solid	Yes	DMSO/H <sub>2</sub> O Recrystallisation
Cu-PADA-Ph-Me	B	61%	Brown solid	Yes	DMSO/H <sub>2</sub> O Recrystallisation
Cu-BDO-NH <sub>2</sub> -NH <sub>2</sub>	A	46%	Brown solid	No <sup>69, 77, 123, 145, 164</sup>	
Cu-BDO-NH <sub>2</sub> -(Me) <sub>2</sub>	B	53%	Brown solid	Yes	

Cu-BDO-Me-Me	K. Martin's method	72%	Brown solid	No <sup>6, 69, 70, 76, 77, 123, 141, 145, 146, 164, 172, 177</sup>	DMSO/H <sub>2</sub> O Recrystallisation
Cu-BDO-Me-NH <sub>2</sub>	B	59%	Brown solid	Yes	
Cu-PDO-NH <sub>2</sub> -NH <sub>2</sub>	A	58%	Brown solid	No <sup>69, 77, 145, 164</sup>	
Cu-PDO-NH <sub>2</sub> -Me	B	15%	Brown solid	Yes	
Cu-PDO-NH <sub>2</sub> -(Me) <sub>2</sub>	A	43%	Brown solid	Yes	DMSO/H <sub>2</sub> O Recrystallisation
Cu-PDO-NH <sub>2</sub> -Et	A	43%	Brown solid	Yes	DMSO/H <sub>2</sub> O Recrystallisation
Cu-PDO-Me-Me	A	16%	Black solid	No <sup>69, 77, 145, 164</sup>	Unsure if desired complex was obtained
Cu-PDO-Me-NH <sub>2</sub>	A	54%	Brown solid	Yes	DMSO/H <sub>2</sub> O Recrystallisation
Cu-PDO-Et-Et	A	49%	Brown solid	Yes	
Cu-PDO-Et-NH <sub>2</sub>	A	34%	Brown solid	Yes	DMSO/H <sub>2</sub> O Recrystallisation

**Table 3.2.2.1.** A table summarising which general method was used for the synthesis of each complex.

### **3.2.3. Characterisation data for copper bis(thiosemicarbazone) complexes**

#### **Copper bis(thiosemicarbazone) complexes with H/H on the backbone**

##### **Cu-GLY-Et-Et:**

**IR (neat):** cm<sup>-1</sup>= 3325 (m), 2970 (w), 2926 (w), 2878 (w), 1516 (s), 1435 (s), 1416 (s), 1385 (m), 1371 (m), 1339 (s), 1290 (m), 1234 (s), 1200 (s), 119 (m), 1092 (m), 1055 (m), 1012 (m), 926 (w), 860 (m), 824 (w), 760 (w), 685 (m), 602 (m), 509 (s), 455 (m), 419 (m). **Raman (neat), laser = 623.81 nm:** cm<sup>-1</sup>= 1579 (w), 1537 (s), 1443 (s), 1342 (w), 1298 (w), 1221 (w), 1053 (w), 1018 (s), 684 (w), 605 (m), 499 (w). **Melting point:** >220 °C (decomposed). **UV-Vis absorptions:** λ<sub>max</sub>/nm (DMSO) 320 (ε/dm<sup>3</sup> mol<sup>-1</sup> cm<sup>-1</sup> 20 000), 370 (sh), 498 (9 200) and 540 (sh). **Mass spectrometry (ESI):** m/z (Calc.) 322.0096 (322.0096) {M + H<sup>+</sup>}.



### Cu-GLY-Ph-Ph:

**IR (neat):**  $\text{cm}^{-1}$  = 3416 (w), 3325 (w), 3051 (w), 1597 (w), 1541 (m), 1520 (m), 1493 (m), 1452 (m), 1420 (s), 1315 (m), 1244 (m), 1175 (s), 1153 (m), 899 (w), 870 (m), 826 (w), 745 (s), 687 (s), 610 (m), 583 (m), 542 (m), 501 (m). **Raman (neat), laser = 623.81 nm:**  $\text{cm}^{-1}$  = 3055 (w), 3043 (w), 2973 (w), 2949 (w), 2896 (w), 2869 (w), 2850 (w), 2534 (w), 2454 (w), 2161 (w), 2134 (w), 2035 (w), 1953 (w), 1932 (w), 1594 (w), 1526 (s), 1447 (s), 1420 (s), 1310 (w), 1249 (w), 1174 (w), 1075 (w), 1007 (m), 921 (w), 897 (w), 819 (w), 630 (w), 606 (w), 506 (w), 387 (w), 288 (w). **UV-Vis absorptions:**  $\lambda_{\text{max}}/\text{nm}$  (DMSO) 322 ( $\epsilon/\text{dm}^3 \text{mol}^{-1} \text{cm}^{-1}$  17 900), 406 (16 100), 508 (14 000) and 560 (sh).

### Copper bis(thiosemicarbazone) complexes with Me/H on the backbone

#### Cu-PADA-Me-Me

**IR (neat):**  $\text{cm}^{-1}$  = 3325 (m), 3269 (m), 3256 (m), 1531 (s), 1449 (m), 1400 (m), 1381 (s), 1348 (m), 1238 (m), 1225 (m), 1179 (m), 1123 (m), 924 (m), 872 (w), 808 (w), 773 (w), 664 (w), 592 (w), 474 (s), 433 (s), 428 (s). **Raman (neat), laser = 532.00 nm:**  $\text{cm}^{-1}$  = 2979 (w), 2918 (w), 2703 (w), 2122 (w), 2057 (w), 1550 (w), 1512 (w), 1471 (s), 1370 (w), 1246 (w), 1178 (w), 996 (w), 924 (w), 776 (w), 662 (w), 591 (w). **UV-Vis absorptions:**  $\lambda_{\text{max}}/\text{nm}$  (DMSO) 316 ( $\epsilon/\text{dm}^3 \text{mol}^{-1} \text{cm}^{-1}$  19 400), 360 (sh), 488 (7 000) and 540 (sh).

#### Cu-PADA-Me-Ph

**IR (neat):**  $\text{cm}^{-1}$  = 3294 (m), 1597 (w), 1547 (m), 1524 (s), 1497 (m), 1458 (s), 1435 (s), 1391 (s), 1368 (m), 1344 (m), 1317 (m), 1248 (m), 1219 (s), 1194 (s), 1179 (s), 1134 (m), 1123 (m), 926 (m), 897 (w), 881 (w), 808 (w), 758 (s), 687 (s), 664 (m), 631 (m), 610 (m), 586 (m), 507 (m), 446 (m), 419 (m). **Raman (neat), laser = 623.81 nm:**  $\text{cm}^{-1}$  = 1595 (w), 1540 (s), 1519 (m), 1466 (s), 1425 (w), 1348 (w), 1311 (w), 1242 (w), 1218 (m), 1131 (w), 993 (w), 922 (w), 820 (w), 664 (w), 590 (m), 485 (w), 358 (w). **Elemental analysis:** Found: **C**, 38.9; **H**, 3.7; **N**, 22.6. Calc. for  $\text{Cu}_1\text{C}_{12}\text{H}_{14}\text{N}_6\text{S}_2$ : **C**, 39.0; **H**, 3.8; **N**, 22.7%. **Melting point:** >220 °C (decomposed). **UV-Vis absorptions:**  $\lambda_{\text{max}}/\text{nm}$  (DMSO) 320 ( $\epsilon/\text{dm}^3 \text{mol}^{-1} \text{cm}^{-1}$  18 900), 378 (13 100), 496 (9 700) and 540 (sh). **Mass spectrometry (ESI):**  $m/z$  (Calc.) 370.0092 (370.0096) {M + H<sup>+</sup>}.

#### Cu-PADA-Et-(Me)<sub>2</sub>

**IR (neat):**  $\text{cm}^{-1}$  = 3321 (m), 2965 (w), 2926 (w), 1514 (s), 1483 (m), 1462 (s), 1391 (m), 1366 (s), 1339 (s), 1310 (s), 1258 (m), 1234 (s), 1179 (s), 1138 (s), 1059 (m), 1013 (m), 916 (m), 862 (m), 826 (m), 800 (m), 658 (m), 594 (m), 525 (s), 474 (s). **Raman (neat), laser = 632.81 nm:**  $\text{cm}^{-1}$  = 1589 (w), 1538 (m), 1482 (s), 1460 (m), 1373 (w), 1312 (m), 1225 (m), 1008 (m), 931 (m), 661 (w), 632 (w),

596 (m), 351 (w). **Elemental analysis:** Found: **C**, 32.3; **H**, 4.7; **N**, 25.2. Calc. for  $\text{Cu}_1\text{C}_9\text{H}_{16}\text{N}_6\text{S}_2$ : **C**, 32.2; **H**, 4.8; **N**, 25.0%. **UV-Vis absorptions:**  $\lambda_{\text{max}}/\text{nm}$  (DMSO) 320 ( $\epsilon/\text{dm}^3 \text{ mol}^{-1} \text{ cm}^{-1}$  21 500), 360 (sh), 492 (9 500) and 540 (sh). **Mass spectrometry (ESI):**  $m/z$  (Calc.) 336.0255 (336.0252)  $\{\text{M} + \text{H}^+\}$ .

#### Cu-PADA-Ph-NH<sub>2</sub>

**IR (neat):**  $\text{cm}^{-1}$  = 3289 (m), 3073 (m), 1632 (w), 1591 (m), 1541 (m), 1497 (s), 1408 (s), 1368 (s), 1319 (s), 1256 (m), 1244 (m), 1184 (s), 1150 (s), 928 (m), 891 (m), 864 (m), 847 (m), 820 (m), 750 (s), 735 (m), 685 (s), 640 (m), 617 (m), 600 (m), 584 (s), 505 (s), 463 (s). **Raman (neat), laser = 623.81 nm:**  $\text{cm}^{-1}$  = 1528 (s), 1470 (s), 1431 (m), 1314 (w), 1237 (m), 1185 (w), 996 (w), 929 (w), 670 (w), 618 (w), 599 (w), 359 (w), 300 (w). **Elemental analysis:** Found: **C**, 37.2; **H**, 3.3; **N**, 23.4. Calc. for  $\text{Cu}_1\text{C}_{11}\text{H}_{12}\text{N}_6\text{S}_2$ : **C**, 37.1; **H**, 3.4; **N**, 23.6%. **UV-Vis absorptions:**  $\lambda_{\text{max}}/\text{nm}$  (DMSO) 314 ( $\epsilon/\text{dm}^3 \text{ mol}^{-1} \text{ cm}^{-1}$  21 000), 372 (13 300), 494 (9 600) and 540 (sh). **Mass spectrometry (ESI):**  $m/z$  (Calc.) 355.9935 (355.9939)  $\{\text{M} + \text{H}^+\}$ .

#### Cu-PADA-Ph-Me

**IR (neat):**  $\text{cm}^{-1}$  = 3279 (w), 3213 (w), 2932 (w), 1597 (m), 1582 (w), 1545 (m), 1493 (s), 1433 (s), 1346 (s), 1321 (s), 1279 (s), 1244 (m), 1196 (s), 1148 (s), 1043 (m), 934 (m), 891 (w), 847 (m), 822 (m), 745 (s), 685 (s), 610 (m), 584 (m), 503 (s), 484 (m). **Raman (neat), laser = 623.81 nm:**  $\text{cm}^{-1}$  = 1576 (m), 1507 (s), 1470 (s), 1429 (m), 1383 (w), 1351 (w), 1312 (w), 1273 (m), 1243 (m), 1192 (w), 994 (w), 932 (m), 676 (w), 600 (m), 542 (w), 479 (w), 368 (w), 130 (w). **Elemental analysis:** Found: **C**, 38.9; **H**, 3.7; **N**, 22.6. Calc. for  $\text{Cu}_1\text{C}_{12}\text{H}_{14}\text{N}_6\text{S}_2$ : **C**, 39.0; **H**, 3.8; **N**, 22.7%. **UV-Vis absorptions:**  $\lambda_{\text{max}}/\text{nm}$  (DMSO) 318 ( $\epsilon/\text{dm}^3 \text{ mol}^{-1} \text{ cm}^{-1}$  20 600), 380 (sh), 492 (10 100) and 540 (sh). **Mass spectrometry (ESI):**  $m/z$  (Calc.) 370.0092 (370.0096)  $\{\text{M} + \text{H}^+\}$ .

#### Copper bis(thiosemicarbazone) complexes with Me/Me on the backbone

##### Cu-BDO-NH<sub>2</sub>-NH<sub>2</sub>

**IR (neat):**  $\text{cm}^{-1}$  = 3402 (w), 3285 (m), 3144 (m), 1628 (m), 1593 (m), 1541 (w), 1479 (m), 1421 (s), 1360 (m), 1304 (m), 1217 (s), 1186 (m), 1138 (m), 1078 (m), 995 (m), 835 (m), 716 (m), 658 (m), 602 (m), 515 (m), 473 (s), 457 (s). **Raman (neat), laser = 623.81 nm:**  $\text{cm}^{-1}$  = 1533 (s), 1470 (m), 1367 (w), 1290 (s), 1182 (m), 1003 (w), 829 (m), 705 (w), 606 (w), 394 (w), 340 (w). **UV-Vis absorptions:**  $\lambda_{\text{max}}/\text{nm}$  (DMSO) 310 ( $\epsilon/\text{dm}^3 \text{ mol}^{-1} \text{ cm}^{-1}$  23 400), 350 (sh), 476 (6 400) and 530 (sh).

##### Cu-BDO-NH<sub>2</sub>-(Me)<sub>2</sub>

**IR (neat):**  $\text{cm}^{-1}$  = 3426 (w), 3289 (w), 3157 (w), 2918 (w), 1622 (m), 1589 (w), 1541 (m), 1499 (m), 1439 (m), 1387 (s), 1362 (s), 1296 (s), 1258 (s), 1217 (s), 1171 (s), 1140 (m), 1115 (s), 1055 (s), 999 (m), 908 (s), 841 (s), 762 (m), 706 (m), 610 (m), 596 (m), 515 (m), 430 (s). **Raman (neat), laser =**

**532.00 nm:**  $\text{cm}^{-1}$  = 2837 (w), 2807 (w), 2144 (w), 1901 (w), 1804 (w), 1598 (w), 1543 (m), 1497 (m), 1298 (s), 1263 (w), 1204 (w), 1003 (w), 921 (w), 846 (w), 602 (w). **Elemental analysis:** Found: **C**, 29.7; **H**, 4.2; **N**, 25.9. Calc. for  $\text{Cu}_1\text{C}_8\text{H}_{14}\text{N}_6\text{S}_2$ : **C**, 29.85; **H**, 4.4; **N**, 26.1%. **UV-Vis absorptions:**  $\lambda_{\text{max}}/\text{nm}$  (DMSO) 313 ( $\epsilon/\text{dm}^3 \text{mol}^{-1} \text{cm}^{-1}$  17 900), 350 (sh), 481 (6 700) and 540 (sh). **Mass spectrometry (ESI):**  $m/z$  (Calc.) 322.0097 (322.0096) {M + H<sup>+</sup>}.

#### Cu-BDO-Me-Me

**IR (neat):**  $\text{cm}^{-1}$  = 3327 (m), 3267 (w), 1530 (s), 1460 (m), 1385 (s), 1246 (m), 1223 (s), 1159 (m), 1078 (m), 841 (m), 606 (m), 540 (m), 507 (s), 456 (s), 438 (s). **Raman (neat), laser = 632.81 nm:**  $\text{cm}^{-1}$  = 3331 (w), 1602 (w), 1552 (s), 1488 (s), 1388 (w), 1371 (w), 1325 (m), 1264 (m), 1242 (m), 1185 (w), 994 (w), 841 (m), 773 (w), 600 (m), 452 (w), 437 (w), 352 (m), 325 (w), 292 (w), 184 (w). **Raman (neat), laser = 532.00 nm:**  $\text{cm}^{-1}$  = 2158 (w), 2097 (w), 1930 (w), 1556 (s), 1492 (s), 1444 (w), 1372 (w), 1328 (m), 1266 (w), 1245 (m), 996 (w), 843 (w), 773 (w), 603 (m), 451 (w), 441 (w). **Melting point:** >270 °C (decomposed). **UV-Vis absorptions:**  $\lambda_{\text{max}}/\text{nm}$  (DMSO) 314 ( $\epsilon/\text{dm}^3 \text{mol}^{-1} \text{cm}^{-1}$  22 100), 350 (sh), 476 (7 200) and 530 (sh).

#### Cu-BDO-Me-NH<sub>2</sub>

**IR (neat):**  $\text{cm}^{-1}$  = 3458 (w), 3321 (m), 3287 (w), 3136 (w), 1626 (m), 1549 (m), 1504 (m), 1443 (s), 1396 (m), 1364 (m), 1344 (s), 1287 (s), 1221 (s), 1188 (m), 1150 (m), 1099 (m), 1057 (m), 1038 (m), 984 (m), 841 (m), 756 (w), 733 (m), 700 (m), 629 (m), 610 (m), 563 (m), 527 (m), 509 (s), 419 (s). **Raman (neat), laser = 632.81 nm:**  $\text{cm}^{-1}$  = 1542 (m), 1496 (s), 1379 (w), 1284 (s), 1184 (w), 998 (w), 837 (w), 697 (w), 609 (w), 588 (w), 390 (w), 346 (w), 316 (w), 271 (w), 253 (w), 138 (w). **Melting point:** >266 °C (decomposed). **UV-Vis absorptions:**  $\lambda_{\text{max}}/\text{nm}$  (DMSO) 314 ( $\epsilon/\text{dm}^3 \text{mol}^{-1} \text{cm}^{-1}$  22 500), 350 (sh), 476 (6 900) and 520 (sh). **Mass spectrometry (ESI):**  $m/z$  (Calc.) 307.9935 (307.9939) {M + H<sup>+</sup>}.

#### Copper bis(thiosemicarbazone) complexes with Me/Et on the backbone

##### Cu-PDO-NH<sub>2</sub>-NH<sub>2</sub>

**IR (neat):**  $\text{cm}^{-1}$  = 3447 (w), 3377 (w), 3273 (w), 3102 (w), 1630 (m), 1618 (m), 1589 (m), 1533 (w), 1477 (m), 1423 (s), 1327 (m), 1294 (m), 1236 (w), 1211 (m), 1181 (m), 1138 (m), 1059 (w), 1022 (w), 943 (w), 841 (w), 789 (w), 716 (m), 594 (m), 527 (m), 486 (m), 420 (s). **Raman (neat), laser = 632.81 nm:**  $\text{cm}^{-1}$  = 1588 (w), 1529 (s), 1467 (m), 1374 (w), 1325 (w), 1289 (m), 1237 (w), 1182 (w), 1079 (w), 1024 (w), 1000 (w), 946 (w), 841 (w), 788 (w), 705 (w), 600 (w), 393 (w), 338 (w), 260 (w), 174 (m). **UV-Vis absorptions:**  $\lambda_{\text{max}}/\text{nm}$  (DMSO) 312 ( $\epsilon/\text{dm}^3 \text{mol}^{-1} \text{cm}^{-1}$  23 500), 350 (sh), 480 (6 700) and 530 (sh).

### Cu-PDO-NH<sub>2</sub>-Me

**IR (neat):** cm<sup>-1</sup>= 32292 (w), 3146 (w), 1626 (w), 1541 (m), 1518 (w), 1479 (m), 1445 (m), 1391 (m), 1335 (w), 1217 (m), 1190 (m), 1152 (m), 1107 (w), 1061 (w), 951 (w), 779 (w), 727 (w), 592 (m).

**Raman (neat), laser = 532.00 nm:** cm<sup>-1</sup>= 2127 (w), 2075 (w), 1537 (m), 1515 (m), 1480 (w), 1335 (m), 1249 (m), 1025 (w), 794 (w), 604 (m). **Elemental analysis:** Found: **C**, 29.7; **H**, 4.3; **N**, 26.0. Calc. for Cu<sub>1</sub>C<sub>8</sub>H<sub>14</sub>N<sub>6</sub>S<sub>2</sub>: **C**, 29.85; **H**, 4.4; **N**, 26.1%. **UV-Vis absorptions:** λ<sub>max</sub>/nm (DMSO) 312(ε/dm<sup>3</sup> mol<sup>-1</sup> cm<sup>-1</sup> 11 300), 350 (sh), 480 (4 100) and 530 (sh). **Mass spectrometry (ESI):** *m/z* (Calc.) 322.0135 (322.0096) {M + H<sup>+</sup>}.

### Cu-PDO-NH<sub>2</sub>-(Me)<sub>2</sub>

**IR (neat):** cm<sup>-1</sup>= 3360 (w), 3285 (w), 3129 (w), 3129 (w), 2931 (w), 1632 (m), 1585 (w), 1537 (m), 1493 (m), 1456 (s), 1389 (s), 1321 (m), 1300 (s), 1258 (s), 1240 (s), 1213 (s), 1169 (s), 1115 (s), 1061 (m), 957 (m), 910 (m), 847 (w), 795 (m), 706 (m), 631 (m), 598 (m), 536 (s), 517 (s), 496 (s), 428 (s). **Raman (neat), laser = 532.00 nm:** cm<sup>-1</sup>= 1590 (w), 1536 (w), 1497 (w), 1320 (w), 1302 (w), 1247 (w), 633 (w), 598 (w). **Melting point:** >220 °C (decomposed). **Elemental analysis:** Found: **C**, 32.4; **H**, 4.8; **N**, 24.9. Calc. for Cu<sub>1</sub>C<sub>9</sub>H<sub>16</sub>N<sub>6</sub>S<sub>2</sub>: **C**, 32.2; **H**, 4.8; **N**, 25.0%. **UV-Vis absorptions:** λ<sub>max</sub>/nm (DMSO) 314 (ε/dm<sup>3</sup> mol<sup>-1</sup> cm<sup>-1</sup> 23 400), 350 (sh), 484 (8 800) and 530 (sh). **Mass spectrometry (ESI):** *m/z* (Calc.) 336.0247 (336.00252) {M + H<sup>+</sup>}.

### Cu-PDO-NH<sub>2</sub>-Et

**IR (neat):** cm<sup>-1</sup>= 3347 (w), 3157 (w), 2963 (w), 1628 (w), 1587 (w), 1537 (m), 1506 (m), 1476 (m), 1445 (m), 1416 (s), 1366 (m), 1335 (m), 1310 (m), 1221 (s), 1184 (m), 1142 (m), 1061 (m), 955 (w), 787 (m), 689 (m), 597 (m), 419 (s). **Raman (neat), laser = 632.81 nm:** cm<sup>-1</sup>= 3329 (w), 1584 (w), 1533 (s), 1504 (m), 1479 (s), 1371 (m), 1352 (m), 1330 (m), 1248 (m), 1230 (m), 1172 (m), 1030 (w), 999 (w), 957 (w), 787 (w), 602 (m), 338 (m), 317 (w), 261 (w), 221 (w), 157 (m). **Melting point:** >210 °C (decomposed). **Elemental analysis:** Found: **C**, 32.3; **H**, 4.8; **N**, 24.85. Calc. for Cu<sub>1</sub>C<sub>9</sub>H<sub>16</sub>N<sub>6</sub>S<sub>2</sub>: **C**, 32.2; **H**, 4.8; **N**, 25.0%. **UV-Vis absorptions:** λ<sub>max</sub>/nm (DMSO) 314 (ε/dm<sup>3</sup> mol<sup>-1</sup> cm<sup>-1</sup> 25 500), 350 (sh), 480 (8 200) and 530 (sh). **Mass spectrometry (ESI):** *m/z* (Calc.) 336.0287 (336.0252) {M + H<sup>+</sup>}.

### Cu-PDO-Me-NH<sub>2</sub>

**IR (neat):** cm<sup>-1</sup>= 3281 (w), 3119 (w), 1643 (w), 1622 (w), 1541 (m), 1504 (m), 1441 (s), 1350 (m), 1281 (m), 1240 (m), 1215 (s), 1186 (s), 1150 (m), 1101 (m), 1076 (m), 1028 (m), 943 (m), 800 (m), 719 (m), 638 (m), 615 (m) 471 (s). **Raman (neat), laser = 632.81 nm:** cm<sup>-1</sup>= 1582 (w), 1532 (m), 1497 (s), 1433 (w), 1380 (w), 1321 (w), 1281 (m), 1238 (m), 1190 (w), 1031 (w), 987 (w), 943 (w), 848 (w), 801 (w), 702 (w), 610 (w), 395 (w), 351 (w), 320 (w), 139 (w). **Elemental analysis:** Found:

**C**, 29.8; **H**, 4.5; **N**, 26.0. Calc. for  $\text{Cu}_1\text{C}_8\text{H}_{14}\text{N}_6\text{S}_2$ : **C**, 29.85; **H**, 4.4; **N**, 26.1%. **UV-Vis absorptions**:  $\lambda_{\text{max}}/\text{nm}$  (DMSO) 314 ( $\epsilon/\text{dm}^3 \text{ mol}^{-1} \text{ cm}^{-1}$  16 600), 350 (sh), 478 (5 200) and 520 (sh). **Mass spectrometry (ESI)**:  $m/z$  (Calc.) 322.0092 (322.0096)  $\{\text{M} + \text{H}^+\}$ .

#### **Cu-PDO-Et-Et**

**IR (neat)**:  $\text{cm}^{-1}$  = 3323 (m), 2972 (w), 2928 (w), 2876 (w), 1543 (w), 1506 (m), 1481 (m), 1435 (s), 1381 (m), 1342 (m), 1265 (m), 1234 (m), 1211 (s), 1142 (m), 1096 (m), 1055 (m), 1034 (m), 959 (m), 843 (w), 802 (w), 596 (w), 550 (m), 515 (m), 471 (m), 413 (m). **Raman (neat), laser = 532.00 nm**:  $\text{cm}^{-1}$  = 2149 (w), 2091 (w), 1542 (s), 1484 (s), 1462 (m), 1376 (w), 1333 (m), 1234 (m), 1034 (w), 1002 (w), 959 (w), 605 (w). **Elemental analysis**: Found: **C**, 36.2; **H**, 5.4; **N**, 23.0. Calc. for  $\text{Cu}_1\text{C}_{11}\text{H}_{20}\text{N}_6\text{S}_2$ : **C**, 36.3; **H**, 5.5; **N**, 23.1%. **UV-Vis absorptions**:  $\lambda_{\text{max}}/\text{nm}$  (DMSO) 316 ( $\epsilon/\text{dm}^3 \text{ mol}^{-1} \text{ cm}^{-1}$  21 600), 360 (sh), 480 (7 200) and 530 (sh). **Mass spectrometry (ESI)**:  $m/z$  (Calc.) 364.0560 (364.0565)  $\{\text{M} + \text{H}^+\}$ .

#### **Cu-PDO-Et-NH<sub>2</sub>**

**IR (neat)**:  $\text{cm}^{-1}$  = 3374 (w), 3339 (m), 3152 (w), 2972 (w), 1630 (m), 1593 (w), 1539 (w), 1508 (m), 1479 (m), 1437 (s), 1381 (m), 1329 (m), 1304 (m), 1261 (w), 1236 (m), 1211 (s), 1173 (m), 1142 (m), 1103 (m), 1032 (m), 951 (m), 841 (w), 820 (w), 802 (w), 731 (m), 600 (m), 540 (m), 505 (s), 484 (s), 415 (s). **Raman (neat), laser = 632.81 nm**:  $\text{cm}^{-1}$  = 1591 (w), 1533 (s), 1482 (m), 1460 (m), 1374 (w), 1355 (w), 1324 (m), 1299 (m), 1228 (m), 1171 (w), 1033 (m), 951 (w), 840 (w), 778 (w), 602 (w), 336 (w), 265 (w), 165 (m). **Elemental analysis**: Found: **C**, 32.3; **H**, 4.8; **N**, 24.9. Calc. for  $\text{Cu}_1\text{C}_9\text{H}_{16}\text{N}_6\text{S}_2$ : **C**, 32.2; **H**, 4.8; **N**, 25.0%. **UV-Vis absorptions**:  $\lambda_{\text{max}}/\text{nm}$  (DMSO) 314 ( $\epsilon/\text{dm}^3 \text{ mol}^{-1} \text{ cm}^{-1}$  22 100), 350 (sh), 480 (7 100) and 530 (sh). **Mass spectrometry (ESI)**:  $m/z$  (Calc.) 336.0297 (336.0252)  $\{\text{M} + \text{H}^+\}$ .

#### **Unexpected results**

##### **Cu-PADA-Et-Et**

**IR (neat)**:  $\text{cm}^{-1}$  = 3271 (w), 2967 (w), 2872 (w), 1499 (m), 1422 (m), 1375 (m), 1337 (s), 1229 (s), 1157 (s), 1086 (s), 800 (m), 521 (s). **Raman (neat), laser = 532.00 nm**:  $\text{cm}^{-1}$  = 1483 (s), 1235 (m). **UV-Vis absorptions**:  $\lambda_{\text{max}}/\text{nm}$  (DMSO) 306, 450.

##### **Cu-PDO-Me-Me**

**IR (neat)**:  $\text{cm}^{-1}$  = 3321 (w), 3265 (w), 1530 (m), 1479 (m), 1454 (m), 1402 (m), 1383 (m), 1217 (m), 1157 (m), 655 (m), 577 (s), 484 (s). **Raman (neat), laser = 632.81 nm**:  $\text{cm}^{-1}$  = 1543 (m), 1586 (m), 1477 (s), 1372 (w), 1344 (m), 1245 (s), 1025 (w), 988 (w), 954 (w), 842 (w), 808 (w), 762 (w), 593

(m), 527 (w), 440 (w), 359 (w), 332 (w). **UV-Vis absorptions:**  $\lambda_{\text{max}}$ /nm (DMSO) 312, 360 (sh), 480 and 530 (sh).

### **3.2.4. Spectral examples of copper bis(thiosemicarbazone) complexes**

#### **Cu-PADA-Me-Ph**

Figure 3.2.4.1., figure 3.2.4.2. and figure 3.2.4.3. show an example of a FTIR spectrum, a Raman spectrum and a mass spectrum of the complex Cu-PADA-Me-Ph.

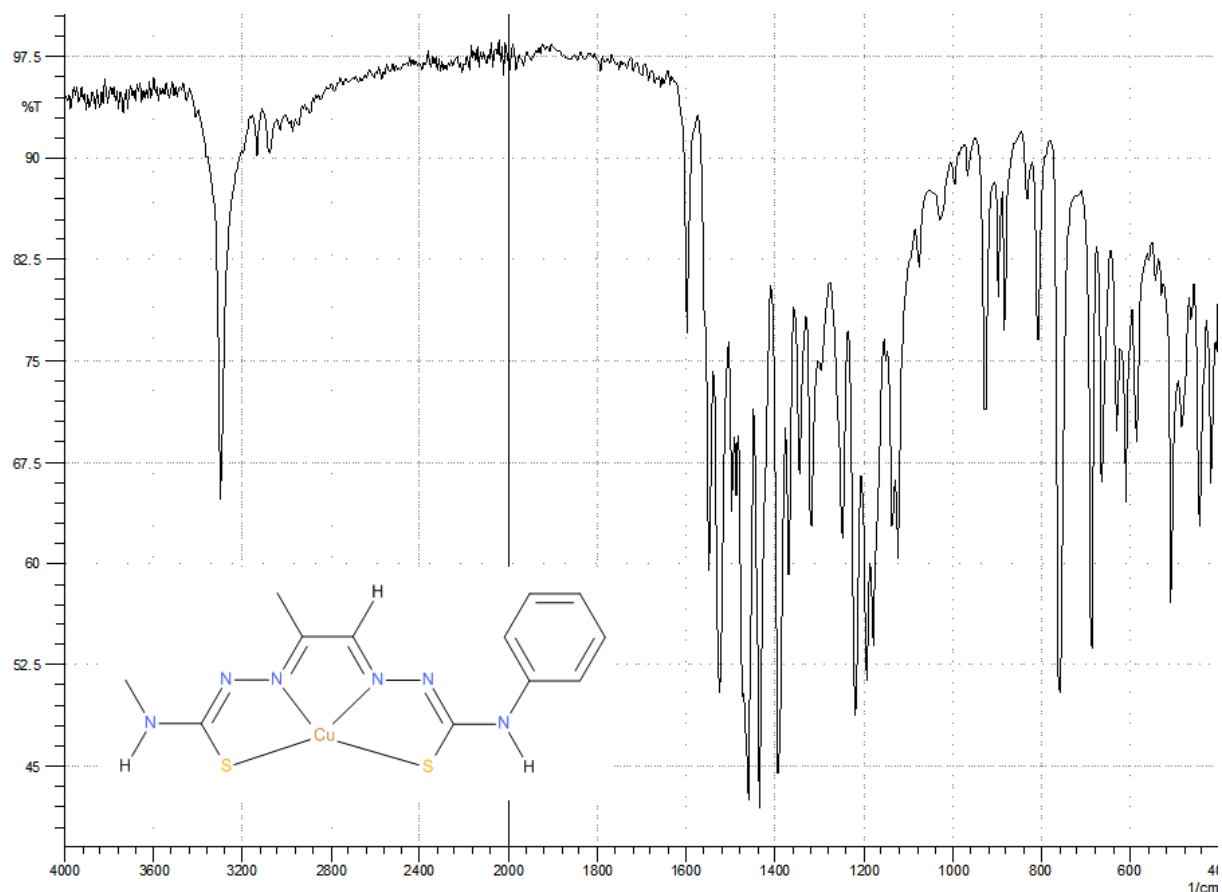


**Figure 3.2.4.1.** A FTIR spectrum of Cu-PADA-Me-Ph. This complex was synthesised by reacting PADA-Me-Ph with copper (II) acetate.

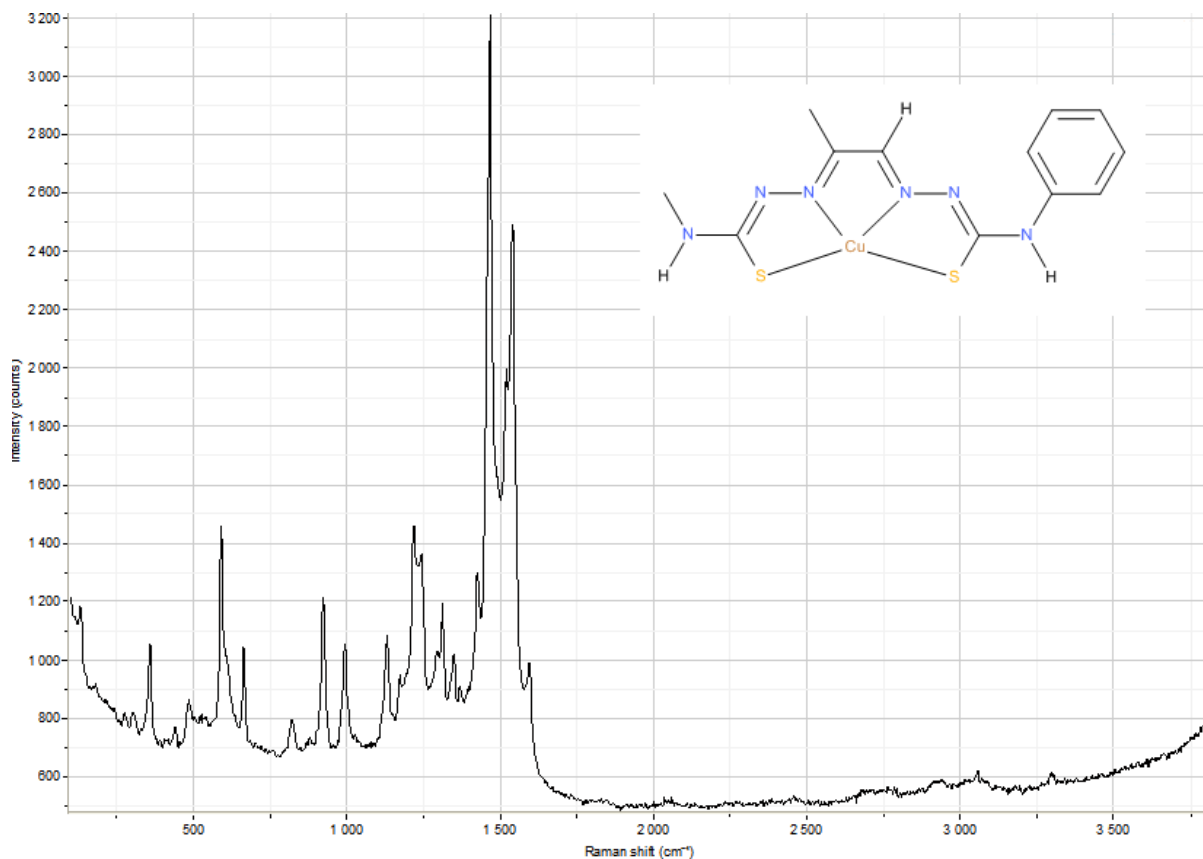


**Figure 3.2.4.2.** A Raman spectrum of Cu-PADA-Me-Ph.

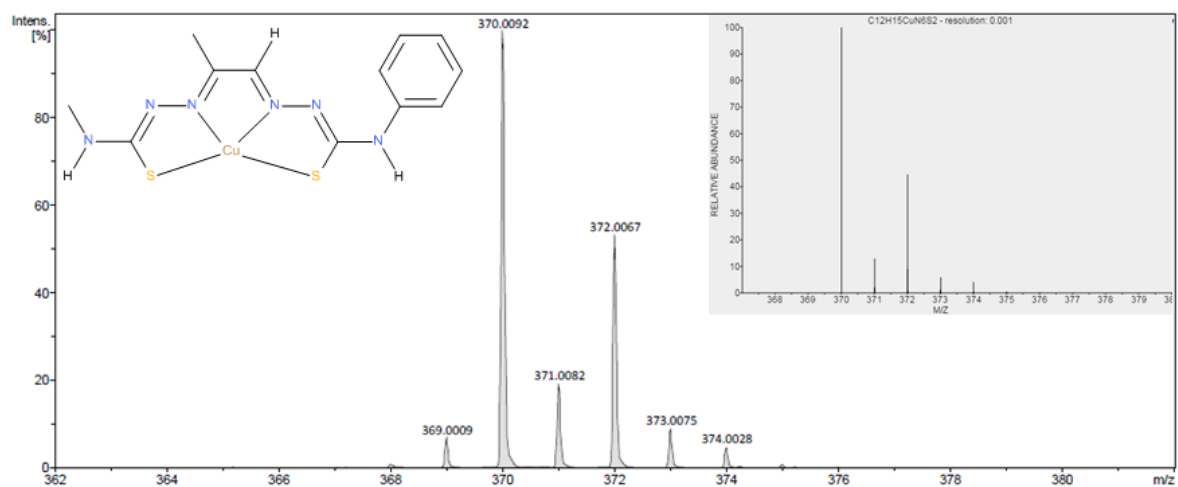


**Figure 3.2.4.3.** A mass spectrum of Cu-BDO-Me-NH<sub>2</sub>. The spectrum in the top right hand corner is the predicted expected spectrum of the  $M + H^+$  ion of Cu-BDO-Me-NH<sub>2</sub> generated by ChemCalc.<sup>213</sup>

## Cu-PDO-Et-Et

Figure 3.2.4.4., figure 3.2.4.5. and figure 3.2.4.6. show an example of a FTIR spectrum, a Raman spectrum and a mass spectrum of the complex Cu-PDO-Et-Et.

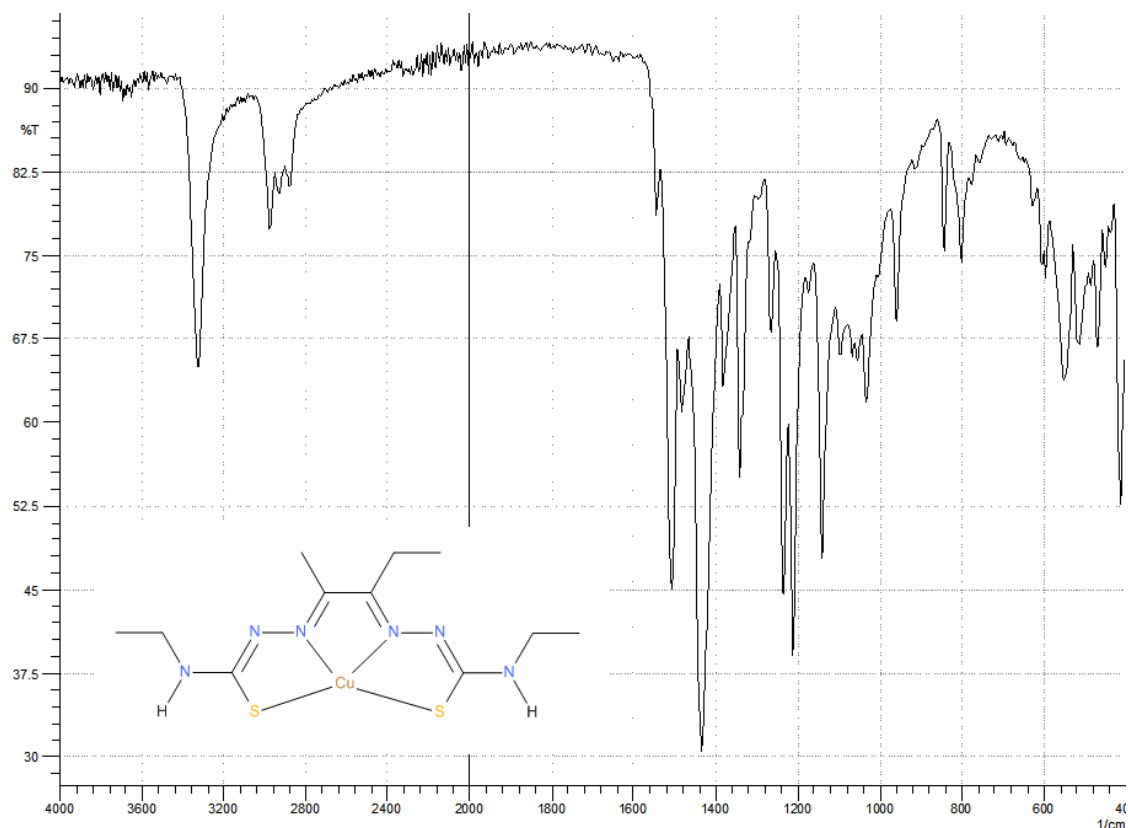


**Figure 3.2.4.4.** A FTIR spectrum of Cu-PDO-Et-Et. This complex was synthesised by reacting PDO-Et-Et with copper (II) acetate.

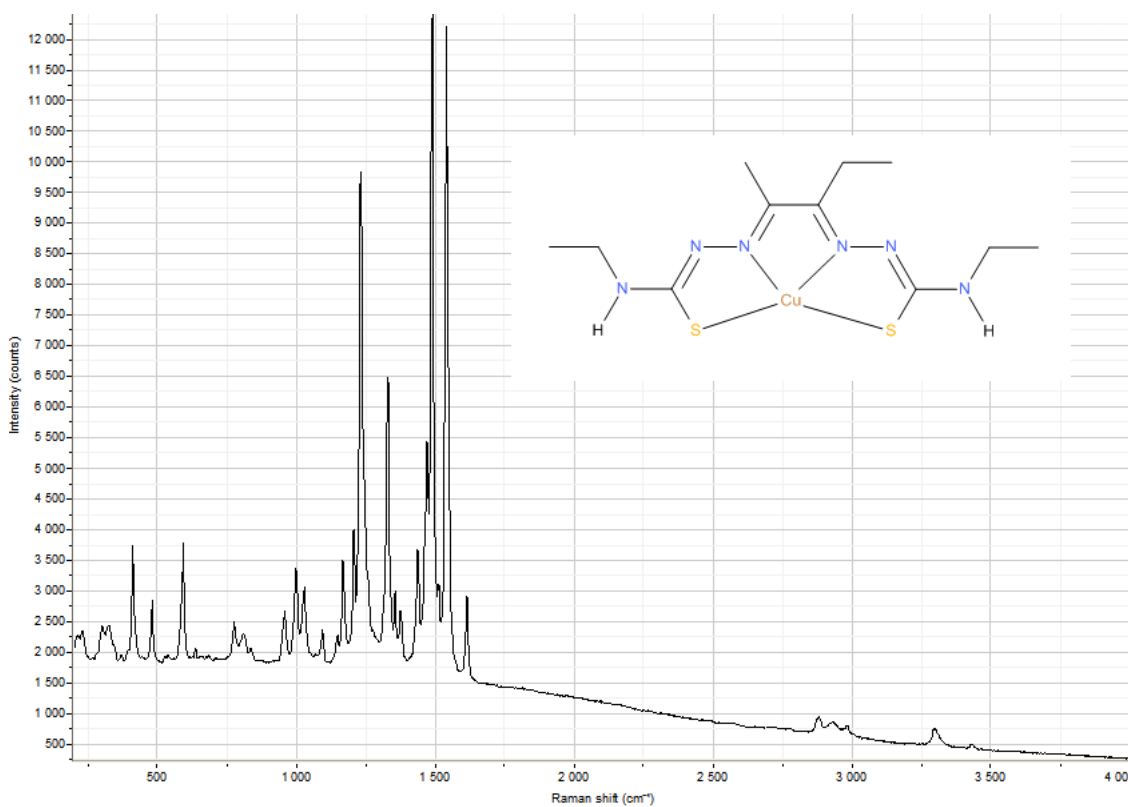


**Figure 3.2.4.5.** A Raman spectrum of Cu-PADA-Et-Et.



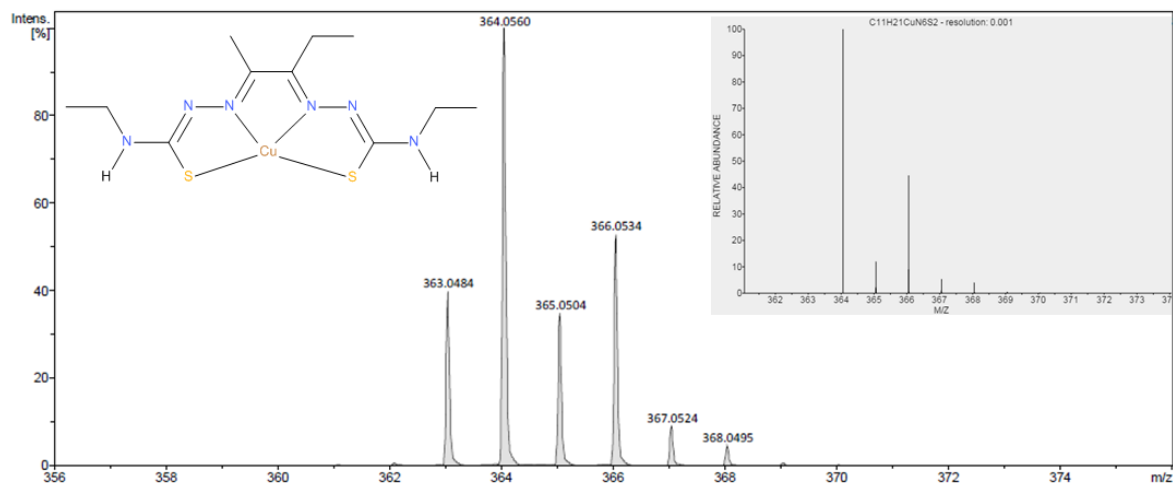


**Figure 3.2.4.6.** A mass spectrum of Cu-PDO-Et-Et. The spectrum in the top right hand corner is the predicted expected spectrum of the  $M + H^+$  ion of Cu-PDO-Et-Et generated by ChemCalc.<sup>213</sup>

### Reduction potentials

Table 3.2.4.7. illustrates the Cu(II/I) reduction potentials of selected copper complexes.

<b>Complex</b>	<b><math>E_{1/2}</math> Cu(II/I) (V) (Non-normalised)</b>	<b><math>E_{1/2}</math> Cu(II/I) (V) (normalised against ferrocene)</b>
Cu-GLY-Me-Me*	-0.24	-0.96
Cu-GLY-Et-Et	-0.37	-1.06
Cu-PADA-Me-(Me) <sub>2</sub>	-0.39	-1.01
Cu-PADA-Ph-Ph	-0.29	-0.88
Cu-PADA-Et-Me	-0.37	-1.08
Cu-PADA-Me-Ph	-0.24	-0.93
Cu-PADA-Ph-Me	-0.33	-1.04
Cu-PADA-Et-Ph	-0.31	-1.06
Cu-BDO-Me-Me	-0.51	-1.12
Cu-BDO-Et-Et	-0.37	-1.13
Cu-BDO-Me-NH <sub>2</sub>	-0.19	-1.12
Cu-BDO-Me-O-Ph*	-0.46	-1.24
Cu-BDO-Me-(Me) <sub>2</sub> *	-0.41	-1.05
Cu-BDO-NH <sub>2</sub> -(Me) <sub>2</sub>	-0.50	-1.13
Cu-BDO-Me-Et-(Me) <sub>2</sub> *	-0.49	-1.11
Cu-BDO-Me-But-NH <sub>2</sub> *	-0.62	-1.30
Cu-BDO-NH <sub>2</sub> -NH <sub>2</sub>	-0.37	-1.11
Cu-PDO-Me-Me	-0.60	-1.14
Cu-PDO-Et-Et	-0.47	-1.13
Cu-PDO-NH <sub>2</sub> -Me	-0.36	-1.13
Cu-PDO-Et-NH <sub>2</sub>	-0.51	-1.14
Cu-PDO-NH <sub>2</sub> -NH <sub>2</sub>	-0.49	-1.16
Cu-PDO-NH <sub>2</sub> -Et	-0.48	-1.11
Cu-PDO-Me-NH <sub>2</sub>	-0.42	-1.13
Cu-PDO-NH <sub>2</sub> -(Me) <sub>2</sub>	-0.44	-1.10
Cu-DTS*	-0.58	-1.12

**Table 3.2.4.7.** Copper (II/I) reduction potentials for copper bis(thiosemicarbazone) complexes, obtained by Julia Baguña Torres from the Division of Imaging Sciences & Biomedical Engineering at King's College London. The potentials were obtained using cyclic voltammetry using a glassy carbon electrode as the working electrode, a silver wire electrode as the reference one and a platinum wire electrode as the auxiliary electrode. The complexes marked with (\*) were synthesised by Julia. Cu-DTS:  $Q_1=Et$ ,  $Q_2=Et$ ,  $R_1=H$ ,  $R_2=H$ ,  $R_3=H$ ,  $R_4=H$ . Cu-BDO-Me-Et-(Me)<sub>2</sub>:  $Q_1=Me$ ,  $Q_2=Me$ ,  $R_1=Me$ ,  $R_2=H$ ,  $R_3=H$ ,  $R_4=C_2H_4-N(Me)_2$ . Cu-BDO-Me-But-NH<sub>2</sub>:  $Q_1=Me$ ,  $Q_2=Me$ ,  $R_1=Me$ ,  $R_2=H$ ,  $R_3=H$ ,  $R_4=C_4H_8-NH_2$ . Cu-BDO-Me-O-Ph:  $Q_1=Me$ ,  $Q_2=Me$ ,  $R_1=Me$ ,  $R_2=H$ , the  $R_3$ & $R_4$  positions are taken up with a single phenyl ring directly bound to the terminal carbon. Cu-BDO-Me-O-Ph also has an oxygen instead of a sulphur atom on the  $R_3/R_4$  side.

### **3.2.5. Discussion**

Except for a few unexpected results, all the reactions produced a brown solid with relatively good yields, normally between 40-60%. The method was relatively straight forward and conveniently formed a brown precipitate that could be easily filtered off. Out of the twenty copper complexes made nine were symmetric and eleven were dissymmetric. Out of these twenty, twelve complexes are believed to be novel. The symmetric ligands were firstly made in order to test if the method of synthesis was suitable for all the range of complexes with their solubilities.

Unfortunately due to the paramagnetic properties of copper, the resulting copper complexes yielded NMR spectra of very poor quality that contained very broad peaks from which little useful information could be extracted. This meant that it was not possible to rely on NMR for confirming if the complexes have been synthesised. Melting point data was taken on only a selection of complexes, the selected complexes were chosen in order to incorporate complexes with a diverse range structural of substituents. It was found that it was very hard, due to the dark brown colour of the samples, to identify the precise stage of decomposition. It was noticed upon heating that the sample's colour turns blacker. When heating is continued the solid sample would melt to form a dark black liquid. As this transition was the easiest to observe this was the point which was reported as the decomposition temperature. For the six samples that were analysed this decomposition was observed between 210-266°C. L. Ackerman *et al.*<sup>80</sup> have reported successfully obtaining melting points of nickel and copper derivatives of the PADA backbone ( $Q_1=Me$ ,  $Q_2=H$ ) however none these complex were synthesised during this project. The most similar copper complexes L. Ackerman obtained had melting points between 204-210°C.

Obtaining infrared spectra of all the copper complexes was extremely straight forward when using the Golden Gate Diamond ATR attachment. This meant that highly quality spectra could be taken of all the complexes relatively quickly and easily. L.J. Ackerman *et al.*<sup>80</sup> and D. West *et al.*<sup>78</sup> both published some infrared data on copper bis(thiosemicarbazones) . From these two articles the only copper complex that was also made during this project was Cu-BDO-Me-Me of which the IR data was in close agreement. Peak assignments given in the literature<sup>78, 80, 207, 208</sup> were used to look

for similar peak locations in the previously unreported complexes. All complexes had peaks in the region of  $3450\text{-}3250\text{ cm}^{-1}$ ,  $1550\text{-}1420\text{ cm}^{-1}$ ,  $840\text{-}700\text{ cm}^{-1}$  and  $500\text{-}415\text{ cm}^{-1}$  corresponding to R-N-H, C=N, C-S and Cu-N bonds respectively. The Cu-S bond appears around  $300\text{-}315\text{ cm}^{-1}$  which is outside the range recorded when collecting the infrared spectra. IR data for Cu-GLY-Ph-Ph was also located within the literature<sup>172</sup> which also agreed with the data obtained in this project.

Collecting suitable Raman spectra of the complexes was a little more challenging. It was found that the complexes are relatively sensitive to laser light often resulting in the burning of the sample. This was observed when using the red laser (632.81 nm) with a filter that blocked less than 50% of the laser light or 10% of the light when using the blue laser (472.98 nm). Unlike with the characterisation of the bis(thiosemicarbazone) ligands, with the related copper complexes it seems that there is no one laser that can be used for all. Even with complexes with minor structural differences it was observed that some may fluoresce while the others would not fluoresce when exposed to the same colour laser. It does not seem possible to predict the best colour laser to use by just looking at the structure of the complex in order to give a respectable spectrum, free of fluoresce. It was found that when analysing the copper complexes, the red (632.81 nm) laser was a good starting point and when the red laser did not give an acceptable spectrum it was best to turn to the green (532.00 nm) laser. The resulting spectra obtained were of mixed quality, some spectra had very strong, sharp peaks with a relatively flat base line while other spectra contained very weak peaks, some of which were very broad and with an often messy or rising baseline.

Due to the large number of copper complexes that were synthesised CHN analysis was only ran on complexes that were believed to be novel. The first round of CHN analysis, disappointingly only three out of the nine samples sent came back with acceptable percentages. It is expected this could be due to either impurities being brought out of solution upon precipitation or solvent molecules/ acetate molecules being incorporated in to the complex, thus giving rise to the diverse results. A study by M. Shebl *et al.*<sup>214</sup> looked into relatively similar complexes where it was found that the anion of the copper salt they used to make the copper complexes also co-ordinated to the copper alongside the main complex. Particularly it was reported the acetate ion behaving in this way by co-ordinating to copper that was already bound to a tri-dentate ligand and a mono-dentate water molecule.

Evidence in the NMR spectra of the zinc bis(thiosemicarbazone) complexes, which are reported later in this Chapter, has also shown a presence of what is thought to be acetate molecule acting as a ligand. It was not possible to utilise NMR in order to elucidate the cause of the divergence in the CHN analysis, neither was it possible to use IR and Raman to determine the cause of the discrepancy.

The copper complexes were purified using a DMSO/H<sub>2</sub>O recrystallisation method. Other solvents were tested (ethanol, methanol, dichloromethane, acetonitrile) but it was found that the copper complexes were poorly soluble in these solvents and consequently full dissolution was not achieved. The copper complexes were dissolved in the minimum volume of DMSO and double the volume of water was pipetted down the side of the test tube in order to form a layer of water on top of the DMSO. The solution was then allowed to diffuse over the course of a week. The product was then recovered by filtration and washed with water and diethyl ether. The solid allowed to dry overnight in air. It was discovered that if the water was not allowed to diffuse with the DMSO layer slowly over a couple of days then the resulting precipitate would be very fine and thus very hard to recover via filtration. The slow recrystallisation method used the purification step was relatively inefficient, with yields typically between 20-30%. Despite the low yields the purifications were highly successful with six out of the eight recrystallised product giving acceptable CHN results.

Mass spectra of all dissymmetric copper complexes were obtained. All the copper complexes tested were detected as M+ H<sup>+</sup> and the theoretical m/z values were in close agreement with the experimental results. The theoretical m/z values were calculated by ChemCalc.<sup>213</sup> The isotope patterns of the spectra obtained all matched the predicted pattern produced by ChemCalc. Figures 3.2.4.3. and 3.2.4.6. illustrate examples of the mass spectrum of Cu-PADA-Me-Ph and Cu-PDO-Et-Et respectively. In the top right hand corner of both the spectra is the ChemCalc predicted spectra. An additional peak was observed in the majority of the spectra which was not present in the predicted spectra, this extra peak has an m/z value of roughly 1.008 lower than the main m/z peak. This peak is expected to attribute to the M<sup>+</sup> ion without the additional proton.

UV-visible absorption spectra were obtained from DMSO solutions of each of the synthesised copper bis(thiosemicarbazone) complexes. It was decided to record the spectra from 285-800nm in order to stay outside the absorption range of DMSO. The UV-vis absorption spectra obtained had strong similarity between them. Every spectrum showed two absorptions, the first maxima was between 498-450 nm with an extinction coefficient of around 6-10,000 dm<sup>3</sup> mol<sup>-1</sup> cm<sup>-1</sup>, a shoulder around 530 nm was always present. The second was between 306-318 nm with an extinction coefficient of around 21-23,000 dm<sup>3</sup> mol<sup>-1</sup> cm<sup>-1</sup>, a shoulder around 350 nm was always present. With complexes containing a phenyl group the shoulder around 350 nm would often increase in absorbance so that it resembled an extra peak with an extinction coefficient ranging from 13-15,000 dm<sup>3</sup> mol<sup>-1</sup> cm<sup>-1</sup>.

There is a little UV-visible data in the literature<sup>57, 172</sup>, whose  $\lambda_{\max}$  and  $\epsilon$  values are within agreement. A study on nickel bis(thiosemicarbazone) complexes by Ackerman *et al.*<sup>80</sup> suggests that for all the d<sup>9</sup> copper bis(thiosemicarbazone) complexes analysed the absorption between

498-450 nm is due to a d-d transition<sup>80</sup> and the absorption between 306-318nm is due to metal-to-ligand transfer.<sup>57</sup>

There were two unexpected results, these were Cu-PDO-Me-Me and Cu-PDO-Et-Et. Despite the same method being followed as the rest of the copper complexes, there is doubt that the expected complexes had been obtained. Concerns were first experienced when the products were obtained were both dark brown/ black in colour and that they were formed in unusually low yields. This appearance was also noticed when using the Raman's microscope to focus the laser. In the case of Cu-PADA-Et-Et the Infrared spectrum had very poorly defined peaks and the Raman spectrum has a very broad peak at  $1489\text{ cm}^{-1}$ , with no other distinguishable peaks against a rolling base line. With Cu-PDO-Me-Me the infrared spectrum also had only a few peaks, with low intensity when compared to the baseline. Surprisingly the Raman spectrum looks relatively sensible when compared to the spectra of the other copper complexes. It is suspected that both these samples decomposed somehow during the reaction yielding these black samples. If these samples mostly contained degraded products which do not absorb much infrared radiation, this would explain the poor infrared spectra. A reason why Cu-PDO-Me-Me still gave a Raman spectrum could be that if the laser was fortuitously focused on an area of sample where some of the non-degraded product was, due to Raman's ability to take spectra of a very small area of the sample the rest of the degraded sample may not have had much influence on the resulting spectrum.

The reduction potential data for the copper bis(thiosemicarbazone) ligands (Table 3.2.4.7.) indicates that out of all the complexes tested, the complexes with Me/Et on the backbone (except Cu-PDO-NH<sub>2</sub>-Et) all have Cu (II/I) reduction potentials lower than Cu-BDO-Me-Me (-1.12V, referenced to ferrocene), Cu-BDO-NH<sub>2</sub>-(Me)<sub>2</sub> also has a lower reduction potential than Cu-BDO-Me-Me with -1.13V. Cu-BDO-Me-O-Ph (Q<sub>1</sub>=Me, Q<sub>2</sub>=Me, R<sub>1</sub>=Me, R<sub>2</sub>=H, the R<sub>3</sub>&R<sub>4</sub> positions are taken up with a single phenyl ring directly bound to the terminal carbon. Cu-BDO-Me-O-Ph also has an oxygen instead of a sulphur atom on the R<sub>3</sub>/R<sub>4</sub> side) and Cu-BDO-Me-But-NH<sub>2</sub> (Q<sub>1</sub>=Me, Q<sub>2</sub>=Me, R<sub>1</sub>=Me, R<sub>2</sub>=H, R<sub>3</sub>=H, R<sub>4</sub>= C<sub>4</sub>H<sub>8</sub>-NH<sub>2</sub>) have a significantly lower reduction potential than Cu-BDO-Me-Me, with a reduction potential of -1.24V and -1.30V, respectively. J. Dearling et al.<sup>77</sup> reports that Cu-BDO-Me-Me (Cu-ATSM) with a Cu(II/I) reduction potential of -0.59V (referenced to Ag/AgCl) had the greatest hypoxia selectively at 60 minutes post injection out of the range of symmetric copper complexes tested. The paper by J. Dearling et al.<sup>77</sup> shows a strong relationship between the reduction potential of a copper complex and its hypoxia selectivity. Different electrodes and references were used in this project, making direct comparison of the reduction potentials impossible. However, it is possible to suggest that based on their reduction potentials copper complexes with Me/Et on the backbone as well as Cu-BDO-NH<sub>2</sub>-(Me)<sub>2</sub>, Cu-BDO-Me-O-Ph

and Cu-BDO-Me-But-NH<sub>2</sub> would be good candidates for further screening in order to establish their hypoxia selectivity. PADA related dissymmetric complexes containing Ph substituents on the terminal amines may also be of interest for hypoxia selectivity testing because J. Dearling<sup>77</sup> reported that despite Cu-PADA-Ph-Ph having a high reduction potential it still had a little hypoxia selectivity. This may mean that even though PADA based copper complexes containing phenyl substituents may have relatively high reduction potentials they still may be hypoxia selective.

In the same paper Cu-GLY-Me-Me (Cu-GTSM) is reported to be non-hypoxia selective. If this idea is transferred to this data set, with GLY-Me-Me having a reduction potential of -0.96V then Cu-PADA-Me-Ph and Cu-PADA-Ph-Ph with reduction potentials of -0.93 and -0.88 respectively, may be good candidates for evaluating their accumulation and retention with in the brain. It is worth noting that for all the complexes tested with Me/H on their backbone they had lower reduction potentials than those with either Me/Me or Me/Et on their backbone. This suggests that even though complexes with Me/H on their backbone may have a higher reduction potential than GLY-Me-Me, if their other pharmacokinetics are favourable, such as lipophilicity, they may still be candidates for evaluation as brain imaging agents.

Unfortunately at the time of writing LogP data was not available for the above complexes, so in order for the suggested complexes to remaining strong candidates for further testing their logP values will have to be favourable for their respective uses. J. Dearling<sup>77</sup> reports a graph which can be found in the introduction of this thesis (Figure 1.6.2.1.6.). From this graph there seems to be a slight trend. For complexes with the same backbone, the ones with more lipophilic substituents on the terminal amines have slightly higher hypoxia selectivity. With this trend in mind it would be sensible to suggest that, in regards to hypoxia selectivity, PDO based copper complexes with more lipophilic substituents such as dimethyl and ethyl may have higher hypoxia selectivity than PDO complexes with NH<sub>2</sub> and methyl on the terminal amines.

### **3.3. Zinc bis(thiosemicarbazone) complexes**

#### **3.3.1. Reaction overview**

The complex formation process for zinc complexes is the same as for the copper complexes. The pro-ligand is de-protonated to un-cover the ligand which when reacted with a zinc (II) salt, forms a complex by chelating between the two sulphur atoms and the lone pairs from both the imine nitrogen atoms in order to yield a square planar, tetradentate complex (Figure 3.3.1.1.).

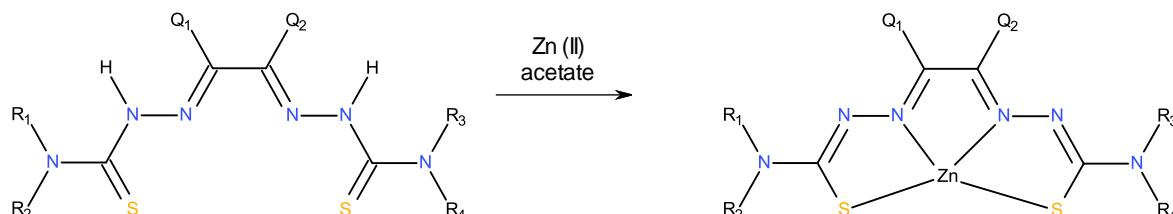


**Figure 3.3.1.1.** The general reaction for the synthesis of zinc bis(thiosemicarbazone) complexes.

#### **3.3.2. Synthesis of zinc bis(thiosemicarbazone) complexes**

##### **Method selection:**

A few studies have previously looked at synthesising zinc bis(thiosemicarbazone) complexes which resulted in a small number of articles in the literature that could be used as a starting point when devising methods for forming zinc bis(thiosemicarbazone) complexes in milligram to gram quantities. Two articles were identified by J. Holland *et al.*<sup>57</sup> and S. Kadowaki *et al.*<sup>75</sup> which report a method that involves the chosen bis(thiosemicarbazone) ligand being refluxed in methanol with zinc acetate. An alternative study by L. Ackerman *et al.*<sup>80</sup> was found, the study itself does not cover the synthesis of zinc bis(thiosemicarbazone) complexes but it does cover the synthesis of the related copper and nickel complexes. L. Ackerman reports a similar reflux reaction but the solvent of choice was ethanol. A number of articles report methods that are also comparable to the ones used by J. Holland and L. Ackerman with the main difference being that the authors ran the reaction under a N<sub>2</sub> atmosphere.<sup>76, 83, 84</sup>

As all the methods are very similar in that a chosen bis(thiosemicarbazone) ligand is refluxed in either ethanol or methanol in the presence of a zinc salt it was chosen that the methods by J. Holland and L. Ackerman would be tried out, alongside the method used in the formation of the copper complexes in order to see if it could be adapted. Due to limitations in the lab facilities available it was decided not to pursue conducting the reactions under a N<sub>2</sub> atmosphere.

**Copper derived method:**

BDO-Me-Me (0.312 g, 0.012 mol) was added to a NaOH solution (1M, 25 mL, 50 °C), the minimum amount of DMF was added in order to achieve full dissolution. Anhydrous zinc (II) acetate (0.257 g, 0.014 mol) was dissolved in de-ionised water (10 mL). The solutions were combined and left to stir over night (whilst cooling down to room temperature). Water was added to try to form a precipitate. The volume of the solvent was reduced via rotary evaporation by roughly 9/10 th's and returned to the fridge overnight. When no precipitate was formed the reaction solution was allowed to evaporate in air over the weekend. The crystalline solid was recovered by filtration and washed with methanol (3 x 20 mL) and a little di-ethyl ether. The solid was dried in air. A white crystalline solid (0.366 g) was recovered.

**L. Ackerman's method:**

BDO-Me-Me (0.312 g, 0.0012 mol) was added to ethanol (30 mL), anhydrous zinc (II) acetate (0.257 g, 0.0014 mol) was added to the suspension. The suspension was then brought under reflux (2 hours). The precipitate was recovered via filtration, washed with ethanol (1 x 30 mL) and diethyl ether (5 x 30 mL). The solid was dried in air. A yellow solid (0.282 g) was recovered (73% yield).

**J. Holland's method:**

BDO-Me-Me (0.312 g, 0.0012 mol) was added to methanol (30 mL). Anhydrous zinc (II) acetate (0.257 g, 0.0014 mol) was added to the suspension. The suspension was then brought under reflux (4 hours). The precipitate was recovered via filtration, washed with methanol (2 x 20 mL) and diethyl ether (3 x 20 mL). The solid was dried in air. A yellow solid (0.199 g) was recovered (51% yield).

**Discussion**

The copper derived method was not successful because when a precipitate was finally produced, the white crystalline solid did not give a NMR spectrum. It is thought that the solid produced is likely to contain mostly sodium hydroxide. Both the L. Ackerman and J. Holland methods produced the desired products in acceptable yields and NMR confirmed that the products were present in high purity. The L. Ackerman product contained no sight of unreacted ligand but the J. Holland product had a small presence of unreacted BDO-Me-Me which was estimated to be less than 1 %.



As the L. Ackerman method produced a slightly purer product with a higher yield than the J. Holland method, it was decided that the L. Ackerman method was the method that would be used in the synthesis of the remaining zinc complexes.

### **General methods:**

Depending on the amount of the ligand that was available the general methods used was either:

#### **General method A:**

The chosen bis(thiosemicarbazone) ligand ( X g, 0.0006 mol) was added to ethanol (15 mL). Anhydrous zinc (II) acetate (0.128 g, 0.0007 mol) was added to the suspension. The suspension was then brought to reflux (2 hours). The precipitate was recovered via filtration, washed with ethanol (1 x 15 mL) and diethyl ether (5 x 15 mL). The solid was dried in air.

#### **General method B:**

The chosen bis(thiosemicarbazone) ligand ( X g, 0.0004 mol) was added to ethanol (10 mL). Anhydrous zinc (II) acetate (0.092 g, 0.0005 mol) was added to the suspension. The suspension was then brought to reflux (2 hours). The precipitate was recovered via filtration, washed with ethanol (1 x 10 mL) and diethyl ether (5 x 10 mL). The solid was dried in air.

#### **General method C:**

The chosen bis(thiosemicarbazone) ligand ( X g, 0.0003 mol) was added to ethanol (7.5 mL). Anhydrous zinc (II) acetate (0.073 g, 0.0004 mol) was added to the suspension. The suspension was then brought to reflux (2 hours). The precipitate was recovered via filtration, washed with ethanol (1 x 7.5 mL) and diethyl ether (5 x 7.5 mL). The solid was dried in air.

The method used for each complex is summarised in table 3.3.2.1., along with the reaction yield and appearance of the product.

<b>Complex</b>	<b>General method used</b>	<b>Yield</b>	<b>Appearance of product</b>	<b>Believed to be novel</b>	<b>Comments</b>
<b>Zn-GLY-Et-Et</b>	<b>A</b>	<b>62%</b>	<b>Orange solid</b>	<b>No<sup>76, 180</sup></b>	
<b>Zn-GLY-Ph-Ph</b>	<b>A</b>	<b>85%</b>	<b>Orange solid</b>	<b>No<sup>76, 180</sup></b>	
<b>Zn-PADA-Me-Me</b>	<b>A</b>	<b>48%</b>	<b>Yellow solid</b>	<b>No<sup>202</sup></b>	
<b>Zn-PADA-Me-Ph</b>	<b>B</b>	<b>21%</b>	<b>Orange solid</b>	<b>Yes</b>	
<b>Zn-PADA-Et-(Me)<sub>2</sub></b>	<b>A</b>	<b>42%</b>	<b>Orange solid</b>	<b>Yes</b>	

Zn-PADA-Et-Ph	A	26%	Orange solid	Yes	
Zn-PADA-Ph-Ph	B	49%	Orange solid	Yes	
Zn-PADA-Ph-NH <sub>2</sub>	C	33%	Yellowish Orange solid	Yes	Expected acetate ligand Yield (28%)
Zn-PADA-Ph-Me	B	48%	Orange solid	Yes	
Zn-BDO-NH <sub>2</sub> -NH <sub>2</sub>	A	69%	Yellow solid	No <sup>202, 215</sup>	
Zn-BDO-NH <sub>2</sub> -(Me) <sub>2</sub>	B	64%	Yellow solid	Yes	Expected acetate ligand Yield (54%)
Zn-BDO-Me-Me	L. Ackerman's method	73%	Yellow solid	No <sup>75, 76, 189</sup>	
Zn-BDO-Me-NH <sub>2</sub>	B	55%	Yellow solid	No <sup>83</sup>	
Zn-PDO-NH <sub>2</sub> -NH <sub>2</sub>	A	53%	Yellow solid	Yes	Expected ethanol ligands Yield (40%)
Zn-PDO-NH <sub>2</sub> -Me	B	51%	Yellow solid	Yes	
Zn-PDO-NH <sub>2</sub> -(Me) <sub>2</sub>	A	9%	Yellow solid	Yes	
Zn-PDO-NH <sub>2</sub> -Et	A	33%	Yellow solid	Yes	
Zn-PDO-Me-NH <sub>2</sub>	A	34%	Yellow solid	Yes	
Zn-PDO-Et-Et	A	38%	Yellow solid	Yes	
Zn-PDO-Et-NH <sub>2</sub>	A	33%	Yellow solid	Yes	A small quantity of acetate ligand expected

**Table 3.3.2.1.** summarises which general method was used for the synthesis of each complex.

### **3.2.3. Characterisation data for zinc bis(thiosemicarbazone) complexes**

#### **Zinc bis(thiosemicarbazone) complexes with H/H on the backbone**

##### **Zn-GLY-Et-Et**

**<sup>1</sup>H NMR** (DMSO-*d*<sub>6</sub>, 400 MHz): δ= 8.01 (s, 1 H, C-NH), 7.90 (s, 1 H, C-NH), 7.50 (s, 2 H, N=C-H), 3.49 (m, 4 H, H<sub>2</sub>C-NH), 1.01 (m, 6 H, H<sub>2</sub>C-CH<sub>3</sub>). **<sup>13</sup>C {<sup>1</sup>H} NMR** (DMSO-*d*<sub>6</sub>, 100 MHz): δ= 177.7 (C-S), 135.3 (C=N), 38.24 (N-CH<sub>2</sub>), 37.36 (N-CH<sub>2</sub>), 15.25 (H<sub>2</sub>C-CH<sub>3</sub>), 14.89 (H<sub>2</sub>C-CH<sub>3</sub>). **IR (neat)**: cm<sup>-1</sup>= 3296 (w), 3246 (w), 3036 (w), 2980 (w), 2922 (w), 1541 (m), 1495 (m), 1468 (m), 1443 (m), 1420 (m), 1389 (m), 1375 (m), 1342 (m), 1244 (s), 1163 (s), 1080 (s), 1045 (s), 930 (m), 916 (m), 826 (m), 766 (m), 704 (m), 644 (m), 629 (m), 561 (m), 488 (m). **Raman (neat), laser = 784.15 nm**: cm<sup>-1</sup>= 1573 (s), 1520 (w), 1502 (w), 1469 (w), 1452 (w), 1425 (w), 1393 (w), 1174 (s), 1167 (s), 929 (w), 919 (w), 719 (w), 464 (w), 413 (w), 332 (w), 291 (w), 274 (w), 236 (w). **UV-Vis absorptions**: λ<sub>max</sub>/nm (DMSO) 328 (ε/dm<sup>3</sup> mol<sup>-1</sup> 9 700) and 440 (sh), 458 (43 700).

##### **Zn-GLY-Ph-Ph**

**<sup>1</sup>H NMR** (DMSO-*d*<sub>6</sub>, 400 MHz): δ= 9.68 (s, 2 H, Ph-NH), 7.78 (s, 2 H, N=C-H), 7.71 (d, 4 H, H<sub>(2,6)</sub> aryl, J = 7.6 Hz), 7.21 (t, 4 H, H<sub>(3,5)</sub> aryl, J = 7.6 Hz), 6.92 (t, 2 H, H<sub>(4)</sub> aryl, J = 7.6 Hz). **<sup>13</sup>C {<sup>1</sup>H} NMR** (DMSO-*d*<sub>6</sub>, 100 MHz): δ= 176.34 (C-S), 141.09 (C<sub>(1)</sub> aryl), 138.46 (C=N), 128.93 (C<sub>(3,5)</sub> aryl), 122.70 (C<sub>(4)</sub> aryl), 121.24 (C<sub>(2,6)</sub> aryl). **IR (neat)**: cm<sup>-1</sup>= 3370 (w), 1595 (w), 1541 (m), 1495 (m), 1449 (m), 1400 (s), 1325 (s), 1298 (m), 1252 (s), 1177 (m), 1088 (m), 1067 (m), 1028 (w), 918 (m), 893 (w), 868 (w), 841 (w), 808 (m), 746 (s), 685 (s), 611 (m), 586 (m), 557 (m), 501 (s), 438 (w). **Raman (neat), laser = 784.15 nm**: cm<sup>-1</sup>= 1568 (m), 1541 (m), 1473 (m), 1461 (m), 1430 (w), 1365 (w), 1319 (w), 1257 (w), 1175 (w), 1146 (s), 1121 (w), 997 (w), 921 (w), 837 (w), 691 (w), 523 (w), 412 (w), 359 (w), 268 (w). **Melting point**: >270 °C (decomposed). **UV-Vis absorptions**: λ<sub>max</sub>/nm (DMSO) 348 (ε/dm<sup>3</sup> mol<sup>-1</sup> 13 400) and 472 (23 200).

#### **Zinc bis(thiosemicarbazone) complexes with Me/H on the backbone**

##### **Zn-PADA-Me-Me**

**<sup>1</sup>H NMR** (DMSO-*d*<sub>6</sub>, 400 MHz): δ= 7.54 (s, 1 H, N=CH), 7.41 (s, 1 H, H<sub>3</sub>C-NH), 7.22 (s, 1 H, H<sub>3</sub>C-NH), 2.78, 6 H, HN-CH<sub>3</sub>), 2.06 (s, 3 H, N=C-CH<sub>3</sub>). **<sup>13</sup>C {<sup>1</sup>H} NMR** (DMSO-*d*<sub>6</sub>, 100 MHz): δ= 29.79 (HN-CH<sub>3</sub>), 16.32 (N=C-CH<sub>3</sub>). **IR (neat)**: cm<sup>-1</sup>= 3374 (m), 3204 (w), 2924 (m), 1585 (w), 1514 (s), 1433 (m), 1402 (s), 1342 (s), 1271 (s), 1233 (s), 1184 (s), 1136 (m), 1115 (m), 1053 (s), 986 (m), 922 (m), 853 (m), 795 (m), 723 (m), 669 (s), 598 (m), 581 (m), 546 (m), 523 (s), 453 (s), 428 (m). **Raman (neat), laser = 784.15 nm**: cm<sup>-1</sup>= 1608 (w), 1574 (w), 1526 (m), 1495 (s), 1486 (s), 1376 (w), 1271 (m), 1242 (m), 1199 (m), 986 (w), 921 (m), 852 (w), 722 (w), 662 (w), 601 (w), 580 (m), 867 (w), 452 (w), 431 (w), 380 (w), 339 (w), 275 (w). **Elemental analysis**: Found: C, 27.3; H, 3.85; N, 26.9. Calc. for

Zn<sub>1</sub>C<sub>7</sub>H<sub>12</sub>N<sub>6</sub>S<sub>2</sub>: **C**, 27.15; **H**, 3.9; **N**, 27.1%. **UV-Vis absorptions**:  $\lambda_{\text{max}}$ /nm (DMSO) 326 ( $\epsilon/\text{dm}^3 \text{ mol}^{-1} \text{ cm}^{-1}$  13 800) and 444 (13 000).

#### Zn-PADA-Me-Ph

**<sup>1</sup>H NMR** (DMSO-*d*<sub>6</sub>, 400 MHz):  $\delta$ = 9.48 (s, 1 H, Ph-NH), 7.76 (s, 1 H, N=CH), 7.72 (m, 2 H, **H**<sub>(2,6)</sub> aryl), 7.43 (s, 1 H, CH<sub>3</sub>-NH), 7.43 (t, 2 H, **H**<sub>(3,5)</sub> aryl, J= 7.2 Hz), 6.89 (d, 1 H, **H**<sub>(4)</sub> aryl, J= 7.2 Hz), 2.81 (s, 3 H, N-CH<sub>3</sub>), 2.10 (s, 3 H, N=C-CH<sub>3</sub>). **<sup>13</sup>C {<sup>1</sup>H} NMR** (DMSO-*d*<sub>6</sub>, 100 MHz):  $\delta$ = 141.87 (**C**=N), 141.35 (**C**<sub>(1)</sub> aryl), 128.86 (**C**<sub>(3,5)</sub> aryl), 122.31 (**C**<sub>(4)</sub> aryl), 120.88 (**C**<sub>(2,6)</sub> aryl), 29.69 (N-CH<sub>3</sub>), 16.26 (N=C-CH<sub>3</sub>). **IR (neat)**:  $\text{cm}^{-1}$ = 3451 (w), 3267 (w), 3130 (w), 3071 (w), 1597 (w), 1545 (m), 1493 (m), 1477 (m), 1450 (m), 1416 (s), 1398 (s), 1348 (m), 1319 (m), 1308 (m), 1263 (m), 1242 (m), 1221 (s), 1171 (s), 1130 (s), 1072 (m), 1030 (m), 997 (m), 959 (m), 922 (m), 895 (m), 885 (m), 831 (m), 824 (m), 795 (m), 743 (s), 683 (s), 658 (m), 617 (s), 584 (s), 501 (s), 474 (m), 430 (m). **Raman (neat), laser = 632.81 nm**:  $\text{cm}^{-1}$ = 3273 (w) 1619 (w), 1602 (w), 1549 (m), 1536 (s), 1477 (s), 1454 (m), 1516 (m), 1370 (w), 1347 (w), 1318 (w), 1310 (m), 1246 (m), 1225 (m), 1187 (w), 1132 (m), 1034 (w), 996 (w), 923 (m), 831 (w), 656 (w), 618 (w), 591 (w), 583 (w), 472 (w), 457 (w), 348 (w). **Elemental analysis**: Found: **C**, 38.8; **H**, 3.9; **N**, 22.6. Calc. for Zn<sub>1</sub>C<sub>12</sub>H<sub>14</sub>N<sub>6</sub>S<sub>2</sub>: **C**, 39.0; **H**, 3.8; **N**, 22.7%. **UV-Vis absorptions**:  $\lambda_{\text{max}}$ /nm (DMSO) 342 ( $\epsilon/\text{dm}^3 \text{ mol}^{-1} \text{ cm}^{-1}$  18 200) and 450 (15 800). **Mass spectrometry (ESI)**: *m/z* (Calc.) 371.0093 (371.0091) {M + H<sup>+</sup>}.

#### Zn-PADA-Et-(Me)<sub>2</sub>

**<sup>1</sup>H NMR** (DMSO-*d*<sub>6</sub>, 400 MHz):  $\delta$ = 7.53 (s, 1 H, N=CH), 7.28 (s, 1 H H<sub>2</sub>C-NH), 3.15 (s, 6 H, HN-(CH<sub>3</sub>)<sub>2</sub>), 2.05 (s, 3 H, N=C-CH<sub>3</sub>), 1.06 (t, 3 H, H<sub>2</sub>C-CH<sub>3</sub>, J= 7.2 Hz). **<sup>13</sup>C {<sup>1</sup>H} NMR** (DMSO-*d*<sub>6</sub>, 100 MHz):  $\delta$ = 180.44 (**C**-S), 137.31 (**C**=N), 37.46 (N-CH<sub>2</sub>), 16.27 (N=C-CH<sub>3</sub>), 15.16 (H<sub>2</sub>C-CH<sub>3</sub>). **IR (neat)**:  $\text{cm}^{-1}$ = 3304 (m), 2970 (w), 2928 (w), 2870 (w), 1514 (m), 1508 (m), 1437 (s), 1375 (s), 1339 (s), 1317 (s), 1263 (s), 1248 (s), 1217 (s), 1179 (s), 1128 (s), 1053 (m), 934 (m), 907 (s), 891 (s), 818 (m), 723 (m), 650 (m), 621 (m), 613 (m), 586 (m), 559 (m), 540 (m), 457 (m), 417 (s). **Raman (neat), laser = 632.81 nm**:  $\text{cm}^{-1}$ = 3304 (w), 1611 (w), 1541 (s), 1499 (s), 1482 (s), 1450 (s), 1404 (w), 1378 (w), 1369 (w), 1321 (s), 1249 (w), 1219 (s), 1182 (w), 1133 (w), 1122 (w), 1002 (m), 931 (s), 892 (w), 725 (w), 651 (w), 586 (m), 493 (w), 456 (w), 418 (w), 332 (w), 279 (w). **Elemental analysis**: Found: **C**, 32.1; **H**, 4.7; **N**, 25.0. Calc. for Zn<sub>1</sub>C<sub>9</sub>H<sub>16</sub>N<sub>6</sub>S<sub>2</sub>: **C**, 32.0; **H**, 4.8; **N**, 24.9%. **UV-Vis absorptions**:  $\lambda_{\text{max}}$ /nm (DMSO) 322 ( $\epsilon/\text{dm}^3 \text{ mol}^{-1} \text{ cm}^{-1}$  11 900) and 454 (13 700). **Mass spectrometry (ESI)**: *m/z* (Calc.) 337.0272 (337.0248) {M + H<sup>+</sup>}.

#### Zn-PADA-Et-Ph

**<sup>1</sup>H NMR** (DMSO-*d*<sub>6</sub>, 400 MHz):  $\delta$ = 9.46 (s, 1 H, Ph-NH), 7.75 (s, 1 H, N=CH), 7.71 (m, 2 H, **H**<sub>(2,6)</sub> aryl), 7.47 (s, 1 H H<sub>2</sub>C-NH), 7.19 (t, 2 H, **H**<sub>(3,5)</sub> aryl, J=7.2 Hz), 6.88 (dd, 1 H, **H**<sub>(4)</sub> aryl, J=7.2 Hz), 3.4-3.3

(under water peak, 2 H expected,  $H_2C-NH$ ), 2.08 (s, 3 H,  $N=C-CH_3$ ), 1.07 (t, 3 H,  $H_2C-CH_3$ ,  $J=7.6$  Hz).  $^{13}C \{^1H\}$  NMR (DMSO- $d_6$ , 100 MHz):  $\delta=175.60$  (C-S), 141.88 (C=N), 141.35 ( $C_{(1)}$  aryl), 128.84 ( $C_{(3,5)}$  aryl), 122.28 ( $C_{(4)}$  aryl), 120.85 ( $C_{(2,6)}$  aryl), 37.45 (N- $CH_2$ ), 16.22 (N=C- $CH_3$ ), 15.08 ( $H_2C-CH_3$ ). IR (neat):  $cm^{-1}=3418$  (w), 3267 (m), 3071 (w), 1595 (m), 1541 (m), 1481 (s), 1450 (s), 1416 (s), 1312 (s), 1242 (s), 1223 (s), 1165 (s), 1134 (s), 928 (m), 901 (m), 800 (m), 748 (s), 689 (s), 642 (s), 615 (s), 588 (s), 478 (s). Raman (neat), laser = 632.81 nm:  $cm^{-1}=3278$  (w), 1601 (w), 1537 (s), 1482 (s), 1461 (s), 1415 (s), 1338 (w), 1314 (m), 1246 (m), 1222 (m), 1180 (w), 1138 (w), 1002 (w), 930 (m), 821 (w), 659 (w), 613 (w), 589 (w), 478 (w), 413 (w). Elemental analysis: Found: C, 40.4; H, 4.1; N, 21.7. Calc. for  $Zn_1C_{13}H_{16}N_6S_2$ : C, 40.5; H, 4.2; N, 21.8%. UV-Vis absorptions:  $\lambda_{max}/nm$  (DMSO) 334 ( $\epsilon/dm^3 mol^{-1} cm^{-1}$  12 600) and 456 (17 900). Mass spectrometry (ESI):  $m/z$  (Calc.) 385.0249 (385.0248)  $\{M + H^+\}$ .

### Zn-PADA-Ph-Ph

$^1H$  NMR (DMSO- $d_6$ , 400 MHz):  $\delta=9.64$  (s, 1 H, Ph-NH), 9.50 (s, 1 H, Ph-NH), 7.83 (s, 1 H, N=CH), 7.78 (m, 2 H,  $H_{(2,6)}$  aryl), 7.72 (m, 2 H,  $H_{(2,6)}$  aryl), 7.22 (t, 4 H,  $H_{(3,5)}$  aryl,  $J=7.6$  Hz), 6.91 (m, 2 H,  $H_{(4)}$  aryl), 2.22 (s, 3 H, N=C- $CH_3$ ).  $^{13}C \{^1H\}$  NMR (DMSO- $d_6$ , 100 MHz):  $\delta=176.64$  (C-S), 173.92 (C-S), 147.32 (C=N), 143.53 (C=N), 141.15 ( $C_{(1)}$  aryl), 141.00 ( $C_{(1)}$  aryl), 128.93 ( $C_{(3,5)}$  aryl), 128.90 ( $C_{(3,5)}$  aryl), 122.65 ( $C_{(4)}$  aryl), 122.19 ( $C_{(4)}$  aryl), 121.21 ( $C_{(2,6)}$  aryl), 120.61 ( $C_{(2,6)}$  aryl), 16.94 (N=C- $CH_3$ ). IR (neat):  $cm^{-1}=3422$  (m), 3414 (m), 3022 (w), 1597 (m), 1547 (w), 1516 (m), 1491 (m), 1472 (m), 1452 (m), 1410 (s), 1352 (m), 1308 (m), 1252 (m), 1233 (m), 1184 (m), 1138 (s), 1074 (m), 1028 (m), 932 (m), 908 (m), 893 (m), 845 (m), 822 (m), 745 (s), 685 (s), 652 (m), 611 (m), 586 (m), 540 (m), 498 (s), 422 (m). Raman (neat), laser = 632.81 nm:  $cm^{-1}=3416$  (w), 3051 (w), 1622 (w), 1602 (w), 1545 (s), 1526 (s), 1466 (s), 1430 (w), 1406 (w), 1351 (w), 1313 (w), 1237 (s), 1180 (w), 1140 (w), 996 (w), 934 (m), 845 (w), 662 (w), 613 (w), 595 (w), 476 (w), 355 (w). Elemental analysis: Found: C, 46.9; H, 3.7; N, 19.3. Calc. for  $Zn_1C_{17}H_{16}N_6S_2$ : C, 47.1; H, 3.7; N, 19.4%. UV-Vis absorptions:  $\lambda_{max}/nm$  (DMSO) 344 ( $\epsilon/dm^3 mol^{-1} cm^{-1}$  13 100) and 462 (21 400). Mass spectrometry (ESI):  $m/z$  (Calc.) 433.0241 (433.0247)  $\{M + H^+\}$ .

### Zn-PADA-Ph-NH<sub>2</sub>

$^1H$  NMR (DMSO- $d_6$ , 400 MHz):  $\delta=9.34$  (s, 1 H, Ph-NH), 7.77 (m, 2 H,  $H_{(2,6)}$  aryl), 7.54 (s, 1 H, N=CH), 7.36 (s, 2 H, C-NH), 7.19 (t, 2 H,  $H_{(3,5)}$  aryl,  $J=7.2$  Hz), 6.86 (t, 1 H,  $H_{(4)}$  aryl,  $J=7.2$  Hz), 2.17 (s, 3 H, N=C- $CH_3$ ).  $^{13}C \{^1H\}$  NMR (DMSO- $d_6$ , 100 MHz):  $\delta=177.13$  (C-S), 172.93 (C-S), 147.94 (C=N), 141.71 (C=N), 135.66 ( $C_{(1)}$  aryl), 128.88 ( $C_{(3,5)}$  aryl), 121.85 ( $C_{(4)}$  aryl), 120.33 ( $C_{(2,6)}$  aryl), 17.02 (N=C- $CH_3$ ). IR (neat):  $cm^{-1}=3402$  (w), 3316 (w), 1612 (m), 1537 (m), 1514 (m), 1495 (m), 1456 (m), 1408 (s), 1327 (m), 1314 (m), 1256 (w), 1233 (w), 1192 (w), 1150 (m), 1026 (w), 928 (w), 901 (w), 851 (w), 814 (w), 752 (m), 691 (m), 615 (m), 552 (m), 503 (m), 465 (m). Raman (neat), laser = 632.81 nm:

$\text{cm}^{-1}$  = 2918 (w), 1635 (w), 1600 (w), 1551 (s), 1516 (m), 1474 (m), 1376 (w), 1334 (w), 1312 (w), 1229 (m), 1193 (w), 1155 (w), 999 (w), 930 (w), 850 (w), 741 (w), 698 (w), 647 (w), 617 (w), 599 (w), 539 (w), 493 (w), 360 (w), 324 (w), 302 (w). **Melting point:** >250 °C (decomposed). **UV-Vis absorptions:**  $\lambda_{\text{max}}/\text{nm}$  (DMSO) 328 ( $\epsilon/\text{dm}^3 \text{ mol}^{-1} \text{ cm}^{-1}$  9 600) and 452 (12 900).

### Zn-PADA-Ph-Me

**$^1\text{H}$  NMR** (DMSO- $d_6$ , 400 MHz):  $\delta$  = 9.36 (s, 1 H, Ph-NH), 7.77 (m, 2 H,  $\text{H}_{(2,6)}$  aryl), 7.63 (s, 2 H,  $\text{H}_3\text{C-NH}$  and N=CH), 7.20 (t, 2 H,  $\text{H}_{(3,5)}$  aryl,  $J=7.2$  Hz), 6.87 (t, 1 H,  $\text{H}_{(4)}$  aryl,  $J=7.2$  Hz), 2.78 (s, 3 H, N- $\text{CH}_3$ ), 2.18 (s, 3 H, N=C- $\text{CH}_3$ ).  **$^{13}\text{C}$  { $^1\text{H}$ } NMR** (DMSO- $d_6$ , 100 MHz):  $\delta$  = 141.71 ( $\text{C}_{(1)}$  aryl), 128.90 ( $\text{C}_{(3,5)}$  aryl), 121.89 ( $\text{C}_{(4)}$  aryl), 120.34 ( $\text{C}_{(2,6)}$  aryl), 17.02 (N=C- $\text{CH}_3$ ). **IR (neat):**  $\text{cm}^{-1}$  = 3316 (w), 3265 (w), 3210 (w), 3125 (w), 3051 (w), 3005 (w), 2916 (w), 1597 (m), 1543 (m), 1504 (s), 1493 (s), 1464 (s), 1429 (s), 1352 (s), 1319 (s), 1302 (s), 1240 (m), 1200 (s), 1182 (m), 1173 (m), 1148 (m), 1119 (m), 1076 (m), 1042 (m), 932 (m), 868 (m), 845 (m), 820 (m), 750 (s), 387 (m), 675 (m), 627 (m), 608 (m), 592 (m), 581 (m), 530 (m), 503 (m), 469 (m), 419 (m). **Raman (neat), laser = 632.81 nm:**  $\text{cm}^{-1}$  = 3319 (w), 3034 (w), 1616 (w), 1599 (w), 1540 (w), 1507 (s), 1462 (s), 1427 (w), 1382 (w), 1316 (m), 1298 (m), 1243 (s), 1184 (m), 994 (w), 933 (s), 869 (w), 845 (w), 720 (w), 668 (w), 609 (w), 593 (m), 535 (w), 461 (w), 414 (w), 384 (w), 353 (w), 328 (w), 287 (w), 239 (w). **Elemental analysis:** Found: C, 38.85; H, 3.8; N, 22.6. Calc. for  $\text{Zn}_1\text{C}_{12}\text{H}_{14}\text{N}_6\text{S}_2$ : C, 38.8; H, 3.8; N, 22.6%. **Melting point:** >270 °C (decomposed). **UV-Vis absorptions:**  $\lambda_{\text{max}}/\text{nm}$  (DMSO) 330 ( $\epsilon/\text{dm}^3 \text{ mol}^{-1} \text{ cm}^{-1}$  13 100) and 454 (18 800). **Mass spectrometry (ESI):**  $m/z$  (Calc.) 371.0093 (371.0091) {M + H $^+$ }.

### Zinc bis(thiosemicarbazone) complexes with Me/Me on the backbone

#### Zn-BDO-NH $_2$ -NH $_2$

**$^1\text{H}$  NMR** (DMSO- $d_6$ , 400 MHz):  $\delta$  = 6.83 (s, 4 H, C-NH), 2.13 (s, 6 H, N=C- $\text{CH}_3$ ).  **$^{13}\text{C}$  { $^1\text{H}$ } NMR** (DMSO- $d_6$ , 100 MHz):  $\delta$  = 178.48 (C-S), 144.75 (C=N), 14.48 (N=C- $\text{CH}_3$ ). **IR (neat):**  $\text{cm}^{-1}$  = 3395 (w), 3283 (w), 3138 (w), 1632 (m), 1603 (m), 1533 (w), 1472 (m), 1427 (m), 1356 (m), 1290 (m), 1211 (m), 1184 (m), 1144 (m), 1070 (m), 1045 (m), 988 (m), 827 (m), 737 (w), 710 (m), 598 (m), 588 (m), 525 (m), 476 (m), 420 (s). **Raman (neat), laser = 632.81 nm:**  $\text{cm}^{-1}$  = 1611 (w), 1532 (s), 1476 (m), 1420 (w), 1287 (s), 1214 (w), 1188 (m), 1004 (w), 823 (w), 704 (w), 598 (w), 392 (w), 310 (w), (fluorescence present). **UV-Vis absorptions:**  $\lambda_{\text{max}}/\text{nm}$  (DMSO) 308 ( $\epsilon/\text{dm}^3 \text{ mol}^{-1} \text{ cm}^{-1}$  10 900) and 434 (9 500). **Mass spectrometry (ESI):**  $m/z$  (Calc.) 294.9793 (294.9778) {M + H $^+$ }.

#### Zn-BDO-NH $_2$ -(Me) $_2$

**$^1\text{H}$  NMR** (DMSO- $d_6$ , 400 MHz):  $\delta$  = 6.86 (s, 2 H, C-NH), 3.14 (s, 6 H, N-( $\text{CH}_3$ ) $_2$ ), 2.15 (s, 3 H, N=C- $\text{CH}_3$ ), 2.12 (s, 3 H, N=C- $\text{CH}_3$ ).  **$^{13}\text{C}$  { $^1\text{H}$ } NMR** (DMSO- $d_6$ , 100 MHz):  $\delta$  = 178.38 (C-S), 178.12 (C-S), 145.25 (C=N), 144.78 (C=N), 40.62-39.36 (under solvent peak, N-( $\text{CH}_3$ ) $_2$ ), 11.96 (N=C- $\text{CH}_3$ ), 11.70 (N=C-

**CH<sub>3</sub>**). **IR (neat):**  $\text{cm}^{-1}$  = 3422 (w), 3283 (w), 3159 (w), 2916 (w), 1622 (m), 1601 (m), 1541 (m), 1501 (m), 1433 (s), 1389 (s), 1375 (s), 1364 (s), 1294 (s), 1261 (s), 1207 (m), 1165 (s), 1136 (m), 1107 (m), 1055 (m), 903 (s), 835 (s), 758 (m), 700 (m), 619 (m), 590 (m), 567 (w), 519 (m), 478 (m), 457 (m), 432 (s). **Raman (neat), laser = 632.81 nm:**  $\text{cm}^{-1}$  = 2916 (w), 1609 (w), 1543 (m), 1508 (s), 1466(w), 1434 (w), 1375 (w), 1327 (w), 1293 (s), 1264 (w), 1205 (w), 1171 (w), 1141 (w), 1006 (w), 989 (w), 835 (w), 752 (w), 698 (w), 626 (w), 567 (w), 588 (w), 567 (w), 429 (w), 380 (w), 335 (w), 294 (w). **Elemental analysis:** Found: **C**, 29.6; **H**, 4.4; **N**, 25.8. Calc. for  $\text{Zn}_1\text{C}_8\text{H}_{14}\text{N}_6\text{S}_2$ : **C**, 29.7; **H**, 4.7; **N**, 26.0%. **Melting point:** >250 °C (decomposed). **UV-Vis absorptions:**  $\lambda_{\text{max}}/\text{nm}$  (DMSO) 314 ( $\epsilon/\text{dm}^3 \text{mol}^{-1} \text{cm}^{-1}$  12 600) and 442 (12 900).

### Zn-BDO-Me-Me

**<sup>1</sup>H NMR** (DMSO-*d*<sub>6</sub>, 400 MHz):  $\delta$  = 7.15 (s, 2 H, H<sub>3</sub>C-NH), 2.79 (m, 6 H, HN-CH<sub>3</sub>), 2.16 (s, 6 H, N=C-CH<sub>3</sub>). **<sup>13</sup>C {<sup>1</sup>H} NMR** (DMSO-*d*<sub>6</sub>, 100 MHz):  $\delta$  = 176.3 (C-S), 145.8 (C=N), 29.74 (HN-CH<sub>3</sub>), 14.42 (N=C-CH<sub>3</sub>). **IR (neat):**  $\text{cm}^{-1}$  = 3333(w), 2922 (w), 2882 (w), 1557 (w), 1522 (s), 1493 (s), 1452 (s), 1402 (m), 1379 (s), 1369 (s), 1219 (s), 1157 (s), 1119 (m), 1074 (m), 982 (m), 833 (s), 793 (w), 768 (m), 596 (m), 538 (m), 645 (s), 449 (s), 442 (s), 417 (s). **Raman (neat), laser = 632.81 nm:**  $\text{cm}^{-1}$  = 3333 (w), 1611 (w), 1547 (m), 1492 (s), 1461 (w), 1368 (w), 1327 (m), 1251 (m), 1188 (w), 992 (w), 837 (w), 769 (w), 585 (w), 433 (w), 334 (w), 298 (w). **Melting point:** >310 °C (decomposed). **UV-Vis absorptions:**  $\lambda_{\text{max}}/\text{nm}$  (DMSO) 314 ( $\epsilon/\text{dm}^3 \text{mol}^{-1} \text{cm}^{-1}$  14 000) and 432 (13 400).

### Zn-BDO-Me-NH<sub>2</sub>

**<sup>1</sup>H NMR** (DMSO-*d*<sub>6</sub>, 400 MHz):  $\delta$  = 7.16 (1 H, H<sub>3</sub>C-NH), 6.86 (s, 2 H, C-NH), 2.77 (m, 3 H, HN-CH<sub>3</sub>), 2.15 (s, 3 H, N=C-CH<sub>3</sub>), 2.12 (s, 3 H, N=C-CH<sub>3</sub>). **<sup>13</sup>C {<sup>1</sup>H} NMR** (DMSO-*d*<sub>6</sub>, 100 MHz):  $\delta$  = 178.47 (C-S), 144.60 (C=N), 29.72 (HN-CH<sub>3</sub>), 14.46 (N=C-CH<sub>3</sub>). **IR (neat):**  $\text{cm}^{-1}$  = 3464 (w), 3404 (w), 3352 (m), 3277 (w), 3134 (m), 1628 (m), 1607 (w), 1547 (m), 1516 (m), 1487 (m), 1431 (s), 1396 (s), 1375 (s), 1315 (m), 1300 (m), 1223 (s), 1184 (m), 1153 (m), 1094 (m), 1057 (m), 999 (m), 982 (m), 831 (s), 727 (s), 696 (m), 654 (m), 588 (m), 522 (m), 501 (m), 444 (s). **Raman (neat), laser = 632.81 nm:**  $\text{cm}^{-1}$  = 3351 (w), 2927 (w), 1614 (w), 1538 (s), 1483 (s), 1454 (w), 1425 (w), 1317 (m), 1302 (m), 1264 (w), 1236 (m), 1192 (m), 999 (w), 831 (w), 785 (w), 718 (w), 653 (w), 593 (w), 450 (w), 394 (w), 325 (m), 290 (w). **UV-Vis absorptions:**  $\lambda_{\text{max}}/\text{nm}$  (DMSO) 312 ( $\epsilon/\text{dm}^3 \text{mol}^{-1} \text{cm}^{-1}$  13 900) and 432 (12 800).

### Zinc bis(thiosemicarbazone) complexes with Me/Et on the backbone

#### Zn-PDO-NH<sub>2</sub>-NH<sub>2</sub>

**<sup>1</sup>H NMR** (DMSO-*d*<sub>6</sub>, 400 MHz):  $\delta$  = 6.86 (d, 4 H, C-NH), 2.63 (q, 2H, C-CH<sub>2</sub>, J = 7.2 Hz), 2.14 (s, 3 H, N=C-CH<sub>3</sub>), 0.99 (t, 3 H, C-CH<sub>2</sub>-CH<sub>3</sub>, J = 7.2 Hz). **<sup>13</sup>C {<sup>1</sup>H} NMR** (DMSO-*d*<sub>6</sub>, 100 MHz):  $\delta$  = 178.75 (C-S),

178.50 (C-S), 149.17 (C=N), 144.13 (C=N), 20.83 (C-CH<sub>2</sub>), 14.21 (N=C-CH<sub>3</sub>), 11.34 (C-CH<sub>2</sub>-CH<sub>3</sub>). **IR (neat)**: cm<sup>-1</sup>= 3294 (w), 3165 (w), 2974 (w), 1630 (w), 1599 (m), 1537 (w), 1416 (s), 1323 (m), 1298 (m), 1242 (w), 1204 (m), 1175 (m), 1144 (m), 1043 (m), 943 (m), 874 (m), 837 (m), 789 (m), 706 (s), 588 (m), 536 (m), 469 (m). **Raman (neat), laser = 632.81 nm**: cm<sup>-1</sup>= 1618 (w), 1537 (s), 1454 (w), 1325 (w), 1295 (m), 1243 (w), 1208 (w), 1183 (m), 1025 (w), 995 (w), 946 (w), 789 (w), 708 (w), 591 (w), 390 (w), 307 (w), 242 (w), 219 (w). **Elemental analysis**: Found: **C**, 27.3; **H**, 4.0; **N**, 26.9. Calc. for Zn<sub>1</sub>C<sub>7</sub>H<sub>12</sub>N<sub>6</sub>S<sub>2</sub>: **C**, 27.15; **H**, 3.9; **N**, 27.1%. **UV-Vis absorptions**: λ<sub>max</sub>/nm (DMSO) 312 (ε/dm<sup>3</sup> mol<sup>-1</sup> cm<sup>-1</sup> 12 000) and 438 (10 000).

#### Zn-PDO-NH<sub>2</sub>-Me

**<sup>1</sup>H NMR** (DMSO-*d*<sub>6</sub>, 400 MHz): δ= 7.18 (s, 1 H, C-NH), 6.87 (s, 2 H, H<sub>3</sub>C-NH), 2.77 (m, 3 H, HN-CH<sub>3</sub>), 2.64 (q, 2H, C-CH<sub>2</sub>, J= 7.6 Hz), 2.13 (s, 3 H, N=C-CH<sub>3</sub>), 1.00 (t, 3 H, C-CH<sub>2</sub>-CH<sub>3</sub>, J=7.6 Hz). **<sup>13</sup>C {<sup>1</sup>H} NMR** (DMSO-*d*<sub>6</sub>, 100 MHz): δ= 178.47 (C-S), 144.04 (C=N), 29.79 (HN-CH<sub>3</sub>), 20.93 (C-CH<sub>2</sub>), 14.22 (N=C-CH<sub>3</sub>), 10.83 (C-CH<sub>2</sub>-CH<sub>3</sub>). **IR (neat)**: cm<sup>-1</sup>= 3445 (w), 3399 (w), 3275 (w), 3140 (w), 2972 (w), 2928 (w), 1624 (w), 1605 (w), 1541 (m), 1489 (m), 1425 (s), 1395 (s), 1333 (m), 1294 (m), 1231 (m), 1204 (m), 1180 (m), 1148 (m), 1098 (m), 1059 (m), 953 (m), 841 (m), 787 (m), 772 (m), 723 (m), 646 (m), 621 (m), 596 (m), 532 (m), 501 (m), 459 (m), 415 (s). **Raman (neat), laser = 632.81 nm**: cm<sup>-1</sup>= 3446 (w), 2972 (w), 2923 (w), 1611 (w), 1538 (m), 1492 (s), 1426 (w), 1397 (w), 1331 (w), 1298 (w), 1244 (w), 1233 (w), 1206 (w), 1184 (w), 1153 (w), 1083 (w), 989 (w), 954 (w), 840 (w), 783 (w), 594 (w), 429 (w), 396 (w), 328 (w), 244 (w). **Elemental analysis**: Found: **C**, 29.8; **H**, 4.5; **N**, 25.9. Calc. for Zn<sub>1</sub>C<sub>8</sub>H<sub>14</sub>N<sub>6</sub>S<sub>2</sub>: **C**, 29.7; **H**, 4.4; **N**, 26.0%. **UV-Vis absorptions**: λ<sub>max</sub>/nm (DMSO) 314 (ε/dm<sup>3</sup> mol<sup>-1</sup> cm<sup>-1</sup> 13 900) and 436 (12 800). **Mass spectrometry (ESI)**: *m/z* (Calc.) 323.0102 (323.0091) {M + H<sup>+</sup>}.

#### Zn-PDO-NH<sub>2</sub>-(Me)<sub>2</sub>

**<sup>1</sup>H NMR** (DMSO-*d*<sub>6</sub>, 400 MHz): δ= 6.87 (s, 2 H, C-NH), 3.15 (s, 6 H, N-(CH<sub>3</sub>)<sub>2</sub>), 2.66 (q, 2H, C-CH<sub>2</sub>, J= 7.6 Hz), 2.14 (s, 3 H, N=C-CH<sub>3</sub>), 1.02 (t, 3 H, C-CH<sub>2</sub>-CH<sub>3</sub>, J=7.6 Hz). **<sup>13</sup>C {<sup>1</sup>H} NMR** (DMSO-*d*<sub>6</sub>, 100 MHz): δ= 178.40 (C-S), 178.31 (C-S), 149.70 (C=N), 144.23 (C=N), 20.96 (C-CH<sub>2</sub>), 14.20 (N=C-CH<sub>3</sub>), 10.71 (C-CH<sub>2</sub>-CH<sub>3</sub>). **IR (neat)**: cm<sup>-1</sup>= 3418 (w), 3285 (w), 3157 (w), 2922 (w), 1620 (w), 1597 (w), 1539 (m), 1495 (m), 1429 (m), 1391 (s), 1327 (m), 1298 (m), 1265 (s), 1244 (m), 1207 (s), 1169 (m), 1142 (m), 1107 (m), 1053 (m), 949 (m), 905 (s), 839 (m), 785 (m), 745 (m), 700 (m), 669 (m), 617 (m), 588 (m), 482 (s), 461 (s), 432 (s). **Raman (neat), laser = 632.81 nm**: cm<sup>-1</sup>= 3285 (w), 2919 (w), 1603 (w), 1539 (s), 1500 (s), 1457 (m), 1443 (m), 1385 (w), 1367 (w), 1330 (s), 1302 (s), 1266 (w), 1244 (m), 1207 (w), 1174 (w), 1081 (w), 1029 (w), 996 (w), 951 (w), 905 (w), 842 (w), 783 (w), 740 (w), 700 (w), 672 (w), 620 (w), 588 (m), 495 (w), 430 (w), 400 (w), 379 (w), 327 (w), 290 (w), 259



(w). **Elemental analysis:** Found: **C**, 32.1; **H**, 4.7; **N**, 24.75. Calc. for  $Zn_1C_9H_{16}N_6S_2$ : **C**, 32.0; **H**, 4.8; **N**, 24.9%. **UV-Vis absorptions:**  $\lambda_{max}/nm$  (DMSO) 318 ( $\epsilon/dm^3 mol^{-1} cm^{-1}$  12 200) and 446 (13 000).

#### Zn-PDO-NH<sub>2</sub>-Et

**<sup>1</sup>H NMR** (DMSO-*d*<sub>6</sub>, 400 MHz):  $\delta$ = 7.23 (s, 1 H, H<sub>2</sub>C-NH, J= 6.0 Hz), 6.84 (s, 2 H, C-NH), 3.31 (m, 2 H, HN-CH<sub>2</sub>), 2.64 (q, 2H, C-CH<sub>2</sub>, J= 7.6 Hz), 2.14 (s, 3 H, N=C-CH<sub>3</sub>), 1.06 (t, 3 H, N-CH<sub>2</sub>-CH<sub>3</sub>, J=7.6), 1.00 (t, 3 H, C-CH<sub>2</sub>-CH<sub>3</sub>, J=7.6 Hz). **<sup>13</sup>C {<sup>1</sup>H} NMR** (DMSO-*d*<sub>6</sub>, 100 MHz):  $\delta$ = 178.44 (C-S), 144.13 (C=N), 37.56 (HN-CH<sub>2</sub>), 20.95 (C-CH<sub>2</sub>), 15.27 (N-CH<sub>2</sub>-CH<sub>3</sub>), 14.20 (N=C-CH<sub>3</sub>), 11.01 (C-CH<sub>2</sub>-CH<sub>3</sub>). **IR (neat):**  $cm^{-1}$ = 3422 (m), 3285 (w), 3161 (w), 2976 (w), 2932 (w), 2870 (w), 1603 (m), 1541 (m), 1466 (s), 1425 (s), 1383 (m), 1369 (m), 1350 (m), 1329 (m), 1296 (m), 1231 (m), 1204 (s), 1171 (m), 1144 (m), 1059 (m), 951 (m), 783 (m), 723 (m), 656 (w), 530 (w), 442 (s). **Raman (neat), laser = 784.15 nm:**  $cm^{-1}$ = 1614 (m), 1539 (s), 1490 (s), 1468 (m), 1423 (m), 1368 (m), 1350 (m), 1328 (m), 1299 (m), 1243 (m), 1231 (m), 1206 (m), 1178 (m), 1030 (w), 990 (w), 953 (w), 782 (w), 719 (w), 655 (w), 594 (w), 585 (w), 409 (w), 391 (w), 344 (w), 290 (w). **Elemental analysis:** Found: **C**, 32.2; **H**, 4.6; **N**, 24.8. Calc. for  $Zn_1C_9H_{16}N_6S_2$ : **C**, 32.0; **H**, 4.8; **N**, 24.9%. **UV-Vis absorptions:**  $\lambda_{max}/nm$  (DMSO) 314 ( $\epsilon/dm^3 mol^{-1} cm^{-1}$  12 900) and 438 (12 100). **Mass spectrometry (ESI):** *m/z* (Calc.) 337.0276 (337.0248) {M + H<sup>+</sup>}.

#### Zn-PDO-Me-NH<sub>2</sub>

**<sup>1</sup>H NMR** (DMSO-*d*<sub>6</sub>, 400 MHz):  $\delta$ = 7.16 (s, 1 H, H<sub>3</sub>C-NH), 6.88 (s, 2 H, C-NH), 2.78 (m, 3 H, HN-CH<sub>3</sub>), 2.63 (q, 2H, C-CH<sub>2</sub>, J= 7.6 Hz), 2.17 (s, 3 H, N=C-CH<sub>3</sub>), 0.99 (t, 3 H, C-CH<sub>2</sub>-CH<sub>3</sub>, J=7.6 Hz). **<sup>13</sup>C {<sup>1</sup>H} NMR** (DMSO-*d*<sub>6</sub>, 100 MHz):  $\delta$ = 178.76 (C-S), 149.74 (C=N), 29.73 (HN-CH<sub>3</sub>), 20.83 (C-CH<sub>2</sub>), 14.18 (N=C-CH<sub>3</sub>), 11.36 (C-CH<sub>2</sub>-CH<sub>3</sub>). **IR (neat):**  $cm^{-1}$ = 3242 (m), 3103 (m), 2967 (w), 1643 (m), 1547 (m), 1508 (m), 1435 (s), 1366 (s), 1327 (s), 1283 (s), 1242 (m), 1204 (s), 1180 (s), 1148 (s), 1096 (m), 1074 (s), 1030 (s), 943 (s), 839 (m), 799 (m), 745 (m), 698 (m), 658 (s), 611 (s), 584 (s), 530 (s), 465 (s). **Raman (neat), laser = 632.81 nm:**  $cm^{-1}$ = 3252 (w), 1607 (w), 1545 (w), 1508 (s), 1430 (w), 1379 (w), 1327 (w), 1288 (m), 1243 (m), 1206 (w), 1186 (w), 1031 (w), 984 (w), 943 (w), 843 (w), 799 (w), 701 (w), 591 (w), 525 (w), 386 (w), 320 (w), 229 (w). **Elemental analysis:** Found: **C**, 29.7; **H**, 4.3; **N**, 26.0. Calc. for  $Zn_1C_8H_{14}N_6S_2$ : **C**, 29.7; **H**, 4.4; **N**, 26.0%. **Melting point:** >245 °C (decomposed). **UV-Vis absorptions:**  $\lambda_{max}/nm$  (DMSO) 314 ( $\epsilon/dm^3 mol^{-1} cm^{-1}$  12 800) and 436 (11 800). **Mass spectrometry (ESI):** *m/z* (Calc.) 323.0102 (323.0091) {M + H<sup>+</sup>}.

#### Zn-PDO-Et-Et

**<sup>1</sup>H NMR** (DMSO-*d*<sub>6</sub>, 400 MHz):  $\delta$ = 7.21 (s, 2 H, H<sub>2</sub>C-NH), 3.36-3.32 (under water peak, 4 H expected, HN-CH<sub>2</sub>), 2.64 (q, 2H, C-CH<sub>2</sub>, J= 7.2 Hz), 2.16 (s, 3 H, N=C-CH<sub>3</sub>), 1.06 (t, 6 H, N-CH<sub>2</sub>-CH<sub>3</sub>, J=7.2), 1.01 (t, 3 H, C-CH<sub>2</sub>-CH<sub>3</sub>, J=7.2 Hz). **<sup>13</sup>C {<sup>1</sup>H} NMR** (DMSO-*d*<sub>6</sub>, 100 MHz):  $\delta$ = 37.48 (HN-CH<sub>2</sub>),

20.95 (C-CH<sub>2</sub>), 15.29 (N-CH<sub>2</sub>-CH<sub>3</sub>), 14.12 (N=C-CH<sub>3</sub>), 11.02 (C-CH<sub>2</sub>-CH<sub>3</sub>). **IR (neat):** cm<sup>-1</sup>= 3429 (w), 3296 (m), 2970 (w), 2932 (w), 2872 (w), 1539 (w), 1516 (m), 1429 (s), 1325 (m), 1258 (m), 1223 (m), 1202 (s), 1140 (m), 1092 (m), 1020 (m), 951 (m), 833 (m), 802 (m), 575 (m). **Raman (neat), laser = 632.81 nm:** cm<sup>-1</sup>= 3294 (w), 2928 (w), 2879 (w), 1611 (w), 1539 (s), 1487 (s), 1469 (m), 1435 (w), 1373 (w), 1354 (w), 1328 (m), 1229 (s), 1205 (w), 1166 (w), 1093 (w), 1027 (w), 996 (w), 958 (w), 807 (w), 774 (w), 591 (w), 479 (w), 410 (w), 323 (w), 299 (w). **Elemental analysis:** Found: **C**, 36.1; **H**, 5.5; **N**, 23.1. Calc. for Zn<sub>1</sub>C<sub>11</sub>H<sub>20</sub>N<sub>6</sub>S<sub>2</sub>: **C**, 36.1; **H**, 5.5; **N**, 23.0%. **UV-Vis absorptions:** λ<sub>max</sub>/nm (DMSO) 316 (ε/dm<sup>3</sup> mol<sup>-1</sup> cm<sup>-1</sup> 13 600) and 440 (13 800). **Mass spectrometry (ESI):** m/z (Calc.) 365.0583 (365.0561) {M + H<sup>+</sup>}.

#### **Zn-PDO-Et-NH<sub>2</sub>**

**<sup>1</sup>H NMR** (DMSO-*d*<sub>6</sub>, 400 MHz): δ= 7.14 (s, 1 H, H<sub>2</sub>C-NH), 6.75 (s, 2 H, C-NH), 3.31 (m, 2 H, HN-CH<sub>2</sub>), 2.61 (q, 2H, C-CH<sub>2</sub>, J= 7.2 Hz), 2.15 (s, 3 H, N=C-CH<sub>3</sub>), 1.05 (t, 3 H, N-CH<sub>2</sub>-CH<sub>3</sub>, J=7.2), 0.97 (t, 3 H, C-CH<sub>2</sub>-CH<sub>3</sub>, J=7.2 Hz). **<sup>13</sup>C {<sup>1</sup>H} NMR** (DMSO-*d*<sub>6</sub>, 100 MHz): δ= 178.63 (C-S), 149.70 (C=N), 37.48 (HN-CH<sub>2</sub>), 20.83 (C-CH<sub>2</sub>), 15.13 (N-CH<sub>2</sub>-CH<sub>3</sub>), 14.12 (N=C-CH<sub>3</sub>), 11.31 (C-CH<sub>2</sub>-CH<sub>3</sub>). **IR (neat):** cm<sup>-1</sup>= 3424 (w), 3283 (w), 3163 (w), 2978 (w), 2870 (w), 1603 (m), 1543 (m), 1477 (m), 1466 (m), 1425 (s), 1371 (m), 1329 (m), 1298 (m), 1258 (m), 1233 (m), 1204 (s), 1171 (m), 1146 (m), 1022 (m), 945 (m), 839 (m), 802 (m), 775 (m), 725 (m), 654 (m), 588 (m), 538 (m), 438 (s), 432 (s). **Raman (neat), laser = 784.15 nm:** cm<sup>-1</sup>= 1614 (w), 1541 (s), 1492 (s), 1465 (w), 1423 (w), 1372 (w), 1355 (w), 1327 (w), 1303 (w), 1259 (w), 1234 (m), 1204 (m), 1156 (w), 1023 (w), 999 (w), 947 (w), 839 (w), 803 (w), 777 (w), 719 (w), 589 (w), 412 (w), 382 (w), 320 (w), 287 (w). **Elemental analysis:** Found: **C**, 31.7; **H**, 4.7; **N**, 24.7. Calc. for Zn<sub>1</sub>C<sub>9</sub>H<sub>16</sub>N<sub>6</sub>S<sub>2</sub>: **C**, 32.0; **H**, 4.8; **N**, 24.9%. **UV-Vis absorptions:** λ<sub>max</sub>/nm (DMSO) 314 (ε/dm<sup>3</sup> mol<sup>-1</sup> cm<sup>-1</sup> 13 900) and 436 (12 800). **Mass spectrometry (ESI):** m/z (Calc.) 337.0245 (337.0248) {M + H<sup>+</sup>}.

### **3.3.4. Spectral examples of zinc bis(thiosemicarbazone) complexes**

#### **Zn-PADA-Et-(Me)<sub>2</sub>**

Figure 3.3.4.1-5. shows a <sup>1</sup>H and <sup>13</sup>C NMR, FTIR, Raman and mass spectrum of the complex Zn-PADA-Et-(Me)<sub>2</sub>.

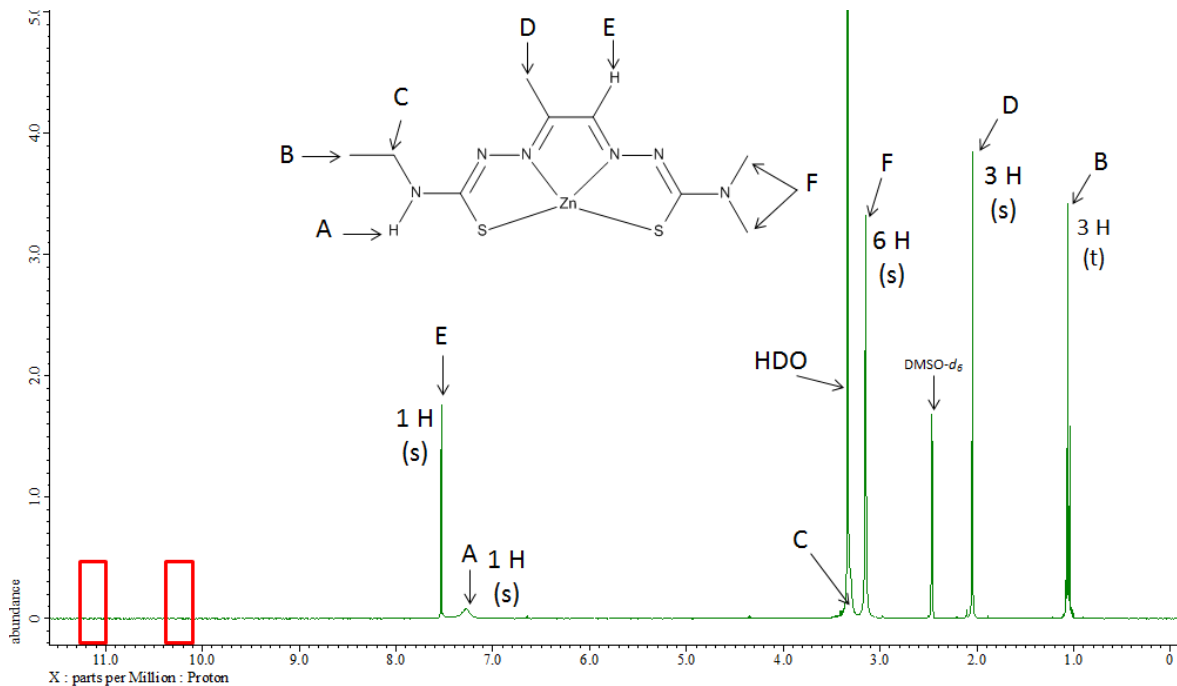


**Figure 3.3.4.1.** An assigned proton NMR spectrum of the complex  $\text{Zn-PADA-Et-(Me)}_2$ . The red boxes illustrates the location of the N-N-H protons would be if there was any PADA-Et-(Me)<sub>2</sub> ligand present. Environment C is located underneath the water peak, this has been shown with other complexes where a HMQC NMR spectrum has been acquired, this has been covered in more detail the discussion section.

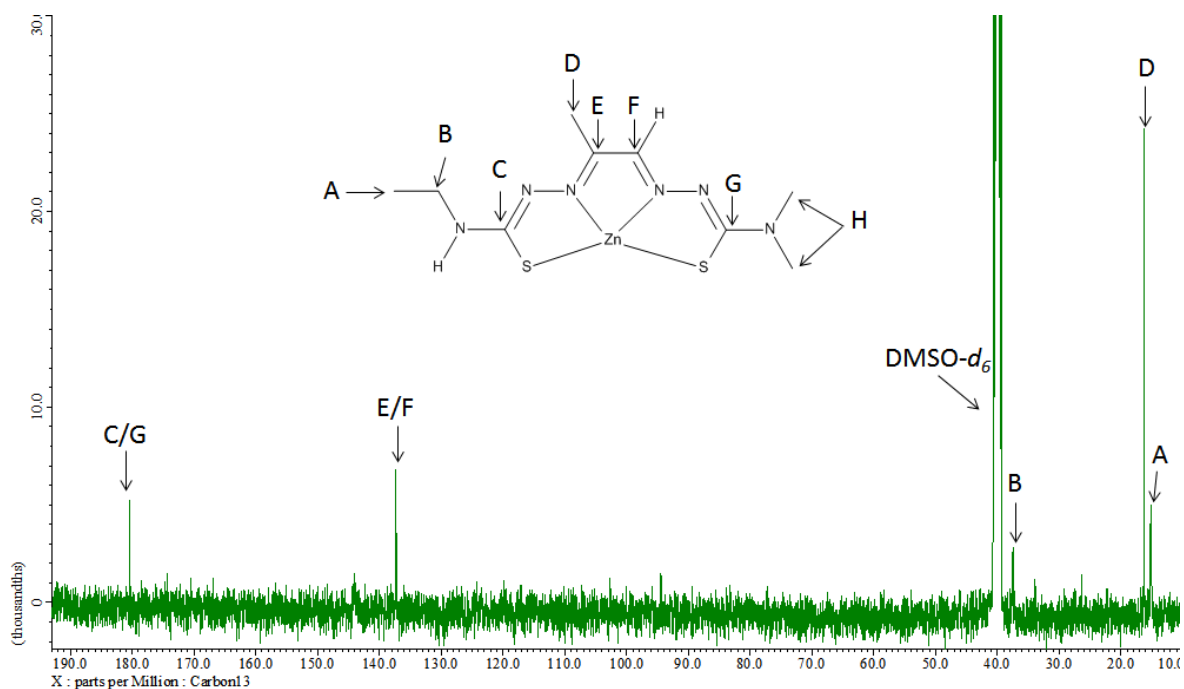


**Figure 3.3.4.2.** An assigned carbon NMR spectrum of the complex  $\text{Zn-PADA-Et-(Me)}_2$ . It is believed that environment H is not visible because the signal is particularly weak, instead of it being completely absent or under the DMSO- $d_6$  solvent peak. It is unclear if the peaks at 180.44 ppm and 137.31 ppm are both or one of environments C/G and E/F respectively.

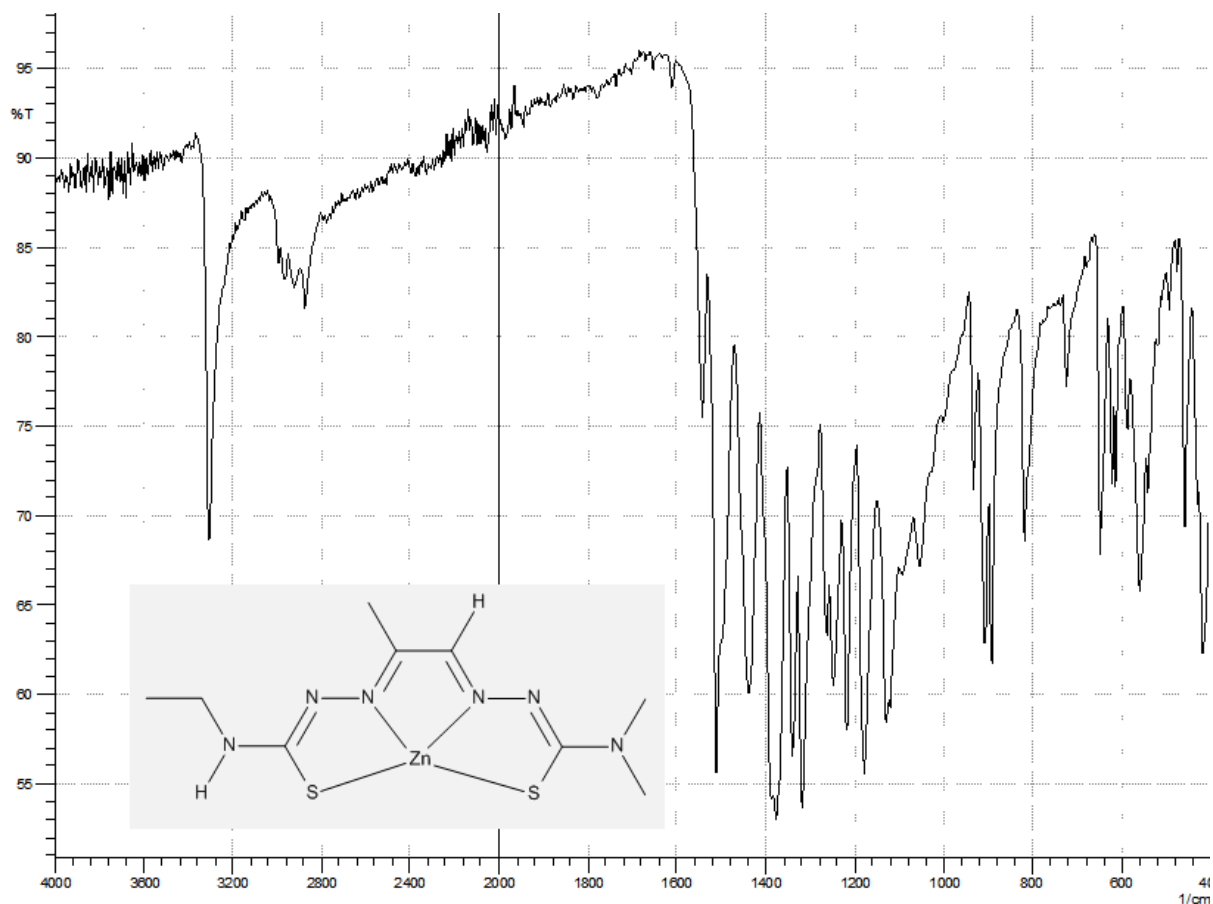


**Figure 3.3.4.3.** A FTIR spectrum of the complex  $\text{Zn-PADA-Et-(Me)}_2$ . This complex was synthesised by reacting  $\text{PADA-Et-(Me)}_2$  with zinc (II) acetate in refluxing ethanol.

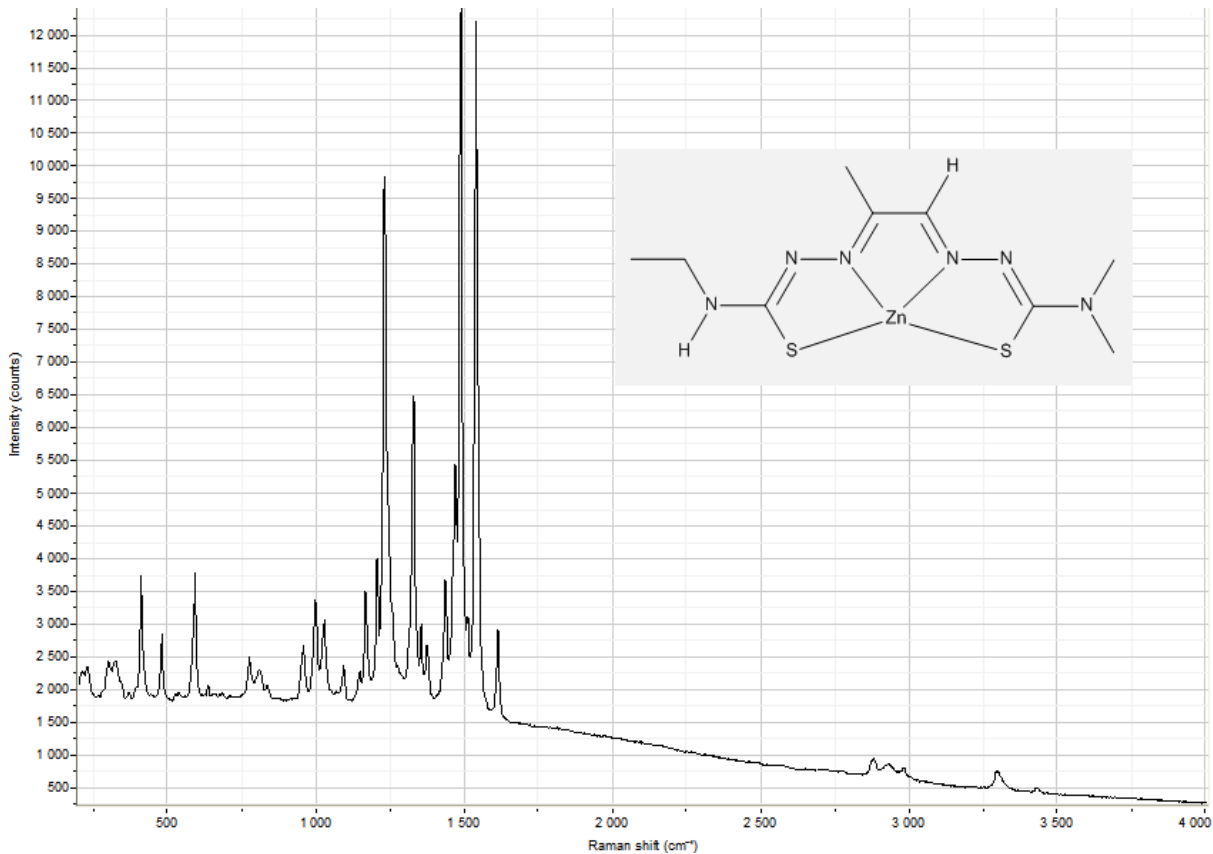


**Figure 3.3.4.4.** A Raman spectrum of the complex  $\text{Zn-PADA-Et-(Me)}_2$ .

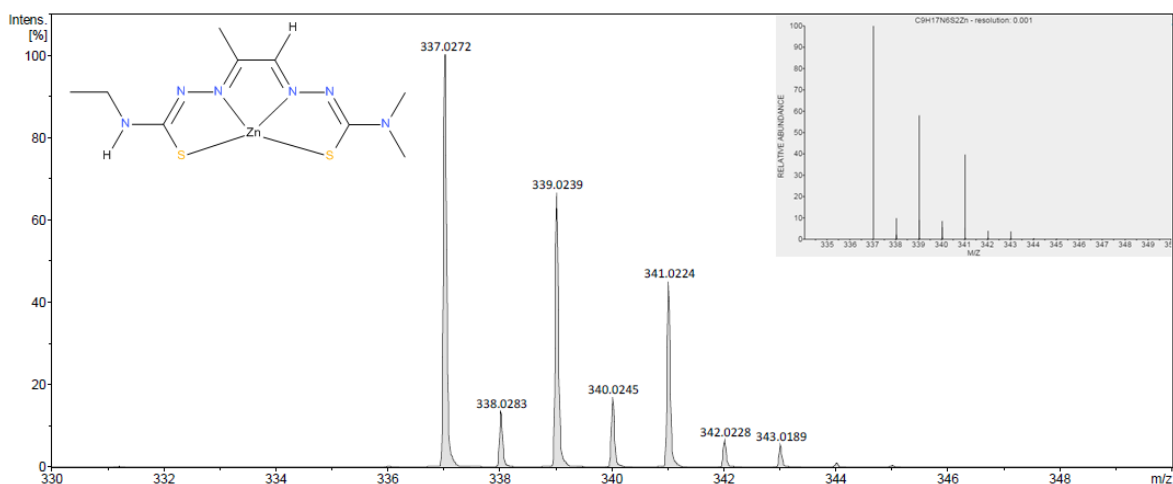


**Figure 3.3.4.5.** A mass spectrum of Zn-PADA-Et-(Me)<sub>2</sub>. The spectrum in the top right hand corner is the predicted expected spectrum of the M + H<sup>+</sup> ion of Zn-PADA-Et-(Me)<sub>2</sub> generated by ChemCalc.<sup>213</sup>

### Zn-PDO-NH<sub>2</sub>-Et

Figure 3.3.4.6-11. shows a <sup>1</sup>H, <sup>13</sup>C and HMQC NMR, FTIR, Raman and mass spectrum of the complex Zn-PDO-NH<sub>2</sub>-Et.

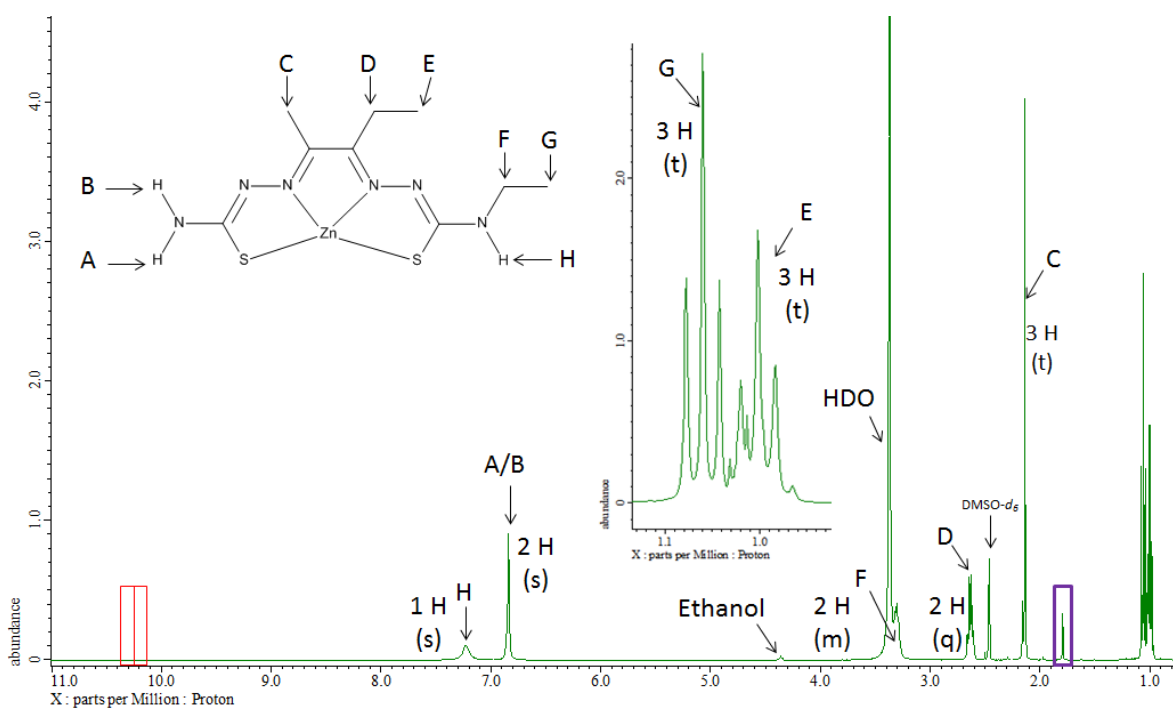


**Figure 3.3.4.6.** An assigned proton NMR spectrum of the complex Zn-PDO-NH<sub>2</sub>-Et. The red boxes illustrate the location of the N-N-H protons would be if there was any PDO-NH<sub>2</sub>-Et ligand present. Environment F is overlapped by the water peak, this has been shown with the HMQC NMR spectrum below (Figure 3.3.4.3.). The purple box shows the presence of an extra peak, which is thought to be due to some acetate forming part of the complex, this is discussed further in unexpected results.

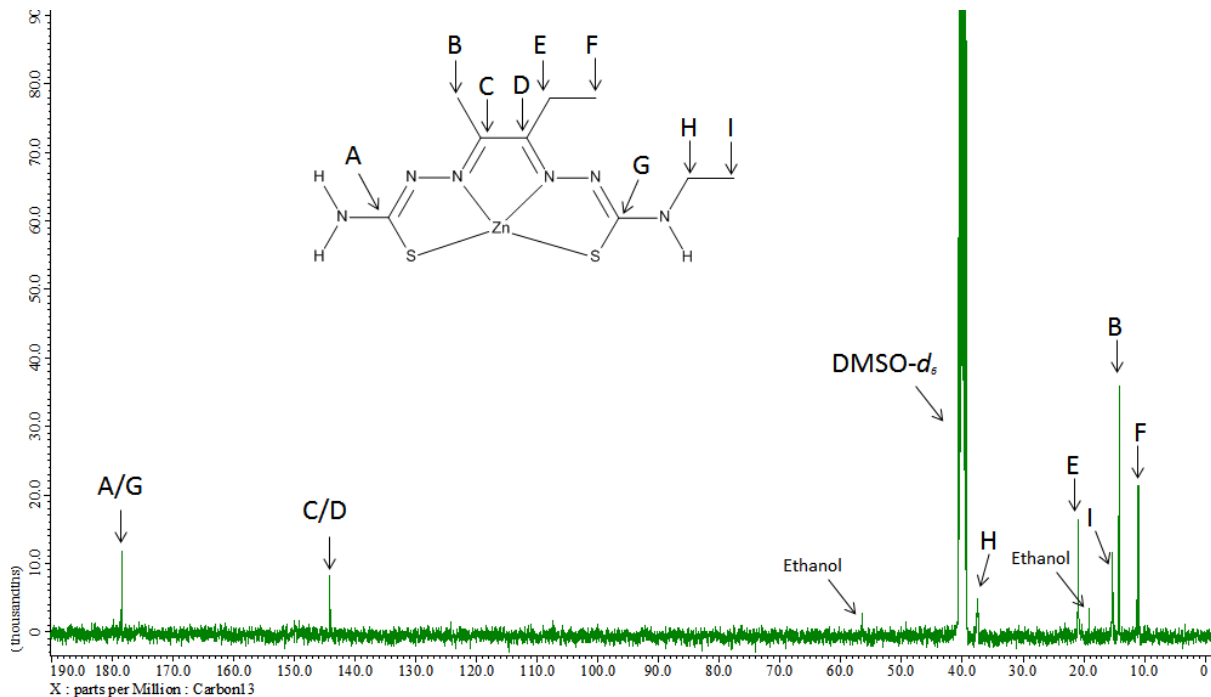


**Figure 3.3.4.7.** An assigned carbon NMR spectrum of the complex Zn-PDO-NH<sub>2</sub>-Et.

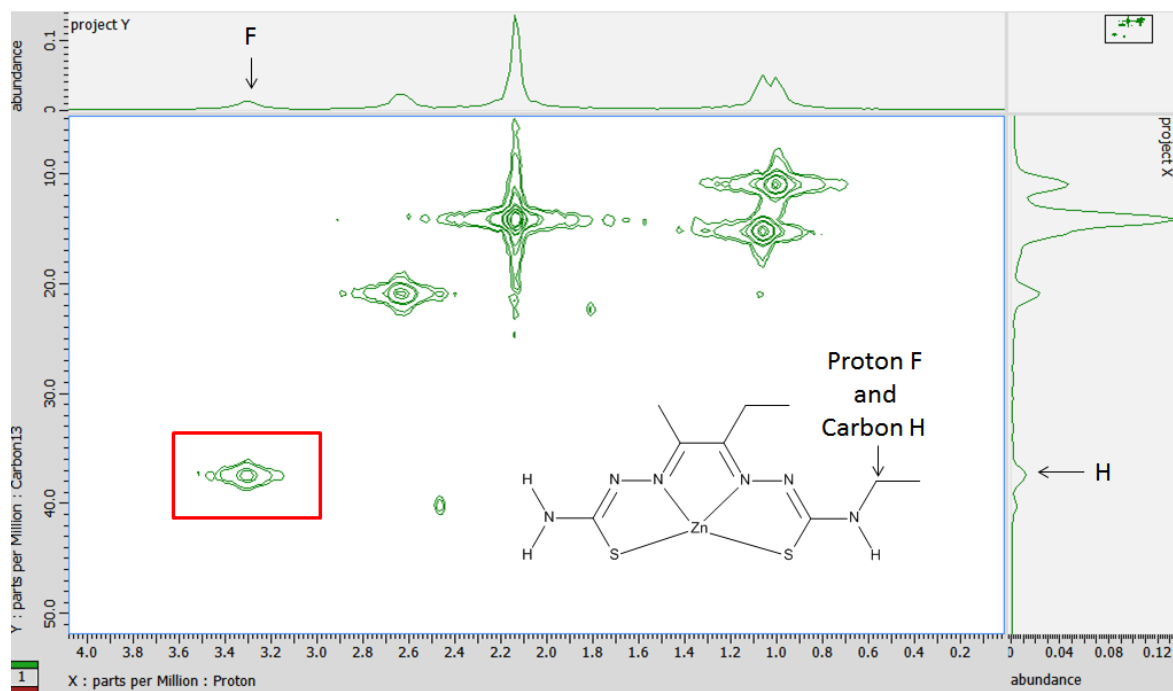


**Figure 3.3.4.8.** A HMQC NMR spectrum of the complex Zn-PDO-NH<sub>2</sub>-Et. The red box highlights the coupling between the carbon environment H to the hydrogen environment F which is very close to the position where a water peak would be. This shows that the signal for proton will be found underneath the water peak.

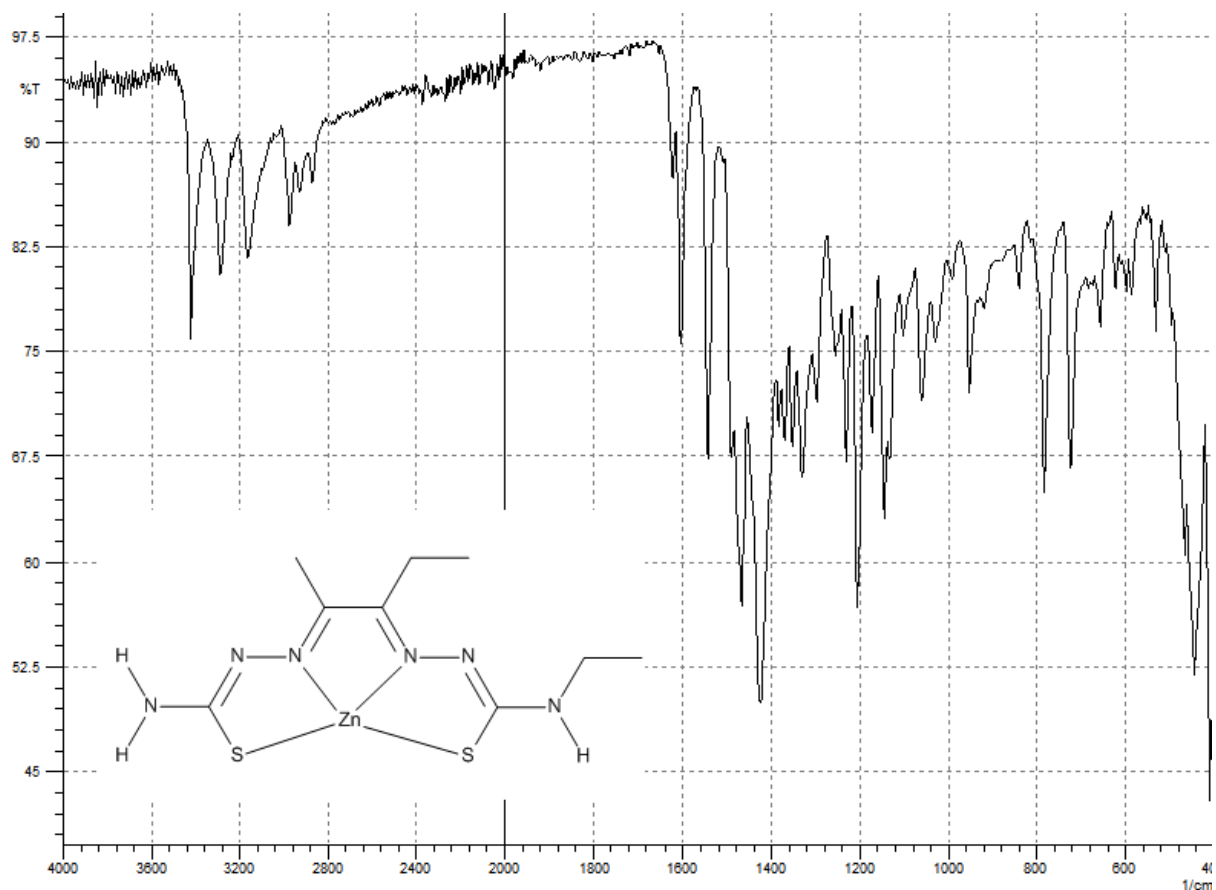


**Figure 3.3.4.9.** A FTIR spectrum of the complex Zn-PDO-NH<sub>2</sub>-Et. This complex was produced by reacting PDO-NH<sub>2</sub>-Et with zinc (II) acetate in refluxing ethanol.

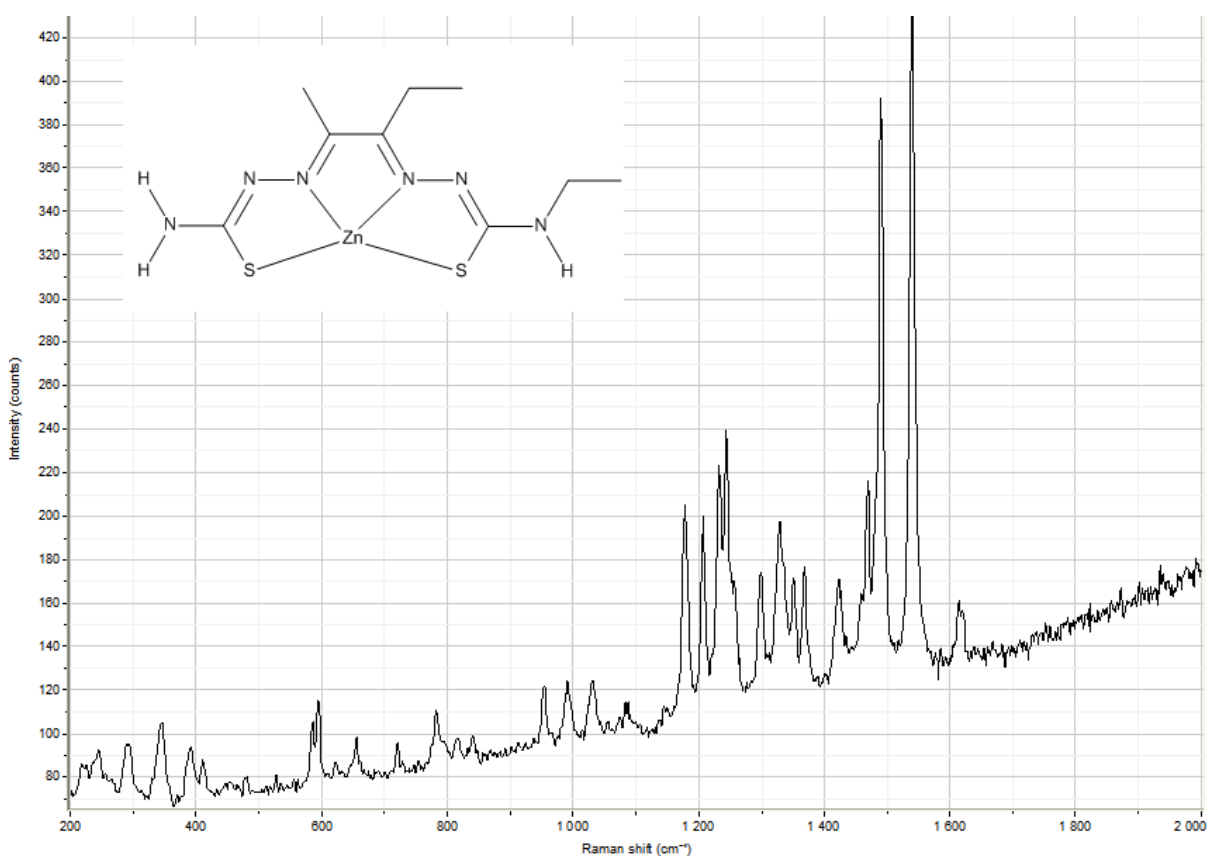


**Figure 3.3.4.10.** A Raman spectrum of the complex Zn-PDO-NH<sub>2</sub>-Et.

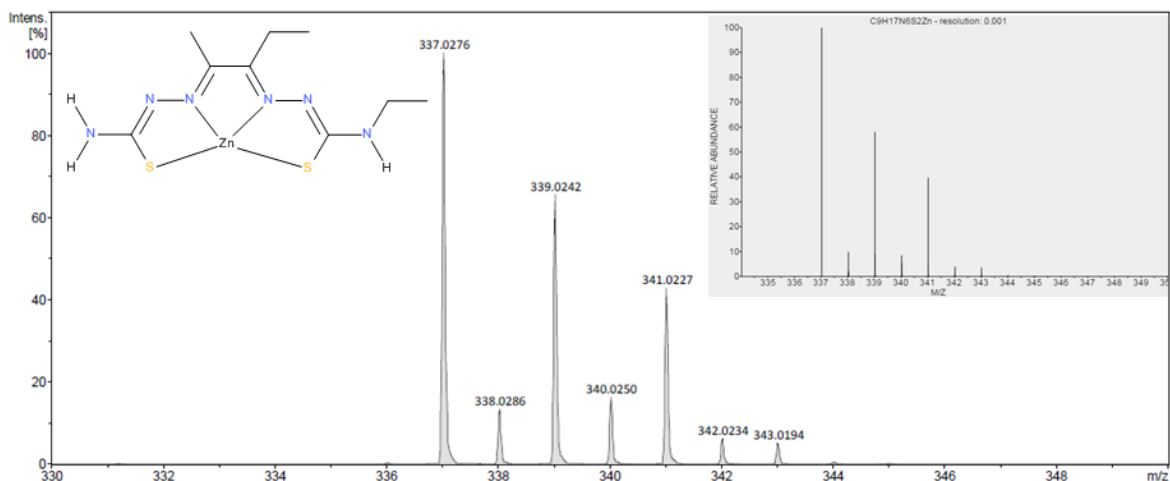


**Figure 3.3.5.11.** A mass spectrum of Zn-PDO-NH<sub>2</sub>-Et. The spectrum in the top right hand corner is the predicted expected spectrum of the  $M + H^+$  ion of Zn-PDO-NH<sub>2</sub>-Et generated by ChemCalc.<sup>213</sup>

### 3.3.5. Discussion

All the zinc bis(thiosemicarbazone) complex forming reactions produced yellow or orange solids with yields that on the whole were slightly poorer than the yields for the copper bis(thiosemicarbazone) complexes, but they were still acceptable. The majority of the complexes yields where in the range of 30-70%. The entire range of yields experienced was 9-85%. The main factor that seems to dictate the yield is the lipophilicity of the resulting complex, which would dictate how readily the complex will dissolve in boiling ethanol. There seems to be a rough correlation between the complexes with lipophilic substituents on the backbone or side arms and lower reaction yields. If in future it became desirable to improve the reaction yields, it may be possible to improve these yields by using an alternative reaction solvent that is slightly less lipophilic, for example methanol. This may increase the yield of the more lipophilic complexes but may reduce the yields of the more hydrophilic complexes.

As zinc is diamagnetic, it was possible to use NMR in order to analyse if the zinc complex had been successfully synthesised. The Zn-BDO-Me-Me NMR data obtained closely matches to the data reported by J. Holland *et al.*<sup>91</sup> Some problems were encountered during the analysis of the resulting complexes. In the proton spectra it was observed that most of the peaks experienced a chemical shift as well as some broadening of the peaks which in some cases caused the expected splitting pattern to be obscured. It was found that the proton peak from the CH<sub>2</sub> group from the ethyl substituent on the side arm was often shifted to a lower chemical shift so that the peak was situated fully or partially underneath the proton peak of water as shown in figures 3.3.4.6. and 3.3.4.7. The example of a peak of GLY-Et-Et being obscured by the water peak was also reported by P. Donnelly *et al.*<sup>76</sup>



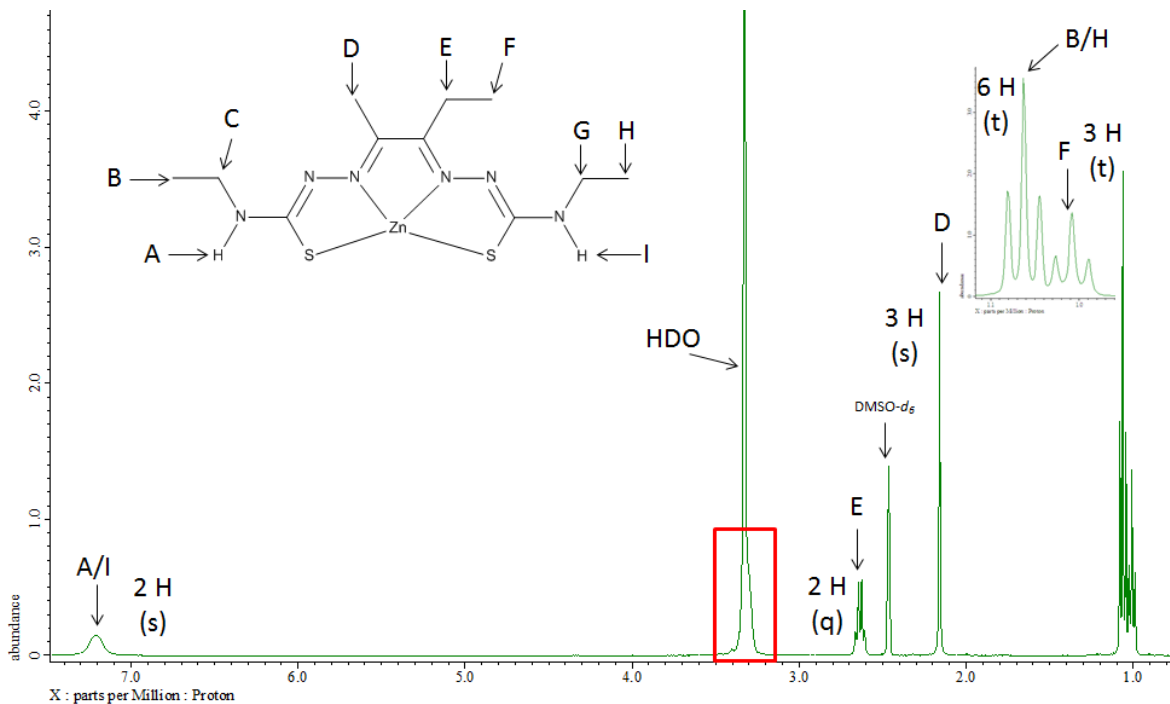


**Figure 3.3.4.6.** An assigned proton NMR spectrum of the complex Zn-PDO-Et-Et. The red box illustrates that the protons environments C and G are expected to be located underneath the water peak at 3.33 ppm.

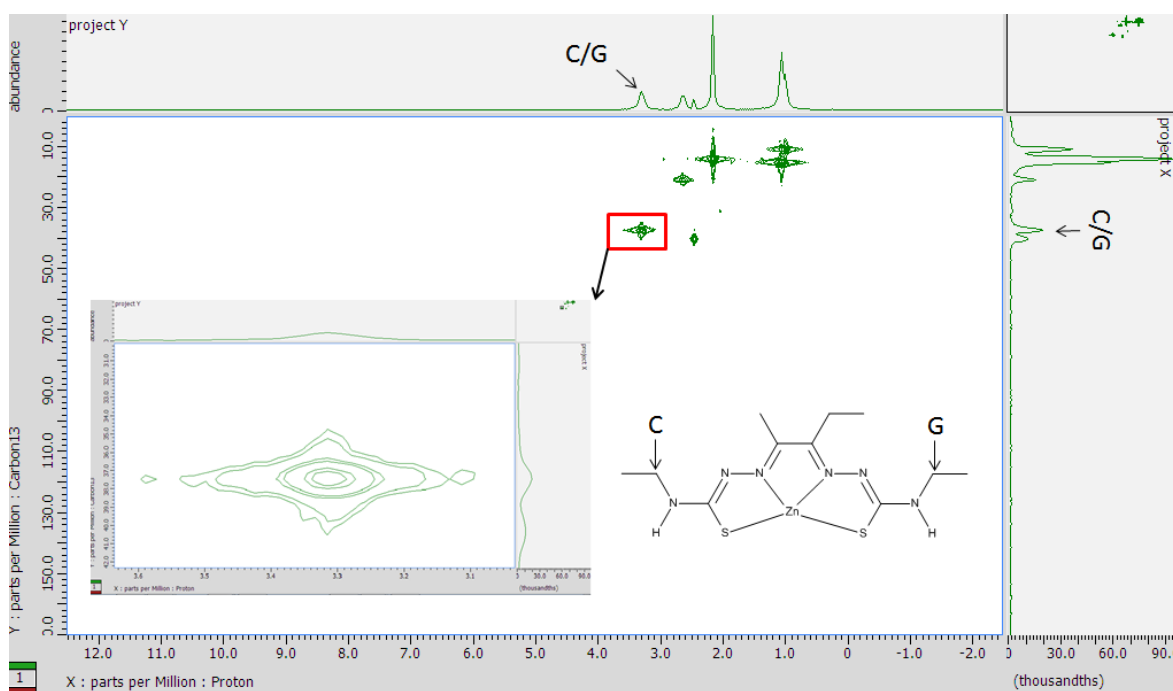


**Figure 3.3.4.7.** A HMQC NMR spectrum of the complex Zn-PDO-Et-Et. The carbon peak found at 37.48 ppm that relates to the carbon environments C and G have a coupling (illustrated by the red box) to the proton peak at 3.32 ppm which is normally were the water peak is found.

A similar problem was sometimes observed in the carbon spectra of the dimethyl side arm, where the peak was shifted to a lower chemical shift so that it was located underneath the DMSO- $d_6$  solvent peak, an specific example of this would be Zn-BDO-NH<sub>2</sub>-(Me)<sub>2</sub>. It was also noticed that a lot more sample had to be dissolved in order to obtain an acceptable spectrum than if a NMR spectrum was ran of the corresponding ligands. This did not cause much problem in the proton

NMR but caused some peaks in the carbon NMR not to be detected despite dissolving a relatively large amount of sample. This caused some carbon NMR data to not be reported in the characterisation section. When the carbon peak was particularly weak or broad the chemical shifts were only reported to one decimal place instead of two. Carbon environments that were directly bound to a nitrogen atom or a sulphur atom seem to be particularly prone to being too weak to be detected, presumably this is due to the relaxation time of the environments being particularly long. The addition of the relaxation agent chromium(III) acetylacetonate ( $\text{Cr}(\text{acac})_3$ ) was tried in order to see the carbon spectra could be improved. At first only a tip of a micro spatulas worth of  $\text{Cr}(\text{acac})_3$  was added to a sample before analysis, then a second sample with as much  $\text{Cr}(\text{acac})_3$  added as possible was ran. Unfortunately the addition of the chromium(III) acetylacetonate resulted in a weaker carbon spectra on both accounts. A report of the proton NMR spectra of Zn-GLY-Ph-Ph and Zn-Gly-Et-Et was found in the literature<sup>76</sup> were the data very closely agreed with the data obtained in this project.

It was very easy and straight forward to quickly obtain high quality infrared spectra of the zinc complexes when using the Golden Gate Diamond ATR attachment. No previously reported infrared data for zinc bis(thiosemicarbazone) complexes was found. By using data reported on similar copper and nickel complexes<sup>78, 80</sup> and text books on vibrational spectroscopy<sup>207, 208</sup> peaks that are in the regions of  $3470\text{-}3200\text{ cm}^{-1}$ ,  $1550\text{-}1450\text{ cm}^{-1}$ ,  $800\text{-}680\text{ cm}^{-1}$  and  $500\text{-}410\text{ cm}^{-1}$  are likely to correspond to R-N-H, C=N, C-S and Zn-N bonds, respectively.

As with the copper complexes, obtaining suitable Raman spectra of the zinc complexes was not possible by just using one laser. It was found that when analysing the zinc complexes the red (632.81 nm) laser was a good starting point and when the red laser did not give an acceptable spectrum, changing to the near infrared (784.15 nm) laser would normally give an improved spectrum. When the near infrared laser was used the spectrum was only recorded between 200 and  $2000\text{ cm}^{-1}$  because it was observed that very little useful information could be extracted from the spectrum between 2000 and  $4000\text{ cm}^{-1}$ . The majority of zinc complexes gave more than acceptable spectra, with strong sharp peaks and a relatively flat baseline, only a few complexes giving weaker spectra but the majority of these still contained sharp peaks. M. Betts *et al.*<sup>137</sup> reported using Raman spectroscopy for characterising Zn-ATSM (Zn-BDO-Me-Me) for the application of transmetalation (please refer to Chapter 4). Besides this report, it is believed that no comprehensive Raman characterisation data for neither zinc nor copper bis(thiosemicarbazone) complexes has been reported. That Raman spectrum of Zn-ATSM reported by M. Betts and co-workers<sup>137</sup> shows a very strong resemblance to the Raman spectrum of Zn-BDO-Me-Me that was synthesised.

Similarly to the copper complexes, due to the large number of zinc complexes that were synthesised CHN analysis was only run on complexes that were believed to be novel. The first round of CHN analysis was significantly more successful than the copper CHN results with ten out of the eleven coming back with acceptable percentages. It is believed that during the reaction the zinc complexes continuously dissolved and precipitated out of the boiling ethanol, effectively acting as a purification step as well. Two samples show signs of a large presence of what is thought to be an acetate molecule acting as a second ligand, this is explored in section 3.4. below. A preliminary study was carried out with Zn-BDO-Me-Me in order to discover if it was possible to purify the zinc complexes by recrystallisation. A range of solvents mixtures were tried in order to achieve full dissolution of the complexes, these included methanol, ethanol, dichloromethane and dimethyl-sulfoxide. It was found that DMSO, hot ethanol or hot methanol could be used to dissolve the complexes. Warm dichloromethane or warm acetonitrile partially dissolved the complexes, but full dissolution was only achieved on the addition of a few drops of dimethyl-sulfoxide. It was discovered that whilst the complex was relatively easy to get in to solution it was particularly difficult to get the complex to recrystallise out, neither cooling the solutions or adding a solvent that it was perceived the complex would not be soluble in (petroleum spirit 40-60 °C, diethyl ether and water) yielded a successful recrystallisation. About 20 different combinations were tried without success. As most the CHN results came back acceptable and most the NMR spectra showed little or no sign of impurity, the pursuit for a recrystallisation method was discontinued. It is expected that due to the range of solubility zinc bis(thiosemicarbazone) complexes can possess finding a recrystallisation method that is quick, straight forward and that can be applied to the whole range of zinc bis(thiosemicarbazone) complexes will be particularly challenging.

As zinc complexes are able to be analysed by NMR for characterisation purposes and due to the large number of zinc complexes synthesised mass spectrometry was not utilised routinely as a form of characterisation, mass spectra of only a handful of compounds were collected to show that mass spectrometry could be used to aid identification of the zinc complexes. Similarly to the copper complexes both zinc complexes were detected as  $M+H^+$  and were in close agreement to the theoretical  $m/z$  values and isotope pattern as calculated by ChemCalc.<sup>213</sup> Figures 3.3.4.5. and 3.3.4.11. illustrate examples of the mass spectrum of Zn-PADA-Et-(Me)<sub>2</sub> and Zn-PDO-NH<sub>2</sub>-Et respectively. In the top right hand corner of both the spectra is the ChemCalc<sup>213</sup> predicted spectra.

As with the copper complexes, melting point data was taken on a selection of zinc complexes, again the selected complexes were chosen in order to incorporate complexes with a diverse range structural of substituents. Instead of melting all zinc complexes seemed to decompose upon heating. It was observed that when the yellow zinc complexes were heated they would become

darker orange in colour as the temperature increased. If the decomposition temperature had not been reached then on cooling of the sample the colour would revert back to yellow. Due to this effect it was a lot harder to monitor with the complexes that were orange to start with. Upon decomposition the samples would turn to a brownish orange colour and would not revert back to their initial colour when cooled. For the six samples that was analysed this decomposition was observed between 245-310°C. J. Holland et al.<sup>57</sup> also reported that similar zinc complexes decomposed above 230°C.

UV-visible absorption spectra were obtained from DMSO solutions of each of the synthesised zinc bis(thiosemicarbazone) complexes. It was decided to record the spectra from 285-800nm in order to stay outside the absorption range of DMSO. The UV-vis absorption spectra obtained had strong similarity between them. Every spectrum showed two absorptions, the first with maxima between 432-472nm and the second between 308-348nm. The vast majority of the extinction coefficient were found to be around 12,000-14,000  $\text{dm}^3 \text{mol}^{-1} \text{cm}^{-1}$ , with some being as low as 9,500 and others being as high as 23,000. However, there does seem to be a trend that the complex will have a higher extinction coefficient if a phenyl group is present presumably due to the effect of addition conjugation within the complex. One spectrum that seems to lie outside the trend is the spectrum of Zn-Gly-Et-Et while having a maximum absorption at 458nm with an extinction coefficient of 9,700  $\text{dm}^3 \text{mol}^{-1} \text{cm}^{-1}$  which is within the expected range, the second absorption at 328nm which has an extinction coefficient of over 43,600  $\text{dm}^3 \text{mol}^{-1} \text{cm}^{-1}$  which is significantly higher than any other extinction coefficient measured. The only previously reported UV-vis data on zinc bis(thiosemicarbazone) complexes is for Zn-BDO-Me-Me<sup>137</sup> which are in close accord with the experimental data.

### **3.4. Unexpected results**

#### **3.4.1. Acetate ligand**

It was noticed in the NMR spectra of some of the zinc complexes that extra peaks were present. Zn-PADA-Ph-NH<sub>2</sub> and Zn-PADA-BDO-NH<sub>2</sub>-(Me)<sub>2</sub> are complexes with the presence of these extra peaks are the most obvious, however the majority of zinc complexes that were made show no noticeable signs of these extra peaks.

The NMR spectra of Zn-PADA-Ph-NH<sub>2</sub> (Figures 3.4.1.1-3.) illustrate the presence of these extra peaks.

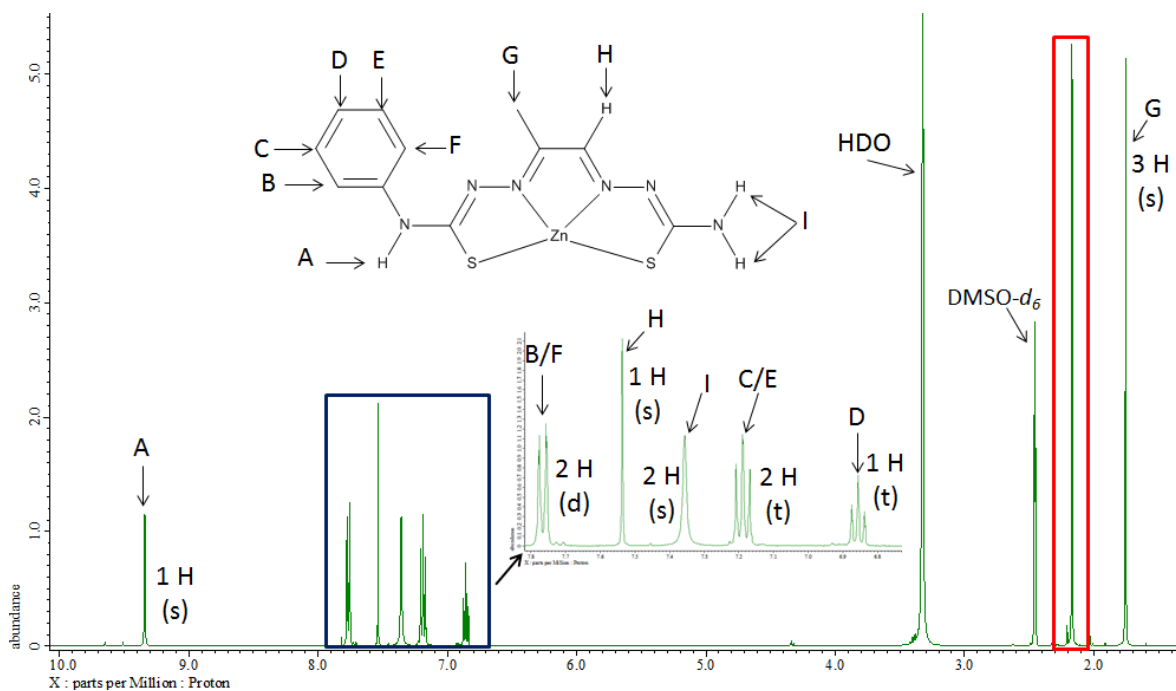


**Figure 3.4.1.1.** An assigned proton NMR spectrum of the complex Zn-PADA-Ph-NH<sub>2</sub>. The red box highlights the extra peak at 1.76 ppm with an integral equal to 3 protons.

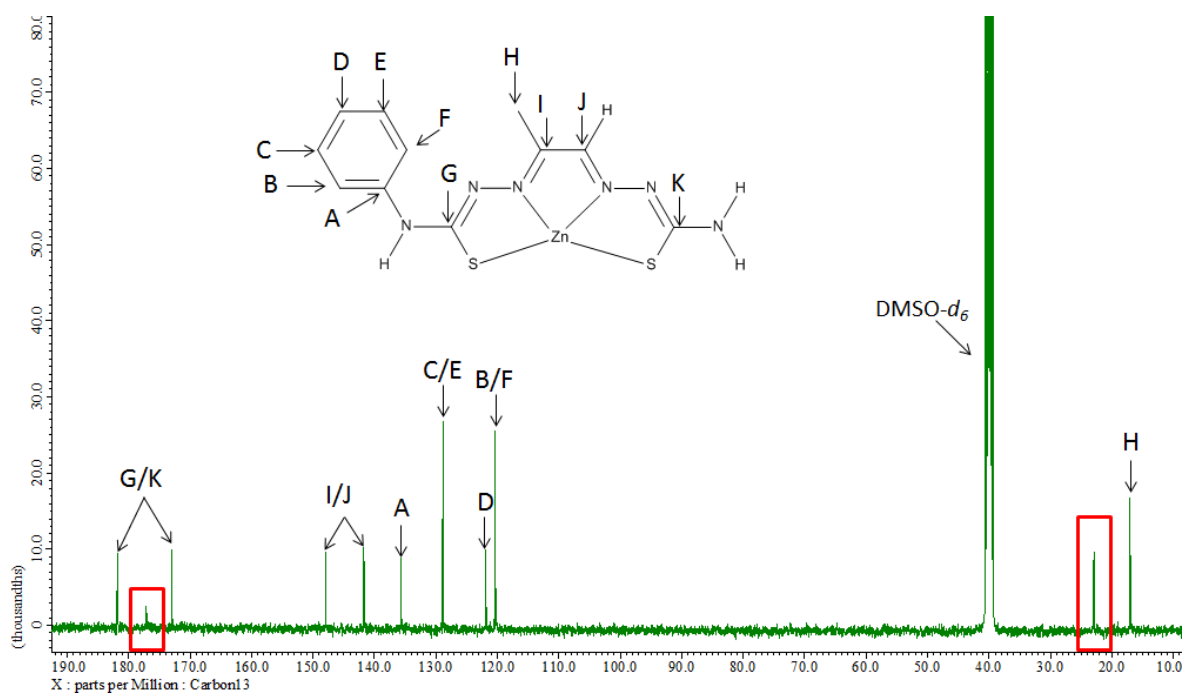


**Figure 3.4.1.2.** An assigned carbon NMR spectrum of the complex Zn-PADA-Ph-NH<sub>2</sub>. The red box highlights the extra peaks at 22.94 and 177.13 ppm.

A HMQC NMR spectrum (Figure 3.4.1.3.) was also run in order to investigate what the new proton and carbon environments are bonded to.

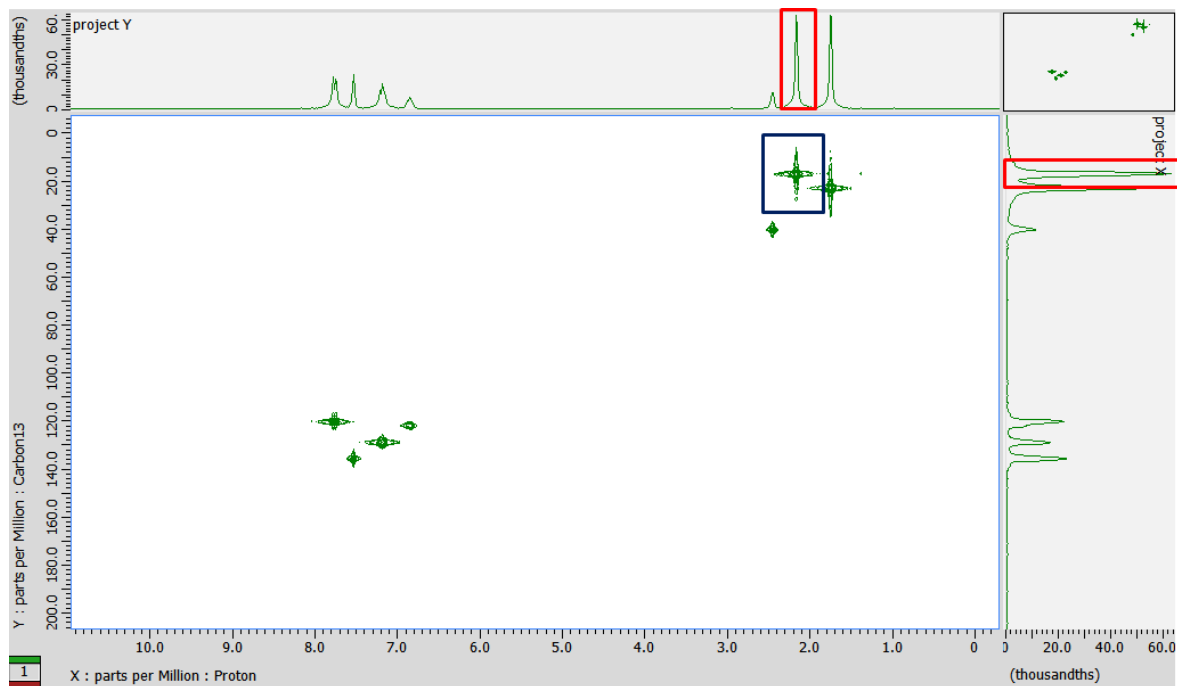


**Figure 3.4.1.3.** A HMQC NMR spectrum of the complex Zn-PADA-Ph-NH<sub>2</sub>. This spectrum is showing that the extra proton peak at 1.76 ppm and carbon peak at 22.94 ppm (red boxes) have a strong coupling (blue box) to each other. There are no other couplings between any other peaks and the new additional peaks.

## Discussion

Based on the evidence from the NMR spectra it is thought that the extra peaks are coming from an acetate ion that is also co-ordinating with the zinc atom. Other possible candidates for the extra ligands based on what is present in the reaction mixture could be ethanol or an ethoxide ion.

The proton NMR spectrum (Figure 3.4.1.1.) shows one extra singlet peak at 1.76 ppm with an integral of 3 protons. The carbon NMR spectrum (Figure 3.4.1.2.) shows two extra peaks at 22.94 ppm and 177.13 ppm and the HMQC spectrum (Figure 3.4.1.3.) confirms that the protons giving rise to the singlet at 1.76 ppm are bound to the carbon giving rise to the peak at 22.94. The NMR spectra therefore suggest that the molecule these extra peaks are arising from has hydrogens attached to a carbon, which by looking at their chemical shifts is likely to be an alkyl group, most possibly a methyl group depending on how much confidence is drawn from the integral of the proton peak. There is also evidence of a second carbon atom which does not seem to have any hydrogen atoms bound to it and due to the large chemical shift of the carbon peak there is a suggestion that the carbon has an electronegative atom attached to it, maybe in the form of a carbonyl group. For comparison a proton and carbon NMR spectra was taken of zinc (II) acetate, the resulting proton spectra contained a singlet at 1.80 ppm and the carbon showed two environments one at 23.05 ppm and the other at 177.47 ppm. All the observations from the NMR spectra supports that the extra ligand is an acetate ion.

Similar observations were observed in the NMR spectra of the complex Zn-BDO-NH<sub>2</sub>-(Me)<sub>2</sub>. A HMBC NMR spectrum (Figure 3.4.1.4) was ran in order to establish if the acetate is coordinated to the zinc or bound to another part of the complex.

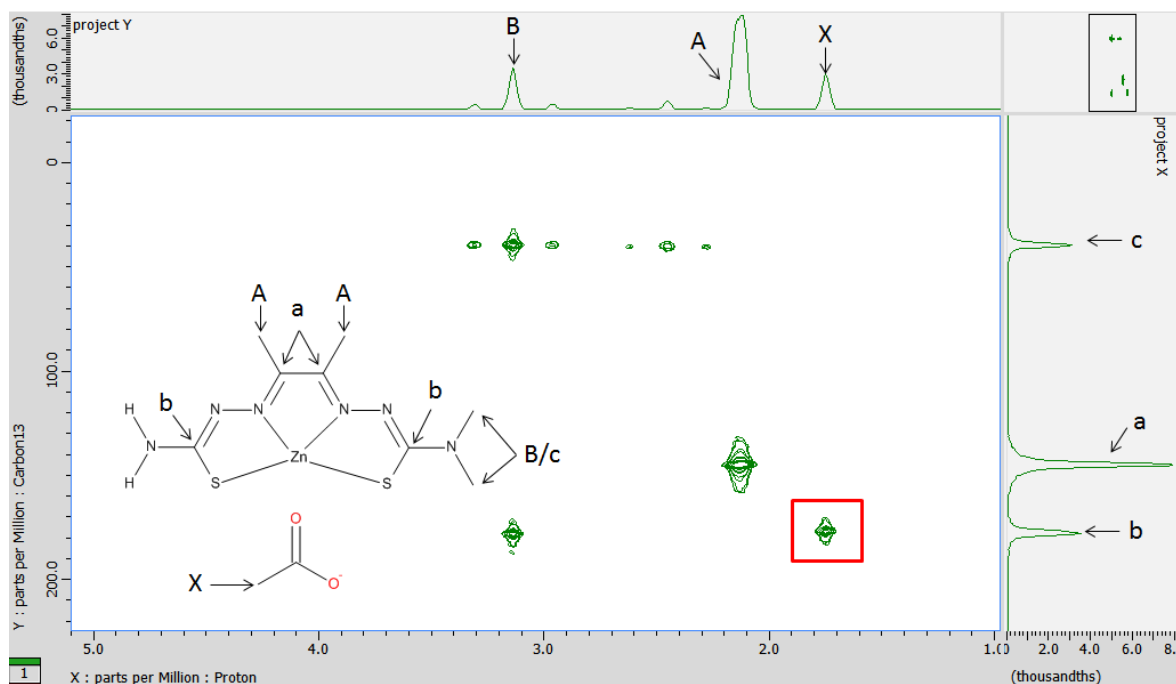


**Figure 3.4.1.4.** A HMBC NMR spectrum of the complex Zn-BDO-NH<sub>2</sub>-(Me)<sub>2</sub>.

At the first instance the HMBC NMR spectrum (Figure 3.4.1.4) of the complex Zn-BDO-NH<sub>2</sub>-(Me)<sub>2</sub> shows that there could be long range coupling between the methyl protons of the acetate ion and the C-S groups of the bis(thiosemicarbazone) ligand suggesting that the acetate may be coordinating directly to the zinc ion. However, if this is the case it is a bit suspicious that a coupling can be seen 6 bonds away and that there is not coupling between the protons at X and the carboxylate carbon environment. It is expected that the carbon environments b, of which in a standard carbon NMR spectrum forms two peaks at 182.16 ppm and 179.35 ppm, cannot be resolved in the HMBC spectrum and hence resemble just one peak. The carboxylate found at 177.47 ppm may also of merged with peak b, so instead of the red box showing a coupling with the acetate ion and the zinc complex it is actually showing the coupling between the X protons and its carboxylate carbon who's peak happens to lie under the peak attributing to carbon environment b.

On consulting the infrared spectra of the complexes that are expected to have the extra acetate ligand there are no obvious extra peaks compared to other zinc complexes. Zinc (II) acetate has acetate ions bound via the acetates oxygen to a Zn<sup>2+</sup> ion,<sup>216</sup> this Zn-O bond is similar to what is expected to be formed in the case of when an acetate molecule acts as a ligand to the zinc bis(thiosemicarbazone) complexes. A reference IR spectrum of zinc (II) acetate gives a strong C=O stretch at 1539cm<sup>-1</sup>, off course once bound to zinc complex the C=O position is expected to shift a

little but this value gives an idea of the rough area of the IR spectrum that the C=O stretch of the acetate compound would arise. The C=O peak was chosen because it is likely that due to its characteristic strong absorbance it would be the environment that would be most visible in the spectra of the Zn complexes. IR spectra of all zinc bis(thiosemicarbazone) complexes contain peaks with wavenumbers in the 1500's to low 1600's. Due to this it was not possible to confirm the presence of the expected acetate group with infrared spectroscopy. Unfortunately neither Zn-PADA-Ph-NH<sub>2</sub> or Zn-BDO-NH<sub>2</sub>-(Me)<sub>2</sub> formed crystalline products meaning X-ray diffraction could not be utilised to gather further information about the products.

In the literature there is evidence that zinc atoms are willing to form complexes with five coordinate bonds.<sup>217</sup> This principle was exploited in a study by H Betts *et al.*<sup>137</sup> for the transmetalation reaction with zinc bis(thiosemicarbazone) complexes with copper to form copper bis(thiosemicarbazone) complexes. This application is explored further in the next Chapter. However, if it is the case that acetate ion has bound to the zinc of the above complexes then the resulting complex would mean that zinc is in the 3+ oxidation state, which is not feasible. If the ligand happens to be singly de-protonated instead of doubly de-protonated then the zinc in the resulting complex would be in the 2+ oxidation state. This extra proton would be visible in the proton NMR spectrum (probably around 9-11 ppm) with an integral of 1 proton but there is no extra proton peak in either of the proton NMR spectra of Zn-PADA-Ph-NH<sub>2</sub> or Zn-BDO-NH<sub>2</sub>-(Me)<sub>2</sub>. An alternative explanation could be that the acetate ion is actually an acetic acid molecule, as acetic acid is neutral this would keep the zinc in the sensible oxidation state of 2+. Unfortunately the spectroscopic data does not support the presence of the acetic acid. The infrared spectra of both samples do not contain a broad O-H peak nor do their NMR proton spectra contain an extra peak around 12 ppm, which would indicate the presence of a hydroxyl group. An acetic acid reference NMR shows that the carboxylate carbon should be present around 172 ppm instead 177 ppm. This coupled with a literature search which failed to identify any previously reported cases of just an acetic acid molecule acting as a ligand to a zinc ion produces doubt that the impurity can be an acetic acid molecule.

To summarise, the spectroscopic data suggests a complex with an extra acetate ligand but which would result in a zinc ion with an unrealistic oxidation state. Whilst an acetic acid ligand would give a sensible oxidation state for zinc but the spectroscopic data does not support the presence of the acetic acid molecule. Within the time frame of this project it has not been possible to definitively identify the possible extra molecule in the samples Zn-PADA-Ph-NH<sub>2</sub> or Zn-BDO-NH<sub>2</sub>-(Me)<sub>2</sub>.



### 3.4.2. Ethanol ligand

The complex Zn-PDO-NH<sub>2</sub>-NH<sub>2</sub> also seems to only be isolated with an impurity, but in this case it is believed that the impurity is an ethanol molecule. The proton and carbon NMR spectra of this complex show a strong presence of peaks attributing to ethanol. The proton NMR integrals of these peaks suggest that the ethanol impurity is about 1:1 ethanol to complex (Figure 3.4.2.1.).

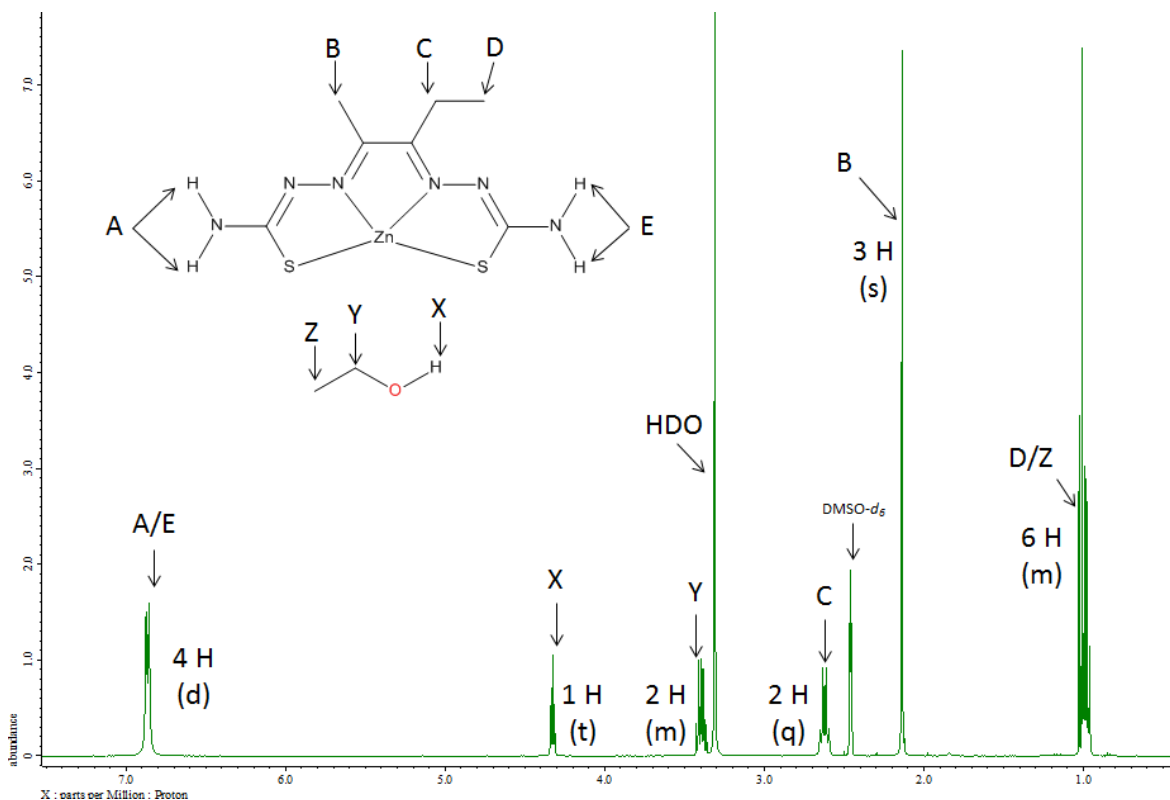


**Figure 3.4.5.1.** An assigned proton NMR spectrum of Zn-PDO-NH<sub>2</sub>-NH<sub>2</sub>. This shows the presence of the extra environments X, Y and Z which are thought to be due to the presence of ethanol.

A second NMR was run on the same sample to ascertain if the ethanol is uniformly spread through the dry solid. The NMR integrals were almost identical to the first NMR integrals which suggest that ethanol is uniformly distributed in the product either as a bound ligand or a co-recrystallized product. The use of HMBC NMR did not show evidence of any coupling to the ethanol molecules and the zinc complex. The IR spectrum of the sample contains peaks at 2974, 1043 and 874 cm<sup>-1</sup> which are close to the peak positions in the ethanol reference spectrum (2972, 1045 and 880 cm<sup>-1</sup>) suggesting that ethanol is present in the sample.

However, despite ethanol consistently being observed by NMR experiments, the CHN analysis results were correct for the complex without an ethanol impurity. It may be the case that during the heating of the sample in the CHN instrumentation the ethanol evaporated off from the sample before the combustion of the sample took place hence giving the result correct for the sample minus any ethanol.

Element	Expected without ethanol (%) (Zn <sub>1</sub> C <sub>7</sub> H <sub>12</sub> N <sub>6</sub> S <sub>2</sub> )	CHN result re- run (%)
Carbon	27.15	27.3
Nitrogen	3.91	4.0
Hydrogen	27.1	26.9

**Table 3.4.5.2.** Expected and obtained CHN results for Zn-PDO-NH<sub>2</sub>-NH<sub>2</sub>.

It is feasible to say that complex Zn-PDO-NH<sub>2</sub>-NH<sub>2</sub> has successfully been synthesised and depending on which analytical method is used, there may also be ethanol as an impurity.

### **3.5. Conclusions**

Bis(thiosemicarbazone) pro-ligands readily chelate with either copper or zinc 2+ ions to form the corresponding bis(thiosemicarbazone) complex. 18 copper complexes and 20 zinc complexes have been successfully synthesised with varying substituents on the imine backbone and terminal amines. There is ambiguity if the complexes Cu-PADA-Et-Et and Cu-PDO-Me-Me have been successfully made, which warrants further investigation if these complexes become of particular interest. It is believed that 12 of the copper complexes and 14 of the zinc complexes are novel. The complexes have been characterised by infra-red spectroscopy and Raman spectroscopy. Zinc complexes have been subjected to NMR spectroscopy. Selected complexes have also been characterised by elemental analysis and mass spectrometry. Some of the zinc complexes seem to have the propensity to encompass reagent impurities making it not possible to isolate the pure complex. It is important that this is kept in mind as it is unclear if the presence of any impurity would affect the transmetalation reaction explored in Chapter 4. Despite the bis(thiosemicarbazone) complexes being of interest since the 1950's<sup>57, 58</sup> the literature is still incomplete in regards to characterisation data. Hopefully this Chapter goes some way to fill this gap in this knowledge.

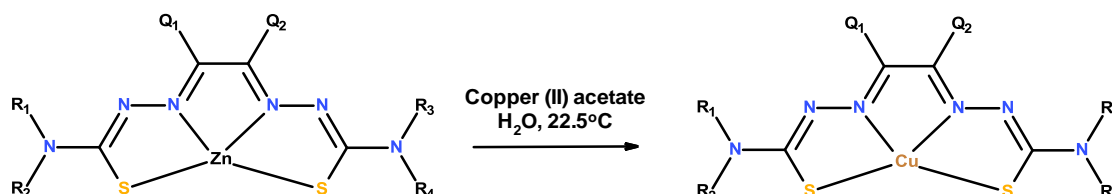
Cyclic voltammetry testing of a range of copper complexes has suggested groups of complexes which would be of interest for further biological screening. For the application of hypoxia imaging, complexes Me/Et on the backbone as well as Cu-BDO-NH<sub>2</sub>-(Me)<sub>2</sub>, Cu-BDO-Me-O-Ph and Cu-BDO-Me-But-NH<sub>2</sub> would be good candidates for further testing in order to obtain their hypoxia selectivity. For the application of copper metabolism imaging within the brain, complexes with Me/H on the backbone particularly, Cu-PADA-Me-Ph and Cu-PADA-Ph-Ph are good contenders for further testing in order to establish their accumulation and retention within the brain. Good candidates have been initially identified based only on their reduction potentials however, in light of further pharmacokinetic data such as lipophilicity, there may be a requirement to revise the list of candidates for further testing.

## 4. Transmetalation of bis(thiosemicarbazone) complexes.

### 4.1. Introduction

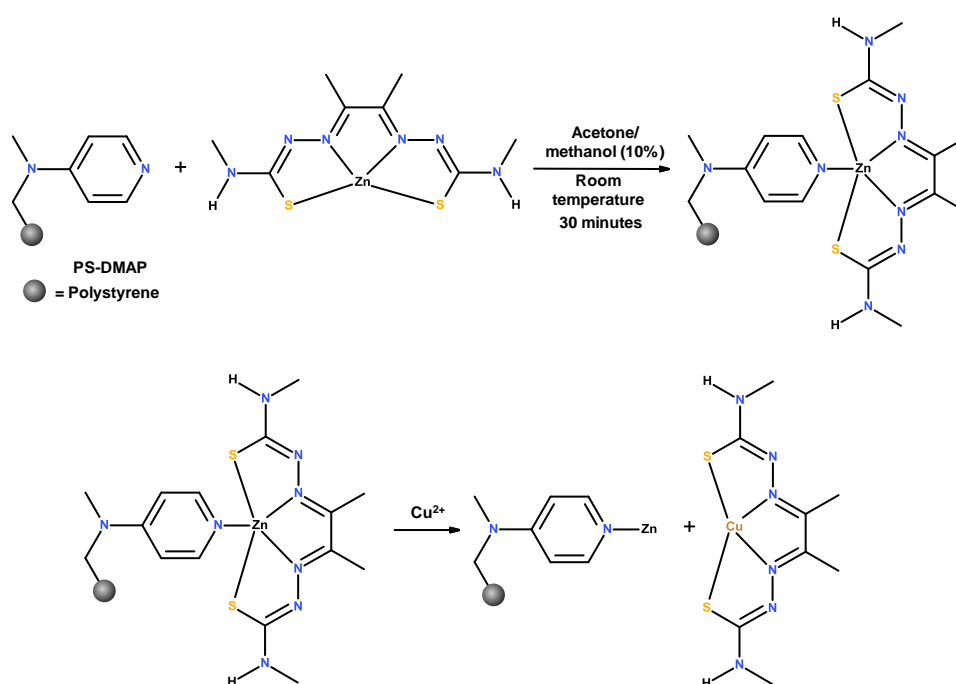
J.Holland *et al.*<sup>57</sup> used zinc bis(thiosemicarbazone) complexes as a precursor for desired copper bis(thiosemicarbazone) complexes by reacting them with copper acetate in water. This reaction is illustrated in Figure 4.1.1.

**Figure 4.1.1.** Formation of a copper bis(thiosemicarbazone) complex by transmetalation, based on<sup>57</sup>.



This synthetic approach could be very useful in the quick, clean synthesis of radio-copper complexes, particularly if the copper isotope has a short half live. This method was taken one step forward by H. Betts *et al.*<sup>137</sup> who attached the zinc bis(thiosemicarbazone) complex to a solid support and eluted the desired radio-copper complex by the addition of a [<sup>64</sup>Cu]Cu-acetate solution. This approach is illustrated in figure 4.1.2. A. Aphaiwong<sup>194</sup> and co-workers tested a number of different polymers for zinc-copper bis(thiosemicarbazone) transmetalation reactions. They concluded out of the polymers that they tested a pyridine functionality is optimal. The authors also stated that further work to improve loading and release of metal ligands from their polymeric supports is warranted.

**Figure 4.1.2.** The formation of a copper bis(thiosemicarbazone) complex by using polymer bound zinc bis(thiosemicarbazone) complexes to undergo transmetalation reactions with copper, based on<sup>137</sup>.





combined and stirred solution for 5 minutes. The solution changed rapidly to a brown coloured solution. Water (9 mL) was added to the solution. The precipitate was recovered by filtration. The product was washed with water (10 mL), ethanol (10 mL) and diethyl ether (10 mL). The product was left to dry. A brown solid (0.008 g) was recovered (48% yield).

#### **Cu-PADA-Me-Me**

0.012g (0.00004 mol) of Zn-PADA-Me-Me was dissolved in DMSO (1 mL). 0.010g (0.00005 mol) of copper acetate monohydrate was dissolved in deionised water (0.5 mL). The solutions were combined and stirred solution for 5 minutes. The solution changed rapidly to a brown coloured solution. Water (3 mL) was added to the solution. The precipitate was recovered by filtration. The product was washed with water (10 mL) and diethyl ether (10 mL). The product was left to dry. A brown solid (0.012 g) was recovered (97% yield).

#### **Cu-BDO-NH<sub>2</sub>-NH<sub>2</sub>**

0.021g (0.00007 mol) of Zn-BDO-NH<sub>2</sub>-NH<sub>2</sub> was dissolved in DMSO (2.5 mL). 0.016g (0.00008 mol) of copper acetate monohydrate was dissolved in deionised water (0.5 mL). The solutions were combined and stirred solution for 5 minutes. The solution changed rapidly to a brown coloured suspension. The precipitate was recovered by filtration. The product was washed with water (10 mL), ethanol (10 mL) and diethyl ether (10 mL). The product was left to dry. A brown solid (0.011 g) was recovered (53% yield).

#### **Cu-BDO-Me-Me**

0.050g (0.00015 mol) of Zn-BDO-Me-Me was dissolved in DMSO (2 mL). 0.034g (0.00017 mol) of copper acetate monohydrate was dissolved in deionised water (1 mL). The solutions were combined and stirred solution for 5 minutes. The solution changed rapidly to a brown coloured suspension. The precipitate was recovered by filtration. The product was washed with water (10 mL), ethanol (10 mL) and diethyl ether (10 mL). The product was left to dry. A brown solid (0.040 g) was recovered (82% yield).

#### **Cu-PDO-Et-Et**

0.019g (0.00005 mol) of Zn-PDO-Et-Et was dissolved in DMSO (1 mL). 0.012g (0.00006 mol) of copper acetate monohydrate was dissolved in deionised water (0.5 mL). The solutions were combined and stirred solution for 5 minutes. The solution changed rapidly to a brown coloured suspension. The precipitate was recovered by filtration. The product was washed with water (10 mL), ethanol (10 mL) and diethyl ether (10 mL). The product was left to dry. A brown solid (0.012 g) was recovered (64% yield).

### **Cu-PADA-Et-(Me)<sub>2</sub>**

0.027g (0.00008 mol) of Zn-PADA-Et-(Me)<sub>2</sub> was dissolved in DMSO (1 mL). 0.018g (0.00009 mol) of copper acetate monohydrate was dissolved in deionised water (1 mL). The solutions were combined and stirred for 5 minutes. The solution changed rapidly to a brown colour. The precipitate was recovered by filtration and was washed with water (10 mL) and diethyl ether (10 mL). The product was left to dry. A brown solid (0.026 g) was recovered (91% yield).

### **Cu-PADA-Ph-Me**

0.020g (0.00005 mol) of Zn-PADA-Ph-Me was dissolved in DMSO (1 mL). 0.012g (0.00006 mol) of copper acetate monohydrate was dissolved in deionised water (1 mL). The solutions were combined and stirred for 5 minutes. The solution changed rapidly to a brown colour. The precipitate was recovered by filtration and was washed with water (10 mL) and diethyl ether (10 mL). The product was left to dry. A brown solid (0.009 g) was recovered (49% yield).

### **Cu-PDO-Me-NH<sub>2</sub>**

0.026g (0.00008 mol) of Zn-PDO-Me-NH<sub>2</sub> was dissolved in DMSO (1 mL). 0.018g (0.00009 mol) of copper acetate monohydrate was dissolved in deionised water (1 mL). The solutions were combined and stirred for 5 minutes. The solution changed rapidly to a brown colour. The precipitate was recovered by filtration and was washed with water (10 mL) and diethyl ether (10 mL). The product was left to dry. A dark brown solid (0.019 g) was recovered (74% yield).

## **4.2.2. Characterisation data for the transmetalated copper complexes.**

### **Cu-GLY-Et-Et**

**IR (neat):**  $\text{cm}^{-1}$  = 3325 (m), 2970 (w), 2926 (w), 1518 (s), 1437 (s), 1416 (s), 1385 (m), 1371 (m), 1339 (s), 1290 (m), 1234 (s), 1202 (s), 1190 (s), 1119 (m), 1092 (m), 1055 (m), 1013 (m), 926 (w), 860 (m), 824 (w), 760 (w), 685 (m), 604 (m), 597 (m). **Raman (neat), laser = 632.81 nm:**  $\text{cm}^{-1}$  = 1582 (w), 1539 (m), 1445 (s), 1342 (w), 1300 (w), 1219 (w), 1055 (w), 1019 (m), 684 (w), 606 (w), 500 (w). **Mass spectrometry (ESI):**  $m/z$  (Calc.) 322.0096 (322.0115) {M + H<sup>+</sup>}.

### **Cu-PADA-Me-Me**

**IR (neat):**  $\text{cm}^{-1}$  = 3325 (m), 3273 (m), 2924 (w), 2886 (w), 1531 (s), 1449 (s), 1379 (s), 1348 (m), 1240 (m), 1223 (m), 1179 (s), 1132 (m), 924 (m), 870 (m), 808 (m), 775 (w), 664 (m), 613 (m). **Raman (neat), laser = 532.00 nm:**  $\text{cm}^{-1}$  = 2972 (w), 2915 (w), 2056 (w), 1548 (w), 1514 (w), 1470 (s), 1245 (w), 1180 (w), 997 (w), 924 (w), 663 (w), 590 (w). **Mass spectrometry (ESI):**  $m/z$  (Calc.) 307.9939 (307.9954) {M + H<sup>+</sup>}.

### Cu-BDO-NH<sub>2</sub>-NH<sub>2</sub>

**IR (neat):**  $\text{cm}^{-1}$  = 3404 (m), 3287 (m), 3146 (m), 1628 (s), 1593 (m), 1539 (w), 1479 (m), 1422 (s), 1362 (m), 1304 (m), 1217 (s), 1186 (m), 1138 (m), 1078 (m), 995 (m), 835 (m), 748 (w), 718 (m), 673 (m), 658 (m), 602 (m), 517 (m). **Raman (neat), laser = 632.81 nm:**  $\text{cm}^{-1}$  = 1534 (s), 1470 (m), 1367 (w), 1290 (s), 1182 (m), 1003 (m), 829 (m), 705 (w), 606 (w), 395 (w), 339 (w). **Mass spectrometry (ESI):**  $m/z$  (Calc.) 293.9783 (293.9805) {M + H<sup>+</sup>}.

### Cu-BDO-Me-Me

**IR (neat):**  $\text{cm}^{-1}$  = 3321 (s), 2928 (w), 1524 (s), 1495 (m), 1468 (s), 1385 (s), 1242 (m), 1223 (s), 1188 (m), 1157 (m), 1117 (m), 1078 (m), 841 (m), 773 (w), 606 (m), 546 (s), 509 (m). **Raman (neat), laser = 532.00 nm:**  $\text{cm}^{-1}$  = 1556 (s), 1492 (s), 1328 (m), 1265 (m), 1244 (m), 842 (w), 603 (m). **Mass spectrometry (ESI):**  $m/z$  (Calc.) 322.0096 (322.0113) {M + H<sup>+</sup>}.

### Cu-PDO-Et-Et

**IR (neat):**  $\text{cm}^{-1}$  = 3321 (m), 2974 (w), 2930 (w), 2874 (w), 1543 (w), 1506 (m), 1481 (m), 1433 (s), 1381 (m), 1342 (m), 1265 (w), 1234 (s), 1211 (s), 1140 (m), 1096 (w), 1055 (w), 1034 (w), 959 (w), 843 (w), 802 (w), 596 (w), 546 (m), 515 (w). **Raman (neat), laser = 532.00 nm:**  $\text{cm}^{-1}$  = 1540 (s), 1483 (s), 1466 (m), 1333 (m), 1233 (m), 605 (w). **Mass spectrometry (ESI):**  $m/z$  (Calc.) 364.0565 (364.0579) {M + H<sup>+</sup>}.

### Cu-PADA-Et-(Me)<sub>2</sub>

**IR (neat):**  $\text{cm}^{-1}$  = 3323 (m), 2966 (w), 1514 (s), 1483 (m), 1464 (s), 1391 (s), 1368 (s), 1339 (s), 1310 (s), 1258 (s), 1237 (s), 1179 (s), 1140 (s), 1059 (m), 1022 (w), 916 (m), 862 (m), 826 (m), 800 (w), 658 (m), 625 (m), 594 (m), 544 (m), 527 (m), 474 (m). **Raman (neat), laser = 632.81 nm:**  $\text{cm}^{-1}$  = 1591 (w), 1539 (m), 1507 (w), 1482 (s), 1460 (m), 1373 (w), 1312 (m), 1225 (m), 1010 (m), 930 (m), 660 (w), 595 (m), 511 (w), 376 (w), 350 (w). **Mass spectrometry (ESI):**  $m/z$  (Calc.) 336.0252 (336.0238) {M + H<sup>+</sup>}.

### Cu-PADA-Ph-Me

**IR (neat):**  $\text{cm}^{-1}$  = 3314 (w), 3194 (w), 2974 (w), 1599 (w), 1530 (m), 1481 (s), 1456 (s), 1435 (s), 1383 (s), 1354 (m), 1317 (m), 1244 (m), 1233 (m), 1192 (m), 1177 (s), 1146 (s), 1126 (m), 1026 (w), 935 (w), 895 (w), 866 (w), 812 (w), 754 (s), 689 (m), 669 (m), 631 (m), 583 (m), 507 (m), 492 (w), 449 (m), 436 (m). **Raman (neat), laser = 632.81 nm:**  $\text{cm}^{-1}$  = 1578 (w), 1508 (s), 1471 (s), 1430 (w), 1313 (w), 1273 (w), 1243 (m), 1193 (w), 995 (w), 932 (m), 676 (w), 601 (m), 542 (w), 479 (w), 369 (w). **Mass spectrometry (ESI):**  $m/z$  (Calc.) 370.0096 (370.0068) {M + H<sup>+</sup>}.

## Cu-PDO-Me-NH<sub>2</sub>

**IR (neat):**  $\text{cm}^{-1}$  = 3287 (m), 3121 (m), 2971, (m), 1643 (w), 1628 (w), 1614 (w), 1589 (w), 1543 (m), 1504 (m), 1435 (s), 1435 (m), 1354 (m), 1319 (m), 1277 (s), 1238 (m), 1213 (s), 1184 (s), 1148 (s), 1101 (m), 1076 (s), 1028 (s), 943 (s), 847 (m), 800 (m), 750 (m), 708 (m), 640 (m), 613 (s), 594 (s), 532 (s), 474 (s). **Raman (neat), laser = 632.81 nm:**  $\text{cm}^{-1}$  = 1586 (w), 1539 (m), 1500 (s), 1436 (w), 1384 (w), 1320 (w), 1282 (m), 1239 (m), 1188 (w), 1032 (w), 987 (w), 945 (w), 846 (w), 802 (w), 706 (w), 611 (w), 395 (w), 351 (w), 322 (w). **Mass spectrometry (ESI):**  $m/z$  (Calc.) 322.0096 (322.0051)  $\{M + H^+\}$ .

### 4.2.3. Spectral comparisons

Figures 4.2.3.1-4.2.3.4. illustrates the IR and Raman spectral comparisons of the copper complexes that have been synthesised in Chapter 3 and the copper complexes made via the transmetalation approach. Figures 4.2.3.5-6. illustrates the mass spectra of the copper complexes synthesised by the transmetalation method.

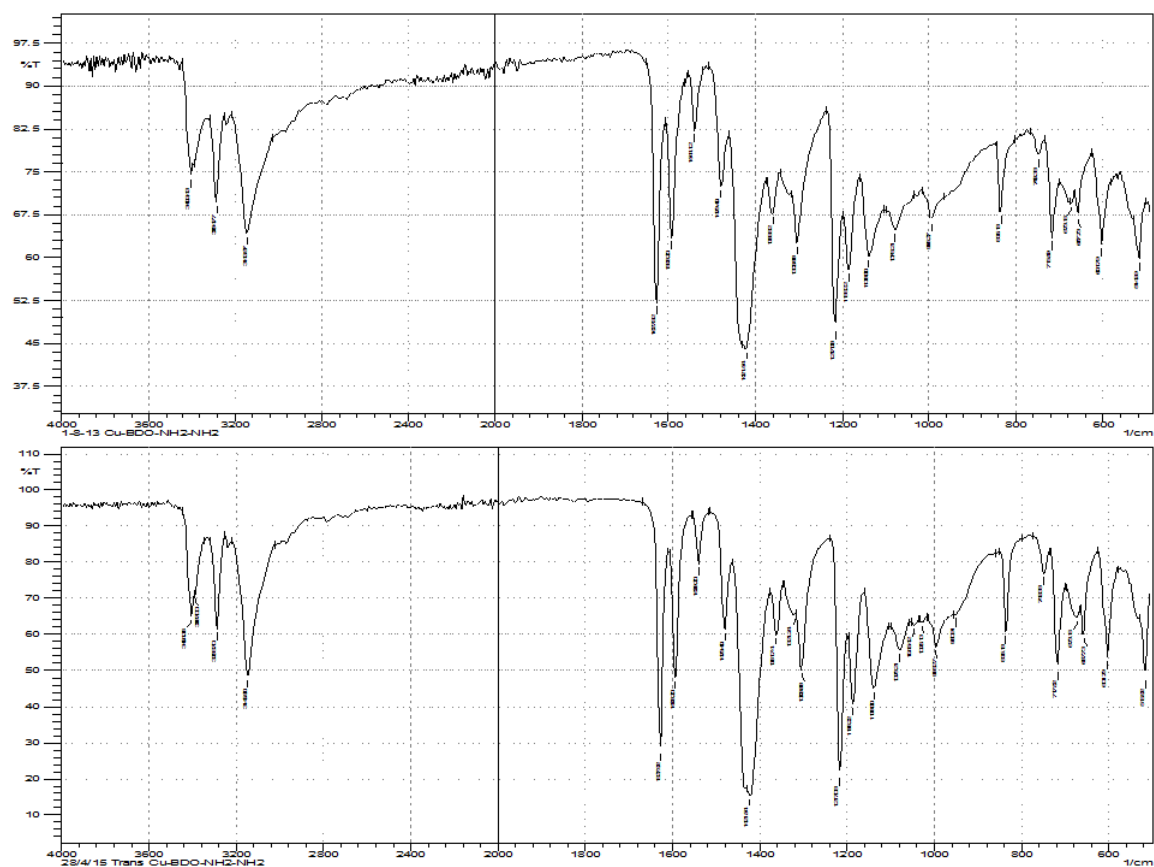


**Figure 4.2.3.1.** A comparison of the infrared spectra of Cu-BDO-NH<sub>2</sub>-NH<sub>2</sub> synthesised via the method in chapter3 (top) and Cu-BDO-NH<sub>2</sub>-NH<sub>2</sub> synthesised via the transmetalation approach (bottom).



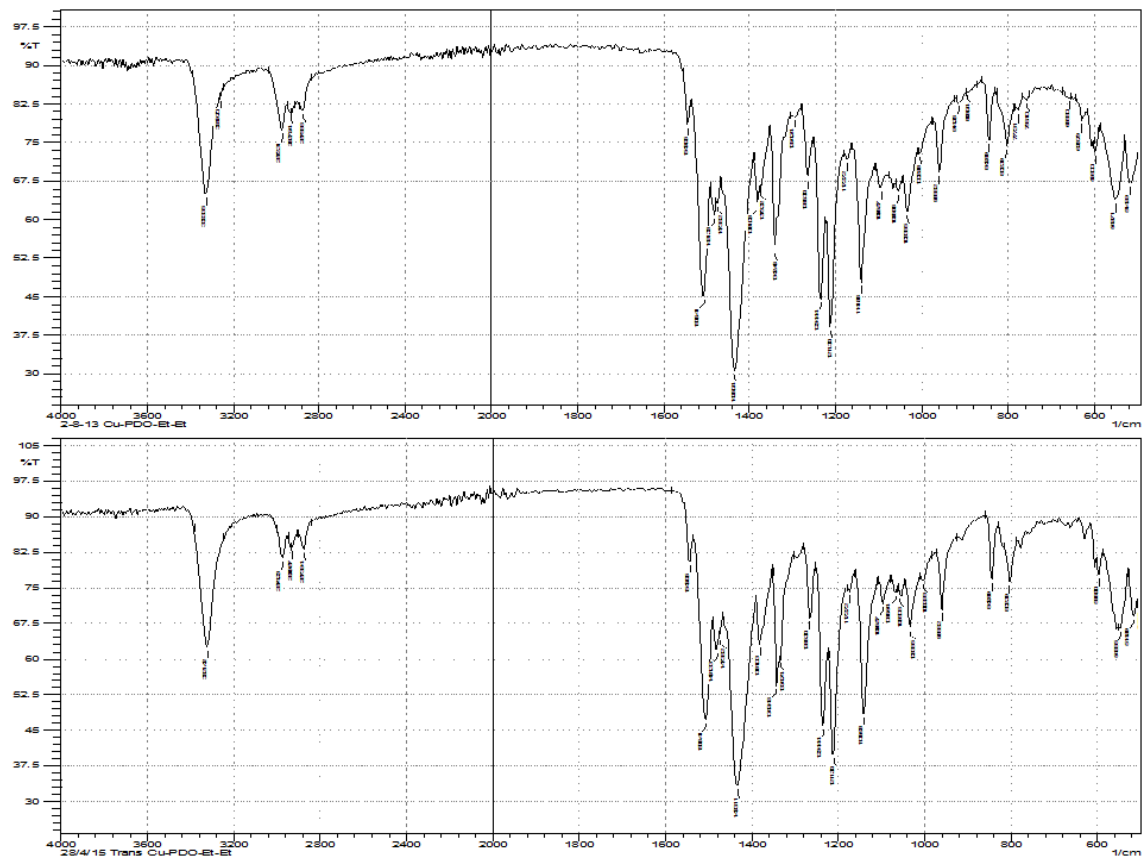


**Figure 4.2.3.2.** A comparison of the infrared spectra of Cu-PDO-Et-Et synthesised via the method in chapter 3 (top) and Cu-PDO-Et-Et synthesised via the transmetalation approach (bottom).

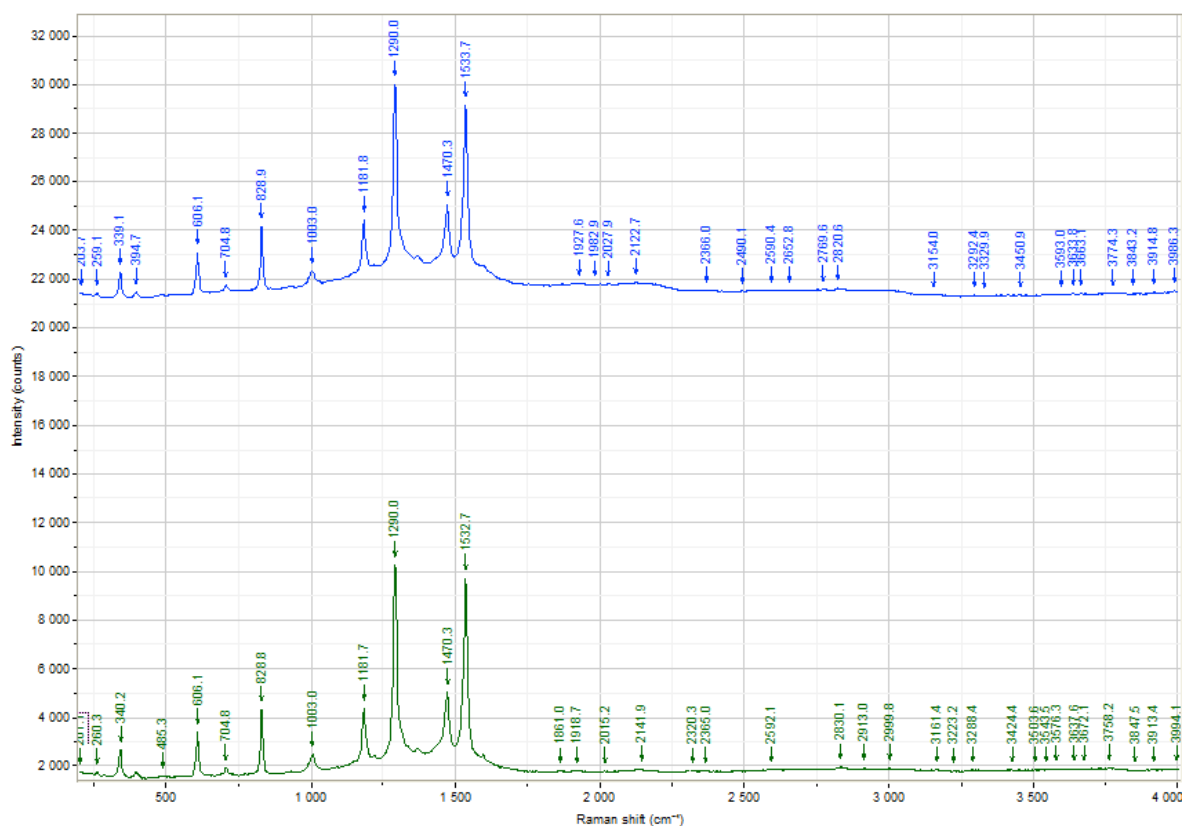


**Figure 4.2.3.3.** A comparison of the Raman spectra of Cu-BDO-NH<sub>2</sub>-NH<sub>2</sub> synthesised via the method in chapter 3 (green) and Cu-BDO-NH<sub>2</sub>-NH<sub>2</sub> synthesised via the transmetalation approach (blue).

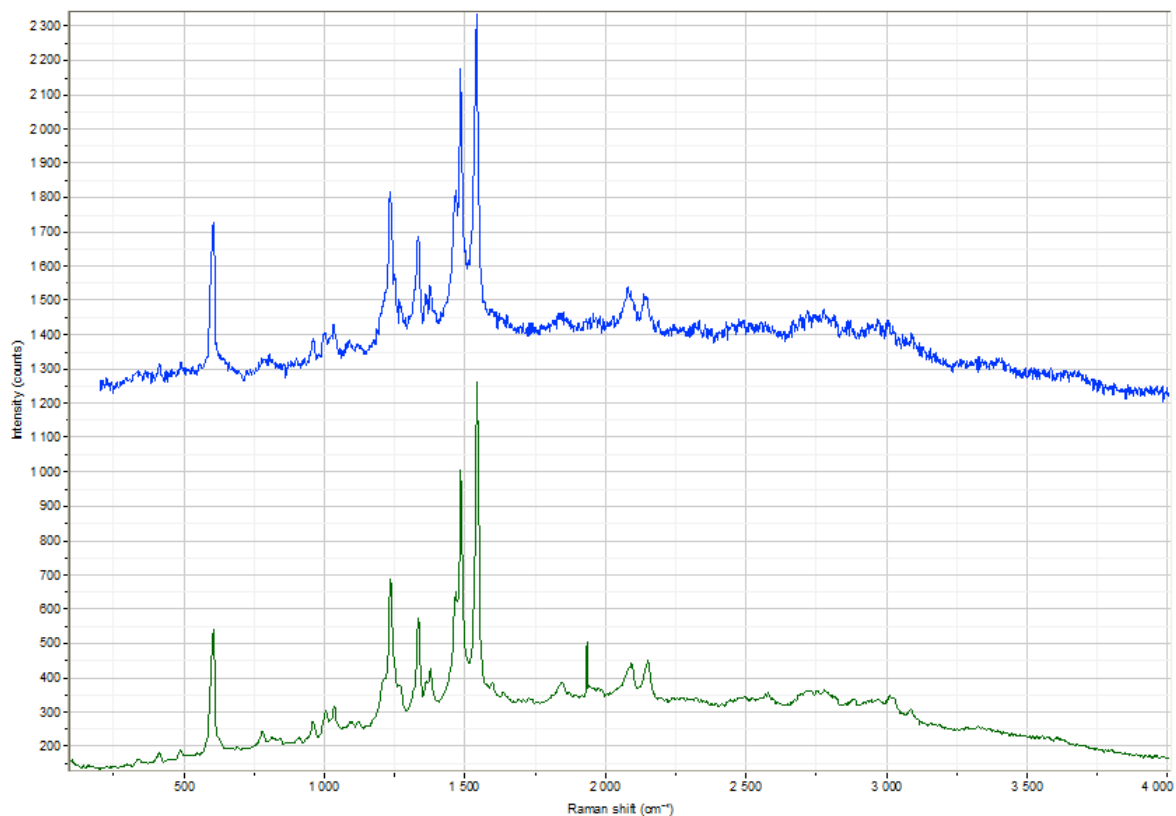


**Figure 4.2.3.4.** A comparison of the infrared spectra of Cu-PDO-Et-Et synthesised via the method in chapter 3 (green) and Cu-PDO-Et-Et synthesised via the transmetalation approach (blue). The peak labels have not been included as it was not possible to label the spectra sensibly by using the software. The very sharp peak in the green spectra just below 2000 wavenumbers is believed to be an artefact and not a real peak from the sample.

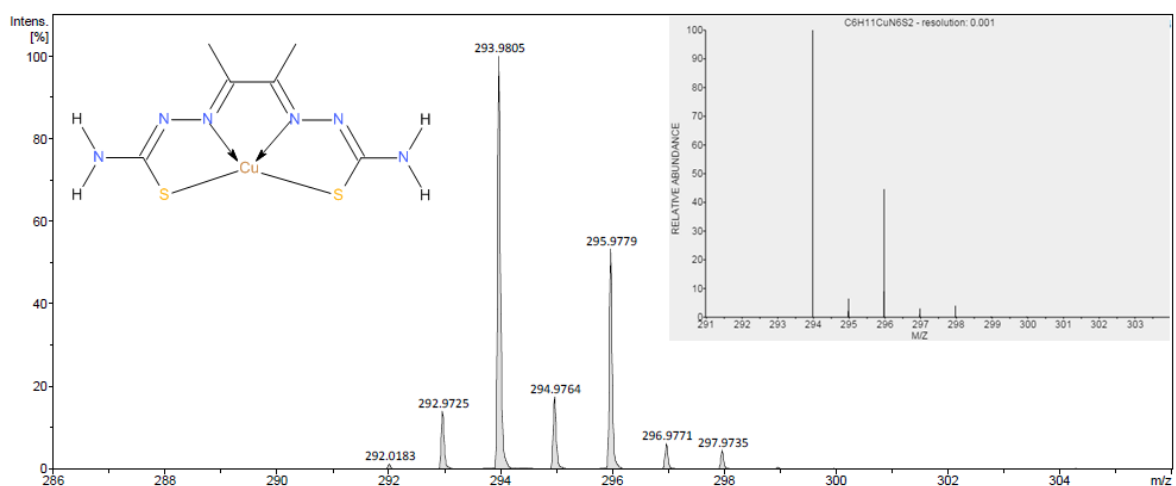


**Figure 4.2.3.5.** A mass spectrum of Cu-BDO-NH<sub>2</sub>-NH<sub>2</sub> synthesised by the transmetalation approach. The spectrum in the top right hand corner is the predicted expected spectrum of the M + H<sup>+</sup> ion of Cu-BDO-NH<sub>2</sub>-NH<sub>2</sub> generated by ChemCalc.<sup>213</sup> The peak at 1.008 m/z unit below the M + H<sup>+</sup> ion (292.9725) is expected to be the M<sup>+</sup> ion.

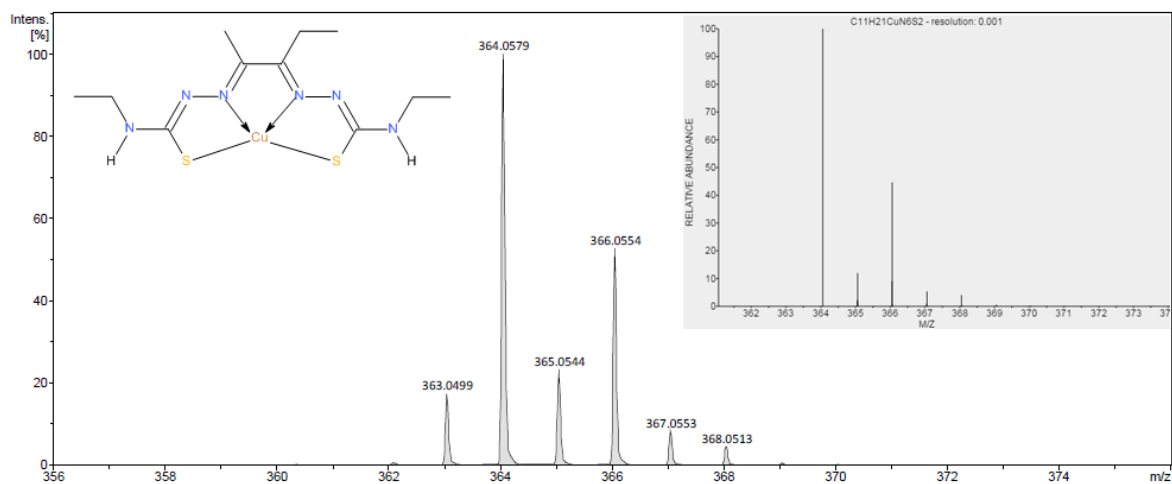


**Figure 4.2.3.6.** A mass spectrum of Cu-PDO-Et-Et synthesised by the transmetalation approach. The spectrum in the top right hand corner is the predicted expected spectrum of the  $M + H^+$  ion of Cu-PDO-Et-Et generated by ChemCalc.<sup>213</sup> The peak at 1.008 m/z unit below the  $M + H^+$  ion (363.0499) is expected to be the  $M^+$  ion.

#### **4.2.4. Discussion**

The transmetalation reaction for the sample of symmetric and dissymmetric zinc complexes tested was found to be particularly straight forward. Upon addition of the copper acetate solution the reaction mix turned very rapidly to brown which was indicative of a copper complex being formed. The reactions either yield a precipitate upon addition of the copper solution or upon further addition of water to the reaction mixture. The product recovered was of sufficient quantities in order to obtain characterisation data by infrared spectroscopy, Raman spectroscopy and mass spectrometry, for the purposes of identifying it as the expected copper complex.

The use of infra-red spectroscopy was particularly simple for establishing if the transmetalation reaction was successful. For all complexes tested, the infrared spectra of the copper complexes synthesised in Chapter 3 bore very strong similarities to the transmetalated copper complexes. The spectral examples of two complexes (Cu-PDO-Et-Et and Cu-BDO-NH<sub>2</sub>-NH<sub>2</sub>) are shown above (Figure 4.2.3.1. and Figure 4.2.3.2.) were the infrared spectra of the relevant copper complex that was synthesised in Chapter 3 is compared to the resulting product of the transmetalation reactions. There are very strong similarities between the spectra. When the individual peak wavenumbers were compared (Table 4.2.4.1.) a large number of peaks in both spectra were positioned at exactly the same wavenumbers (to 2 decimal places) and for the peaks that are not located at exactly the same wavenumber the discrepancy is only between 2-3 wavenumbers. So by using infrared spectroscopy alone it suggests that the transmetalation reactions have been successful.

Cu-PDO-Et-Et			Cu-BDO-NH <sub>2</sub> -NH <sub>2</sub>		
Chapter 3 Cu-PDO-Et-Et (cm <sup>-1</sup> )	Transmetalated Cu-PDO-Et-Et (cm <sup>-1</sup> )	Difference (cm <sup>-1</sup> )	Chapter 3 Cu-BDO -NH <sub>2</sub> -NH <sub>2</sub> (cm <sup>-1</sup> )	Transmetalated Cu-BDO-NH <sub>2</sub> - NH <sub>2</sub> (cm <sup>-1</sup> )	Difference (cm <sup>-1</sup> )
3323.35	3321.42	1.93	3402.43	3404.36	1.93
2972.31	2974.23	1.92	3284.77	3286.70	1.93
2927.94	2929.87	1.93	3143.97	3145.90	1.93
<b>1543.05</b>	<b>1543.05</b>	<b>0</b>	<b>1627.92</b>	<b>1627.92</b>	<b>0</b>
<b>1506.41</b>	<b>1506.41</b>	<b>0</b>	<b>1593.20</b>	<b>1593.20</b>	<b>0</b>
<b>1481.33</b>	<b>1481.33</b>	<b>0</b>	1541.12	1539.20	1.92
1435.04	1433.11	1.93	<b>1479.40</b>	<b>1479.40</b>	<b>0</b>
<b>1381.03</b>	<b>1381.03</b>	<b>0</b>	<b>1421.54</b>	<b>1421.54</b>	<b>0</b>
<b>1342.46</b>	<b>1342.46</b>	<b>0</b>	1359.82	1361.74	1.92
<b>1265.30</b>	<b>1265.30</b>	<b>0</b>	<b>1303.88</b>	<b>1303.88</b>	<b>0</b>
<b>1234.44</b>	<b>1234.44</b>	<b>0</b>	<b>1217.08</b>	<b>1217.08</b>	<b>0</b>
<b>1211.30</b>	<b>1211.30</b>	<b>0</b>	<b>1186.22</b>	<b>1186.22</b>	<b>0</b>
1141.86	1139.93	1.93	<b>1138.00</b>	<b>1138.00</b>	<b>0</b>
<b>1095.57</b>	<b>1095.57</b>	<b>0</b>	<b>1078.21</b>	<b>1078.21</b>	<b>0</b>
<b>1055.06</b>	<b>1055.06</b>	<b>0</b>	<b>995.27</b>	<b>995.27</b>	<b>0</b>
<b>1033.85</b>	<b>1033.85</b>	<b>0</b>	<b>835.18</b>	<b>835.18</b>	<b>0</b>
<b>958.62</b>	<b>958.62</b>	<b>0</b>	<b>748.38</b>	<b>748.38</b>	<b>0</b>
<b>842.89</b>	<b>842.89</b>	<b>0</b>	715.59	717.52	1.93
<b>802.39</b>	<b>802.39</b>	<b>0</b>	<b>657.73</b>	<b>657.73</b>	<b>0</b>
<b>596.00</b>	<b>596.00</b>	<b>0</b>	<b>601.79</b>	<b>601.79</b>	<b>0</b>
549.71	545.85	3.86	514.99	516.92	1.93

**Table 4.2.4.1.** Showing the comparison of the twenty largest peaks in the infrared spectra shown in Figure 4.4.3.1. and Figure 4.4.3.2. Cu-PDO-Et-Et and Cu-BDO-NH<sub>2</sub>-NH<sub>2</sub> represents the copper complexes that were made in chapter 3 whilst transmetalated Cu-PDO-Et-Et and transmetalated Cu-BDO-NH<sub>2</sub>-NH<sub>2</sub> represents the copper complexes synthesised by the transmetalation approach. The emboldened numbers highlight were exact matches were obtained.

Using Raman spectroscopy was not as straight forward as using infrared spectroscopy. All the spectra obtained from the transmetalated copper complexes did show strong resemblances to the Raman spectra of the respective copper complexes synthesised in Chapter 3, examples for Cu-PDO-Et-Et (Figure 4.2.3.4.) and Cu-BDO-NH<sub>2</sub>-NH<sub>2</sub> (Figure 4.2.3.3.) are included. However, despite using the same acquisition parameters as in Chapter 3 for the Raman, the resulting spectra of

most the transmetalated complexes were significantly weaker. This meant that less peaks could be use in the comparison of the Raman spectra of the transmetalated copper complexes and copper complexes synthesised in Chapter 3. The comparison data for the example spectra (Figure 4.2.3.3-4.) is tabulated below (Table 4.2.4.2.) where despite fewer exact matches than the infrared results the differences in peaks wavenumbers are still small, on average around 1-2 wavenumbers. Raman spectroscopy further supports that the expected copper complexes have been successfully synthesised by the transmetalation approach.

Cu-PDO-Et-Et			Cu-BDO-NH <sub>2</sub> -NH <sub>2</sub>		
Chapter 3 Cu-PDO-Et-Et (cm <sup>-1</sup> )	Transmetalated Cu-PDO-Et-Et (cm <sup>-1</sup> )	Difference (cm <sup>-1</sup> )	Chapter 3 Cu-BDO -NH <sub>2</sub> -NH <sub>2</sub> (cm <sup>-1</sup> )	Transmetalated Cu-BDO-NH <sub>2</sub> - NH <sub>2</sub> (cm <sup>-1</sup> )	Difference (cm <sup>-1</sup> )
1541.9	1539.7	2.2	1532.7	1533.7	1.0
1484.3	1482.5	1.8	<b>1470.3</b>	<b>1470.3</b>	<b>0</b>
1461.8	1466.2	4.4	<b>1290.0</b>	<b>1290.0</b>	<b>0</b>
1333.1	1332.6	0.5	1181.7	1181.8	0.1
1234.0	1233.2	0.8	<b>1003.0</b>	<b>1003.0</b>	<b>0</b>
604.6	604.7	0.1	828.8	828.9	0.1
			<b>704.8</b>	<b>704.8</b>	<b>0</b>
			<b>606.1</b>	<b>606.1</b>	<b>0</b>
			393.5	394.7	1.2
			340.2	339.1	1.1

**Table 4.2.4.2.** Showing the comparison of the largest peaks in the Raman spectra shown in Figure 4.4.3.1. and Figure 4.4.3.2. Cu-PDO-Et-Et and Cu-BDO-NH<sub>2</sub>-NH<sub>2</sub> represents the copper complexes that were made in chapter 3 whilst transmetalated Cu-PDO-Et-Et and transmetalated Cu-BDO-NH<sub>2</sub>-NH<sub>2</sub> represents the copper complexes synthesised by the transmetalation approach. The emboldened numbers highlight where exact matches were obtained.

All the transmetalated copper complexes were analysed by mass spectrometry. All complexes yielded a mass spectrum that was in accord to the molecular ion m/z value and the isotopic distribution as predicted by ChemCalc<sup>213</sup> for the relevant copper complex. Examples of Cu-PDO-Et-Et and Cu-BDO-Me-Me synthesised by the transmetalation approach are illustrated above (Figure 4.2.3.5 and Figure 4.2.3.6.). This data coupled with the supporting infrared and Raman data strongly supports that transmetalation reactions were successful.

### **4.3. Zinc complexes + pyridine**

Initial investigations were undertaken in order to establish if pyridine can act as a 5<sup>th</sup> ligand with the zinc ion within a zinc bis(thiosemicarbazone) complex. Besides H. Betts<sup>137</sup> and co-workers other reports of similar ligands to pyridine being bound to the zinc atom of a bis(thiosemicarbazone) complex have also been found. S. Pascu *et al.*<sup>191</sup> used ligands containing two nitrogen atoms (4,4'-bispyridyl and 1,4-diazabicyclo[2.2.2]octane) in order to link two zinc complexes together by forming a bond between the nitrogen of the ligand bridge and the zinc atom of the zinc complex. Unfortunately no IR, NMR or Raman data was reported. V. Bocokic *et al.*<sup>190</sup> has also reported co-ordinating phosphine based pyridine ligands to the zinc atom of a zinc bis(thiosemicarbazone) complex.

#### **4.3.1. Methods**

Three different methods were tried to see if it was possible to synthesise the complex Zn-BDO-Me-Me-pyridine. One approach was adding the pyridine at the same time as zinc (II) acetate was reacted with the ligand BDO-Me-Me and the other two were adding the pyridine to the complex Zn-BDO-Me-Me. The methods that were followed are:

##### **Approach 1:**

BDO-Me-Me (0.312 g, 0.0012 mol) was added to ethanol (15 mL). Anhydrous zinc (II) acetate (0.257 g, 0.0014 mol) along with pyridine (0.49 mL, 0.479 g, 0.0061 mol) was added to the suspension. The suspension was then brought to reflux (2 hours). The precipitate was recovered via filtration, washed with ethanol (1 x 30 mL) and di-ethyl ether (5 x 30 mL). The solid was dried in air. A yellow solid (0.196 g) was recovered (35% yield).

##### **Approach 2:**

Zn-BDO-Me-Me (0.194 g, 0.0006 mol) was dissolved in DMSO (2 mL). Pyridine (0.06 mL, 0.059 g, 0.0007 mol) was added to the solution and left to stir overnight. Water (5 mL) was added to solution. The precipitate was recovered via filtration, washed with ethanol (1 x 10 mL) and di-ethyl ether (5 x 10 mL). The solid was dried in air. A yellow solid (0.125 g) was recovered (52% yield).

##### **Approach 3:**

Zn-BDO-Me-Me (0.194 g, 0.0006 mol) was added to ethanol (15 mL). Pyridine (0.06 mL, 0.059 g, 0.0007 mol) was added to the suspension. The suspension was then brought to reflux (2 hours).

The precipitate was recovered via filtration, washed with ethanol (3 x 10 mL) and di-ethyl ether (3 x 10 mL). The solid was dried in air. A yellow solid (0.111 g) was recovered.

It was found via NMR spectroscopy that approach 1 and 2 both yielded the desired product while approach 3 mostly yielded the complex Zn-BDO-Me-Me with only a small proportion of the desired product.

Approach 2 was then used to attach pyridine to four more zinc complexes as it is believed to be the most versatile when investigating if pyridine can chelate to a range of zinc complexes with varying substituents. Complexes with bulky phenyl substituents were particularly of interest to investigate if the extra steric hindrance due to the phenyl functionality would impede the bonding of the pyridine to zinc.

#### **Zn-PADA-Me-Me-Pyridine**

Zn-PADA-Me-Me (0.0031 g, 0.0001 mol) was dissolved in DMSO (1.5 mL). Pyridine (0.1 mL, 0.10 g, 0.0012 mol) was added to the solution and left to stir overnight. Water (10 mL) was added to the solution. The precipitate was recovered via filtration, washed with water (10 x 2 mL). The solid was dried in air. An orange solid (0.012 g) was recovered (31% yield).

#### **Zn-PADA-Ph-Ph-Pyridine**

Zn-PADA-Ph-Ph (0.013 g, 0.00003 mol) was dissolved in DMSO (0.5 mL). Pyridine (0.1 mL, 0.10 g, 0.0012 mol) was added to the solution and left to stir overnight. Water (5 mL) was added to the solution. The precipitate was recovered via filtration, washed with water (5 x 2 mL). The solid was dried in air. An orange solid (0.005 g) was recovered (32% yield).

#### **Zn-GLY-Ph-Ph-Pyridine**

Zn-GLY-Ph-Ph (0.0126 g, 0.0003 mol) was dissolved in DMSO (2 mL, warm). Pyridine (0.03 mL, 0.30 g, 0.037 mol) was added to the solution and left to stir overnight. Water (10 mL) was added to the solution. The precipitate was recovered via filtration, washed with water (10 x 2 mL). The solid was dried in air. A bright orange solid (0.123 g) was recovered (82% yield).

#### **Zn-BDO-NH<sub>2</sub>-NH<sub>2</sub>-Pyridine**

Zn-BDO-NH<sub>2</sub>-NH<sub>2</sub> (0.059 g, 0.0002 mol) was dissolved in DMSO (3 mL, warm). Any insoluble particulates were removed by filtration. Pyridine (0.2 mL, 0.20 g, 0.025 mol) was added to the solution and left to stir overnight. Water (10 mL) was added to the solution. The precipitate was recovered via filtration, washed with water (5 x 2 mL). The solid was dried in air. A yellow solid (0.037 g) was recovered (49% yield).

### 4.3.2. Characterisation data for zinc complexes with pyridine

#### Zn-BDO-Me-Me- Pyridine

$^1\text{H NMR}$  (DMSO- $d_6$ , 400 MHz):  $\delta$ = 8.49 (m, 2 H,  $H_{(2,6)}$  pyridyl), 7.79 (m, 2 H,  $H_{(4)}$  pyridyl), 7.39 (m, 2 H,  $H_{(3,5)}$  pyridyl), 7.18 (s, 2 H,  $H_3\text{C-NH}$ ), 2.79 (m, 6 H,  $\text{HN-CH}_3$ ), 2.26 (s, 6 H,  $\text{N=C-CH}_3$ ).  $^{13}\text{C}\{^1\text{H}\}$  NMR (DMSO- $d_6$ , 100 MHz):  $\delta$ = 149.72 ( $C_{(2,6)}$  pyridyl), 137.57 ( $C_{(4)}$  pyridyl), 124.90 ( $C_{(3,5)}$  pyridyl), 29.81 ( $\text{HN-CH}_3$ ), 14.47 ( $\text{N=C-CH}_3$ ). **IR (neat)**:  $\text{cm}^{-1}$ = 3273 (w), 3217 (w), 3001 (w), 2938 (w), 1603 (w), 1530 (m), 1510 (m), 1476 (m), 1447 (m), 1396 (m), 1337 (m), 1250 (s), 1213 (s), 1157 (m), 1072 (s), 1040 (s), 1013 (m), 974 (m), 839 (m), 760 (m), 694 (s), 648 (m), 635 (m), 590 (m), 446 (s). **Raman (neat), laser = 632.81 nm**:  $\text{cm}^{-1}$ = 3285 (w), 1613 (w), 1544 (s), 1513 (s), 1478 (m), 1377 (w), 1337 (w), 1285 (m), 1254 (m), 1217 (w), 1190 (w), 1037 (w), 1013 (w), 989 (w), 841 (w), 795 (w), 726 (w), 592 (w), 538 (w), 448 (w), 375 (w), 334 (w), 289 (w). **Elemental analysis**: Found: **C**, 38.8; **H**, 4.6; **N**, 24.3. Calc. for  $\text{Zn}_1\text{C}_{13}\text{H}_{19}\text{N}_7\text{S}_2$ : **C**, 38.8; **H**, 4.75; **N**, 24.3%. **UV-Vis absorptions**:  $\lambda_{\text{max}}/\text{nm}$  (DMSO) 314 ( $\epsilon/\text{dm}^3 \text{mol}^{-1} \text{cm}^{-1}$  12 600) and 434 (12 800).

#### Zn-PADA-Me-Me-Pyridine

$^1\text{H NMR}$  (DMSO- $d_6$ , 400 MHz):  $\delta$ = 8.50 (m, 2 H,  $H_{(2,6)}$  pyridyl), 7.77 (m, 2 H,  $H_{(4)}$  pyridyl), 7.55 (s, 1 H,  $\text{N=CH}$ ), 7.43 (s, 1 H,  $H_3\text{C-NH}$ ), 7.38 (m, 2 H,  $H_{(3,5)}$  pyridyl), 7.24 (s, 1 H,  $H_3\text{C-NH}$ ), 2.78, 6 H,  $\text{HN-CH}_3$ ), 2.06 (s, 3 H,  $\text{N=C-CH}_3$ ).  $^{13}\text{C}\{^1\text{H}\}$  NMR (DMSO- $d_6$ , 100 MHz):  $\delta$ = 149.91 ( $C_{(2,6)}$  pyridyl), 137.11 ( $C_{(4)}$  pyridyl), 124.66 ( $C_{(3,5)}$  pyridyl), 29.80 ( $\text{HN-CH}_3$ ), 16.32 ( $\text{N=C-CH}_3$ ). **IR (neat)**:  $\text{cm}^{-1}$ = 3210 (w), 3007 (w), 1603 (w), 1533 (m), 1499 (m), 1464 (w), 1447(w), 1396(w), 1333(w), 1271 (s), 1215 (m), 1184 (s), 1128 (m), 1072 (m), 1042 (m), 1015 (m), 918 (m), 881 (m), 692 (s), 665 (m), 635 (m), 596 (m). **Raman (neat), laser = 632.81 nm**:  $\text{cm}^{-1}$ = 1608 (w), 1546 (m), 1501 (s), 1470 (s), 1397 (w), 1374 (w), 1276 (w), 1226 (m), 1188 (m), 1131 (w), 996 (w), 921 (m), 882 (w), 666 (w), 585 (w), 544 (w), 455 (w), 338 (w). **Elemental analysis**: Found: **C**, 37.1; **H**, 4.5; **N**, 25.1. Calc. for  $\text{Zn}_1\text{C}_{12}\text{H}_{17}\text{N}_7\text{S}_2$ : **C**, 37.1; **H**, 4.5; **N**, 25.2%. **UV-Vis absorptions**:  $\lambda_{\text{max}}/\text{nm}$  (DMSO) 320 ( $\epsilon/\text{dm}^3 \text{mol}^{-1} \text{cm}^{-1}$  14 200) and 447 (12 000).

#### Zn-PADA-Ph-Ph-Pyridine

$^1\text{H NMR}$  (DMSO- $d_6$ , 400 MHz):  $\delta$ = 9.65 (s, 1 H,  $\text{Ph-NH}$ ), 9.51 (s, 1 H,  $\text{Ph-NH}$ ), 8.50 (m, 2 H,  $H_{(2,6)}$  pyridyl), 7.76 (m, 6 H,  $\text{N=CH}$ ,  $H_{(2,6)}$  aryl,  $H_{(4)}$  pyridyl), 7.35 (m, 2 H,  $H_{(3,5)}$  pyridyl), 7.21 (t, 4 H,  $H_{(3,5)}$  aryl,  $J = 7.6$  Hz), 6.90 (m, 2 H,  $H_{(4)}$  aryl), 2.21 (s, 3 H,  $\text{N=C-CH}_3$ ).  $^{13}\text{C}\{^1\text{H}\}$  NMR (DMSO- $d_6$ , 100 MHz):  $\delta$ = 176.64 (**C-S**), 173.92 (**C-S**), 150.10 ( $C_{(2,6)}$  pyridyl), 147.31 (**C=N**), 141.54 (**C=N**), 141.15 ( $C_{(1)}$  aryl), 141.00 ( $C_{(1)}$  aryl), 136.78 ( $C_{(4)}$  pyridyl), 128.90 ( $C_{(3,5)}$  aryl), 124.49 ( $C_{(3,5)}$  pyridyl), 122.63 ( $C_{(4)}$  aryl), 122.16 ( $C_{(4)}$  aryl), 121.19 ( $C_{(2,6)}$  aryl), 120.60 ( $C_{(2,6)}$  aryl), 16.94 ( $\text{N=C-CH}_3$ ). **IR (neat)**:  $\text{cm}^{-1}$ = 3364 (w), 3312 (w), 1591 (w), 1522 (m), 1493 (m), 1464 (m), 1450 (m), 1393 (s), 1308 (m), 1250 (m), 1225



(m), 1190 (m), 1140 (m), 1074 (m), 1040 (m), 1015 (m), 930 (m), 899 (m), 826 (m), 746 (s), 691 (s), 650 (m), 635 (m), 615 (m). **Raman (neat), laser = 632.81 nm:**  $\text{cm}^{-1}$  = 1600 (w), 1543 (s), 1526 (s), 1466 (s), 1429 (w), 1403 (w), 1347 (w), 1309 (w), 1231 (m), 1136 (w), 997 (w), 931 (m), 661 (w), 624 (w), 594 (w), 504 (w), 466 (w), 230 (w). **Elemental analysis:** Found: **C**, 51.5; **H**, 4.0; **N**, 19.0. Calc. for  $\text{Zn}_1\text{C}_{22}\text{H}_{21}\text{N}_7\text{S}_2$ : **C**, 51.5; **H**, 4.1; **N**, 19.1%. **UV-Vis absorptions:**  $\lambda_{\text{max}}/\text{nm}$  (DMSO) 343 and 462.

### Zn-GLY-Ph-Ph-Pyridine

**$^1\text{H}$  NMR** (DMSO- $d_6$ , 400 MHz):  $\delta$  = 9.68 (s, 2 H, Ph-NH), 8.52 (m, 2 H,  $H_{(2,6)}$  pyridyl), 7.79 (m, 3 H, N=C-H,  $H_{(4)}$  pyridyl), 7.72 (d, 4 H,  $H_{(2,6)}$  aryl,  $J$  = 7.6 Hz), 7.38 (m, 2 H,  $H_{(3,5)}$  pyridyl), 7.22 (t, 4 H,  $H_{(3,5)}$  aryl,  $J$  = 7.2 Hz), 6.92 (t, 2 H,  $H_{(4)}$  aryl,  $J$  = 7.2 Hz).  **$^{13}\text{C}$   $\{^1\text{H}\}$  NMR** (DMSO- $d_6$ , 100 MHz):  $\delta$  = 176.42 (C-S), 149.90 ( $C_{(2,6)}$  pyridyl), 141.09 ( $C_{(1)}$  aryl), 138.46 (C=N), 137.18 ( $C_{(4)}$  pyridyl), 128.92 ( $C_{(3,5)}$  aryl), 124.70 ( $C_{(3,5)}$  pyridyl), 122.72 ( $C_{(4)}$  aryl), 121.28 ( $C_{(2,6)}$  aryl). **IR (neat):**  $\text{cm}^{-1}$  = 1593 (w), 1531 (w), 1495 (w), 1447 (w), 1393 (w), 1315 (m), 1283 (m), 1242 (m), 1169 (m), 1069 (w), 1040 (w), 1001 (w), 880 (w), 750 (m), 691 (m), 633 (m), 588 (m). **Raman (neat), laser = 784.15 nm:**  $\text{cm}^{-1}$  = 1598 (w), 1523 (s), 1452 (s), 1418 (s), 1313 (w), 1300 (w), 1245 (w), 1176 (w), 1158 (w), 1001 (s), 606 (w), 589 (w), 476 (w). **Elemental analysis:** Found: **C**, 50.5; **H**, 3.8; **N**, 19.6. Calc. for  $\text{Zn}_1\text{C}_{21}\text{H}_{19}\text{N}_7\text{S}_2$ : **C**, 50.55; **H**, 3.8; **N**, 19.7%. **UV-Vis absorptions:**  $\lambda_{\text{max}}/\text{nm}$  (DMSO) 351 ( $\epsilon/\text{dm}^3 \text{mol}^{-1} \text{cm}^{-1}$  13 500) and 472 (25 400).

### Zn-BDO-NH<sub>2</sub>-NH<sub>2</sub>-Pyridine

**$^1\text{H}$  NMR** (DMSO- $d_6$ , 400 MHz):  $\delta$  = 8.48 (m, 2 H,  $H_{(2,6)}$  pyridyl), 7.79 (m, 2 H,  $H_{(4)}$  pyridyl), 7.39 (m, 2 H,  $H_{(3,5)}$  pyridyl), 6.86 (s, 4 H, C-NH), 2.12 (s, 6 H, N=C-CH<sub>3</sub>).  **$^{13}\text{C}$   $\{^1\text{H}\}$  NMR** (DMSO- $d_6$ , 100 MHz):  $\delta$  = 178.50 (C-S), 149.75 ( $C_{(2,6)}$  pyridyl), 144.78 (C=N), 137.40 ( $C_{(4)}$  pyridyl), 124.79 ( $C_{(3,5)}$  pyridyl), 14.48 (N=C-CH<sub>3</sub>). **IR (neat):**  $\text{cm}^{-1}$  = 3368 (w), 3291 (w), 3121 (w), 1626 (w), 1603 (m), 1537 (w), 1416 (s), 1290 (m), 1207 (m), 1177 (m), 1138 (m), 1067 (m), 1040 (m), 988 (m), 827 (m), 752 (m), 692 (s), 633 (m), 596 (m). **Raman (neat), laser = 632.81 nm:**  $\text{cm}^{-1}$  = 1666 (w), 1537 (s), 1464 (m), 1289 (s), 1214 (w), 1183 (m), 997 (w), 827 (w), 603 (w), 389 (w), 309 (w). **Elemental analysis:** Found: **C**, 32.8; **H**, 4.4; **N**, 24.3. Calc. for  $\text{Zn}_1\text{C}_{11}\text{H}_{15}\text{N}_7\text{S}_2$ : **C**, 35.25; **H**, 4.0; **N**, 26.2%. **UV-Vis absorptions:**  $\lambda_{\text{max}}/\text{nm}$  (DMSO) 308 ( $\epsilon/\text{dm}^3 \text{mol}^{-1} \text{cm}^{-1}$  13 800) and 433 (12 400).

### 4.3.3. Spectral and X-ray diffraction illustrations of Zn-BDO-Me-Me-Pyridine

Figure 4.3.3.1-4. shows examples of a proton and carbon NMR spectra, a FTIR spectrum and a Raman spectrum of Zn-BDO-Me-Me-Pyridine. Figures 4.3.3.5-8. displays the X-ray diffraction data obtained from the crystal structure of Zn-BDO-Me-Me-pyridine.

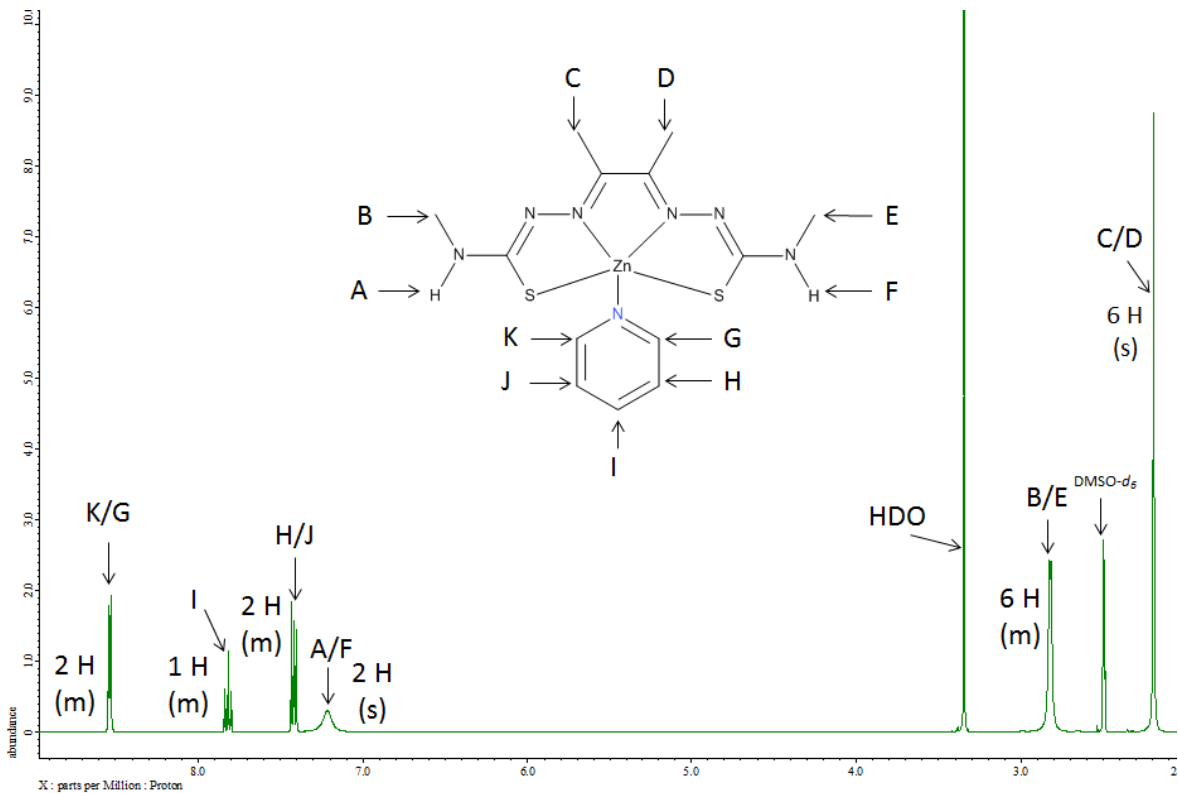


**Figure 4.3.3.1.** An assigned proton NMR spectrum of Zn-BDO-Me-Me-Pyridine. This adduct was synthesised by reacting Zn-BDO-Me-Me with pyridine.

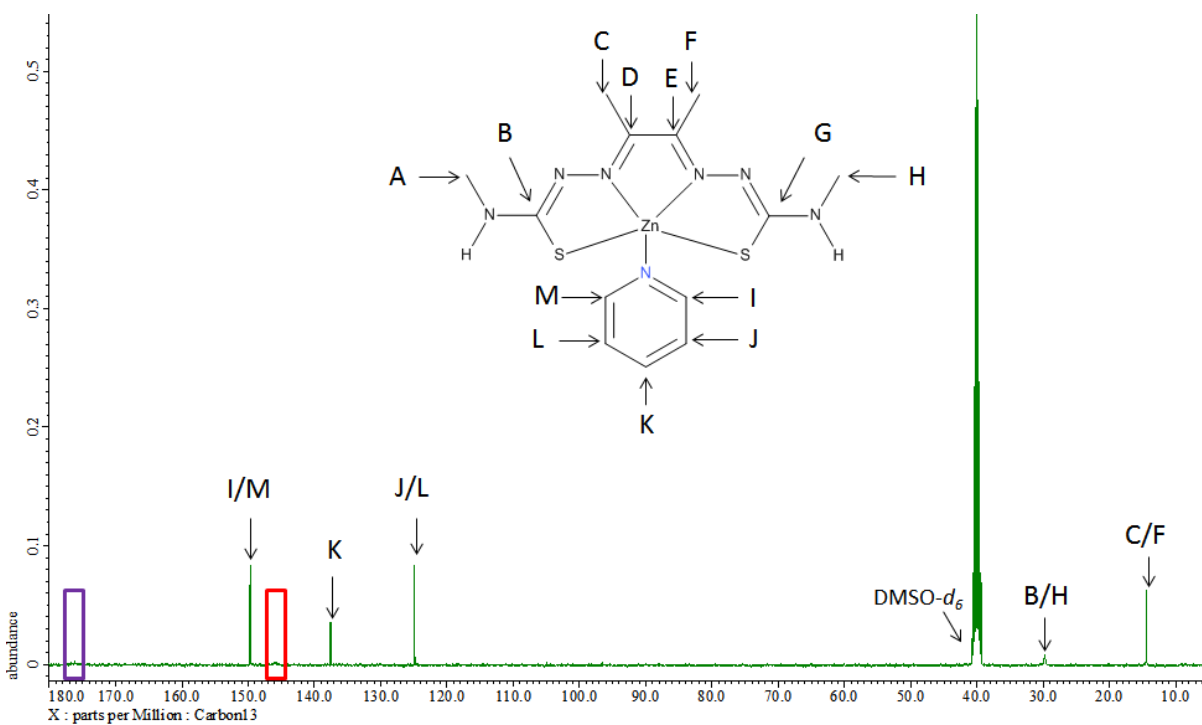


**Figure 4.3.3.2.** A assigned carbon NMR spectrum of Zn-BDO-Me-Me-Pyridine. The purple and red boxes highlights two very faint peaks which potentially could be environments B/G and D/E respectively.

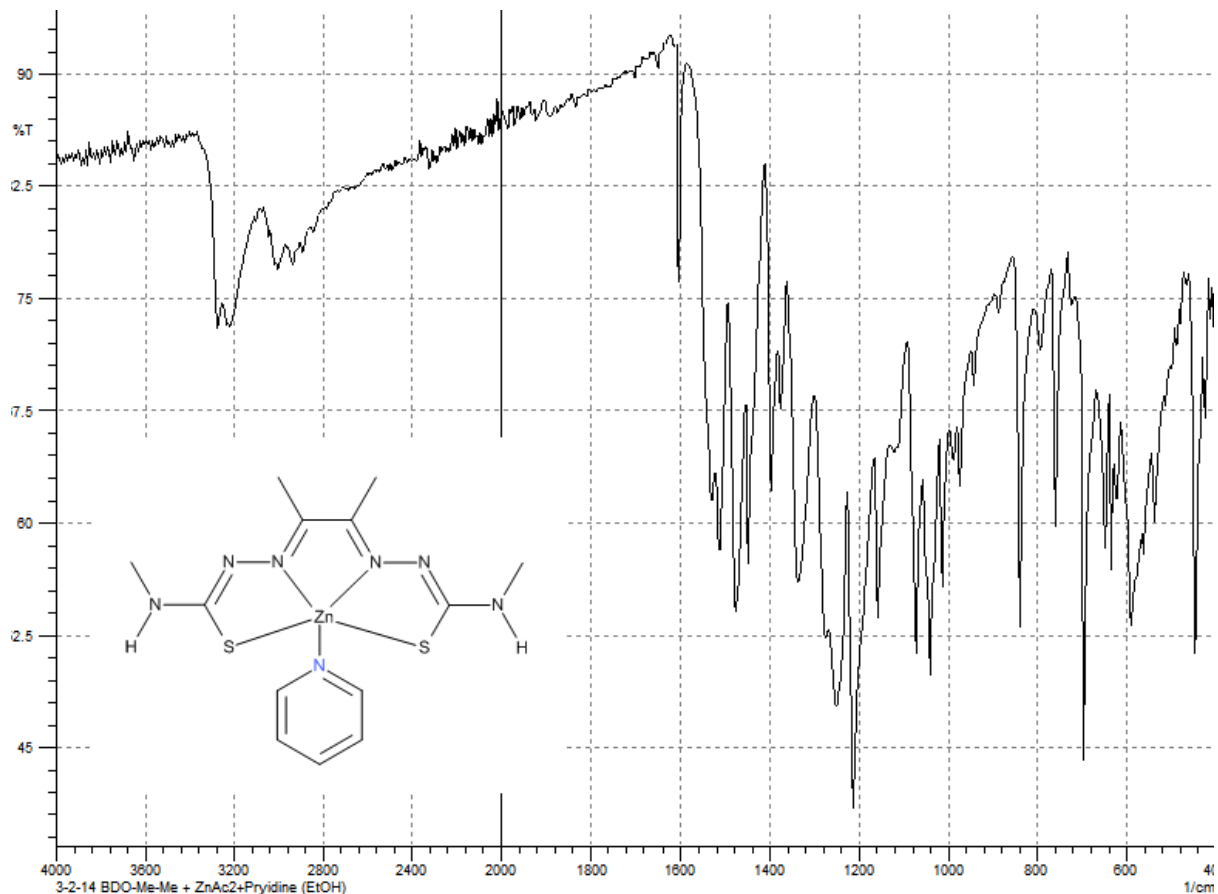


**Figure 4.3.3.3.** A FTIR spectrum of Zn-BDO-Me-Me-Pyridine.

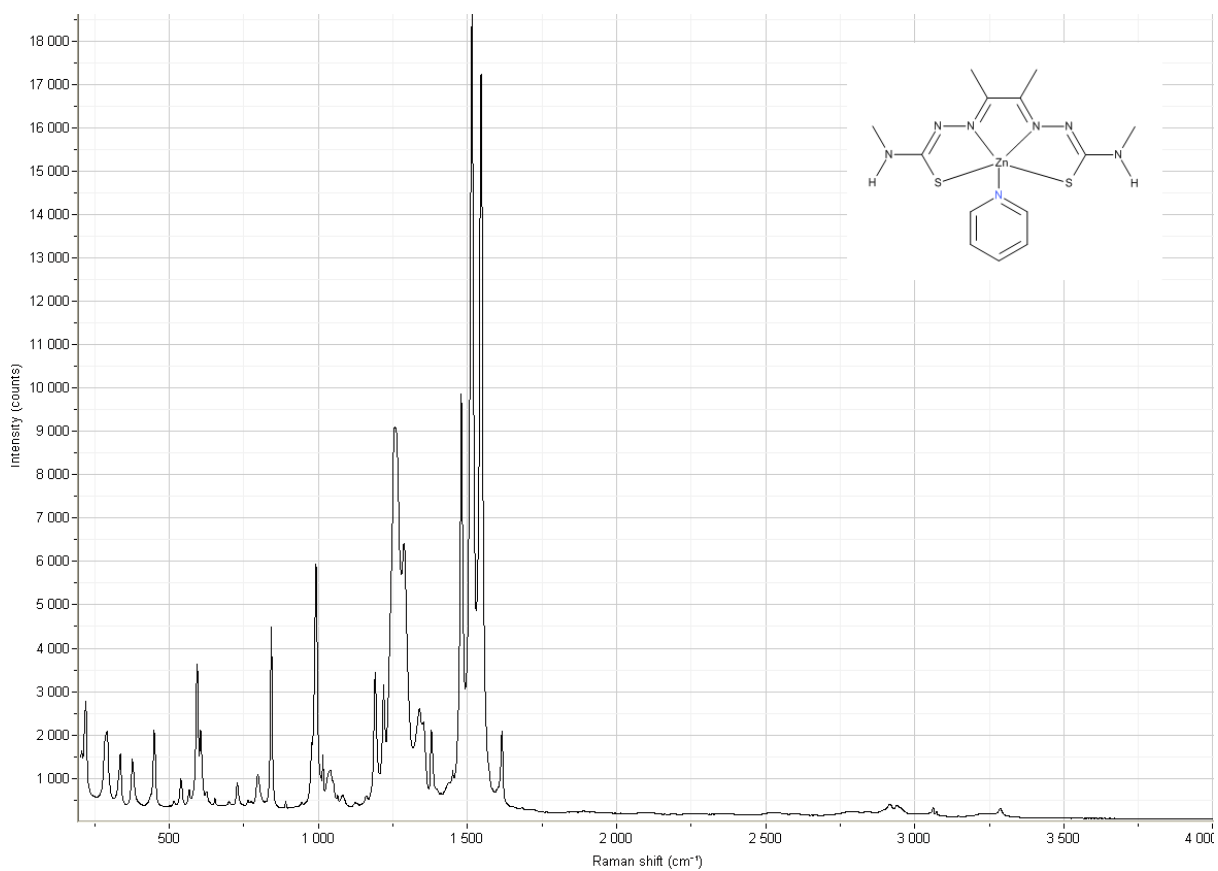


**Figure 4.3.3.4.** A Raman spectrum of Zn-BDO-Me-Me-Pyridine.

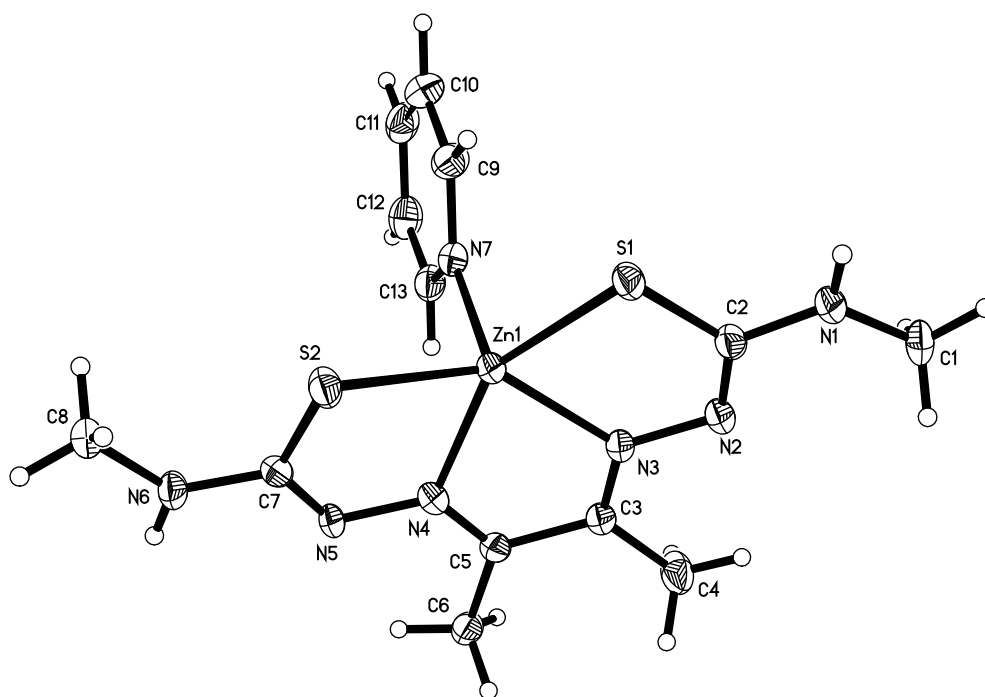


**Figure 4.3.3.5** The X-ray crystal structure of Zn-BDO-Me-Me-pyridine showing that the pyridine is bound between the zinc of Zn-BDO-Me-Me and the nitrogen of the pyridine in the axial position.

Atom	Atom	Length/Å	Atom	Atom	Length/Å
Zn1	S1	2.3635(6)	N4	C5	1.288(3)
Zn1	S2	2.3718(6)	N5	C7	1.337(3)
Zn1	N3	2.1218(18)	N6	C7	1.344(3)
Zn1	N4	2.1241(17)	N6	C8	1.452(3)
Zn1	N7	2.0900(18)	N7	C9	1.341(3)
S1	C2	1.760(2)	N7	C13	1.341(3)
S2	C7	1.738(2)	C3	C4	1.491(3)
N1	C1	1.450(3)	C3	C5	1.482(3)
N1	C2	1.347(3)	C5	C6	1.495(3)
N2	N3	1.372(3)	C9	C10	1.385(3)
N2	C2	1.321(3)	C10	C11	1.385(4)
N3	C3	1.294(3)	C11	C12	1.379(4)
N4	N5	1.369(2)	C12	C13	1.382(3)

**Table 4.3.3.6.** Bond lengths for the crystal structure of Zn-BDO-Me-Me-pyridine.

Atom	Atom	Atom	Angle/°	Atom	Atom	Atom	Angle/°
S1	Zn1	S2	113.40(2)	C7	N6	C8	125.71(19)
N3	Zn1	S1	80.75(5)	C9	N7	Zn1	118.66(15)
N3	Zn1	S2	144.85(5)	C13	N7	Zn1	123.45(15)
N3	Zn1	N4	74.45(7)	C13	N7	C9	117.86(19)
N4	Zn1	S1	150.39(5)	N1	C2	S1	114.89(16)
N4	Zn1	S2	80.36(5)	N2	C2	S1	127.89(17)
N7	Zn1	S1	102.52(5)	N2	C2	N1	117.2(2)
N7	Zn1	S2	101.09(5)	N3	C3	C4	124.0(2)
N7	Zn1	N3	107.07(7)	N3	C3	C5	114.89(18)
N7	Zn1	N4	100.05(7)	C5	C3	C4	120.98(18)
C2	S1	Zn1	95.38(7)	N4	C5	C3	114.89(18)
C7	S2	Zn1	94.57(7)	N4	C5	C6	124.51(19)
C2	N1	C1	123.16(19)	C3	C5	C6	120.51(18)
C2	N2	N3	111.67(18)	N5	C7	S2	127.03(16)
N2	N3	Zn1	123.07(13)	N5	C7	N6	114.16(19)
C3	N3	Zn1	117.35(14)	N6	C7	S2	118.75(17)
C3	N3	N2	119.53(18)	N7	C9	C10	122.9(2)
N5	N4	Zn1	120.87(13)	C11	C10	C9	118.4(2)
C5	N4	Zn1	117.43(14)	C12	C11	C10	119.1(2)
C5	N4	N5	121.53(18)	C11	C12	C13	118.9(2)
C7	N5	N4	112.29(17)	N7	C13	C12	122.8(2)

**Table 4.3.3.7.** Bonding angles for the crystal structure of Zn-BDO-Me-Me-pyridine.

Crystal data	
Chemical formula	[Zn(C <sub>8</sub> H <sub>14</sub> N <sub>6</sub> S <sub>2</sub> )(C <sub>5</sub> H <sub>5</sub> N)]
<i>M<sub>r</sub></i>	402.84
Crystal system, space group	Monoclinic, <i>P2<sub>1</sub>/n</i>
Temperature (K)	150
<i>a</i> , <i>b</i> , <i>c</i> (Å)	10.1466 (2), 13.9076 (3), 12.7775 (3)
$\beta$ (°)	104.756 (2)
<i>V</i> (Å <sup>3</sup> )	1743.64 (7)
<i>Z</i>	4
Radiation type	Cu <i>K</i> $\alpha$
$\mu$ (mm <sup>-1</sup> )	4.27
Crystal size (mm)	0.26 × 0.04 × 0.02
Data collection	
Diffractometer	Agilent SuperNova Dual Source diffractometer with an Atlas detector
Absorption correction	Multi-scan ( <i>CrysAlis PRO</i> ; Agilent, 2014)
<i>T<sub>min</sub></i> , <i>T<sub>max</sub></i>	0.775, 1.000
No. of measured, independent and observed [ <i>I</i> > 2 $\sigma$ ( <i>I</i> )] reflections	12050, 3445, 3020
<i>R<sub>int</sub></i>	0.041
( <i>sin</i> $\theta$ / $\lambda$ ) <sub>max</sub> (Å <sup>-1</sup> )	0.622
Refinement	
<i>R</i> [ <i>F</i> <sup>2</sup> > 2 $\sigma$ ( <i>F</i> <sup>2</sup> )], <i>wR</i> ( <i>F</i> <sup>2</sup> ), <i>S</i>	0.031, 0.074, 1.04
No. of reflections	3445
No. of parameters	212
H-atom treatment	H-atom parameters constrained
$\Delta\rho_{\max}$ , $\Delta\rho_{\min}$ (e Å <sup>-3</sup> )	0.36, -0.42

**Table 4.3.3.8.** Experimental details for the collection of the crystal structure of Zn-BDO-Me-Me-pyridine. Computer programs: *CrysAlis PRO*<sup>218</sup>, *SHELXS97*<sup>219</sup>, *SHELXL2014*<sup>220</sup> and *OLEX2*.<sup>221</sup>

#### **4.3.4. Discussion**

The chelation of an additional pyridine ligand to the zinc atom of a zinc bis(thiosemicarbazone) complex was successfully undertaken. For the complexes Zn-BDO-Me-Me, Zn-PADA-Me-Me, Zn-PADA-Ph-Ph and Zn-GLY-Ph-Ph one pyridine molecule coordinates with the zinc atom of the chosen zinc bis(thiosemicarbazone) complex. This is backed up by the proton integrals of NMR spectra and CHN analysis. However, with Zn-BDO-NH<sub>2</sub>-NH<sub>2</sub> the proton NMR spectra suggests that one pyridine is bound to the zinc atom of the complex but the CHN results are out by up to 2%, which suggest that the complex has not been made pure. It was also attempted to co-ordinate pyridine with Zn-GLY-Et-Et. In this case the NMR suggested that pyridine is present with in the product but in a ratio of 2:1 (complex: pyridine) and the CHN analysis also was out by a few percent. Even though the last two complexes were not recovered with one pyridine chelated to one zinc atom, they still confirm the aim of this investigation which was to determine if pyridine is able to complex to zinc bis(thiosemicarbazone) complexes. It is believed that BDO-Me-Me, PADA-Me-Me, Zn-PADA-Ph-Ph and GLY-Ph-Ph with the pyridine adduct are novel.

In order to establish if pyridine was indeed bound to the zinc of the complexes instead of being contained within the lattice of the product it was hoped that HMBC NMR experiments would show some through bond coupling. However, the only through bonding couplings observed with the hydrogen environments of pyridine was just to the pyridines carbon environments. It was also attempted to detect through space interactions between the pyridine and the rest of complex by running a NOESY NMR experiment. Couplings were observed between the different environments of the pyridine. The complexes also showed couplings between the different environments of the complex however, no through space coupling was observed between the pyridine and the rest of the complex.

When the pyridine proton environments are compared to the proton NMR spectrum (Figure 4.3.4.1.) of Zn-BDO-Me-Me-Pyridine and pyridine it is possible to see that the peaks have shifted. Protons in environment A have shifted by about -0.05 ppm (values taken from the middle of each peak), and proton environments C and B have both shifted by around +0.08 ppm. The presence of the changes in chemical shift suggests that the pyridine protons must be in a slightly different chemical environment. Thus, supporting that the pyridine may be chelated to the zinc ion of the zinc bis(thiosemicarbazone) complex. The splitting of the pyridine peaks of Zn-BDO-Me-Me-Pyridine has also become more complicated. It is thought that this is due to the pyridine molecules binding to the zinc in slightly different orientations in space.

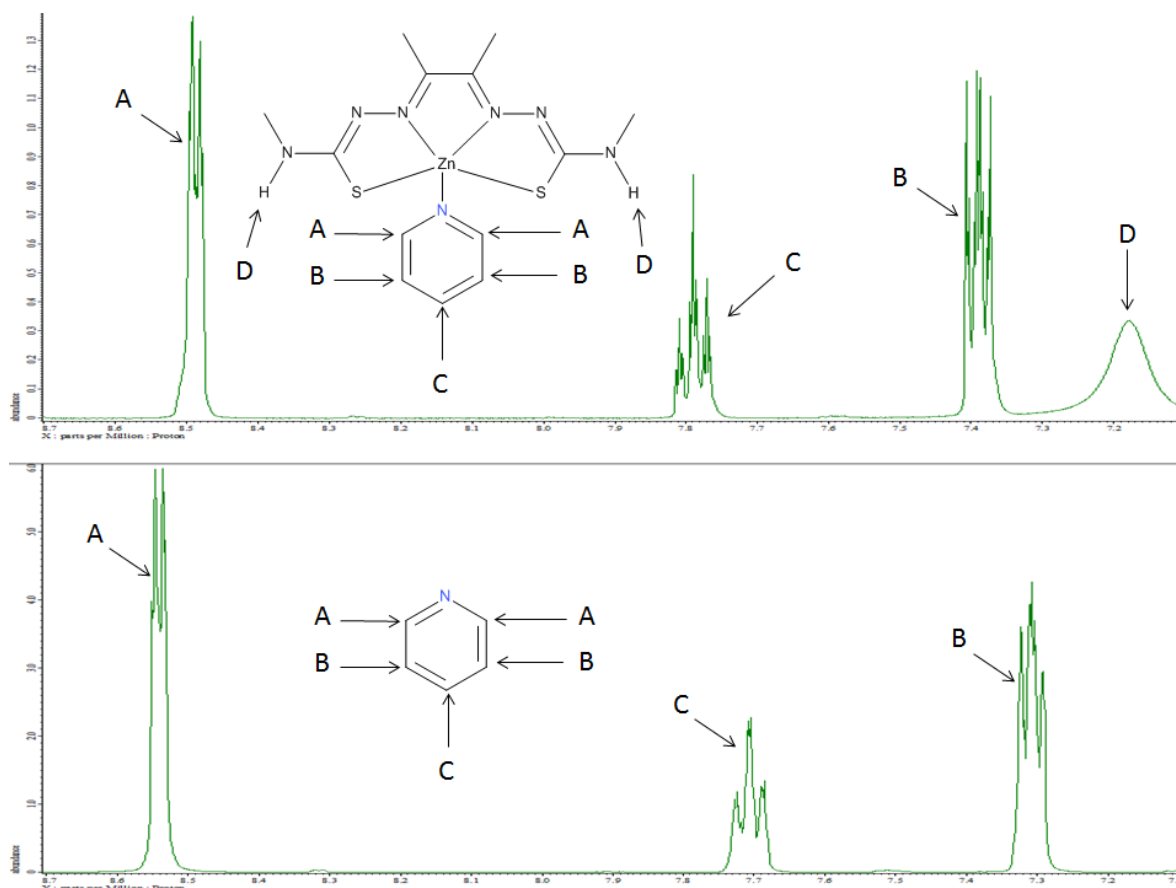


**Figure 4.3.4.1.** A comparison proton NMR spectra of Zn-BDO-Me-Me-Pyridine (top) and pyridine which has been zoomed in to highlight the pyridine proton environments in the two molecules. In both spectra the DMSO-  $d_6$  peak is position at 2.459 ppm.

It was attempted to obtain a mass spectrum of Zn-BDO-Me-Me-Pyridine but the results showed only Zn-BDO-Me-Me without the presence of the pyridine. It is expected that during ionisation in the mass spectrometer the pyridine molecule gets stripped from the complex. A similar observation was reported by E. Lopez-Torres *et al.*<sup>222</sup> where two absent nitrate groups were observed in the mass spectrum of their zinc benzyl bis(thiosemicarbazone) complexes.

Vibrational spectroscopy was used in order to show the presence of the pyridine within the zinc complex. Infrared spectra of the product (Figure 4.3.4.2.) suggests that the pyridine is present as it shows peaks that are only found in the pyridine spectra and peaks that are only found in the zinc bis(thiosemicarbazone) complex. It was observed that the more substituted the zinc complexes were the harder it was to find regions of the infra-red spectrum from the product which could only be attributed to the pyridine. This was particularly to case for phenyl substituents on the terminal amine, which make sense as the phenyl substituent shares similar bonds to parts of the pyridine ligand. A similar situation was also encountered with Raman spectroscopy as illustrated in the comparison spectra of pyridine, Zn-PADA-Me-Me and Zn-PADA-Me-Me-Pyridine (Figure 4.3.4.3.).

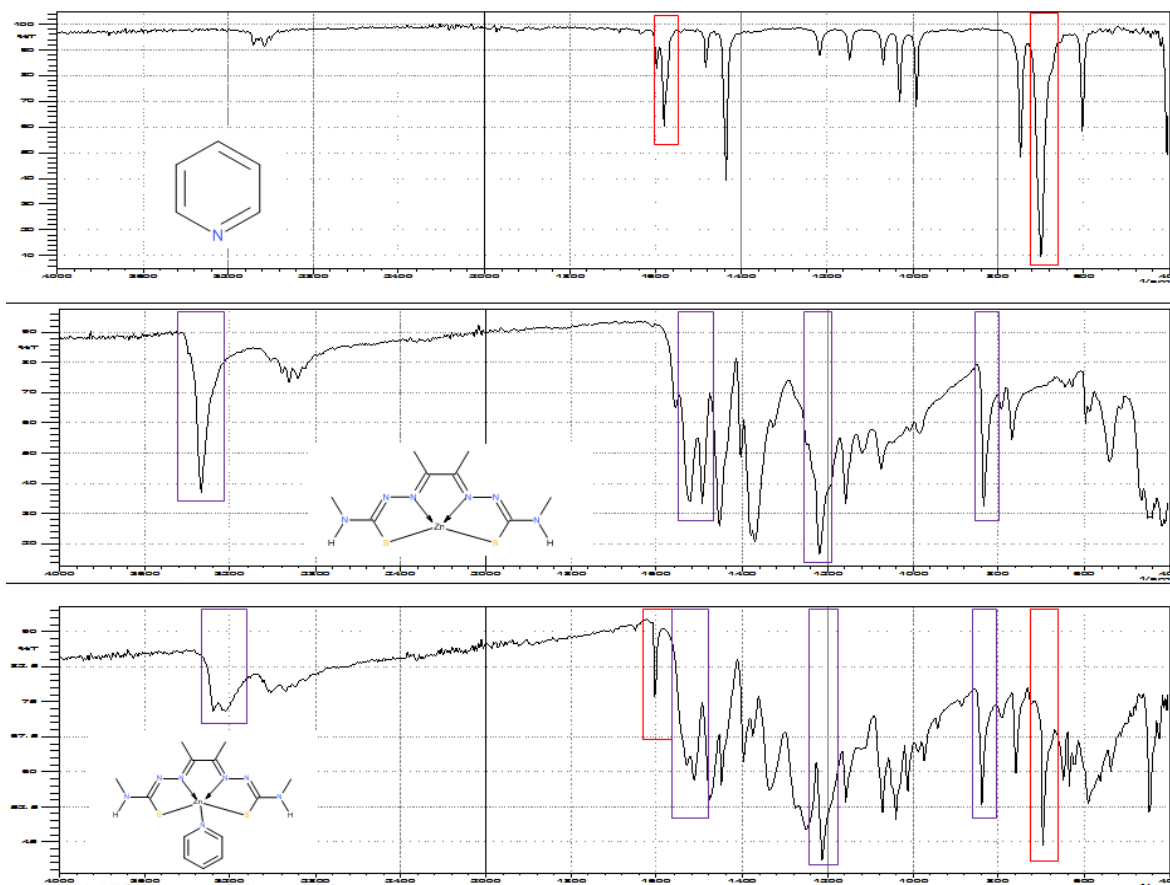


**Figure 4.3.4.2.** A comparison of the infra-red spectra of pyridine, Zn-BDO-Me-Me and Zn-BDO-Me-Me-Pyridine. The red boxes highlight the similar peaks between pyridine and Zn-BDO-Me-Me-Pyridine. The purple boxes highlight the similar peaks between Zn-BDO-Me-Me and Zn-BDO-Me-Me-Pyridine.

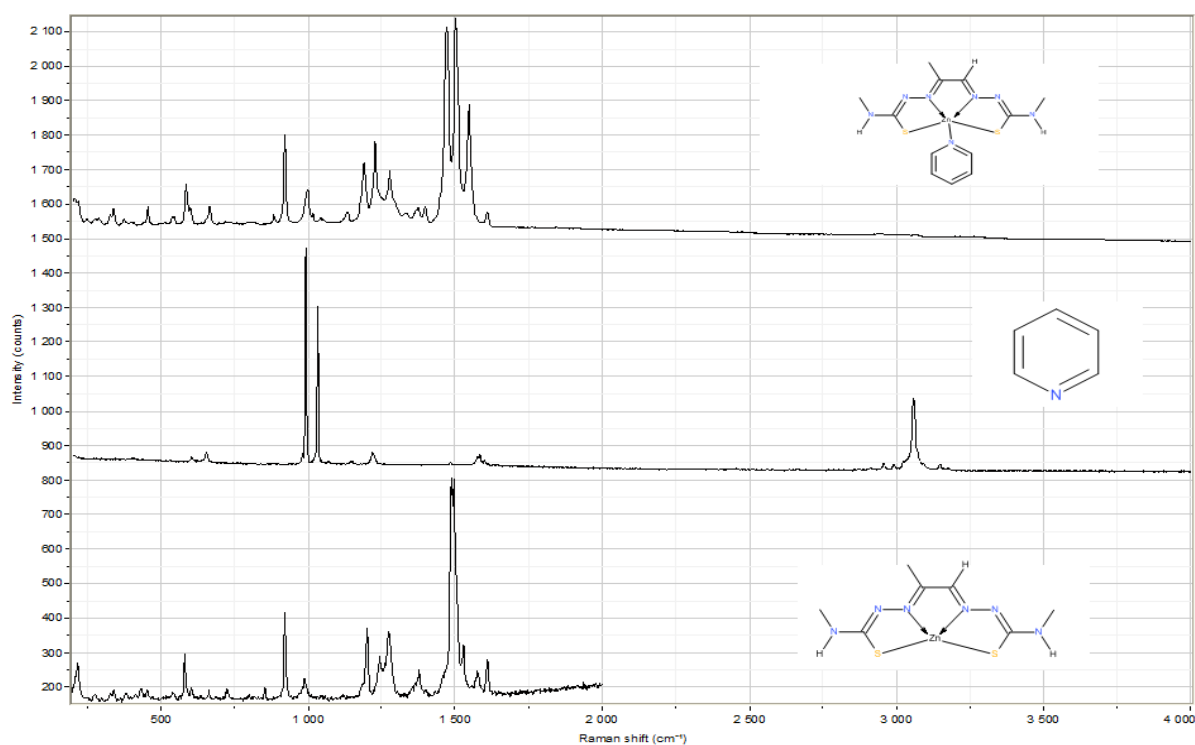


**Figure 4.3.4.3.** A comparison of the Raman spectra of pyridine, Zn-PADA-Me-Me and Zn-PADA-Me-Me-Pyridine. The spectrum of Zn-PADA-Me-Me was obtained by using an infrared laser (784.15 nm) and only up to  $2000\text{ cm}^{-1}$ .



Reports<sup>223-225</sup> in the literature suggests that the zinc-nitrogen bond, where the nitrogen is part of a pyridine ligand, can be found in an infrared or Raman spectrum at around 200-260 cm<sup>-1</sup>. Unfortunately 200 cm<sup>-1</sup> is below the detection range of the infrared spectrometer used. The Raman spectra were collected up to 200 cm<sup>-1</sup> which do show peaks in the region reported for Zn-N bonds. However, it not possible to say with any level of certainty that these peaks are due to the Zn-N bond of the pyridine coordinating with the zinc atom as the zinc atom is also bound to the bis(thiosemicarbazone) ligand via two Zn-N bonds.

The UV-vis spectra of the zinc complexes with the pyridine adduct was taken. The spectra obtained were all very similar to the zinc complexes without the pyridine adduct. The position of the  $\lambda_{\text{max}}$  varied only by a couple of nanometres which could be due to error in the labelling of the peak by the software. It seems that the presence of the pyridine adduct does not have much of an effect on the UV-vis spectrum of the resulting zinc complex.

The complex Zn-PADA-Ph-Ph-pyridine was re-synthesised with aim of sending the sample for analysis by X-ray diffraction, the integrals of proton NMR suggested that despite the same method being followed the product had two equivalents of pyridine per zinc bis(thiosemicarbazone) complex. This result seems to suggest that the number of pyridines that chelate to a zinc complex may be variable however, even though the number of pyridines may differ this still shows that pyridine is able to chelate to a zinc atom of a bis(thiosemicarbazone) complex. It was later decided that Zn-PADA-Ph-Ph-pyridine produced a product in the form of a powder which was not suitable for X-ray diffraction studies. Zn-BDO-Me-Me-pyridine did produce a crystalline product which was sent off to UCL for X-ray diffraction studies which generated an X-ray crystal structure (Figure 4.3.3.5).

The crystal structure data is in close agreement when the bonding lengths (Table 4.3.3.6.) and bonding angles (Table 4.3.3.7.) are compared to published data on related complexes.<sup>57, 191</sup> The crystal structure very strongly supports that the nitrogen of the pyridine adduct does indeed co-ordinate with the zinc atom with the Zn-BDO-Me-Me complex in the axial position. H. Betts *et al.*<sup>137</sup> has published some X-ray crystal data on Zn-BDO-Me-Me that has been co-ordinated with dimethylaminopyridine (DMAP), a table tabulating the zinc bonds lengths within this complex can be found below (Table 4.3.5.4.).

Bond	Bond length (H.Betts <sup>137</sup> )	Bond length (This project)
Zn1-S1	2.3725 (7) Å	2.3635 (6) Å
Zn1-S2	2.3946 (6) Å	2.3718 (6) Å
Zn-N3	2.117 (2) Å	2.1218 (18) Å
Zn-N4	2.112 (2) Å	2.1241 (17) Å
Zn-N7	2.0688 (19) Å	2.0900 (18) Å

**Table 4.3.5.4.** A comparison of the zinc bond lengths in Zn-BDO-Me-Me-pyridine and Zn-BDO-Me-Me-DMAP as reported by H.Betts<sup>137</sup> and co-workers. Estimated standard deviations (esd) are shown in parentheses.

Table 4.3.5.4. shows that despite the pyridine/DMAP ligands having slightly different structures the bonding lengths between the zinc ion and nitrogen and sulphur atoms are similar. In both cases the bond length between the zinc and the nitrogen of the pyridine (Zn-N7) is slightly shorter than the bond length between the zinc and imine nitrogen's. The crystal structure illustration (Figure 4.3.3.5.) shows that the zinc atom is a little bit above the N<sub>2</sub>S<sub>2</sub> plane, the distance between the zinc atom and the N<sub>2</sub>S<sub>2</sub> plane has not been established in this project but in the case of Zn-BDO-Me-Me-DMAP it was reported to be 0.517 Å.<sup>137</sup>

#### **4.4. Zn-BDO-Me-Me on PS-DMAP and PVP**

After establishing that pyridine can form a fifth coordinate bond with a zinc in a bis(thiosemicarbazone) complex the next step was to bind a chosen complex (Zn-BDO-Me-Me) to both the polymer supports. It was desirable to create a polymer-complex binding method that could be easily applied to all of the synthesised zinc complexes, as all these zinc complexes are readily soluble in DMSO it was decided to use a variation of approach 2, which was used in the Zn-BDO-Me-Me + pyridine reactions.

##### **4.4.1. Methods**

###### **Zn-BDO-Me-Me + PS-DMAP**

Zn-BDO-Me-Me (0.089 g, 0.00027 mol) was dissolved in DMSO (8 mL). Polystyrene bound Dimethylaminopyridine (0.029 g) was added to the solution and left to stir (2 days). The product was recovered via filtration, washed with diethyl ether (5 x 10 mL). The solid was dried in air. An orange solid (0.033 g) was recovered.

###### **Zn-BDO-Me-Me + PVP**

Zn-BDO-Me-Me (0.089 g, 0.00027 mol) was dissolved in DMSO (8 mL). Poly-(4-vinylpyridine) (0.029 g) was added to the solution and left to stir (2 days). The product was recovered via

filtration, washed with diethyl ether (5 x 10 mL). The solid was dried in air. A yellow solid (0.018 g) was recovered.

#### **4.4.2. Infra-red and Raman analysis of the products**

As the products could not be readily analysed by NMR spectroscopy due to the insolubility of the product, IR and Raman spectroscopy were the principle techniques used to analyse the products.

##### **Zn-BDO-Me-Me on PS-DMAP**

**IR (neat):**  $\text{cm}^{-1}$  = 3260 (w), 2924 (w), 1611 (m), 1510 (m), 1454 (m), 1375 (s), 1346 (s), 1281 (m), 1211 (s), 1155 (m), 1109 (m), 1013 (s), 949 (m), 928 (m), 853 (s), 806 (s), 768 (m), 700 (s), 530 (s), 446 (s). **Raman (neat), laser = 632.81 nm:**  $\text{cm}^{-1}$  = 1610 (w), 1540 (m), 1474 (m), 1372 (w), 1321 (m), 1282 (m), 1228 (m), 1183 (m), 1030 (m), 1000 (m), 986 (m), 856 (m), 775 (m), 668 (m), 594 (m), 564 (m), 445 (s), 431 (s), 328 (s).

Figures 4.4.2.1. and 4.4.2.2. shows stacked infra-red and Raman spectra of the product, Zn-BDO-Me-Me and the PS-DMAP.

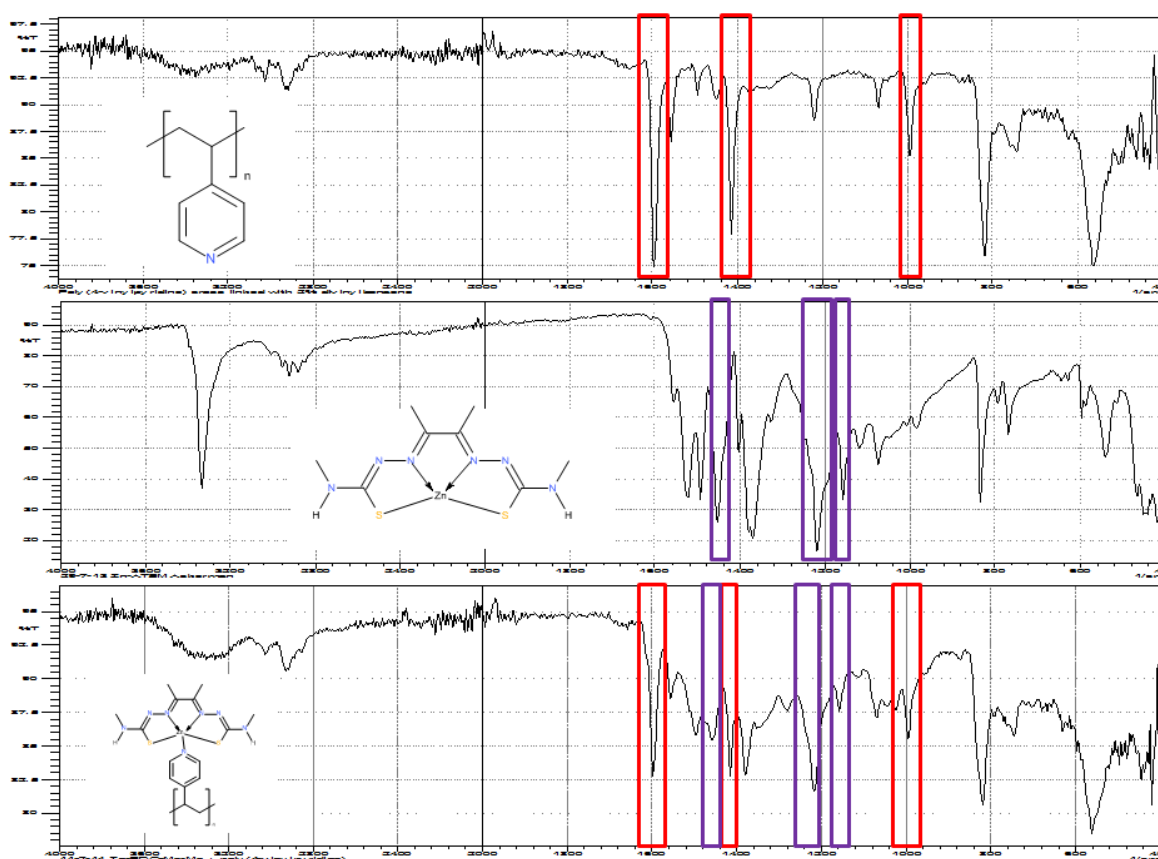


**Figure 4.4.2.1.** A comparison of the infra-red spectra of PS-DMAP, Zn-BDO-Me-Me and Zn-BDO-Me-Me on PS-DMAP. The red boxes highlight the similar peaks between PS-DMAP and Zn-BDO-Me-Me on PS-DMAP. The purple boxes highlight the similar peaks between Zn-BDO-Me-Me and Zn-BDO-Me-Me on PS-DMAP.

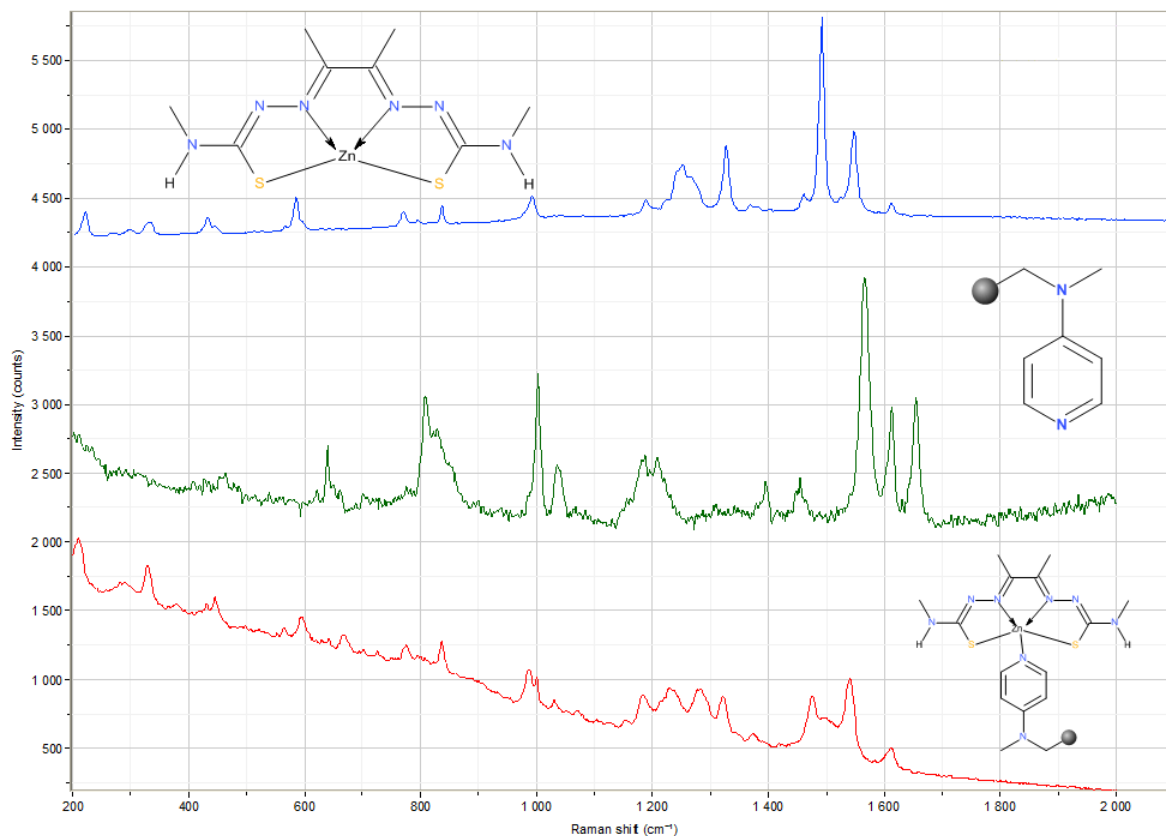


**Figure 4.4.2.2.** A comparison of the Raman spectra of PS-DMAP (green), Zn-BDO-Me-Me (blue) and Zn-BDO-Me-Me on PS-DMAP (red).

### Zn-BDO-Me-Me on PVP

**IR (neat):**  $\text{cm}^{-1}$  = 3285 (w), 2920 (w), 1595 (m), 1555 (m), 1493 (m), 1458 (m), 1414 (m), 1379 (m), 1279 (m), 1215 (s), 1157 (m), 1069 (m), 1043 (m), 1024 (m), 993 (m), 818 (m), 743 (m), 561 (s).

**Raman (neat), laser = 632.81 nm:**  $\text{cm}^{-1}$  = 3051 (w), 1610 (s), 1542 (s), 1499 (s), 1481 (s), 1324 (s), 1283 (s), 1237 (s), 993 (s), 838 (s), 668 (s), 594 (s), 429 (s), 332 (s).

Figure 4.4.2.3. and 4.4.2.4. shows stacked infra-red and Raman spectra of the product, Zn-BDO-Me-Me and the unbound PVP.

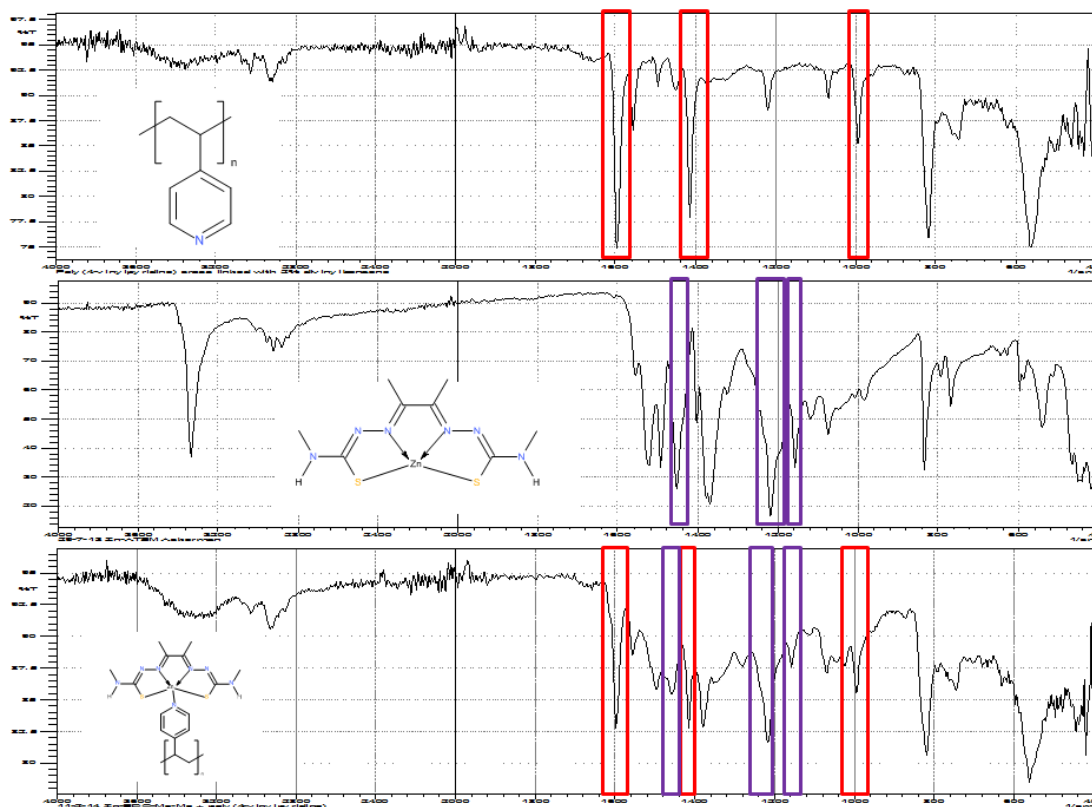


**Figure 4.4.2.3.** A comparison of the infra-red spectra of PVP, Zn-BDO-Me-Me and Zn-BDO-Me-Me on PVP. The red boxes highlight the similar peaks between PVP and Zn-BDO-Me-Me on PVP. The purple boxes highlight the similar peaks between Zn-BDO-Me-Me and Zn-BDO-Me-Me on PVP.

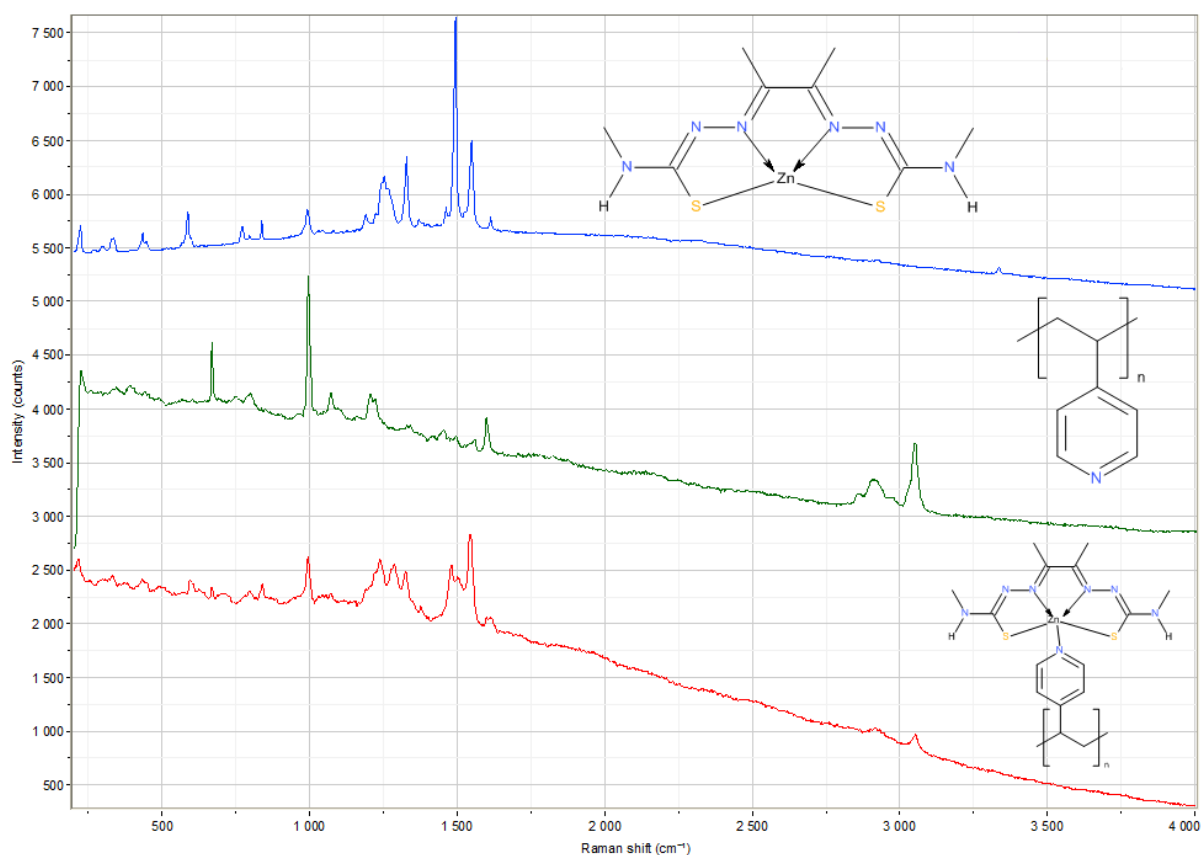


**Figure 4.4.2.4.** A comparison of the Raman spectra of PVP (green), Zn-BDO-Me-Me (blue) and Zn-BDO-Me-Me on PVP (red).

A blank procedure was run in order to look at the effect that solvents used in the reaction have on the polymer. The chosen polymer was added to DMSO and left to stir overnight. The polymer was then recovered via filtration and washed with 5 lots of 10 mL of diethyl ether. The polymer was then left to dry in air. With the poly-(4-vinylpyridine) very minimal change was observed in the IR or Raman spectra of the product when compared to the reference spectra of stock polymer. The IR spectrum of dimethylaminopyridine however, suggests that either the polymer was still wet or that the solvents have interacted with the polymer in some way as peaks for diethyl ether and DMSO were observed in the spectrum. The Raman spectrum of dimethylaminopyridine had extra peaks even though these were not directly attributed to solvents. It is suspected that the presence of solvents in the polymer would not adversely affect the linking reaction between polymer and zinc complex but it should still be noted as it may give rise to variations in the products spectra.

The attempts to bind Zn-BDO-Me-Me to the pyridine based polymer supports DMAP and PVP seem to be successful. In both cases the infrared spectrum in the final loaded polymer contains peaks which can be attributed to both the Zn-BDO-Me-Me complex and the unloaded polymer. Through Raman spectroscopy it was found a lot harder to identify peaks that are likely to attribute to both the Zn-BDO-Me-Me complex and the unloaded polymer. This is mostly likely due to the Raman spectra containing weaker peaks which were less prominent against the baseline. However there are slight signs of the two individual components being present in the polymers which are expected to be loaded with the zinc complex. Given more time, further investigations into optimising the Raman acquisition parameters may solve this issue and hopefully produce more compelling evidence that the polymers are bound with the Zn-BDO-Me-Me.

Attempts to bind a selection of zinc bis(thiosemicarbazone) complexes to both the polymers PS-DMAP and PVP were undertaken. However by just using infrared and Raman spectroscopy alone it was not possible to say confidently that the zinc complexes were successfully loaded on to the polymers and due to time constraints of this project it was not possible to pursue this further. The results of the investigations earlier in this chapter about the proof of concept of zinc bis(thiosemicarbazone) complexes being able to bind to pyridine functionalised polymers are positive. Therefore further investigations into the loading of different bis(thiosemicarbazone) complexes on both the PS-DMAP and PVP polymer support is warranted.

A preliminary transmetalation reaction was carried out on a sample of the PS-DMAP and PVP which were loaded with Zn-BDO-Me-Me. The hope was that upon the addition of a copper acetate solution the reaction mix would turn to a brown colour suggesting the formation of Cu-BDO-Me-Me. Both the loaded polymers were stirred in a 0.1 M solution of copper (II) acetate for 3 days. Control experiments were ran where each of the polymers free of Zn-BDO-Me-Me were

also stirred for 3 days in a 0.1 M solution of copper (II) acetate. The resulting solutions of the PVP loaded with Zn-BDO-Me-Me and the controls all were the same colour as the starting solutions however for all the solutions appeared a slightly lighter blue. The PS-DMAP loaded with Zn-BDO-Me-Me produced a solution which was a little greener in colour than the starting solution.

It is hard to tell if the PVP polymer was able to undergo the transmetalation reaction. Without knowing the loading of each polymer with Zn-BDO-Me-Me it is not possible to know the best concentration of copper (II) acetate solution to use. It is expected that even if Zn-BDO-Me-Me bound to both the polymers did undergo transmetalation, the amount of Cu-BDO-Me-Me produced may not be enough to inflect a noticeable colour change within the initial blue solution. Further investigation is required for both polymers where a method that needs to be developed that can produce a transmetalated copper complex in a suitable quantity in order to allow characterisation of the product. Once this is established then the reaction conditions can be optimised for the production of the radio-copper complexes for diagnostic imaging.

## **4.5. Conclusions**

It was found that for a selection of five symmetric and three dissymmetric zinc bis(thiosemicarbazone) complexes that they underwent transmetalation with copper (II) acetate very rapidly in order to form the corresponding copper bis(thiosemicarbazone) complex. Using infrared, Raman spectroscopy and mass spectrometry the identity of the products were confirmed as the expected copper complexes. There is no reason not to expect the transmetalation reaction would work for any of the other zinc complexes synthesised in chapter 3.

Attempts to chelate a pyridine ligand to the zinc ion of a selected zinc bis(thiosemicarbazone) complexes was also successful. Out of the six of the selected zinc complexes, four bound with one pyridine molecule in order to form what is believed to be four novel complexes. It was found that the remaining two zinc complexes bound to pyridine in a different ratio than one to one. Despite this, all six selected zinc complexes demonstrated that pyridine is able to bind via the zinc ion of a zinc bis(thiosemicarbazone) complex in a range of zinc complexes. A crystal structure of Zn-BDO-Me-Me with the pyridine adduct was successfully obtained via X-ray diffraction which further demonstrated that pyridine can form a fifth coordinate bond with the zinc core of the zinc bis(thiosemicarbazone) complex.

Attempts were undertaken to attach a zinc bis(thiosemicarbazone) complex to the pyridine functionalised polymers DMAP and PVP. It is believed that this is the first study with using PVP as a polymer platform for the transmetalation reaction for zinc bis(thiosemicarbazone) complexes. It

is expected that Zn-BDO-Me-Me as been successfully attached to the both DMAP and PVP. Infrared and Raman spectroscopy supports that this is the case, however it was found that the evidence collected by Raman spectroscopy was not as compelling as the evidence collected by infrared spectroscopy. Attempts to load alternative zinc bis(thiosemicarbazone) complexes on both DMAP and PVP were undertaken however the results from IR and Raman spectroscopy were not convincing in terms of if the zinc complex had bound to the polymers. If more time was available then this would most certainly be an area which is worth pursuing further.

Preliminary transmetalation reactions have been under taken but the results were inconclusive. Much more investigation is called for before the polymer based transmetalation reaction can be utilised to produce radio-copper tracers for the full range of copper complexes synthesised in this project.



## **Overall conclusions and future work**

Thirty bis(thiosemicarbazone) ligands have been successfully synthesised, of which seventeen of these are dissymmetric ligands. It is believed that 13 ligands are novel. Experience showed that the exploitation of carbonyl reactivity was a superior approach compared to the synthesis via the acetal protection method. This is because using this method a mono-substituted-3-thiosemicarbazone intermediate could be synthesised in a good yield with a relatively high level of purity. A particularly convenient point is that the intermediate precipitates out of solution which made recovery very straight forward. The acetal protection method on the other hand required two steps to create the same mono-substituted-3-thiosemicarbazone intermediate which normally required DMF as a solvent which had to be removed. The critical disadvantages about this method are that the yields were often low and that after the DMF was removed a sludge like product was left over which was very difficult to work with. However, this being said the protection approach could have the potential to synthesise ligands with Me/Et on the backbone free of isomeric impurities. If biological screening data shows that this was vital for the optimisation of imaging quality then one area of future investigation would be synthesising ligands with Me/Et on the backbone via the acetal protection approach, or by using another protecting group. This could also be applied to complexes with or H/H on the backbone, if they become of interest. In the terms of the first aim and the first objective of this project (page 46), which relates to being able to synthesise dissymmetric bis(thiosemicarbazone) ligands, it can be said that they have been achieved. However in the future, depending on the results of the biological data, there may be a call to expand this aim and objective so that they cover synthesising a wider range of ligands with substituents different from those which were made during this project. There may also be an interest in attaching pendant arms to the ligands in order to impart further desirable properties on to the complex. All efforts have been made in order to design a generic synthesis method that can be used to make a range of bis(thiosemicarbazone) ligands. This has been achieved for the most part. However, ligands from each subclass explored during this thesis still possess unique challenges for their clean synthesis. In our hands attempts to create dissymmetric ligands with hydrogen atoms on the di-imine backbones were unsuccessful.

Project aim 2 and objective 2, called for the synthesis of a range of symmetric ligands containing each backbone (H/Me, Me/Me and Me/Et) for comparison both in characterisation and biological screening. A total of 13 symmetric ligands have been synthesised which covers the range of substituents used in the synthesis of the dissymmetric ligands. All of the symmetric ligands have been fully characterised.

In terms of objective 3, partial optimisation of each synthetic step was undertaken in order to produce products with the highest yield and purity in the least number of manipulations. Whenever possible the reactions would be carried out in more biologically compatible solvents, such as water and ethanol, if purity and yield were not compromised.

The ligands were successfully chelated with zinc or copper 2+ ions in order to yield the resulting zinc or copper bis(thiosemicarbazone) complexes, respectively. Eighteen copper complexes were synthesised of which twelve are expected to be novel and out of the twenty zinc complexes that were produced, fourteen are believed to be first reported in this thesis. If there was a call for a copper or zinc complex that had not been synthesised but the related ligand had been made during this project, it is expected that this could be done by following the methods established in this project. In respects to the initial aim and objectives of this project which relates to complex synthesis (aim 3, objective 4 & 5), it is regarded that these have been successfully met as it is believed that the synthetic methods reported can be applied to entire library of ligands produced in this project. Even though in some cases complications may be encountered as some complexes maybe susceptible to forming a fifth coordinate bond with solvent or reagent molecules. Investigations in to synthesising copper bis(thiosemicarbazone) complexes by transmetalating the zinc from a zinc bis(thiosemicarbazone) complex precursor with copper have been under taken. Early results suggest that the transmetalation reaction works for a range of zinc bis(thiosemicarbazone) complexes. A handful of zinc bis(thiosemicarbazone) complexes containing a pyridine adduct have also been synthesised and characterised for the investigation of carrying out the transmetalation reaction on pyridine based solid supports. A previously reported polymer alongside a cheaper, more readily available polymer support has been loaded with a zinc complex. Initial spectroscopic data shows promising results. Preliminary transmetalation reactions using the polymer support were inconclusive.

Further investigation in to the transmetalation reaction on the polymer supports is warranted. The key areas of interest would be loading both PS-DMAP and PVP with a large range of zinc complexes and verifying if the zinc complexes successfully bind to the polymers. In order to verify binding optimisation of spectroscopic techniques, particularly Raman, may be required. Identifying the level of loading of each zinc complex on both polymers would be valuable information for optimisation of the transmetalation process. Once all this is achieved, work on development of a generic and simple method for the transmetalation of zinc complexes on a polymer support, which can be applied to the range of complexes synthesised in this project would provide a very convenient method for synthesising the related radio-copper complexes for future biological screening.

Additional work on identifying the impurity, expected to be related to the acetate ion, found in a number of zinc complexes can be pursued as well as verifying if this impurity is also present in any of the copper complexes. If a reagent impurity is present in the related zinc complex ascertaining if it interferes with the transmetalation reaction would be of interest. If a reagent impurity was found to be present in a copper complex, a key thing to gather would be if the impurity can be removed via purification techniques. If this is not possible then whether the impurity has an effect, either positively or negatively, on the pharmacokinetics of the complex in regards to imaging hypoxia or copper metabolism in the brain.

All intermediates, ligands and complexes, both novel and previously reported, were comprehensively characterised by a range of techniques, which has filled some gaps in the reported literature. Due to restrictions in resources and time, it was not possible to obtain mass spectrometry and CHN data on all complexes and ligands made in this project however it was possible to obtain this data for the vast majority of the novel compounds. It is regarded that aim 4 and objective 6 of this project have been mostly achieved.

The Cu (II/I) reduction potential data collected on a selection of the copper complexes showed that complexes with Me/Et on the back bone had lower reduction potentials than Cu-BDO-Me-Me, this may suggest that they have greater hypoxia selectivity than Cu-BDO-Me-Me and therefore are good candidates for further testing for hypoxia selectivity. Unfortunately at the time of writing no lipophilicity data was available but if a trend observed in a paper by J. Dearling *et al.*<sup>77</sup> PDO based copper complexes with more lipophilic substituents such as dimethyl and ethyl may have higher hypoxia selectivity than PDO complexes with NH<sub>2</sub> and methyl on the terminal amines. Objectives 7, 8 and 9 are regarded as being partially achieved. Future work in order to meet the remainder of the objectives would be to collect lipophilicity values for the copper complexes, particularly the copper complexes identified by their reduction potentials as good candidates.

Due to the lack of personnel and recurrent problems in radio-copper supply, it has not been possible to directly measure hypoxia selectivity or brain accumulation/retention. So in this regard it has not been possible to meet the biological screening components of objective 8 and 9. Assuming that the required personnel and radio-copper is available to screen candidate compounds, future experiments would be to establish if the dissymmetric compounds synthesised in this project are superior imaging agents for hypoxia by testing them in the isolated heart model.

The hypothesis of this thesis was:

The use of radio labelled dissymmetric copper bis(thiosemicarbazone) complexes offers the opportunity to achieve superior imaging capabilities in diagnostic imaging of hypoxia by positron emission tomography, than currently used symmetric copper bis(thiosemicarbazone) complexes.

Even though the work in this thesis has made progress towards showing that dissymmetric copper bis(thiosemicarbazone) complexes have a potential to offer superior imaging capabilities, without the direct measuring of their hypoxia selectivity it is not possible to prove or disprove this hypothesis at this point in time. However, with a little further biological screening it should possible to comment further on this hypothesis.

## Bibliography

- 1 A. H. Elgazzar, *A Concise Guide to Nuclear Medicine*, Springer, 2011.
- 2 S. Vallabhajosula, *Molecular Imaging: Radiopharmaceuticals for PET and SPECT*, Springer, 2009.
- 3 P. Blower, *Dalton Trans.*, 2006, **6**, 1705-1711 (DOI:10.1039/b516860k).
- 4 P. J. Blower, *Transit. Met. Chem.*, 1997, **23**, 109-112.
- 5 P. F. Sharp, H. G. Gemmell and A. D. Murray, *Practical nuclear medicine*, 2005.
- 6 B. M. Paterson and P. S. Donnelly, *Chem. Soc. Rev.*, 2011, **40**, 3005-3018 (DOI:10.1039/c0cs00215a).
- 7 R. Zimmermann, *Nuclear Medicine: Radioactivity for Diagnosis and Therapy*, EDP Sciences, 2007.
- 8 G. Malviya and T. K. Nayak, *Curr. Pharm. Biotechnol.*, 2013, **14**, 669-682 (DOI:10.2174/1389201014666131226104750).
- 9 J. Knuuti and H. Tuunanen, *Q. J. Nucl. Med. Mol. Imag.*, 2010, **54**, 168-176.
- 10 L. J. Brown, D. R. Bouvet, S. Champion, A. M. Gibson, Y. Hu, A. Jackson, I. Khan, N. Ma, N. Millot, H. Wadsworth and R. C. D. Brown, *Angew. Chem. Int. Ed.*, 2007, **46**, 941-944 (DOI:10.1002/anie.200603394).
- 11 N. Wagner, A. Bosshart, J. Failmezger, M. Bechtold and S. Panke, *Angew. Chem. Int. Ed.*, 2015, **54**, 4182-4186 (DOI:10.1002/anie.201411279).
- 12 R. Baskar, K. A. Lee, R. Yeo and K. W. Yeoh, *Int. J. Med. Sci.*, 2012, **9**, 193-199 (DOI:10.7150/ijms.3635).
- 13 R. J. Kowalsky, *Radiopharmaceuticals in nuclear medicine practice*, Norwalk, Conn., Appleton & Lange, 1987.
- 14 G. K. Von Schulthess, *Molecular Anatomic Imaging: PET-CT and SPECT-CT Intergrated Modality Imaging*, Lippincott Williams & Wilkins, 2007.
- 15 S. Pascu and J. Dilworth, *J. Labelled Compd. Radiopharm.*, 2014, **57**, 191-193 (DOI:10.1002/jlcr.3196).
- 16 A. J. H. A. Scholte, C. J. Roos and J. M. Van Werkhoven, *EuroIntervention*, 2010, **6**, G94-G100.
- 17 I. N. Fleming, F. J. Gilbert and P. J. Blower, *Nucl. Med. Commun.*, 2012, **33**, 1-3 (DOI:10.1097/MNM.0b013e32834c6411).
- 18 D. Brasse and A. Nonat, *Dalton Trans.*, 2015, **44**, 4845-4858 (DOI:10.1039/C4DT02911A).
- 19 S. Puttick, C. Bell, N. Dowson, S. Rose and M. Fay, *Drug Discov. Today*, 2015, **20**, 306-317 (DOI:10.1016/j.drudis.2014.10.016).
- 20 G. Smith, L. Carroll and E. O. Aboagye, *Mol. Imaging. Biol.*, 2012, **14**, 653-666 (DOI:10.1007/s11307-012-0590-y).

- 21 R. Yao, R. Lecomte and E. S. Crawford, *J. Nucl. Med. Technol.*, 2012, **40**, 157-165 (DOI:10.2967/jnmt.111.098632).
- 22 S. Kajander, A. Saraste, H. Ukkonen and J. Knuuti, *EuroIntervention*, 2010, **6**, G87-G93.
- 23 P. J. Blower, J. S. Lewis and J. Zweit, *Nucl. Med. Biol.*, 1996, **23**, 957-980 (DOI:10.1016/s0969-8051(96)00130-8).
- 24 T. J. Wadas, E. H. Wong, G. R. Weisman and C. J. Anderson, *Curr. Pharm. Des.*, 2007, **13**, 3-16 (DOI:10.2174/138161207779313768).
- 25 E. Bodio, M. Boujtita, K. Julienne, P. Le Saec, S. G. Gouin, J. Hamon, E. Renault and D. Deniaud, *ChemPlusChem*, 2014, **79**, 1284-1293 (DOI:10.1002/cplu.201402031).
- 26 B. M. Zeglis, J. L. Houghton, M. J. Evans, N. Viola-Villegas and J. S. Lewis, *Inorg. Chem.*, 2014, **53**, 1880-1899 (DOI:10.1021/ic401607z).
- 27 B. Wangler, R. Schirrmacher, P. Bartenstein and C. Wangler, *Mini-Rev. Med. Chem.*, 2011, **11**, 968-983 (DOI:10.2174/138955711797068445).
- 28 E. I. Solomon, D. E. Heppner, E. M. Johnston, J. W. Ginsbach, J. Cirera, M. Qayyum, M. T. Kieber-Emmons, C. H. Kjaergaard, R. G. Hadt and L. Tian, *Chem. Rev.*, 2014, **114**, 3659-3853 (DOI:10.1021/cr400327t).
- 29 R. Hueting, *J. Label. Compd. Radiopharm.*, 2014, **57**, 231-238 (DOI:10.1002/jlcr.3155).
- 30 B. E. Kim, T. Nevitt and D. J. Thiele, *Nat. Chem. Biol.*, 2008, **4**, 176-185 (DOI:10.1038/nchembio.72).
- 31 P. S. Donnelly, Z. Xiao and A. G. Wedd, *Curr. Opin. Chem. Biol.*, 2007, **11**, 128-133 (DOI:10.1016/j.cbpa.2007.01.678).
- 32 C. Duncan, L. Bica, P. J. Crouch, A. Caragounis, G. E. Lidgerwood, S. J. Parker, J. Meyerowitz, I. Volitakis, J. R. Liddell, R. Raghupathi, B. M. Paterson, M. D. Duffield, R. Cappai, P. S. Donnelly, A. Grubman, J. Camakaris, D. J. Keating and A. R. White, *Metallomics*, 2013, **5**, 700-714 (DOI:10.1039/c3mt20231c).
- 33 E. Gaggelli, H. Kozlowski, D. Valensin and G. Valensin, *Chem. Rev.*, 2006, **106**, 1995-2044 (DOI:10.1021/cr040410w).
- 34 P. Chen, A. M. Keller, C. P. Joshi, D. J. Martell, N. M. Andoy, J. J. Benítez, T. Y. Chen, A. G. Santiago and F. Yang, *Biochemistry*, 2013, **52**, 7170-7183 (DOI:10.1021/bi400597v).
- 35 G. Cerchiaro, T. M. Manieri and F. R. Bertuchi, *Metallomics*, 2013, **5**, 1336-1345 (DOI:10.1039/c3mt00136a).
- 36 N. Arnal, G. R. Morel, M. J. T. De Alaniz, O. Castillo and C. A. Marra, *Int. J. Alzheimer's Dis.*, 2013, **2013**, 1-15 (DOI:10.1155/2013/414817).
- 37 N. Arnal, L. Dominici, M. J. T. D. Tacconi and C. A. Marra, *Nutrition*, 2014, **30**, 96-106 (DOI:10.1016/j.nut.2013.06.009).
- 38 A. N. Prasad, S. Levin, C. A. Rupa and C. Prasad, *Brain and Development*, 2011, **33**, 866-876 (DOI:10.1016/j.braindev.2011.08.002).

- 39 J. Woodward, *Medicine*, 2015, **43**, 234-238 (DOI:10.1016/j.mpmed.2015.01.011).
- 40 J. M. Trocello, E. Broussolle, N. Girardot-Tinant, M. Pelosse, A. Lachaux, C. Lloyd and F. Woimant, *Rev. Neurol.*, 2013, **169**, 936-943 (DOI:10.1016/j.neurol.2013.05.002).
- 41 P. J. Blower, *Dalton Trans.*, 2015, **44**, 4819-4844 (DOI:10.1039/C4DT02846E).
- 42 E. A. Mathez, J. D. Blacic, J. Beery, C. Maggiore and M. Hollander, *Geophys. Res. Lett.*, 1984, **11**, 947-950.
- 43 J. P. Holland, R. Ferdani, C. J. Anderson and J. S. Lewis, *PET Clinics*, 2009, **4**, 49-67 (DOI:10.1016/j.cpet.2009.04.013).
- 44 A. H. Asad, S. V. Smith, S. Chan, C. M. Jeffery, L. Morandea and R. I. Price, 2012, **1509**, 91-95 (DOI:10.1063/1.4773947).
- 45 Y. Fujibayashi, K. Wada, H. Taniuchi, Y. Yonekura, J. Konishi and A. Yokoyama, *Biol. Pharm. Bull.*, 1993, **16**, 146-149.
- 46 Y. Ng, J. L. Lacy, J. W. Fletcher and M. A. Green, *Appl. Radiat. Isot.*, 2014, **91**, 38-43 (DOI:10.1016/j.apradiso.2014.05.006).
- 47 B. M. Paterson, P. Roselt, D. Denoyer, C. Cullinane, D. Binns, W. Noonan, C. M. Jeffery, R. I. Price, J. M. White, R. J. Hicks and P. S. Donnelly, *Dalton Trans.*, 2014, **43**, 1386-1396 (DOI:10.1039/c3dt52647j).
- 48 T. J. Wadas, E. H. Wong, G. R. Weisman and C. J. Anderson, *Chem. Rev.*, 2010, **110**, 2858-2902 (DOI:10.1021/cr900325h).
- 49 B. M. Paterson, K. Alt, C. M. Jeffery, R. I. Price, S. Jagdale, S. Rigby, C. C. Williams, K. Peter, C. E. Hagemeyer and P. S. Donnelly, *Angew. Chem., Int. Ed.*, 2014, **53**, 6115-6119 (DOI:10.1002/anie.201402613).
- 50 R. J. Browning, V. Rajkumar, R. B. Pedley, R. J. Eckersley and P. J. Blower, *J. Labelled Compd. Radiopharm.*, 2014, **57**, 279-284 (DOI:10.1002/jlcr.3157).
- 51 F. Peng, X. Lu, J. Janisse, O. Muzik and A. F. Shields, *J. Nucl. Med.*, 2006, **47**, 1649-1652.
- 52 K. R. Zinn, T. R. Chaudhuri, T. P. Cheng, J. S. Morris and W. A. Meyer Jr, *Cancer*, 1994, **73**, 774-778.
- 53 F. Szelecsényi, G. Blessing and S. M. Qaim, *Appl. Radiat. Isot.*, 1993, **44**, 575-580.
- 54 J. Zweit, A. M. Smith, S. Downey and H. L. Sharma, *Int J Rad Appl Instrum A*, 1991, **42**, 193-197.
- 55 I. Novak-Hofer and P. A. Schubiger, *Eur. J. Nucl. Med.*, 2002, **29**, 821-830 (DOI:10.1007/s00259-001-0724-y).
- 56 J. A. Odonoghue, M. Bardies and T. E. Wheldon, *J. Nucl. Med.*, 1995, **36**, 1902-1909.
- 57 J. P. Holland, F. I. Aigbirhio, H. M. Betts, P. D. Bonnitcha, P. Burke, M. Christlieb, G. C. Churchill, A. R. Cowley, J. R. Dilworth, P. S. Donnelly, J. C. Green, J. M. Peach, S. R. Vasudevan and J. E. Warren, *Inorg. Chem.*, 2007, **46**, 465-485 (DOI:10.1021/ic0615628).

- 58 M. Christlieb, H. J. Cloughton, A. R. Cowley, J. M. Heslop and J. R. Dilworth, *Transit. Met. Chem.*, 2006, **31**, 88-92 (DOI:10.1007/s11243-005-6354-7).
- 59 L. Alsop, A. R. Cowley, J. R. Dilworth, P. S. Donnelly, J. M. Peach and J. T. Rider, *Inorg. Chim. Acta*, 2005, **358**, 2770-2780 (DOI:10.1016/j.ica.2005.03.027).
- 60 R. P. Vieira and H. Beraldo, in *Ligand Design in Medicinal Inorganic Chemistry*, ed. T. Storr, Wiley & Sons Ltd, 2014, p. 175-204.
- 61 C. Neuberg and W. Neimann, *Chem. Ber.*, 1902, **35**, 2054-2056.
- 62 V. C. Barry, M. L. Conalty, C. N. O'Callaghan and D. Twomey, *Proc. R. Ir. Acad., Sect. B*, 1967, **65**, 309-324.
- 63 V. C. Barry, M. L. Conalty and J. F. O'Sullivan, *Cancer Research*, 1966, **26**, 2165-2168.
- 64 G. J. Van Giessen and H. G. Petering, *J. Med. Chem.*, 1968, **11**, 695-699.
- 65 M. Christlieb, A. R. Cowley, J. R. Dilworth, P. S. Donnelly, B. M. Paterson, H. S. R. Struthers and J. M. White, *Dalton Trans.*, 2007, , 327-331 (DOI:10.1039/b612907b).
- 66 M. Christlieb and J. R. Dilworth, *Chem. -Eur. J.*, 2006, **12**, 6194-6206 (DOI:10.1002/chem.200501069).
- 67 P. McQuade, K. E. Martin, T. C. Castle, M. J. Went, P. J. Blower, M. J. Welch and J. S. Lewis, *Nucl. Med. Biol.*, 2005, **32**, 147-156 (DOI:10.1016/j.nucmedbio.2004.10.004).
- 68 T. C. Castle, R. I. Maurer, F. E. Sowrey, M. J. Went, C. A. Reynolds, E. J. L. McInnes and P. J. Blower, *J. Am. Chem. Soc.*, 2003, **125**, 10040-10049 (DOI:10.1021/ja035737d).
- 69 P. J. Blower, M. J. Went, K. E. Martin and G. E. Smith, *J. Label. Compd. Radiopharm.*, 2007, **50**, 354-359 (DOI:10.1002/jlcr.1195).
- 70 K. Y. Djoko, B. M. Paterson, P. S. Donnelly and A. G. McEwan, *Metallomics*, 2014, **6**, 854-863 (DOI:10.1039/c3mt00348e).
- 71 T. S. Lobana, R. Sharma, G. Bawa and S. Khanna, *Coord. Chem. Rev.*, 2009, **253**, 977-1055 (DOI:10.1016/j.ccr.2008.07.004).
- 72 A. I. Matesanz, J. M. Pérez, P. Navarro, J. M. Moreno, E. Colacio and P. Souza, *J. Inorg. Biochem.*, 1999, **76**, 29-37 (DOI:10.1016/s0162-0134(99)00105-1).
- 73 B. M. Paterson, J. A. Karas, D. B. Scanlon, J. M. White and P. S. Donnelly, *Inorg. Chem.*, 2010, **49**, 1884-1893 (DOI:10.1021/ic902204e).
- 74 Y. Fujibayashi, H. Taniuchi, Y. Yonekura, H. Ohtani, J. Konishi and A. Yokoyama, *J. Nucl. Med.*, 1997, **38**, 1155-1160.
- 75 S. Kadowaki, M. Munekane, Y. Kitamura, M. Hiromura, S. Kamino, Y. Yoshikawa, H. Saji and S. Enomoto, *Biol. Trace Elem. Res.*, 2013, **154**, 111-119 (DOI:10.1007/s12011-013-9704-x).
- 76 P. S. Donnelly, A. Caragounis, T. Du, K. M. Laughton, I. Volitakis, R. A. Cherny, R. A. Sharples, A. F. Hill, Q. X. Li, C. L. Masters, K. J. Barnham and A. R. White, *J. Biol. Chem.*, 2008, **283**, 4568-4577 (DOI:10.1074/jbc.M705957200).



- 77 J. L. J. Dearling, J. S. Lewis, G. E. D. Muller, M. J. Welch and P. J. Blower, *J. Biol. Inorg. Chem.*, 2002, **7**, 249-259 (DOI:10.1007/s007750100291).
- 78 D. X. West, J. S. Ives, G. A. Bain, A. E. Liberta, J. ValdesMartinez, K. H. Ebert and S. HernandezOrtega, *Polyhedron*, 1997, **16**, 1895-1905 (DOI:10.1016/s0277-5387(96)00468-8).
- 79 J. K. Lim, C. J. Mathias and M. A. Green, *J. Med. Chem.*, 1997, **40**, 132-136 (DOI:10.1021/jm9605703).
- 80 L. J. Ackerman, P. E. Fanwick, M. A. Green, E. John, W. E. Running, J. K. Swearingen, J. W. Webb and D. X. West, *Polyhedron*, 1999, **18**, 2759-2767 (DOI:10.1016/s0277-5387(99)00173-4).
- 81 L. J. Ackerman, D. X. West, C. J. Mathias and M. A. Green, *Nucl. Med. Biol.*, 1999, **26**, 551-554 (DOI:10.1016/s0969-8051(99)00020-7).
- 82 G. Buncic, J. L. Hickey, C. Schieber, J. M. White, P. J. Crouch, A. R. White, Z. G. Xiao, A. G. Wedd and P. S. Donnelly, *Aust. J. Chem.*, 2011, **64**, 244-252 (DOI:10.1071/ch10463).
- 83 M. Christlieb, H. S. R. Struthers, P. D. Bonnitcha, A. R. Cowley and J. R. Dilworth, *Dalton Trans.*, 2007, , 5043-5054 (DOI:10.1039/b705087a).
- 84 S. C. Lim, K. A. Price, S. F. Chong, B. M. Paterson, A. Caragounis, K. J. Barnham, P. J. Crouch, J. M. Peach, J. R. Dilworth, A. R. White and P. S. Donnelly, *J. Biol. Inorg. Chem.*, 2010, **15**, 225-235 (DOI:10.1007/s00775-009-0587-4).
- 85 R. Hueting, M. Christlieb, J. R. Dilworth, E. G. Garayoa, V. Gouverneur, M. W. Jones, V. Maes, R. Schibli, X. Sun and D. A. Tourwe, *Dalton Trans.*, 2010, **39**, 3620-3632 (DOI:10.1039/b925128f).
- 86 D. G. Calatayud, E. Lopez-Torres and M. A. Mendiola, *Polyhedron*, 2013, **54**, 39-46 (DOI:10.1016/j.poly.2013.02.025).
- 87 J. S. Casas, M. V. Castano, E. E. Castellano, J. Ellena, M. S. Garcia-Tasende, A. Gato, A. Sanchez, L. M. Sanjuan and J. Sordo, *Inorg. Chem.*, 2002, **41**, 1550-1557 (DOI:10.1021/ic0111942).
- 88 M. A. Blanco, E. Lopez-Torres, M. A. Mendiola, E. Brunet and M. T. Sevilla, *Tetrahedron*, 2002, **58**, 1525-1531 (DOI:10.1016/s0040-4020(02)00016-9).
- 89 A. Diaz, I. Garcia, R. Cao, H. Beraldo, M. M. Salberg, D. X. West, L. Gonzalez and E. Ochoa, *Polyhedron*, 1997, **16**, 3549-3555 (DOI:10.1016/s0277-5387(97)00119-8).
- 90 D. G. Calatayud, E. Lopez-Torres and M. A. Mendiola, *Eur. J. Inorg. Chem.*, 2013, **2013**, 80-90 (DOI:10.1002/ejic.201200815).
- 91 J. P. Holland, P. J. Barnard, S. R. Bayly, H. M. Betts, G. C. Churchill, J. R. Dilworth, R. Edge, J. C. Green and R. Hueting, *Eur. J. Inorg. Chem.*, 2008, **2008**, 1985-1993 (DOI:10.1002/ejic.200701351).
- 92 P. A. Waghorn, M. W. Jones, M. B. M. Theobald, R. L. Arrowsmith, S. I. Pascu, S. W. Botchway, S. Faulkner and J. R. Dilworth, *Chem. Sci.*, 2013, **4**, 1430-1441 (DOI:10.1039/c2sc21489j).
- 93 A. R. Cowley, J. R. Dilworth, P. S. Donnelly, J. M. Heslop and S. J. Ratcliffe, *Dalton Trans.*, 2007, , 209-217 (DOI:10.1039/b612142j).
- 94 J. R. Dilworth, S. I. Pascu, P. A. Waghorn, D. Vullo, S. R. Bayly, M. Christlieb, X. Sun and C. T. Supuran, *Dalton Trans.*, 2015, **44**, 4859-4873 (DOI:10.1039/C4DT03206C).

- 95 R. Hueting, V. Kersemans, M. Tredwell, B. Cornelissen, M. Christlieb, A. D. Gee, J. Passchier, S. C. Smart, V. Gouverneur, R. J. Muschel and J. R. Dilworth, *Metallomics*, 2015, **7**, 795-804 (DOI:10.1039/c4mt00330f).
- 96 B. A. Gingras, T. Suprunchuk and C. H. Bayley, *Can. J. Chem.*, 1962, **40**, 1053-1059.
- 97 A. I. Matesanz and P. Souza, *Inorg. Chem. Commun.*, 2013, **27**, 5-8 (DOI:10.1016/j.inoche.2012.10.022).
- 98 R. N. Prabhu and R. Ramesh, *Tetrahedron Lett.*, 2013, **54**, 1120-1124 (DOI:10.1016/j.tetlet.2012.12.070).
- 99 T. Ismail, D. D. Rossouw, P. Beukes, J. P. Slabbert and G. S. Smith, *Inorg. Chem. Commun.*, 2013, **33**, 154-157 (DOI:10.1016/j.inoche.2013.04.025).
- 100 M. Cindrić and M. Rubčić, *Croat. Chem. Acta*, 2012, **85**, 505-513 (DOI:10.5562/cca2153).
- 101 H. R. Modi and N. K. Sharma, *Asian J. Chem.*, 2010, **22**, 2485-2490.
- 102 H. Yan, P. Chellan, T. Li, J. Mao, K. Chibale and G. S. Smith, *Tetrahedron Lett.*, 2013, **54**, 154-157 (DOI:10.1016/j.tetlet.2012.10.115).
- 103 E. Lopez-Torres and M. A. Mendiola, *J. Organomet. Chem.*, 2013, **725**, 28-33 (DOI:10.1016/j.jorganchem.2012.11.032).
- 104 N. S. H. N. Moorthy, N. M. F. S. A. Cerqueira, M. J. Ramos and P. A. Fernandes, *Recent Pat. Anti-Cancer Drug Discovery*, 2013, **8**, 168-182.
- 105 H. Kurihara, N. Honda, Y. Kono and Y. Arai, *Curr. Med. Chem.*, 2012, **19**, 3282-3289 (DOI:10.2174/092986712801215964).
- 106 M. E. Shelton, M. A. Green, C. J. Mathias, M. J. Welch and S. R. Bergmann, *J. Nucl. Med.*, 1989, **30**, 1843-1847.
- 107 T. Zhang, S. K. Das, D. R. Fels, K. S. Hansen, T. Z. Wong, M. W. Dewhirst and G. Vlahovic, *Am. J. Roentgenol.*, 2013, **201**, W698-W706 (DOI:10.2214/ajr.12.9698).
- 108 K. Y. Djoko, P. S. Donnelly and A. G. McEwan, *Metallomics*, 2014, **6**, 2250-2259 (DOI:10.1039/c4mt00226a).
- 109 K. A. Krohn, J. M. Link and R. P. Mason, *J. Nucl. Med.*, 2008, **49**, 129S-148S (DOI:10.2967/jnumed.107.045914).
- 110 S. E. Lapi, T. F. Voller and M. J. Welch, *PET Clinics*, 2009, **4**, 39-47 (DOI:10.1016/j.cpet.2009.05.009).
- 111 S. E. Rademakers, P. N. Span, J. H. A. M. Kaanders, F. C. G. J. Sweep, A. J. van der Kogel and J. Bussink, *Mol. Oncol.*, 2008, **2**, 41-53 (DOI:10.1016/j.molonc.2008.03.006).
- 112 O. J. Kelada and D. J. Carlson, *Radiat. Res.*, 2014, **181**, 335-349 (DOI:10.1667/rr13590.1).
- 113 I. Serganova, J. Humm, C. Ling and R. Blasberg, *Clin. Cancer Res.*, 2006, **12**, 5260-5264 (DOI:10.1158/1078-0432.ccr-06-0517).

- 114 D. Hennessey, L. M. Martin, A. Atzberger, T. H. Lynch, D. Hollywood and L. Marignol, *Urol. Oncol. : Semin. Orig. Invest.*, 2013, **31**, 1106-1116 (DOI:10.1016/j.urolonc.2011.10.008).
- 115 Q. N. Do, J. S. Ratnakar, Z. Kovács and A. D. Sherry, *ChemMedChem*, 2014, **9**, 1116-1129 (DOI:10.1002/cmdc.201402034).
- 116 R. H. Thomlinson and L. H. Gray, *Br. J. Cancer*, 1955, **9**, 539-549.
- 117 R. Wijsman, J. H. A. M. Kaanders, W. J. G. Oyen and J. Bussink, *Q. J. Nucl. Med. Mol. Imag.*, 2013, **57**, 244-256.
- 118 J. R. Ballinger, *Semin. Nucl. Med.*, 2001, **31**, 321-329.
- 119 J. Lanzen, R. D. Braun, B. Klitzman, D. Brizel, T. W. Secomb and M. W. Dewhirst, *Cancer Res.*, 2006, **66**, 2219-2223 (DOI:10.1158/0008-5472.can-03-2958).
- 120 X. Geets, V. Grégoire and J. A. Lee, *Q. J. Nucl. Med. Mol. Imag.*, 2013, **57**, 271-282.
- 121 C. J. Koch and S. M. Evans, *Semin. Nucl. Med.*, 2015, **45**, 163-176 (DOI:10.1053/j.semnuclmed.2014.10.004).
- 122 E. M. Hammond, M. C. Asselin, D. Forster, J. P. B. O'Connor, J. M. Senra and K. J. Williams, *Clinical Oncology*, 2014, **26**, 277-288 (DOI:10.1016/j.clon.2014.02.002).
- 123 J. P. Holland, J. C. Green and J. R. Dilworth, *Dalton Trans.*, 2006, , 783-794 (DOI:10.1039/b512656h).
- 124 J. Overgaard, *Int. J. Radiat. Biol.*, 1989, **56**, 801-811 (DOI:10.1080/09553008914552081).
- 125 G. Schwarz, *Münchener Med Wochenschr*, 1909, **24**, 1-2.
- 126 D. Gambino, *Curr. Med. Chem.*, 2010, **17**, 3616-3631 (DOI:10.2174/092986710793213797).
- 127 D. Thorwarth, D. Mönnich and D. Zips, *Q. J. Nucl. Med. Mol. Imag.*, 2013, **57**, 235-243.
- 128 D. Zips, K. Zöphel, N. Abolmaali, R. Perrin, A. Abramyuk, R. Haase, S. Appold, J. Steinbach, J. Kotzerke and M. Baumann, *Radiother. Oncol.*, 2012, **105**, 21-28 (DOI:10.1016/j.radonc.2012.08.019).
- 129 L. S. Mortensen, J. Johansen, J. Kallehauge, H. Primdahl, M. Busk, P. Lassen, J. Alsner, B. S. Sørensen, K. Toustrup, S. Jakobsen, J. Petersen, H. Petersen, J. Theil, M. Nordmark and J. Overgaard, *Radiother. Oncol.*, 2012, **105**, 14-20 (DOI:10.1016/j.radonc.2012.09.015).
- 130 C. Yip, P. J. Blower, V. Goh, D. B. Landau and G. J. R. Cook, *Eur. J. Nucl. Med. Mol. Imaging*, 2015, (DOI:10.1007/s00259-015-3009-6).
- 131 P. Vaupel, K. Schienger, C. Knoop and M. Höckel, *Cancer Res.*, 1991, **51**, 3316-3322.
- 132 S. E. Lapi, J. S. Lewis and F. Dehdashti, *Semin. Nucl. Med.*, 2015, **45**, 177-185 (DOI:10.1053/j.semnuclmed.2014.10.003).
- 133 S. E. Rademakers, J. Lok, A. J. van der Kogel, J. Bussink and J. H. A. M. Kaanders, *BMC Cancer*, 2011, **11** (DOI:10.1186/1471-2407-11-167).

- 134 M. R. Horsman, L. S. Mortensen, J. B. Petersen, M. Busk and J. Overgaard, *Nat. Rev. Clin. Oncol.*, 2012, **9**, 674-687 (DOI:10.1038/nrclinonc.2012.171).
- 135 M. Piert, H. J. Machulla, M. Picchio, G. Reischl, S. Ziegler, P. Kumar, H. J. Wester, R. Beck, A. J. B. McEwan, L. I. Wiebe and M. Schwaiger, *J. Nucl. Med.*, 2005, **46**, 106-113.
- 136 J. L. J. Dearling and A. B. Packard, *Nucl. Med. Biol.*, 2010, **37**, 237-243 (DOI:10.1016/j.nucmedbio.2009.11.004).
- 137 H. M. Betts, P. J. Barnard, S. R. Bayly, J. R. Dilworth, A. D. Gee and J. P. Holland, *Angew. Chem.-Int. Edit.*, 2008, **47**, 8416-8419 (DOI:10.1002/anie.200801936).
- 138 M. P. S. Dunphy and J. S. Lewis, *J. Nucl. Med.*, 2009, **50**, 106S-121S (DOI:10.2967/jnumed.108.057281).
- 139 K. A. Wood, W. L. Wong and M. I. Saunders, *Nucl. Med. Biol.*, 2008, **35**, 393-400 (DOI:10.1016/j.nucmedbio.2008.02.002).
- 140 G. Mees, M. Sathekge, A. Maes and C. Van de Wiele, *Curr. Pharm. Des.*, 2014, **20**, 2308-2318 (DOI:10.2174/13816128113196660662).
- 141 K. A. Price, P. J. Crouch, I. Volitakis, B. M. Paterson, S. Lim, P. S. Donnelly and A. R. White, *Inorg. Chem.*, 2011, **50**, 9594-9605 (DOI:10.1021/ic201334q).
- 142 H. Taniuchi, Y. Fujibayashi, H. Okazawa, Y. Yonekura, J. Konishi and A. Yokoyama, *Biol. Pharm. Bull.*, 1995, **18**, 1126-1129.
- 143 F. Shaughnessy, E. Mariotti, K. P. Shaw, T. R. Eykyn, P. J. Blower, R. Siow and R. Southworth, *EJNMMI Research*, 2014, **4** (DOI:10.1186/s13550-014-0040-8).
- 144 P. J. Barnard, S. R. Bayly, J. P. Holland, J. R. Dilworth and P. A. Waghorn, *Q. J. Nucl. Med. Mol. Imag.*, 2008, **52**, 235-244.
- 145 J. L. J. Dearling, J. S. Lewis, D. W. McCarthy, M. J. Welch and P. J. Blower, *Chem. Commun.*, 1998, , 2531-2532.
- 146 R. I. Maurer, P. J. Blower, J. R. Dilworth, C. A. Reynolds, Y. Zheng and G. E. D. Mullen, *J. Med. Chem.*, 2002, **45**, 1420-1431 (DOI:10.1021/jm0104217).
- 147 R. Hueting, V. Kersemans, B. Cornelissen, M. Tredwell, K. Hussien, M. Christlieb, A. D. Gee, J. Passchier, S. C. Smart, J. R. Dilworth, V. Gouverneur and R. J. Muschel, *J. Nucl. Med.*, 2014, **55**, 128-134 (DOI:10.2967/jnumed.113.119917).
- 148 Y. Fujibayashi, C. S. Cutler, C. J. Anderson, D. W. McCarthy, L. A. Jones, T. Sharp, Y. Yonekura and M. J. Welch, *Nucl. Med. Biol.*, 1999, **26**, 117-121 (DOI:10.1016/s0969-8051(98)00049-3).
- 149 J. S. Lewis, T. L. Sharp, R. Laforest, Y. Fujibayashi and M. J. Welch, *J. Nucl. Med.*, 2001, **42**, 655-661.
- 150 J. S. Lewis, P. Herrero, T. L. Sharp, J. A. Engelbach, Y. Fujibayashi, R. Laforest, A. Kovacs, R. J. Gropler and M. J. Welch, *J. Nucl. Med.*, 2002, **43**, 1557-1569.
- 151 N. Takahashi, Y. Fujibayashi, Y. Yonekura, M. J. Welch, A. Waki, T. Tsuchida, N. Sadato, K. Sugimoto and H. Itoh, *Ann. Nucl. Med.*, 2000, **14**, 323-328.

- 152 J. S. Lewis, R. Laforest, F. Dehdashti, P. W. Grigsby, M. J. Welch and B. A. Siegel, *J. Nucl. Med.*, 2008, **49**, 1177-1182 (DOI:10.2967/jnumed.108.051326).
- 153 S. R. Bayly, R. C. King, D. J. Honess, P. J. Barnard, H. M. Betts, J. P. Holland, R. Hueting, P. D. Bonnitza, J. R. Dilworth, F. I. Aigbirhio and M. Christlieb, *J. Nucl. Med.*, 2008, **49**, 1862-1868 (DOI:10.2967/jnumed.108.054015).
- 154 P. Barnard, S. Bayly, H. Betts, P. Bonnitza, M. Christlieb, J. Dilworth, J. Holland and S. Pascu, *Q. J. Nucl. Med. Mol. Imag.*, 2008, **52**, 174-184.
- 155 J. S. Lewis, D. W. McCarthy, T. J. McCarthy, Y. Fujibayashi and M. J. Welch, *J. Nucl. Med.*, 1999, **40**, 177-183.
- 156 T. J. Bradshaw, S. R. Bowen, N. Jallow, L. J. Forrest and R. Jeraj, *J. Nucl. Med.*, 2013, **54**, 1931-1937 (DOI:10.2967/jnumed.113.121921).
- 157 P. Burgman, J. A. O'Donoghue, J. S. Lewis, M. J. Welch, J. L. Humm and C. C. Ling, *Nucl. Med. Biol.*, 2005, **32**, 623-630 (DOI:10.1016/j.nucmedbio.2005.05.003).
- 158 H. Yuan, T. Schroeder, J. E. Bowsher, L. W. Hedlund, T. Wong and M. W. Dewhirst, *J. Nucl. Med.*, 2006, **47**, 989-998.
- 159 K. S. C. Chao, W. R. Bosch, S. Mutic, J. S. Lewis, F. Dehdashti, M. A. Mintun, J. F. Dempsey, C. A. Perez, J. A. Purdy and M. J. Welch, *Int. J. Radiat. Oncol. Biol. Phys.*, 2001, **49**, 1171-1182 (DOI:10.1016/s0360-3016(00)01433-4).
- 160 K. I. Matsumoto, L. Szajek, M. C. Krishna, J. A. Cook, J. Seidel, K. Grimes, J. Carson, A. L. Sowers, S. English, M. V. Green, S. L. Bacharach, W. C. Eckelman and J. B. Mitchell, *Int. J. Oncol.*, 2007, **30**, 873-881.
- 161 S. Carlin, H. Zhang, M. Reese, N. N. Ramos, Q. Chen and S. A. Ricketts, *J. Nucl. Med.*, 2014, **55**, 515-521 (DOI:10.2967/jnumed.113.126615).
- 162 M. Bourgeois, H. Rajerison, F. Guerard, M. Mougin-Degraef, J. Barbet, N. Michel, M. Cherel, A. Faivre-Chauvet and J. F. Gestin, *Nucl. Med. Rev.*, 2011, **14**, 90-95 (DOI:10.5603/NMR.2011.00022).
- 163 V. Kersemans, B. Cornelissen, R. Hueting, M. Tredwell, K. Hussien, P. D. Allen, N. Falzone, S. A. Hill, J. R. Dilworth, V. Gouverneur, R. J. Muschel and S. C. Smart, *Plos One*, 2011, **6** (DOI:10.1371/journal.pone.0025911).
- 164 M. G. Handley, R. A. Medina, E. Mariotti, G. D. Kenny, K. P. Shaw, R. Yan, T. R. Eykyn, P. J. Blower and R. Southworth, *J. Nucl. Med.*, 2014, **55**, 488-494 (DOI:10.2967/jnumed.113.129015).
- 165 R. M. Bell, M. M. Mocanu and D. M. Yellon, *J. Mol. Cell. Cardiol.*, 2011, **50**, 940-950 (DOI:10.1016/j.yjmcc.2011.02.018).
- 166 K. Imahashi, K. Morishita, H. Kusuoka, Y. Yamamichi, S. Hasegawa, K. Hashimoto, Y. Shirakami, M. Kato-Azuma and T. Nishimura, *J. Nucl. Med.*, 2000, **41**, 1102-1107.
- 167 M. G. Handley, R. A. Medina, R. L. Paul, P. J. Blower and R. Southworth, *Nucl. Med. Commun.*, 2013, **34**, 1015-1022 (DOI:10.1097/MNM.0b013e328363f25e).
- 168 M. G. Handley, R. A. Medina, E. Nagel, P. J. Blower and R. Southworth, *J. Mol. Cell. Cardiol.*, 2011, **51**, 640-650 (DOI:10.1016/j.yjmcc.2011.07.005).

- 169 J. S. Lewis, R. Laforest, T. L. Buettner, S. K. Song, Y. Fujibayashi, J. M. Connett and M. J. Welch, *Proc. Natl. Acad. Sci. U. S. A.*, 2001, **98**, 1206-1211 (DOI:10.1073/pnas.98.3.1206).
- 170 T. J. Bradshaw, S. Yip, N. Jallow, L. J. Forrest and R. Jeraj, *Int. J. Radiat. Oncol. Biol. Phys.*, 2014, **89**, 399-405 (DOI:10.1016/j.ijrobp.2014.02.016).
- 171 M. A. Cater, H. B. Pearson, K. Wolyniec, P. Klaver, M. Bilandzic, B. M. Paterson, A. I. Bush, P. O. Humbert, S. La Fontaine, P. S. Donnelly and Y. Haupt, *ACS Chem. Biol.*, 2013, **8**, 1621-1631 (DOI:10.1021/cb400198p).
- 172 D. Palanimuthu, S. V. Shinde, K. Somasundaram and A. G. Samuelson, *J. Med. Chem.*, 2013, **56**, 722-734 (DOI:10.1021/jm300938r).
- 173 Y. Sato, T. Tsujikawa, M. Oh, T. Mori, Y. Kiyono, S. Fujieda, H. Kimura and H. Okazawa, *Clin. Nucl. Med.*, 2014, **39**, 1027-1032 (DOI:10.1097/RLU.0000000000000537).
- 174 D. J. Williamson, S. Ejaz, S. Sitnikov, T. D. Fryer, S. J. Sawiak, P. Burke, J. C. Baron and F. I. Aigbirhio, *Nucl. Med. Biol.*, 2013, **40**, 338-344 (DOI:10.1016/j.nucmedbio.2012.11.012).
- 175 T. J. Nowak and A. G. Handford, *Pathophysiology: Concepts and Applications for Health Care Professionals*, McGraw-Hill, 2004.
- 176 J. L. Hickey and P. S. Donnelly, *Coord. Chem. Rev.*, 2012, **256**, 2367-2380 (DOI:10.1016/j.ccr.2012.03.035).
- 177 C. Lambert, H. Beraldo, N. Lievre, A. Garnier-Suillerot, P. Dorlet and M. Salerno, *J. Biol. Inorg. Chem.*, 2013, **18**, 59-69 (DOI:10.1007/s00775-012-0949-1).
- 178 P. J. Crouch and K. J. Barnham, *Acc. Chem. Res.*, 2012, **45**, 1604-1611 (DOI:10.1021/ar300074t).
- 179 J. L. Hickey, S. Lim, D. J. Hayne, B. M. Paterson, J. M. White, V. L. Villemagne, P. Roselt, D. Binns, C. Cullinane, C. M. Jeffery, R. I. Price, K. J. Barnham and P. S. Donnelly, *J. Am. Chem. Soc.*, 2013, **135**, 16120-16132 (DOI:10.1021/ja4057807).
- 180 K. A. Price, A. Caragounis, B. M. Paterson, G. Filiz, I. Volitakis, C. L. Masters, K. J. Barnham, P. S. Donnelly, P. J. Crouch and A. R. White, *J. Med. Chem.*, 2009, **52**, 6606-6620 (DOI:10.1021/jm9007938).
- 181 P. J. Crouch, W. H. Lin, P. A. Adlard, M. Cortes, V. Lal, G. Filiz, K. A. Perez, M. Nurjono, A. Caragounis, T. Du, K. Loughton, I. Volitakis, A. I. Bush, Q. X. Li, C. L. Masters, R. Cappai, R. A. Cherny, P. S. Donnelly, A. R. White and K. J. Barnham, *Proc. Natl. Acad. Sci. U. S. A.*, 2009, **106**, 381-386 (DOI:10.1073/pnas.0809057106).
- 182 Y. Biran, C. L. Masters, K. J. Barnham, A. I. Bush and P. A. Adlard, *J. Cell. Mol. Med.*, 2009, **13**, 61-86 (DOI:10.1111/j.1582-4934.2008.00595.x).
- 183 J. R. Dilworth and R. Hueting, *Inorg. Chim. Acta*, 2012, **389**, 3-15 (DOI:10.1016/j.ica.2012.02.019).
- 184 M. T. Fodero-Tavoletti, V. L. Villemagne, B. M. Paterson, A. R. White, Q. X. Li, J. Camakaris, G. O'Keefe, R. Cappai, K. J. Barnham and P. S. Donnelly, *J. Alzheimer's Dis.*, 2010, **20**, 49-55 (DOI:10.3233/jad-2010-1359).

- 185 S. Lim, B. M. Paterson, M. T. Fodero-Tavoletti, G. J. O'Keefe, R. Cappai, K. J. Barnham, V. L. Villemagne and P. S. Donnelly, *Chem. Commun.*, 2010, **46**, 5437-5439 (DOI:10.1039/c0cc01175d).
- 186 J. P. Holland, M. W. Jones, P. D. Bonnitcha, J. S. Lewis and J. R. Dilworth, *New J. Chem.*, 2009, **33**, 1845-1852 (DOI:10.1039/b902895a).
- 187 B. R. Roberts, N. K. H. Lim, E. J. McAllum, P. S. Donnelly, D. J. Hare, P. A. Doble, B. J. Turner, K. A. Price, S. C. Lim, B. M. Paterson, J. L. Hickey, T. W. Rhoads, J. R. Williams, K. M. Kanninen, L. W. Hung, J. R. Liddell, A. Grubman, J. F. Monty, R. M. Llanos, D. R. Kramer, J. F. B. Mercer, A. I. Bush, C. L. Masters, J. A. Duce, Q. X. Li, J. S. Beckman, K. J. Barnham, A. R. White and P. J. Crouch, *J. Neurosci.*, 2014, **34**, 8021-8031 (DOI:10.1523/jneurosci.4196-13.2014).
- 188 B. M. Hybertson, B. Gao, S. K. Bose and J. M. McCord, *Mol. Asp. Med.*, 2011, **32**, 234-246 (DOI:10.1016/j.mam.2011.10.006).
- 189 A. R. Cowley, J. Davis, J. R. Dilworth, P. S. Donnelly, R. Dobson, A. Nightingale, J. M. Peach, B. Shore, D. Kerr and L. Seymour, *Chem. Commun.*, 2005, , 845-847 (DOI:10.1039/b417206j).
- 190 V. Bocokic, M. Lutz, A. L. Spek and J. N. H. Reek, *Dalton Trans.*, 2012, **41**, 3740-3750 (DOI:10.1039/c2dt12096h).
- 191 S. I. Pascu, P. A. Waghorn, T. D. Conry, B. Lin, H. M. Betts, J. R. Dilworth, R. B. Sim, G. C. Churchill, F. I. Aigbirhio and J. E. Warren, *Dalton Trans.*, 2008, , 2107-2110 (DOI:10.1039/b802806k).
- 192 K. Matsumoto, Y. Fujibayashi, Y. Arano, K. Wada and A. Yokoyama, *Int J Rad Appl Instrum B*, 1992, **19**, 33-38.
- 193 H. Saji, A. Saiga, Y. Iida, Y. Magata and A. Yokoyama, *J. Labelled Compd. Radiopharm.*, 1993, **33**, 127-135 (DOI:10.1002/jlcr.2580330207).
- 194 A. Aphaiwong, M. G. Moloney and M. Christlieb, *J. Mater. Chem.*, 2012, **22**, 24627-24636 (DOI:10.1039/c2jm34942f).
- 195 C. S. Tai, *Radiopharmaceutical copper thiosemicarbazone complexes*, University of kent, 2007.
- 196 J. R. Dilworth, J. M. Peach, J. M. Heslop and P. S. Donnelly, *Preparation of transition metal thiosemicarbazone derivative complexes for medical imaging and therapy*, WO 2007003944, World, 2007.
- 197 M. Olea, R. Fatima and R. Garcia-Villanova, *Ars Pharm.*, 1978, **19**, 181-188.
- 198 V. C. Barry, J. Byrne, M. L. Conalty and J. F. O'Sullivan, *Proc. R. Ir. Acad. [B]*, 1967, **65**, 269-284.
- 199 P. A. Barrett and D. E. Bays, *Thiosemicarbazones and their Preparation*, GB 966849, Great Britain, 1964.
- 200 Sigmaaldrich.com, *Methylglyoxal-1,1-dimethyl acetal ≥97%*, <http://www.sigmaaldrich.com/catalog/product/aldrich/170216?lang=en&region=GB>, (Last accessed 06/2015).
- 201 Sigmaaldrich.com, *Methylglyoxal solution ~40% in H<sub>2</sub>O*, <http://www.sigmaaldrich.com/catalog/product/sigma/m0252?lang=en&region=GB>, (Last accessed 06/2015).

- 202 D. T. Minkel, C. Chan Stier and D. H. Petering, *Mol. Pharmacol.*, 1976, **12**, 1036-1044.
- 203 K. Horiuchi, T. Tsukamoto, M. Saito, M. Nakayama, Y. Fujibayashi and H. Saji, *Nucl. Med. Biol.*, 2000, **27**, 391-399.
- 204 A. R. Cowley, J. R. Dilworth, P. S. Donnelly, E. Labisbal and A. Sousa, *J. Am. Chem. Soc.*, 2002, **124**, 5270-5271 (DOI:10.1021/ja012668z).
- 205 J. Adams and R. Shepherd, *Tetrahedron Lett.*, 1968, , 2747-2750.
- 206 G. Buncic, P. S. Donnelly, B. M. Paterson, J. M. White, M. Zimmermann, Z. Xiao and A. G. Wedd, *Inorg. Chem.*, 2010, **49**, 3071-3073 (DOI:10.1021/ic902370a).
- 207 P. J. Larkin, *Infrared and Raman Spectroscopy: Principles and Spectral Interpretation* , Elsevier, Oxford, 2011.
- 208 G. Socrates, *Infrared and Raman Characteristic Group Frequencies: Tables and Charts*, Wiley, 2001.
- 209 Z. Afrasiabi, P. Stovall, K. Finley, A. Choudhury, C. Barnes, A. Ahmad, F. Sarkar, A. Vyas and S. Padhye, *Spectrochim. Acta, Part A*, 2013, **114**, 114-119 (DOI:10.1016/j.saa.2013.04.122.).
- 210 H. Beraldo, L. P. Boyd and D. X. West, *Transit. Met. Chem.*, 1998, **23**, 67-71 (DOI:10.1023/A:1006958018049).
- 211 K. E. Martin, BSc, University of Kent, 2003.
- 212 S. Stringer, BSc, University of Kent, 2006.
- 213 L. Patiny and A. Borel, *J. Chem. Inf. Model.*, 2013, **53**, 1223-1228 (DOI:10.1021/ci300563h).
- 214 M. Shebl, M. A. Ibrahim, S. M. E. Khalil, S. L. Stefan and H. Habib, *Spectrochim. Acta, Part A*, 2013, **115**, 399-408 (DOI:10.1016/j.saa.2013.06.075).
- 215 X. Zhong, P. An, M. Liu, J. Zhang and J. Huang, *Hainan Yixueyuan Xuebao*, 2010, **16**, 817-819.
- 216 J. N. Van Niekerk, F. R. Schoening and J. H. Talbot, *Acta Cryst.*, 1953, **6**, 720-723 (DOI:10.1107/S0365110X53002015).
- 217 S. Bhattacharyya, S. B. Kumar, S. K. Dutta, E. R. T. Tiekink and M. Chaudhury, *Inorg. Chem.*, 1996, **35**, 1967-1973.
- 218 Agilent Technologies, *CrysAlis PRO*, Yarnton, England, 2014.
- 219 G. M. Sheldrick, *Acta Cryst.*, 2008, **A64**, 12-122.
- 220 G. M. Sheldrick, *Acta Cryst.*, 2015, **C71**, 3-8.
- 221 O. V. Dolomanov, L. J. Bourhis, R. J. Gildea, J. A. K. Howard and H. Puschmann, *J. Appl. Cryst.*, 2009, **42**, 339-341.
- 222 E. López-Torres, M. A. Mendiola, J. Rodríguez-Procopio, M. T. Sevilla, E. Colacio, J. Ma Moreno and I. Sobrados, *Inorg. Chim. Acta*, 2001, **323**, 130-138 (DOI:10.1016/S0020-1693(01)00607-7).



223 S. Akyüz, A. B. Dempster, R. L. Morehouse and S. Suzuki, *J. Mol. Struct.*, 1973, **17**, 105-125 (DOI:10.1016/0022-2860(73)85047-1).

224 D. A. Thornton, *Coord. Chem. Rev.*, 1990, **104**, 251-295.

225 S. Akyüz, A. B. Dempster, J. E. D. Davies and K. T. Holmes, *Dalton Trans.*, 1976, , 1746-1749 (DOI:10.1039/DT9760001746).

### Appendix 1 Materials used

<b>Name</b>	<b>Quantity</b>	<b>Supplier</b>	<b>CAS number</b>	<b>Purity</b>
<b>Acetone</b>	2.5l	Fisher Scientific	67-68-5	>99%
<b>Acetonitrile</b>	2.5l	Fisher Chemicals	75-05-8	99.99%
<b>2,3 Butanedione</b>	100ml	Aldrich	431-03-8	97%
<b>Copper acetate monohydrate</b>	500g	Fisons Scientific Equipment	142-71-2	99%
<b>Diethyl ether</b>	2.5l	Fisher Scientific	60-29-7	99.98%
<b>3,3-Dimethoxy-2-butanone</b>	25g	Acros organics	21983-72-2	98%
<b>Dimethyl aminopyridine on polystyrene crosslinked with 2% divinyl benzene</b>	5g	Aldrich	82942-26-5	
<b>Dimethyl sulfoxide</b>	500ml	Fisher Scientific	67-68-5	99.99%
<b>Dimethyl sulfoxide D-6</b>	10g	Cambridge isotope laboratories inc	2206-27-1	99.9%
<b>4,4-Dimethyl-3-thiosemicarbazide</b>	1g	Aldrich	6926-58-5	98%
<b>Ethanol (absolute)</b>	2.5l	Fisher Scientific	64-17-5	99.99%
<b>4-Ethyl-3-thiosemicarbazide</b>	25g	Aldrich	13431-34-0	97%
<b>Glyoxal solution</b>	100g	Sigma-Aldrich	107-22-2	40% wt in H <sub>2</sub> O
<b>Hydrochloric acid</b>	2.5l	Fisher Scientific	7647-01-0	32%
<b>Lithium tetraflouroborate</b>	10g	Alfa Aesar	14283-07-9	98%
<b>Lithium tetraflouroborate</b>	10g	Aldrich	14283-07-9	98%
<b>Magnesium sulfates</b>	2Kg	Aldrich	7487-88-9	97%

<b>Methyl glyoxal-1,1-dimethyl acetal</b>	25g	Acros Organics	6342-56-9	97+%
<b>Methanol</b>	2.5l	Fisher Scientific	67-56-1	99.99%
<b>4-Methyl-3-thiosemicarbazide</b>	50g	Aldrich	6610-29-3	97%
<b>Molecular Sieves (3Å)</b>	1Kg	Sigma-Aldrich	308080-99-1	
<b>N,N-Dimethyl formamide</b>	2.5l	Fisher Scientific	68-12-2	99%
<b>2,4-Pentanedione</b>	250ml	Aldrich	123-54-6	99+%
<b>4-Phenylthiosemicarbazide</b>	10g	Aldrich	5351-69-9	99%
<b>Poly (4-vinyl pyridine) crosslinked with 2% divinyl benzene</b>	25g	Aldrich	9017-40-4	
<b>Pyridine</b>	100ml	Sigma-Aldrich	110-86-1	99.8%
<b>Sodium carbonate</b>	500g	Aldrich	497-19-8	97%
<b>Sodium hydroxide</b>	1Kg	Fisher Scientific	1310-73-2	99%
<b>Thiosemicarbazide</b>	100g	Aldrich	79-19-6	99%
<b>Zinc acetate</b>	25g	Aldrich	557-34-6	99.99%

## **Appendix 2 Instrumental conditions**

Instrumentation and conditions used for analysis of the bis(thiosemicarbazone) ligands, intermediates and their corresponding copper and zinc complexes.

### **NMR spectroscopy conditions**

A Jeol JNM ECS400 Nuclear Magnetic Resonance Spectrometer was used.

<sup>1</sup>H: Field strength: 9.4 T (400 MHz), X freq: 400 MHz, scans: 8.

<sup>13</sup>C: Field strength: 9.4 T (400 MHz), X freq: 101 MHz, scans: 1024.

### **Infrared spectroscopy conditions**

A Shimadzu IR Affinity-1 Fourier Transform Infrared Spectrometer with a Golden Gate Diamond Attenuated Total Reflectance (ATR) attachment was used.

Range: 400 cm<sup>-1</sup>-4000 cm<sup>-1</sup>, number of scans: 16, resolution: 4.0, measurement mode: % transmittance

### **Raman spectroscopy conditions**

A LABRAM HR800 Raman Spectrometer was used.

### **Bis(thiosemicarbazone) ligands & monosubstituted-3-thiosemicarbazone intermediates:**

**Red laser:** Laser: 632.81 nm, range: 200 cm<sup>-1</sup>-4000 cm<sup>-1</sup>, hole: 800, slit: 100, grating: 600, filter: 10 %, accumulation time: 2 seconds, accumulations: 5.

### **Copper bis(thiosemicarbazone) complexes:**

**Red laser:** Laser: 632.81 nm, range: 200 cm<sup>-1</sup>-4000 cm<sup>-1</sup>, hole: 800, slit: 100, grating: 600, filter: 10 %, accumulation time: 20 seconds, accumulations: 4.

**Green laser:** Laser: 532.00 nm, range: 200 cm<sup>-1</sup>-4000 cm<sup>-1</sup>, hole: 800, slit: 100, grating: 1800, filter: 0.1 %, Accumulation time: 2 seconds, Accumulations: 5.

### **Zinc bis(thiosemicarbazone) complexes:**

**Red laser:** Laser: 632.81 nm, range: 200 cm<sup>-1</sup>-4000 cm<sup>-1</sup>, hole: 800, slit: 100, grating: 600, filter: 10 %, accumulation time: 2 seconds, accumulations: 5.

**Near infrared:** Laser: 784.15 nm, range: 200 cm<sup>-1</sup>-2000 cm<sup>-1</sup>, hole: 200, slit: 100, grating: 600, filter: 10 %, accumulation time: 2 seconds, accumulations: 5.

### **Elemental analysis conditions**

A Thermo Scientific (Carlo Erba) Flash 2000 Elemental Analyser was used which was configured for %CHN. The samples were run by Stephen Boyer from London Metropolitan University's Elemental Analysis Service.

### **Melting point analysis conditions**

A Stuart SMP10 melting point apparatus was used.

An initial melting point was obtained by using the fast ramp rate (20°C per min). The apparatus was allowed to cool by 30°C and a fresh sample was heated up using the slow ramp rate (2 °C per min).

### **UV-vis spectroscopy conditions**

A Shimadzu UV-1800 UV Spectrophotometer was used.

Scan Range: 285-800nm, Scan Speed: slow, Solvent: DMSO, Cuvette: Quartz, 1 cm path length.

### **Mass spectrometry conditions**

A Bruker micrO<sub>2</sub>-TOF-Q mass spectrometer was used.

Samples were dissolved in DMSO at a concentration of 1 mg/ml before being diluted 1 in 100 in methanol. 10 µl of sample was injected into a flowing stream of 10 mM ammonium acetate in 95% methanol in water (flow rate: 0.02 ml/min) and the flow directed into the electrospray source of the spectrometer. Mass spectra were acquired in the positive ion mode and data processed in Bruker's Compass Data Analysis software utilising a lock mass.

Source type: ESI, Scan begin: 100 m/z, Scan end: 1250 m/z, Ion polarity: positive, Set capillary: 4500 V, Set end plate offset: -100 V, Set Collision Cell RF: 150.0 Vpp, Set nebulizer: 0.4 Bar, Set dry heater: 180°C, Set dry gas: 4.0 l/min, Set divert valve: Source.

### **Reduction potential measurement conditions:**

The reduction potentials were gathered by Julia Baguña Torres from the Division of Imaging Sciences & Biomedical Engineering at King's College London. The potentials were obtained using cyclic voltammetry using a glassy carbon electrode as the working electrode, a silver wire electrode as the reference one and a platinum wire electrode as the auxiliary electrode. The values were normalised against ferrocene.